

Finite Element Simulation of Hip Joint Replacement under Static and Dynamic Loading

By

Hussam El-Din F. El-Shiekh, B.Sc.

This thesis is submitted to Dublin City University as the fulfillment of the requirement for the award of the degree of

Doctor of Philosophy

Supervisors

Professor M. S. J. Hashmi, Ph.D. D.Sc.

and

Dr. B. J. MacDonald, Ph.D.

**School of Mechanical and Manufacturing Engineering
Dublin City University**

March 2002

REFERENCE

DECLARATION

I hereby certify that this material, which I now submit for assessment on the programme of study leading to the award of *Doctor of Philosophy*, is entirely my own work and has not been taken from the work of others save and to the extent that such work has been cited and acknowledged within the text of my work.

Signed: _____



Hussam El-Din El-Sheikh

ID: 98970283

Date: 13th August 2002

Dedication

This thesis is dedicated to my mother, Salima and my father, Brigadier Fathi and also to my fiancée, Rania.

Acknowledgments

Many individuals have come to my assistance during the present work. I offer many thanks to all, and in particular I would like to acknowledge the contributions of:

Prof. M.S.J. Hashmi, Head of School of Mechanical & Manufacturing Engineering at Dublin City University, and Dr. Bryan Mac Donald, my academic supervisors, who bestowed me the opportunity to work in a stimulating research environment, for their continued support, guidance, encouragement, and their excellent supervision throughout the course of this project.

I would also like to record my appreciation to Dr. Brian McNamara, Senior Lecturer in School of Mechanical and Manufacturing Engineering, DCU, for his helpful advice and guidance during the early stages of the project.

I thank Mr Liam Domican and Mr. Keith Hickey for their help in the provision of software and computer facilities.

To my fellow research students in the School of Mechanical and Manufacturing Engineering.

I would like to convey my sincere thanks to my family, my mum and my dad, without whose support and encouragement this thesis would not have been written. Thanks are due to my siblings for their encouragement and up-lifting confidence in my ability and who continually inspired me.

Finally, all praises to God almighty for enabling me to complete this work.

Hussam El-Din El-Sheikh

Finite Element Simulation of Hip Joint Replacement under Static and Dynamic Loading

Hussam El-Din Fathi El'Shiekh

ABSTRACT

The objective of this work is to develop methods for the structural analysis of orthopaedic implants. The central argument is that, if stress distributions are interpreted in the context of failure models of the component materials, significant advantages can be made in our ability to design these devices. The artificial hip joint is used throughout as an example.

The finite element method was used as a structural analysis tool and its applicability was discussed. Validity and accuracy were assessed and results were compared with previous experimental and finite element studies. By comparing stress distributions with failure criteria for prosthesis and cement, the suitability of proposed design changes were assessed and guidelines for materials selection were presented. Prediction of bone stresses were also given for different prosthesis designs in the region of the artificial hip joint where bone adaption contributes to failure. Thereafter the focus was on utilizing a new technique to develop a new hip prosthesis model.

This study was divided into two parts according to the loading type. In this regard the stress field in the artificial hip components (prostheses, cement mantle, and bone) is analysed statically and dynamically to assess the implant longevity. In this static analysis all the simulations were conducted by assuming the peak loads during the normal gait at a particular time (static loads). The aim was to study the effects of a set of variables within which an optimal prosthesis design can be made by means of finite element analysis to qualify and quantify the stresses and the strains in natural and treated human femur for different cases of implantation. Until now, models developed to predict stresses in total hip replacements have been generally poorly validated. This could be because all the pre-clinical simulations were performed statically, that is by selecting the greatest load at a particular time of the activity cycle. The second part of the study was aimed to take into consideration, in designing total hip replacement, another factor belongs to the patient activity (stamping, jumping, walking, etc) and the effect of impact over the prosthesis head during these activity into the prosthesis performance. This study considered the prosthesis hip deformation with time, dynamic loads study. The elimination of impact cracking was considered by studying the effect of using "damper" trapped between the grooved prosthesis collar and the bone. Material selection of the total hip replacements was also investigated under the dynamic loading. The approaches of prosthesis fixation have been studied, too. This study was conducted by constructing three-dimensional finite element model for a femur implanted with a cemented prosthesis with a representative physiological loading condition by using the LS-DYNA3D software.

Nomenclature

Symbol	Definition	Dimension
l	Element characteristic length	m
t	Time	seconds
AHJ	Artificial Hip Joint	-
THP	Total Hip Prosthesis	-
$B^{(m)}$	Strain-displacement matrix for element m	-
C	Sonic wave propagation velocity	m/s
F	Force	N
f^B	Force per unite volume	N/m ³
f^S	Surface tractions	N/m ²
$H^{(m)}$	displacement interpolation matrix or shape function for element m .	-
K	Global stiffness matrix	-
R	Load vector	N
U	Virtual displacements	m
\bar{U}	Displacement in global X direction	m
\hat{U}	Vector of the three global displacement components	m
\dot{U}	Vector of the nodal point velocities	m/s
\ddot{U}	nodal point accelerations	m/s ²
\bar{V}	Displacement in global Y direction	m
V_e	Element volume	m ³
\bar{W}	Displacement in global Z direction	m

Greek

α	Number of hourglass mode	-
τ	Virtual stress	N/m ²
ε	Virtual strain	-
κ	Damping property parameter	-
ρ	Density	Kg/m ³
Γ	Hourglass shape vector	-

Superscript

B	Body	-
S	Surface	-
T	Transpose of a Matrix	-
eff	Effective	-
<i>i</i>	Point in space	-
t	Time	second
V	Volum	-

Contents

<i>Section No.</i>	<i>Description</i>	<i>Page No.</i>
	Declaration	i
	Dedication	ii
	Acknowledgments	iii
	Abstract	iv
	Nomenclature	v
	Contents	vii
Chapter 1	Background and Introductory Materials	1
1.1.	Historical View	1
1.2.	The Anatomy of Long Bone	2
1.3.	Functional Adaptation of Bone (Bone Remodeling)	7
1.4.	Bone as a Composite Material	10
1.4.1.	Elasticity and Strength of Bone	10
1.4.2.	Anisotropy of Bone	12
1.4.3.	Failure Criteria of Bone	12
1.5.	Biomechanics of the Lower Extremity	13
1.5.1.	Rigid Body Biomechanics	13
1.5.2.	Stresses and Strains	20
1.5.3.	Statics of the Lower Extremity	24
1.5.3.1.	Bipedal Stance	24
1.5.3.2.	Monopodal Stance	25
1.5.4.	Dynamics of the Lower Extremity	26
1.5.4.1.	Slow Motion	26
1.5.4.2.	High Speed and Acceleration	27
1.5.5.	Mechanics of the Hip Joint	28
1.5.5.1.	Equilibrium Conditions	28

1.5.5.1.1.	Equilibrium in Bipedal Stance	28
1.5.5.1.2.	Equilibrium in Monopodal Stance	29
1.5.5.2.	Stressing of the Hip Joint	29
1.5.5.2.1.	Stress Distribution in the Articular Surfaces	29
1.5.5.2.2.	Stress distribution in the Femoral neck	34
1.6.	Total Hip Prosthesis (THP)	35
1.6.1.	The Femoral Stem	37
1.6.2.	The Shoulder on the Femoral Stem	39
1.6.3.	Head Position – Neck Length and Neck Angle	40
1.6.4.	Head Diameter	41
1.6.5.	Use of Acrylic Cement	42
1.6.6.	Acetabular Component	43
1.6.7.	The Spherical Bearing	47
1.6.8.	Design Criteria for the Hip Endoprotheses	49
1.6.9.	Materials Combinations in Total Hip Joint Replacements	51
1.7.	Structural Stress Analysis	51
1.7.1.	Methods of Analysis	52
1.7.1.1.	Experimental Methods	52
1.7.1.1.1.	Electrical Strain Gauge	53
1.7.1.1.2.	Photoelastic Analysis Technique	55
1.7.1.2.	Closed –Form Theories	56
1.7.1.2.1.	Bar Theory	57
1.7.1.2.2.	Compound-Bar Theory	57
1.7.1.2.3.	Beam Theory	61
1.7.1.2.4.	Torsion of Circular Shafts	63
1.7.1.2.5.	Combined Loading of Slender Bodies	65
1.7.1.3.	Finite Element Methods	67
1.8.	Introduction to the Present work	72
1.9.	Objectives of the Present Work	75

1.9.1.	First Part: Static Analysis	75
1.9.2.	Second Part: Dynamic Analysis	76
Chapter 2	Literature Review	78
2.1.	General View	78
2.2.	The Dilemma of Bone Stress Shielding and Prosthesis Loosing	82
2.3.	The Effect of Material Selection on Prosthesis Performance	83
2.4.	The Effect of the Prosthesis Geometry on its Performance	85
2.5.	The Effect of Prosthesis Collar on its Performance	89
2.6.	Prosthesis Stability	90
2.7.	Frictional Heating in the Total Hip Implants	93
2.8.	Wear Behaviour in Total Hip Replacement	94
2.9.	Failure of Hip Prosthesis Components	95
2.10.	Relative Studies	97
2.11.	Closing Remarks	100
Chapter 3	Finite Element Analysis	102
3.1.	Introduction	102
3.2.	The Finite Element Method	102
3.2.1.	General Theory	103
3.2.2.	Non Linearities	107
3.2.3.	Solution Methodology	107
3.3.	ANSYS Theoretical Methods	110
3.3.1.	Solution Procedures	110
3.3.2.	Large Strain Theory	112
3.3.3.	Element Formulation	114
3.4.	LS-DYNA3D Theoretical Methods	114
3.4.1.	Solution Methodology	114
3.4.2.	Element Formulation	115

3.4.3.	Contact Algorithm	117
3.4.4.	Friction	119
3.5.	Summary of Chapter 3	120
Chapter 4	Static Loading Simulation	121
4.1.	Introduction	121
4.2.	Statement of the Problem	122
4.3.	Study of the Stress Distribution in The Intact Femur	123
4.3.1.	F.E. Model of Proximal Femur	123
4.3.2.	Material Properties	126
4.3.3.	Loading	126
4.3.4.	F.E. Model Validation	129
4.3.5.	Results	132
4.4.	Finite Element Stress Analysis of the AHJ	138
4.4.1.	Introduction	138
4.4.2.	Geometry modelling	138
4.4.2.1.	Treated Femur Implanted by AHJ	138
4.4.2.2.	Loading and Restraints	140
4.4.2.3.	Material Properties	140
4.4.3.	Global Stress Results	140
4.4.3.1.	Prosthesis Stem	141
4.4.3.2.	Cement Layer	141
4.5.	Parametric Analysis	145
4.5.1.	Material Selection in the Design of the Femoral Component of Cemented Total Hip Replacement	145
4.5.1.1.	Introduction	145
4.5.1.2.	The Effect of Prosthesis Materials on Prosthesis Stresses	146
4.5.1.3.	The Effect Cement Materials on the Prosthesis Stresses	146
4.5.1.4.	The Effect of Prosthesis Materials on the Cement	148

	Stresses	
4.5.1.5.	The effect of Cement Materials on the Cement Stresses	148
4.5.1.6.	The Effect of Cemented AHJ materials Combination on the Bone Cortex Stress Distributions	150
4.5.1.7.	Analysis of A.H.J. Using Stress Data for Material Selection	151
4.5.2.	Design of Artificial Hip Replacement consists of Two Materials to Control Stress Shielding And Migration Phenomenon	156
4.5.3.	Role of the Collar (Calcar Support) on the Femoral Stem of Cemented Total Hip Replacements	171
4.5.4.	Effect of Prosthesis Length Stem	186
4.5.5.	The Effect of the Stem Thickness	189
4.6	Summery of the Chapter	193
Chapter 5	A Comparison Study between Static and Dynamic Loading, and stress-based criteria reliability	194
5.1.	Introduction	194
5.2.	Finite Element Model	195
5.3.	Material Properties	196
5.4.	Loading Conditions	196
5.5.	Results	198
5.5.1.	Deformation Pattern	198
5.5.2.	Contours and Peak Stresses	199
5.5.3.	Axial Stresses	201
5.5.4.	Percentage of elements of prosthesis components at a given stress	203
Chapter 6	Dynamic Loading Simulation	205
6.1.	Objective	205
6.2.	Design Methodology	207
6.3.	Geometry Modelling	208
6.3.1.	Prosthesis and cement	209

6.3.2.	Damper	209
6.3.3.	Femur	210
6.4.	Boundary Conditions and loads applied	210
6.5.	Material proposed	211
6.6.	Simulation Results and Analysis	211
6.6.1.	The Effect of Design Features	212
6.6.1.1.	Prosthesis Displacements	212
6.6.1.2.	Hip components Axial Stress	213
	(A) Stem Prosthesis Stresses	213
	(B) Neck Prosthesis Stresses	221
	(C) Cement Mantle Stresses	223
	(D) Bone Cortex Stresses	226
6.6.2.	The Effect of Prosthesis material	228
6.6.2.1.	Hip components Axial Stress	229
	(A) Stem Prosthesis Stresses	229
	(B) Neck Prosthesis Stresses	230
	(C) Cement Mantle Stresses	230
	(D) Bone Cortex Stresses	233
6.6.3.	Would the proximal bound fixation alleviate the stress shielding in the bone?	235
6.6.3.1.	Stress Analysis	235
	(A) Neck and stem prosthesis stresses	235
	(B) Cement Mantle Axial Stress	237
	(C) Bone Cortex Axial Stress	240
6.6.4.	Is the damper solution to alleviate the impulse loads?	241
6.6.4.1.	Stress Analysis	241
	(A) Neck and stem prosthesis stresses	241
	(B) Cement Mantle Axial Stress	244
	(C) Bone Cortex Axial Stress	245

Chapter 7	Discussion	247
7.1.	Static Loading Simulation	249
7.1.1.	F.E. Model Validation.	249
7.1.2.	F.E. Model of Intact Proximal Femur	249
7.1.3.	Finite Element Stress Analysis of the AHJ	250
7.1.4.	Material Selection in the Design of the Femoral Component of Cemented Total Hip Replacement	250
7.1.5.	Design of Artificial Hip Replacement consists of Two Materials to Control Stress Shielding and Migration Phenomenon	251
7.1.6.	Role of the Collar on the Femoral Stem of Cemented Total Hip Replacements	252
7.1.7.	Effect of Prosthesis Length Stem	256
7.1.8.	Effect of Stem Thickness	256
7.2.	A Comparison Study between Static and Dynamic Loading, and Stress-Based Criteria Reliability	257
7.3.	Dynamic Loading Simulation	258
7.3.1.	The Effect of Design Features	258
7.3.2.	The Effect of Skirt-Collared Prosthesis Material	259
7.3.3.	Would the Proximal Bound Fixation Alleviate the Stress Shielding in the Bone?	261
7.3.4.	Is the Damper Solution to Alleviate the Impulse Loads?	262
Chapter 8	Conclusion and Proposal for Future Work	263
8.1.	Static loading simulation	263
8.1.1.	Finite element model	263
8.1.2.	Material Selection in the Design of the Femoral Component of Cemented Total Hip Replacement	263
8.1.3.	Design of Artificial Hip Replacement consists of Two Materials to Control Stress Shielding and Migration Phenomenon	264
8.1.4.	Role of the Collar on the Femoral Stem of Cemented Total Hip Replacements	264
8.1.5.	Effect of Prosthesis Length Stem	265
8.1.6.	Effect of Stem Thickness	265

8.2.	A Comparison Study between Static and Dynamic Loading, and Stress-Based Criteria Reliability	266
8.3.	Dynamic Loading Simulation	266
8.3.1.	The Effect of Design Features	266
8.3.2.	The Effect of Skirt-Collared Prosthesis Material	266
8.3.3.	Would the Proximal Bound Fixation Alleviate the Stress Shielding in the Bone?	267
8.3.4.	Is the Damper Solution to Alleviate the Impulse Loads?	267
8.4.	Recommendation for Further Work	267
8.5.	Thesis Contribution	268
References		269
Appendix 1	Publication	293

Chapter One

Background and Introductory Materials

1.1. Historical View

Biomechanics entails the application of methods and principles of engineering mechanics to biological structures and medical problems. As such, it is not a new field of endeavor. Early efforts in this area date back to Aristotle, Leonardo da Vinci, and Galileo. Significant contributions to the understanding of human body mechanics were also made in the last century and the first half of this century. Biomechanics has many fields of application, including orthopedic and cardiovascular surgery, traumatology, dentistry, rehabilitation, and sports, and is closely interwoven with basic medical sciences such as biophysics and medical physics, physiology, functional anatomy, and biomaterials. It can be considered a subbranch of biomedical engineering (or bioengineering) and a branch of biomechanical engineering, as engineering mechanics is one basic science of mechanical engineering.

After World War II and during the last two decades especially, a proliferation in biomechanics activities has occurred. This development was triggered and enhanced by two separate events. In the first place, engineering mechanics has advanced tremendously through the development of computers and computer methods. As a result the complex mechanical behavior of biological tissues and structures can now be realistically described and successfully analyzed. Secondly, increasing emphasis is being put close surgical reconstruction of body functions in the disabled and the sick. The augmentation in routine applications of artificial joints and new fracture fixation devices in orthopedic surgery is a good example. Long-term success of these devices and other reconstructive operations requires designs and surgical techniques that are based on a sound understanding of human body musculoskeletal mechanics.

In this chapter basic concepts and a general background of biomechanics are covered.

1.2. The Anatomy of Long Bone

Figure 1.1 shows a sketch of a long bone. It consists of a shaft (diaphysis) with an expansion (metaphysis) at each end. In an immature animal, each metaphysis is surmounted by an epiphysis, which is united to its metaphysis by a cartilaginous growth plate (epiphyseal plate). At the extremity of each epiphysis, a specialized covering of articular cartilage forms the gliding surface of the joint (articulation). The coefficient of dry friction between the articulate cartilages of a joint is very low (can be as low as 0.0026, probably the lowest of any known solid material); hence the cartilage covering makes an efficient joint [89, 310].

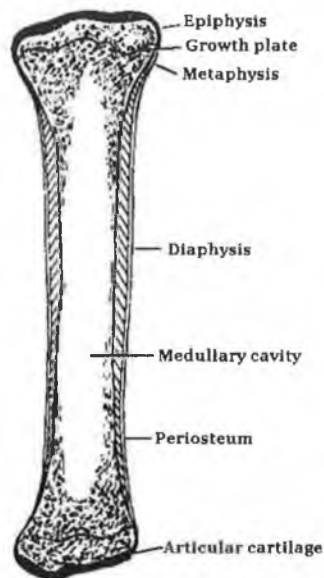


Figure 1.1: parts of a long bone [194].

The growth plate, as its name indicates, is the place where calcification of cartilage takes place. At the cessation of growth, the epiphysis, composed of cancellous bone, become fused with the adjacent metaphyses. The outer shell of the metaphyses and epiphyses is a thin layer of cortical bone continuous with the compactum of the diaphysis. The diaphysis is a hollow tube. Its walls are composed of dense cortex (compactum), which is thick throughout the extent of the diaphysis but tapers off to become the thin shell of each metaphysis. The central space (medulla or medullary cavity) within the diaphysis contains the bone marrow [89].

Covering the entire external surface of a mature long bone, except for the articulation, is the periosteum. The inner layer of the periosteum contains the highly active cells that produce circumferential enlargement and remodeling of the growing

long bone; hence it is called the OSTEOGENIC LAYER. After maturity, this layer consists chiefly of capillary blood vessel network. The outer layer of the periosteum is fibrous and comprises almost the entire periosteum of a mature bone. In event of injury to a mature bone, some of the resting cells of the inner periosteal layer become osteogenic.

Over most of the diaphysis, the periosteum is tenuous and loosely attached, and the blood vessels therein are capillary vessels. At the expanded ends of long bones, however, ligaments are attached firmly and can convey blood vessels of larger size. The same is true at the ridges along the diaphyses, where heavy fascial septa are attached. Thus when is spoken about the mechanical properties of bone, must specify which part of the bone are talking about ,Table 1.1, [89].

When examined microscopically, the bone material is seen to be a composite. Figure 1.2 shows Ham's sketch [103] of the basic structure of compact bone. The basic unit is the Haversian system or osteon. In the center of an artery or vein. These blood vessels are connected by transverse channels called Volkmann's canals.

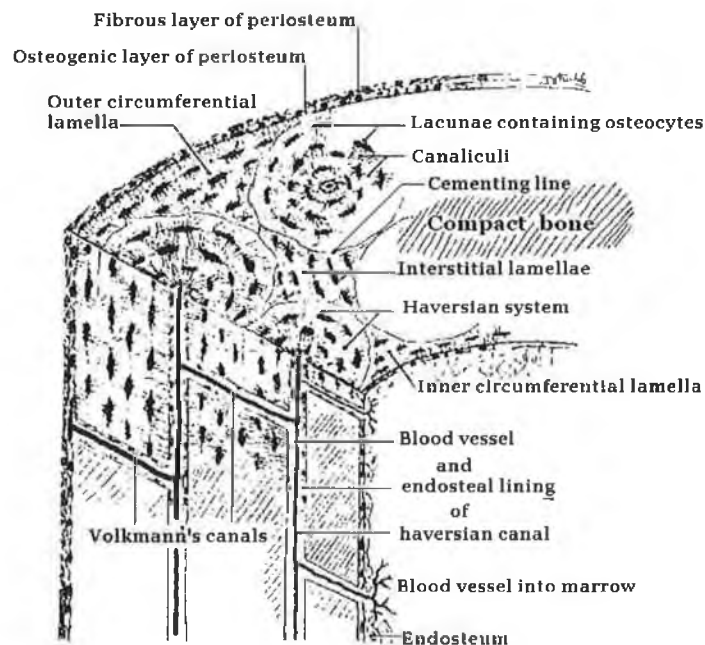


Figure 1.2: The basic structure of compact bone [106].

The two major classes of bone, cortical and cancellous, are constructed of tissue that consists predominantly of extra-cellular material termed “matrix”. It is the matrix, which gives bone its structural strength. The matrix itself is comprised of a

strong brittle mineral phase called HYDROXYAPATITE [$\text{Ca}_{10}(\text{PO}_4)_2\text{OH}$] and a soft organic phase most of which is a protein called collagen. The term “matrix” is used here in the histological sense to refer to material outside the cell rather than in the material science sense. Bone tissue could be simplified into three components [206]; a mineral phase, an organic phase, and a porous phase which is filled with liquids. Porosity varies between about 10% - 30% for cortical bone and 30% - 90% for cancellous bone [299].

The microstructure of bone refers to the way these three basic components are assembled. Ascenzi [10] in a brief review presents these as a hierarchy of four orders, as in Figure 1.3. In sequence of decreasing size they are:

- 1) The gross shape of the bone and arrangement of its pores.
- 2) The preliminary mesostructural units, termed “osteons” and the interstitial bone coming between them. Part (d) of Figure 1.3 shows a schematic representation where it can be seen that osteons consist of concentric laminae pressed together. There are about 20 – 30 such laminae in each osteon. An osteon is of the order of 0.15-mm diameter and up to 1 – 2 cms long and it has a “Haversian” canal along its axis via which nourishment is supplied to the bone cells. Therefore consists of laminates. However, laminates do not have to arrange themselves cylindrically into osteons and such bone is called lamellar bone [299]. Ongoing in the living bone is a continual process of destruction and reconstruction whereby old osteons are

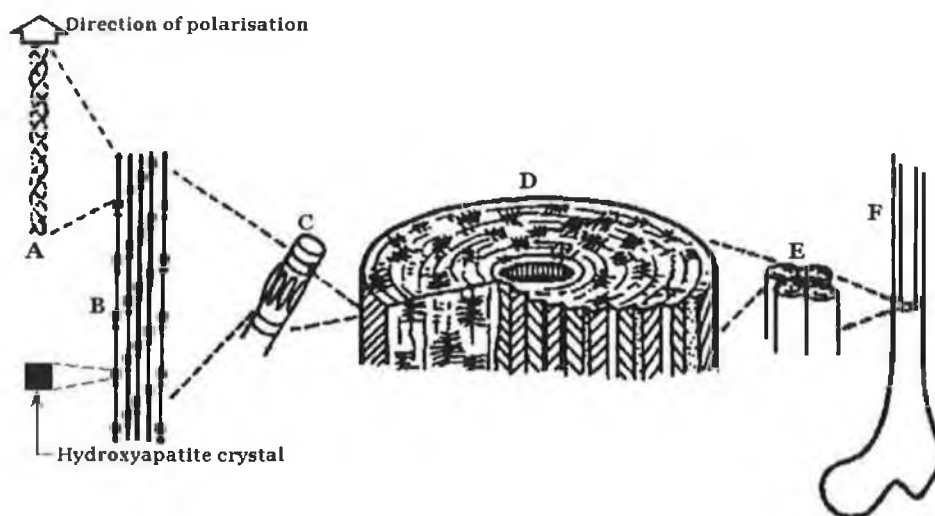


Figure 1.3: The hierarchies of bone structure: A, B, and C constitute the fourth order; D shows an osteon (third and second order); and F shows the first order [227].

resorbed and new ones are laid down around a new Haversian canal. This is termed osteonal remodeling. Osteons directly, and hence present at the start of remodeling, are termed “primary” osteons and those formed due to remodeling are called “secondary” osteons. Hence, after osteonal remodeling, fragments of old osteons lie between the new ones and they are said to lie “interstitially”: The boundary between a secondary osteon and the interstitial osteon fragments is a “cement line” about 1 – 5 μm wide, the exact morphology of which is still not entirely clear [32].

- 3) The third order consists of the laminae themselves. They are about 7 μm thick [299] and consist of collagen bundles that are variously oriented to the central axis of the osteon. Ascenzi and Bonucci [9] observed three classes of laminae: those whose collagen fiber bundles are predominantly longitudinal, those with circumferentially oriented bundles and those with alternate fibers. Martin and Ishida [171] found that the orientation of collagen has considerable influence on the static strength of cortical bone. Ascenzi and Benvenuti [8] observed that, at the boundary between successive laminae, the predominant fiber bundle direction does not change abruptly but there is an intermediate system of criss-crossed fibres making an angle of 45° with the adjacent bundles on either side. The significance of collagen bundle orientation is that their distribution in the shafts of bones is such that they can best resist the local stress state [10]. The hydroxyapatite crystals are precipitated into the collagen fibres. Sasaki et al. [229] observed that the x-axes of the hydroxyapatite crystal rods are predominantly oriented circumferentially. Ascenzi et al. [8] also reported that the ratio of longitudinal to transverse oriented hydroxyapatite increases the more calcified the tissue.
- 4) The fourth order refers to the molecular pattern of the inorganic and organic substances [207].

In order to understand the biological aspects of bone remodeling, some description of the cellular basis of the process is needed. Three types of cells are active on the bone surfaces (both internal pore surfaces and the external surface) to create new bone. “Osteoblasts” synthesize bone matrix by first secreting a protein called topolagen which polymerizes into collagen fibrils. When this is complete the

Osteoblasts precipitate hydroxyapatite crystals. Osteoblasts then become osteocytes and carry out various vital biomechanical activities. Osteocytes eventually become ineffective and, perhaps with Osteoblasts, they form osteoclasts. It is the osteoclasts that go on to effect the resorption of the osteon, as shown schematically in Figure 1.4.

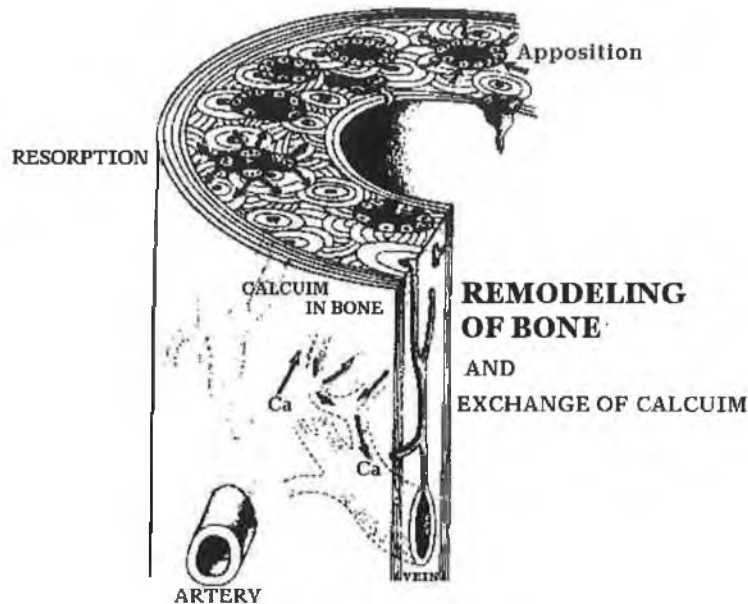


Figure 1.4: Conceptual drawing of the remodeling of bone by apposition, resorption, and calcium exchange [121].

This process is, in some way, influenced by the stress state in the bone tissue. Possible mechanisms for this have been comprehensively reviewed by Trehan [264]. He proposes that there are many “theoretical pathways” but only two “principles of operation” namely the piezoelectric principal and the chemical principal. The piezoelectric principal [14] involves the hypothesis that the cellular processes noted above are influenced by electric potential. Two proposed pathways are: firstly that the collagen is piezoelectric caused by molecular shifts under an applied shear stress, or secondly that the load affects the solubility of the hydroxyapatite – either directly or indirectly via pressure from the extracellular fluid – thereby changing calcium ion concentration and generating streaming potentials [108]. The chemical hypothesis, on the other hand [136], is that the increased extra cellular calcium concentration, caused by a decrease in hydroxyapatite solubility on loading, directly triggers osteoclast activity.

Briefly, remodeling (or adaptation) processes can be defined as mechanisms by which the bone adapts its histological structure to the changes in long term

loading. It is assumed that the bone has Mechano-Receptors or sensors distributed throughout the tissue [218].

We can see, therefore, that the bone remodeling process is effected by complex biochemical reactions, and furthermore that the biological mechanism by which loading influences these reactions is not completely understood. McNamara and Prendergast [177] suggested a mechanical model for bone remodeling based on damage accumulation that can explain the net-effect [177, 214]. The McNamara and Prendergast model change the view away from the biological perspective described above to some alternative perspective from which the process can be explained by a mathematical model.

1.3. Functional Adaptation of Bone (Bone Remodeling)

Living bone is continually undergoing processes of growth, reinforcement and resorption. These processes are termed collectively “remodeling”. The remodeling processes in living bone are mechanisms by which the bone adapts its histological structure to changes in long term loading. Bone adapts its external shape and internal structure in response to the mechanical forces it is required to support. It is well known principle of orthopedics that prolonged straining of a bone tends to make the bone stronger, that is to say, stiffer and denser. This why a person in later stages of recovery from broken leg is encouraged to walk on his healing limb. Conversely, a living bone not subjected to its accustomed strain level will, in time, become weaker, that is to say, less stiff and more porous [55].

The remodeling processes (loosening) is a significant problem which threaten the success of the total hip replacement due to the mismatch between the bone and the implant material, as we will see later. Understanding and predicting remodeling properties of living bone are particularly important for the proper design of prosthetic devices which contact bone tissue.

Recent researches have focused on obtaining the biomechanical signal, which drives the adaptation process. The signal is associated with either:

- (a) microdamage in the bone, or
- (b) strain in the mineralized bone tissue.

It was assumed that the bone has mechano-receptors or sensors distributed throughout the tissue. The mechano-receptors sense the biomechanical signal and emit a chemical (or electrical) stimulus which generates a new activity pattern for the osteoclasts (bone resorbing cells) and osteoblasts (bone forming cells). As bone changing shape in response to new forces, the stimulus emitted by the mechano-receptors until the bone assumes a suitable shape to carry the new load [218].

But how are the Sensors Activated? There are two possible mechanisms relating sensor activation to mechanical loads:

- (a) Deformations of the lacunae under load. This causes fluid flow in the lacunae, which stimulates the osteocytes [151].
- (b) Microdamage in the form of inter-constituent microcracks. Microcracks stimulate the sensors, either by altering the local tissue deformation [172], or by changing the biochemical environment in the tissue by release of growth factors [74, 151].

For a microdamage signal, microcracks will continue to accumulate if the repair rate is insufficient to mend the damage as it is formed (such a phenomenon can cause stress fractures). In this case, the motive for adaptation is to re-obtain an acceptable amount of microdamage in the bone tissue.

The most frequently used method to verify whether hypertrophy or atrophy has occurred in a bone due to its use or disuse is by means of x ray, which measures the opacity of bone, which in turn is proportional to the mineral content of the bone. Another way is to measure wave transmission velocity and vibration modes of the bone as a means to determine the density of the bone. Results obtained by these methods have generally supported the idea of functional adaptation.

Changes in bone may take place slowly (in months or years) due to the action of the bone cells (osteoclasts for resorption; osteoplasts for apposition), or rapidly (in days) due to the uptake of mineral salts. These processes are illustrated in a sketch made by Kummer [148], Figure 1.4. Julius Wolff [218] first advanced the idea that living bones change according to the stress and strain acting in them. Evans [76] concluded that clinical and experimental evidence indicated that compressive stress stimulates the formation of the new bone and is an important factor in fracture healing. Dietrick et al. [67] conducted an experiment on remodeling in humans by

immobilizing some volunteers from the waist down in plaster casts for periods from 6 to 8 weeks. During this study their urine, faces, and blood were analyzed for organics such as creatine and inorganics such as calcium and phosphorous. Four days after the plaster casts removed the subjects resumed normal activity. The chemical analysis indicated that during the immobilization, their bodies suffered a net loss of bone calcium and phosphorous. After normal activity had been resumed, the mineral loss phenomenon was reversed and the body regained calcium and phosphorous. Hert et al. [114, 300] concluded further that intermittent stresses is a morphogenic stimulus to functional adaptation of bone, and that the effect of compressive stress is the same as that of tensile stress. Woo et al. [290] and Torino et al. [262] showed that remodeling due rigid plat fixation in dogs occurs by thinning the femoral diaphysis cortex rather than by induced osteoporosis in the cortex. In other words, it is primary surface remodeling.

McNamara [177] proposes that bone is an optimized structure according to strength considerations and that the stimulus for remodeling is change in the amount of damage in bone from its equilibrium level, denoted $\Delta\omega$. He formulated the remodeling rule as follows:

$$dX/dN = C \Delta\omega \quad (5)$$

where X denotes the extent of bone deposition or resorption and C is a rate constant. The stimulus for remodeling is the difference between the new damage rate and the steady-state value:

$$\text{Remodeling Stimulus} = d\omega/dN - (d\omega/dN)_{ss} \quad (6)$$

The author then goes on to note that damage, in the form of the number and size of microcracks, will accumulate in the material, and will also be repaired over time. The excess of the bone's damage, after an increase in load, or deficit, after a decrease in load, can be obtained by integrating the mismatch at any bone surface:

$$dX/dt = \int (\text{Remodeling Stimulus}) dt \quad (7)$$

where (dX/dt) is the rate of change of position at any bone surface [178].

1.4. Bone as a Composite Material

Bone material is a composite of collagen and hydroxyapatite. Apatite crystals are very stiff and strong. The Young's modulus of fluorapatite along the axis is about 165 GPa. This may be compared with the Young's modulus of steel, 200GPa, and Aluminum (6061 alloy), 70GPa. Collagen does not obey Hooke's law exactly, but its tangent modulus is about 1.24GPa. The Young's modulus of bone (18GPa in tension in human femur) is intermediate between that of apatite and collagen. But as a good composite material, the bone's strength is higher than that of either apatite or collagen, because the softer component prevents the stiff one from brittle cracking, while the stiff component prevents the soft one from yielding.

The mechanical properties of a composite material (Young's modulus, shear modulus, viscoelastic properties, and especially the ultimate stress and strain at failure) depend not only on the composition, but also on the structure of the bone (the geometric shape of the components, bond between fibers and matrix, and bonds at points of contact of the fibers) [198].

1.4.1. Elasticity and Strength of Bone

Bone is hard and has a stress-strain relationship similar to many engineering materials. Hence a stress analysis of bone can be made in a way similar to the usual engineering structural analysis. Figure 1.5 shows the stress-strain relationship of a human femur subjected to uniaxial tension.

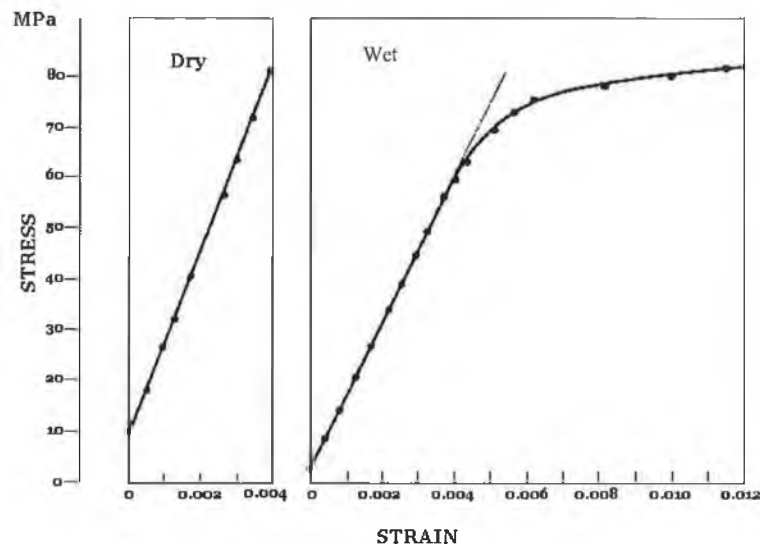


Figure 1.5: Stress-strain curves of human femoral bone [81].

It is seen that dry bone is brittle and fails at a strain of 0.4%; but wet bone is less so, and fails at a strain of 1.2%. Figure 1.5 suggests that Hooke's law is applicable for a limited range of strains.

Table 1.1 gives the mechanical properties of wet compact bone of human bone. It is seen that the ultimate strength and ultimate strain in compression are larger than the corresponding values in tension for all the bones, whereas the modulus of elasticity in tension is larger than that in compression. The difference in the mechanical properties in tension and compression is caused by nonhomogeneous anisotropic composite structure of bone, which also causes different ultimate strength values when a bone is tested in other loading conditions. Thus, for adult human femoral compact bone, the ultimate bending strength is 160 MPa, and the ultimate shear strength in torsion is 54.1 ± 0.6 MPa, whereas the modulus of elasticity in torsion is 3.2 GPa.

Table 1.1: Mechanical properties of wet compact bone in tension, compression, and torsion parallel to axis for human (20 – 39 years) [89].							
Ultimate Tensile Strength (MPa)		Ultimate Percentage Elongation		Modulus of Elasticity in Tension (GPa)			
Femur	124 \pm 1.1	Femur	1.41	Femur	17.6		
Tibia	174 \pm 1.2	Tibia	1.50	Tibia	18.4		
Humerus	125 \pm 0.8	Humerus	1.43	Humerus	17.5		
Radius	152 \pm 1.4	Radius	1.5	Radius	18.9		
Ultimate Percentage Contraction		Ultimate Compressive Strength (MPa)		Ultimate Shear Strength (MPa)		Torsional Modulus of Elasticity (GPa)	
Femur	1.85 \pm 0.04	Femur	170 \pm 4.3	Femur	54 \pm 0.6	Femur	3.2

It is also well known that the strength of bone varies with the age and sex, the location of the bone, the orientation of the load, the strain rate and the test condition (whether it is dry or wet). The strain rate effect may be especially significant, with higher ultimate strength being obtained at higher strain rate. The strength and modulus of elasticity of spongy (concellous) bone are much smaller than those of compact bone [294].

1.4.2. Anisotropy of Bone

Lotz et al. [160] analyzed the anisotropic mechanical properties of the metaphyseal bone. Cowin [56], and Reilly and Burstein [220] analyzed these properties of the diaphyseal bone. Both used the transverse isotropic model. Major differences exist, Table 1.2:

Table 1.2: Mechanical properties of the metaphyseal bone		
Properties	Diaphyseal cortical shell	Metaphyseal cortical shell
$E_{\text{longitudinal}}$ (MPa)	17000	9650
$E_{\text{transverse}}$ (MPa)	11500	5470
ρ density (g cm ⁻³)	1.95	1.62
Reference	Reilly et al. [220]	Lotz et al. [160]

Here E is the Young's modulus, ρ is the mass density, and the subscripts refer to directions.

1.4.3. Failure Criteria of Bone

Lotz et al. [160] used von Mises' yield criterion for cortical bone, and von Mises and Hoffman's yield criterion for trabecular bone. The Hoffman [117] failure theory assumes linear terms to account for different tensile and compressive strengths, and has been demonstrated to fit experimental trabecular bone data well [254]. Assuming isotropy, the criterion is given by:

$$C_1(\sigma_2 - \sigma_3)^2 + C_2(\sigma_3 - \sigma_1)^2 + C_3(\sigma_1 - \sigma_2)^2 + C_4 \sigma_1 + C_5 \sigma_2 + C_6 \sigma_3 = 1 \quad (8)$$

Where;

$$C1 = C2 = C3 = 1 / [2 St . Sc] \quad (9)$$

$$C4 = C5 = C6 = [St - Sc] / [St . Sc] \quad (10)$$

Here σ_1 , σ_2 , σ_3 are the principal stresses, and S_t and S_c are the ultimate strengths in tension and compression, respectively. If S_t and S_c are equal, then Eq.(8) reduces to the von Mises yield criterion. These criteria will overestimate the strength under hydrostatic compression. Lotz et al. [160] found that the strains at failure predicted by the von Mises criterion do not correspond well with measured values, but yield and fracture were accurately predicted for two femora tested [198].

1.5. Biomechanics of the Lower Extremity

Engineering mechanics can be divided into rigid body mechanics (dynamics, kinematics, and statics), fluid mechanics, and solid mechanics. The aim of this section is to discuss a few aspects that are of importance in the identification and evaluation of forces on human body parts.

1.5.1. Rigid Body Biomechanics

Forces in the musculoskeletal system are generated by gravity, muscle action, acceleration and deceleration of body parts, and joint restraints. These forces cause motion in the system and deformation of skeletal parts. Because the deformations are small when compared to the gross motions, they are usually neglected when forces and gross motions are analyzed. In other words, the skeletal parts are assumed rigid in that case.

The study of this forces and motions between rigid bodies is called kinetics, and the analysis of motions alone is called kinematics. If a rigid body is at rest, or moving with constant speed (no accelerations), its external forces form an equilibrium system. The study of this condition is called statics. The principles of statics are formulated in the law of Newton.

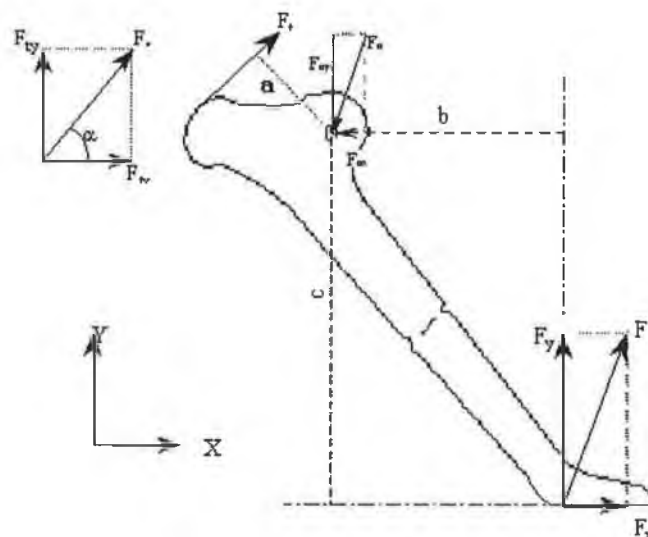


Figure 1.6: A free body diagram of the foot in a specific position. Achilles tendon, ankle, and floor reaction forces are drawn and decomposed in their x and y component. Moment arms (a , b , c) to the joint instantaneous center of rotation are shown.

Consider the example shown in Figure 1.6 by which the ankle joint and

Achilles tendon forces in the foot during gait are evaluated. In order to facilitate our analysis, a number of simplifying assumptions are made:

1. Although the structure to be analyzed (the foot) is not at rest and probably not moving at a constant speed. It is assumed that acceleration forces can be neglected when compared to muscle, joint restraint, and floor reaction forces (in other words, the problem is assumed quasistatic). For the same reason gravity forces is neglected.
2. Regard the foot in subsequent positions of gait; in each position the foot it is assumed to be a rigid body, taking into account its specific configuration (geometry) at that time.
3. All forces is assumed to work in one plane. Owing to these three assumptions one can now apply two-dimensional (2-D) statics.

The next step is to identify all relevant external forces working on the body. For that reason the body (the foot in the position shown in Figure 1.6) is freed from its environment, replacing all environmental restraints by forces. Forces are vector quantities and are characterized by orientation, magnitude, and point of application. External forces on the foot are expected at three locations: the Achilles tendon insertion, the ankle joint, and the foot-floor contact region. The orientation and the point of application of the tendon force (F_t) are known (from X-rays), but the magnitude is not. For the ankle joint force (F_a), only the point of application is known. For the ground reaction force (F), the point of application is known, but not the orientation, nor the magnitude. Thus, there are five unknowns: the magnitudes of F , F_t , and F_a and the orientations of F and F_a . Since each force can be decomposed in vector components, the nature of the unknowns can be changed. For example, the ground reaction force can be decomposed in a force in the x direction (F_x) and a force in the y direction (F_y), a force system that is equivalent to the original force F (which is the vector sum of F_x and F_y). In the same way F_a is decomposed in F_{ax} and F_{ay} . Still there are five unknowns (the magnitudes of F_t , F_x , F_y , F_{ax} , and F_{ay}) but of a different nature. The entity of the body under consideration, freed from its environment, in which the environmental restraints are represented by forces (as shown in Figure 1.6), is called a free body diagram.

The last step is to evaluate the unknown forces by applying the equilibrium conditions: a body is in equilibrium when the vector sum of all external forces is zero and when the sum of the moments of all forces with respect to one arbitrarily chosen point is zero.

This condition gives three equations in a 2-D case:

1. Sum of forces in x direction = 0.
2. Sum of forces in y direction = 0.
3. Sum of force moments = 0.

In order to apply the first two conditions, F_t must be resolved in the x and y directions. From the geometric configuration it follows: $F_{tx} = F_t \cos\alpha$ and $F_{ty} = F_t \sin\alpha$, in which α is known. Applying the equilibrium conditions:

4. $F_x - F_{ax} + F_t \cos\alpha = 0$.
5. $F_y - F_{ay} + F_t \sin\alpha = 0$.
6. $F_t \cdot a - F_y \cdot b - F_x \cdot c = 0$.

Since there are five unknowns and only three equations, this system can not be solved unless two unknowns are eliminated by other means. Such a force system is called indeterminate. A method of obtaining more information is to measure magnitude and orientation of the ground reaction force F (and thus F_x , and F_y), for instance, by using a force plate. Then, reducing the number of unknowns to three, which can be evaluated from the three equations.

It is evident that this example is a simple one, at least it was made simple by introducing a number of assumptions. In reality the problem may be three-dimensions (3-D), while a number of additional muscle tendons and ligamentous restraints may load the body as well. Dynamic aspects may play a role too. In other words, the solution found in this way can not be more than a rough estimate.

Nevertheless, the example serves to illustrate a number of aspects that are of importance in biomechanics force analysis:

- The introduction of specific assumptions about the mechanical behavior of the system considered, in order to facilitate the analysis or even make it possible

(These assumptions must, however, be realistic with respect to the required validity of the results.)

- The development of free body diagram by identifying the under consideration and isolating it from its environment, replacing the environmental restraints by forces.
- The application of geometric data (for instance from X-ray) and the nature of connections to determine as many characteristics of the external forces as possible (The nature of the tendon insertion is recognized to estimate the point of application and the orientation of the Achilles forces. The nature of the ankle joint is used to determine the point of application of the ankle force. A characterization of several types of connections and their specific force systems is shown in Figure 1.7).
- The application of equilibrium conditions to calculate the unknowns: three equations in 2-D problem, six in a 3-D problem (Vector decomposition of forces in the directions of the coordinate axes is usually necessary.)
- The fact that forces system may be indeterminate, so that unknowns will have to be eliminated by other means, for instance by using experimental data or more sophisticated mathematical criteria.

	Connection	Symbol	Unknowns		Connection	Symbol	Unknowns
A				C			
B				D			

Figure 1.7: Characterization of unknown loading variables in kinematic connections of structures to their environment. (a) Rigid Fixation [two forces and one moment]; (b) hinge [two forces or one force with unknown orientation]; (c) tendon or cable [one force in the direction of the tendon]; and (d) frictionless sliding [one force perpendicular to the sliding surfaces].

The last aspect is a problem in musculoskeletal biomechanics research specifically [37]. The number of muscles and joint/ligamentous restraints working on

the individual bones is large, while the experimental means available to measure these forces are of limited applicability and accuracy. Electromyography can be used to estimate muscle action, but only to a limited extent. Force plates can be applied to evaluate ground reaction forces on the foot, and center-of-gravity analysis can be used for gravity force determination on body parts. In dynamic performances for instance, acceleration forces in gait on body parts can be calculated by rough approximation from motion patterns. The experimental methods and the equilibrium equations available however, are not sufficient in most cases to obtain a complete and dependable estimate of all muscle and joint forces

Alternative criteria have been used as well: minimal joint forces, optimal control function, and others; the results usually differ for each criterion chosen. Although, the present knowledge about forces in human joints is of an approximate nature and limited to a few specific functions (e.g. gait). Evidently, a rotational approach to artificial joint design by the application of mechanics analysis is hampered by this lack of quantitative knowledge.

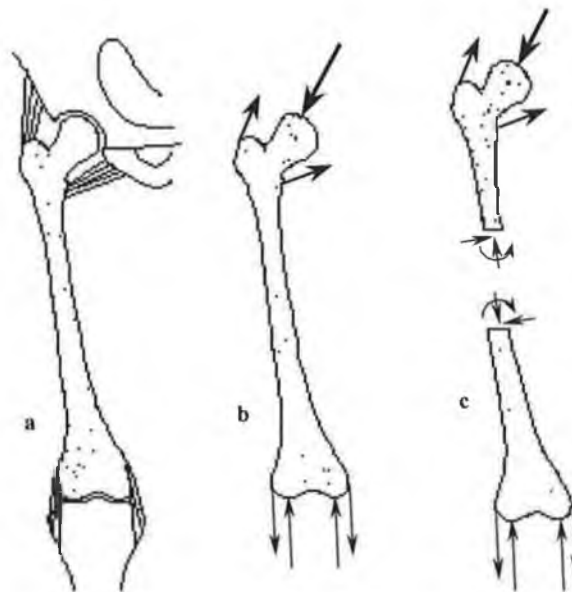


Figure 1.8: (a) A femur developed in (b) a free body diagram, and (c) free body diagrams of two parts of that bone. The principal of cutting is applied in the latter case by introducing a loading system of two forces and a moment at the site of the (imaginary) cut.

Developing a free body diagram is a very important step in all problems of force and stress analysis. All subsequent steps depend on this diagram; an error made here will be reflected in the validity of the eventual conclusions. The crucial aspect

of this step is freeing the body from its environment and replacing the connections by forces and moments to take their influences into account. To analyze a part of a body the principle of cutting is applied as illustrated in Figure 1.8. A free body diagram of the femur, Figure 1.8a, is developed by freeing this bone from its environment and replacing all environmental connections by forces, taking into account the kinematic characteristics of the restraints, Figure 1.8b. A free body may comprise only a part of the bone as well if for instance the bone is cut as shown in Figure 1.8c. The mechanical influence of the removed part must be taken into account by introducing forces and couples. These forces and couples represent the internal loads within the material, at the site of the cut. Due to the “action = reaction” law, the forces and couples must be equal but opposite in sign on either side of the cut. The nature of the sectional loading system is equal to that of a rigid fixation (two forces and a couple in a 2-D problem, Figure 1.7).

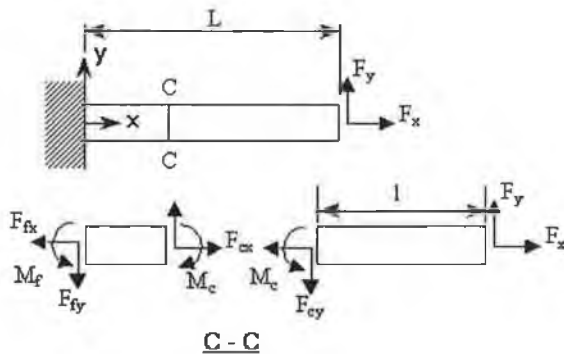


Figure 1.9: Internal loads in a cantilever beam, loaded extremely by a transverse and an axial force. The internal forces and moments at an arbitrary chosen site can be calculated using equilibrium conditions.

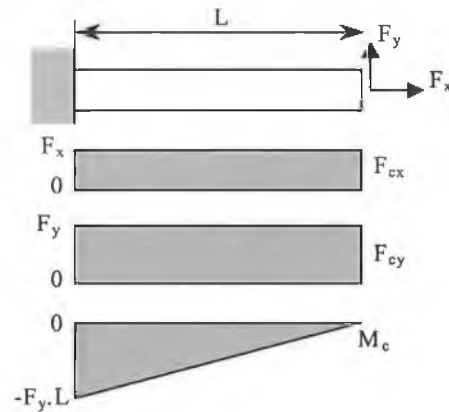


Figure 1.10: Internal forces and moment diagrams of the beam in Figure 4.4. the loads are shown as a functions of the longitudinal coordinate x . the internal forces are constant throughout the beam; the internal moment varies linearly, with a maximum in absolute value at the fixation site.

The sectional, internal loads are used to free a part of a body in a free body diagram for a subsequent force analysis, in which these loads are evaluated. Consider the cantilever beam in Figure 1.9, loaded by an axial (F_x) and a transverse (F_y) force. The beam is first freed from its fixation by introducing the forces F_{fx} and F_{fy} and the moment M_f . applying equilibrium conditions:

$$x \text{ direction: } F_x - F_{fx} = 0, \text{ hence } F_{fx} = F_x$$

y direction: $F_y - F_{fy} = 0$, hence $F_{fy} = F_y$

moments: $M_f + F_y.L = 0$, hence $M_f = -F_y.L$

Apparently, M_f works in the opposite direction as drawn, as witnessed by the negative sign. If the internal loads in the beam at cross section C-C is wanted to evaluate, the beam must be cut at that location and the cross-sectional loads F_{cy} , F_{cx} , and M_c introduced. Applying the equilibrium conditions, that is $F_{cx} = F_x$, $F_{cy} = F_y$, and $M_c = -F_y.L$. If this is carried out for varying L , the internal load distribution is obtained, giving the cross-sectional loads throughout the beam in diagram, as shown in Figure 1.10. Evidently, the internal axial and transverse forces are constant throughout the beam, while the internal moment varies from zero to maximal at the fixation site. These forces and moment diagrams are often applied for beam-like structures for design and analysis purposes. It is evident in this example that the greatest structure strength is required at the fixation site.

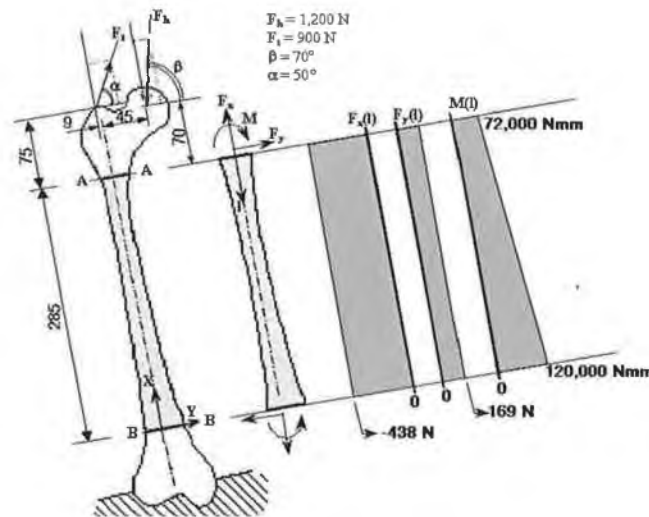


Figure 1.11: Internal forces and moment diagrams of a femoral diaphysis. All forces are assumed to act in one plane. Dimensions are shown in millimeters. From the abduction tendon force magnitude (F_t) and direction (α), the hip force magnitude (F_h) and direction (β), and the geometric configuration, the internal loads at section AA (F_x , F_y , and M) are calculated using equilibrium conditions. These are the external loads of the freed bone piece AA – BB in which, just as in Figure 1.9, internal forces and moment as functions of the location (l) are calculated.

Another example of this procedure is worked out in Figure 1.11, with respect to the femoral shaft. In this problem it is assumed that the abductor muscles are active only and that all forces work in one plane (2-D problem). The analysis is carried out in steps, starting from the free body diagram of the femur (in which all knee forces are lumped into three loading variables):

1. Decompose the external forces in x and y directions.
2. Develop a free body diagram of the femoral shaft by evaluating the loads at Sections A-A and B-B.
3. Calculate the cross-sectional loads in the shaft as a function of L.
4. Draw the diagram for the internal load distribution, based on step 3.

1.5.2. *Stresses and Strains*

When a piece of material is subject to loading it deforms. Although the deformation may be invisible to the naked eye it is always present. The molecules resist deformation through mutual bonds that generate internal loads. In solid mechanics which studies this deformational behavior under loading, the local deformations are represented by strain; the internal loads are represented by stress. In the analyses of these phenomena in structures (called structural analysis), the principles of continuum theory are usually applied. Although the materials out of which a structure is made are not truly continuous at a molecular or even a microscopic level, the mechanical behavior of structures can usually be described and predicted with methods that neglect discontinuities on a smaller scale. Within the frame of continuum theory, materials are regarded as indefinitely divisible and thus variables as stresses and strains can be defined in an indefinitely small point. This assumption of material continuity is sometimes quite adequate, as in metals, and sometimes rather rough, as for instance, in trabecular bone.

Strain is relative deformation (a change in dimension relative to the original dimension); stress is an amount of force per unit area; both are local phenomena. To define the stress state in a point of a structure, an arbitrary plane was chosen in that part Figure 1.12a. On this plane works a certain internal load that, divided by the plane area, is represented by a certain amount of stress (σ). The stress can be decomposed into a component normal to the plane (σ_n , called direct stress) and one parallel to the plane (τ , called shear stress). Thus, the stress state in that point its fully characterized by three variables: one direct-stress component (σ_n), one shear-stress component (τ), and the orientation (α) of the plane with respect to an external (x-y)

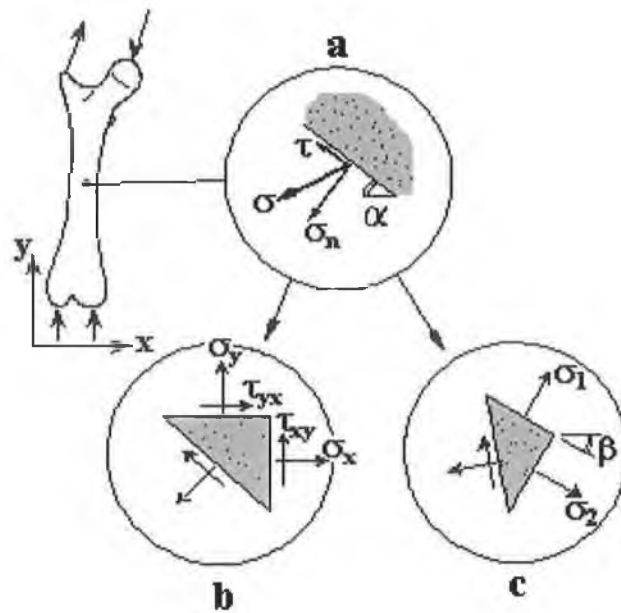


Figure 1.12: Characterization of a 2-D stress state.

- (a) In a geometric point by three variables (direct stress, shear stress components, and plane orientation).
- (b) Alternative characterization with respect to fixed planes.
- (c) By principal stresses.

reference system. This characterization of stress in a point can be worked into two alternative representations that are commonly used. In the first one, Figure 1.12b, two planes are chosen parallel to the external coordinate axes (an x-plane and a y-plane). On these plates direct-stress components (σ_x and σ_y) and shear-stress components (τ_{xy} and τ_{yx}) are found again. It can be proven that this system of stress components on nonarbitrarily chosen planes is equivalent with that of Figure 1.12a and also that $\tau_{xy} = \tau_{yx}$. The third representation, Figure 1.12c, is based on the fact that two perpendicular planes can be found on which only direct stresses exist (σ_1 and σ_2). These are called the principal stresses in that point concerned, while the orientation of the planes is characterized by the principal-stress orientation (β) with respect to the external coordinate system. In summary, the stress state in a point of a structure is characterized by either the magnitudes of two direct stress and one shear-stress component (σ_x , σ_y , and τ_{xy}) or by the magnitudes of two principal-stress components and the principal-stress orientation (σ_1 , σ_2 , and β). Compressive and tensile stress both are direct stresses, compressive denoted with a negative sign and tensile with a positive sign. Although their influences on materials might differ, mathematically they are not treated separately.

Like a 2-D stress state is characterized by three stress components, a 3-D stress state is characterized by six: the magnitudes of the three direct-stress and three shear-stress components. Of course, all structures are in fact 3-D, but quite often the stress state can be adequately represented by a 2-D approximation. The six components of a 3-D stress state are illustrated in Figure 1.13. Parallel to the representation of a 2-D stress state as in Figure 1.12b, an infinitesimal small cube in the material was regarded, the sides of which align with external (x-y-z) reference system. On each of the three planes work one direct-stress and two shear-stress components. In this case, too, it can be proven that $\tau_{xy} = \tau_{yx}$, $\tau_{xz} = \tau_{zx}$, and $\tau_{yz} = \tau_{zy}$. Hence, the stress state in the point concerned is fully characterized by six independent variables, three direct- and three shear-stress components.

The local state of deformation in a material is represented by strain, in much the same as internal loading is represented by stress, and defined again with respect to an infinitesimal small cube, a geometric point. There are two types of strain, Figure 1.14: direct strain (ϵ), describing the relative changes in length of the cube ribs, and shear strain (γ), describing the angular distortion. Comparable to the stress state, the local strain state in a material is fully determined by six independent strain variables (i.e., ϵ_x , ϵ_y , ϵ_z , γ_{xy} , γ_{xz} , γ_{yz}) in a 3-D case and by three (i.e., ϵ_x , ϵ_y , γ_{xy}) in a 2-D case.

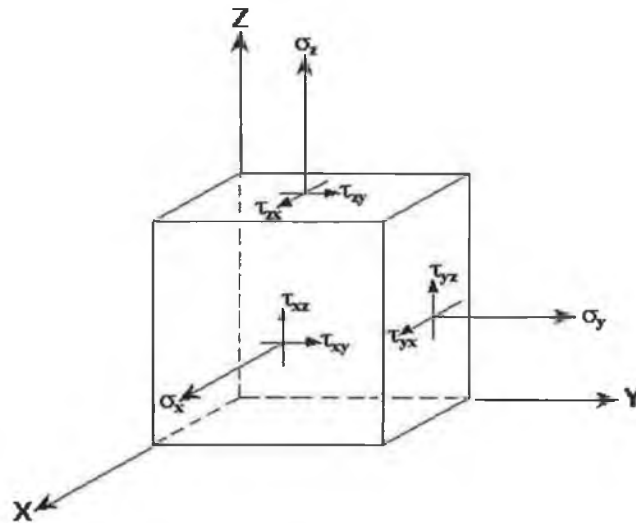


Figure 1.13: Characterization of 3-D stress state in a geometric point with respect to fixed (x, y, z) planes in nine stress components. Because $\tau_{xy} = \tau_{yx}$, etc., the number of independent stress variables is reduced to six.

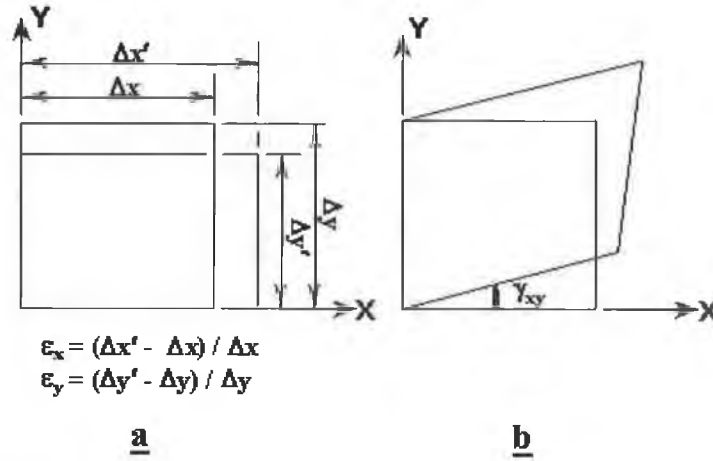


Figure 1.14: Illustration of strain components in two dimensions.

- (a) The direct strains (ϵ_x, ϵ_y) represent relative dimensional changes of the infinitesimal cube.
 (b) The shear strain ($\gamma_{xy} = \gamma_{yx}$) represent the direction of the cube.

The stress and strain states in a point of a structure are related to each other through the mechanical (elastic) properties of the materials concerned. These relations are expressed in constructive equations which mathematically relate the stress to strain components. The forms of these equations depend on the nature of the material, as discussed in the next section. Their simplest forms are for linear elastic, isotropic, and homogeneous materials as metals,

$$\epsilon_x = \{\sigma_x - \nu(\sigma_y + \sigma_z)\} / E$$

$$\epsilon_y = \{\sigma_y - \nu(\sigma_x + \sigma_z)\} / E$$

$$\epsilon_z = \{\sigma_z - \nu(\sigma_x + \sigma_y)\} / E$$

$$\gamma_{xy} = 2 \cdot \tau_{xy} (1 + \nu) / E$$

$$\gamma_{xz} = 2 \cdot \tau_{xz} (1 + \nu) / E$$

$$\gamma_{yz} = 2 \cdot \tau_{yz} (1 + \nu) / E$$

In which E and ν are the elastic constants of the material concerned, the Young's modulus (or modulus of elasticity) and the Poisson's ratio, respectively. These relations are also known as Hooke's law. It is evident that when the material properties are known (E and ν), the strains can be directly calculated from the stresses and vice versa, using these formulas. The expression $E / 2(1 + \nu)$ appearing (in reversed form) in the equations is usually denoted with the symbol G and called the shear modulus of the material concerned.

1.5.3. Statics of the Lower Extremity

The most important requirement of statics is that the center of gravity of a body must be on a vertical line passing through its area of support, Figure 1.15. This means that for a standing man the gravity vertical line falls within an area between the points of support.

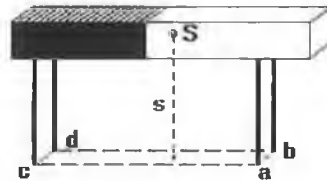


Figure 1.15: Heavy bar, supported by four legs (a to d). The vertical, *s*, from the center of gravity, *S*, must fall within the area of support.

1.5.3.1. Bipedal Stance

The supporting area in bipedal stance is delimited by the tangents to the convexities of the standing surfaces, Figure 1.16. The foot of the gravity vertical line within this area may vary in relation to the actual posture of the whole body. If a symmetrical stance is presumed, the body weight is distributed on both legs equally.



Figure 1.16: Area of support at various postures of a standing man. *S* = position of the gravity vertical.

Top: "military bearing"

Center: "easy bearing"

Bottom: "normal posture"

What is meant by the term "body weigh" will depend on the part of the leg to be considered.

With regard to the level of the hip joints the weight to be considered is the sum of the masses of trunk, head, and both arms. Pauwels [202] calls this part of the total body mass G_4 , because it is composed of four partial masses, Figure 1.17. Thus,

the primary loading of each hip joint is $G_4/2$. At the level of the knee joints, the weight G_4 is augmented by the weights of both thighs etc.

The important fact in the statics of bipedal stance is the absence of any tilting moment in the frontal plane, since the gravity vertical line of the mass borne lies between the two supporting extremities. Although in the sagittal plane the gravity vertical line generally falls in front of or behind the hip or knee axis, Figure 1.18, thus tending to end or extend these joints, the contraction of antagonistic muscles is necessary to prevent those movements.

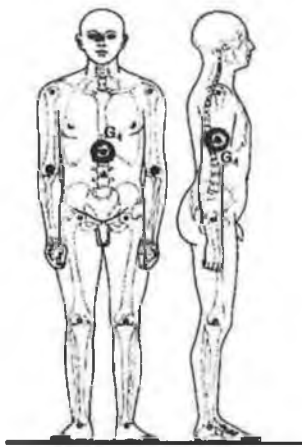


Figure 1.17: Position of the partial mass G_4 of the human body.

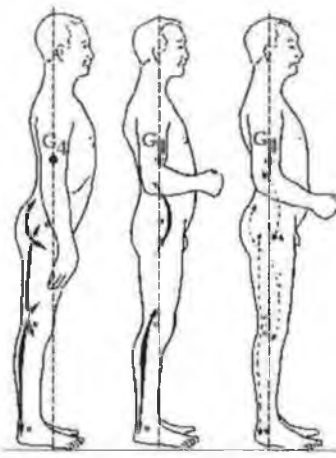


Figure 1.18: Position of the center of gravity, G_4 , relative to the main joints of the lower extremity.

A: Military bearing.

B: Easy bearing.

C: Normal posture.

In A and B the principal muscles for the balance of the hip and knee joint are indicated by black arrows. In C "ready-for-action" muscles are indicated.

1.5.3.2. Monopodal Stance

When the body is supported on only one leg, its center of gravity, S_6 , has to be balanced vertically above the bearing area of the foot, Figure 1.19. This fact determines the posture as a whole including the posture of the leg, joint positions etc.

With regard to the hip joint of the supporting leg, the center of gravity, S_5 , has to be considered, and the moment of the mass G_5 must be balanced in the joint by means of the abductor muscles. Magnitude and direction of the joint resultant then depend on the:

- direction and tension of the hip-abductors,
- posture of the pelvis, and

- length and posture of the leg.

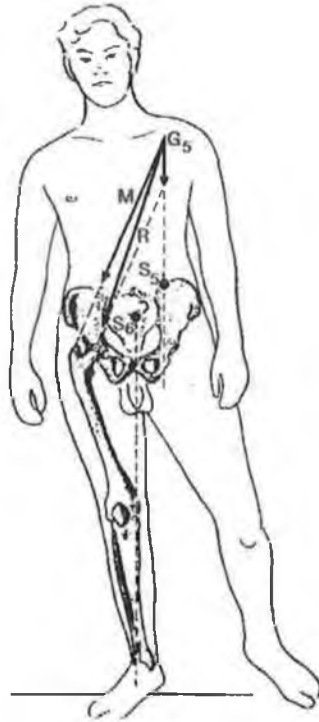


Figure 1.19: Man standing on his right leg. The gravity vertical line from S_6 falls in the supporting area of the right foot. The weight G_5 is to be balanced in the right hip joint.
M: Abductor muscles of the right hip.
R: Hip resultant.
S₅: Center of gravity of the body mass to be borne in the right hip joint [147].

Moreover, direction and tension of the abductor muscles are related to the lever arm of the load (depending, among other things, on the width of the pelvis), to the length of the femoral neck and trochanter, and to the angle between neck and shaft, Figure 1.20. Furthermore, it must be remembered that the posture of the leg is strictly determined by the position of S_6 , on account of the equilibrium conditions.

1.5.4. Dynamics of the Lower Extremity

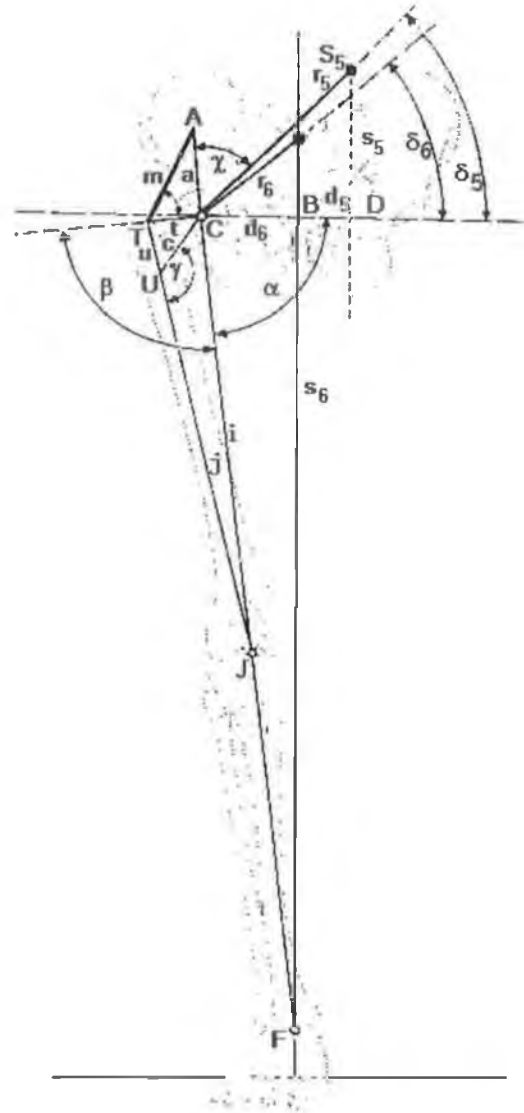
The dynamic stressing of the skeleton is, in principle, similar to the static stressing. Differences between the two may concern magnitudes and directions of the forces, but the equilibrium conditions at the joints are still valid.

1.5.4.1. Slow Motion

When the change of speed is so slow that the internal forces involved are negligible, the subsequent stages of the movement may be considered as static.

Figure 1.20: Some distances and angles in the human pelvis and leg skeleton.

A: insertion of abductors at the pelvis,
a: distance AC,
B: intersection of S_6 with a horizontal through C,
C: center of the hip joint,
c: length of the femoral neck (distance CU),
D: intersection of S_5 with the horizontal through C,
 d_5 : distance DC;
 d_6 : distance BC;
F: center of the ankle joint;
i: distance CF;
J: center of the knee joint;
j: distance JU;
k: distance CS;
m: line of action of the abductors;
 r_5 : distance C S_5 ;
 r_6 : distance C S_6 ;
 S_5 : gravity center of the body mass minus the mass of the supporting leg;
 S_6 : gravity center of the body mass,
 s_5 : vertical from S_5 ;
 s_6 : vertical from S_6 ;
T: apex of the greater trochanter,
t: distance CT;
U: intersection of the line through J and T with the neck-axis;
u: distance TU,
 α : angle between I and the horizontal;
 β : angle between I and t;
 γ : angle between j and c [projection of angle between neck and shaft];
 δ_5 : angle between r_5 and the horizontal;
 δ_6 : angle between r_6 and the horizontal;
 χ : angle between a and r_5 . [5]



1.5.4.2. High Speed and Acceleration

Only higher speeds require considerable accelerations or decelerations. Consequently, inertial forces arise from the accelerated masses. The total “load” acting on the parts of the extremity is then the resultant of the weight of the body (or some of its parts), and the force of inertia. In further considerations, this resultant force takes the place of the load and must be balanced at the levels of the joints by muscular forces. It goes without saying, that the line of action of the total load passes through the area of support, Figure 1.21.

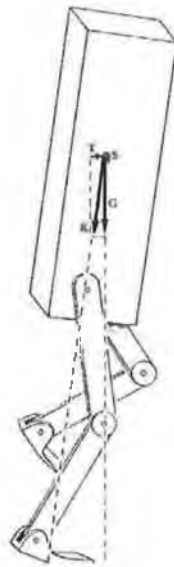


Figure 1.21: "Total load" of an accelerated body.
 G: weight of the body.
 K: "Total load" (resultant of G and T).
 S: Center of gravity.
 T: Force of inertia.

1.5.5. Mechanics of the Hip Joint

To a first approximation, the hip joint may be considered as an ideal spherical joint. This implies three degrees of freedom for rotation and consequently three main axes for abduction-adduction, extension-flexion, and internal-external rotation movements. There is virtually no degree of freedom for translation.

1.5.5.1. Equilibrium Conditions

The equilibrium conditions of a spherical joint are relatively easy to determine on account of its practically unlimited rotational ability: since the sum of all rotational moments must be zero, the resultant of all forces must pass through the geometrical center of the joint.

1.5.5.1.1. Equilibrium in Bipedal Stance

Theoretically, instable equilibrium without any muscle action should be possible in bipedal stance. In every case, the resultant of the stressing forces is directed vertically in the projection on a frontal plane.

In a sagittal plane, the gravity line of S_4 can pass through the articular center, or behind the joint, or in front of it, depending on the posture of the individual. Thus, either the flexors of the hip (Mm. iliopsoas et rectus femoris) or the extensors (M.

gluteus maximus, ischiocrural muscles) are responsible for the maintenance of equilibrium.

1.5.5.1.2. Equilibrium in Monopodal Stance

As has been mentioned above, in Monopodal support the weight G_5 has to be balanced in the hip joint. This effected by the abductor muscles.

The resultant of the forces can be determined from the known vector of the load G_5 and the position and direction of the muscular force M [202, 203]. The position of the latter is given by the fact that the equilibrium conditions require the forces G_5 and M to be in the same plane as the articular center C , Figure 1.19. This “plane of stressing” deviates from the sagittal plane through the joint by a very small angle, which can be neglected. The exact direction of the muscular force M is not so easy to determine [64]. It is commonly believed that the force exerted by the abductors (*Mm. glutei medius et minimus*) is directed from the apex of the trochanter to the center of the surface of origin of these muscles.

In addition to this difficulty, the magnitude and inclination of the hip resultant, R , depend on virtually all the morphological parameters of the skeleton of the lower extremity including the pelvis [5].

1.5.5.2. Stressing of the Hip Joint

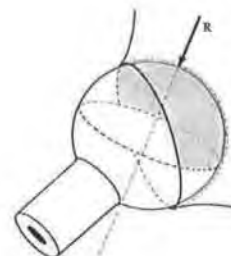
In the following considerations it shall be presumed that in synovial joints friction is negligible, and the pressure is not hydrostatic. Under these considerations, the stresses on the articular surface are normal stresses and are proportional to the normal forces transmitted from one articulating element to the other.

1.5.5.2.1. Stress Distribution in the Articular Surfaces

Since there is no reason to assume that stress distributions in the acetabulum and femoral head should be different in any particular position of the joint, the stresses in but one component, the acetabulum, may be considered. Furthermore, attention will be paid only to monopodal stance or the supporting phase of the gait, because this represents the situation of maximal articular stress.

As is demonstrated in Figure 1.22, in a spherical joint, the area of support need not be identical with the area of contact nor with the anatomical articular surface. The supporting area is delimited either by the borders of the anatomical articular surface or by a principal circle on the sphere, comparable to the equator on the globe if the point of penetration of the stressing force R (the hip resultant) is taken as the "pole".

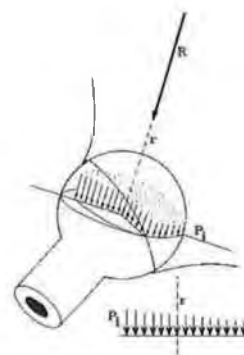
Figure 1.22: The supporting area of a spherical joint as a "spherical biangle". The spherical head may be converted by cartilage : anatomical surface, its contact with the socket comprises the area of contact, shadowed biangle : area of support.
 R : hip resultant, penetrating the joint at the "pole".



With this assumption one may say that below the equator no normal forces can be transmitted from the socket to the articular head and that where the border of the socket lies above the equator, it delineates the area of force transmission. It goes without saying that for reasons of equilibrium, the pole cannot go outside the border of the area of contact.

For theoretical calculation of the stresses, the hip resultant is divided into partial forces distributed in such a way that the sums of rotational moments of opposite sides everywhere are equal to zero, Figure 1.23.

Figure 1.23: Division of the hip resultant, R , into partial forces P_i . The distribution of the P_i takes place in a plane, perpendicular to the line of action r of R [146].



If P_i are the partial forces, then:

$$R = \sum P_i, \quad (11)$$

and, assuming an elastic, but not visibly deformable material, the principal stresses in the articular surface are proportional to the normal components of P_i :

$$\sigma_i \propto -P_i \cdot \sin \alpha \quad (12)$$

where α_i is the angle between P_i and the equator (angle of latitude).

If the principal circle through the pole and the apex of the border of the socket is taken as the “zero meridian” and the angle of inclination of the acetabular border to the equatorial plane may be ρ , the smallest angle α on the zero meridian will be (Figure 1.24):

$$\alpha_0 = \rho \quad (13)$$

This angle increases as the resultant, R , approaches the acetabular border. Because of the fact that the sum of all moments have to be equal to zero, the stresses must increase in the area between R and the border of the surface of contact. Consequently, increasing angle ρ means increasing stresses at the articular border, Figure 1.24.

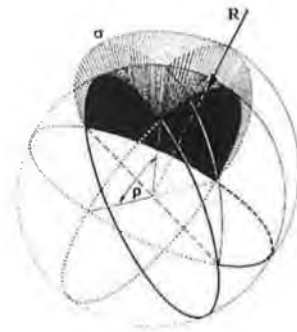


Figure 1.24: Stress distribution in a spherical joint.

R : Hip resultant.

ρ : Angle between the plane of the border of the socket and the equatorial plane [146].

Since the magnitudes of the transmitted normal forces, and consequently the normal stresses, depend on the angle α , the stresses will be greater and equal to the partial force P_i at the pole, and will decrease to zero at the equator, Figures 1.25 to 1.27.

Theoretically, an elastic layer like the articular cartilage should be able to distribute the stresses over a great part of the supporting surface to an almost uniform magnitude.

This is particularly so when the articulating head is a little bit wider than the socket and touches first the border of the acetabulum and relieves the roof of socket [96].

It may be presumed that the radius of the head is somewhat greater than the radius of the socket, but that the double layer of compressible cartilage is able to compensate the incongruity, Figure 1.28. Furthermore, the stresses arising from the compression of the cartilage at the border of the socket may be exactly as greater as

the maximal stress at the pole, Figure 1.29. The superposition of the two diagrams (1. from compression of the cartilage, due to incongruity, and 2. from the loading of the joint) then gives a uniform stress over the entire area of support.

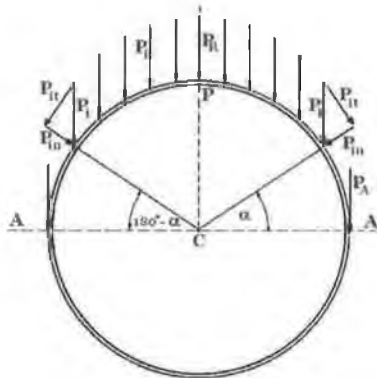


Figure 1.25: Determination of the normal forces P_{in} from the partial forces P_i . Each force P_i can be divided into the normal component P_{in} and the tangential component P_{it} . The relation of P_{in} to P_{it} depends on the "latitude". [147]

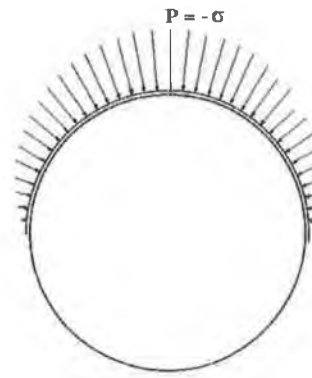


Figure 1.26: Distribution of the normal forces P_{in} in a spherical joint. The maximum $P_{in} = P_i$ lies on the pole, on the equator $P_{in} = 0$. [147]

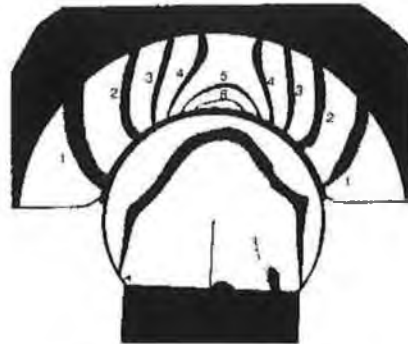


Figure 1.27: Stress distribution in a spherical joint as determined by a photo-elastic experiment. The numbers indicate the orders of interference fringes. They are proportional to the local stresses.

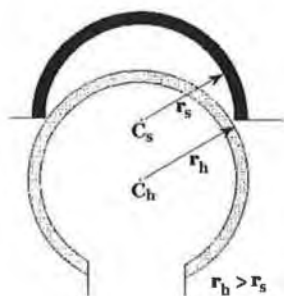


Figure 1.28: Incongruent ball-and-socket joint. Both articular surfaces are covered by an elastic layer.
 C_h and C_s : Center of head and socket respectively.
 r_h and r_s : Radii of head and socket. [146]

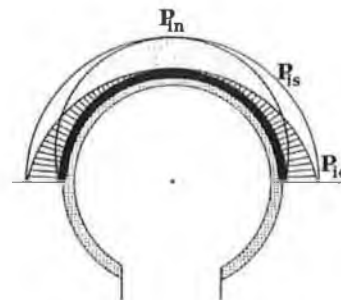


Figure 1.29: Stress distribution in an incongruent ball-and-socket joint with elastic layer on both surfaces.
 P_{ic} : Normal stresses due to compression of the cover.
 P_{in} : Normal stresses due to loading.
 P_{is} : Sum of P_{in} and P_{ic} (uniform over the whole area of support). [146]

Pauwels [202, 203] has maintained that the densification in the subchondral

bone exactly reflect the stress distribution in the joint, assuming that bone formation and calcification are everywhere proportional to the actual stresses. In a normal hip joint the roof of the socket has a very compact bone structure, Figures 1.30 and 1.31. Its uniform height indicates that the stresses must be distributed uniformly, probably due to the articular cartilage. If the hip resultant is shifted towards the acetabular border, the stress diagram becomes triangular in shape, Figure 1.32, and the densification in the acetabulum shows the same contour, Figure 1.33.



Figure 1.30: Stress distribution in the normal human hip joint. [202]



Figure 1.31: Bony condensation in the acetabular roof. [202]



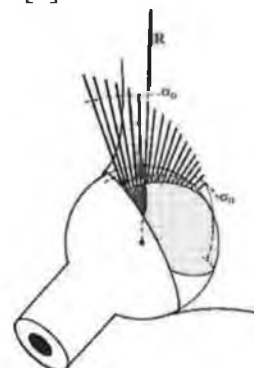
Figure 1.32: Triangular stress diagram in a hip joint with laterally shifted force R . [202]



Figure 1.33: Triangular condensation in the acetabular roof of a hip joint with subluxation of the head. [202]

Such an unequal stress distribution may influence the development of the articular cartilage. There are many arguments in favor of the assumption that cartilage can exist only if the mechanical stresses do not exceed certain limits, Figure 1.34. Beyond the upper limit, σ_o , cartilage degenerates with the symptoms of arthritis; below the minimal stress, σ_u , it undergoes involution and, generally, is replaced by bone tissue [5].

Figure 1.34: Reaction of the articular cartilage to the magnitude of stresses. Cartilage develops and is preserved in the area between the lower limit σ_u and the upper limit σ_o . Beyond σ_o cartilage is destroyed, below σ_u it disappears due to ossification. [146]



This reaction of cartilage determines the shape of articular surfaces, so that it may be said that all areas of support in every position of the joint must be covered with cartilage in case the stresses stay between σ_u and σ_o .

Following this theory, artificial surfaces of joint of joints can be constructed. Presumed is an area of support, shaped as spherical biangle, delimited by the acetabular border and part of the equator, Figure 1.22. When the joint resultant, R, shifts on the articular surface, the supporting area changes its position in the same way [5].

1.5.5.2.2. Stress distribution in the Femoral neck

The femoral neck is stressed by the same hip resultant, R, that stresses the articular surface, Figure 1.35a. since the line of action of the force passes oblique to its axis, the femoral neck is stressed by bending. In a femur with normal angle between neck and shaft, the eccentricity of the stressing force is so great that, at the middle of the neck relatively high compressive stresses arise in the medial wall and somewhat lower tensile stresses in the lateral wall, Figure 1.35b.

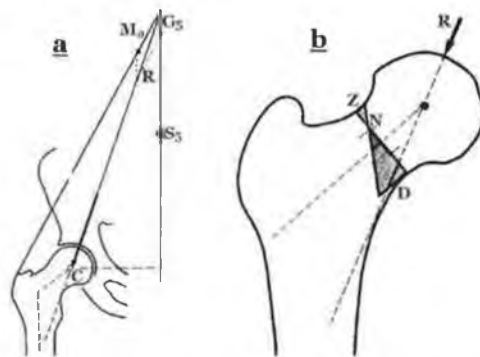


Figure 1.35: Stressing of the femoral neck with normal angle between neck and shaft. (a) Determination of the hip resultant, R, from G_5 and M_a . (b) Distribution of stresses in a cross-section at the middle of the neck. D: compressive stresses, R: stressing force, N: no-loaded line, Z: tensile stresses.

In coxa vara, the bending moment for the femoral neck increases, Figure 1.36a, and consequently the bearing parts of the cancellous bone at the lateral side is reinforced, Figure 1.36b.

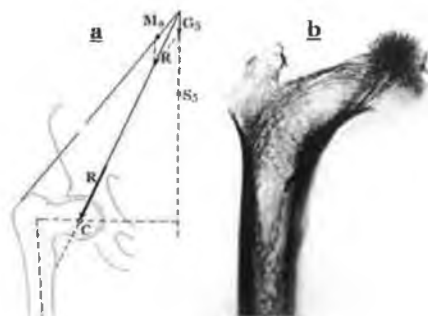


Figure 1.36: Increased bending stress in coxa vara.
a) Determination of the hip resultant, R, from G_5 and M_a .
b) Radiograph of a coxa vara (Note the reinforced tension bearing parts at the lateral contour of the neck!).

A certain erection of the neck can lead to a position where the line of action of the hip resultant intersects with the border of the marrow space at the middle of the neck, Figure 1.37. Under these conditions, the no-loaded line falls within the lateral contour.

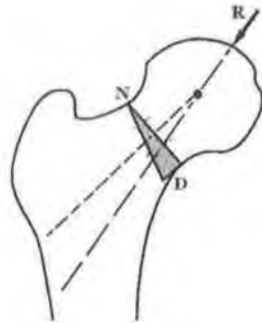


Figure 1.37: Stressing of the femoral neck by a force R just at the top of the roof.
 D: Compressive stresses in the medial wall of the neck.
 N: Neutral fiber in the lateral wall.

Extreme of the neck as in coxa valga can reduce the bending moment almost to zero, Figure 1.38a. if the line of action of the stressing force passes through the neck axis, the cross-section is stressed by pure compression of uniform magnitude, Figure 1.38b.

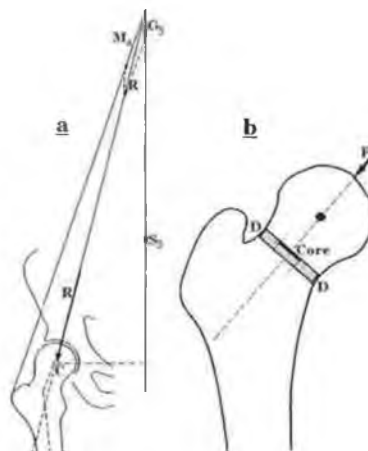


Figure 1.38: Stress distribution in the femoral neck of an extreme coxa valga..
 c) Determination of the hip resultant, R , from G_5 and M_a .
 d) Axial position of the force R and uniform distribution of compressive stresses D .

1.6. Total Hip Prosthesis (THP)

A great many hip replacement designs have been put forward since the first recorded attempts of Thomas Gluck in 1890 [230] and Wiles in 1938 [282], but very few have gained general acceptance. The present survey is restricted to modern designs which are known to be in general use, or have potential for becoming so.

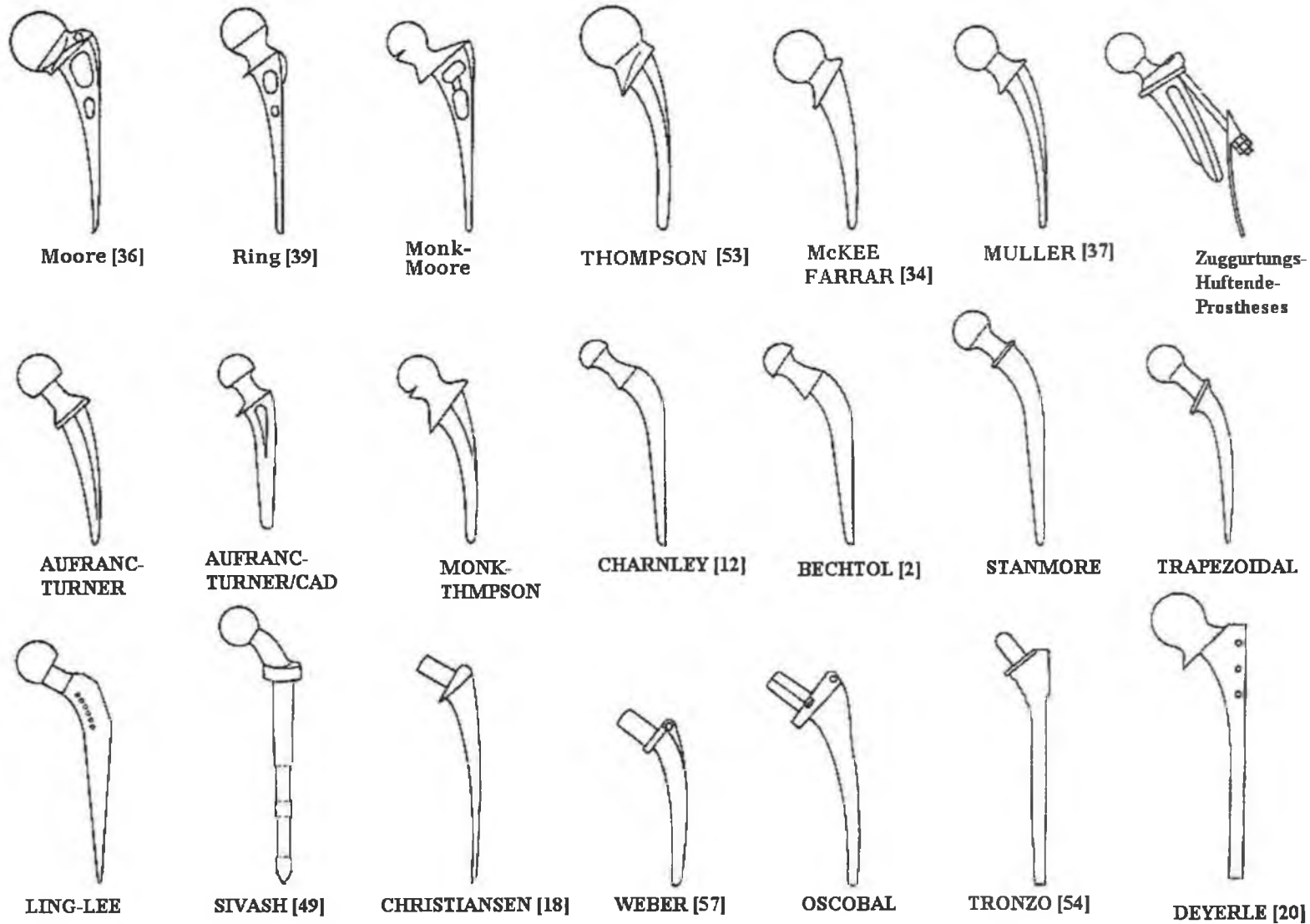


Figure 1.39: Line drawing of various femoral stem designs.

All total hip replacements to date mimic the natural joint with an essentially hemispherical bearing cup set in the acetabulum, and a matching sphere attached to the femur in place of the original head. There are many ideas shared between the various designs, and differences between particular brands are due as much to the particular combination of ideas as to unique features. In order to facilitate comparisons and identify significant features, subsequent discussion is made under the headings:

- (i) Femoral stem.
- (ii) Shoulder on femoral stem.
- (iii) Head position – neck length and angle.
- (iv) Head diameter.
- (v) Use of acrylic cement.

1.6.1. The Femoral Stem

The function of the femoral component is to position the replacement ball relative to the femur and transmit the loads on it to the supporting bone. Many varied designs have been tried in the past [288], but experience has led to the use of a tapered or parallel stem extending about one-quarter of the way down the femoral medullary cavity. The stem shapes for 21 prostheses at present available are shown in Figure 1.39. Typical cross sections for some of these are shown in Figure 1.40. The frost-Ring and Sbarbaro are not shown, as these use the same stem design as Moore. Moore and Thompson produced their prosthesis before the introduction of acrylic cement by Charnley in 1960. The Ring design was introduced later, but the inventor has steadfastly refrained from adopting acrylic because of the uncertainties and risks [222].

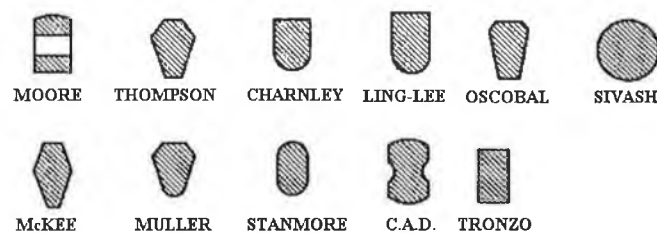


Figure 1.40: Cross sections of prosthesis stem one-third distance from shoulder.

The stem length depends to some extent on the planned position of resection on the femoral neck. Thus, the Moore appears to have a longer stem than the Thompson, although the head-tip length is the same. The extremes on the chart are

the Weber, which is smaller than others, and the long-stemmed Sivash, Tronzo, and Deyerle for use without acrylic. The Howse is a prosthesis for small patients. All standard current models can be considered of similar length, with the non-acrylic cement models slightly longer, when compared with longer devices such as intermedullary nails of the special long-stemmed versions now available.

All stems are smaller at the distal end than at the medial end, and are curved in some way on the medial side to match the shape of the calcar, with the exception of the Sivash which uses a circular reamed seat.

The Moore style [184] has been used in other total hip replacements not employing acrylic cement – Ring, Monk, and Sbarbaro, and with the Urist cup. It is used with cement in some cases [245] and is still currently available as a femoral head prosthesis. The Thompson [260] femoral head replacement is a companion to the Moore as a femoral head prosthesis because of its different neck configuration. The style has now been used with slightly modifications in many total hip prosthesis designs. The design was developed for use without cement, but is now widely used in conjunction with it.

The Sivash, Tronzo, and Deyerle are more recent and indicate an attempt to gain maximum load transfer area. Sivash uses a long, gently tapering, round femoral stem with elongated holes to provide locking by bone ingrowth. The vertical load transfer is aided by a broad circular collar which rests on a prepared site on the lower neck. The stem is hammered into a reamed intermedullary cavity of the same shape to ensure a tight fit. It must be presumed that the friction from the right fit at insertion is adequate to prevent any rotation of the stem in its socket until sufficient bone ingrowth into the slots on the stem has taken place. The Tronzo uses a long rectangular cross-section stem with stepped shoulders resting against the calcar. Deyerle [66] uses a similar form, but with a smooth surface resting against the calcar, and the addition of three large transfixation bolts antero-posterior through the bone and upper end of the femoral prosthesis.

Designs using acrylic cement are all subsequent to 1968. Charnley [40] was the first to use the material, and others soon followed. It appears that the shape of the stem is less critical when acrylic cement is employed, because a good fit against the

bone and potentially good transfer is possible for almost any shape stem. Charnley [38, 43] initially used a Moore stem, but brokerages occurred. Later, his now well-known stem shape was adopted and this has been in use for more than 32 years. The new shape is consistent with the change from cast cobalt-chromium alloy to a forging, in this case of stainless steel. The Stanmore design is similar, but has a slightly larger collar at the base of the neck and is rounded on both the lateral and medial sides of the stem, whereas the Charnley is flat on the lateral side.

The McKee-Farrat and Stanmore designs adopted the use of acrylic soon after Charnley, and since that time Müller [187] and the others shown in Figure 1.39 [4, 49, 235, 236, 243, 246, 265, 276]. Further, many designs are now available with a range of sizes and forms of femoral stem, and some manufacturers provide an extra-long version (Bechtol, Charnely, McKee-Farrar, Minneapolis, and Christianson) for salvage procedures. Despite the variety of designs available, there does not appear to be any rationale of published grounds for the size and forms chosen, other than the experience of the surgeons, which by now is not inconsiderable.

1.6.2. The Shoulder on the Femoral Stem

The nature of the transition between the femoral stem and the head and neck portion varies a great deal. The shoulder which opposes the cut end of the neck of the femur may be quite large as on the earlier femoral head replacement of Moore and Thompson, or merely an abrupt change in section shape as on the Charnley or Bechtol, or completely absent as in the case of the Ling-Lee. The angle between the face of the shoulder and the shaft of the femur will influence the nature of any load transfer to be the cut neck of the femur. The angle between the shoulder and the prosthesis stem is difficult to specify precisely, because of the curved nature of the stem. Most prostheses are made with an angle of about 45° [70], but the actual value has little meaning since the angle to the femoral shaft may vary by as much as 10° either way, depending on the angle of insertion of the stem in the femur.

The angle between the prosthesis femoral neck and the prosthesis stem or the femoral shaft can likewise be recorded, but is of doubtful significances. The crucial information is in the position of the prosthetic femoral head in relation to the rest of

the femur, and this depends on the position of insertion as well as on the shape of the prosthesis.

The importance of the neck flange on the femoral prosthesis component varies according to use of acrylic bone cement. When cement is not used, a substantial portion of the joint force is transmitted to the femur through the flange onto the cut neck [80, 213]. As absorption of the cut neck takes place, the prosthesis 'sinks' down into the femur [70].

In this case, discussion of the force transfer to the cut neck is very significant. Where cement is used, little if any load is transmitted to the cut neck. Charnley et al. [44] observed a 37.2% incidence of resorption away from the flange without loosening, confirming the adequacy of load through the cement in the medulary cavity. Experimental evidence supports this view [245, 280, 291].

Where acrylic cement is not used, it seems appropriate that the shoulder should be at right angles to the direction of maximum load, to avoid any lateral force component acting against the calcar. Thus, an angle of 60° is required between the prosthesis shaft and the shoulder. The Aufranc-Turner and Christiansen are the nearest to this, but generally the value is in the range 30-45°. The Sivash does not use the cut neck at all, and has a reamed seat at right angles to the femoral shaft.

1.6.3. Head Position – Neck Length and Neck Angle

Neck length and neck angle are difficult to define and measure in comparative terms, and are not, in themselves, worthy of accurate description. The position of the head of the prosthesis in relation to the femoral shaft can be influenced to considerable degree by the surgeon.

Reduced femoral neck diameter increases the range of movement and extends the overall life of the system, Figure 1.41. Consequently, the moment at which the neck will impinge upon the rim of the cup is delayed. This minimizes chock loading of the cup and extends the fixation life of the acetabular component.

Many suppliers offer a selection of neck length to permit selection of the best femoral position in relation to the hip and surrounding muscles. Charnley advise the alternative procedure of trochanter shift to adjust abductor tension and improve hip

mechanics. Designs using trunnion bearing (Christiansen, Oscoball, Tronzo, and Weber-Huggier) provide a convenient selection of neck lengths with the advantage that final selection can be made in the later stages of the operation [29, 311].

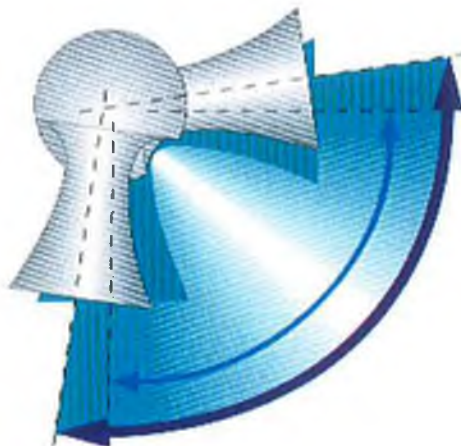


Figure 1.41: Reduced diameter neck increases the range of movement and extends the overall life of the system.

1.6.4. Head Diameter

Head diameters on total hip replacement prosthesis vary from 22 mm for Charnley and Bechtol series to 51 mm for the Sbarbaro [29, 70, 311]. In general, the larger diameters allow a greater range of movement and reputedly greater resistance to dislocation, while smaller sizes claim lower friction. Designs derived from femoral head replacement tend to have the larger diameters, and models using plastic acetabular cups must, of necessity, use smaller diameters to permit sufficient wall thickness for strength and wear requirements. All heads, with the exception of the aluminum oxide ceramic head, are now made of metal and are of a size to match the requirements of the acetabular component.

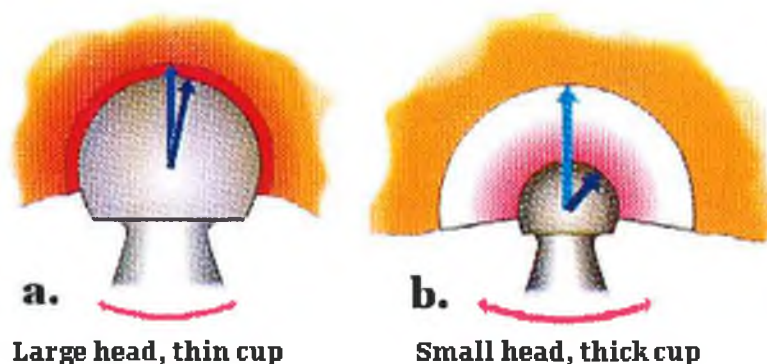


Figure 1.42: A small articulating in a thick cup significantly reduces the risk of socket migration. Stress is diffused and the risk of localized cement failure is diminished.

The principal of low frictional torque arthroplasty means a minimization of the torsional forces at work in implant loosening. Torque loading of the cement-bone interface is at its lowest when a small diameter prosthetic femoral head is articulated of socket, Figure 1.42. With lower turning, or loosening forces applied directly to the cement, the potential life of the implant is extended [85]. Photo-elastic studies demonstrate different patterns of stress between large head/thin cup and small head/thick cup designs. In Figure 1.42 (a) stresses are concentrated over a 90° quadrant and are 1.5 times higher. In Figure 1.42 (b) they are diffused and distributed evenly across the surface of the socket. The effect is to prevent localized movement between cement and bone, which would lead eventually to a histiocyte reaction and bone cavitation followed by loosening [224].

Current technology allows for the addition of a femoral cup at some stage after the insertion of a femoral head prosthesis. Initially, metal-metal total hip replacements were produced as matched pairs [175], but improvements in production methods now permit interchangeability between cups and head of the same nominal diameter. Meanwhile it has been found that a metal-nonmetal head-cup combination gives better results in terms of wear and heat due to friction. Van Lenthe et al. [276] analyzed four head-cup material combinations (aluminum oxide ceramic, cobalt chromium alloy, and high density polyethylene) and concluded that high density polyethylene cups are unlikely to provoke problems, but that metal-metal and ceramic-ceramic combinations need the lowest possible friction coefficients to prevent tissue necrosis. When a femoral head prosthesis is used as a preliminary treatment, however, the size of the head is determined by the acetabulum, and matching cups fitted at a later stage must then match the original head. Trunnion heads overcome the problem by allowing replacement of the head without disturbing fixation of the stem.

In vivo measurements show that hip implants heat up during activity [20, 95]. It is hypothesized that this is due to friction between head and cup. It may cause thermal damage to soft tissues and bone, and eventually may cause implant loosening [276].

1.6.5. Use of Acrylic Cement

The use of acrylic cement in providing improved fixity of the femoral stem

has been widely accepted. The major mechanical improvement is that the connection between the prosthesis and the femur is much stiffer. Charnley and Kettlewell [47] showed that without the use of acrylic cement, the femoral stem movement in the femur when subjected to an axial load was 2.56 mm per kN. However, when acrylic was used, the movement decreased to 0.11 mm per kN. Without the use of cement the lack of stiffness would be related to the necessary clearances between bone and prosthesis. If the cavity were very accurately reamed, the joint would be more satisfactory. However, such an ideal circumstance is very difficult to achieve.

There are substantial difficulties associated with the use of acrylic cement:

- a) The orthopedic bone cement is a PMMA which is obtained by mixing prepolymerized powder with liquid monomer. The polymerization is an exothermic autocatalytic reaction. de Wijn et al. [63] reported an overall initial expansion of 2 to 5% due to expansion of enclosed air and vaporized monomer bubbles. Subsequently, there is a contraction due to dimensional changes of the polymerizing mass and thermal shrinkage upon cooling. The clinical significance of the contraction is that it may provoke a gap between the bone and the cement and that the hoop stresses generated by shrinking around a much stiffer stem may create cracking of the cement mantle at the time of operation [181].
- b) The possibility of thermal necrosis due to rising temperatures at the bone cement interface during polymerization. The generation of necrosing temperatures was usually possible for cement thicknesses in excess of 5 mm [237].
- c) The polymerization is never complete: there remains some 1 to 2% residual monomer. This monomer, methylmethacrylate, is cytotoxic. Willert and Semlitsch [284] consider the amount released into the tissue potentially capable of causing tissue necrosis.

1.6.6. Acetabular Component

The nature of the acetabular component varies a great deal with the method of fixation. The Ring (and the Frost derivative), Sbarbaro, Sivash, and Tronzo have been developed for use without acrylic bone cement. The Ring [222] design uses 75

mm cancellous bone screw directed from the acetabulum up the weight bearing line of the ilium. The rear of the cast cobalt-chromium alloy cup is conical in shape, and fits accurately into a specially reamed seat in the acetabulum, the Tronzo design [266] uses a triflange spike with a serrated head placed in a similar position to the Ring screw, although not as deep. The acetabular cup is driven into a prepared hole, and rotation is prevented by three additional short spikes on the back of the cup. Sbarbaro uses four tines only and a peripheral flange to minimize migration of the cup into the reamed acetabulum. The design differs from all others in that it is not a complete cup but more horseshoe shaped. In complete contrast, the Sivash [243] design depends on sharp circumferential petals that are embedded in the reamed acetabular cancellous bone. It is claimed that the implant stimulates growth of bone into and around the slots and grooves in the acetabular component. Insertion appears difficult, with very little margin for error. The Frost variation of Ring's design [88] differs from all others in using fibrocartilage as the bearing surface. The threaded stem of the Ring cup is replaced by a smooth rod, and additional shoulders added to the rear of the cup. The unit is thus rotate about its longitudinal axis on a bed of fibrocartilage formed between the bone and the cup. The mechanical bearing situation is comparable with designs using a free ball on a trunnion, except that the cup moves instead of the ball.

Where acrylic bone cement is used, the only requirements of the outside of the cup are that the cup is mechanically strong enough, the external diameter is appropriate to the size of socket in which it must fit, and the acrylic can mechanically bond to it. The most crucial variables are in the hands of the surgeon – the preparation of the bony socket, the selection of the acetabular component of the prosthesis, correct manipulation of the cement, and the correct angular positioning in relation to the rest of the body.

The external diameter of the acetabular components is dependent primarily on the size of cavity available. This is much less critical where acrylic bone cement is used. External diameters of cups vary from 37 mm to 57 mm for use with, and 65 mm for use without, acrylic bone cement, with most suppliers providing a choice of two or three. The interchangeability of cups and femoral components is a prerequisite for such selection procedures to be economically feasible. The wear on metal-metal

artificial joint is important because of the resultant increase in coefficient of friction and tissue reaction to the resultant wear debris [231, 286].

The basic hemispherical cup has been modified in several ways. The Aufranc-Turner and Harris designs employ an eccentric cavity to increase the wear thickness available, and the Harris and Deyerle also supply the option of a metal socket for the plastic cup, so that replacement may be made without disturbance to the cup fixation. Charnley has a 'long posterior wall' acetabular cup to reduce the likelihood of posterior dislocation (British Patent No. 1,296,162), and Ling-Lee uses a similar modification. The Howse-Arden design uses a cup in which the cavity extends slightly beyond the half-sphere, so that the metal head is retained firmly in position in much the same way as the glenoid labrum on a normal hip. The design of long posterior wall of the socket gives maximum head coverage and minimize the risk of dislocation [298], Figure 1.43.

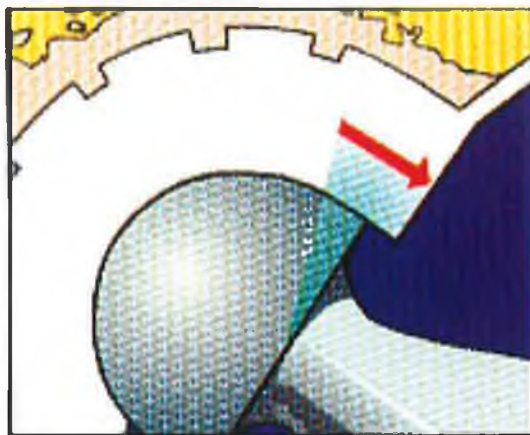


Figure 1.43: The long posterior wall of the socket gives maximum head coverage and minimize the risk of dislocation.

The maximum range of movement possible for an artificial hip with the ball remaining seated in the cup is determined by the positions of contact between the rim of the cup and the neck of the femoral component. Repeated contact in this region may lead to loosening of one or more components, usually the cup. The limitations to design can be readily appreciated from the geometry. The maximum cup extent for rigid metal cups is half a sphere, and most cups are of this extent. Oscobal and Sbarbaro are relieved around a portion of the cup circumference, and the Sivash uses a captive ball which reduces the range to 88°. Plastic cups allow an occasional small extension beyond the hemisphere through the greater elasticity of the edge. The

Howse and Monk designs takes advantage of the idea to provide improved retention between the ball and cup. The Buchholtz St. Georg cup is segmentally relieved about 45° to extend the range by 20°.

The greater the thickness of the neck in relation to the ball diameter, the smaller the range of the prosthesis. The greatest range will be obtained when the neck cross section is a minimum at the point of impingement on the cup, and the ball diameter is the greatest. The minimum neck thickness is dictated by strength considerations, while the maximum head diameter is restricted by the size of the reamed acetabulum. The Aufranc-Turner elliptical neck and the Zimmer Trapezoidal 28 (designed by Amstutz and Walker) appear to have been designed for maximum range of movement in flexion and extension. The advantages gained from optimization of cup diameter are not very great, however. The maximum ranges calculated from prosthesis head and neck diameters in Table 1.3.

Table 1.3: Maximum angular range of movement for total hip prosthesis designs			
Design	Ball diameter [mm]	Neck diameter [mm]	Range [degree]
Aufranc-Turner	n.a.*	n.a.	120
Bechtol	n.a.	n.a.	128
Charnley	22	13	108
McKee-Farrar	35	19	114
Müller	32	15	124
Oscobal	44 ±3 mm relief on cup	30	102
Sivash	n.a.	n.a.	88
Stanmore	n.a.	n.a.	113

* n.a: not available for measurment.

The importance of maximum range will depend on the youth and vigour of the patient, and the accuracy of positioning of the acetabular cup. While the Sivash might justifiably be criticized for its limited range, it is very doubtful if the differences between the other models listed significant.

The incidence of dislocation after primary total hip arthroplasty (THA) is reported to be between 0.6% and 9.5% [142]. Charnley [41], has put forward the idea that a large diameter ball and socket would be less likely to dislocate than a small

diameter joint, on the ground that the ball would need to be moved out a greater distance to escape the cup. Additional concerns exist for hard-hard articulations such as ceramic-ceramic or metal-metal because ceramic and metal are much less deformable than polyethylene. Klabunde and Portman [142] reported that the metal-metal combination are less sensitive to dislocation. When the hip joint force is almost parallel to the face of the cup, the dangers of dislocation are greatest. Such an event is principally resisted by the action of muscles and ligaments.

1.6.7. The Spherical Bearing

All total hip replacement designs under review are based on a simple ball-and-socket joint as in the normal hip, with the ball mounted on the femur and a matching socket set in the pelvis. In addition, the Christiansen [49], Tronzo [266], and Weber [276], designs introduce an extra degree of freedom into the joint by mounting the ball on a trunnion attached to the top of the femoral stem. All joints fall into one of two classifications: metal on metal, or metal on plastic.

The all-metal bearings use the larger diameters and the metal-on-plastic types tend to be smaller. The smallest is the Charnley at 22 mm diameter, and the largest by Sbarbaro at 51 mm diameter. The Charnley design [46] is based on the concept of minimum friction force, but this also complied with the criterion of minimum volumetric wear within restrictions of resistance to dislocation and rate of head penetration through the cup. The McKee-Farrar and other metal-on-metal designs are based on the concept of minimum wear and hence, long life. Charnley, and van Lenthe [276], claim that wear on high density polyethylene cups is not excessive, while the proponents of metal-on-metal types consider that friction is not excessive [4, 223].

A future design factor supporting the small head in the Charnley prosthesis is that a greater thickness of plastic can be accommodated in the acetabulum. This is desirable in order to achieve a reasonable wear life, since it is the plastic which wears in preference to the metal.

Metal-on-metal bearings for joint replacements have gained from two significant areas of study. Pin-on-disc and hip simulator studies demonstrated that cast cobalt-chromium alloy was the only one suitable for metal-on-metal bearings [21, 71, 72]. Besong et al. [21] identified the importance of the contact area between

the ball and socket in determining the frictional character of the joint. Contact near the rim of the cup produced a wedging action which produced higher friction and greater likelihood of loosening of the prosthesis. the simulator studies at Stanmor clearly demonstrated that the metal-plastic bearings had less friction by up to five times, and it was recognized that excessive joint friction can cause loosening [232]. The all-metal joint has been retained because of the greater wear rate experienced by polyethylene cups and long-term uncertainty of the reaction with this material in the body. Histological studies have shown that there is an effect due to a cellular reaction on the wear or abrasion particles of polyethylene and cement [285], Figure 1.44.

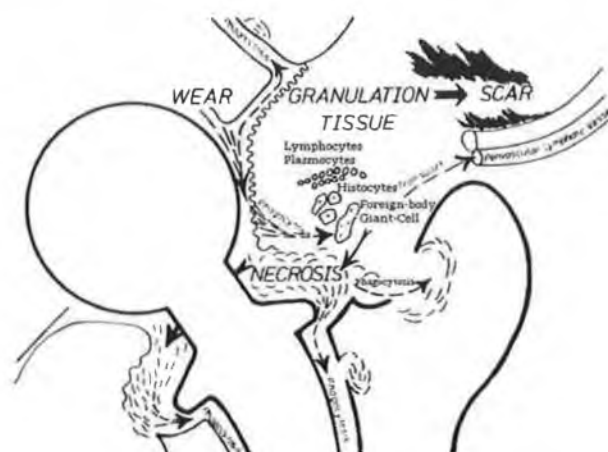


Figure 1.44: Schematic representation of loosening by tissue reaction on wear and abrasion particles [285].

These particles initiate a foreign body reaction and result in the formation of granulation tissue, including macrophages and foreign body giant cells. When the amount of particles is small, they may be eliminated via the perivascular lymph spaces. However, when this transport system is insufficient to handle the volume, the foreign-body reaction may extend to the whole environment surrounding the joint including the calcar region and the cement bone interface. Thus, in addition to impairing calcar stability, the foreign body reaction on wear and abrasion particles may provoke loosening as well [285]. The amount of wear debris produced by all-metal joint is much less than metal-on-plastic joint, but Freeman suggests that the cobalt-chromium alloy debris is more toxic than that from polyethylene, and demonstrated 10 times greater concentration of metallic ions in the surrounding tissue for all-metal joints.

Tunnion head prostheses were first introduced to reduce the wear on the

acetabulum by femoral head replacements but were later incorporated in total hip replacement designs [29]. The removable central element provides an opportunity to adjust the femoral fixation of the prosthesis, and to replace worn parts without destroying the fixation. On the debit side, the trunnion requires a more complex implant with increased cost, and closed reduction after dislocation is extremely difficult.

Charnley [40] adopted small diameter heads on P.T.F.E. cups in the first place to minimize friction. Studies of the wear of hip sockets of this material after revision, and mathematical treatment of the problem, indicated that the 22 mm heads produced less wear debris than larger heads. Below a certain size, the rate of penetration into the socket by the head became too rapid [46]. The wear rate of P.T.F.E. was found to be excessive, and it produced an irritant sludge. Ultra-high-molecular-weight polyethylene was used instead and is now widely used as a bearing material in joint replacement for the human body.

1.6.8. Design Criteria for the Hip Endoprotheses

Figure 1.45 collects and illustrates some a controversial design criteria for an “ideal stem”. The diameters of the articulating ball (A) ranges from 22 to 36 mm in THR with a certain predominance of 32 mm. Balls larger than 32 mm will certainly disappear during the coming years because they afford a larger socket and hence need more bone removal at the critical acetabular implantation site. Smaller ball diameters,

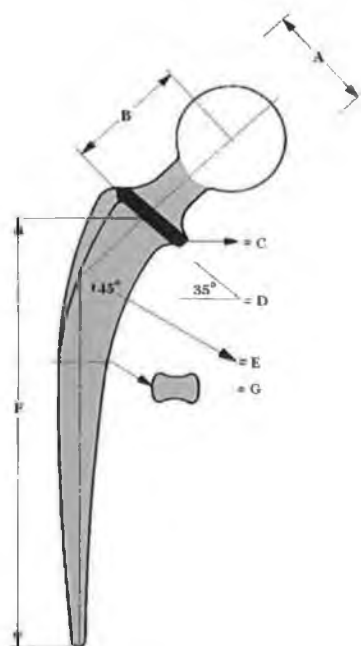


Figure 1.45: Line drawing of essential design criteria for an ideal cemented stem design in THR [70].

however, have a significantly higher rate of spontaneous postoperative dislocation.

Many THR devices offer three different neck lengths (B). The short-neck design should nearly never be used as it limits the postoperative range of motion considerably (earlier contact of calcar or minor trochanter and socket in flexion/adduction or of greater trochanter and the lateral pelvic wall in fixation/abduction). The results as to pain relief and range of motion are not satisfactory with short-neck prosthesis and can be avoided in most cases by better surgical technique. Long-neck prostheses, which are most often used in the attempt to restore leg length equality, tend to loosen earlier than standard medium-neck length prostheses. This can easily be explained by the lengthening of the lateral lever arm of the hip joint by using a long neck. This increases the load of the femoral prosthesis and the torque at the calcar area. Both parameters increase the risk of loosening of the femoral component through chronic overload of the bone-implant interface.

The calcar support of a femoral prosthesis (C) is another area of dispute. The basis of large calcar supports of femoral components is taken from static and dynamic loading experiments of cadaver femora with post-mortem implanted prostheses. Clinical experience has shown that many cemented femora components subside during the years and do not loosen. This is considerably impeded by a large calcar support of the prosthesis. A smaller calcar support, which allows for a rest of the prosthesis on the cement cuff only and therefore does not prevent the prosthesis from settling during interface remodeling is the optimum solution. It combines the advantages already mentioned for small calcar supports with a better load distribution on the cement cuff and a minor risk of splitting of the cement cuff by sinking into it.

Biomechanical studies have stressed the importance of a neck support of 35 to 30° and a neck-shaft angle between 135 and 145° (valgus position, D and E in Figure 1.45). A valgus prosthesis together with a long neck is, however, considering the aforementioned argument; a dangerous prosthesis considering the risk of persisting pain and early loosening as it exaggerates the positive effects of this proposal. Lowering of the neck support angle from originally 45 to 30° reduces the torque at this area during every load cycle, a femoral lateral lever arm. Both improvements only within this "physiologic range" are considered to reduce the risk of loosening.

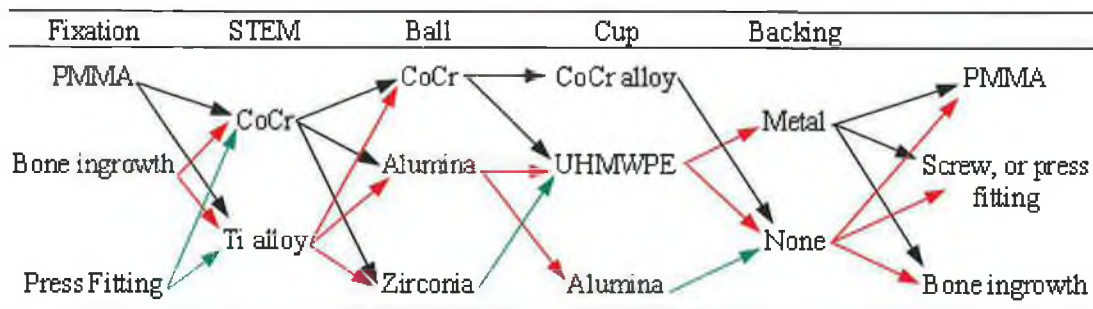
The length of the intramedullary stem of the femoral prosthesis (F) varies in a large scale from 12 to 18 cm for standard prosthesis. Theoretically the problem of mechanical loosening is only postponed by lengthening of the prosthesis.

The rigidity of femoral stem prosthesis is not only a matter of the material used, but also a matter of the square diameter of the stem and its shape (G). Presently T or H-shapes being the most stable against repeated bending are most popular. Flanging of the stem also contributes to augmenting the strength of the femoral component. The finite element model of the artificial hip of present work was built up in the strength of these data.

1.6.9. Materials Combinations in Total Hip Joint Replacements

Table 1.4 illustrates the most frequently used combinations of material in total hip replacement [196]:

Table 1.4: Possible Combinations of Total Hip Replacement



UHMWPE = Ultra-high-molecular-weight polyethylene

1.7. Structural Stress Analysis

A structure is a geometric configuration of materials created to withstand loads. Structural analyses are performed to predict stresses occurring within the loaded structure, with the objective to evaluate the adequacy of its design and materials in fulfilling its load-bearing functions. The stress distribution in a structure depends on four aspects:

- The magnitude and configuration of the external loads, the loading conditions.
- The geometry of the structure.
- The material properties.

- d) The physical nature of connections with the environment (boundary conditions) and between different materials (interface conditions).

For a structural stress analysis, these aspects must be described, either mathematically (in a theoretical stress analysis) or physically (in experimental stress analysis). This description is called a model of the structure. The development of the model is probably the most difficult and crucial step in the analysis.

Roughly, the objectives can be divided into three categories. In the first, design evaluation, are those analyses aimed at testing the mechanical performance of a specific design. A possible question, in this case, is simply whether the design, which could be an implant, will fail or not, based on quantitative criteria known. Another possibility in this category is to compare a specific design to another or previous one. The “model” in this case may be the structure itself, a prototype on which stresses are experimentally determined, simulating the loading environment for which it is intended. The second category, design optimization, is directed at investigating the effects of design parameters (geometry, material) on the stress distribution. Such an analysis may be aimed at a true mathematical optimization; e.g., to evaluate the one stem shape of a total hip replacement for which acrylic cement stresses are minimal or it may be limited to investigate a few shapes to establish trends from which design decisions are made. For design optimization purposes, parametric analysis will usually be applied, investigating the isolated influences of structural properties on the stress distribution by subsequent variation of parameters. Theoretical methods are suitable for parametric analyses in particular. Obviously, the borderline between the first and the second category is not very strict, nor is it between the second and the third, basic research. This category includes all analyses aimed at finding fundamental concepts with respect to the shape and function of the structure itself. Examples in this category are those pertaining to stress-related architecture and remodeling of bone; effects of material characteristic (such as anisotropy, viscoelasticity), geometry, and loading on stress distributions; development of special techniques for the analysis of biological tissues; principals of load transmission in bone-prosthesis structures; stress-related interface behavior; and so on. Parametric analysis is a major tool category.

The procedure of stress analysis can thus be divided into four steps: structure identification and assessment of objectives, model development (including the collection of required data), analysis process, result validation and interpretation. Several decisions have to be made in the execution of these steps, the consequences of which are closely interrelated. The central issue in the whole process is the model, the characteristics of which affect all steps.

1.7.1. Methods of Analysis

1.7.1.1. Experimental Methods

To understand the principles of experimental stress analysis, it must be appreciated that stresses cannot be determined in direct measurements. Just like heat becomes manifest by its effects only (temperature changes), stresses are abstract concepts that must be determined indirectly, by measuring their effects (i.e., deformations). Nor can strains be measured directly as they are (as stresses) defined in an infinitesimal small geometric point. Most experimental methods measure displacements between points, which are calculated to strain (in this case an average value over the measured region), and later to stresses (using the constitutive equations of the materials concerned). With few exceptions (e.g., 3-D photoelasticity and Moire fringe techniques), all methods can be applied to either a prototype or a laboratory model of a structure. Again with the exception of 3-D photoelasticity, all methods are suitable for evaluating stresses at the free surfaces of structures only. In some methods, measuring devices are applied to the surface (e.g., extensometers, electrical strain gauges); in some the surfaces are applied with strain sensitive coatings (e.g., brittle or photoelastic coatings), while in others the displacements are registered directly with photographic or laser techniques (e.g., Moire, holography, interferometry). In biomechanics (hard-tissue) analysis, there are only two techniques frequently applied: strain gauges and photoelasticity.

1.7.1.1.1. Electrical Strain Gauge

Electrical strain gauges are based on the principle that the resistance of a material changes when stretched. The gauge consists of a small electrical coil that is glued on the surface of the structure, in a certain orientation. The change in voltage

over the coil is directly proportional to the length of the gauge in its specific direction. If a state of uniaxial stress (or uniaxial strain) occurs in the structure and the gauge orientation coincide with that of the stress, the measured strain (ϵ) can be calculated directly to stress (σ), using Young's modulus (E) of the material ($\sigma = E\epsilon$). In general, however, a state of plane stress presides at a structure's free surface. The plane stress state is fully characterized by three independent variables (e.g., the values of two direct stresses and a shear stress or two principal stresses and principal stress orientation). To completely determine all stress variables in this case, use can be made of a strain rosette, which essentially consists of three coils registering strains in three different orientations, Figure 1.46. The three measured values are calculated to principal strain magnitudes and orientation, and subsequently to principal stresses.

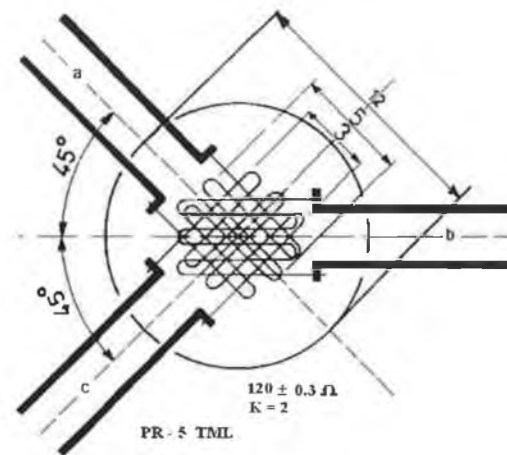


Figure 1.46: A strain rosette with three filaments (a, b, and c). the coils that are the actual measuring devices are shown (measured region. 3 mm). The thick lines represent the connections to the measuring equipment.

Disadvantage of this approach:

Obviously, stresses in structures can be calculated from strains only if the constitutive equations of the material are known. Because the strain gauge averages strain over a certain region (however small that may be), high stress gradients and local stress concentrations can usually not be determined adequately.

Strain gauge has frequently been used for stress analyses of bones, in vivo [127] and in vitro [124]. The limitations of this experimental approach are that to obtain a complete characterization of the stress distribution, many rosettes (100 in this case) have to be applied. Gluing these to the bone surface and connecting them

to the electronic measuring equipment is a time-consuming endeavor, which may take more than half a year' work. Moreover, the equipment needed is expensive, since so much measuring data must be collected automatically. In view of the time periods needed for preparation and experiment, the bone has to be embalmed with formalin, which affects its material properties. Hence, the experimental bone is merely a rough physical model of the original living bone. Examining the influences of load changes on the stresses is easily done, but variation of the material properties or the geometry of the model is impossible short of starting a new experiment. In addition, stresses can be determined on the outside surface of the bone only, whereas no information is obtained from within the material. In contrast, a theoretical technique as the finite element method is more suitable for a complete stress evaluation of irregular streetcars. Nevertheless, experiments are necessary to provide reference data for the development of mathematical models, whereas some problems are more suitable for an experimental approach.

1.7.1.1.2. Photoelastic Analysis Technique

Another technique which has been used frequently in hard-tissue biomechanics is that of photoelastic analysis [179]. This method uses the principle that deformation patterns become visible as fringes in certain plastic when illuminated by a polarized light source. The difference between indexes of refraction are proportional to the maximal shear stresses in the material. A disadvantage of the method (if not applied as a coating) is that it can only be used in a physical models, to be made out of the photoelastic material with given (unchangeable) mechanical properties. A photoelastic model can be 2-D, in which case the fringes are directly visible and are quantified by photographic means, or 3-D, in which case the fringes have to be "frozen" at high temperatures and the model cut to evaluate the results. Contrary to other methods of experimental stress analysis, this technique also provides information inside the material of the model. Nevertheless, it has almost completely been replaced by finite element methods. In other hand, photoelastic methods can be useful to locate stress concentrations and to evaluate the influences of complex boundary conditions that are difficult to model mathematically. An example is in Figure 1.47. The structure shown is simple (2-D) model, representing the general characteristics of an implant, fixated in the medullary canal of a bone with

acrylic cement. The cement layer is represented in the model by layers of photoelastic material. The aluminum structure is U-shaped to take the structural integrity between upper and lower “bone” slabs into account. A transverse load applied and the photograph shows the resulting fringe patterns in the photoelastic material. Each fringe represents one refraction index increase in the maximal shear stress.

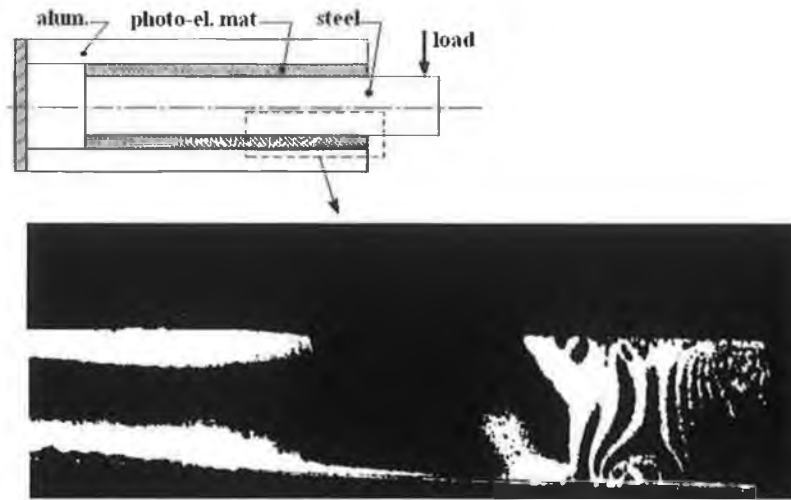


Figure 1.47: Local photoelastic fringes in a general model of an intramedullary fixation system. The fringes represent lines of equal maximal shear stress in the photoelastic material that represents acrylic cement.

1.7.1.2. Closed-Form Theories

The essence of closed-form solutions is that stress and strain values are expressed directly in the parameters describing the structural aspects. Examples of closed-form theories that are frequently applied in biomechanics are linear-elastic bar theory, beam theory, and torsion shaft theory. All three are valid for slender, prismatic bodies whose length is much larger than the thickness, made out of linear-elastic, isotropic, and homogeneous materials, loaded in axial tension or compression, transverse forces or bending, and torsion, respectively. These theories are available for 2-D and 3-D structures, uniform and variable cross-sections, and straight and curved bodies.

Closed-form solutions are attractive for obtaining rapid, approximative solutions for certain problems. They often give a direct insight into relations between essential structural parameters and stress behavior. Their application is cheap and rapidly leads to results, and they are therefore often applied to obtain first-order reference solutions for more advanced experimental and numerical analysis. Many of

the closed-form theories traditionally applied, however, in particular those that are mathematically complex, have become obscure in the recent past because of much greater potential of finite element analysis.

1.7.1.2.1. Bar Theory

The essential feature of bar theory is that a plane cross section remains plane after the load is applied and parallel to the plane as it was before deformation. As a consequence, the stress state is Uniaxial, uniformly distributed over a cross section and throughout the bar. From these two equations, $\sigma = F/A$ and $\epsilon = \sigma/E$, it follows immediately that $\epsilon = F/EA$. The entity EA thus governs the deformation of the bar and is called the axial rigidity, a structural parameter combining material and geometrical properties. In order for the bar cross sections to deform parallel to their original shape, the force must apply in the center of gravity of the section. Close to the point of force application, the stress distribution is distributed by end effects (Figure 1.48, left side): some length is needed for the stress distribution to become uniform.

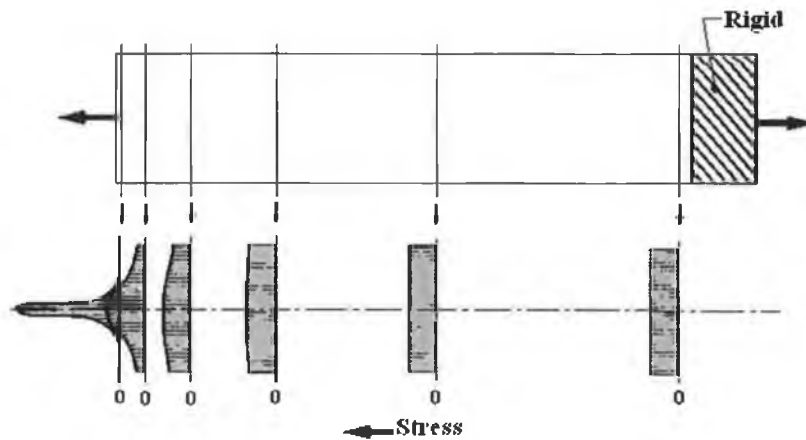


Figure 1.48: The force that loads the bar on a small area (left) engenders end effects in the bar: the stress distribution in the bar cross sections (shown below) becomes uniform only after a certain length. the Rigid block on the right side transmits a uniform stress distribution immediately. Due to requirements of equilibrium, the average stress must be the same in all sections ($\sigma_{av} = F/A$).

1.7.1.2.2. Compound-Bar Theory

Assume a bar as shown in Figure 1.49a, a combination of two bars with different material properties, loaded in tension. End effects are eliminated by a rigid blocks at the ends. In compound-bar theory, it is assumed that the cross sections of the bar as a whole remain plane and parallel, a condition imposed here through the

rigid blocks. This condition implies that the strain (ϵ) is uniformly distributed over a cross section. Therefore, the stress by necessity is not. In material 1, by applying the constitutive equation: $\sigma_1 = E_1 \cdot \epsilon$, and in material 2: $\sigma_2 = E_2 \cdot \epsilon$; since E_1 and E_2 differ, σ_1 and σ_2 cannot be equal either (Figure 1.49b). As it is known, the total internal force in a cross section must be F , but how larger are the internal forces in each material in each individual bar (Figure 1.49c)? obviously $F_1 = A_1 \cdot \sigma_1$ and $F_2 = A_2 \cdot \sigma_2$. By assuming that the load (F), the material properties (E_1 and E_2), and the geometry (A_1 and A_2) of this structure are given. To evaluate the stresses (σ_1 and σ_2) the five equations should be considered:

$$\text{Equilibrium: } F_1 + F_2 = F \quad (1)$$

$$\text{Constitutive eq.: } \sigma_1 = E_1 \cdot \epsilon \quad (2)$$

$$\text{And } \sigma_2 = E_2 \cdot \epsilon \quad (3)$$

$$\text{Bar theory: } F_1 = A_1 \cdot \sigma_1 \quad (4)$$

$$\text{and } F_2 = A_2 \cdot \sigma_2 \quad (5)$$

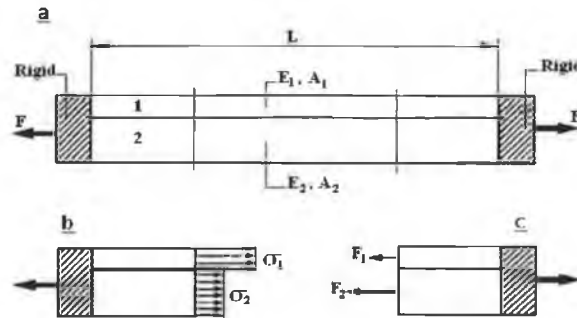


Figure 1.49: (a) A compound bar loaded in tension. the strain in the bar is uniform owing to the rigid blocks on the sides. (b) Due to differences in cross-sectional areas (A_1 and A_2) and Young's moduli (E_1 and E_2) of the individual bars, the stresses differ. Evidently, (c) each bar carries a part of the load.

Hence, the five unknowns (F_1 , F_2 , σ_1 , σ_2 , and ϵ) can be evaluated from Equations 2, 4, 3 and 5:

$$F_1 = A_1 \cdot E_1 \cdot \epsilon \quad \text{and} \quad F_2 = A_2 \cdot E_2 \cdot \epsilon$$

Hence ,

$$\frac{F_1}{F_2} = \frac{A_1}{A_2} \cdot \frac{E_1}{E_2}$$

Combining this with Equation 1, it follows:

$$F_1 = \frac{A_1 : E_1}{A_1 : E_1 + A_2 : E_2} : F$$

$$F_2 = \frac{A_2 : E_2}{A_1 : E_1 + A_2 : E_2} : F$$

and applying Equation 4 and 5 again,

$$\hat{U}_1 = \frac{E_1}{A_1 : E_1 + A_2 : E_2} : F \quad \hat{U}_2 = \frac{E_2}{A_1 : E_1 + A_2 : E_2} : F$$

Apparently, the internal load in each individual bar depends on the ratio between its own axial rigidity and the axial rigidity of the compound bar. This means that when bar 1 is flexible and bar 2 is stiff ($E_1.A_1 \ll E_2.A_2$), most of the load will be carried by bar 2, and vice versa. This is a prove that explain why most of the load carried by the artificial hip joint.

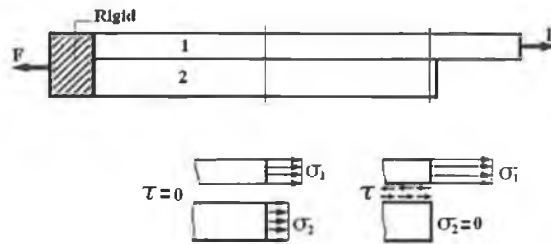


Figure 1.50: A compound bar as in Figure 1.49, but this time the load applies to Bar 1, as a consequence of which load transmission takes place through shear stresses (τ) from Bar 1 to Bar 2. This "end effect" (shear lag) vanishes after a certain length, and from there on the compound bar behaves in accordance with compound bar theory.

It can be proven, qualitatively, that there is no shear stress at the connection between the two bars in the above case. Hence, whether they are connected or not is irrelevant. This situation changes when only one of the bars is loaded at the end, Figure 1.50. Then an end effect occurs, which is a result of load transmission from bar 1 to bar 2. At the right-hand side, all loads are applied to bar 1. Then gradually it is transferred to bar 2 by shear stresses at the connection, the interface, between the two bars. After a specific length the end effect vanishes and the internal loads in the two bars are divided as calculated above. In other words, from there on the structure again acts according to compound bar theory. The consequences of this load transfer mechanism for the internal loads in the two bars separately and the shear stresses at the interface are shown schematically in Figure 1.51. The length of the load-transmission region depends on the structural properties of both bars.

Lets now assume that the forces are applied to each bar separately, Figure 1.52a. In that case the end effects occur on each side. When the fixation length (L) is described, the load transmission regions will eventually meet. From a certain length, Figure 1.52b, the interface shear stress does not vanish anymore between the ends,

but has a more or less uniform value over the full fixation length. In that case, the shear stress approximately equals the force divided by the fixation area ($\tau = F/d.l$, where d is the thickness of the bars). What is to be learned from this example is that one has to be careful with the notation that stress “is force divided by area”. This is only true on a local basis. It is not universally so that when “the area is enlarged the stress decreases”. Enlarging the fixation length of the bars in Figure 1.52a has no effect on the magnitude of the shear stresses; the load transmission regions only separate further in that case.

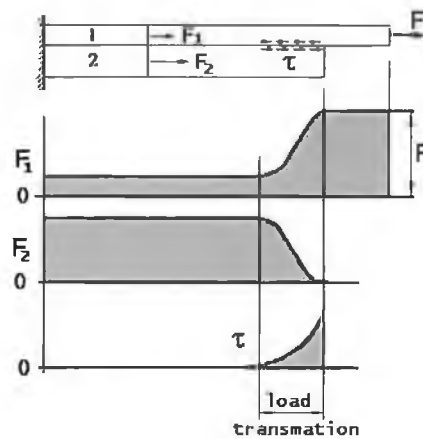


Figure 1.51: Internal load distribution in the compound bar of Figure 1.50. Internal forces in the separate bars (F_1 and F_2) and the interface shear stress are shown along the length. The load transmission phenomenon (shear lag) is evident.

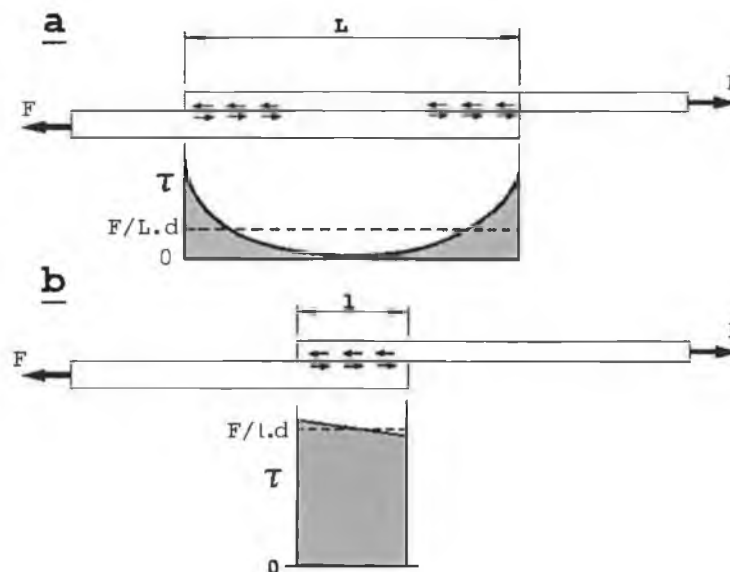


Figure 1.52: A compound bar as in Figure 1.50 and 1.51, but this time the loads apply to each bar separately on either side. load transmission (as in Figure 1.51) occurs (a) on each side and vanishes toward the middle region of the fixation, as witnessed by the shear stress distribution. (b) If the fixation length decrease, the load transmission regions meet and the shear stress becomes more or less uniform. In both cases the average shear stress equals force divided by area ($F/L.d$ and $F/l.d$, respectively). However, elongating the fixation in the first example (a) only serves to separate the load transmission regions further, whereas the peak stresses will not decrease.

1.7.1.2.3. Beam Theory

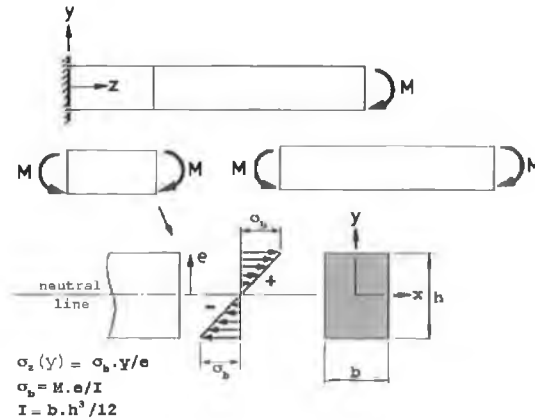


Figure 1.53: A cantilever beam loaded in pure bending. the stress distribution in a cross section is nonuniform, but linear. Stresses are zero in the neutral line. The bending resistance of the beam depends on the second moment of inertia (I), which depends on the cross-section geometry.

A beam is a slender, prismatic body loaded in pure bending or bending by transverse forces. The essential feature of beam theory is that plane cross sections remain plane (but not parallel) after the load is applied. As in the bar theory, the stress state is uniaxial, but the stresses are not uniformly distributed over a cross section. Consider the case of pure bending by a moment M , Figure 1.53. Equilibrium conditions dictate that the only nonzero internal load in an arbitrary cross section is a bending moment (M). Thus, the stress distribution in the cross section is such as to have a zero axial force and a nonzero bending moment as resultants. Furthermore, the stress distribution must be linear because the strain distribution is linear in view of the fact that plane cross section sections remain plane after deformation. These requirements can only be fulfilled by a stress distribution as shown in Figure 1.53. The stress is zero in one point. The collection of these points in all cross sections of the beam is called the natural line. The stresses are negative (compression) on one side of this line and positive (tension) on the other. It can be shown that the stress value at a given point with distance y from the neutral line:

$$\sigma = M \cdot y / I$$

in which I is the static (or second) moment of inertia (SMI) of the cross section in the plane considered. I depends on geometrical parameters only. In the case of a rectangular cross section, as in the example of Figure 1.53:

$$I = b \cdot h^3 / 12$$

The maximal stress value in the section (in absolute value equal on either side because the section is symmetric) is often called the bending stress (σ_b). obviously,

$$\sigma_b = M \cdot e / I$$

in which e is the maximal value of y (in Figure 1.53 $e = h / 2$).

The SMI plays an important role in bending of beams, comparable to that of the cross-sectional area in axial loading. The angular deflection ϕ of cross section after load application in bending equals:

$$\phi = M / E I$$

where E is the Young's modulus of the material. Thus, the deflection is governed by the value EI , a structural parameter called the flexural rigidity of the beam. It plays a role in beam theory and compound beam theory comparable to that of the axial rigidity (EA) in bar theory.

If a beam is loaded by a transverse force, Figure 1.54, the nonzero internal loads in a cross section are a bending moment (M) and a transverse force. The bending moment in this case is not distributed uniformly throughout the beam, but depends on the distance to the force line of application: $M = F l$. the internal transverse force at all sections equals the external force F . the internal bending moment M represents an axial stress distribution completely equal to that discussed previously for the case of pure bending. The internal transverse force represents a shear stress distribution that is parabolic.

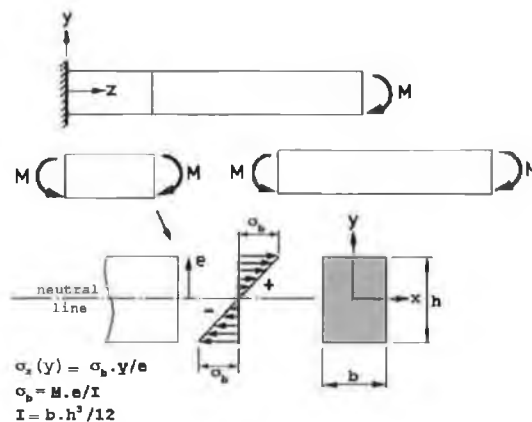


Figure 1.53: A cantilever beam loaded in pure bending. the stress distribution in a cross section is nonuniform, but linear. Stresses are zero in the neutral line. The bending resistance of the beam depends on the second moment of inertia (I), which depends on the cross-section geometry.

1.7.1.2.4. Torsion of Circular Shafts

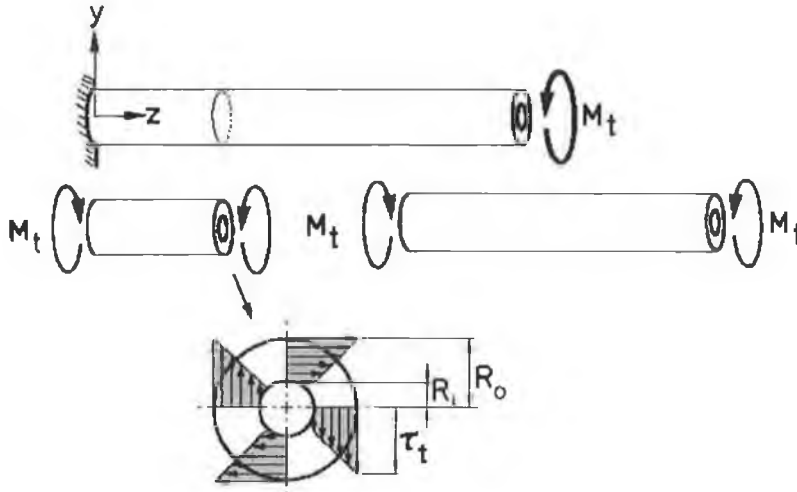


Figure 1.55: A circular, hollow shaft loaded in torsion. In each cross section works a torsional moment which is the resultant of a shear stress distribution in the plane of the section. The magnitude of the stress is proportional to the distance to the central axis.

It was assumed a straight long and slender shaft of uniform axisymmetric (circular) cross section, loaded in torsion and made out of a linear elastic, isotropic, and homogeneous material, Figure 1.55. In simple torsion theory it is assumed, again, that plane cross sections remain plane after application of the load. The torque (M_t) results in an angular twisting of the shaft around the longitudinal axis. The only internal load in the cross sections, uniformly distributed along the shaft, is the moment M_t , which represents a shear stress distribution in the plane of the section; all other stress components in the cross section are zero. The shear stress increases from zero at the center to maximal at the periphery is calculated from:

$$\tau = M_t \cdot r / I_p$$

in which r is the radius to the point concerned, and I_p is the polar moment of inertia.

In general $I_p = I_{\max} + I_{\min}$, hence for a massive circular cross section:

$$I_p = \frac{\pi}{2} R^4$$

and for a hollow tube,

$$I_p = \frac{\pi}{2} (R_o^4 - R_i^4)$$

where R_o is the outer and R_i is the inner radius. Obviously, the maximal shear stress in a cross section is:

$$\tau_t = \frac{M_t \cdot R_o}{I_p}$$

If θ is denoted as the angular twist per unit length of the shaft, it can be shown that:

$$\theta = \frac{M_t}{G \cdot I_p}$$

in which G is a material parameter called the “shear modulus”, to be calculated from Young’s modulus and Poisson’s ratio according to $G = E / 2 \cdot (1 + \nu)$. In analogy to beam and bar theory, the value GI_p , which govern the angular twist, is called the “torsional rigidity” of the shaft. It is evident from the formulas for I_p that material on the periphery of the section contributes most to the structural rigidity, comparable to bending. Hollow shaft is able to produce significantly more torsional rigidity than a massive one if the amounts of material (the cross-sectional areas) are equal. It must be remarked, however, that when the integrity of the cross section is disturbed, for instance, by holes or cracks, so that it is no longer closed, the torsional rigidity reduces dramatically.

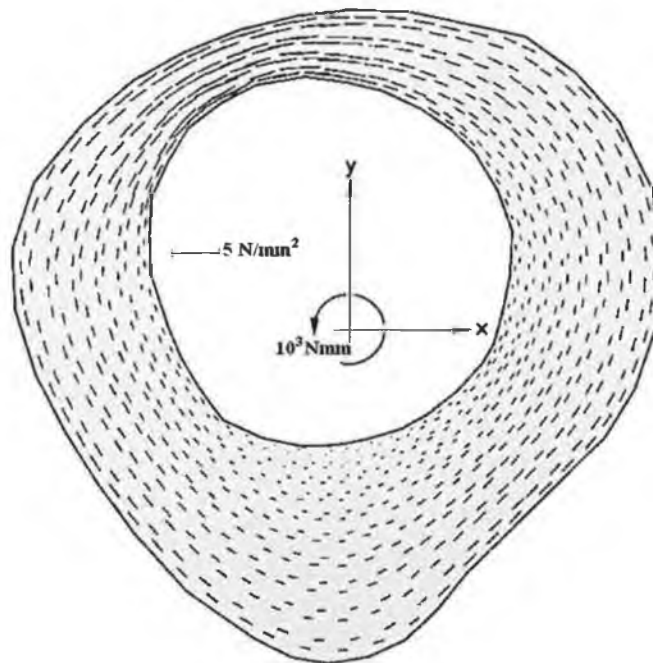


Figure 1.56: Shear stress distribution of a (noncircular) section of a femur loaded by torsional moment, calculated with Saint-Venant's warping theory, using numerical methods. The orientations and lengths of the line pieces represent directions and magnitudes of the stresses. Evidently, the distribution differs from that in Figure 1.55; maximal stresses occur specifically there where the cortical shell is narrow [124].

It is always tempting to use simple closed-form solutions for structures more

complex than the ones they were intended for. In other words, to simplify a model to such an extent that a simple theory can be applied. Although this is not bad in principle and, depending on the objectives, may even represent good engineering practice, it is obvious that the consequences of the simplifying assumptions for the validity of the model should be well understood. Simple torsion theory in particular is rather unforgiving where its underlying assumptions are concerned. Shafts that are not circular in cross section do not yield to the theory, but can be analyzed with Saint-Venant's warping theory [217], which is many times more complex. An example of a shear stress distribution in a femoral cross section loaded by torsion, determined with this theory, is shown in Figure 1.56. For the solution, a numerical process was used. It is evident from these results that although the shape of the section does not deviated dramatically from circular, the shear stresses are not just proportional to the radius. A more precise characterization is that they depend on the width of the cortical shell, being maximal where the section is narrow.

1.7.1.2.5. Combined Loading of Slender Bodies

Loading of slender bodies (as bars and beam) by axial forces, transverse forces, and bending moments results in axial direct stresses, normal to the cross sections. Although transverse forces generate shear stresses as well, the axial direct stresses are usually the most significant ones where chances for failure are concerned. If these loading cases occur in combination, then the stresses in the structure are found by superimposing the stresses as they would result from each loading case separately. This is an important principle in stress analysis, valid for structures in general as long they behave linear elastic.

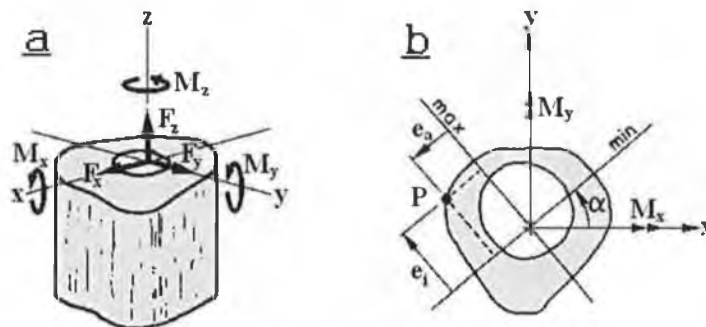


Figure 1.57: (a) 3-D internal loads in a cross section of a femoral diaphysis. The axial force and bending moment produce axial direct stresses in the cross section. (b) The orientation of the bending moments with respect to the principal inertia axes are shown. The axial direct stress in an arbitrarily chosen point P can be calculated by superimposing the separate contributions of the three loads.

Assume a femur as shown in Figure 1.8, loaded by a force on the head and cut (freed) at a particular cross section. Using the principles described previously, the internal (3-D) loading configuration in that section is determined. Generally, it consists of three moments (two bending moments and a torque), an axial force and two transverse forces, Figure 1.57a. Only the bending moments and the axial force produce axial direct stresses, in which we are interested. We assume the femoral shaft to behave as a linear elastic, isotropic, and homogeneous 3-D beam. In other words, we treat the cross section as if it were a part of a bar/beam as we have discussed previously, the only difference being that the cross sectional shape is irregular, Figure 1.57b. To apply the formulas of bar/beam theory, we have to evaluate:

- a) The cross sectional area (A).
- b) The center of gravity location.
- c) The principal inertia axes' orientations (α) with respect to the global (x-y) coordinate system.
- d) The maximal and minimal SMI values (I_{\max} and I_{\min}).

The axial direct stresses (σ_z) are then calculated by superimposing the individual contributions of the axial force and two bending moments. Assume an arbitrary point P in the section, Figure 1.57b). The stress in that point resulting from the axial force (in fact in the whole section, since the stresses as resulting from this force are uniformly distributed) is:

$$\sigma_z = - Fz / A \quad (\text{compression is negative})$$

To calculate the stresses resulting from the bending moments M_x and M_y , these loads must be decomposed in components around the principal inertia axes:

$$M_{\max} = M_y \cos \alpha - M_x \sin \alpha$$

$$M_{\min} = M_y \sin \alpha + M_x \cos \alpha$$

For the contribution to the stress at point P we find:

$$\sigma_z = \frac{M_{\max} \cdot e_a}{I_{\max}} + \frac{M_{\min} \cdot e_i}{I_{\min}}$$

Superimposing the contributions of the axial force and the bending moments gives:

$$\sigma_z = -\frac{F_z}{A} + \frac{e_a}{I_{\max}}(M_y \cos \alpha - M_x \sin \alpha) + \frac{e_i}{I_{\min}}(M_y \sin \alpha + M_x \cos \alpha)$$

Since all loads (F_z , M_x , M_y) and structural parameters (A , I_{\max} , I_{\min} , α) are known, σ_z can be calculated for all points in the section, substituting the appropriate values of e_a and e_i .

Till here, it has been tried to briefly illustrate 3-D beam theory and the execution of theoretical analysis in general:

- Identify the structure (the bone, freed from its environment) and assess the objectives (evaluate axial direct stresses in cross sections to judge the applicability of 3-D beam theory).
- Develop the model (free body diagram, cutting, assumptions of constitutive equations, bar/beam theory, principle of superposition), including the evaluation of required data (area, moments of inertia, loading characteristics).
- Process the analysis (combine the equations to a mathematical solution, calculate stresses in all relevant points).
- Result validation (by comparing with experimental data) and interpretation (yes, the femoral diaphysis does by a certain degree of approximation behave as a 3-D linear elastic, isotropic, and homogeneous beam).

Two final remarks have to be made. First of all, the validation of a model by experimental data is not always necessary [69]. Secondly, if the result are not acceptable, model refinement will have to be carried out by restarting the modeling cycle [69].

1.7.1.3. Finite Element Methods

The use of closed-form theories is limited to structures of relatively simple geometrical and material properties. Only for a very few types of regular structure (e.g., bars, beams, plates, and shells) do these theories yield relatively simple formulas which can be readily solved by hand. The finite element method (FEM) is

essentially a computer method that can be used in principle to calculate stresses in load carrying structures of unlimited complexity, although there are limitations of a practical nature. Nevertheless, the method is preeminently suited for stress analyses of irregular components as bone-prosthesis structures and is meeting increasing interest in biomechanics research [81, 91, 204].

A FEM model describes the four relevant aspects of a structure (loading conditions, geometry, material properties, and boundary/interface conditions) in discrete, numerical form. The central issue is the geometrical description by elements: the structure (or rather, the model) is mathematically divided into a set of connected blocks, or elements, which can have various regular shapes, Figure 1.58. At their corners, faces, or edges, these elements have nodal points by which they are considered to be attached to each other. The type of element used depends on whether a model is 2-D or 3-D and on specific requirements of accuracy.

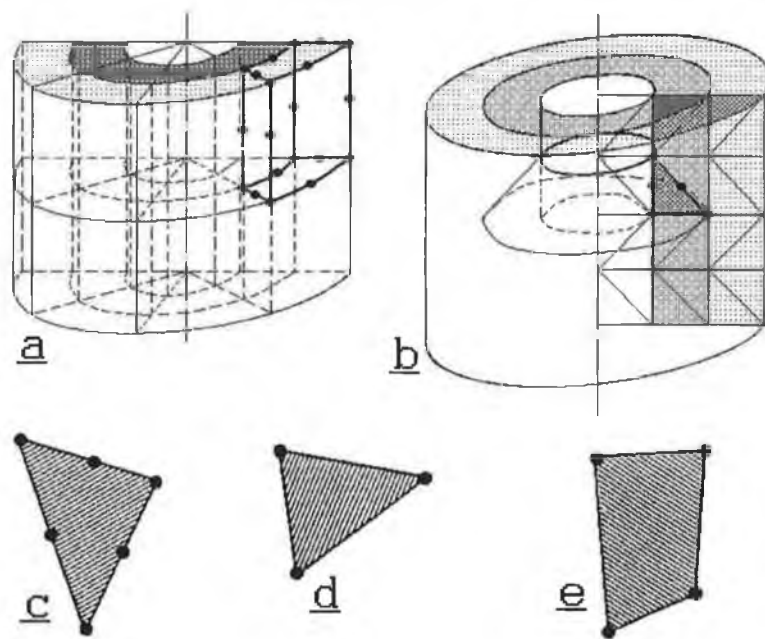


Figure 1.58: Examples of element types used in finite element analysis. (a) 3-D; (b) quasi-3-D; and (c, d, e) 2-D elements. Nodal points are indicated [91].

A few element shapes are shown in Figure 1.58: a 3-D (20-node) hexahedron element (a), suitable for arbitrary 3-D geometries (the elements can be “molded” in any shape, provided they are not overstretched or deteriorated, in one direction) a (quasi) 3-D (6-node) ring element (b) for axisymmetric structures only, two 2-D triangular (c and d), and a 2-D quadrilateral element (e).

After the problem has been discretized, the governing equations for each element are calculated and then assembled to give the system equations. Thus, once the general format of the equations of an element type is derived, the calculation of the equations for each occurrence of that element in the body is straightforward; it is simply a question of substituting the nodal coordinates, material properties and loading conditions of the element into the general format. The individual element equations are assembled to obtain the system equations, which describe the behavior of the body as a whole. These generally take the form:

$$[k] \{U\} = \{F\} \quad (6)$$

where $[k]$ is a square matrix, known as the stiffness matrix; $\{U\}$ is the vector of (unknown) nodal displacements; and $\{F\}$ is the vector of applied nodal forces.

Equation (6) is directly comparable to the equilibrium or load-displacement relationship for a simple one-dimensional spring, where F produces a deflection U in a spring of stiffness k . To find the displacement developed by a given force, the relationship is inverted. The same approach applies to the finite element method; however, before Equation (6) can be inverted and solved for $\{U\}$, some form of boundary condition must be applied. In stress problems, this means that the body must be constrained to prevent it from performing unlimited rigid body motion. The solution of Equation (6) is not trivial in practice because the number of equations involved tends to be very large. It is not unreasonable to have 50 000 equations, and consequently $[k]$ cannot be simply inverted. Fortunately, however, $[k]$ is banded, and techniques have been developed to store and solve the equations efficiently. After solving for the unknown nodal values, it is then simple to use the displacements to find the strains and then the element stresses [82].

Figure 1.59 shows a finite element model of a finger joint prosthesis, of which the material stem is fixated within the medullary canal with a plastic plug. The model is axisymmetric and ring elements are used, Figure 1.58b. The element mesh is usually generated automatically by a computer program, called a "FEM Preprocessor", based on varying amounts of data to be entered by the analyst. This program organizes the mesh numbering, generates a node-point location file (the element numbers and accessory

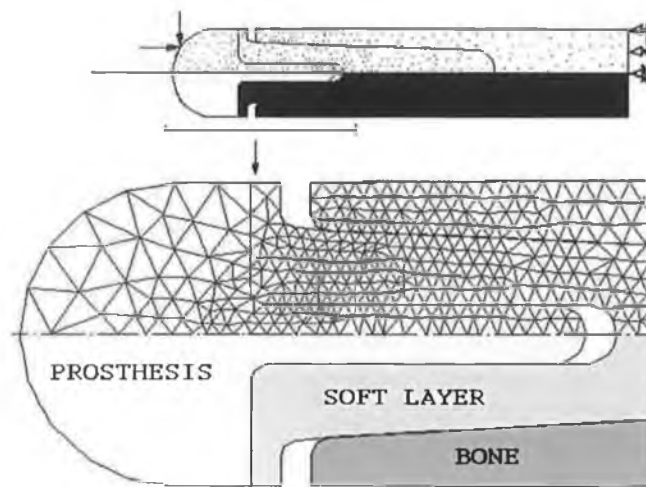


Figure 1.59: *Element mesh in a model of a finger joint fixation system. The elements are axisymmetric, hence only a longitudinal section is shown. The loading is nonaxisymmetric [121].*

modal point numbers), and a nodal-point coordinate file (the nodal-point numbers and their coordinates in an external reference system). In these two files the element mesh is completely characterized. The FEM program further requires an element characteristics file (for each element, its material properties, such as Young's modulus and Poisson's ratio in a linear elastic, isotropic problem, and in the case of a 2-D model, its thickness), a loading file, and a displacement file. The loading file contains the numbers of the nodal points at which forces are introduced to the structure, the direction of these forces, and their magnitudes. The displacement file characterizes the kinematic boundary conditions. The model in Figure 1.59, for instance, is considered to be connected to the environment (supported, fixed) on the right-hand side, and the displacements of the nodal points concerned are prescribed as zero (suppressed). A nodal-point coupling file handles the characterization of the connections between nodes of different materials (regions or substructures). The stem in Figure 1.59, for example, is able to slide within the plug, for which the nodal points at the interface are disconnected in that direction (but not in transverse direction).

Based on this information, the FEM program calculates the displacements of all nodal points (which characterize the deformation of the loaded structure) and the stresses in all nodes or in the element centroids. The solution is obtained numerically through a set of linear equations, equal to the amount of degrees of freedom in the model: the number of nodal points times the number of displacement components in each node (two in a 2-D, three in a 3-D model). The computer time and memory

space required for a problem progressively depends on the number of degree of freedom. A time-efficient element mesh is of crucial importance, since computer capacity is the only practical limit to the level of model complexity feasible. The nodal point displacements and stresses calculated by the FEM program are presented in tabular printed form and in graphs of different kinds. These graphs are usually prepared by "FEM postprocessors"; computer programs that rearrange or adapt the output data according to the uses' specifications.

The most difficult steps in FEM analyses are the creation of the model and the interpretation of results in the light of the model limitation. Accuracy is mainly a question of adequate (local) mesh density. Convergence checks (repeating the calculations with a finer mesh) are always feasible, but sometimes expensive. Judging the validity of results requires a realistic assessment of model limitations. Often some results are more realistic than others, depending on how sensitive a certain stress value is to certain assumption. For instance, it has been shown [127] that when the interfaces in models of the femoral hip joint fixation structure are assumed rigidly bonded (and in reality they are loose) the most significant stem and bone stress results are still realistic, but the cement layer and interface stresses represent reality only in a rough relative sense. Sometimes it is intuitively obvious how a certain assumption affects a certain result. Sometimes this influence can be estimated from existing information or from simple analytical considerations. Often, however, this influence is simply unknown and should be established through appropriate research. This can be done by mean of parametric analysis, for instance, comparing 2-D with 3-D models, isotropic assumptions with anisotropic assumptions, and so on. Another possibility is the use of verifying experiments on laboratory models, which may be simulated in FEM models to compare theoretical with experimental results.

Eventually, the stress results will be judged as to what they actually indicate. This is often a problem when the objective of an analysis entails the prevention of possible failure in connection with structural design. It was, for instance, established in several analyses that cement failure in femoral hip joint prostheses is most likely to occur either on the proximal side or at the distal tip [3], where the cement stresses reach maximal values. It has also been established that proximal cement stresses increases on using a more flexible titanium alloy instead of a cobalt-chrome alloy for

the stem, while the distal cement stresses decrease in that case [77, 216]. These facts can be established with structural analyses, however, the decision on what to use depends not only on the outcome of the analysis, but also on which failure mechanism one believes is the most destructive. Although there is more to this question of stem material than simply stated here, this is one example of how different analyses of the same structure can sometimes result in opposite recommendations. Another example concerns the interpretation of stresses in bone, where different authors may reach different conclusions based on comparable analyses, since so little is known about the biological reactions of bone to various kind of stresses [69].

Possibilities of the application of the FEM in biomechanics entail all potential uses of structural analysis, i.e., all cases where a quantitative assessment of stress is required, whether for the investigation of basic mechanisms or for the evaluation of designs and techniques. Its use is not limited to bone, but can be applied to soft tissues as well [69, 204] although poor knowledge about collagenous tissue properties hamper its application as yet. As a numerical computer solution method, the FEM is also applied in biomechanics for problems of heat and mass transfer [127, 261].

1.8. Introduction to the Present work

Since both loosening and fracture of the stem are related to mechanical stresses in the joint, stress analysis may help to reduce the surgical use of mechanically unsound implant constructions, and may also help to improve the design of existing prosthesis. Problems, however, do arise and a hip replacement is not expected to function indefinitely. Problems become more acute as the operation is carried out on younger and more active patients with the requirement for longer service-life under higher loads. The complications that arise most often involve loosening of the femoral stem, although clinical complications such as infection are also reported. Loosening of the prosthesis, although in itself a mechanical phenomenon is caused, at least in part, by biological factors such as soft tissue growth at the bone cement interface or changes in the bone structure of the femur as a result of changed stress patterns. The salient point then, is that failure by loosening

involves an intimate mix of biological and mechanical processes, and full understanding of it would demand a complex bio-mechanical model. Figure 1.60 is an attempt to formalize such a model schematically. This scheme separates the mechanical parameters into two groups. In the first group are the design parameters, which are wholly determined, in principle, by the implant designer. In the second group are the patient parameters, which are largely determined by the activity level and pathology of the individual. The design parameters, combined with the initial value of the patient parameters determine the potential of a joint design to withstand primary mechanical failure which is termed "primary stability". If the deformations within the structure are critical (loosening), or, the stresses within the material or on the interfaces are critical (fracture), then failure will occur. It is difficult to quantify exactly when a failure occurs because a mechanical failure, such as cement fracture, does not necessarily cause a clinical failure and the need for a revision operation. If the stress is not critical then it feeds back to alter the control parameters via biological processes, as depicted in the scheme. these biological processes can deteriorate the structure and as a consequence the selected design parameters are no longer optimal. The extent to which they can remain optimal determines the "secondary stability" of the implant system, which is defined as the potential to withstand rapid mechanical deterioration after mechanical failure or biological adaptations have occurred.

A number of approaches has been used in predicting stresses and strain patterns in biomechanical field including experimental techniques such as strain gauging and photoelastic analysis, and numerical procedures such as the finite element method (FEM) to obtain comprehensive information on the state of stress and strain in the intact and treated femur. The empirical approach of medicine has proved to be unsuitable for improving of biomechanical devices and mathematical models have been developed to simulate the features of real systems and so give us the capacity to predict how they would behave under changed circumstances [70]. The versatile features of FEM analysis when compared to experimental methods in cases that a structure is too complicated for closed-form theories are its potential for evaluating stresses/strains throughout the structure, in and between all materials concerned, and for parametric analysis. Material properties, and loading and

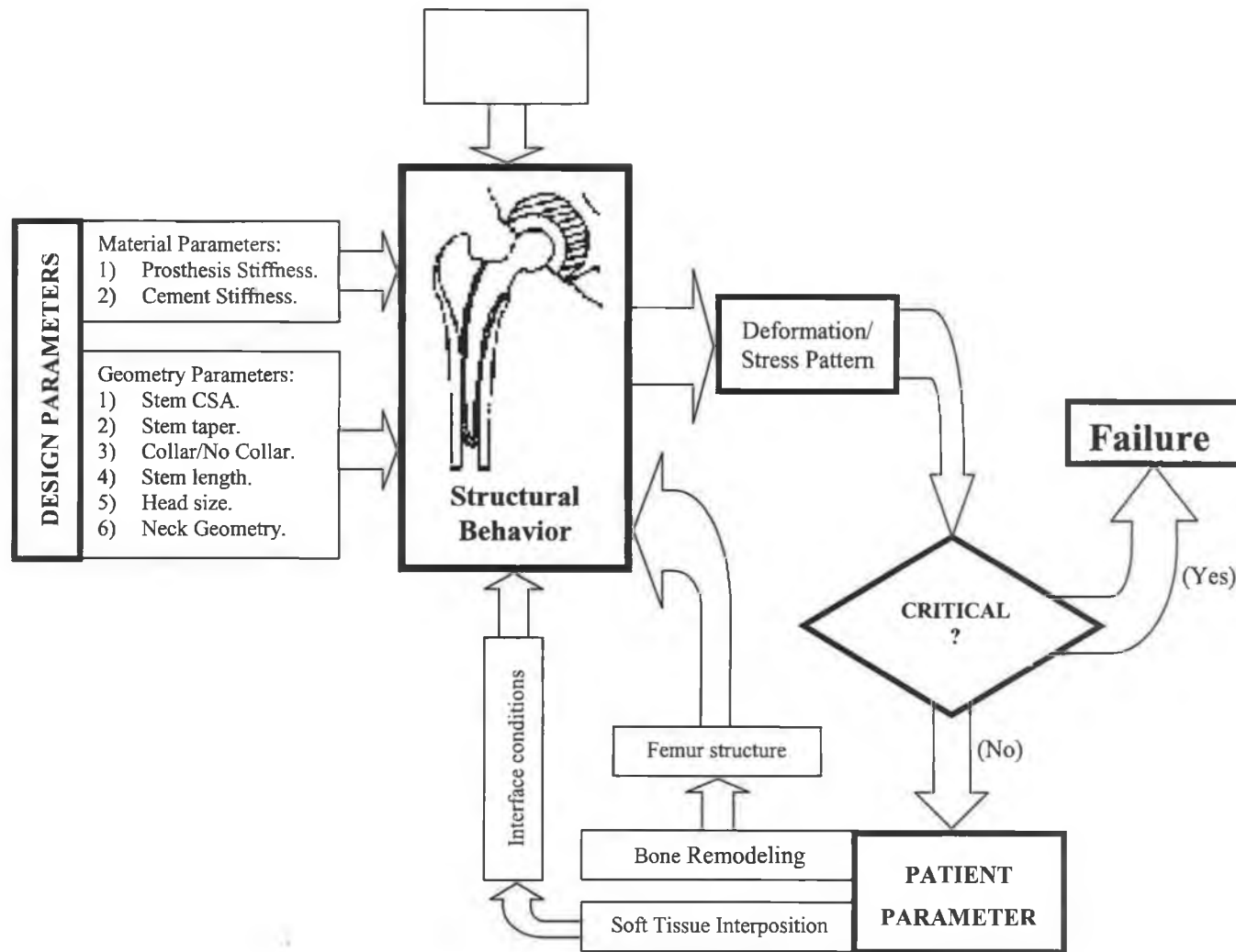


Figure 1.60: A schematic model of the structural behaviour of the artificial hip joint showing three processes: (i) structure behaviour, (ii) bone remodeling, (iii) soft tissue formation.

boundary conditions can readily be varied in order to investigate their influences. For this reason, The finite element method has become a particularly useful tool in analyzing the stresses in structures of complex shapes, loading and material behavior.

Faced with the task of understanding a complex system, it is often useful to extract its most essential features and use them to create a simplified representation, or model of the system. A model allows one to observe more closely the behaviour of the system and to make predictions regarding its performance under altered input conditions and different system parameters. Finite element models are numerical mathematical models – numerical because they rely on computers to find approximate solutions to large sets of equations. Finite element analysis has provided many predictions relevant to orthopaedics. In some cases, these predictions have been compared with physical models to help establish their validity.

1.9. Objectives of the Present Work

This study has been divided into two parts according to the loading type. In this regard the stress field in the artificial hip components (prostheses, cement mantle, and bone) is analyzed statically and dynamically to investigate the effect of the loading pattern on the stress-based criteria to assess implant longevity.

1.9.1. First Part: Static Analysis

In this study all the results were conducted by assuming the peak loads during the normal gait at a particular time (static loads). This project aims to study the effects of a set of variables within which an optimal prosthesis design can be made by means of finite element analysis. F.E.A. is used to qualify and quantify the stresses and the strains in natural and treated human femur for different cases of implantation. However, since both loosening and fracture of the stem are related to mechanical stresses in the joint, stress analysis may help to reduce the surgical use of mechanically unsound implant constructions, and may also help to improve the design of existing prosthesis. There are a number of distinct phases in this project:

<u>First phase:</u>	Includes identification and generation F.E. models of intact and treated femur.
----------------------------	---

- Second phase:** Deals with the effect of the human loads on the stress distribution in the prosthesis, bone and cement and verification.
- Third phase:** Deals with the effects of prosthesis design and material selection.
- Fourth phase:** The conclusion of the last two phases that will give a relationship between different stress in the implant and cement for any combination.

1.9.2. Second Part: Dynamic Analysis

Although pre-clinical validation procedures have significantly improved in the last few years, some important factors, affecting the biomechanical performance of hip implants, are still very difficult to account for. Using a clever combination of numerical models and experiments *in vivo* it is possible today to replicate the major part of the failure scenario previously observed in the clinical practice. However, many important factors are still very difficult to take into account during these studies. In particular, these aspects related to the patient (skeletal anatomy, bone quality, muscles, level of activity or biological response) or to the surgeon (bone surgery, implant position and fit, joint centre relocation or muscle surgery). Until now, models developed to predict stresses in total hip replacements have been generally poorly validated. This could be because all the pre-clinical simulations were performed statically, that is by selecting the greatest load at a particular time of the activity cycle.

The second part of the study was aimed to take into consideration, in designing total hip replacement, that a major factor relates to patient activity (stamping, jumping, walking, etc) and the effect of impact over the prosthesis head during these activities into the prosthesis performance. This study will consider the prosthesis hip deformation with time in a dynamic load study. The elimination of impact cracking will be considered by studying the effect of using a “damper” trapped between the grooved prosthesis collar and the bone. Material selection of the total hip replacements will be improved by interjecting this factor.

This study will be conducted by constructing three-dimensional finite element model for a femur implanted with a cemented prosthesis with a representative physiological loading condition and solved using LS-DYNA.

There are a number of distinct phases in this project:

- 1) An alternative mesh generation, is required to accommodate the loading conditions to be simulated using LS-DYNA.
- 2) A comparison between static and dynamic loading in designing and pre-clinical testing of artificial hip prosthesis (AHP).
- 3) A new AHP design will be studied, which aims to reduce the impact cracking.

Therefore, the simulation of these cases has been carried out using two commercial FE packages ANSYS and LS-DYNA. The simulation results will be verified with some experimental and theoretical results available in the literature.

Chapter Two

Literature Review

2.1. General View

A structure is a geometric configuration of materials created to withstand loads. Structural structure analyses, are performed to predict stresses occurring within the loaded structure, with the objective to evaluate the adequacy of its design and materials in fulfilling its load-bearing functions. The stress distribution in a structure depends on four, and only four, aspects:

- (i) The magnitude and configuration of the external loads, the loading conditions.
- (ii) The geometry of the structure.
- (iii) The material properties.
- (iv) The physical nature of connections with the environment (boundary conditions) and between different material (interface conditions).

For a structural stress analysis, these aspects must be described, either mathematically (in a theoretical stress analysis) or physically (in an experimental stress analysis). This description is called Structure Modeling [69]. The development of the model is probably the most difficult and crucial step in the analysis. The tools of structure analysis can be listed [69]:

- (i) Experimental methods such as photoelasticity, strain gauging, brittle lacquer coating, holography etc.
- (ii) Closed-form theories such as beam theory (beam-on-elastic foundations, composite beams), torsion theory, thin shell/thick shell theory, buckling theory etc.
- (iii) Numerical methods such as finite element methods.

Each method has its own particular usefulness and all have been used in the analysis of biomechanical devices.

Much experimental stress analysis is reported with respect to the AHJ, for example, McNamara et al.[179], Akay and Aslan [3], Oh and Harris [194], McBeath et al. [174], Crowninshield et al. [60], Jacob and Huggler [132], Huiskes et al. [127], Engelhardt and saha [73]. Their results are analyzed with those of the present work in chapters 4 and 6. Little [159] used strain gauges to determine stresses in a model of the knee joint and he outlines how, with difficulty, 3D stress data can be obtained by selecting suitable resins within which the gauges are implanted. Also, Orr [195] and O'Brien [193] used 3D photoelasticity to investigate stresses in stems at different orientations and with different amounts of calcar support. Among Orr's findings were that rotation into various moves the maximum stress site distally and that maximum stress in valgus-oriented stems are less affected by bone loss. Unlike strain gauging, photoelasticity can give a full view of the stress field and this can be useful for qualitative analysis and for identifying stress concentrations [193]. However, Huiskes [125] outlined some difficulties with physical models, particularly that they are not suitable for parametric design analysis.

Closed-form theories are those in which a direct algebraic link is made relating stress to the properties of the structure. Specifically, the properties of a structure are the constitutive law of its material(s), the boundary conditions (connections to the world outside the structure) and its geometric form. Closed-form theories are only practical when these properties can be expressed in straightforward manner. Gola and Gugliotta [94] derived a solution to the set of equations describing the load distribution at a "coupling zone" between two flexible beams and they applied it to a bone/prosthesis structure. Qualitative stress distributions are then obtained. Huiskes [128] gave a comprehensive analysis of intramedullary systems using such theories where it is clear that their use is intended to give "first order reference solution" and to explore the fundamental features of prosthesis design. In an investigation of the coupling between bone and prosthesis he found that the structure divided into three regions: a distal region, a mid-stem region, and a proximal region each of which can be analyzed separately; the ends using beam-on-elastic foundations theory and the middle using composite beam theory. It was proposed that the middle serves only to separate proximal and distal end-

effects and hence that there is no point in extending stem length beyond some limit. Figure 2.1 shows this concept with respect to shear stresses at the stem/cement interface.

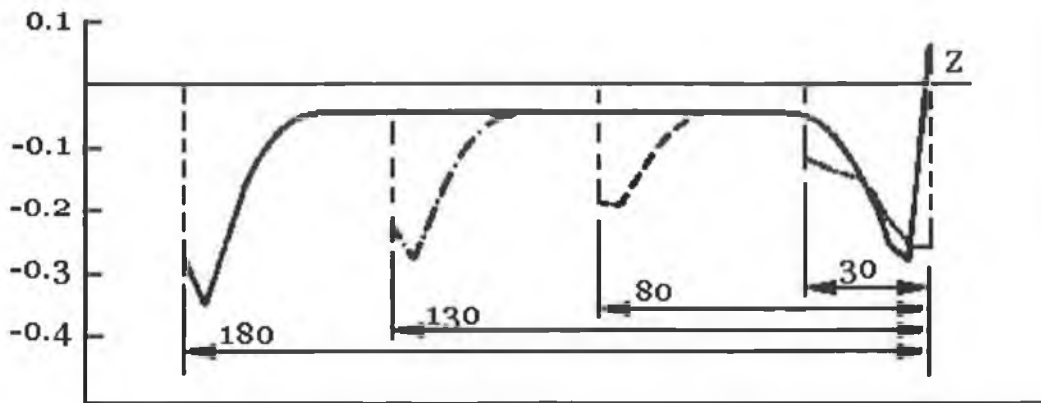


Figure 2.1: Stresses in the cement layer at the cement/bone interface calculated on transverse loading for four stem length [128].

Numerical methods, and particularly the finite element (FE) method, are better suited to the analysis of complex systems. The FE method has been used extensively in orthopedic biomechanics, both for the analysis of specific design and for parametric analysis and as a tool for basic research. A discussion of the theory is presented in chapter 6. By 1983, 2D and axi-symmetric modeling was being superseded by 3D modeling, albeit with limited numbers of elements [121]. Since then, finite element modeling of hip replacement has become commonplace, motivated by the fact that up to 800 000 operations are carried out per year, with several hundred different designs on the market. Table 2.1 details some articles from the literature and it can be seen that FE models have been developed with various purposes in mind and that no model yet envisaged can account for all aspects of the structural behavior. Rohlmann et al. [226] presented the first large 3D model of the hip replacement, calculating stresses in the prosthesis, cement and bone and showing the influence of musculature. Investigating fundamental behavior, Huiskes [128] uses a simple axi-symmetric FE model to illustrate the three structural regions in intramedullary fixation, and shows that prosthesis and cement stresses cannot be reduced simply by increasing stem length.

Table 2.1: Some finite element studies of orthopaedic

No	Author(s)	Year	Focus of study
1	Anriacci et al.	1976	Stem fracture (Effect of Orientation)
2	Svesnsson et al.	1977	Stress analysis of Charnley prosthesis
3	Huiskes	1979	Fundamental aspects
4	Cook et al.	1980	Parametric study (materials) of calcar stresses
5	Hampton et al.	1980	Femoral stem fracture
6	Crowninshield et al.	1980a	Stem cross section (parametric analysis)
7	Crowninshield et al.	1980b	Parametric study (materials, stem length)
8	Sih et al.	1981	Finding cement fracture sites
9	Skinner et al.	1982	Canal plug design
10	Huiskes et al.	1983	Heat conduction/stress analysis
11	Tarr et al.	1983	Parametric study (materials, stem length)
12	Rohlmann et al.	1983	Specific design analysis, loading analysis
13	Lewis et al.	1984	Parametric analysis calcar stresses
14	Fagan and Lee	1986a	Analysis of collar function
15	Fagan and Lee	1986b	Parametric analysis of Exeter design
16	Vichnin and Batterman	1986	Bone fracture
17	Rohlmann et al.	1987	Parametric analysis (materials, stem length)
18	Huiskes and Bocklagen	1989	Numerical optimization of femoral stem
19	Huiskes	1990	Stress transfer patterns with various designs
20	McNamara et al	1992	Prediction of bone adaptation in the ulnar-osteotomized sheep's forelimb using an anatomical model (FE and experimental study)
21	Prendergast and Taylor	1992	Design of intramedullary prostheses to prevent bone loss by using FEA.
22	Verdonschot and Freeman	1993	Pre-clinical testing of hip prosthetic design: a comparison of finite element calculations and laboratory tests.
23	McNamara et al.	1995	Prediction of bone remodeling around hip prosthesis stems based on altered microdamage accumulation in bone tissue
24	Prendergast and Huskies	1996	Microdamage and Osteocyte-Lacuna Strain in Bone: A Microstructural Finite Element Analysis
25	Aky and Aslan	1996	Numerical and experimental stress analysis of a polymeric composite hip joint prosthesis
26	McNamara et al	1997	Relationship between bone-prosthesis bonding and load transfer in total hip reconstruction.
27	Tai-Ming Chu et al.	1997	Finite element stress analysis of the femur with implant utilizing computed tomography
28	Brian Greer	1999	FE modeling and analysis of the proximal femur
29	Chi-Chung Hu et al.	2000	FE analyses for frictional heating in total hip prosthesis
29	El'sheikh et al.	2000	Material selection in the design of the femoral component of cemented total hip replacement.
30	Simões J.A. et al.	2000	Design of a controlled-stiffness composite proximal femoral prosthesis

2.2. The Dilemma of Bone Stress Shielding and Prosthesis Loosening

The natural stress distribution in the femur is significantly altered after total hip arthroplasty (THA). When an implant is introduced, it will carry a portion of the load, causing a reduction of stress in some regions of the remaining bone. This phenomenon is commonly known as stress shielding. In response to the changed mechanical environment the shielded bone will remodel according to Wolf's law, resulting in a loss of bone mass through the biological process called resorption. Resorption can, in turn, cause or contribute to loosening of the prosthesis. The problem is particularly common among younger THA recipients. Beside infection, aseptic loosening is the major post-surgery concern. The bone resorption and fibrous encapsulation associated with aseptic loosening may be caused by:

- a) a bone-implant gap left when inserting the implant [35, 248],
- b) foreign body reactions against debris of polyethylene [52, 283], polymethyl-metacrylate [283, 167], or metal [86, 109, 168],
- c) physiological remodeling [211],
- d) mechanical stress modifications induced by the implant, be it stress shielding [25, 129, 166], or local overloading [122],
- e) a loose implant [34, 249, 267],
- f) mechanical failure of the implant or cement [165], and / or
- g) relative motion across the interface [165].

In general, the stress shielding and prosthesis loosening causative is either as a result of mechanical factors, such as material and design geometry, and/or patient factors such soft tissue growth at the bone cement interface and pathology of the individual.

Because that the mechanical factor is more controllable by either improving the material selected and/or the prosthesis design, this literature survey will be devoted to reveal some researches carried out to overcome this the problem of stress shielding and hence mounted up the prosthesis longevity.

2.3. The Effect of Material Selection on Prosthesis Performance

Further research has described the effect of materials selection on stresses in the various components. It has been shown, for example, A stem of a lower stiffness material (e.g. a titanium alloy compared with a cobalt chrome alloy) will transfer more of the load to the femur proximally, reducing stress shielding, however, this is achieved at the expense of higher load transfer stresses at the cement interfaces with the bone and implant and the risk of cement failure. While the stiffer prostheses generate higher prostheses stresses, lower bulk cement and cement interface stresses [1, 3, 50, 81, 156, 217,227].

To improve the long-term survivability of the femoral component of cemented total hip replacements, the manufacturers of hip systems are constantly assessing new materials for use in the femoral stems and the cement. Although the individual constituents may appear to have satisfactory mechanical properties, it is not until the composite structure of the bone, cement and stem is analyzed that the mechanical properties of the assembly can be determined. Fagan and Lee [81] examined the behavior of the femoral prosthesis when the stem and cement are manufactured from a wide range of different materials. While Prendergast et al. [217] proposed the material selection for the artificial hip structures based on the fatigue strength. Bone loss around femoral hip stems is one of the problems threatening the long-term fixation of uncemented stems. Many believe that this phenomenon is caused by reduced stresses in the bone (stress shielding) [278]. Henn et al. [113] encouraged of using prostheses of low stiffness to reduce the stress shielding. Their results will be discussed in chapter 6.

Huiskes [129] has indicated the importance of material flexibility and its effects on stress shielding and adaptive remodeling of bone. Weinans [277] has applied FEA analysis combined with strain energy density criteria for bone remodeling to evaluate the effects of the material properties of femoral hip components on bone remodeling. The conclusion of these studies is that a more flexible component reduces the change in stress level in bone and consequently bone loss is less. They also showed that cemented fixation, since it combines the stiff stem and more deformable polymer such as polymethylmethacrylate (PMMA), causes less bone resorption and lower interface stresses than noncemented fixation with the same implant material. The effects of stem

stiffness on stress shielding and femoral bone resorption have also been studied experimentally [3, 25, 80, 81, 113, 217]. It was shown that a flexible stem results in more uniform load transfer, less stress shielding, and less bone loss [73, 139, 164]. Recent advances in design and manufacturing technologies of fiber-reinforced composite materials offer strength comparable to that of metals and also more flexibility than metals [61, 244]. The mechanical properties of long-fiber composites are determined by the fibers' orientation and their overall fraction in the composite, and therefore can be varied over a wide range. For instance, carbon fibers embedded in polyetheretherketone (PEEK) or polysulfone, which are biocompatible polymer matrices [287, 279], can have a strength ranging from 70 to 1900 MPa and a stiffness ranging from 10 to 100 GPa [3, 61, 149, 189]. Furthermore, polymer composites have demonstrated biocompatibility, environmental stability, excellent chemical resistance and resistance to repeated sterilization by gamma radiation and steam, and also have good fatigue properties [61, 149, 244]. These advantages have made polymer composites more useful to many orthopaedic implant manufacturers.

Katoozian et al. [104] incorporated in their study material design variables into the optimization of the femoral component of hip prostheses. By assuming that the flexible stem can be used to address the stress shielding and resorption problem, they investigated the use of fiber-reinforced composite material for this purpose. Specifically they employed a numerical optimization procedure to design a fiber-reinforced composite to minimize the potential for remodeling and stress shielding.

Akay and Aslan [3] performed 3D FE stress analysis for an intact and treated femur implanted with a polymeric composite and titanium hip joint replacement for various loading conditions, and then validated by an experimental strain gauge measurements by using a synthetic femurs. The model comprised 2151 elements and 2487 nodes, and meshed with 8-node brick element. They found good agreement between the two methods except in the hoop strain of the femur in the calcar region because of the assumption of the material properties. The stem stresses were lower for the polymeric prosthesis than for the titanium prosthesis. They reported that the maximum stress was in the spigot stem of the titanium prosthesis. And stress generated in the cement was almost

equal for both prostheses although more load was transferred, via cement, to the femur with polymeric prosthesis, and this was interpreted because the load transfer took place over a large area.

The effectiveness of using reinforced fiber composites for the material optimization of hip implants has been demonstrated and general guidelines on some material design aspects of total hip replacement (THR) were proved by Katoozian et al [138], in terms of fiber volume fraction and fiber orientation angles. A modular program was developed to interface the optimization routine with the finite element code. In this study two cases of cemented and non-cemented THR were investigated. In both cases perfectly bonded interfaces were assumed. Two objective functions were defined based on interface failure criteria and bone adaptive remodeling to avoid interface disruption and to reduce the risk of bone loss. The overall results demonstrated the effectiveness of the technique, which can provide meaningful insights into the fiber-reinforced composite material design of orthopaedic implants.

2.4. The Effect of the Prosthesis Geometry on its Performance

The effect of femoral stem design parameters on stresses in the materials and on their interfaces was investigated by Huiskes [128]. Conclusions are listed [121] such as that stem stresses increase in proportion to Young's modulus, and that reducing stem thickness reduces distal cement stresses and increases proximal cement stresses. A thick stem would also reduce the cement layer thickness thus increasing its stress. Hence an optimal proximal cement layer thickness could be expected to exist and Huiskes [128] calculates that a 2 mm thick layer is optimal in a 10 mm diameter idealized bone structure. Brockhurst and Svensson [29] suggested that the prosthesis thickness should be as thick as possible – particularly in the upper half, because in the upper half prosthesis itself carries most of the applied load and to resist fatigue loading. With a higher Young's modulus stem the optimal thickness tends to decrease. Brockhurst and Svensson [29] recommended that the stem of the prosthesis should be as long as possible, because this would result in a reduction in the pressure bearing between the prosthesis and bone and the circumferential stresses in the bone will also be reduced. Also the shear stresses at the

acrylic/bone interface would also be reduced. Crowninshield et al. [58] predicted higher stem stresses for slim stems using a FE model. They and Lewis et al. [156] also predicted that cement stresses are higher proximally and lower distally with a slim stem. Huiskes and Boeklagan [120] set out to optimize the shape of a femoral component so as to minimize cement/bone interface stresses. Using the strain energy density at the cement element integration points along the cement/bone interface as an objective function to be minimized, they find that an optimal femoral component shape features both proximal and distal tapers. Different optimal shapes are predicted for different stem lengths and material Young's moduli. Andriacchi et al. [7] indicated that stem design could be improved by increasing the cross section in the middle one-third of the stem where maximum tensile stresses are found to occur.

Crowninshield et al. [58] using a FE model with 400 elements (no other information given), predicted an increase in maximum tension in the stem and a reduction in maximum tension in the cement with increasing stem length and on this basis reasoned the use of a long stem since cement stresses are critical. Rohlmann et al. [227] used a model with 3663 brick elements resulting in 15,000 degree-of-freedom and in contrast to Crowninshield et al. [58], they conclude "the stress curve may be cut at any level, the resultant stress curve [for the stem] then shows approximately the stress distribution for this stem length". With respect to cement stresses they observe, contrary to Crowninshield et al. [58], a threshold stem length of 100 mm above which increasing stem length does not significantly reduce cement stresses. Therefore it would seem that the early rudimentary FE models may lead to conclusions that neither concur with the theory nor with later more sophisticated FE models.

Makarand et al. [165] suggested that in his study there is a significant benefit from the use of a short stem versus a long stem in terms of the interfacial shear stresses in the bone. He used in his model of the artificial hip prosthesis, Figure 2.2, a proximal plat to distribute the contact load over the entire cross section of the femur and reduce the stress shielding in the cortical bone. In addition, the designed prosthesis was anchored to the bone by means of developed cabling system to help produce a more natural bending load over the cross section of the femur by fixing the trochanter to the implant. The medial

side, a short screw into the stem was used to hold the plate against the medial calcar.

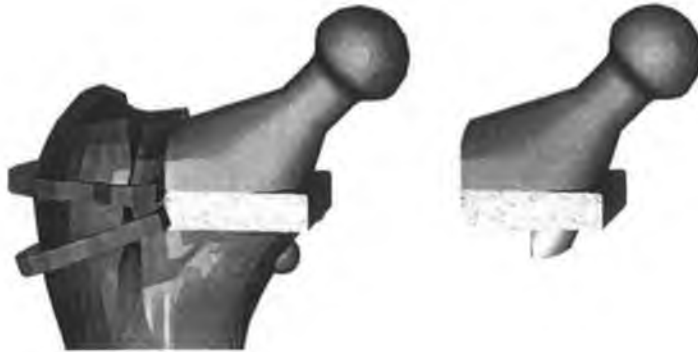


Figure 2.2: Schematic representation of the proposed hip prosthesis designed by Makarand et al. (2000).

Gross and Abel [98] made a comparison and optimization study, by using finite element modeling, for different shapes of hollow stem with those produced using comparable sizes of solid stem, Figure 2.3, with different values of elastic modulus to investigate their effect on stress shielding and the stresses occurred in the proximal femur. They found that the linearly tapered hollow stems achieved an increase in the proximal bone stress of about 22%, which could be a good compromise between acceptable cement stresses and ease of manufacture.

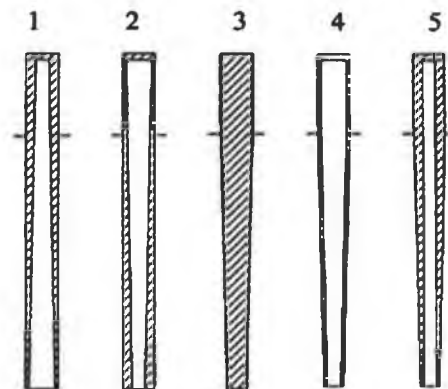


Figure 2.3: Shapes of the five tapered stems as designed by Gross and Abel (2001). The horizontal line shows the line of the resected bone.

Many previous studies have analyzed different stem designs in order to understand their load transfer properties and to look for improvements. Crowninshield et al. [59] found that increasing the cross section of the stem decreased the stress in both the stem and the cement. Katoozian and Davy [137], Huiskes and Boeklagen [120], Yoon et

al. [295] and Hedia et al. [301] used theoretically optimised models to find the best overall external shape of the stem, all achieving similar shapes. Kuiper [144] applied optimisation methods to select the elastic modulus of the stem. Bobyn et al. [26] and Schmidt and Hackenbroch [233] used a parallel walled hollow stem. Engelhardt and Saha [73] and Viceconti et al. [274] lessened the stiffness of the stem by using transverse holes. Täger [257] also used transverse holes to encourage spongiosa ingrowth.

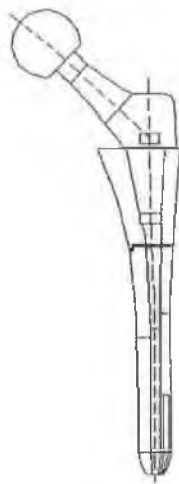


Figure 2.4: Modular hip prosthesis N.D.S.1.

Two recent designs have intimations of a more effective design approach. The modular hip prosthesis N.D.S.1 [92], Figure 2.4, able to realize a good press-fit and a better distribution of cortical loading. NDS1 has been built with respect with different flare proximal femur dimensions; a particular metaphyseal par has been studied to better fit the proximal flare; femoral component stem continue to have a long stem designed to have its axis parallel to the axis of the proximal femoral shaft. The NDS1 hip replacement system has a modular philosophy, with 276 possible combinations. The proximal end of the implant which flares to fill the wider cavity proximally at the intertrochanteric area of the femur is intended to proximalize load transfer and enhance stability of the implant, by a much better load circumferential distribution; an optagonal cross section shape has been choosen to increase contact surface without losing resistance at torque moments during walking loading condition. A final three dotted equally perimetral spaced diapason shaped structure has been chosen as the tip stem to avoid general or particular stress

points on the inner cortical lateral bone, to avoid stress shielding or minor solicitation and demineralization of bone. Modular designs allow for selection of multiple fitting geometrical shapes for proximal femoral flare in order to better restore the normal habitus of the walking patient [92]. In the Howmedica CAD Hip System, the stem has been “designed to withstand the loads” likely to be applied to it, and to this point the work must be commended. Unfortunately, the loading conditions chosen do not take into consideration the prosthesis-bone interaction. The design is thicker than most and well-rounded on the lateral and medial aspects, and makes allowance for head position for the longer-necked versions but not for the difference between straight and curved stems. The basic stem designs are available with Charnley, Müller [187], Harris, and Aufranc Turner designs for the head and acetabular components.

The results presented by Charnley and Kettlewell [47] would suggest that the femoral stem of femoral head replacements should be as short as possible, to minimize relative movement, especially where acrylic cement is not used. Yet, even Charley [39] stated “the trend in development over the years since the Judet prosthesis has been to increase the length of the medullary stem of the femoral prosthesis, and improved results have supported this policy.” As can be seen from Figure 2.4, the trend is for the designs not using acrylic bone cement (N.D.S.1, Deyerle, Tronzo, and Sivash) to be longer than those for use with it.

In contrast to this, Freeman [70] advocated minimization of the area of interface between the prosthesis and bone in order to reduce the incidence of infection. He advocates a spherical metal cup cemented over the trimmed femoral head so that the existing head and neck structure remains intact. Charnley [40] tried this with a PTFE cap, but found ischemic necrosis of the bone inside the cup, and so discarded the idea.

2.5. The Effect of Prosthesis Collar on its Performance

The effect of a collar on the prosthesis stem has also been specifically examined with such models [80, 213]. The prediction is that the collar can create more physiological calcar stresses if it remains in contact with the excised surface of the femur; if it can not remain in contact successfully then it may be better not to have it at all.

Fagan and Lee [80], and Prendergast and Tallor [213] suggest that the collar can never function in transferring the load properly to the femur neck for two reasons. Firstly, it must always contact the bone at localized contact points since the femur can neither be cut perfectly flat nor at the correct angle. Secondly, cement which extrudes from the femoral canal on insertion of the prosthesis, will invariably be caught under the collar, and this thin cement layer will eventually fracture. As regards the effect of a cement layer between femur and collar, Fagan and Lee [80] predicted that it will cause the calcar axial stress to be almost completely reduced to the magnitude of the uncollared prosthesis. Cement stresses are also changed by the presence of a collar where it is seen to reduce proximal cement stresses and have no effect on distal cement stresses [213, 80, 156]. In spite that Fagan and Lee [80], and Lewis et al. [156] conducted to the same results, they presented different conclusions. Fagan and Lee [80] suggest that the collar is a causative factor in bone loss because it affects “the manner in which the stem moves within the cement” whereas Lewis et al. [156] recommend to use a collared prostheses, concluding that we should be aim to design “functioning collar”. Prendergast [213] concluded that a low stiffness prosthesis causes higher tensile hoop stresses if uncollared and higher compressive hoop stresses if collared. And he suggested that in terms of reproducing the intact femur stress state, the use of a low stiffness material with a collar is an optimal prosthesis design.

2.6. *Prosthesis Stability*

Stability of a femoral stem prosthesis is a critical factor in its long-term clinical success. In non-cemented stems, the immediate post-operative, or primary, stability is important because it allows the bone to grow towards the prosthesis stem to interlock it, creating secondary, long-term stability. A previous study developed a protocol to compare the *in vitro* primary stability of rectangular and conical press-fit stem designs using custom-designed micromotion sensors [30]. The study found that both stems exhibited similar amounts of migration, but the cone-shaped stem showed moderately more cyclic motion than the tapered stem, most of which was in the anterior-posterior direction.

In contrast, cemented fixation offers immediate stability from cement-stem and cement-bone bonding, but may deteriorate over time [118]. Many studies have examined ways to improve the long-term clinical success of cemented implants by modifying stem surface characteristics or cementing technique to improve bonding. Ahmed et al. [2] and Stone et al. [253] determined that cement precoating can increase the interface strength because the bonding occurs *ex vivo* and is thus free of any included blood or other contaminants. Cook et al. [53] found that the implant-cement interface strength of porous-coated implants increases with pore size, and they recommend an optimum size of 345 μm . Modifications of the cementing technique, such as preheating the implants [23], distal plugging of the medullary canal and pressurization of the cement [13] and centrifugation of the cement [31], result in a more homogeneous cement mantle, and therefore a stronger cement-stem and cement-bone bond. The ultimate goal of these improvements is to make the implant more stable, and therefore prolong the fatigue life. Although cemented stem fixation is expected to be much more rigid than for uncemented stems, detectable motions may occur under physiologic loading, and excessive motions could damage the cement mantle. Speirs et al. [250] investigated the stability of two cemented hip implants under physiologic loads. The implants were tested *in vitro*, implanted in paired human femurs, and loaded with simulated *in vivo* forces on the femoral head while motions were measured with custom-designed micromotion sensors. The different motion patterns exhibited by the two stems could be used to explain the effect of design features on the stability of the implant.

Axisymmetric finite element models have been used to analysis the relationship between creep of acrylic cement and depending of the cement/metal interface [192, 270]. Using a 2D model of uncemented hip arthroplasty, Kuiper and Huiskes [145] showed that even small amount of bone/implant friction cause the prosthesis to be gripped within the medullary canal, thereby reducing the magnitude of interfacial micromotions. Tensi et al. [259] Report a non-linear analysis of cementless stems which predicted that a more physiological stress transfer occurs if the extent of porous coating is limited to the proximal region, and predicted that low-modulus prosthetic materials would generate unsuitable interface shear stresses. Verdonchot and Huiskes [269] studied the effect of

friction in cemented hip arthroplasty. Keaveny and Bartel [140] used non-linear finite element model of uncemented prostheses to show the influence of the extent of porous coating, and of a collar, on primary load transfer and relative motions in the reconstruction. Similar values of interface motions are calculated using an anisotropic, elastoplastic representation of bone by Rublin et al. [228].

Interface micromotion has, also, been studied by using concentric cylinder geometrical models of intramedullary fixation – the prediction is that reduced prosthesis stiffness causes increased micromotion [107, 225, 242], depending on the amount of interfacial friction and ingrowth. Proximal femoral prostheses are conventionally made of a single material, with constant elastic modulus. These prostheses can only address the micromotion or stress shielding problem. They are unable to address both simultaneously. Simões et al. [242] proposed a novel prosthesis design consisting of a stiff cobalt-chrome core surrounded by a relatively flexible outer layer. And by varying the thickness of the outer layer to control the stiffness of the prosthesis it is possible to obtain a suitable compromise to attenuate both problems, since avoiding them is impossible.

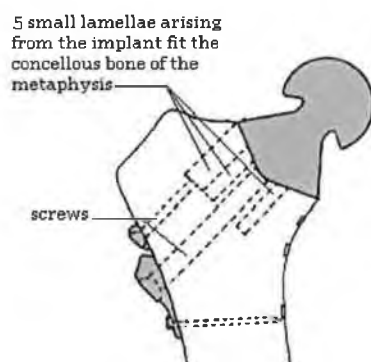


Figure 2.5: Schematic representation of the proposed hip prosthesis designed by Munting and Verhelpen (1995).

The bending displacements in the bone surrounding the stem are reduced because of the relatively high flexural stiffness of the prosthesis. This reduced bending unloads the outer fibers of femur leading to a state of stress shielding. For this reason, recently, new prosthesis design using proximal fixation was developed by Munting and Verhelpen [188] and has shown promising initial results. In this design the prosthesis stem is suppressed and provided metaphyseal fixation of the proximal femur by means of two

bolts and employed fins along the medial border to provide resistance to torsional motion, Figure 2.5. Their in vitro experiments show minimal micromotion and the short-term clinical studies show low initial failure rates.

2.7. Frictional Heating in the Total Hip Implants

In *vivo* measurements show that hip implants heat up to 43.1°C during activity [95]. It hypothesized that this is due to friction between head and cup. And it may cause thermal damage to soft tissues and bone, and eventually may cause implant loosening. Of course the temperature distribution is influenced by implant materials which have different thermal conductivities and frictional coefficients. van Lenthe et al. [268] tried to answer this question by simulating FE model of prosthetic hip with surrounding tissues: “whether temperatures in the tissues can reach critical levels? and how this depends on commonly used implant materials?”. They performed the simulation by selecting different material combination of the hip and cup, and concluded the temperature distribution strongly influenced by soft tissue conductivity. And that polyethylene cups are unlikely to provoke problems, but that metal-metal and ceramic-ceramic combination need the lowest possible friction coefficients to prevent tissue necrosis. Bergmann et al. [20] Observed that the peak temperature in the implant is inside the head. And it varied considerably and rose up to 43.1°C after an hour of walking. And they reported that in order to keep the temperatures low, an implant should have an aluminum ceramic head, a metal backed polyethylene cup, possibly with a ceramic inlay, and a CoCr head in combination with a polyethylene cup is unfavorable. In other hand, Chi-Chung Hu et al. [48] Showed that the major parameters such as applied loading, coefficient of friction, sliding speed, and sliding distance, which affect the elevation of temperature at the bearing surface of UHMWPE cup liner. When the temperature of articulating material is increased, several effects may occur such as the mechanical properties changed, the rate of oxidation increased, and the phase transformation took place. And all of these will influence its frictional behavior of the bearing surface.

Based on the experimental data a finite element model was developed to calculate the temperatures in the tissues surrounding the hip implant to determine whether these

tissues can heat up to critical levels. Various parameters were investigated which could account for the variations in the measured temperatures in the patients, including the perfusion rate in tissues, the volume of synovial fluid, and different implant materials. It was found that the synovial fluid is most endangered by thermal damage and consequent deterioration of lubricating properties. Implants with a cobalt-chromium head and a polyethylene cup are unfavourable as they can elevate the temperature in the synovia to more than 46°C. With regard to thermal properties stems made from cobalt-chromium alloys are superior to titanium stems, by better conducting heat to the femur and minimizing the synovial fluid temperature. Factors determining the temperatures during walking are insufficiently known or cannot be determined in the individual patient. Therefore, the risk of a thermally induced implant loosening cannot currently be estimated. Therefore, general improvements of implant materials and clinical studies on the possibility of implant loosening due to high temperatures are required [19].

2.8. *Wear Behavior in Total Hip Replacement*

Computer simulation techniques are rapidly growing in their application in biomechanical fields. As a result of the high efficiency and reliable results obtained, studies concerning the estimation of structural wear have focused on the utilization of computer programs and numerical methods. In the past few years, Wang et al. [275], Pietrabissa et al. [208], Jin et al. [134] and Maxian et al. [173] used the Hertz theorem to calculate contact stresses on the interface and estimate the wear depth and the wear volume using the simplified Archard's model in different forms. The Hertz contact theorem can be used only for contact bodies with conformal counterface (contact surface) under steady loadings or static loadings. However, the contact status between the hemispherical acetabular cup and the ball shaped femoral head must consider not only the variation of three-dimensional geometry, but also the difference in materials. Forces transmitted to the hip joint are quite complicated and stresses across the counterface between the acetabular cup and the femoral head appear discontinuous and may affect the contact status and wear behavior of the arthroplasty. Therefore, in order to simulate wear behaviors of a polyethylene acetabular cup accurately, Wu J. S.S. et al. [293] propose a

modified Archard's wear formula and history-dependent processes in this study. They constructed finite element models of a pin-on-disk plate and an artificial hip joint that include the appropriate loading and boundary conditions. It is shown that their algorithms are useful and helpful in understanding wear behavior for alternative or new designs of artificial hip joints and even for other analogous structures.

Further investigation into the effect of femoral heads with various sizes suggests that the larger femoral head may induce larger wear volume but gives a smaller wear depth and that wear depth and volume loss are apparently nonlinearly related to the femoral head diameter.

2.9. Failure of Hip Prosthesis Components

The brittle nature of the cement and the many flaws that it contains suggest a fracture mechanics approach to predicting fatigue and fracture, but this difficult because of the multiple materials that are present and the complex geometry [78]. Hedia et al. [111] used 2D the finite element model for predicting the fatigue life of the prosthesis in addition to the stresses developed in the bone, cement and stem. They used different assumptions regarding the form of the idealization, the load conditions, and the interface conditions for deterring stress distributions and resulting fatigue notch factors in the human femur with endoprosthesis. The FE results show that a realistic loading condition without a tension banding force (due to iliotibial tract muscle) always produces the highest fatigue notch factor and von Mises stresses. Also, they realize that full bonded interface is a satisfactory approximation for the real interface conditions because it predicts stress distributions of the correct form without excessive stress condition. Evans [78] demonstrated the potential computational fracture mechanics using boundary element techniques for analyzing biomechanical problems, and shows that it is possible to simulate three-dimensional fatigue crack propagation under complex stress conditions and variable amplitude loading. While using this technique he found that the boundary element approach does have some limitations in biomechanics, since it is not possible to represent poroelastic materials, where fluid flows through the volume of the material, and

varying elastic properties require additional boundaries at each change in stiffness making realistic variation in tissue stiffness difficult and uneconomical.

Repetitive loading causes accumulation of mechanical damage in the cement, leading to the formation of micro-cracks, and as a result the load-carrying capabilities of the cement are reduced and abrasion particles may be formed. Stolk et al. [252] Developed a finite element algorithm to simulate damage accumulation in the cement in a total hip arthroplasty (THA) reconstruction under dynamic loading conditions, using an anisotropic continuum damage mechanics (CDM) approach. They found that debonded stem produced a higher amount of cracks than the bonded stem and this is in agreement with what Harrigan and Harris [107] reported since they used A non-linear analysis of cemented stems.

Andriacchi et al. [7] present two-dimensional FE model used to study the effect of some of the factors leading to early fatigue failure of the femoral stem in total hip prostheses. And they showed that the loss of the proximal stem support at the level of the calcar femoral will result in stem stress levels which can lead to fatigue failure. This conclusion is in agreement with what Zaki et al. [296] conducted to by using 3D FE model.

Hertzler J. et al. [115] used a combination of experimental and computational methods to investigate the fatigue crack propagation process from the stem-PMMA cement interface using a novel torsional loading model. Constructs with thin (1 mm), medium (3 mm) or thick (7 mm) cement mantles were evaluated. Crack growth was stable for all cases and the rate of crack growth diminished with increasing crack length. They deduced that crack growth rate did not depend on mantle thickness ($p>0.05$) over the first 1 mm of crack length, but cracks in thin mantles reached the full thickness of the mantle in the fewest number of loading cycles. The fracture mechanics-based on finite element models indicated decreased stress intensity factors with increasing crack length and were consistent with the experimental findings. They also found that the finite element models provided reasonable predictions of the crack growth process.

Residual stress due to shrinkage of polymethylmethacrylate bone cement after

polymerisation is possibly one factor capable of initiating cracks in the mantle of cemented hip replacements. No relationship between residual stress and observed cracking of cement has yet been demonstrated. Lennon and Prendergast [154] investigated if there is any relationship exists, a physical model has been developed which allows direct observation of damage in the cement layer on the femoral side of total hip replacement. The model contains medial and lateral cement layers between a bony surface and a metal stem; the tubular nature of the cement mantle was ignored. Five specimens were prepared and examined for cracking using manual tracing of stained cracks, observed by transmission microscopy; cracks were located and measured using image analysis. A mathematical approach for the prediction of residual stress due to shrinkage was developed which uses the thermal history of the material to predict when stress-locking occurs, and estimates subsequent thermal stress. The residual stress distribution of the cement layer in the physical model was then calculated using finite element analysis. Their results showed maximum tensile stresses normal to the observed crack directions, suggesting a link between residual stress and preload cracking. The residual stress predicted depends strongly on the definition of the reference temperature for stress-locking. The highest residual stresses (4–7 MPa) are predicted for shrinkage from maximum temperature; in this case, magnitudes are sufficiently high to initiate cracks when the influence of stress raisers such as pores or interdigitation at the bone/cement interface are taken into account. They conclude that the damage accumulation failure scenario begins before weight-bearing due to cracking induced by residual stress around pores or stress raisers.

2.10. *Relative Studies*

Using finite element analyses, Stolk et al. [251] investigated which muscle groups acting around the hip-joint most prominently affected the load distributions in cemented total hip reconstructions with a bonded and debonded femoral stem. The purpose was to determine which muscle groups should be included in pre-clinical tests, predicting bone adaptation and mechanical failure of cemented reconstructions, ensuring an adequate representation of in vivo loading of the reconstruction. Loads were applied as occurring

during heel-strike, mid-stance and push-off phases of gait. The stress/strain distributions within the reconstruction, produced by the hip-joint contact force, were compared to ones produced after sequentially including the abductors, the iliotibial tract and the adductors and vastii. Inclusion of the abductors had the most pronounced effect. They neutralized lateral bending of the reconstruction at heel-strike and increased medial bending at mid-stance and push-off. Bone strains and stem stresses were changed accordingly. Peak tensile cement stresses were reduced during all gait phases by amounts up to 50% around a bonded stem and 11% around a debonded one. Additional inclusion of the iliotibial tract, the adductors and the vastii produced relatively small effects during all gait phases. Their most prominent effect was a slight reduction of bone strains at the level of the stem tip during heel-strike. These results suggest that a loading configuration including the hip-joint contact force and the abductor forces can adequately reproduce in vivo loading of cemented total hip reconstructions in pre-clinical tests.

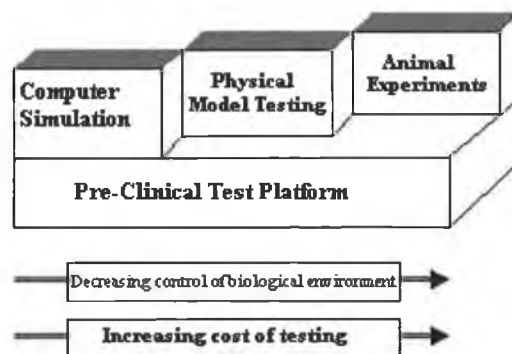


Figure 2.6: Three component of pre-clinical testing: computational modelling, laboratory bench tests, and animal experimentation

The three methods for pre-clinical testing are computational modelling, laboratory bench testing, and animal experimentation. The more the first two are developed, the less reliance needs to be placed on the latter. The three methods may be combined to form a pre-clinical testing platform (see Figure 2.6). Computational methods, usually based on finite element analysis [216], are relatively quick and can be relatively inexpensive; however, finite element methods are entirely reliant on the analyst's understanding of the in vivo situation, and on the capabilities of the finite element codes and the biomechanical algorithms needed to simulate tissue adaptations [215, 216]. Laboratory bench testing may facilitate more reliable testing insofar as factors such as material

properties, interface interactions, etc. are not completely under the experimenter's control. However, experimental models do not simulate tissue reactivity and furthermore can be time-consuming to set up. In this respect, the potential advantages of computer simulation vis-à-vis physical model testing may become considerable, but only if robust simulation algorithms can be developed to predict tissue adaptation (and this is still in the future). In such an eventuality, the potential for creating virtual environments for the testing of implants and medical devices will be possible.

An understanding of how the implant performs in vivo is essential to the development of a pre-clinical test. This information is obtained from a number of sources which include non-invasive diagnostic imaging (X-ray, DEXA, CT, MRI) and retrieval analysis [215]. Retrieval of the implant, either at autopsy or at revision, allows for failure analysis of the implant and histological analysis of the tissues. Implant retrieval at autopsy can be particularly valuable because it allows assessment of the progression towards failure and thus the identification of failure mechanisms before catastrophic failure occurs. However, retrieval of implants is a complex legal area [84]. Once the predominant failure mechanism has been determined and documented for a particular class of devices, a methodology as outlined in Figure 2.7 may be established.

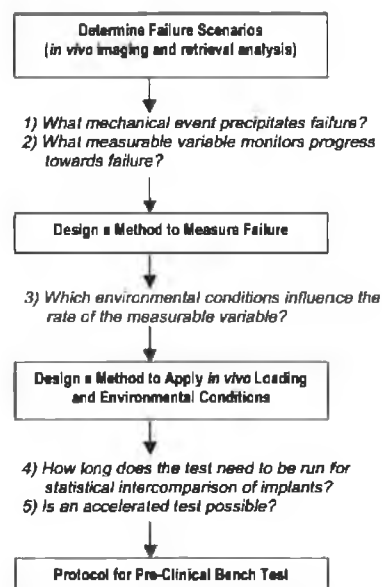


Figure 2.4: Methodology for development of a pre-clinical test for a biomechanical implant or prosthesis

2.11. *Closing Remarks*

The chapter gives a component-by-component assessment of the performance of the artificial hip prosthesis in service and the significant role that mechanical factors play in failure was emphasized. Furthermore, it was noted that as the service-life of the artificial hip prosthesis increases, the complexity of these roles increases greatly because biological factors begin to dominate failure.

The foregoing discussion indicates that because of pronounced technology development the modern surgeon has the opportunity to vary the style and dimensions of a total hip replacement to suit his technique and the particular patient. There are many variables – the stem length, thickness, and shape; the shoulder form, neck length, and head diameter; and the cup material, outer diameter, and external form. The present proliferation of design is a direct consequence of the differences of opinion between surgeons. As a result, for any particular design which will have originated from one school of opinion, there will not be wide range of variations to choose from. It is important, however, that the surgeon has an adequate range of instruments and prostheses at his disposal. It is, therefore, essential that careful rationalization of designs and instrumentation be carried out, both within each design regimen and between different designs.

At the present time, development in total hip and other joint replacements is prevalent, and requires simply the capability for manufacture and a means whereby new ideas or new combination of existing ideas may be tested in patients. With the exception of a few well-directed, thorough, and consequently slowly progressing, investigation, there appears to be very little basis for the many changes in design that have been introduced in the last few years. The fundamental unknowns of implant failure remain: what are the stresses at the interface? What is the nature of the interface under established successful conditions, and why does late infection occur so often?

These are difficult problems and the answers may be a long time coming. In the light of present uncertainties of the fundamental behavior of surgical implants, the proliferation of total hip designs cannot be justified without adequate and reliable

research and development. What justification is there for the use of further modification to a design before the original is fully evaluated? Unless there is very good fundamental reason for expecting a major improvement in the results, any change is open to very valid criticism.

In the next chapter, a new model of the artificial hip prosthesis using finite element analysis will be presented. A different modeling approach is used compared to other 3-D finite element studies. The model is used for primary stability assessment. Subsequent chapters deal with the new approach used as pre-clinical test tool in designing a new artificial hip prosthesis.

Chapter Three

Brief Introduction on Finite Element Analysis

3.1. Introduction

The objective of this chapter is to provide a basic theoretical outline of the numerical methods used to solve the problems as described in later chapters. This chapter is not intended as a text on the finite element method, rather as a description of how the method was utilised here, and hence the reader unfamiliar with the method is referred to the reference section.

3.2. The Finite Element Method

Finite element analysis is the simulation of a physical system (geometry and loading environment) by a mathematical approximation of the real system. Using simple, interrelated building blocks called *elements*, a real system with infinite unknowns is approximated with a *finite* number of unknowns [131]. The basic steps in any finite element analysis consists of the following [183]:

a) Preprocessing Phase

- Create and discretize the solution domain into finite elements; that is, subdivided the problem into nodes and elements.
- Assume a shape function to represent the physical behaviour of an element; that is, an approximate continuous function is assumed to represent the solution of an element.
- Develop equations for element.
- Assemble the elements to present the entire problem. Construct the global stiffness matrix.
- Apply boundary conditions, initial conditions, and loading.

b) Solution Phase

- Solve a set of linear or nonlinear algebraic equations simultaneously to obtain nodal results, such as displacement values at different nodes or temperature values at different nodes in a heat transfer problem.

c) Postprocessing Phase

- Using the nodal values and interpolation functions, other parameters such as strain, stress etc. inside each element may be determined.

3.2.1. General Theory

This section will outline the general theory involved in the finite element method drawing particularly from reference [15]. There are a number of methods available for determining the governing equations of equilibrium for finite element method. One such method is to use the principle of virtual displacements to express the equilibrium of the body. This principle states that the internal virtual work in the body is equal to the external virtual work acting upon the body due to external forces. The internal virtual work is equal to the actual stresses going through the virtual strains. The external work is given by the actual forces going through the virtual displacements. For a three dimensional body subjected to externally applied body forces f^B (force per unit volume), concentrated loads R^i (where i denotes the point of load application), surface tractions f^S , resulting in virtual displacements U , virtual stress τ and virtual strain ε , the principle can be stated as:

$$\int_V \{\bar{\varepsilon}\}^T \{\tau\} dV = \int_V \{\bar{U}\}^T \{f^B\} dV + \int_S \{\bar{U}^S\}^T \{f^S\} dS + \sum_i \{\bar{U}^i\}^T R^i \quad (1)$$

where,

$$\{\bar{\varepsilon}\}^T = [\bar{\varepsilon}_{xx} \quad \bar{\varepsilon}_{yy} \quad \bar{\varepsilon}_{zz} \quad \bar{\gamma}_{xy} \quad \bar{\gamma}_{yz} \quad \bar{\gamma}_{zx}]$$

$$\{\tau\}^T = [\tau_{xx} \quad \tau_{yy} \quad \tau_{zz} \quad \tau_{xy} \quad \tau_{yz} \quad \tau_{zx}]$$

$$\{\bar{U}\}^T = [\bar{U} \quad \bar{V} \quad \bar{W}] \quad \bar{U}, \bar{V} \text{ and } \bar{W} \text{ are displacement in global directions.}$$

$$\{f^B\}^T = [f_x^B \quad f_y^B \quad f_z^B] \quad \text{where B indicates body.}$$

$$\{f^s\}^T = \begin{bmatrix} f_x^s & f_y^s & f_z^s \end{bmatrix}$$

where superscript S indicates surface.

$$\{R^i\} = \begin{bmatrix} R_x^i & R_y^i & R_z^i \end{bmatrix}$$

where superscript i indicates points.

As the problem domain is approximated by an assembly of finite element which are interconnected at nodal points on the element boundaries, the displacements measured within each element are assumed to be a function of the displacements at the nodal points.

$$u^{(m)}(x, y, z) = H^{(m)}(x, y, z) \hat{U} \quad (2)$$

where $H^{(m)}$ is the displacement interpolation matrix or shape function for element m and \hat{U} is a vector of the three global displacement components U_i , V_i and W_i at all nodal points (i.e. if there are N nodes then \hat{U} will be of dimension 3N).

Using this assumption, equilibrium equations that correspond to the nodal point displacements of the assembly of finite elements can be constructed from equations (1) and (2):

$$\sum_m \int_{V^{(m)}} \epsilon^{(m)T} \tau^{(m)} dV^{(m)} = \sum_m \int_{V^{(m)}} \bar{U}^{(m)T} f^{B(m)} dV^{(m)} + \sum_m \int_{S^{(m)}} \bar{U}^{S(m)T} f^{S(m)} dS^{(m)} + \sum_i \bar{U}^{iT} R^i \quad (3)$$

From the assumption on displacements in equation (2) the corresponding element strains can be evaluated as:

$$\epsilon^{(m)}(x, y, z) = B^{(m)}(x, y, z) \hat{U} \quad (4)$$

where $B^{(m)}$ is the strain-displacement matrix for element m . the rows of $B^{(m)}$ are obtained by appropriately differentiating and combining rows of matrix $H^{(m)}$.

The stress within a finite element are related to the element strains and initial stresses by:

$$\tau^{(m)} = C^{(m)} \epsilon^{(m)} + \tau^{I(m)} \quad (5)$$

where $C^{(m)}$ is the matrix relating strain to stress of element m and $\tau^{I(m)}$ are element initial stresses. The material law specified in $C^{(m)}$ for each element can be

that of an isotropic or anisotropic material and can vary from element to element. Using equations (2), (4) and (5) we can rewrite equation (3) as:

$$\bar{U}^T \left[\sum_m \int_{V^{(m)}} B^{(m)T} C^{(m)} B^{(m)} dV^{(m)} \right] \hat{U} = \hat{U}^T \left[\begin{aligned} & \left\{ \sum_m \int_{V^{(m)}} H^{(m)T} f^{B(m)} dV^{(m)} \right\} + \\ & \left\{ \sum_m \int_{S^{(m)}} H^{S(m)T} f^{S(m)} dS^{(m)} \right\} - \\ & \left\{ \sum_m \int_{V^{(m)}} B^{(m)T} \tau^{I(m)} dV^{(m)} \right\} + F \end{aligned} \right] \quad (6)$$

where the surface displacement interpolation matrices $H^{S(m)}$ are obtained from the volume displacement interpolation matrices $H^{(m)}$ in equation (2) by substituting the element surface co-ordinates and F is a vector of the externally applied forces to the nodes of the element assembly. It may be noted that in equation (6) the nodal point displacement vector, \hat{U} , is outside the summation sign as it is independent of the element considered.

In order to obtain the equations for the unknown nodal point displacements from equation (6), the virtual displacement theorem is utilized by imposing unit virtual displacements in turn at all displacement components. This results in $\hat{U}^T = I$ (where I is the identity matrix) and by denoting \hat{U} by U , the equilibrium equation of the element assemblage corresponding to the nodal point displacement is:

$$KU = R \quad (7)$$

the matrix K is the global stiffness matrix and is given by:

$$K = \sum_m \int_{V^{(m)}} B^{(m)T} C^{(m)} B^{(m)} dV^{(m)} \quad (8)$$

the load vector $R = R_B + R_S - R_I + R_C$, where R_B is the effect of element body forces:

$$K = \sum_m \int_{V^{(m)}} H^{(m)T} f^{B(m)} dV^{(m)} \quad (9)$$

R_S is the effect of element surface forces and is given by:

$$R_S = \sum_m \int_{S^{(m)}} H^{S(m)T} f^{S(m)} dS^{(m)} \quad (10)$$

R_I is the effect of element initial stresses and is given by:

$$R_I = \sum_m \int_{V(m)} B^{(m)T} \tau^{I(m)} dV^{(m)} \quad (11)$$

and $R_C = F$ (i.e. the concentrated loads).

Equation (7) is a statement of the static equilibrium of the finite element mesh. In equilibrium considerations, applied forces may vary with time, in which case the displacements may also vary with time. If in reality the loads are applied rapidly, inertia forces must be considered and a dynamic problem must be solved. Using d'Alembert's principle, the element inertia forces may be included as of part of the body forces. In such a cases equation (9) becomes:

$$R_B = \sum_m \int_{V(m)} H^{(m)T} \left[f^{B(m)} - \rho^{(m)} H^{(m)} \ddot{U} \right] dV^{(m)} \quad (12)$$

where $f^{B(m)}$ no longer includes inertial forces, \ddot{U} gives nodal point accelerations and $\rho^{(m)}$ is the mass density of element m . in this case the equilibrium equations are:

$$M\ddot{U} + KU = R \quad (13)$$

where K is the global stiffness matrix, M is the global mass matrix and R and U are time dependant. The global mass matrix is given by:

$$M = \sum_m \int_{V(m)} \rho^{(m)} H^{(m)T} H^{(m)} dV^{(m)} \quad (14)$$

However, in a dynamic analysis some energy is dissipated during vibration, which in vibration analysis is usually taken account of by introducing velocity dependant damping forces. Introducing the damping forces as additional contributions to the body forces changes equation (12) as follows:

$$R_B = \sum_m \int_{V(m)} H^{(m)T} \left[f^{B(m)} - \rho^{(m)} H^{(m)} \ddot{U} - \kappa^{(m)} H^{(m)} \dot{U} \right] dV^{(m)} \quad (15)$$

where \dot{U} is a vector of the nodal point velocities and $\kappa^{(m)}$ is the damping property parameter of element m . in this case the equilibrium equations become:

$$M\ddot{U} + C\dot{U} + KU = R \quad (16)$$

where C is the global damping matrix and can be written as:

$$C = \sum_m \int_{V^{(m)}} \kappa^{(m)} H^{(m)T} dV^{(m)} \quad (17)$$

3.2.2. *Non Linearities*

In the above formulation it was assumed that the displacements of the finite element assembly are small, that the material is linearly elastic and that the boundary conditions remain unchanged during the application of loads. These assumptions have entered the equilibrium equation in the following manner:

- (a) The fact that all integrations have been performed over the original volume of the finite elements implies that displacements must be small. This effects the stiffness matrix, K , and the load vector, R .
- (b) The strain-displacement matrix, B , of each element was assumed to be constant and independent of element displacements.
- (c) The assumption of a linear elastic material is implied in the use of a constant stress-strain matrix, C .
- (d) The unchanged boundary conditions is implied by keeping constant constraint relations for the complete response.

These observations point to the different types of non-linearity that may arise in a finite element analysis:

- (e) Non linearity due to large displacements, large rotations, but small strains.
- (f) Non linearity due to large displacements, large rotations and large strains.
- (g) Material non linearity.
- (h) Non linearity due to contact.

3.2.3. *Solution Methodology*

There are many solution methods available for use with the finite element method, however, as analysis in this work is primarily concerned with non linear analysis, this section will concentrate on solution methodology for non linear problems. The basic problem in a general non linear analysis is to determine the state of equilibrium of the body corresponding to the applied loads. Assuming that the

external loads are described as a function of time, the equilibrium conditions of the finite element assembly can be written as:

$${}^tR - {}^tF = 0 \quad (18)$$

where tR gives the externally applied nodal point forces at time t and the vector tF lists the nodal point forces corresponding to the element stresses, where:

$${}^tR = {}^tR_B + {}^tR_S + {}^tR_C \quad (19)$$

$${}^tF = \sum_m \int_{V^{(m)}} {}^tB^{(m)T} \sigma^{(m)t} dV^{(m)} \quad (20)$$

it may be noted, in reference to equation (20), that in a large deformation analysis the stress and volume of the body at time t be unknown. In a dynamic analysis the vector tR would also include the inertial and damping forces.

Equation (18) must express the equilibrium of the system in the current defined geometry by taking account of all non linearity's and must be satisfied throughout the complete history of load application. The solution process is carried out using a step by step incremental analysis. The basic approach in an incremental solution is to assume that the solution for the discrete time t is known and that the solution for a discrete time $t + \Delta t$ is required, where Δt is a suitably chosen time increment. Thus, at time $t + \Delta t$ equation (18) can be written as:

$${}^{t+\Delta t}R - {}^{t+\Delta t}F = 0 \quad (21)$$

Since the solution at time t is known it can be written that:

$${}^{t+\Delta t}F = {}^tF + F \quad (22)$$

where F is the increment in nodal point forces corresponding to the increment of element displacements and stresses from time t to time $t + \Delta t$. This vector can be approximated using a tangent stiffness matrix tK which corresponds to the geometric and material condition at time t .

$$F \cong {}^tKU \quad (23)$$

where U is the vector of incremental nodal point displacements. By combining (21), (22) and (23) we get:

$${}^tKU = {}^{t+\Delta t}R - {}^tF \quad (24)$$

By solving this equation for U an approximation to the displacements at time $t + \Delta t$ can be calculated:

$${}^{t+\Delta t}U \cong {}^tU + U \quad (25)$$

Having evaluated an approximation to the displacements corresponding to time $t + \Delta t$ an approximation for stresses and corresponding nodal point forces at time $t + \Delta t$ can be obtained. However, because of the approximation expressed in equation (24), such a solution may be subject to significant errors and may be unsuitable. In practice it is frequently necessary to iterate until equation (21) is satisfied to sufficient accuracy.

Different solution procedures exist for the solution of equation (24). In this work the explicit time integration method was used and will be briefly outlined. The most common explicit time integration operator used in non linear dynamic analysis is the central difference operator. The equilibrium of the finite element assembly is considered at time t in order to calculate the displacements at time $t + \Delta t$. Solution is sought for each time step for the equilibrium equation neglecting the effect of damping which may be expressed as:

$$M\ddot{U} = {}^tR + {}^tF \quad (26)$$

where the nodal point force vector tF is evaluated on the basis of the methods used to formulate the material and geometric non linearity's. this involves the choice of element type, the kinematic description and the kinetic description, all of which are problem dependant. The solution for the nodal point displacements at time $t + \Delta t$ is obtained using the central difference approximation for the accelerations as follows:

$$\ddot{U} = \frac{1}{\Delta t^2} \{ {}^{t-\Delta t}U - 2{}^tU + {}^{t+\Delta t}U \} \quad (27)$$

Combining this with equation (26) gives:

$$\frac{M}{\Delta t^2} \{ {}^{t+\Delta t}U \} = {}^tR - {}^tF - \frac{M}{\Delta t^2} \{ {}^{t-\Delta t}U - 2{}^tU \} \quad (28)$$

thus, if ${}^{t-\Delta t}U$ and tU are known then ${}^{t+\Delta t}U$ can be determined from (28). A disadvantage in the use of this method is that for stability, the time step size Δt must be smaller than a critical time step size Δt_{CR} which is equal to T_n / π , where T_n is the smallest period in the finite element assembly.

3.3. ANSYS Theoretical Methods

ANSYS is a general purpose finite element analysis package. It can simulate problems in area of structural mechanics, electromagnetic, heat transfer, fluid dynamics, acoustics and coupled problems. In structural analysis it has the capability to analyse static or dynamic linear and non-linear problems. In addition, ANSYS has a design optimization module based on non-linear optimization theories which in conjunction with finite element procedure can be utilized for the optimization of structural linear or non-linear problems. The simulations carried out in this work are non-linear in nature. The theoretical methods described in the following sub-sections are taken from the manual of ANSYS [143].

3.3.1. Solution Procedures

In ANSYS Newton-Raphson procedure is used for iterative solution of the equilibrium equations. The Newton-Raphson method is a numerical method used by ANSYS to solve a nonlinear system of equations. The Newton-Raphson method is based on applying the load incrementally and iterating to enforce equilibrium at each load increment. In Newton-Raphson procedure an iterative solution is sought for the equation (21) by defining an out-of-balance load vector $\Delta \mathbf{R}_{(i-1)}$ as:

$$\Delta \mathbf{R}_{(i-1)} = \{\mathbf{F}^a\} - \{\mathbf{F}_i^{nr}\} \quad (29)$$

where $\{\mathbf{F}^a\}$ is the vector of applied loads and $\{\mathbf{F}_i^{nr}\}$ is the vector of restoring loads corresponding to the element internal loads. By the virtual displacement principle $\Delta \mathbf{R}_{(i-1)}$ is related as:

$$[\mathbf{K}_i^T] \{\Delta \mathbf{u}_i\} = \Delta \mathbf{R}_{(i-1)} = \{\mathbf{F}^a\} - \{\mathbf{F}_i^{nr}\} \quad (30)$$

and

$$\{\mathbf{u}_{i+1}\} = \{\mathbf{u}_i\} + \{\Delta\mathbf{u}_i\} \quad (31)$$

Both $[\mathbf{K}_i^r]$ and $\{\mathbf{F}_i^{nr}\}$ are evaluated based on the values given by $\{\mathbf{u}_i\}$. The subscripts in the above equations refer to iteration numbers. The final converged solution would be in equilibrium, such that the restoring load vector $\{\mathbf{F}_i^{nr}\}$ would equal to the applied load vector $\{\mathbf{F}^a\}$ or at least to within some tolerance. If the analysis involves path dependent non-linearity such as plasticity, then the solution process requires that some intermediate steps be in equilibrium in order to correctly follow the load path. This is accomplished effectively by specifying a step by step incremental analysis; i.e., the final load vector $\{\mathbf{F}^a\}$ is reached by applying the load in increments and performing the Newton-Raphson iterations at each step.

The incremental time is automatically determined by number of factors such as number of equilibrium iteration needed, time point at which element will have change of status allowable plastic strain increment etc. Depending on the problem, different analysis tools such as adaptive descent and line search method is used to overcome convergence difficulties. Convergence's is assumed when vector norm

$$\|\{\mathbf{R}\}\| < \varepsilon_R \mathbf{R}_{ref} \quad (32)$$

where $\{\mathbf{R}\}$ is the residual vector and

$$\{\mathbf{R}\} = \{\mathbf{F}^a\} - \{\mathbf{F}^{nr}\} \quad (33)$$

ε_R is tolerance (default = 0.001) and \mathbf{R}_{ref} is reference values which is $\|\{\mathbf{F}_a\}\|$ by default. The vector norm used in the analysis is the square root of the sum of the squares value of the terms expressed as,

$$\|\{\mathbf{R}\}\| = \left(\sum \mathbf{R}_i^2 \right)^{\frac{1}{2}} \quad (34)$$

3.3.2. Large Strain Theory

Large strain theory of ANSYS is used for elastic-plastic elements. Let a body has a position vector $\{X\}$ and $\{x\}$ at its undeformed state and deformed state respectively. Then the displacement vector $\{u\}$ would be:

$$\{u\} = \{x\} - \{X\} \quad (35)$$

the deformation gradient defined as $[F] = \frac{d\{x\}}{d\{X\}}$ applied to (35) would give,

$$[F] = [I] + \frac{d\{u\}}{d\{X\}} \quad (36)$$

where the symbol $[]$ stand for matrix and $[I]$ is the identity matrix.

The deformation gradient $[F]$ includes the volume change, the rotation and the shape change of the deforming body. $[F]$ can be separated into a rotation and the shape change matrix using the right polar decomposition theorem.

$$[F] = [R][U] \quad (37)$$

where $[R]$ = rotation matrix.

$[U]$ = right stretch (shape change) matrix.

Once $[U]$ is known, then the logarithmic strain measure can be obtained as:

$$[F] = \ln[U] \quad (38)$$

computationally, the evaluation of (38) is performed by one of the two methods using incremental approximation.

$$[\varepsilon] = \int d[\varepsilon] \cong \sum [\Delta\varepsilon_n] \quad (39)$$

with

$$[\Delta\varepsilon_n] = \ln[\Delta U_n] \quad (40)$$

where n refers to current time step and $[\Delta U_n]$ is the incremental stretch matrix computed from the incremental deformation gradient,

$$[\Delta F_n] = [\Delta R_n][\Delta U_n] \quad (41)$$

where $[\Delta F_n]$ is:

$$[\Delta F_n] = [F_n][F_{n-1}]^{-1} \quad (42)$$

where $[F_n]$ is the deformation gradient at the current time step and $[F_{n-1}]$ is at the pervious time step.

Method 1 for evaluating equation (40) is:

$$[\Delta \epsilon_n] = \sum_{i=1}^3 \ln(\lambda_i) \{e_i\} \{e_i\}^T \quad (43)$$

where, λ_i and $\{e_i\}$ are the eigen value and eigen vector for the i_{th} principal stretch increment of the incremental stretch matrix $[\Delta U_n]$ this method is used for large strain solid elements. For standard solid and shell elements an approximate method is used by evaluating the deformation gradient at the midpoint configuration.

$$[\Delta \epsilon_n] = [R_{1/2}]^T [\Delta \bar{\epsilon}_n] [R_{1/2}] \quad (44)$$

and

$$[\Delta \bar{\epsilon}_n] = [B_{1/2}] \{\Delta u_n\} \quad (45)$$

where, $\{\Delta u_n\}$ is the displacement increment over the time step and $[B_{1/2}]$ is the strain displacement matrix evaluated at the midpoint geometry.

The computed strain increment $\{\Delta \epsilon_n\}$ is then added to the previous strain $\{\Delta \epsilon_{n-1}\}$ to obtain the current total logarithmic strain:

$$[\Delta \epsilon_n] = \{\epsilon_{n-1}\} + \{\Delta \epsilon_n\} \quad (46)$$

the strain is then used in the stress updating procedure in stress-strain relationship matrix.

3.3.3. Element Formulation

The element matrices and load vectors are derived using an updated Lagrangian formulation. The equilibrium equation of this is:

$$[K_i]\Delta u_i = \{F^{app}\} - \{F_i^{nr}\} \quad (47)$$

where $\{F^{app}\}$ is the applied force vector and $\{F_i^{nr}\}$ is the force obtained from Newton-Raphson current trial solution.

The tangent matrix has the form:

$$[K_i] = \int [B_i]^T [D_i] [B_i] dV \quad (48)$$

integrated over the element volume. $[B_i]$ is the strain displacement matrix in terms of current geometry and $[D_i]$ is the current stress-strain matrix.

The Newton-Raphson restoring force,

$$F_i^{nr} = \int [B_i]^T \{\sigma_i\} dV \quad (49)$$

where, $\{\sigma_i\}$ is the current Cauchy stress.

In ANSYS element library there are two dimensional and three dimensional large strain viscoplastic elements. 2-D elements have two integration points in each direction with standard shape functions for linear interpolation. Similarly 3-D elements also have linear shape functions and two integration points in each direction. Gauss quadrature rule for numerical integration procedure is used to evaluate matrix integration required in finite element calculations.

3.4. LS-DYNA3D Theoretical Methods

3.4.1. Solution Methodology

LS-DYNA3D is a general purpose explicit dynamic finite element code for analyzing highly non linear transient dynamic problems. The equilibrium equation of a dynamic problem and the solution process using the central difference method was given above in equations (26), (27) and (28). As mentioned above, the time step size

Δt and its relation to the critical time step size Δt_{CR} is of most importance.

LSDYNA3D calculates the critical time step size from:

$$\Delta t = \frac{l}{C} \quad (50)$$

where l is the characteristic length of the smallest element and C is the sonic wave propagation velocity through the element material. For reasons of stability a scale factor of 0.9 is used to decrease the time step in equation (50). The time step used by LSDYNA3D is therefore given by:

$$\Delta t = 0.9 \frac{l}{C} \quad (51)$$

l and C are calculated in a different manner depending on the element type concerned. In this work eight node solid elements were used for the analyses, in which l is the smallest distance between two neighboring nodes of the smallest element in the model.

The sound wave propagation speed is given by:

$$C = \sqrt{\frac{E(1-\nu)}{(1+\nu)(1-2\nu)\rho}} \quad (52)$$

3.4.2. *Element Formulation*

In this work an eight-node hexahedron solid element was used for the analyses. Volume integration of the elements is carried out using Gaussian quadrature. Both reduced (one point) and full integration options are available. The biggest advantage to reduced integration is the substantial saving in computer time, however, this has to be balanced by the need to control the zero energy modes, called hourglassing modes, which may arise.

Hourglassing is a zero energy mode of deformation that oscillates at a frequency much higher than structures global response. Hourglassing modes may result in stable mathematical states that are not physically possible. They typically have no stiffness and give a zigzag deformation appearance to the finite element

mesh. The hourglass deformation mode in a two dimensional element is shown in Figure 3.1. for illustration.

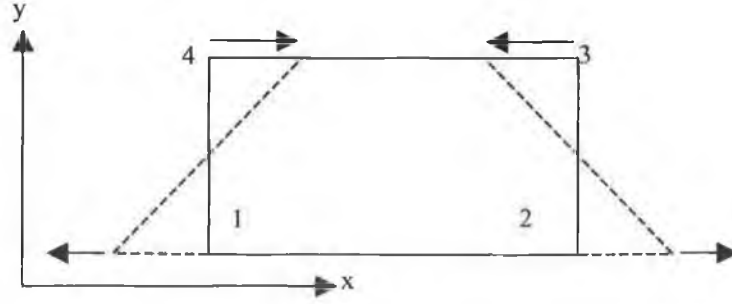


Figure 3.1: Hourglass Deformation Mode.

The origin and consequent implications of the hourglass deformation mode is described in elementary form, with reference to the above figure, by Halliquist and Benson [101]. Suppose nodes 1 and 3 are given a velocity of +1 in the x direction and nodes 2 and 4 are given a velocity of -1 in the x direction, then the element deforms but the velocity gradient of the element is zero. Because the velocity gradient is zero, the element does not develop stresses to oppose the velocities and element may continue to deform in this mode without resistance.

One method of resisting hourglassing modes in to use a viscous damping or a small elastic stiffness capable of stopping the formation of the hourglass modes but having a negligible effect on the stable global nodes. The hourglassing resisting force for a particular node in a particular coordinate direction is dependant to the nodal velocity in that direction. The resisting force in solid elements is given by:

$$f_{i\alpha}^k = a_h h_{i\alpha} \Gamma_{ak} \quad (53)$$

where:

$$a_h = Q_{hg} \rho V_e^{2/3} \frac{C}{4} \quad (54)$$

$$h_{i\alpha} = \sum_{k=1}^8 X_i^k \Gamma_{ak} \quad (55)$$

in which:

α = number of hourglass mode.

$\Gamma_{\alpha k}$ = hourglass shape vectors.

X_i^k = velocity of node k in I direction.

V_e = element volume.

C = speed of sound in material.

Q_{hg} = a constant (usually set between 0.15 and 0.55 [reference 102])

Fully integrated element are less susceptible to hourglass deformation but have the disadvantage of increased computing time. In addition fully integrated elements used in the solution of plasticity problems and other problems where Poisson's ratio approaches 0.5 lock up in the constant column bending modes. In certain situations it has been noted [102] that the cost of using fully integrated elements can be justified by increased reliability and if used sparingly may actually increase the overall speed.

3.4.3. Contact Algorithm

Unlike many implicit finite element formulations, elements are not used to define contact within LS-DYNA3D. Contact is defined using contact surfaces. Contact occurs when one segment of a model's outer surface penetrates another segment. With eighteen different contact types available, contact surface within LS-DYNA3D allow the user to represent a wide range of interactions between surfaces. To properly select a contact surface for a given model it is important to understand the different contact algorithms available. There are three different contact algorithms available: Single surface contact, Nodes to surface contact and Surface contact. In this work the surface to surface contact algorithm was used for all models and will be detailed below.

The surface to surface contact algorithm establishes contact when the surface of one body penetrates the surface of another. The algorithm establishes a fully symmetric contact so that the choice of contact and target surfaces are arbitrary. In order to define surface to surface contact, nodal components or part numbers are required for the contact and target surfaces. The surface to surface contact algorithm is generally used for bodies that have large contact areas and the contact surfaces are

known, as in the processes analysed in this work. The algorithm is based on the penalty method.

The penalty method consists of placing normal interface springs between all penetrating nodes and the contact surface. The interface stiffness is chosen to be approximately the same order of magnitude as the stiffness of the interface element normal to the surface. Contact searching is performed in two steps: global and local searching. In a global search the bucket sort method is used. In the bucket sort algorithm, the three dimensional space occupied by the contact surface is divided into cubes (or “buckets”). Nodes can contact any segment in the same bucket or an adjoining bucket. After the global search has located possible contact, a local search checks for penetration. A node to segment algorithm is used to find the penetration. When a slave node penetrates a master surface, a restoring force f_r , proportional to the penetration depth, l , is generated to restore the node to the contact surface in the normal direction, n . the restoring force may be expressed as:

$$f_r = -kln \quad (56)$$

where k is the master surface stiffness which is independently calculated for each contact surface segment from the bulk modulus, the volume and the surface area of the element. The stiffness is expressed as:

$$k = \frac{(SFSI)KA^2}{V} \quad (57)$$

where K is the bulk modulus, A is the surface area and V is the volume of the element. The scale factor, $SFSI$, may be used to control the stiffness and is generally set to a default value of 0.1.

When a penetrating node stays in contact with the target, it may either stick to the surface or slip along the surface. Friction is provided for stick-slip simulation by a tailored algorithm. The relative slip between the master and slave surfaces is calculated by recording the isoparametric co-ordinates and master segment number for every slave node that is in contact with the master surface. Any distance moved by the slave node is treated as a measure of strain and the radial return algorithm is used to return the tangential force to the yield surface.

As mentioned earlier, the penalty method is implemented in a symmetric manner. When the mesh grading varies along the contact surface, or the surfaces are subject to large distortions, the best choice of master surface may vary along the contact algorithm by allowing each surface to act as both the master and slave surfaces.

3.4.4. Friction

Friction in LS-DYNA3D is based on a Coulomb formulation. If f^* is the trial force, f_n is the normal force, k is the interface stiffness, μ is the coefficient of friction and f^n is the frictional force at time n , then:

$$f^* = f^n - k\Delta e \quad (58)$$

where:

$$\Delta e = r^{n+1}(\xi_c^{n+1}, \eta_c^{n+1}) - r^{n+1}(\xi_c^n, \eta_c^n) \quad (59)$$

in which (ξ_c, η_c) are the contact point coordinates and r represents a master segment that has a unique normal whose direction depends continuously on the points of the corresponding master surface segment.

The friction force at time $n+1$ (i.e. f^{n+1}) needs to be determined. This is given by:

$$f^{n+1} = f^* \text{ if } |f^*| \leq F_y \quad \text{or} \quad f^{n+1} = \frac{F_y f^*}{|f^*|} \text{ if } |f^*| \geq F_y \quad (60)$$

where:

$$F_y = \mu |f_n| \quad (61)$$

An exponential function smoothes the transition between the static and dynamic coefficients of friction where v is the relative velocity between the slave node and the master segment:

$$\mu = \mu_d + (\mu_s - \mu_d) e^{-c|v|} \quad (62)$$

where:

$$v = \frac{\Delta e}{\Delta t} \quad (63)$$

where Δt is the time step size and c is the decay constant.

The interface shear stress that develops as a result of Coulomb friction can be very large and in some cases can exceed the ability of the material to carry the stress. In order to help avoid this situation a further limit is placed on the value of the tangential force:

$$f^{n+1} = \min(f_{Coulomb}^{n+1}, \kappa A_{Master}) \quad (64)$$

where, A_{Master} is the area of the master segment and κ is the viscous coefficient.

3.5. *Summary of Chapter 3*

This chapter presents the theoretical methods utilized in the following analyses and explains how they are implemented in the software used to perform the analyses.

Chapter Four

Static Loading Simulation

4.1. Introduction

The finite element method has become a particularly useful tool in analysing the stresses in structures of complex shapes, loading and material behaviour. An overview of its application in orthopaedics during the last ten years has been presented by Prendergast [216]. For a complete and accurate indication of the stresses in the implant, cement and bone, the model must be three-dimensional. In two-dimensional analysis the hoop stresses in the cement and femur cannot be determined. Furthermore, full three-dimensional loads cannot be applied to a two-dimensional model, and with the increasing evidence of the importance of the anterior-posterior component of the hip reaction in the stressing regime of the joint [79], this is a serious shortcoming. This is also one of the limitations of axisymmetric models, since they cannot represent the transfer of the torsional loads acting on the stem, i.e., they cannot differentiate between implants with circular and rectangular cross-sections.

The finite element method enables a great variety of loading conditions and design variables to be changed easily [29] but it is only an approximate method of solution; it represents the object being modelled as a finite number of degrees of freedom. The model will not converge to the solution of the physical structure under consideration however, unless the model is a precise representation of the structure. The accuracy of a finite element model will depend on the type of element used in the model and the fineness of the mesh, and is best evaluated by observing the convergence of the solution as the number of elements defining the problem is increased. This is particularly difficult however, because the number of the nodes is limited to 32,000 in ANSYS software. The model was built with the largest possible number of elements in order to improve the accuracy of the solution.

The question of how many elements are needed to ensure close convergence

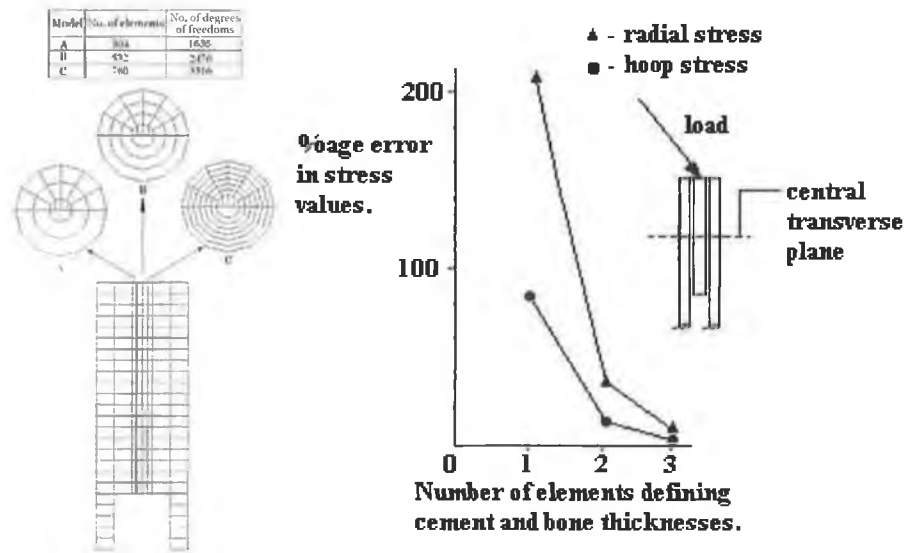


Figure 4.1: A group showing the number of elements against error for the mid-section of a composite beam, after Fagan and Lee [81].

to the true solution is discussed by Zienkiewicz [297]. He suggests that the error in displacement decreases by about a quarter for a doubling of the mesh density. To show that this is approximately true for a finite element model of a bone/cement/metal tube, the results of Fagan and Lee [81] can be quoted. From Figure 4.1 one can see that they show a model of about 3500 degrees of freedom covers to less than 5% for stresses in the mid-diaphysis [73]. The present model of the intact femur has 22,977 degrees of freedom so minimal discretisation error is expected.

4.2. Statement of the Problem

The problem is one of creating a valid model that satisfactorily represents the real structural behaviour of the AHJ system. A balance must be achieved between the complexity of the model and the required results.

The following "model of the AHJ" consists of two parts; firstly the finite element model which gives the stress distributions in the intact femur, and secondly the finite element of the AHJ implanted in the femur. By this one can easily make comparison of the effect of various materials and geometry design of the AHJ on the bone cortex to reach the best design. In this respect this study enables us to study the behaviour of the femoral prosthesis when the stem and cement are manufactured

from a wide range of different materials. From the results, a design aid is developed which estimates the maximum stresses produced in the stem and cement when applied in any material combination. The finite element model is used to provide stress data for the ideal post-operative situation.

4.3. Study of the Stress Distribution in The Intact Femur

The objective here was to generate and validate, by comparison with other validated FE models such as that done by McNamara [179] and Akay [3], a three-dimensional model of the proximal femur for physiological loading conditions in order to study the stress distributions in the intact and treated femur.

4.3.1. F.E. Model of Proximal Femur

A three-dimensional finite element models was generated for this stress analysis by using the ANSYS Software. The essential intact femur geometry was obtained from Istituti Ortopedici Rizzoli (I.O.R.) [97] as an IGES file. This geometry was sectioned parallelly into 79 slices, in which each section contain four splines defining the transverse sections and its surface. This surface model was then 'capped' to form a solid model, which was subsequently sectioned normal to the natural contour of the femur to obtain an appropriate number of sections for mesh discretization. Automatic mesh generation was used to place 24 nodes circumferentially on the external and internal cortices representative of the periosteal and endosteal cortices of the compact bone. The three dimensional elements were placed between every two consecutive slices. 8-noded isoparametric brick elements, 6-noded isoparametric wedge elements, and 4-noded isoparametric tetrahedral elements, Figure 4.2, were used to build two different types of meshing, free mesh and mapped mesh, contains 30,481 elements and 77,31 nodes, and 23,06 elements and 43,69 nodes respectively. The total length of the femur diaphysis was 378 mm and the typical cross-sectional dimension (medial-lateral) was 34 mm. The geometry contained Linea Aspera on the posterior side and the femur displayed a noticeable bow in the anterior-posterior plane. As shown by Pauwes [205], the position of the linea aspera is such as to create minimum resistance to bending [205]. Figure 4.3 illustrates that, when it is oriented in the bending plane, stresses in the bone are

higher. However, when it is oriented approximately 40 degrees to it, the stress is reduced because its position provides further evidence of the functional adaption of bone. Due to its small contribution to the bending stiffness of the overall bone subjected to this type of loading configuration, the spongy bone in the medullary canal was not modelled.

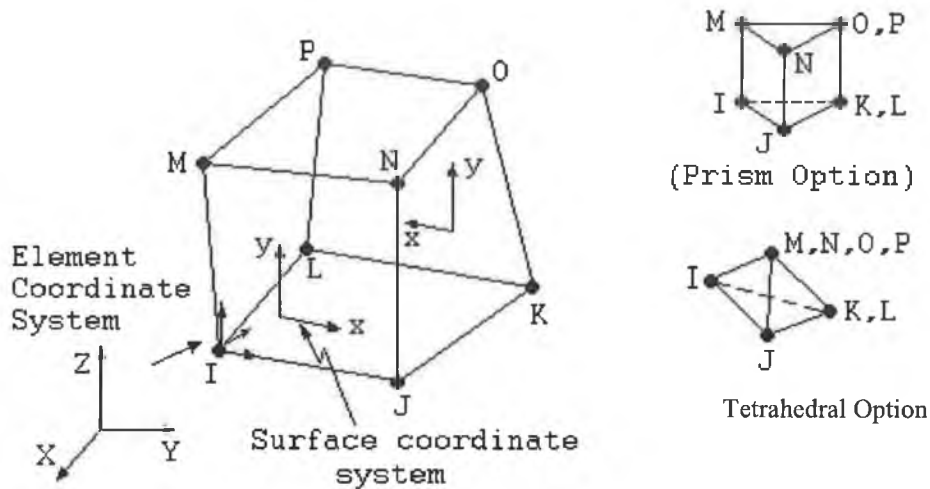


Figure 4.2: SOLID45 is used for 3-d modeling of solid structures. The element is defined by eight nodes having three degrees of freedom at each node: translations in the nodal x, y, and z directions.

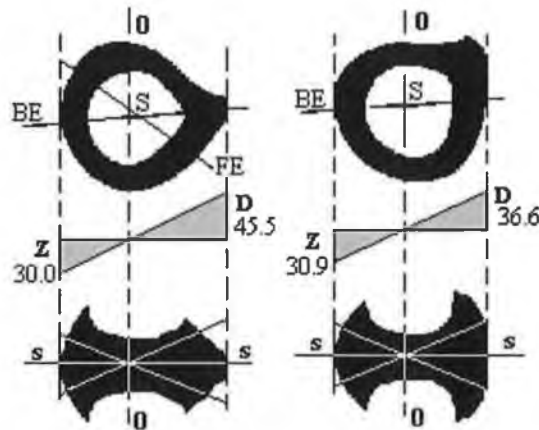


Figure 4.3: A diagrammatic representation of the difference in the resistance to bending of the femur with (i) the linea aspera in the bending plane and (ii) the linea aspera orientated 40 degrees to the bending plane. Maximum stresses are 45.5 [kg/cm²] and 36.6 [kg/cm²] respectively, [205].

The bone cortex was one element thick in each model. Figure 4.4 shows the generated 3-D mesh for the intact femur diaphysis. The respective number of degree of freedom were 22,977 for the model meshed with free mesh SOLID 45, and 12,891 for the mapped mesh of SOLID 45.

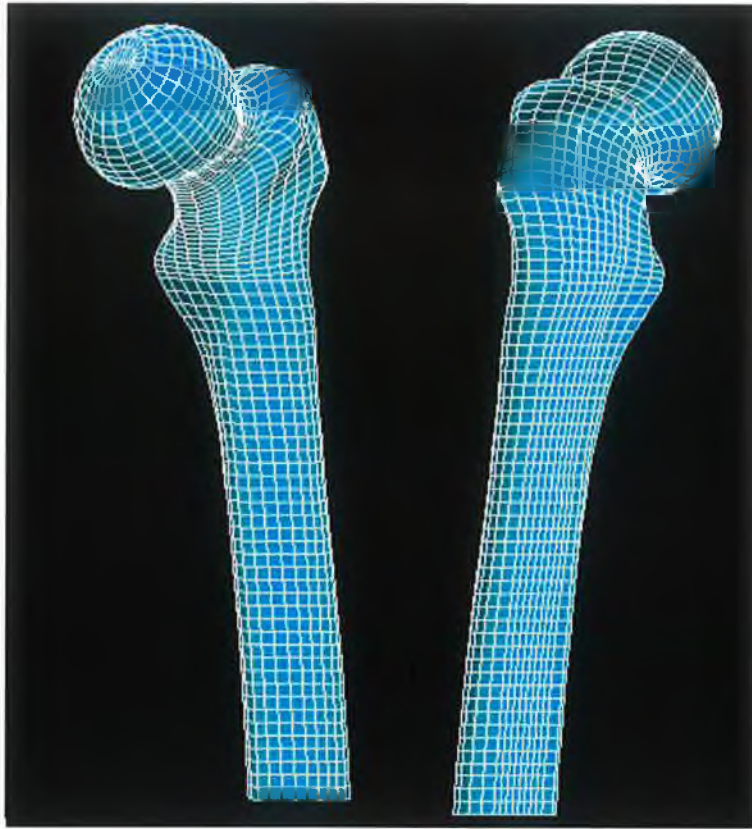


Figure 4.4a: Shows the proximal femur meshed with 8-noded isoparametric brick elements.

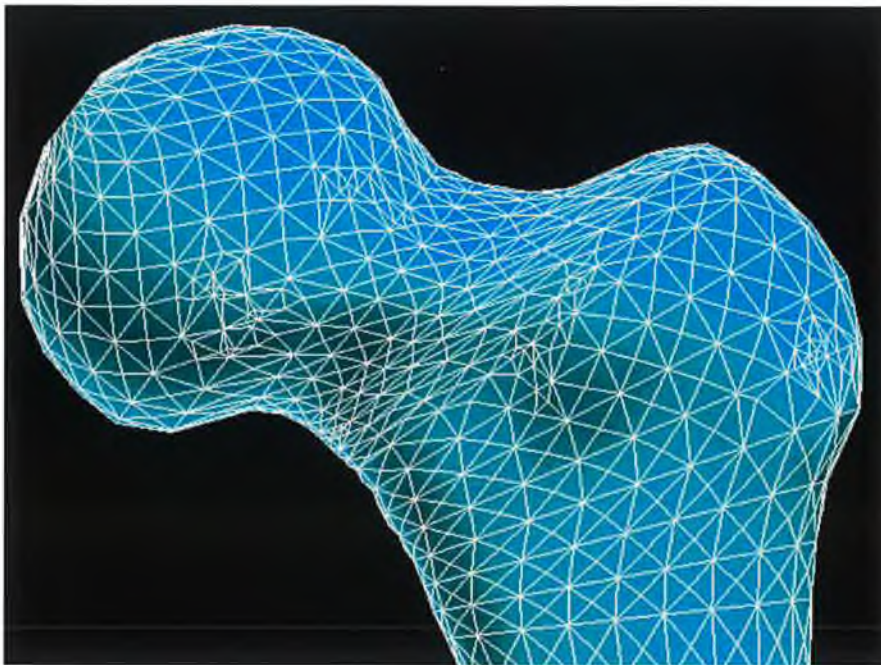


Figure 4.4b: shows the head and the neck of the femur meshed with 6-noded isoparametric prism elements and 4-noded tetrahedral elements.

4.3.2. Material Properties

Human bone is an anisotropic and heterogeneous material [3, 177], which means that its properties depend on the direction and location. In this study the compact bone was assumed as a linear elastic continuum with isotropic properties. The Young's modulus of 16.2 GPa and Poisson's ratio of 0.36 were chosen as representative of bone [219], tested with low / static strain rate $2 \times 10^{-5} \text{S}^{-1}$. The modelling of the cancellous bone was excluded for simplification as tests conducted on cadaveric specimens [170] showed that when the material is modelled as homogenous, the absence of cancellous bone will only minimally affect the stiffness and failure mode of the femur. Theoretical calculations to establish the contribution of the cancellous bone to the system were made for the worst case scenario, i.e., based on a cross sectional profile with minimum cortex thickness and maximum medullary canal size, as found at the greater trochanter level, using the modulus value for the polyurethane foam as documented by the manufacturer. These calculations showed that a maximum error of 1% would occur for a pure compression load while a maximum error of 0.5% would be introduced in a pure bending situation when ignoring the spongy bone. Noting that the strains generated in the femur are mainly due to bending, the magnitude of the error introduced by not modelling the cancellous bone is likely to be minimal.

4.3.3. Loading

As in geometry modeling of the femur one difficulty is the anatomical variation between individuals. A further difficulty is the difference in activity patterns and also that activity patterns may change after hip replacement [200]. However, for the purposes of stress analysis, we do not have to deal with the full complexity because we are only interested in those loads that generate fatigue cycles; namely those generated during gait.

Extensive work on the forces transmitted to the hip during gait has been carried out by Paul [199]. Figure 4.5 shows that the magnitude of the load is up to 4.2 times body weight, which is roughly 3 kN, for a 70 kg person.

For faster walking, larger steps are being taken, loading levels increased considerably. Figure 4.6 shows a schematic diagram of the muscles attached to the

proximal femur from which its complexity can be appreciated.

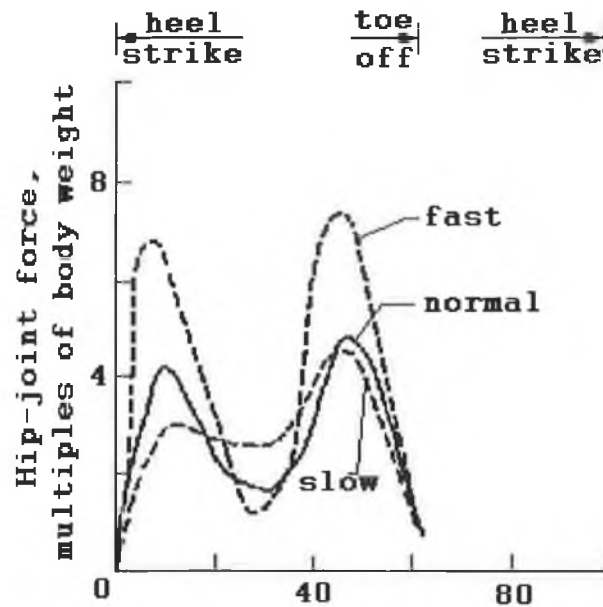


Figure 4.5: Loads on the hip during gait [200].

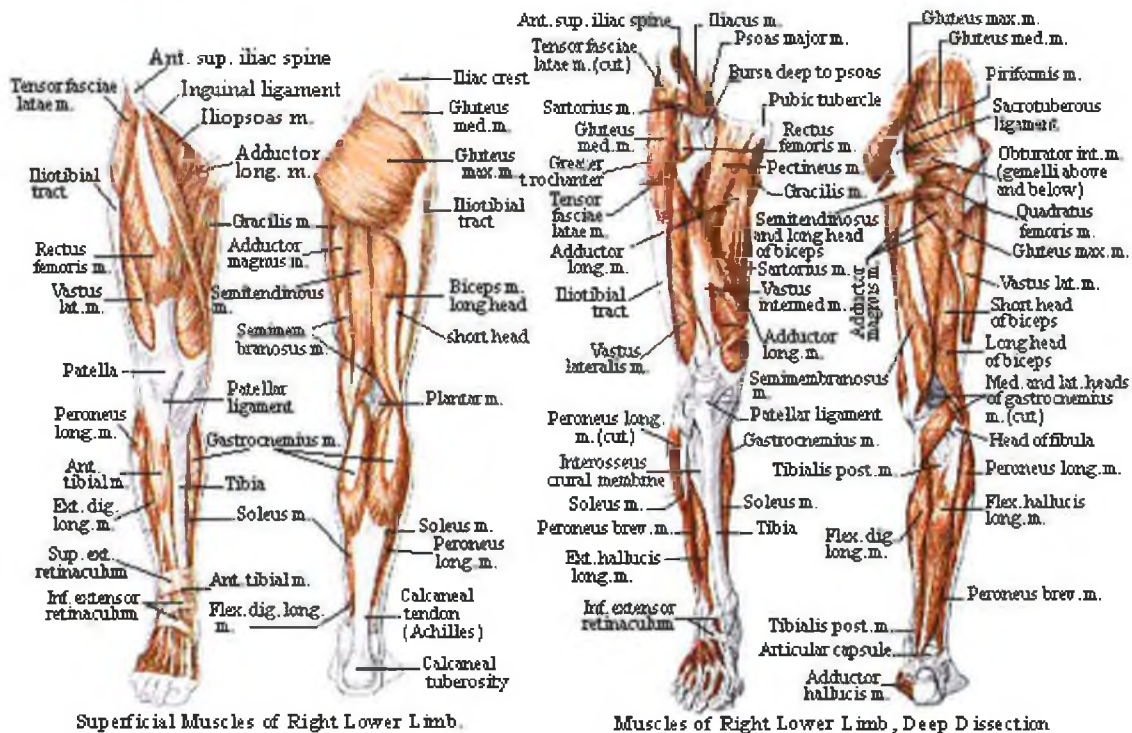


Figure 4.6: Two views of the Lower Limb show the anatomical features and muscle groups [309].

There is another set of ligaments that connect directly from the iliac crest of the acetabulum to the tibia via the greater trochanter. According to Dowson [68] there are some 22 muscles acting to move the femur, in the present finite element

model we only include two; the abductor muscle group (gluteus medius and gluteus minimus) and the ilio-tibial tract. They act to prevent medial tilt and so stabilises the torso during the one-legged stance phase of walking. The results of McLeish and Charnley [176] can be used to estimate the muscle loads. In one of their plots they show that, for a zero degree pelvic angle, the applied load is at approximately 20 degrees to the shaft of the femur. For the same pelvic angle the abductor muscle load is 1.5 times body weight. Using the same body weight as above, this gives a load of approximately 1.15 kN. The ilio-tibial tract load used is 0.25 kN [81, 255]. The results of Rohlmann et al. [226] show that it is important in that it reduces bending of the bone implant structure. Greater ilio-tibial tract forces slightly reduce medial cement compression and lateral prosthesis tension. Furthermore their results do not show the calcar femur stress to be greatly effected by muscle loading.

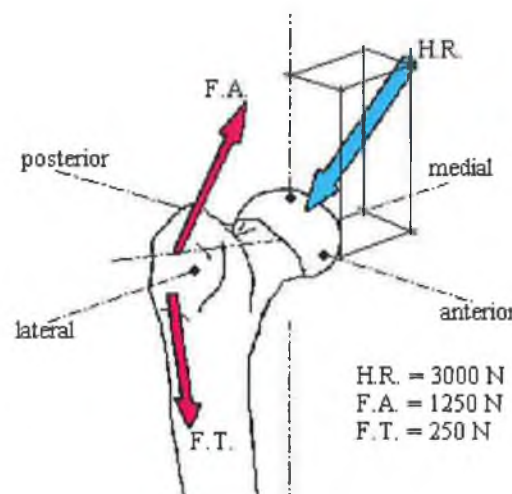


Figure 4.7: Schematic diagram of muscles and hip reaction considered to be acting on the upper femur while walking. **H.R.:** represents the hip-reaction, **F.A.:** represents the abductor muscles and controls the stability of the joint in the coronal plane. **F.T.:** represents the ilio-tibial band that runs from the epicondyles via the greater trochanter to the pelvis.

The point loads applied to the nodes of the finite element model must be such as to do the same work to the structure as the known distributed load. Alex Lennon suggested if there is no interest in studying the stresses in the head (ball) of the implant, then it is sufficient to use a concentrated load on a single node, providing the correct position and line of action is modelled. For the muscles, however, it is usually better to distribute the forces over a number of nodes, especially if there are regions of interest nearby. This is because the attachment of the muscle to the bone can have quite a significant area, and, if modelled as a point load, will lead to

overprediction of stress near the muscle attachment [155]. Point loads representing the body weight were applied over two nodes on the head region, and that representing abductor muscles and iliotibial-tract load were applied over ten nodes for each on the greater trochanter. The schematic diagram of the loading applied to the finite element model is shown in Figure 4.7.

4.3.4. F.E. Model Validation

As a first step, it is important to validate the results of our model to grantee that the subsequent results are close to the reality. For this reason McNamara's Model [179] was selected as a first reference for comparing the results. Consequently, the present model was simulated with the same material and load conditions as that of McNamara who suggested that the material properties were homogeneous and linear elastic (Young's modulus equals to 14.2 GPa and Poisson's ratio equals to 0.3). The distal end of the diaphysis was constrained, and the head of the femur was loaded at an angle of 28° with a load of 1976 N and the abductor-muscle load of 1240 N was applied at an angle of 40° . As mentioned previously two types of mesh are used whereas the reference model was meshed only with 8-noded isoparametric brick elements. The reason for selecting two types of meshing is to attempt to approach the exact result of that of McNamara.

In spite of the fact that all parameters used by McNamara have been applied to the present model, there is one parameter we can not change which is the dimensions of the intact femur of the present work. This will cause the results here to be different than these of McNamara as shown, Figure 4.8. It can be noted that the maximum value of axial strain at the lateral side is at the end of the femur diaphysis (shaft) and the beginning of the greater trochanter and then the axial strain becomes decrease along the diaphysis in the distal direction. Also, it is clear that the F.E. axial strain results of McNamara in the lateral side is close to that meshed with hexahedral elements of the present work.

The axial strain distribution of the medial intact femur of hexahedral elements of the present work is, also, close to that result from numerical analysis of McNamara work. Whereas the maximum axial strain is located in the calcar region of both models.

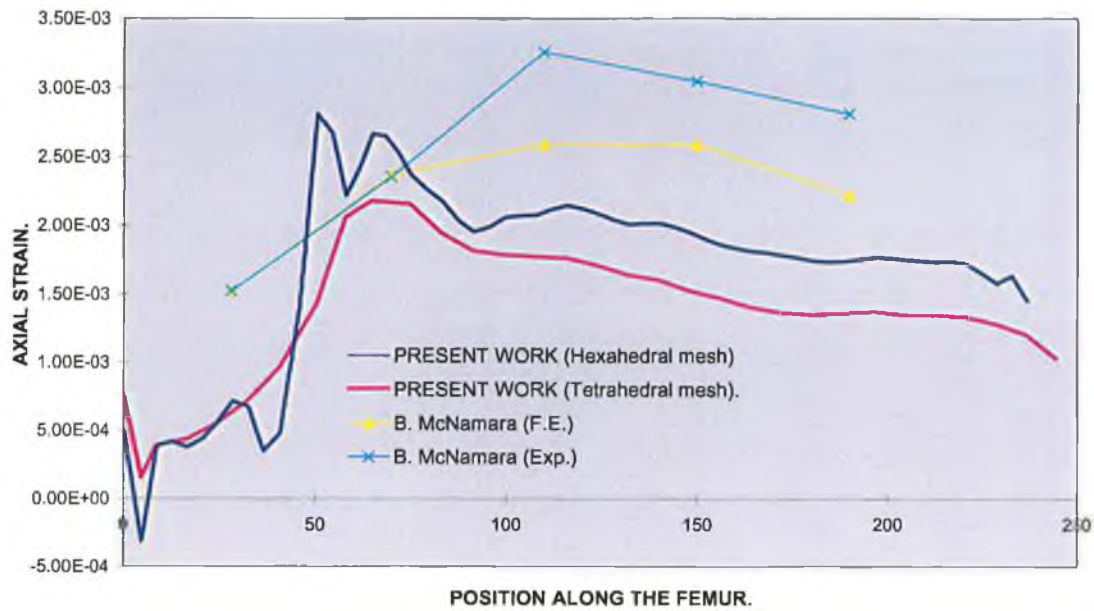


Figure 4.8a: Comparison between the present work and b. McNamara results. This graph shows the axial strains in the lateral side of the intact femur.

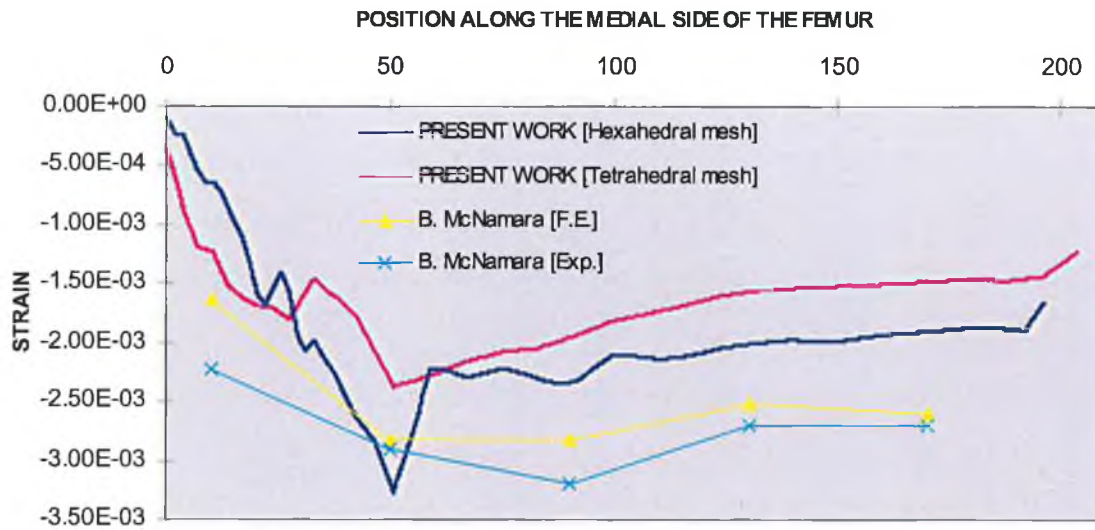


Figure 4.8b: Comparison between the present work results and b. McNamara's results. This graph shows the axial strains at the medial side of the intact femur.

Eventually, a comparison was also made between these results and other published results [3, 50, 73, 194] by using the same material and load conditions as mentioned above. The literature data were adjusted for the magnitude of the loading to make the comparison possible. However, it was not possible to make adjustments for the loading angle variations; therefore these strains are only an approximation,

Figure 4.9. Some of the femurs [73] were loaded with 450 N at an angle of 20° to the shaft of the femur, and the others [3, 60, 194] were loaded at levels of 3000 N, 1012 N and 1000 N with angles of 20° , 15° , and 20° , respectively. The magnitude and the trends of the strains on the medial bone are comparable to those determined by Akay [3] (which is close to the results obtained using tetrahedral elements), Crowninshield et al. [60] (which is close to the results obtained using tetrahedral elements) and by Oh and Harris [194] (which is close to the results obtained using hexahedral elements); also if we take the average values of the two curves of Engelhardt and Saha [73], we can get a curve close to the present work.

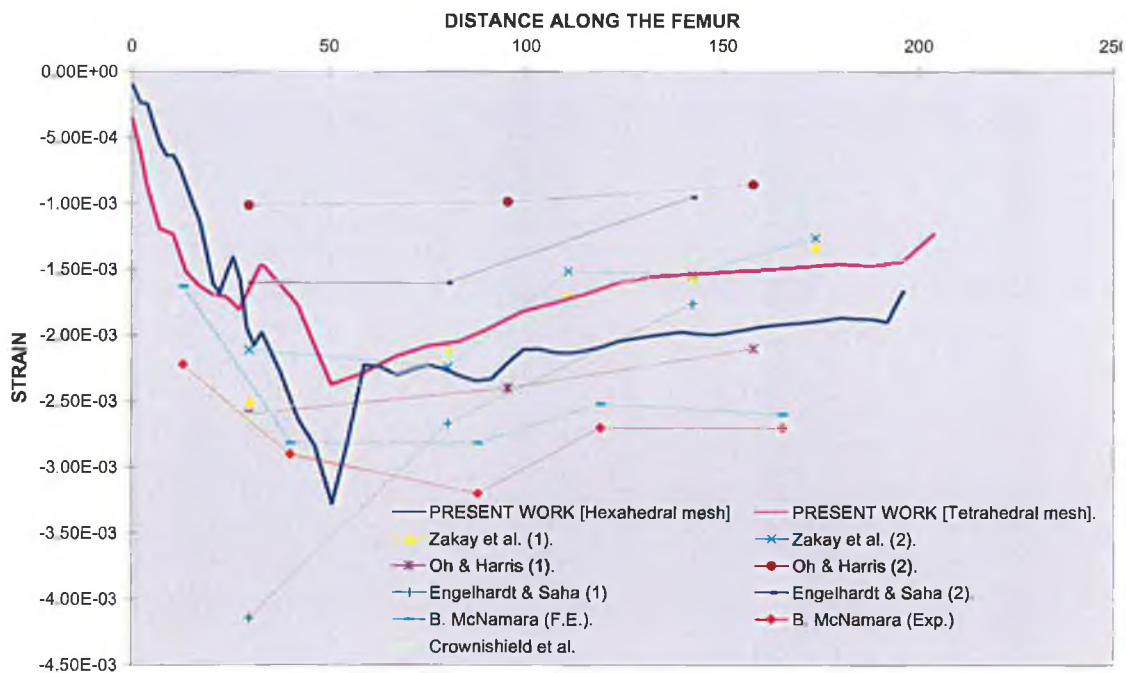


Figure 4.9: Comparison between results of the present work and some published results. this graph shows the variation of strains along over the medial side of an intact femur.

Among these comparison one could conclude that the strains recorded by Akay [3] is close to that obtained using tetrahedral elements, and the strains recorded by Oh and Harris [194] is close to that obtained using hexahedral elements; whereas, the strains recorded by McNamara [179] agree in the calcar region but deviate significantly in the distal region. This deviation may be due to the difference in the geometry dimensions of the intact femur model.

It should be noted that the strain distribution for two femurs of the same

individual (left and right) will be different. Akay and Aslan [3] showed some discrepancy of the strains among individual synthetic intact femurs subjected to the same loading conditions. Szivek and Gealler [256] with the same kind of femurs found a variation of 16 percent among the readings, whereas the strain measurements conducted with the cadaveric femurs produced very high variations, sometimes up to 100 percent. Other works [4, 11] also show significant variations among the strains from different cadaveric femurs (see Fig. 4.9).

4.3.5. Results

Representative strain/stress data for the proximal part of the intact femur when subjected to a force of 3 kN applied vertically to the head with an angle 20° of adduction, abducting force of 1.25 kN applied at an angle of 20° to the vertical over the proximal area of the greater trochanter, and iliotibial-tract load of 250 N applied parallel to the shaft of the femur in a distal direction are shown in Figures 4.10 to 4.15.

Strains/stresses were higher in compression on the concave side than in tension on the convex side and were greater in the coronal plane, Figures 4.10, 4.11 and 4.15, than in sagittal plane, Figure 4.12 and 4.13, and this agrees with Oh et. al. [194], Engelhardt et al. [73] and Aky et al. [3], whereas McNamara et al. [179] when applied only a resultant force on the femur head, second case, found the same results but generally he concluded that the strains on the coronal plane is the greatest.

The distal portion of the posterior part of the neck of the femur was under tension with this loading conditions and the posterior part of the femur distal to the lesser trochanter showed compressive axial strain/stress, as expected from the normal concavity of the posterior aspect of the femur. While in the anterior side there is small fluctuation in the nick but it could be considered as predominately subjected to a compressive axial strain/stress.

These results will be so useful later on when we implant a prosthesis to a femur in the purpose of comparing the stresses/strains distribution round the femur in order to improve the prosthesis design parameters and in study the effect of prosthesis fixation (stress shielding) in attempting to reach to be close to the

stresses/strains distribution of the intact femur. And also to study, for example, the remodelling phenomenon due to stress shielding, McNamara [179] and Prendergast [214].

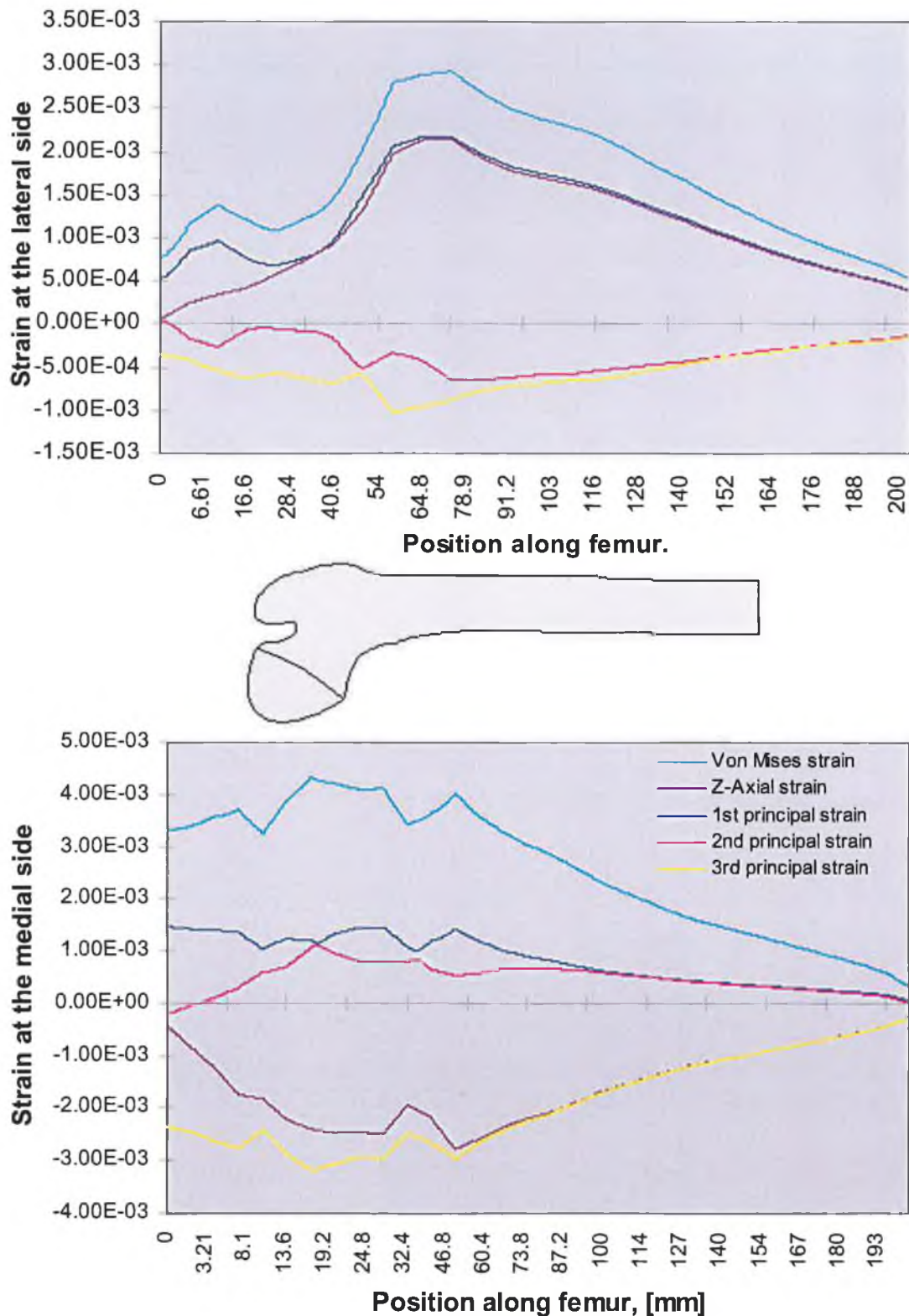


Figure 4.10: The distribution of the predicted strains in the lateral and medial cortices (frontal plane).

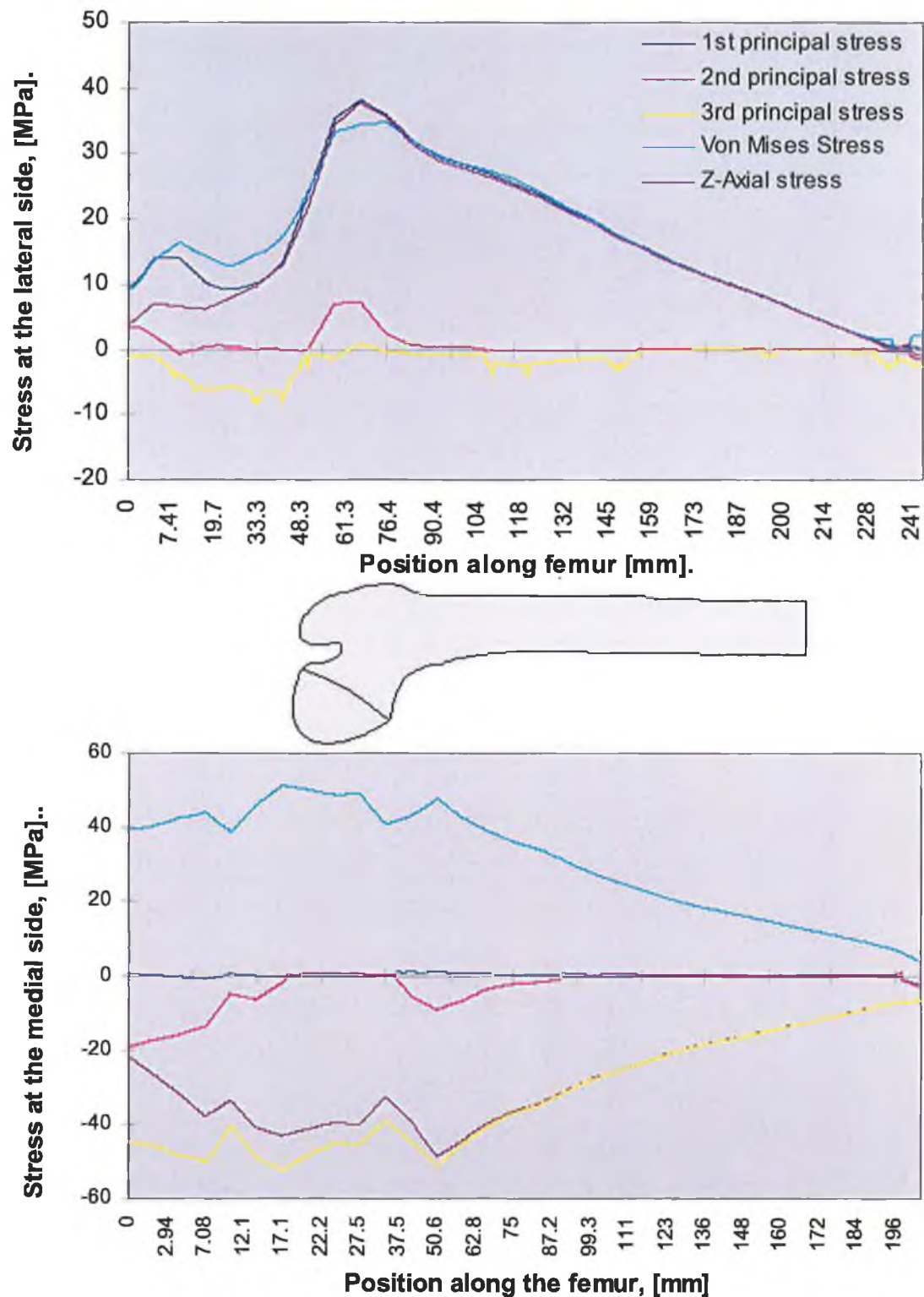


Figure 4.11: The distribution of the predicted stresses in the lateral and medial cortices (frontal plane).

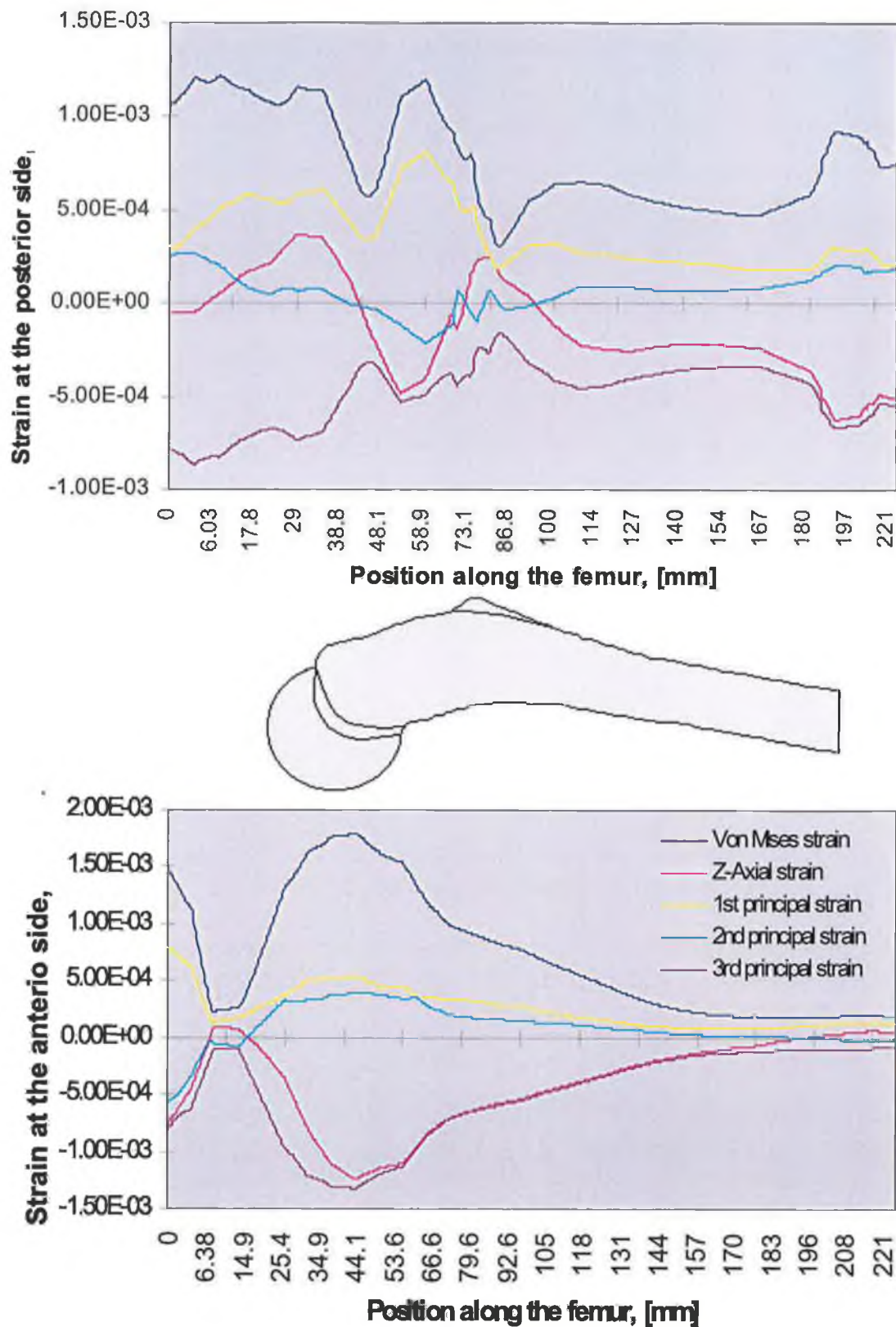


Figure 4.12: The distribution of predicted strains in the anterior and posterior cortices (sagittal plane).

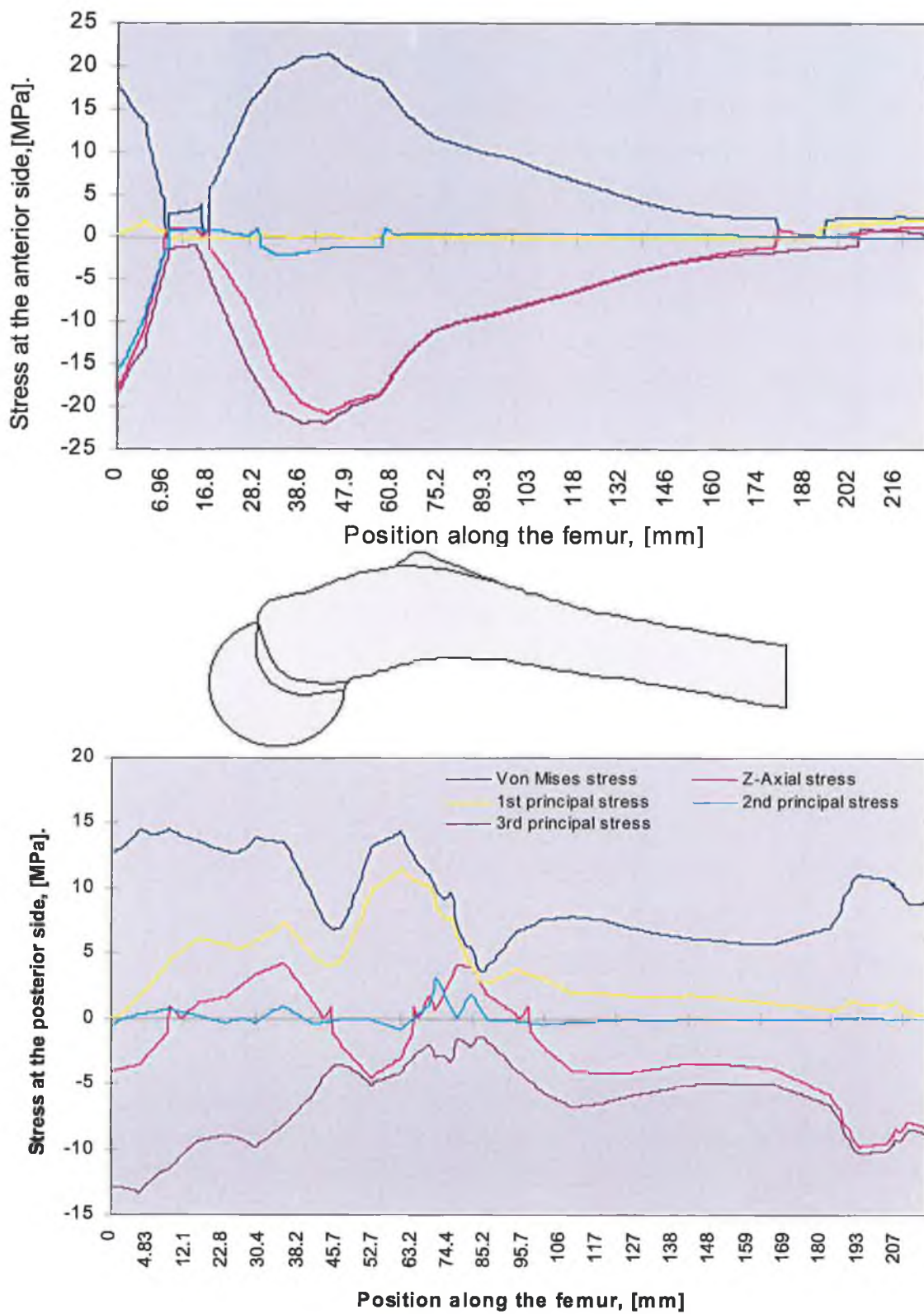


Figure 4.13: The distribution of predicted stresses in the anterior and posterior cortices (sagittal plane).

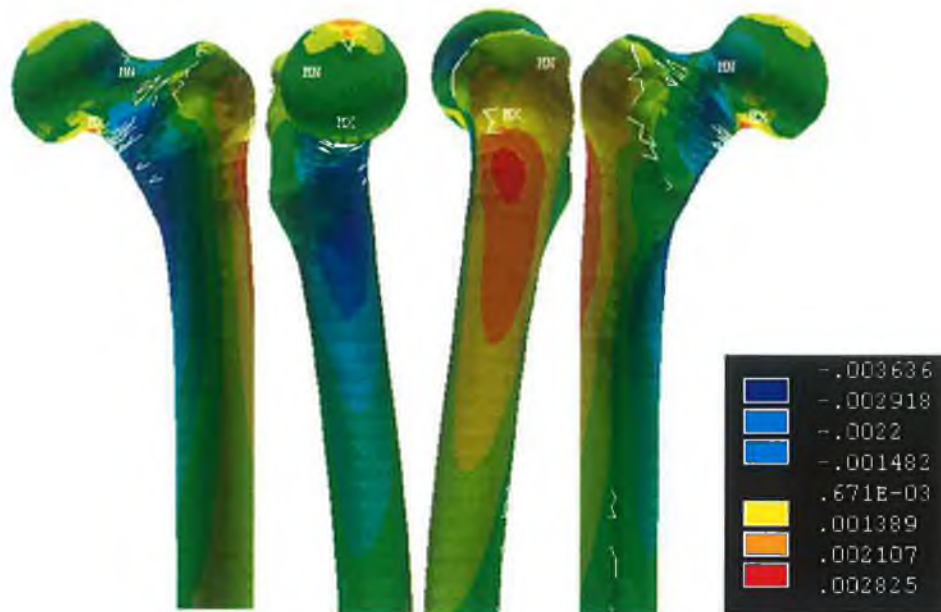


Figure 4.14: The Z-axial proximal femur strain contours. Note that the maximum strains are located in the proximal neck region and this will be so clear in Figure 4.15.



Figure 4.15: The Von Mises proximal femur stress contours shows maximum stresses/strains are located in the proximal neck region.

4.4. Finite Element Stress Analysis of the AHJ

4.4.1. Introduction

This section reports on a finite element stress analysis of the AHJ. The purpose was to develop principles, which could be used as a basis for future hip prosthesis or future design modifications.

The finite element method is used in this section as a tool of structural analysis rather than of structural design since consecutive analysis are used only to accumulate information, the decisions about design changes being left until later. It is not the intention, therefore, to directly develop a new design; the intention is rather to investigate a set of variables within which an optimal design can be found.

In the following sections of this chapter, the effect of materials properties are investigated, together with a study of the prosthesis collar since it is a disputed aspect of prosthesis design. Prosthesis length and thickness are considered because they are design variable which have an observed effect on failure.

4.4.2. Geometry modelling

4.4.2.1. Treated Femur Implanted by AHJ

The same finite element model mentioned in section 4.3.1 was used again here after removing a cavity for the purpose of modelling the AHJ, Figure 4.16. The prosthesis stem was neutrally placed within the medullary canal and encompassed by one layer of elements which represent cement mantle, Figure 4.17. The space between the cement mantle and the inner surface of the femur has been filled with elements that represent the cancellous bone and meshed by the 4-noded isoparametric tetrahedral elements. The rest of the model was meshed with 8-noded isoparametric brick elements. This type of element is characterised by six degrees of freedom at each node. This model contains 11,726 elements, which resulted in 4,118 nodes. The geometry of the bone still contained Linea Aspera on the posterior side and the femur displayed a noticeable bow in the anterior-posterior plane.



Figure 4.16: Finite element modelling of the treated femur.

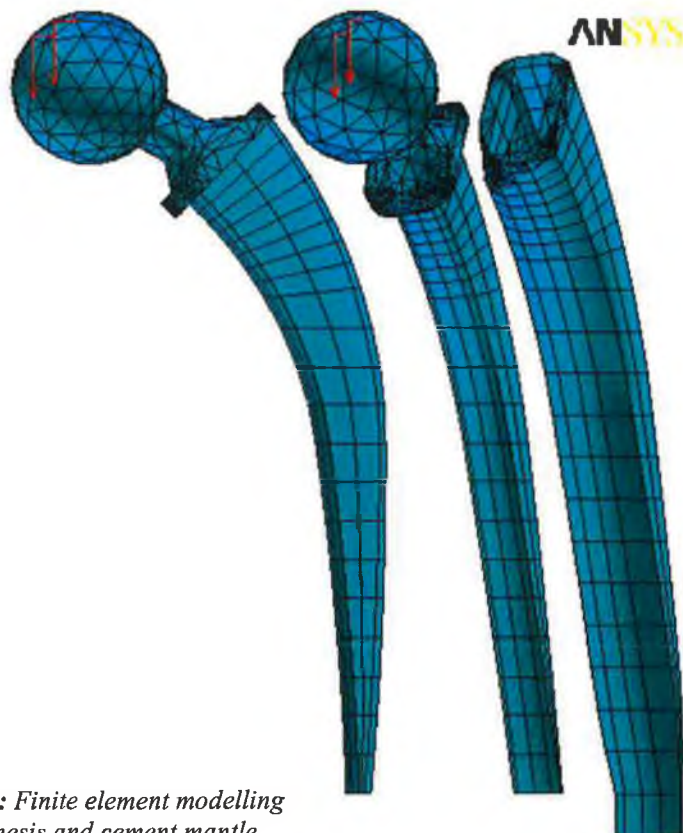


Figure 4.17: Finite element modelling of hip prosthesis and cement mantle.

4.4.2.2. Loading and Restraints

The head prosthesis was loaded at an angle of 20° with a load of 3 kN, which approximates the peak gait load for a 70 kg person during normal walking [200]. An abductor muscle load of 1.25 kN was applied at an angle of 20° to the vertical over the proximal area of the greater trochanter. An ilio tibial-tract load of 250 N was applied parallel to the shaft of the femur, in a distal direction. Restraints were applied to the femur at the distal end.

4.4.2.3. Material Properties

It is easy to change material properties in finite element model. Parametric analysis is limited only by computer time and storage space. Human bone is an anisotropic and heterogeneous material [3], which means that its properties depend on the direction and location. In this study the compact bone was assumed as a linear elastic continuum with isotropic properties. A Young's modulus of 16.2 GPa and Poisson's ratio of 0.36 were chosen as representative of bone [219], tested with low / static strain rate $2 \times 10^{-5} \text{S}^{-1}$. Concellous bone stiffness was taken as 32 MPa.

The prosthesis stiffness values represent a range for four materials varied between 25 GPa and 400 GPa:

- a) Particulate reinforced polymer composite, $E = 25 \text{ GPa}$ and $\nu = 0.35$ [113].
- b) Titanium alloy, Ti-6%Al-4%V, 100 GPa and $\nu = 0.30$ [113].
- c) Chromium cobalt alloy, CoCr, 196 GPa and $\nu = 0.29$ [81].
- d) Alumina ceramic, $E = 400 \text{ GPa}$ and $\nu = 0.24$ [112].

The cement Young's modulus is varied between 2 GPa and 5 GPa representing a rang of material properties for:

- a) Unreinforced PMMA, $E = 2.0 \text{ GPa}$ and $\nu = 0.30$ [110].
- b) Bone particle reinforced PMMA, $E = 2.3 \text{ GPa}$ and $\nu = 0.23$ [197].
- c) Fibre reinforced PMMA, $E = 3.0 \text{ GPa}$ and $\nu = 0.25$ [210].
- d) Preform mesh reinforced PMMA, $E = 5.0 \text{ GPa}$ and $\nu = 0.25$ [182, 258].

4.4.3. Global Stress Results

The results presented in this section are for AHJ combination of 196 GPa and 2.3 GPa for the prosthesis and cement mantle materials, respectively. Because it was

focused in the failures occurred in the prosthesis stem, stresses in the prosthesis head and neck are not reported even though failures do happened there [161].

4.4.3.1. Prosthesis Stem

The stress contours in the prosthesis stem surface are shown in Figures 4.18 and 4.19. Bending is the primary deformation mode in the prosthesis stem. It causes lateral bending stresses of up to 155.7 MPa and a medial compressive stress of up to 175.7 MPa. Note that the both values of von Mises and principal stress in the mentioned Figures are close. Fatigue cracking is most likely to initiate at the site of maximum principal stress, which dominate the middle region of the stem. Cracks can be initiated from large pre-existing defects such as shrinkage cavities in cast prosthesis [90] in which case the propagation direction will be horizontal on the lateral side of the prosthesis.

4.4.3.2. Cement Layer

The stress in the cement mantle is more complex than that in the prosthesis stem. Figures 4.20 and 4.21 show the stress distribution in the cement created by a combination modes. The dominant deformation mode is bending, generating medial compressive and lateral tensile stresses. The cement is also deformed in shear since the prosthesis-cement interface is pushed distally by the prosthesis stem. Furthermore, the cement layer is deformed radially outwards because of the wedging effect of the tapered prosthesis stem, generating hoop stresses.

As Figure 4.22 shows, this principal stress is in the axial direction and would cause cracks to initiate and grow in the lateral to the medial direction. And, also, it shows that these principal stresses are tensile and in the hoop direction. They would cause crack growth to be in the proximal to distal direction.

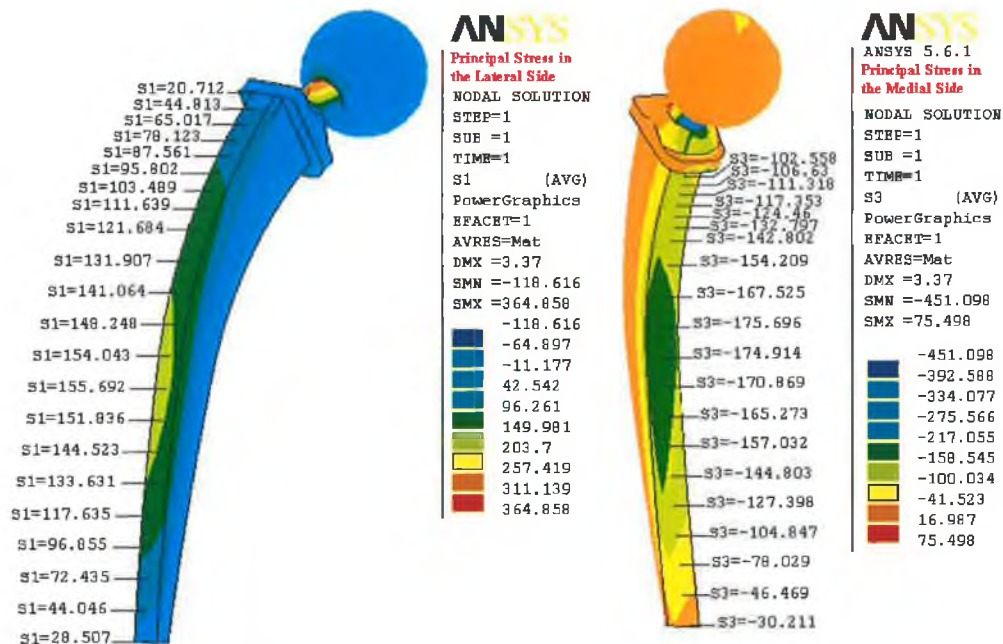


Figure 4.18: The principal stress contours, in MPa, in the hip prosthesis.

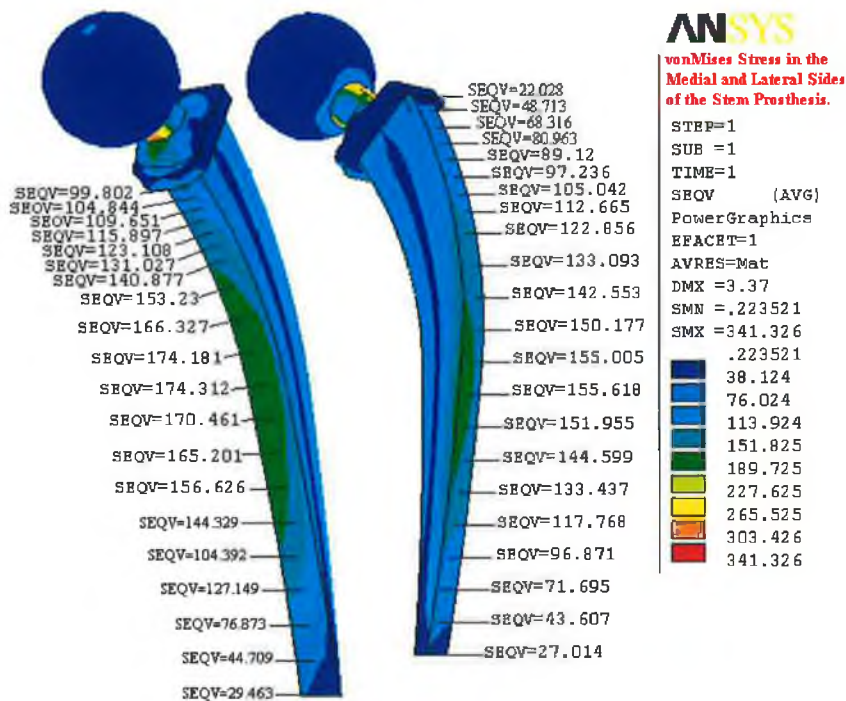


Figure 4.19: vonMises stress contours, in MPa, in the hip prosthesis.

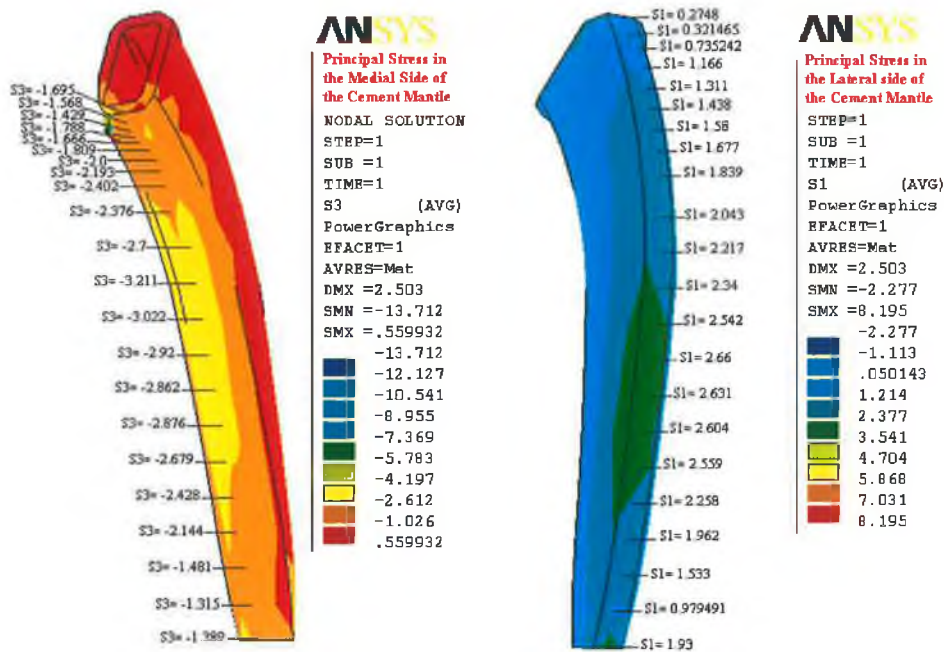


Figure 4.20: The principal stress contours, in MPa, in the cement mantle.

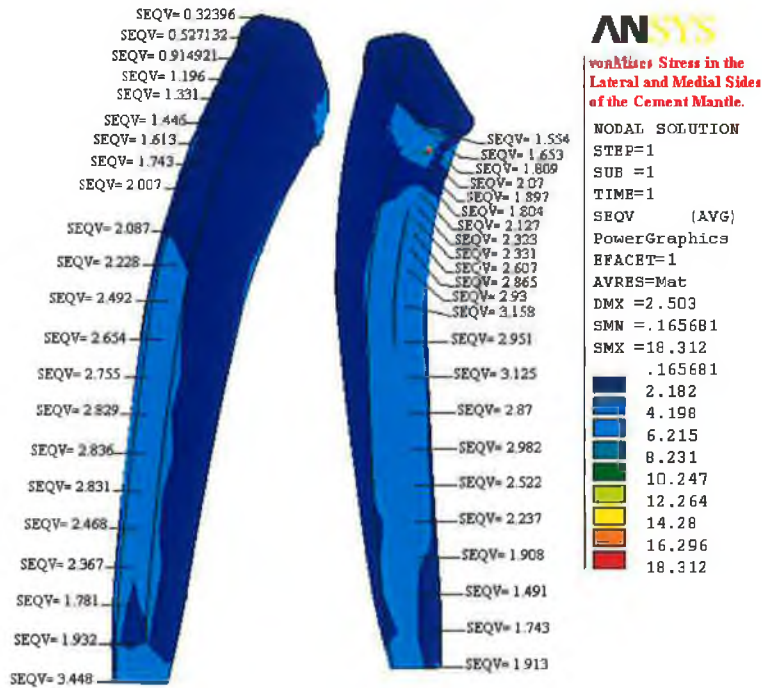


Figure 4.21: vonMises stress contours, in MPa, in the cement mantle.

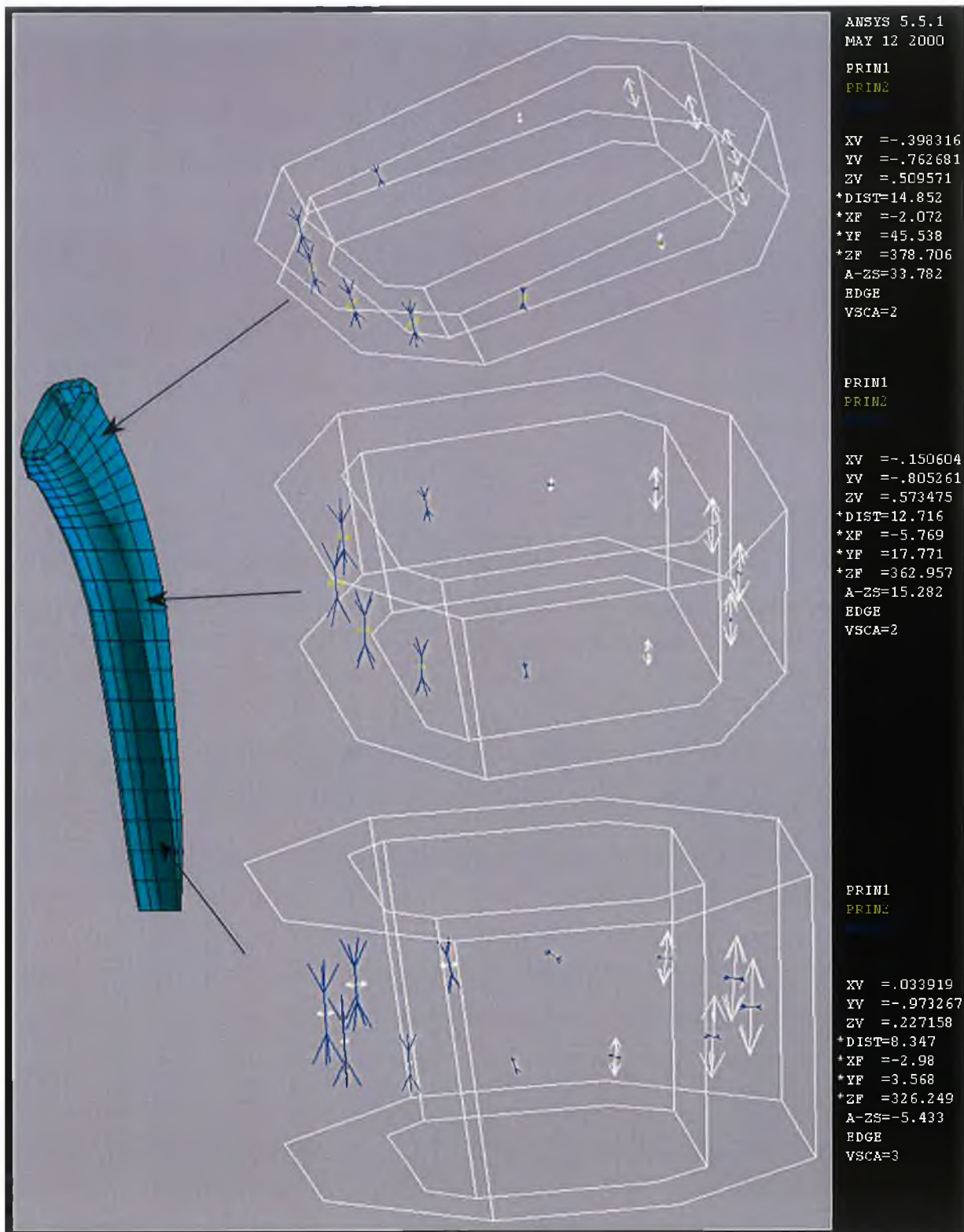


Figure 4.22: Tensile, compressive, and hoop stress vectors across three sections of the cement mantle.

4.5. Parametric Analysis

The results of this section are divided into three parts; firstly the effect of different material properties, mentioned in section 4.4.2.3, are reported aiming to represent this in a mathematical model; secondly effects of design features of AHJ.

4.5.1. Material Selection in the Design of the Femoral Component of Cemented Total Hip Replacement

4.5.1.1. Introduction

A wide range of materials is now available which may be suitable for use in artificial hip joint prostheses, as reviewed by Bonfield [28]. The Young's modulus of the prosthesis material is a critical design variable because, for a given stem geometry design, it largely determines how the load is transferred, via the cement, to the bone.

Prostheses may be used with or without a cement layer to interlock the prosthesis stem into the bone. However, cement is still used in the majority of operations. Reinforcement of the cement has been proposed to increase its strength and toughness; this will result in an increased Young's modulus. To pursue the reinforcement approach, quantitative values for stress within the cement layer are required, because if the cement becomes stiffer, as it will if it is reinforced in some way, then stress in the cement will also increase. However, imagine a situation where the cement becomes stiffer but the toughness does not increase – in this case the Factor of Safety (FOS) in the cement will reduce and the situation will be worse. In this way, if we reinforce the cement, one must make sure that the increased toughness is enough so that the FOS increases. Therefore, the extent by which cement stress increases due to increased cement stiffness must be quantified to ensure that it does not offset the benefits of increased cement toughness. Also, to improve the long-term survivability of the femoral component of cemented total hip replacements, the manufacturers of hip systems are constantly assessing new materials for use in the femoral stems and the cement. Although the individual constituents may appear to have satisfactory mechanical properties, it is not until the composite structure of the bone, cement and stem is analysed, that the true merits of

any new materials can be assessed. This may be achieved by laboratory experiments, where the stresses at a limited number of locations in the stem or bone are recorded, or it may be performed, potentially more thoroughly, using a finite element model. In this section the behaviour of the femoral prosthesis was examined when the stem and cement are manufactured from a wide range of different materials. From the results, a design aid is developed by creating a mathematical model to facilitate the estimation of the maximum stresses produced in the stem and cement when it applied in any material combination.

4.5.1.2. The Effect of Prosthesis Materials on Prosthesis Stresses

Figure 4.23 shows the variation of maximum and minimum principal stresses in the prostheses, which occur at the prosthesis/cement interface, as a function of prosthesis Young's modulus for different artificial hip joint structures. It is obvious that for all AHJ structures the maximum stresses occur medially, for the lower stiffness of 25 GPa (polymer composite) prosthesis the maximum stress is in the neck region under the collar (in the spigot) whereas for the higher stiffness the maximum stress is in the middle third of the stem. Also, one can see that the prosthesis of the lowest Young's modulus behaves as a composite beam.

4.5.1.3. The Effect Cement Materials on the Prosthesis Stresses

Figure 4.24 shows the effect of cement stiffness on the prosthesis stress pattern. The effect of the cement stiffness on the prosthesis stress is very small especially for that of higher Young's modulus where its effect becomes negligible. It is more pronounced on the polymer composite prosthesis. The higher bone cement stiffness the lower the polymer composite prosthesis stresses. The reduction in the polymer composite prosthesis principal stresses, due to increasing the cement stiffness, reaches to about 9% in the proximal stem third. But this effect is negligible in the distal third of the same prosthesis. However the effect, although systematic, is not very significant due to the small stress changes involved.

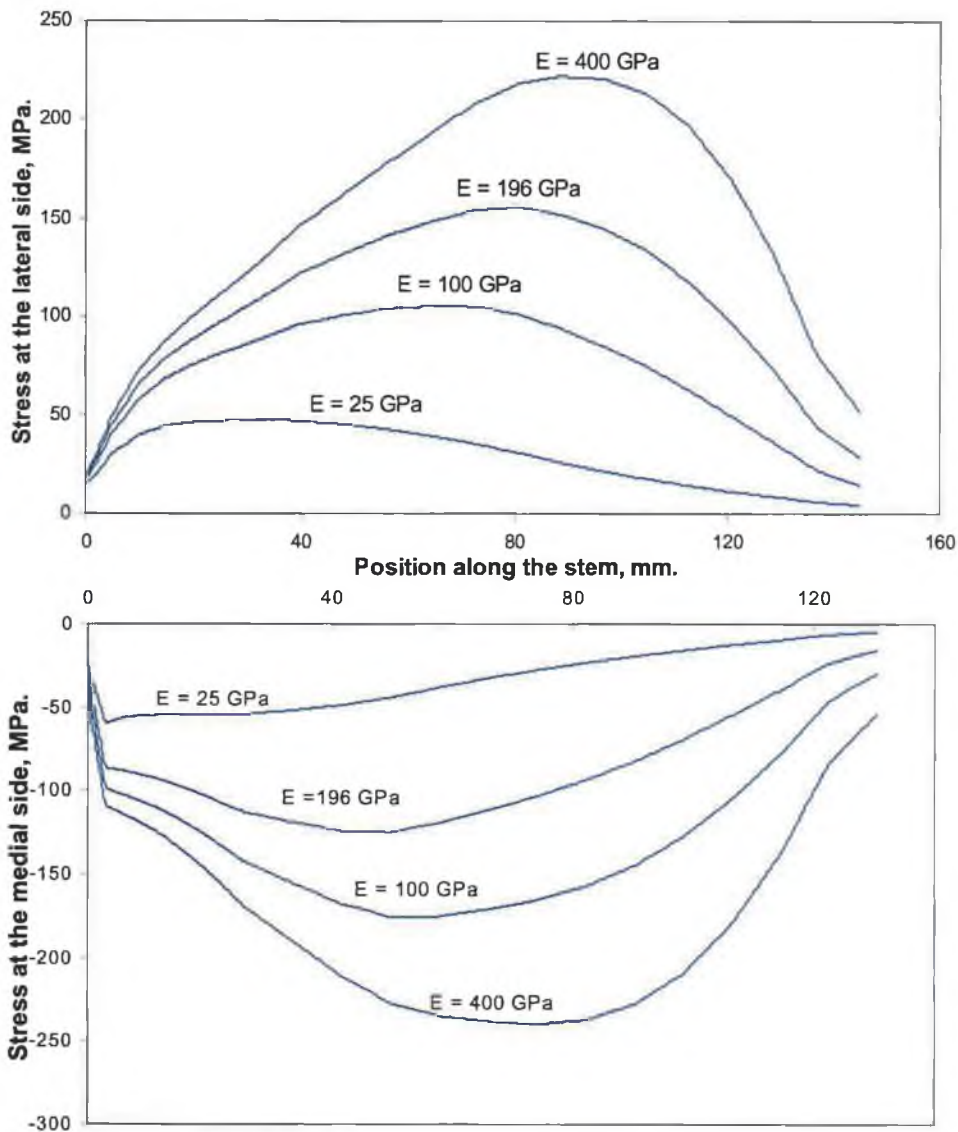


Figure 4.23: Minimum and maximum principal stress distributions, in MPa, in the lateral and medial sides of the stem as a function prosthesis Young's modulus. Cement Young's modulus = 2.0 GPa.

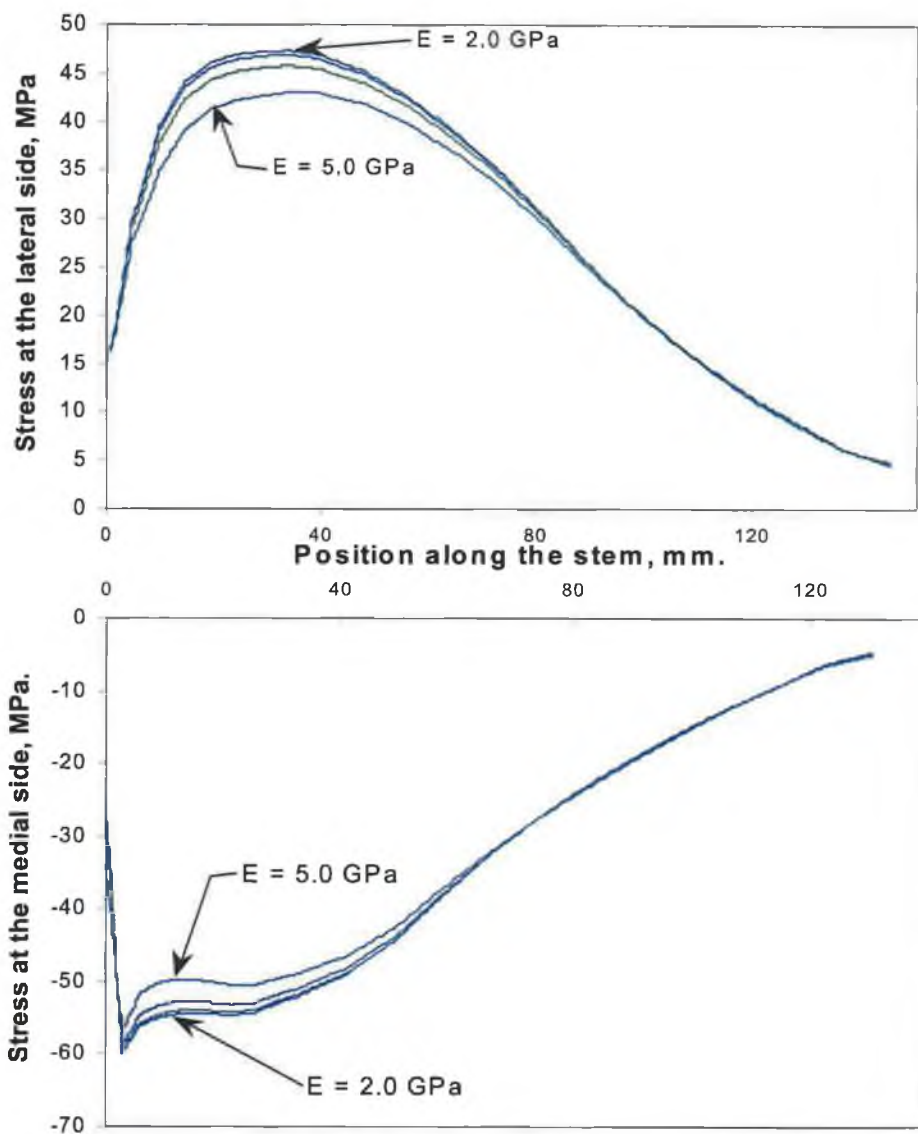


Figure 4.24: Minimum and maximum principal stress distributions, in MPa, in the lateral and medial sides of the stem as a function bone cement Young's modulus. Prosthesis Young's modulus = 25 GPa.

4.5.1.4. The Effect of Prosthesis Materials on the Cement Stresses

Figure 4.25 shows the minimum and maximum stresses in the cement as a function of the prosthesis Young's modulus for different cement materials. In this case the medial side maximum principal stress and the lateral side minimum principal stress are non-zero. As expected, the lateral stresses are tensile and medial stresses are compressive. The maximum stress occurs proximally for the polymer composite prosthesis whereas it is in the middle third for those of high Young's modulus. This means the load transfer occurs proximally with the polymeric prosthesis and distally for the rest with higher stiffness. Decreasing the prosthesis stiffness creates a higher stress in the cement mantle. Therefore, the compliant polymer prosthesis creates higher cement stresses than the other, including the titanium prosthesis. This is because stiffer stems undergo less bending displacements, thereby transferring less stress to the cement layer. However, due to the low stiffness of the polymeric prosthesis, the stem, the cement, and the bone behave as a fibre-reinforced composite such that the load transfer from the stem to the cement and the bone occurs from both ends of the stem and, thus, over a broader surface area.

The lateral tensile and medial compressive stresses in the cement become smaller just beneath the collar of the prosthesis because it transfers the load directly to the neck of the femur. Therefore, there is less pressure on the cement layer just below the collar. Relatively high lateral compressive cement stresses were found at the tip of the prosthesis and they are increased with increasing prosthesis stiffness. This could be because stiffer prostheses are less able to deform and, as a result pivot within the medullary canal generating compressive stress on the lateral cement at the level of the prosthesis tip [3, 217].

4.5.1.5. The effect of Cement Materials on the Cement Stresses

Figure 4.26 shows the minimum and maximum principal stresses in the cement mantle at the bone/cement interface as a function of the cement Young's modulus for different AHJ structures. Maximum tensile stresses on the medial side occur underneath the collar and decrease as the prosthesis stiffness increases. Large compressive stresses also occur at this site and hence, as Bocco et al. [27] reported,

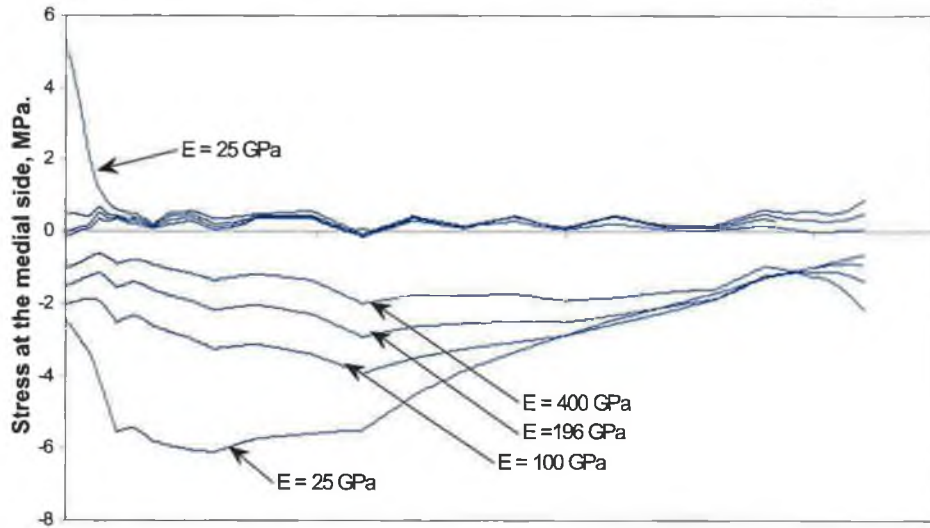
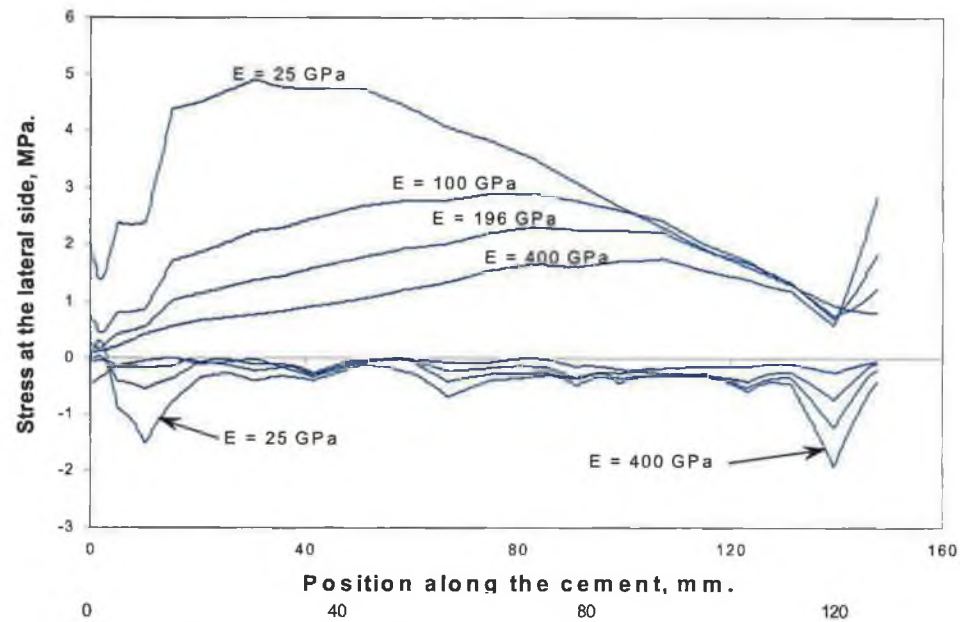


Figure 4.25: Minimum and maximum principal stress distributions, in MPa, in the lateral and medial sides of bone cement as a function prosthesis Young's modulus. Cement Young's modulus = 2.0 GPa.

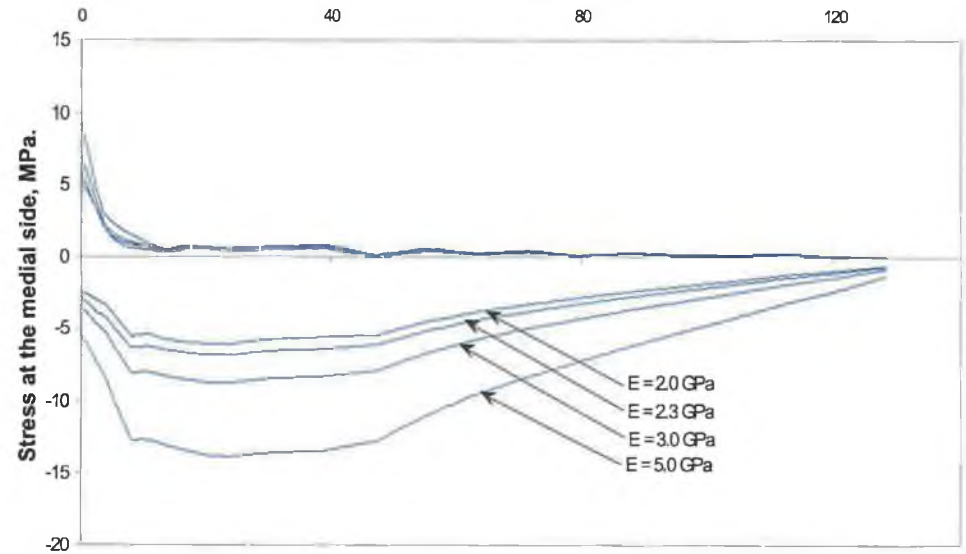
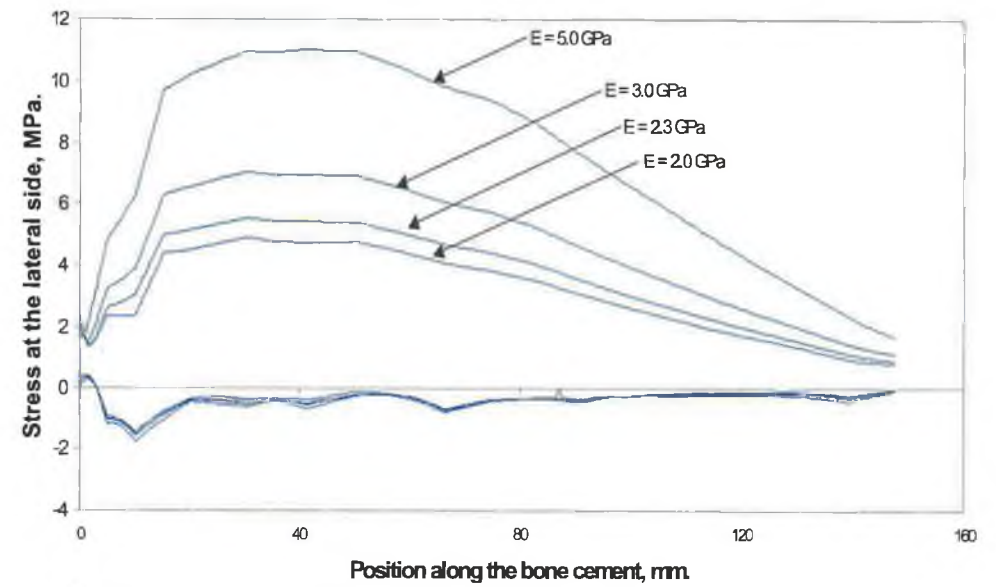


Figure 4.26: Minimum and maximum principal stress distributions, in MPa, in the lateral and medial sides of bone cement as a bone cement Young's modulus. Prosthesis Young's modulus = 25 GPa.

there is a large shear stress which may explain the tendency for cement fragmentation in this position. It can be seen that as the prosthesis Young's modulus increases and the bone cement stiffness decreases the stresses in the bone cement decreases and are more even in distribution. That is because the cement of low stiffness transfers more load to the bone and hence the stresses in the bone will increase as shown in Figure 4.27. Lateral tensile stresses increase with increased cement stiffness. But medial tensile stresses are not affected so much by the increased cement stiffness. Even though, it can be noted from Figure 4.24 that the high modulus cement generates a decrease in the medial tensile stress, possibly because more rigid interlock of the prosthesis results in negligible movement in the medial direction [217].

4.5.1.6. The Effect of Cemented AHJ materials Combination on the Bone Cortex Stress Distributions

Figure 4.27 shows the comparison of stress distributions in the bone cortex for an intact femur with the treated femora. It demonstrates the stress distributions in the treated bone as a function of the prosthesis stiffness for different AHJ structures. The stresses in the bone cortex are so sensitive to the prosthesis material; they increase with decreasing prosthesis Young's modulus, except in the greater trochanter. It can be noted that the compressive stresses are greatly increased with decreasing prosthesis stiffness, till they exceed the physiological stresses in the intact one while in the lateral side they increase till they reach the physiological stress. Rapid disuse atrophy of bone as a sequel to reduced stress has been well reported [177, 214]. An increase in the stress in the bone of the treated femur was noted at the level of the tip of the stem, which then gradually decreases with the same slope of those of intact femur. This increase in the stress in distal area is probably results from the wedge effect of the stem, which creates high hoop stress in this area under the pressure. This is in agreement with study carried out by Oh and Harris [194] and Zaki et al. [296] who found that the principal stresses in the cortical bone of the treated femur are largely exceeded that of the intact femoral bone. On other hand, it was found that the bone is not seriously affected by changes in the stiffness of the cement [81].

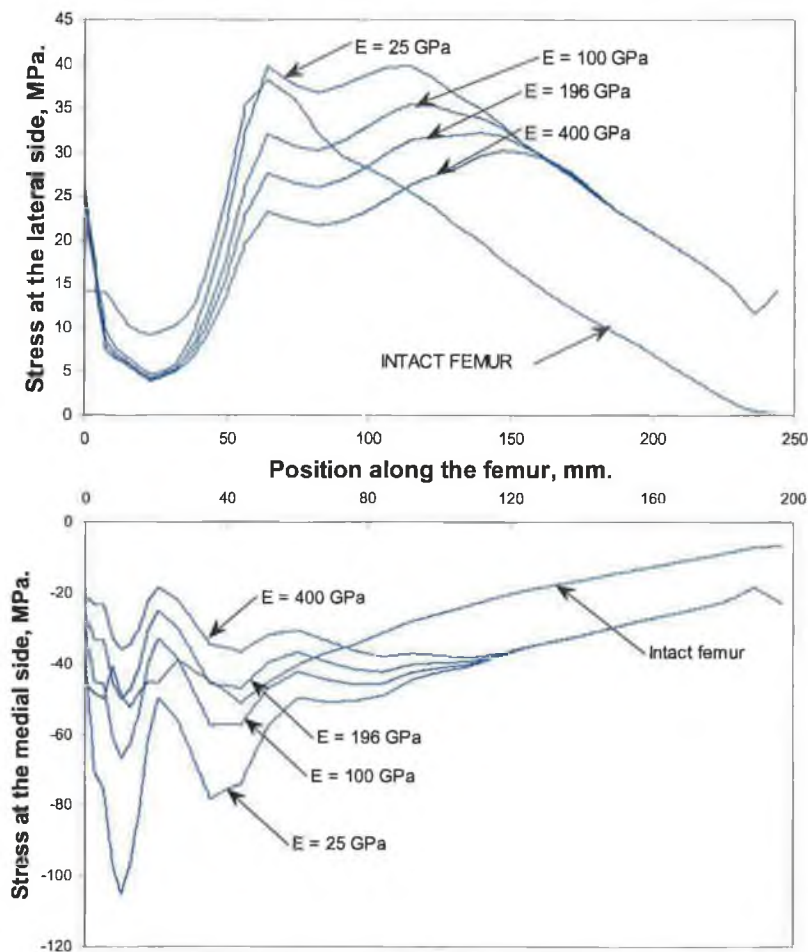


Figure 4.27: Minimum and maximum principal stress distributions, in MPa, in the lateral and medial sides of 1) treated femurs, as a function of prosthesis Young's modulus, 2) an intact femur. Cement Young's modulus = 2.0 GPa.

4.5.1.7. Analysis of AHJ Using Stress Data for Material Selection

The selection of materials for use in hip replacement components is not straightforward, since any implant is introduced into a hostile environment and exposed to a verity of biological and mechanical stresses. The implant material must be biocompatible, as well as being resistant to corrosion itself. Furthermore, the loads encountered by hip prostheses are high and repetitive, up to five to six times the body weight simply during walking [55, 135], with an active person possibly taking over a million steps per year. Generally, the main factor which controls the prosthesis or cement failure is the fatigue stress [81].

According to Henn et al. [113] and Prendergast et al. [217], the important design parameter is not the in-service tensile stress but rather the fatigue limit of the material normalised by the maximum service stress, to give a Factor of Safety. Table

4.1 compares factors of safety for the four prosthesis materials considered. The maximum tensile stresses (in-service tensile stresses) were obtained from Figure 4.28.

Table 4.1: Factor of Safety Estimates for Various Prosthesis materials				
Prosthesis Material	Young's Modulus (GPa)	Max. tensile stress (MPa)	Fatigue Limit (MPa)	Factor -of- Safety
Particulate composite [113]	25	47.36	40	0.8
Fibre composite [50]	50	68.8	75	1.1
Ti-6Al-4V [113]	100	105.49	550	5.2
Ti-6Al-4V (Porous coat) [212]	100	105.49	≈220	2.0
Co-Cr alloy [212]	196	155.9	270 - 670	1.7 - 4.3
Ceramic [100]	400	222.31	≈300	1.3

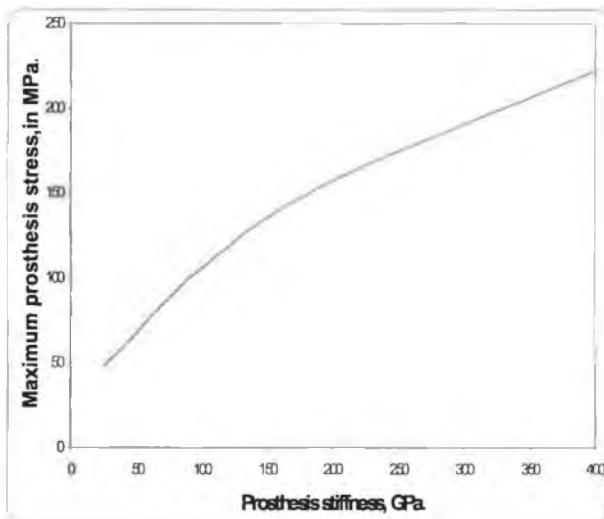


Figure 4.28: Maximum prosthesis stress as a function of prosthesis Young's modulus. Cement stiffness = 2.0 GPa.

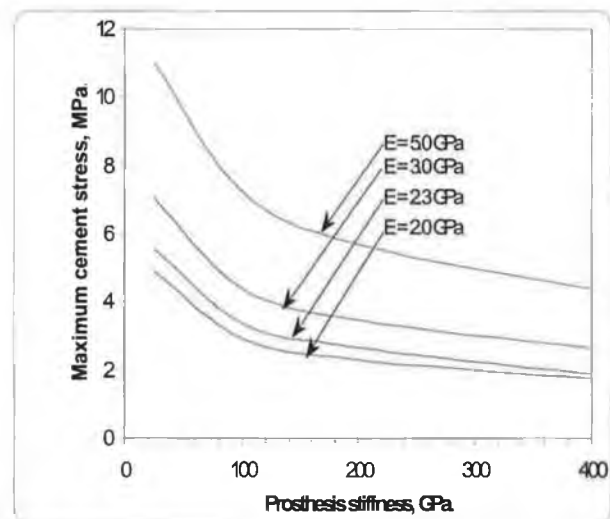


Figure 4.29: Maximum cement stress, in MPa, as a function of prosthesis Young's modulus.

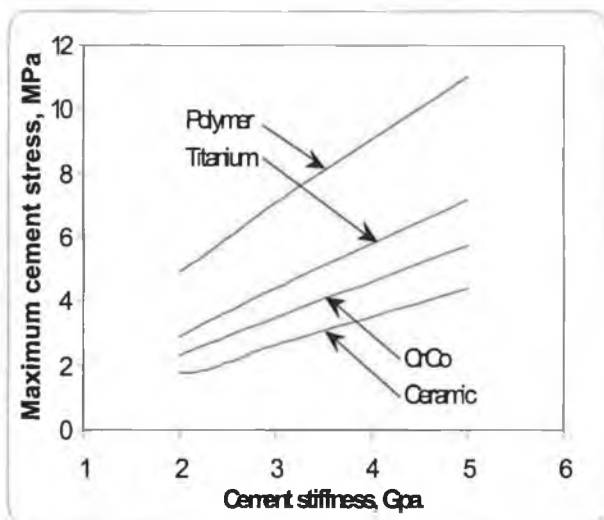


Figure 4.30: Maximum cement stress as a function of cement Young's modulus.

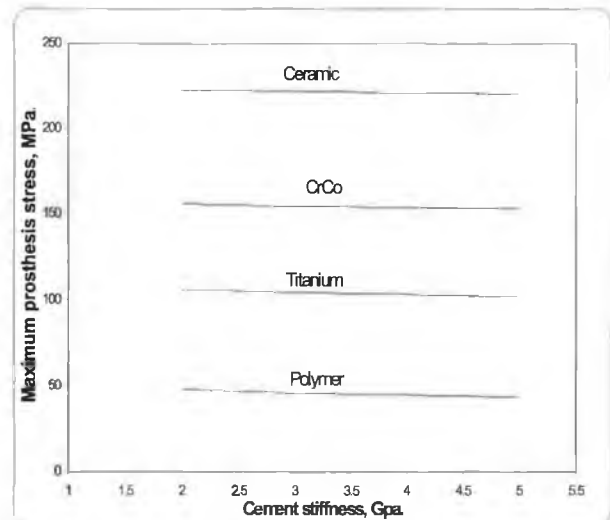


Figure 4.31: Maximum prosthesis stress as a function of cement Young's modulus.

This table shows that the predicted prosthesis fracture probably occurs for the particulate composite, for this particular design, because its Factor-of-Safety is less than unity when it is subjected to an applied load of 3 kN or more. On the other hand, the titanium alloy has the highest Factor-of-Safety. Also, the Cr/Co alloys and ceramics can be usable in spite of their different properties.

Two types of failure could happen to the bone cement. Firstly, there is failure of the cement itself generated by fatigue and generally initiated at flaws. Secondly, failure occurs on the interfaces between the cement and the metal and bone [258]. In this study, failure due to the fatigue only will be considered. The assessment of the cement for different prosthesis materials can be undertaken in a similar way, and it is clarified in Table 4.2.

Table 4.2: Factor of Safety Estimates for Various Cement materials [212]										
Cement Material (PMMA)	Young's Modulus (GPa)	Max. tensile stress (MPa)				Fatigue Limit (MPa)	Factor –of-Safety			
		Poly	Ti	CrCo	Cerm		Poly	Ti	CrCo	Cerm
Unreinforced PMMA	2.76	6.5	4.0	3.1	2.4	10	1.5	2.5	3.2	4.2
Polyester woven	2.8	6.6	4.1	3.2	2.4	60 [258]	9.1	14.6	18.8	25.0
316 s.s woven mesh	2.8	6.6	4.1	3.2	2.4	35	5.3	8.5	10.9	14.6
Knitted carbon fibre	2.8	6.6	4.1	3.2	2.4	40 [258]	6.1	9.8	12.5	16.7
Bone particle	3.50	8.0	5.0	4.0	3.0	11	1.3	2.2	2.75	3.7
Chopped carbon fibre	5.52	12.0	7.9	6.3	4.8	16	1.3	2.0	2.5	3.3

It is observed that as the cement stiffness increases the cement stresses increase. This increase in the cement stress due to the improved stiffness should be accompanied with a satisfactory increase in the toughness and fatigue limit. Some times the increase of cement toughness by reinforcing cement material with fibres leads to relatively small improvements in the material strength [258]. This is also clear from Table 4.2, where the stiffness is increased by 100% by adding chopped carbon fibres but the factor of safety is increased just by 60%. Compared to that polyester reinforcement cement leads to just 1.45% increase in Young's modulus but gave as high as 500% increase in the material toughness and thus it gave a high reliability. The addition of fibres to a polymer to form a composite causes improvements in strength and toughness through two different mechanisms. Firstly, the fibres themselves become stressed, and therefore take some stress away from the polymer. Since the fibre material is generally of high Young's modulus, the fibre

takes proportionally a large amount of stress. Thus failure in the polymer is postponed to higher nominal stress values. The second mechanism concerns the prevention of crack propagation. Brittle polymers such as PMMA invariably fail by propagation of cracks, usually initiated at pre-existing flaws in the material. The presence of fibres inhibits cracking through mechanisms such as fibre/matrix decohesion and crack-spanning by fibres [185], which essentially increase the amount of energy needed to cause propagation, whether in a rapid manner or during fatigue. Table 4.2 gives an indication that the Factor-of-Safety of cement, when polymeric prosthesis is used, is the lowest comparing to the other prosthesis materials. Prendergast [217] recommended not to use polymeric prosthesis as a cemented AHJ. Figure 4.29 shows the effect of prosthesis material stiffness on the stress in the cement layer, increasing prosthesis Young's modulus results in decreasing peak cement stresses. Figure 4.31 shows the effect of the cement stiffness on the prosthesis stresses. It is obvious that the effect is very small.

By referring to Figure 4.30, one can find that the relationship between the cement Young's modulus and the maximum stress for different prosthesis materials is a linear one, since the stresses increase by increasing the cement stiffness for all prosthesis materials used. This linear relationship can be represented by a mathematical equation for the four prosthesis materials:

$$\sigma_{\text{cement}} = 2.0325 E_{\text{cement}} + 0.881; \text{ for a prosthesis of Yong's modulus equal to 25 GPa,}$$

$$\sigma_{\text{cement}} = 1.4264 E_{\text{cement}} + 0.0758; \text{ for a prosthesis of Yong's modulus equal to 100 GPa,}$$

$$\sigma_{\text{cement}} = 1.1389 E_{\text{cement}} + 0.0408; \text{ for a prosthesis of Yong's modulus equal to 196 GPa,}$$

and

$$\sigma_{\text{cement}} = 0.8746 E_{\text{cement}} + 0.0037; \text{ for a prosthesis of Yong's modulus equal to 400 GPa.}$$

From these four equations, one can develop a general equation linking the cement and prosthesis materials to predict maximum stress in the cement for this specific design and construction;

$$\sigma_{\text{cement}} = A \cdot E_{\text{cement}} + B, \quad (1)$$

where,

$$A = -0.4151 \ln(E_{\text{prosthesis}}) + 3.3544, \text{ and} \quad (2)$$

$$B = 415.22 (E_{\text{prosthesis}})^{-1.8655} \quad (3)$$

σ_{cement} , E_{cement} , and $E_{\text{prosthesis}}$ are in GPa.

The relationship between the maximum prosthesis stress and prosthesis Yong's modulus for different AHJ constructions is an exponential one, see Figure 4.28, and it could be represented by the following equation:

$$\sigma_{\text{prosthesis}} = C \cdot (E_{\text{prosthesis}})^D, \quad (4)$$

where,

$$C = -0.453 \cdot E_{\text{cement}} + 8.7405, \text{ and} \quad (5)$$

$$D = 0.0106 \cdot E_{\text{cement}} + 0.5409 \quad (6)$$

$\sigma_{\text{prosthesis}}$, E_{cement} , and $E_{\text{prosthesis}}$ are in GPa.

By these two general equations it is easy to estimate the maximum stress in the cement mantle and in the prosthesis for any combination of cement and prosthesis material used for this particular design, and by knowing the fatigue limit for each material, cement and prosthesis, one can predict the Factor-of-Safety for each when they are used together within the femur.

The above approach to material selection using the fatigue limit is not entirely satisfactory as it does not account for the material damage tolerance. Real materials contain cracks and other defects, which concentrate stress and may initiate fatigue failure. This is particularly true for the cement where defects, such as bubbles, delaminations, and lack of penetration, may be present. Prendergast and Taylor [214] suggested that a more satisfactory approach might be to estimate the maximum defect size, and compare the stress intensity due to it with the fatigue threshold.

4.5.2. Design of a Bi-Material Artificial Hip Replacement to Control Stress Shielding And Migration Phenomenon

Stress shielding of the calcar region of the proximal femur has been a major concern for both engineers and surgeons alike. Studies have shown that flexible stems, with a modulus similar to that of bone, made from designated 'isoelastic' materials increase the load transfer to the calcar region and hence reduce the amount of bone resorption [119]. Since proximal bone resorption has become apparently a problem, different designs of stems embedding the concept of 'isoelasticity' have been developed and clinically tested [6, 33, 133, 186, 191, 263]. Although some studies have reported that flexible stems give good results [6, 33, 186], others have shown that clinical survivorship of these type of prostheses is very poor [133, 190, 263]. Christel et al. [50] clinically tested a carbon-carbon hip prosthesis, but the study has been stopped due to mechanical failures. Prendergast [212] predicted that the use of cemented prosthesis of low stiffness of 25 GPa would cause a 25% decrease in the factor of safety within the cement, therefore he suggested that for polymer composite prosthesis of low stiffness cementless bonding to the bone should be considered. There is broad consensus that these types of prostheses produce large relative micromotion at the interface which are known to cause the formation of an unstable fibrous tissue layer [157, 209] and, therefore, cause high failure rates.

So far it was proved that the polymer composite prosthesis reduces the stress shielding specially in the calcar region, but in the same time it may be liable to failure in the lateral side due to the high fatigues it exposes to. Also it was found that total hip replacement (THR) components are subjected to incompatible design goals as regards prevention of different failure scenarios, therefore, the development of a hip prosthesis must take into account the compromise between established design goals. Stress shielding and migration are two important design objectives that require different solution [238]. According to this information, this study will focus on increasing the long-term reliability and reducing both the stress shielding and micromotion of the prosthesis.

Conventionally prostheses were made of a single material, with constant elastic modulus. These prostheses can only address the stress shielding or

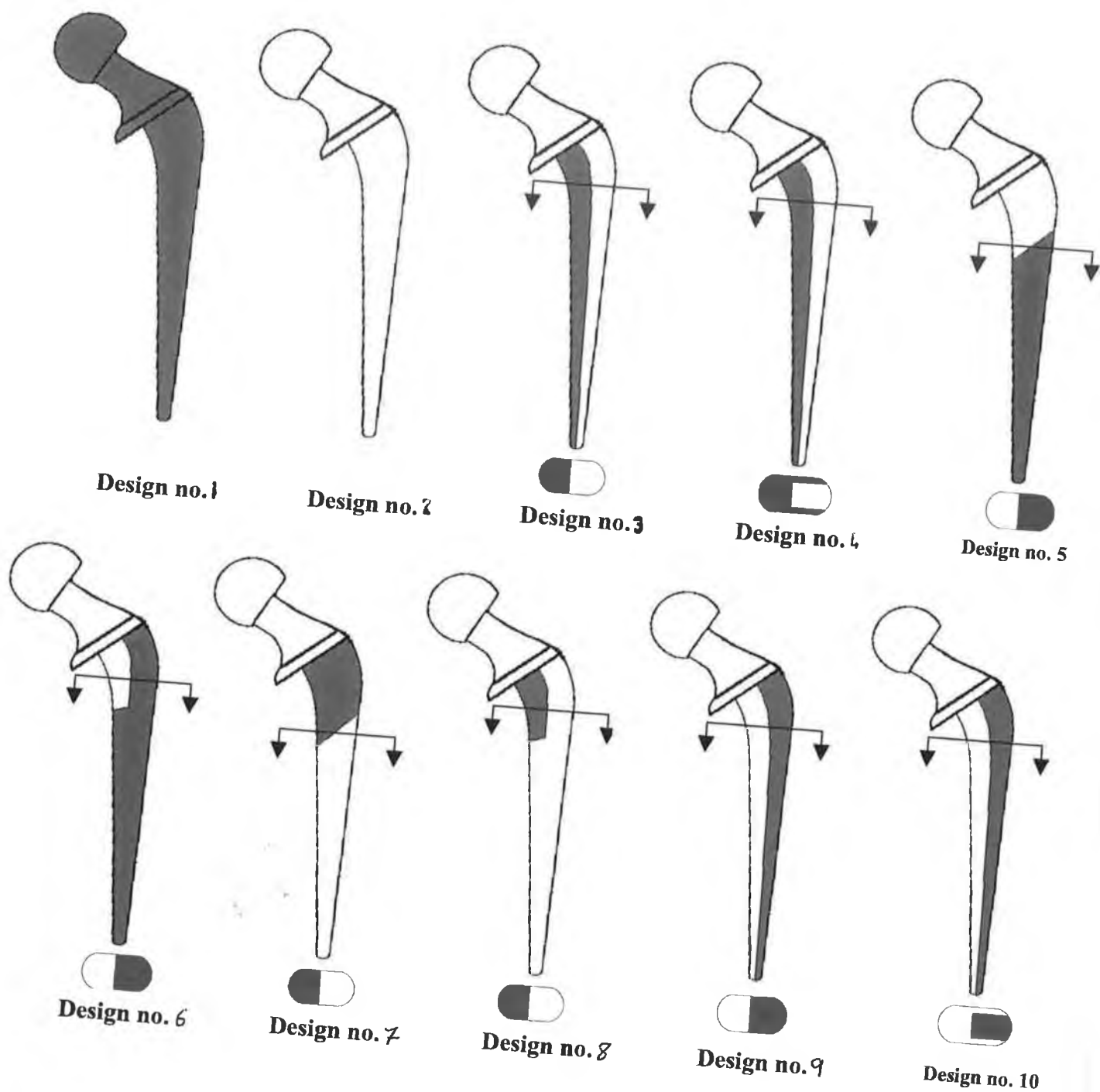




Figure 4.32: Shows the models simulation of the prosthesis stem materials.

 Young's modulus = 25 GPa
 Young's modulus = 196 GPa

micromotion problem. They are unable to address both simultaneously but by making a stem from two different materials of different Young's modulus (one is of low modulus of 25 GPa, and the other will be high of 196 GPa) it is possible to obtain a suitable compromise to attenuate both problems, since avoiding them is impossible [240]. For this study eight different stems designs, Figure 4.32, have been simulated to see into which extent the stresses in the calcar region increased and that at the lateral side of the stem and cement mantle decreased. In other word, the whole performance and quality of the new prosthesis design is going to test it by using FEA software.

Note that the simulation for this study has been carried out on two cases of prosthesis collar contact:

- a) Collared stem with perfect collared-femur contact (ideal case).
- b) Collared stem with collar-cement-femur contact; it was assumed that there is a layer of cement trapped between the collar and the surface of resected femur neck.

Figures 4.33A and B show the stress distribution in the lateral and medial sides in the femur cortex as a function of stem design. Each design for the material combination of the stem gives different stress distributions at the upper half of the femur, while the stress distribution is of the same value in the lower halves. It is always interested to find out the prosthesis design that regenerates stresses in the femur cortex close to that of intact one. The most important region that always suffers from resorption due to stress shielding is the calcar region [212]. From Figure 4.34A and B one can sort the prostheses design, mentioned above, according to minimum stress shielding into:

- 1) Design No. 1,
- 2) Design No. 6,
- 3) Design No. 4,
- 4) Design No. 3,
- 5) Design No. 5,
- 6) Design No. 9, and

- 7) The other either of high stresses shielding in the lateral and medial sides, Design no. 2, or in one of these sides, Designs no. 7 and 8.

In spite of the fact that design no.1 has very low stress shielding it suffers from high migration due to its low Young's modulus. Design no. 6 gave a better compromise of stress distributions in the both sides of the femur cortex. While design no. 3 and 4 gave stress distributions close to that of design 6 in the medial side, whereas the lateral side was in poor agreement. Design no. 5 and 9, in spite of the fact that they gave an satisfactory stress distributions, are in contrast to designs no. 3 and 4, since they offered relatively high stress shielding in the medial side where as it is low in the lateral side. By having a close view to design no. 6, one can find that it is very similar to a prosthesis design invented by Simoes et al. [238] to reduce the stress shielding and migration phenomenon. This design implies Young's modulus varies from being stiff proximally to being flexible distally [81, 135, 201].

These results of stress distributions in the femur cortex for the prosthesis designs mentioned above are not enough in terms of prosthesis performance and quality. The loads encountered by hip prostheses are high and repetitive, up to five to six times the body weight simply during walking [119, 186], with an active person possibly taking over a million steps per year. Generally, the main factor which controls the prosthesis or cement failure is the 'fatigue stress' [81]. Since it is required to know the tension stresses effected in the lateral side of the prostheses and cement wither they exceeded the acceptable limit or not to keep away from the fear of crack initiation in these sides. For this reason the stress values in the lateral and medial side of a stem made of either polymer composite or CrCo has been considered to be easy to compare the changes created by the other eight designs of dual material combinations.

First of all, it is clear from Figure 4.35A and B that the existence of a cement layer between the collar and the resected femur surface serves on increasing the stresses value in the prosthesis stem comparing to that of ideal case. So that it will be focused on the second case, collar-cement-bone contact, because it represent the worse case of stress distributions. For design 5, which is a CrCo extended for 39.4 mm and 25.5 mm down the collar and the rest of the stem is polymer composite, the

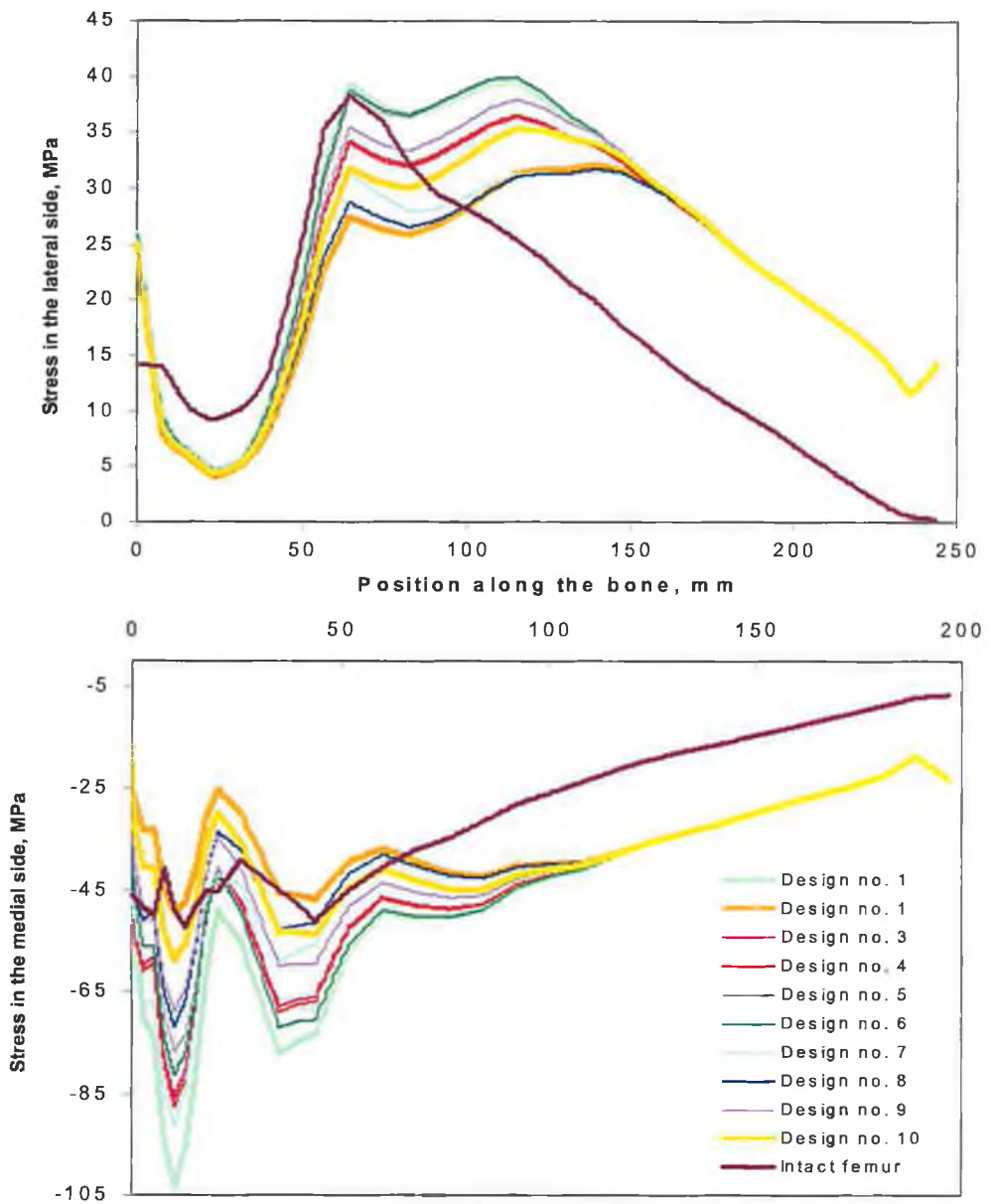


Figure 4.33A: Ideal Contact. Stress distributions in the lateral and medial sides of the femur for different prosthesis designs.

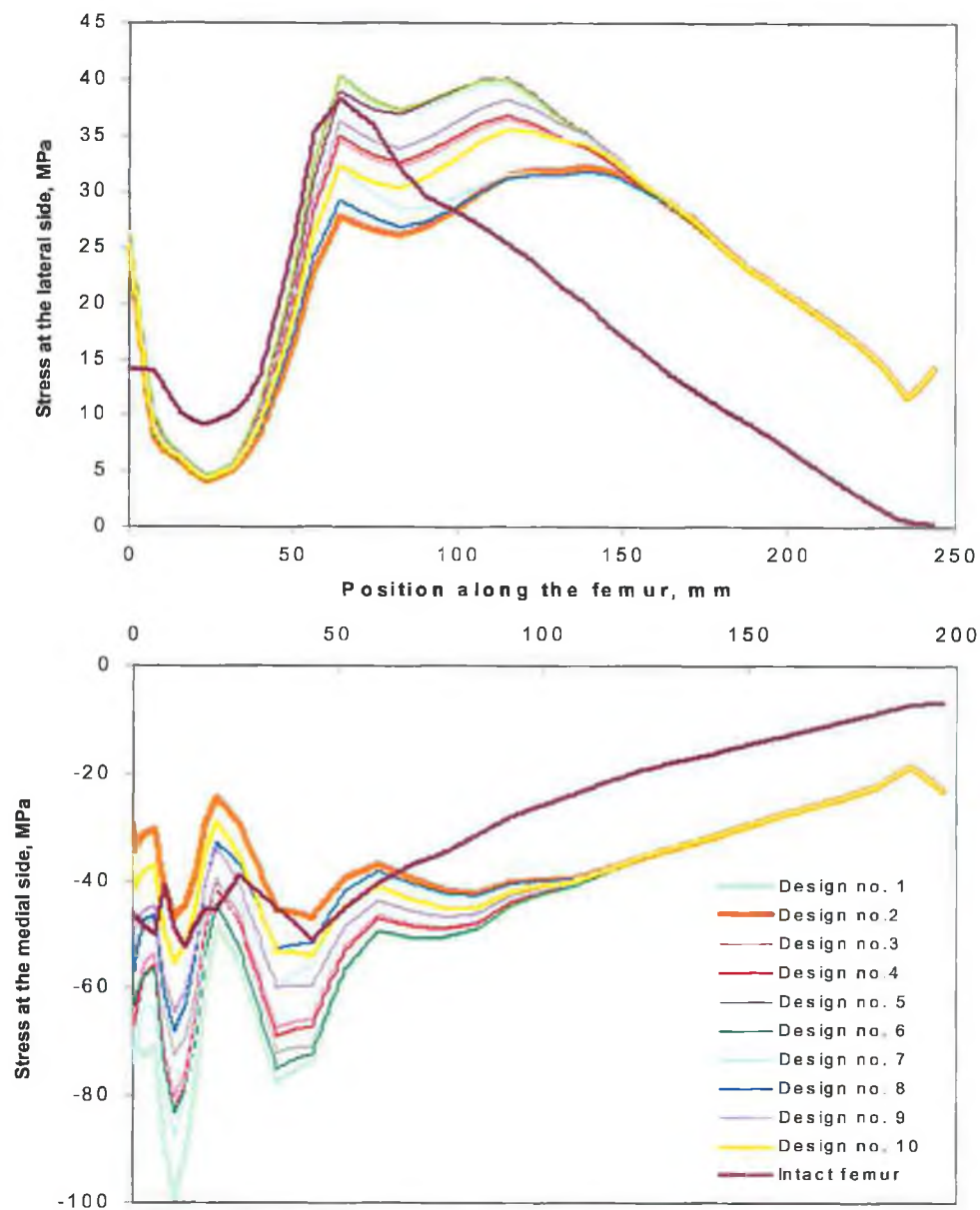


Figure 4.33B: Collar-Cement-Femur Contact. Stress distributions in the lateral and medial sides of the femur for different prosthesis designs.

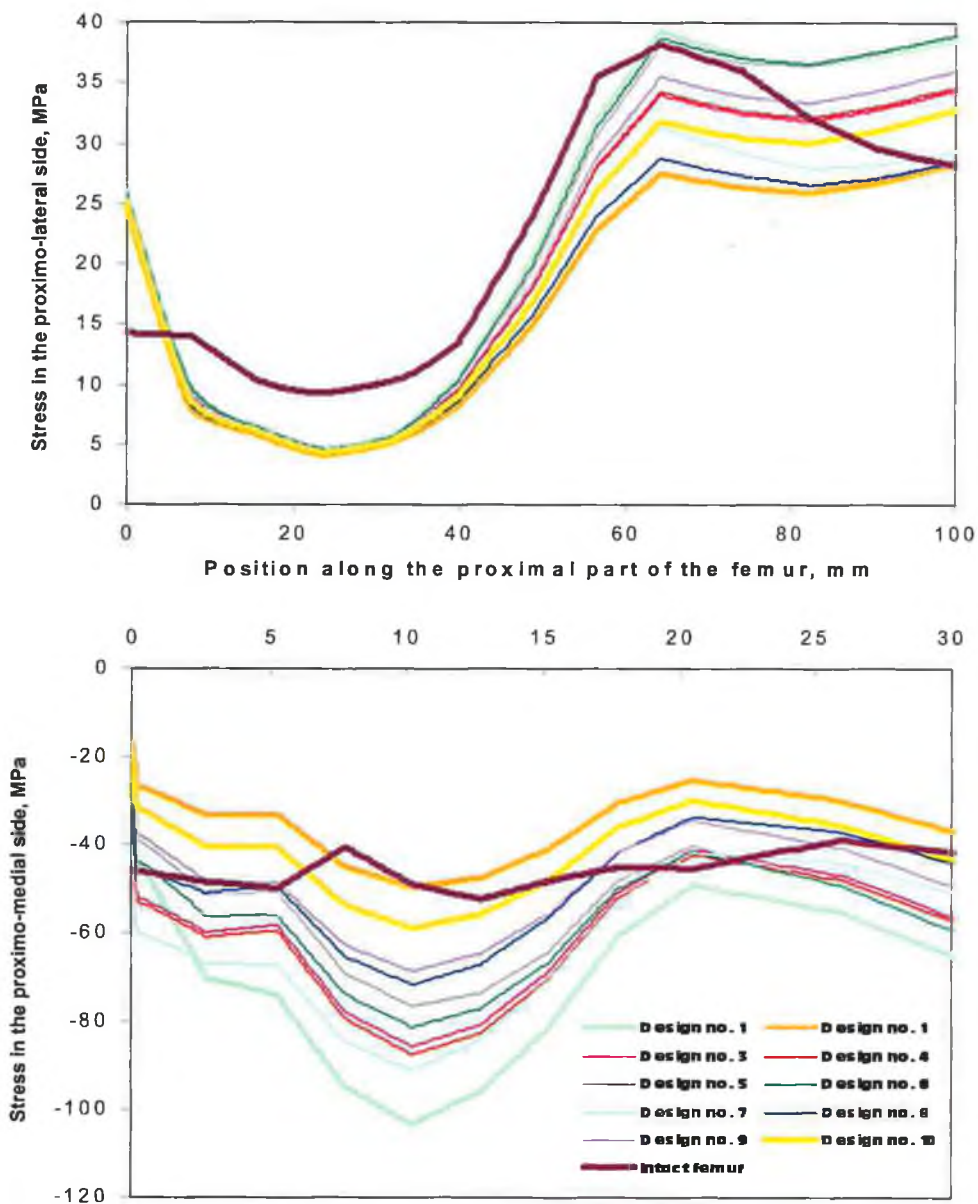


Figure 4.34A: Ideal Contact. Stress distributions in the proximal part for the lateral and medial sides of the femur for different prosthesis designs.

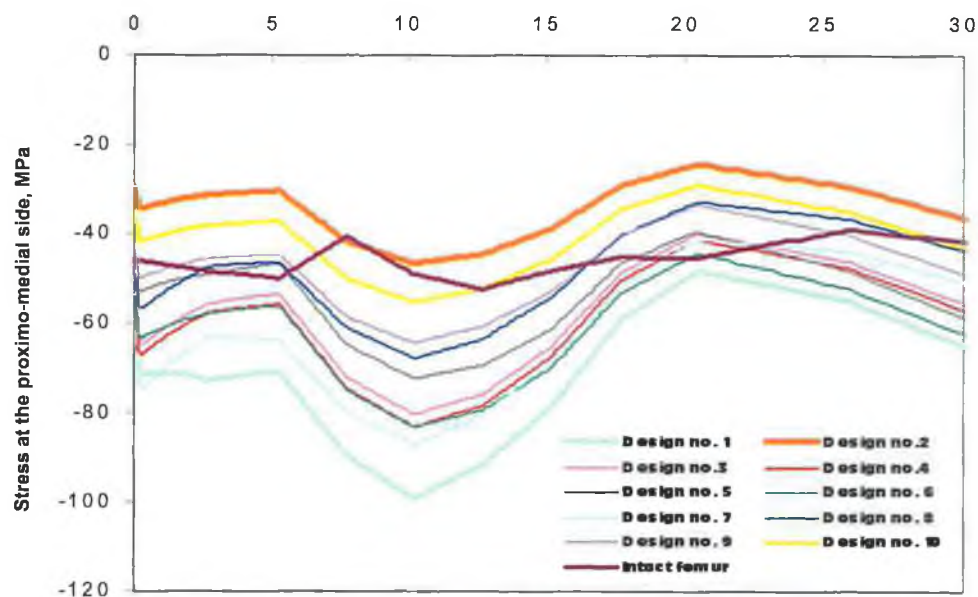
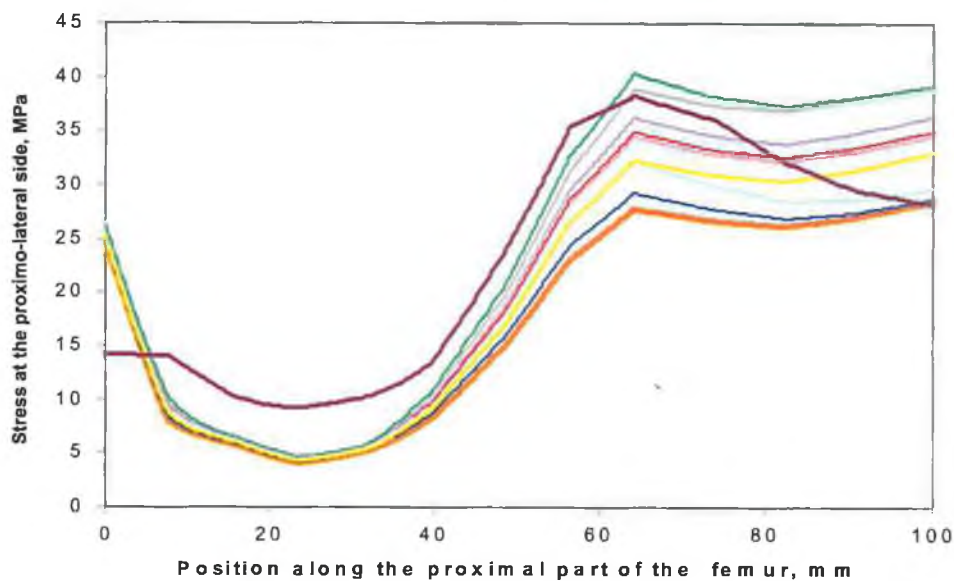


Figure 4.34B: Collar-Cement-Femur Contact. Stress distributions in the proximal part for the lateral and medial sides of the femur for different prosthesis designs.

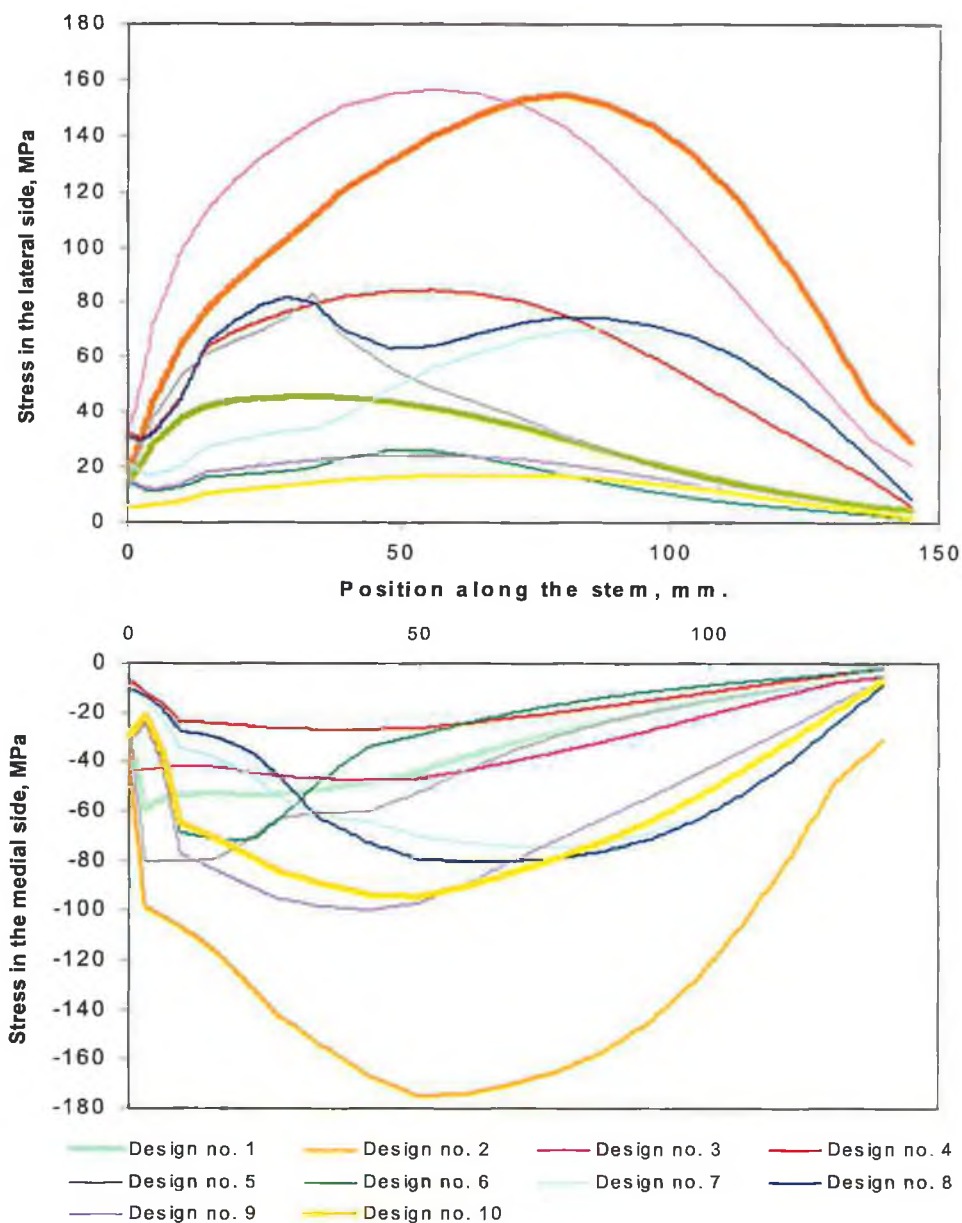


Figure 4.35A: Ideal Contact. Stress distributions in the lateral and medial sides of the stem for different prosthesis designs.

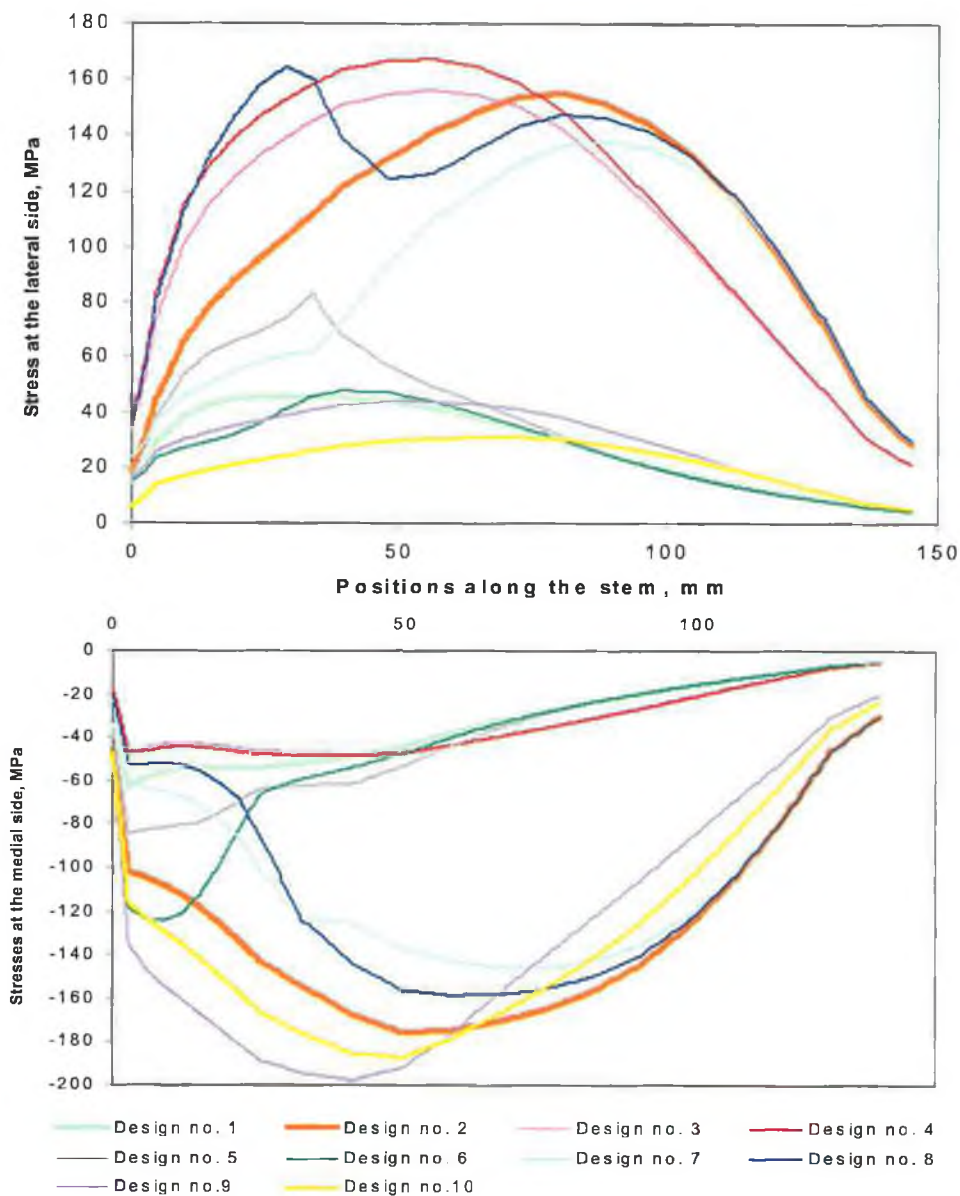


Figure 4.35B: Collar-Cement-Femur Contact. Stress distributions in the lateral and medial sides of the stem for different prosthesis designs.

stress in the lateral side of the CrCo has been reduced compared to that made completely of CrCo (design no. 2). But the stresses created in the polymer composite would be relatively high. Since the maximum tensile stress for the polymer part of the stem is 67.56 MPa, Figure 4.35B, and it is known that the fatigue limit of polymer composite is 40 MPa [113]. So that by dividing the fatigue limit of that material by the maximum tensile stress will give the Factor-Of-Safety (FOS) [51, 217] which is 0.6 for this design. This factor gives an indication that this design is unreliable, since it may be liable to the failure, crack initiation, in the lateral side down the CrCo part of the stem.

Table 4.3 compares factors of safety for the selected prostheses design mentioned above. The maximum tensile stresses were obtained from Figures 4.35A and B.

Table 4.3: Factor of Safety Estimates for stem materials for Different Designs						
Design No.	Young's Modulus GPa	Max. tensile stress MPa		Fatigue Limit MPa	Factor of safety	
		Case 1*	Case 2**		Case 1	Case 2
1	25	45.826	46.107	40 [113]	0.87	0.87
3	196	156.76	155.93	270 [212]	1.7	1.7
4	196	84.635	166.9	270	3.2	1.6
5	25	66.881	67.56	40	0.6	0.6
	196	83.464	81.36	270	3.2	3.3
6	25	26.329	48.045	40	1.5	0.83
9	25	24.232	43.675	40	1.7	0.92

* Collar-femur contact (ideal contact).

** Collar-cement-femur contact.

It is convenient if this compression is made graphically by sorting the design number according to the minimum stress shielding, Figure 4.36. In spite of the fact that Design no. 6 has minimum stress shielding it suffers from low factor-of-safety when a layer of cement trapped between its collar and the cut surface of the femur. It is clear that designs number 4 and 3 made good compromise between the design reliability and minimum stress shielding. Also, this graph shows that sitting the prosthesis collar directly on the bone would increase the factor-of-safety of the selected prosthesis. Figures 4.38 to 4.43 show the stress distributions in the interface of the stem materials for each prosthesis design demonstrated in Figure 4.32. The stress distributions in the interface for the polymer composite for design no. 3 and 4 are shown in Figures 4.38 and 4.39. These graphs shows the tensile stresses in the

interface of the polymer composite, which forms the second material of the stem, are very low and does not exceed 1.2 MPa, so that the factor-of-safety of this material will be high.

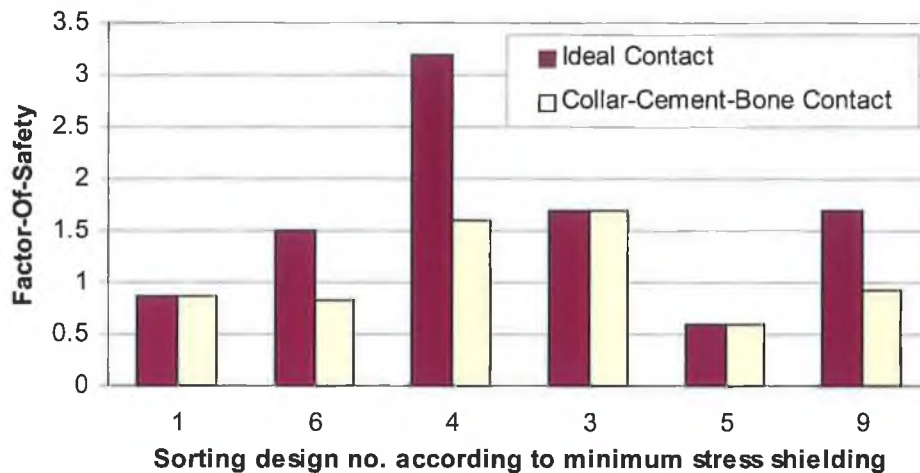


Figure 4.36: Comparison of factor-of-safety for different prosthesis design. Note that prosthesis design number has been sorted in this graph according to the minimum stress shielding results demonstrated in Figures 4.32B and 4.33B.

Figures 4.37A and B show the stress distribution in the cement (of Young's modulus of 2.3 GPa) as a function of stem design. The cement mantle experienced of high stress values in the region that included polymer composite of the stem for different designs. The compliant of polymer material creates higher cement stresses. In the perfect contact of collar to the resected surface of the femur the lateral tensile and medial compressive stresses in the cement become smaller just beneath the collar of the prosthesis because it transfers the load directly to the neck of the femur, Figure 4.37A. Therefore, there is less pressure on the cement layer just below the collar. While in the collar-cement-contact there were high stresses just below the collar in the medial side, Figure 4.37B. This means that the cement layer trapped between the collar and the bone acts as an insulator, resists load transformation to the femur neck. Because design no. 3 and 4 gave a good compromise between the prosthesis mechanical reliability and low stress shielding, it is also good to test their effects on the cement mantle. In this study, failure due to the fatigue only will be considered. The assessment of the cement for prosthesis design no. 3 and 4 can be undertaken in a similar way, and it is clarified in Table 4.4.

Table 4.4: Factor of Safety Estimates for Cement for Different Designs				
Design No.	Cement Young's Modulus (GPa)	Max. tensile stress (MPa)	Fatigue Limit (MPa)	Factor –of- Safety
4	2.3	2.9436	11	3.7
3	2.3	2.8313	11	3.9

It has been made sure that effect of prostheses no. 3 and 4 have no serious effect on the cement mantle as indicated by the factor-of-safety of the cement in table 4.4.

Kuiper and Huiskes [114] and Simoes et al. [239, 241] suggest that the modulus of prosthesis should vary from being stiff proximally to being flexible distally. In the last two decades many researchers have developed and studied composite made hip prostheses [50, 51, 62]. Most of the developed composite material prostheses have been manufactured from laminated composite [65, 113]. Christel et al. [50] developed a hip prosthesis made from carbon fibres infiltrated either with dense pyrolytic carbon or silicon carbide through chemical vapour infiltration. A range of different elastic modulus from 33 to 90 GPa was obtained with these prostheses. Davidson et al. [217] machined Corin C-Fit femoral stems from carbon fibre reinforced plastic (CFRP) laminates. Claes et al. [113] obtained carbon fibre reinforced carbon prostheses from laminates where the carbon fibres were arranged in several layers in angles of 0° , $\pm 45^\circ$ and 90° . These prostheses had a bending strength of 410 MPa and a modulus of elasticity of 76 GPa. Widmer et al. [281] used injection moulding of carbon fibre reinforced polyaryletherketone (PEEK) to obtain anisotropic hip prostheses. A method for manufacturing prostheses with a fibre-reinforced inert plastic is proposed in Hochman US patent [116]. On this regards prosthesis of variable elastic modulus from being stiff proximally to being flexible distally, Figure 4.44; have been simulated to study the performance of this type of prostheses. During this simulation it has been noted that there was not different between the results of collar-bone contact model and the collar-cement-bone contact model, see Figures 4.45, 4.46, and 4.47. The results regard to the level of stress shielding in the bone cortex (Figure 4.45), were not as good as that of designs no. 4 and 3. And

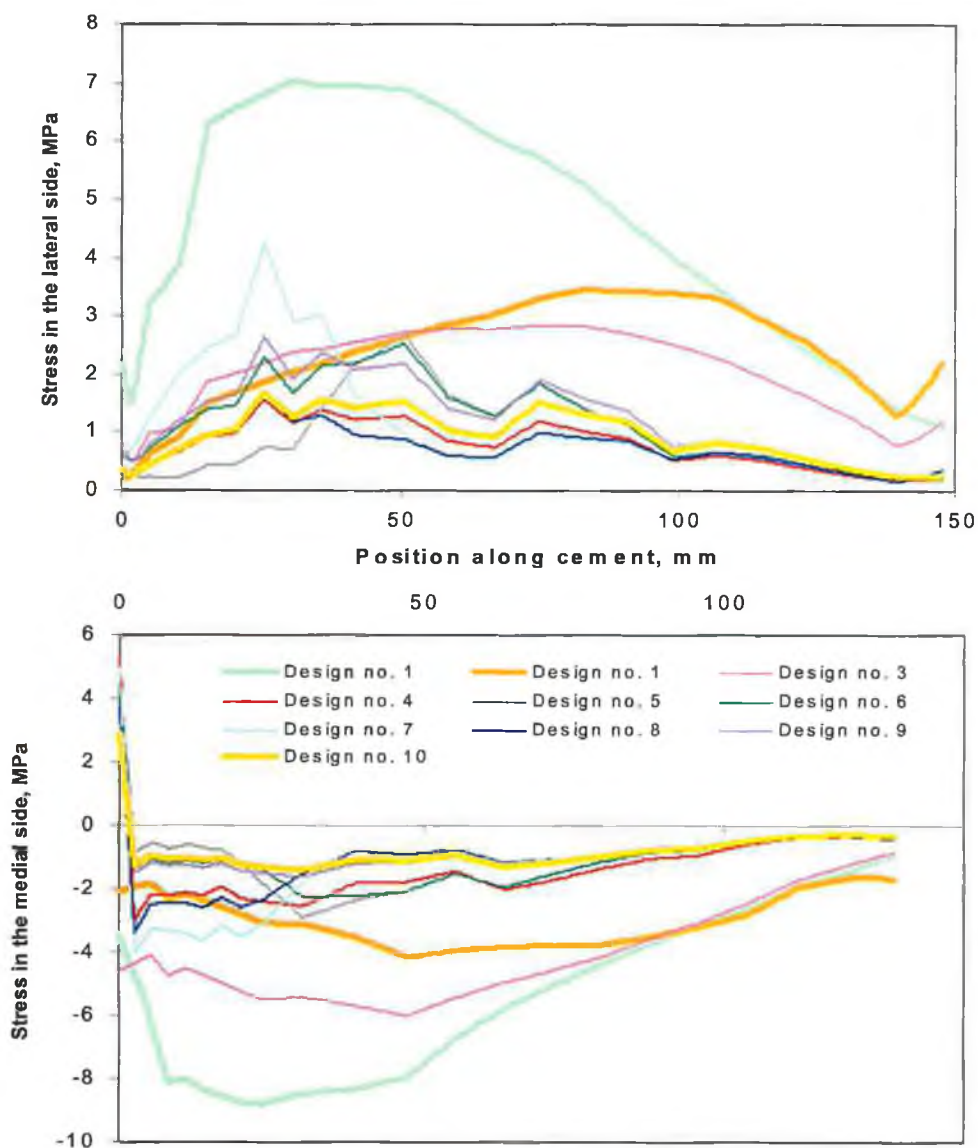


Figure 4.37A: Ideal Contact. Stress distributions in the lateral and medial sides of the cement mantle as a function of different prosthesis designs.

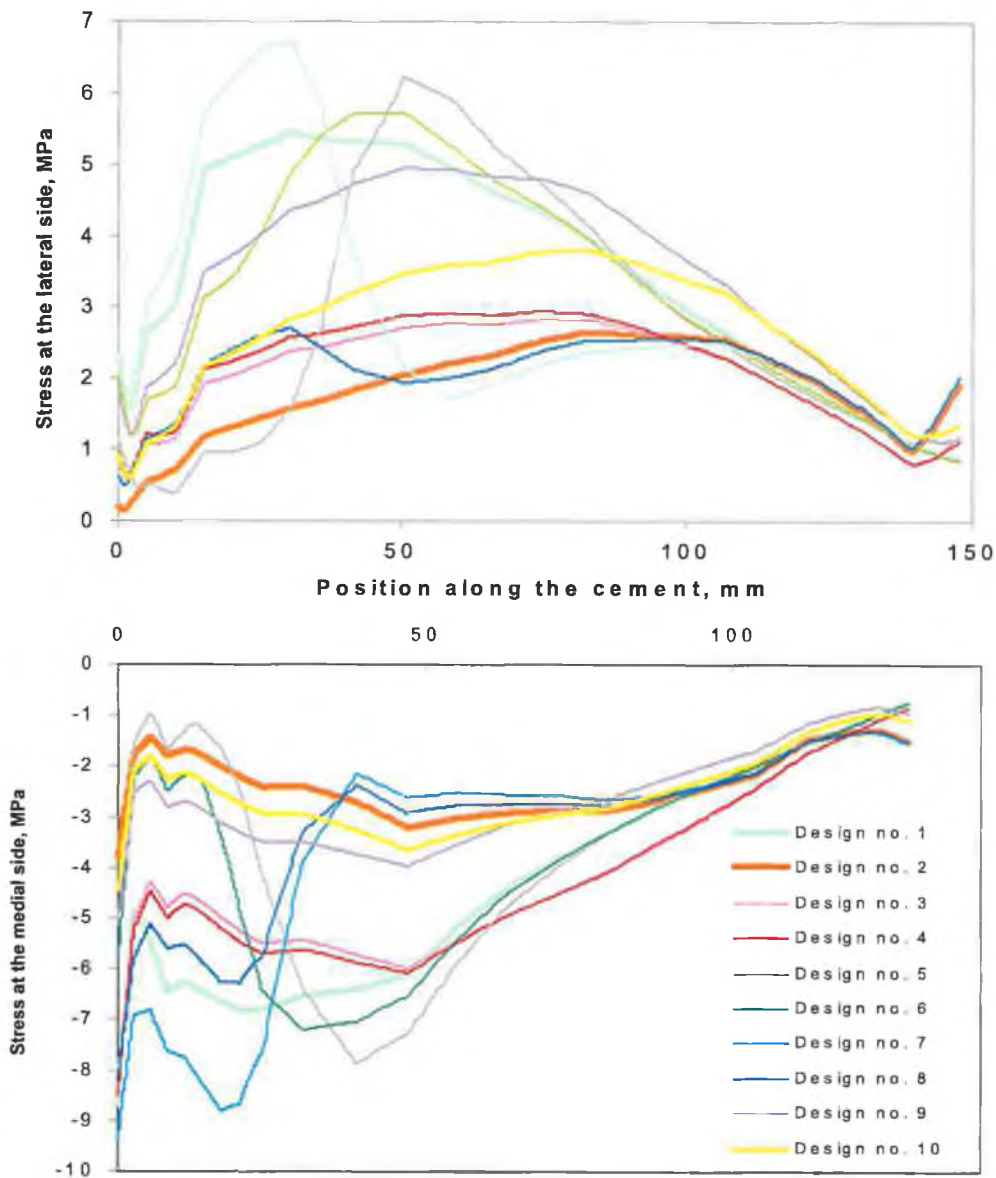


Figure 4.37B: Collar-Cement-Femur Contact. Stress distributions in the lateral and medial sides of the cement mantle as a function of different prosthesis designs.

A) Design No. 3

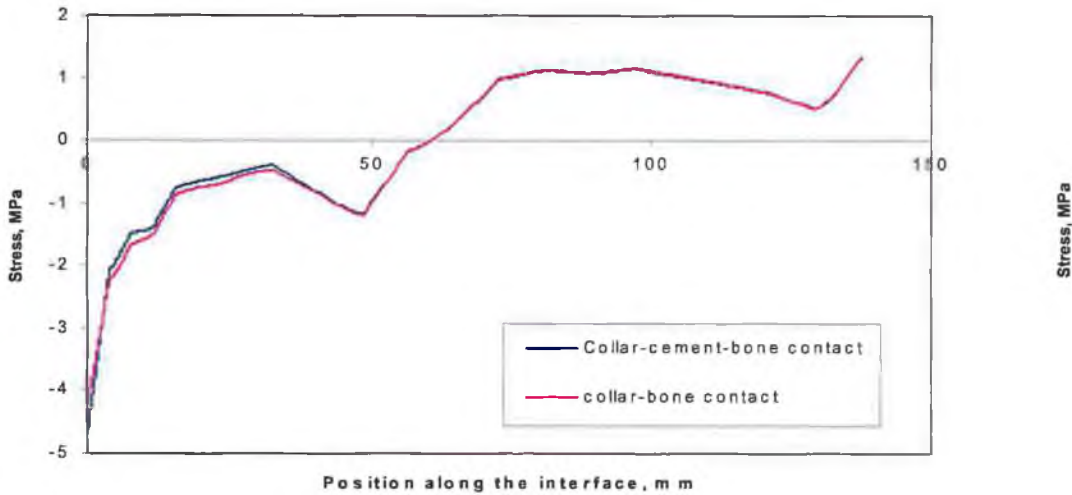


Figure 4.38: Stress distributions in the interference side of the polymer in the stem for the two cases of contact in design no.3.

C) Design No. 6

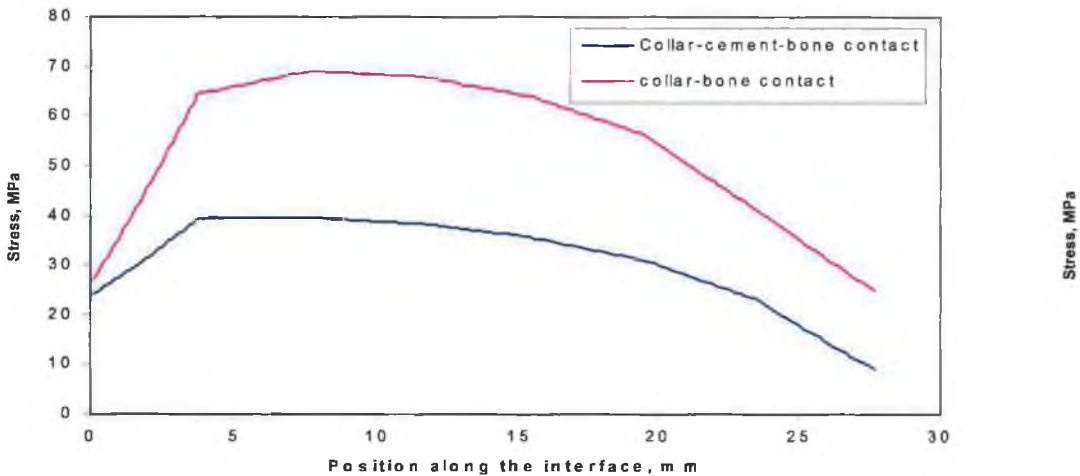


Figure 4.40: Stress distributions in the interference side of the CrCo in the stem for the two cases of contact in design no.6.

B) Design No. 4

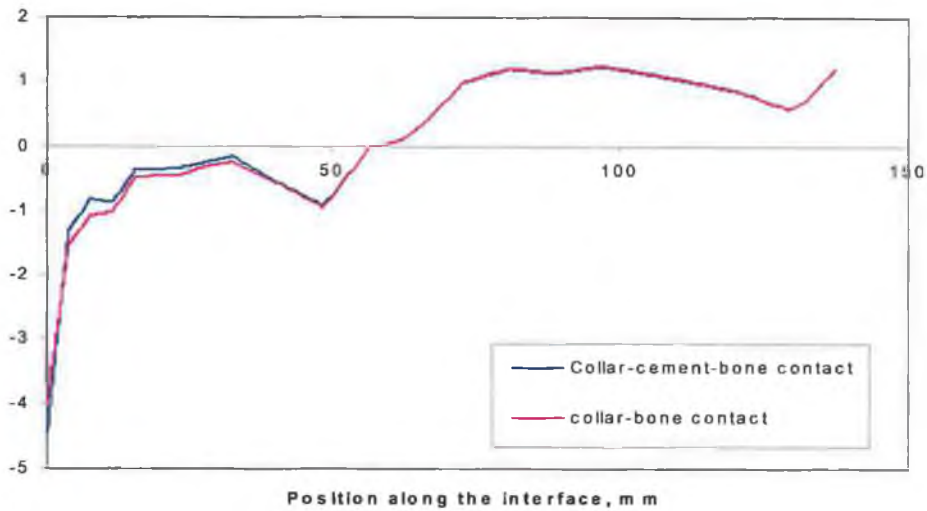


Figure 4.39: Stress distributions in the interference side of the polymer in the stem for the two cases of contact in design no.4.

D) Design No. 8

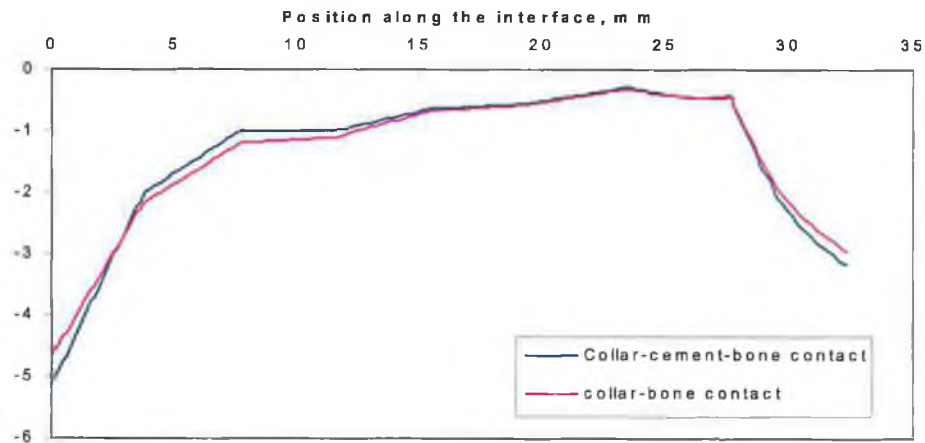


Figure 4.41: Stress distributions in the interference side of the polymer in the stem for the two cases of contact in design no.8.

E) Design No. 9

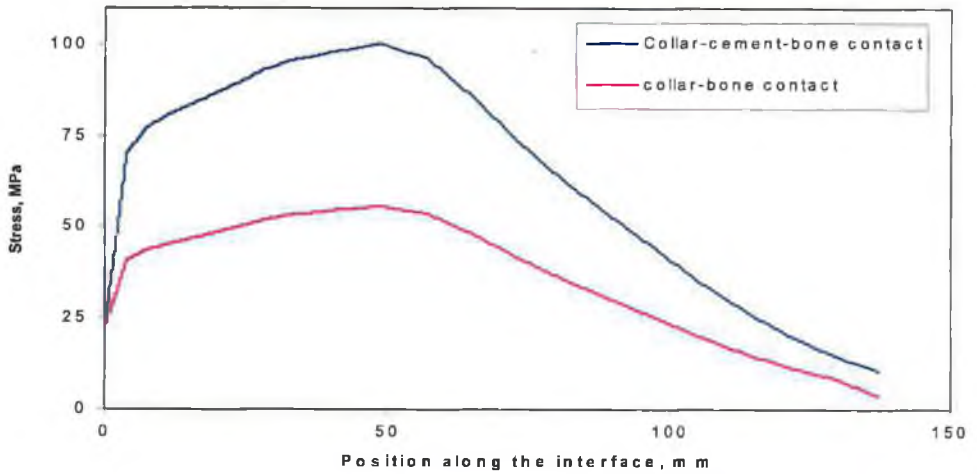


Figure 4.42: Stress distributions in the interference side of the CrCo in the stem for the two cases of contact in design no.9.

F) Design No. 10

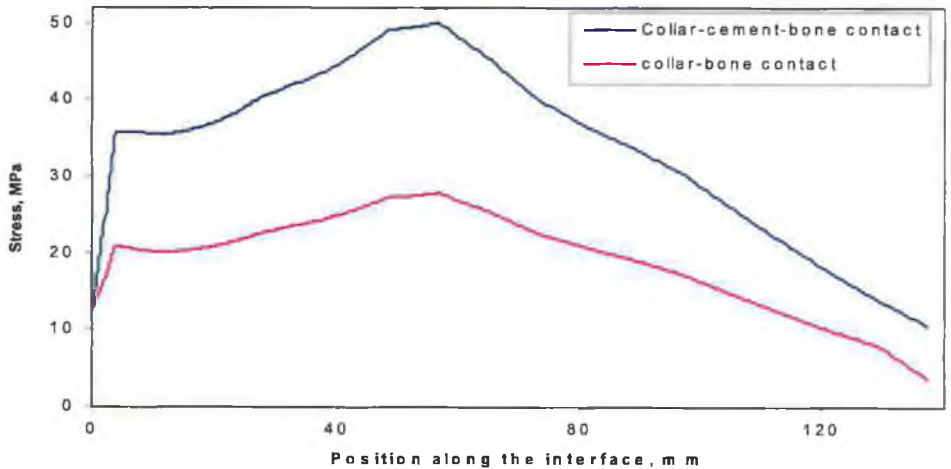


Figure 4.43: Stress distributions in the interference side of the CrCo in the stem for the two cases of contact in design no.10.

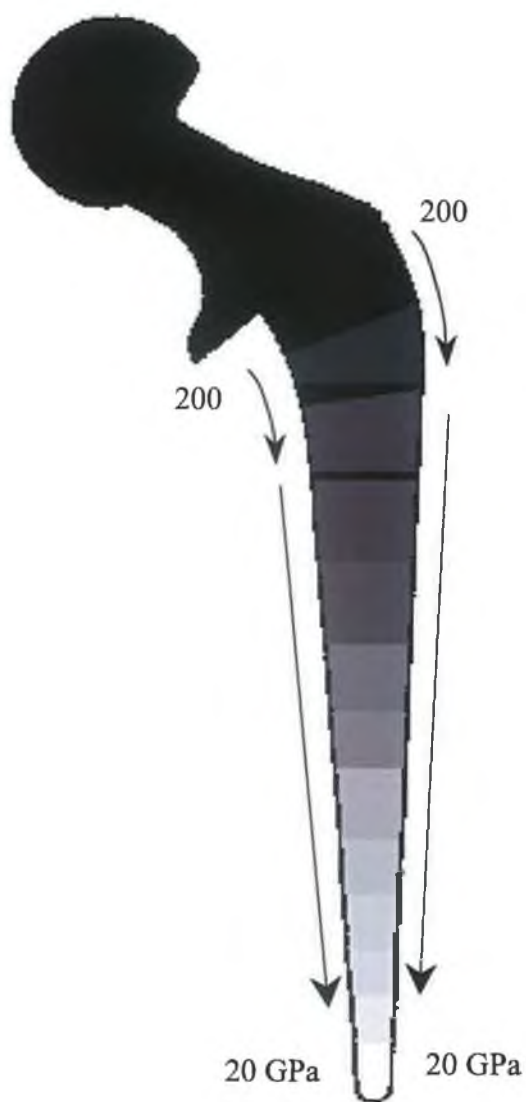


Figure 4.44: Design No. 11, a modified hip prosthesis of declined stiffness along the stem.

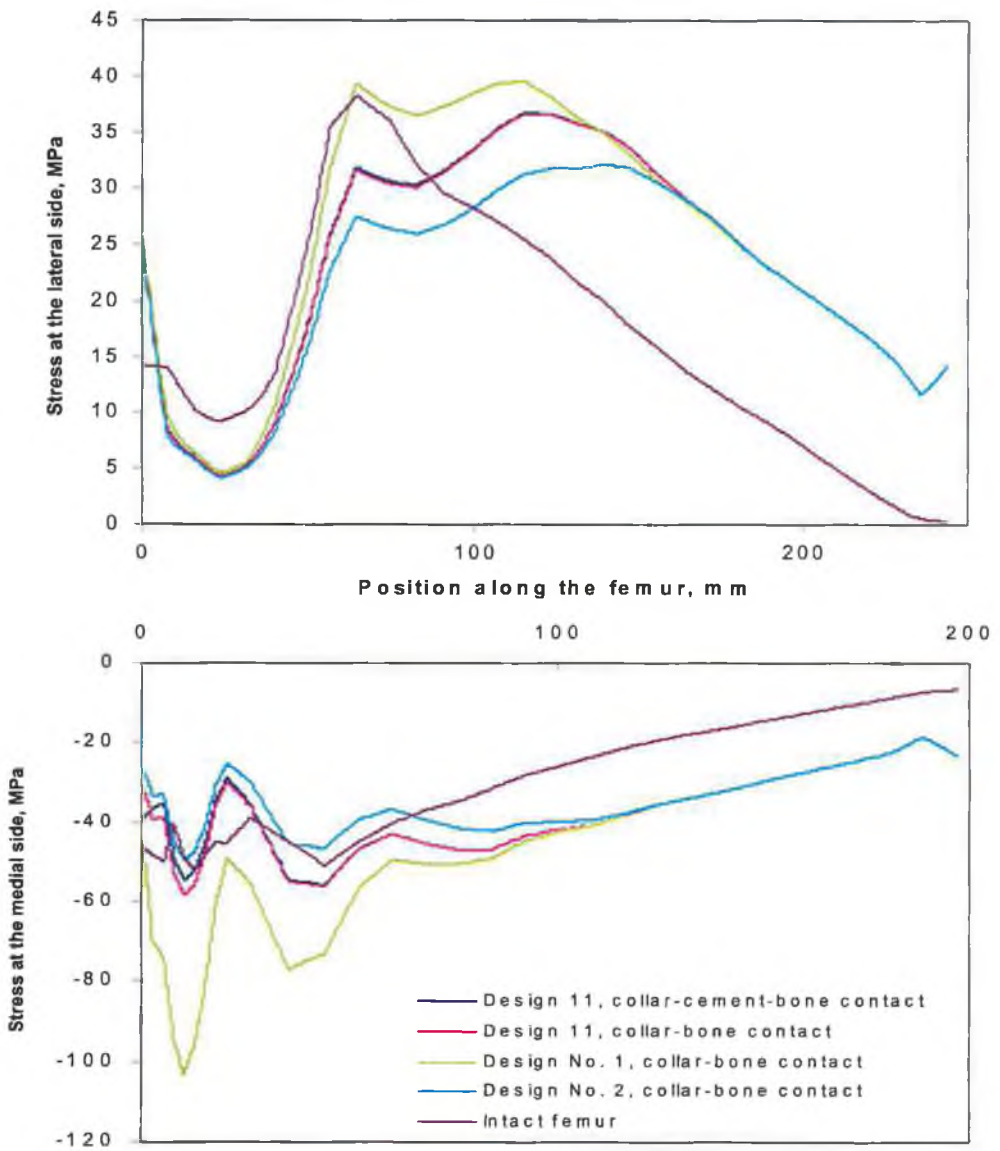


Figure 4.45: Stress distributions in the lateral and medial sides of the femur for different prosthesis designs.

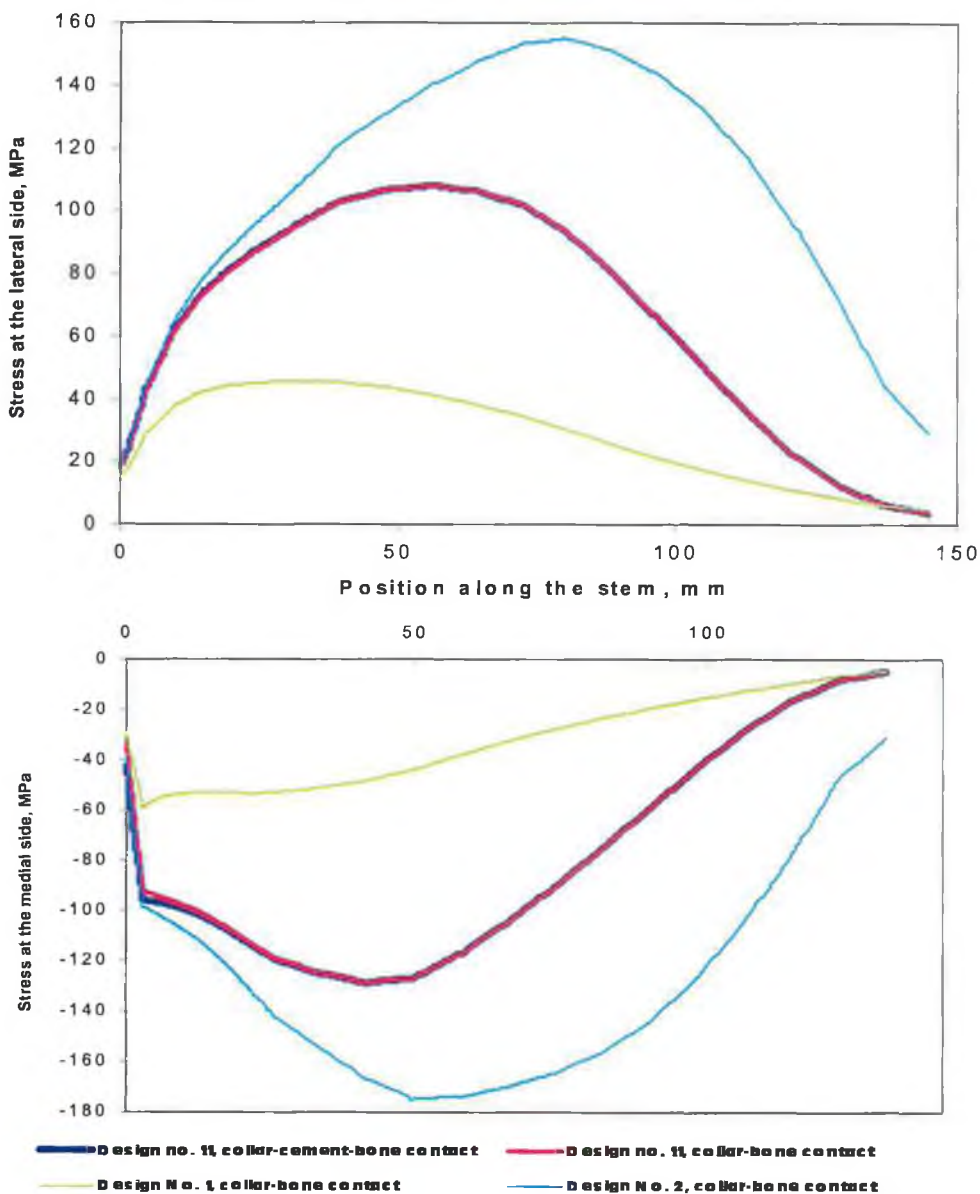


Figure 4.46: Stress distributions in the lateral and medial sides of the prosthesis stem for different prosthesis designs.

these because of the high stiffness that still exist in proximal middle of the prosthesis.

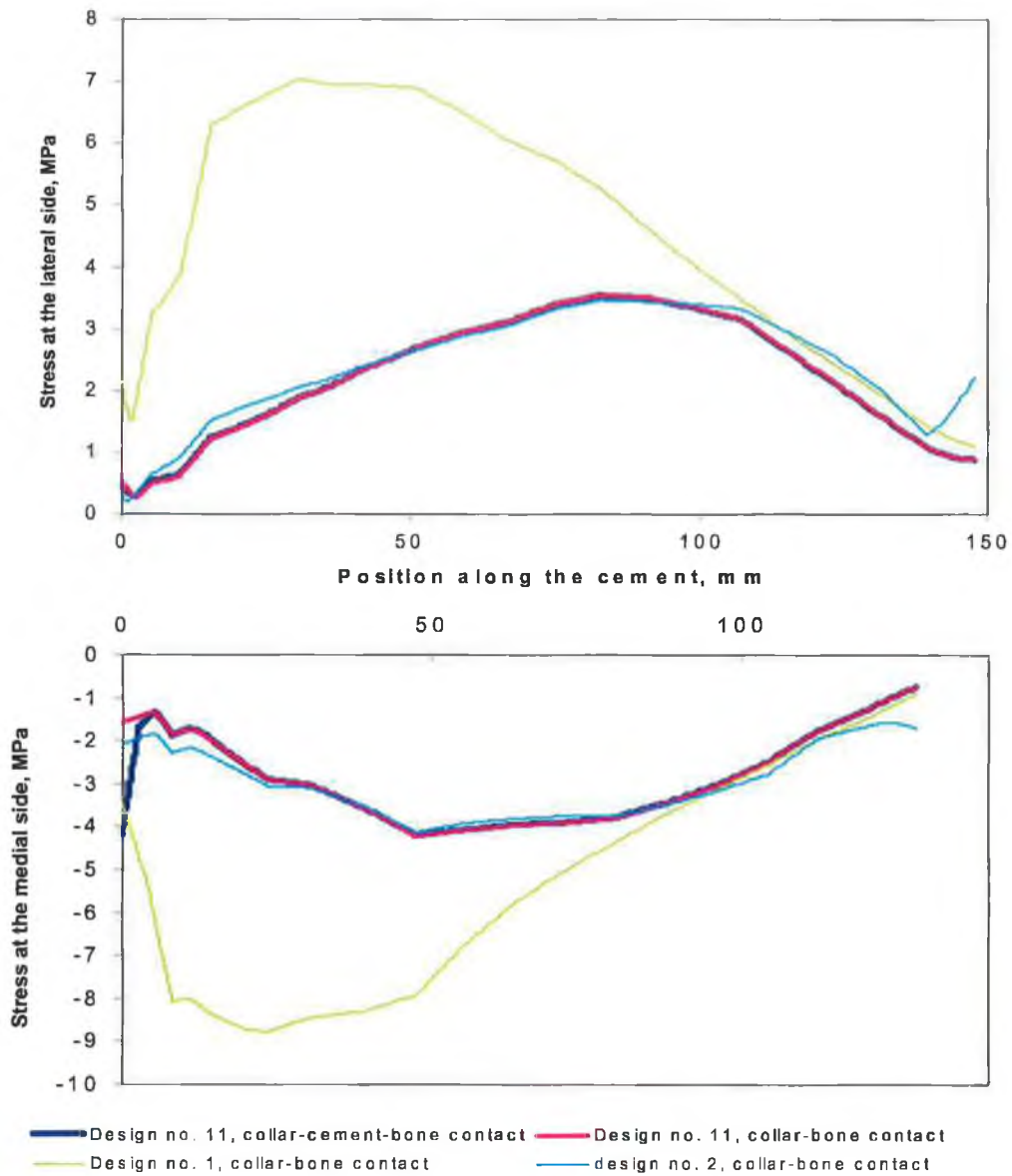


Figure 4.47: Stress distributions in the lateral and medial sides of the cement mantle as a function of different prosthesis designs.

4.5.3. Role of the Collar (Calcar Support) on the Femoral Stem of Cemented Total Hip Replacements

The majority of cemented total hip stems have some kind of collar, which is designed to transmit the more axial components of the hip reaction into the resected neck of the femur and thus load the bone in as natural a manner as possible. Of these collared prostheses, there are three types currently available to surgeons performing total hip replacement:

- The first group reconstructs the proximal femur with an implant which has large collar designed to seat on the neck of the femur and transmit the load directly into the cortex.
- The second type employs a collar that is smaller and designed to seat only on cement. In this design, the load is transferred through the cement to the inner surface of the bone at the medial femoral neck, in the same manner and direction as the trabecular transfer the load to the neck in a natural femur.
- A third design is the completely uncollared version. This prosthesis relies on its wedging action in the cement bed to transfer axial load from the hip reaction through to the femur.

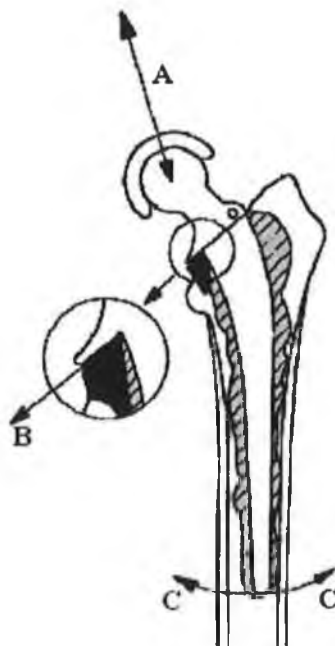


Figure 4.48: The "pendulum theory" of hip endoprosthesis stem loosening.

Large calcar support (collar) areas are aseptically promoted by Oh and Harris [194]; small collar supports are since many years in clinical use in the Charnely and Weber-type femoral stems. No calcar support is demanded by Ling et al. [158]. Clinical experience has shown that many cemented femoral components subside during the years and do not loosen [69]. This is considerably impeded by a large calcar support of the prosthesis. During the course of loosening, this support may be nothing less than the support of a pendulum, Figure 4.48, which enhances loosening by preventing the sinking in and relocking of the prosthesis in the femoral canal. The rationale for no calcar support at all is much better supported by clinical and theoretical data. A small calcar support which allows for a rest of the prosthesis on the cement cuff only and therefore does not prevent the prosthesis from settling during interface remodelling is considered the optimum solution [69]. It combines the advantages already mentioned for small calcar supports with a better load distribution on the cement cuff and a minor risk of splitting of the cement cuff by sinking into it.

However, as the long-term clinical results of replacement operations have become available, the emphasis has changed and the collar is now thought of as a mechanism to load and preserve the medial cortex. The major complications of hip prostheses are loosening and fracture of the femoral of the femoral stem. The causes are numerous, but are thought to include cement fracture and failure of the cement-bone interface, leading to excessive stresses [17, 42, 99]. Loss of proximal support, while maintaining rigid distal fixation is also reported to be a major cause of failure of the joint. In particular, resorption of the medial femoral neck was implicated in the study by Wroblewski [292], which examined the fracture of Charnley prostheses. The necrosis of some bone in the femoral canal after hip replacement is accepted, and thought to be related to a combination of mechanical, chemical and thermal trauma which arises from the preparation of the medullary canal and insertion of the implant [42, 83]. However, the resorption of the bone at the femoral neck is now generally attributed to stress shielding of the bone by the stiff femoral stem [177]. The collar on a femoral stem is now seen to be important, since several mathematical and experimental studies show that it may be capable of restoring some of the stresses to the cortex, and therefore possibly prevent the calcar loss.

The clinical performance of both the collared and uncollared prostheses shows that the resorption of the medial femoral neck is in fact more complicated than this [80]. The most important information comes from the uncollared stem, which are reported to be capable of operating without noticeable bone loss [152]. After the final positioning of the collarless stem, it has been the practice of some surgeons to leave a layer of cement over the resected neck of the femur, forming a non-load bearing pseudo-collar; it is in these replacements, using a collarless stem but with a pseudo-collar of cement, that height loss of the femoral neck is reported [80].

Clinical follow-up of the performance of collared implants shows that resorption of the medial-femoral neck occurs in the majority of patients, both with small and large collared stems. For example, with the smaller collared type, Charnley [42], in his 12-15 year follow-up, reports that calcar loss was 95% of the stems. Implants with a large collar, designed to seat on the resected neck of the femur, have been reported to display resorption of the femoral neck in 70% of all cases after 0.5-11 years of service [52]. In practice there are two reasons why the larger stems cannot function as they are designed to, and which at first appear to be responsible for the bone loss, although experience with other types of stem shows that the causes are more complex. Firstly, for this type of collar to operate efficiently, a uniform degree of contact with the bone must be achieved. It is usual however, for a few localised contact areas to support the collar. This arises from the difficulty of cutting the neck of the femur at precisely the correct angle, and then ensuring that the cut surface is perfectly flat. The areas of the collar not in contact with the bone will be supported by cement which has extruded from the femoral canal during insertion of the stem; this is the second reason why ideal collar-femur contact cannot be achieved. To obtain maximum interlock of the cement with the bone, the medullary canal must be completely filled with bone cement before insertion of the stem. On the introduction of the implant, the cement will be forced out of the canal so that, at the final seating of a collared implant, there will always be a thin layer of cement under the collar [80].

The work presented here is a further examination of the effects of (a) prosthesis Young's modulus, and (b) the collar of cemented total hip stems on stress shielding on the bone cortex. To investigate the differences between the various

types of prosthesis, a finite element model for the following configurations of prostheses for two different materials, Polymer composite and CrCo, was developed, Figure 4.49:

- Case (1)** Collared stem with collar-cement-femur contact; it was assumed that there is a layer of cement trapped between the collar and the surface of resected femur neck.
- Case (2)** Collared stem with perfect collared-femur contact (ideal case).
- Case (3)** Collared stem seats just on the cement cuff, in this case the collar was modelled to be small to fit on the cement cuff.
- Case (4)** Collared stem seats only on the bone; in this case the row of element which is in contact with the bottom surface of the collar was deleted.
- Case (5)** Uncollared prosthesis.

The stresses in the stem, cement and bone were compared for each case. A finite element model of the natural femur before arthroplasty was also produced to act as a reference for the bone stresses predicted by the models of the implanted components.

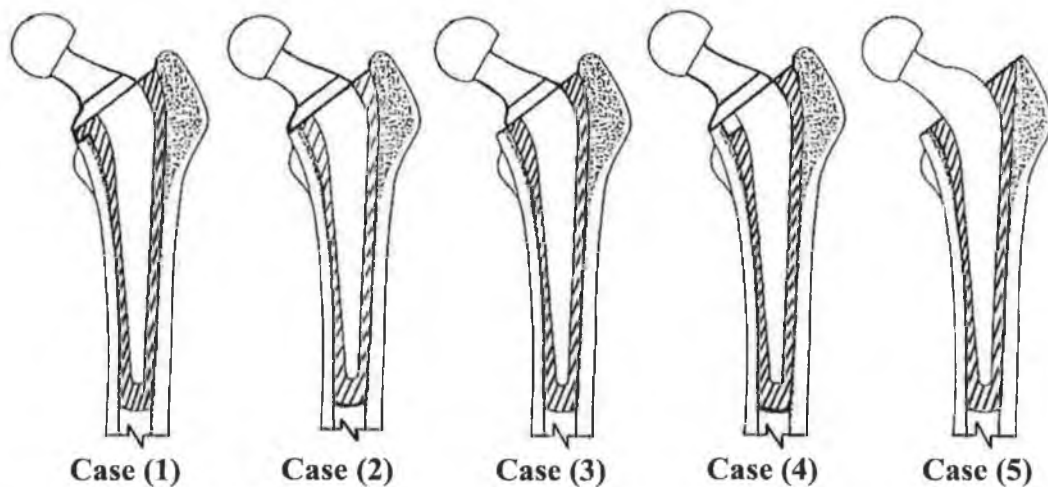


Figure 4.49: The different five artificial hip configurations:

- Case (1): Collared stem with collar-cement-femur contact.*
- Case (2): Collared stem with perfect collared-femur contact (ideal case).*
- Case (3): Collared stem seats just on the cement cuff*
- Case (4): Collared stem seats only on the cut surface of the femoral neck bone.*
- Case (5): Uncollared prosthesis.*

The effect of a collar on the stresses in the stem is demonstrated in Figure 4.50A/B. It is obvious that there is no difference in the stress patterns developed in the lateral and medial sides of the stems for cases 2 and 4, however, they are quite large in comparison to the other cases demonstrated in the same figure. The reason for the high stress in the two mentioned cases is that the collar is assumed to be firmly bonded with the surface of the resected neck. It means there is no chance for rigid prosthesis to move in the medial direction, see Figure 7.2, within the modularly canal once the force is applied on its head. So that the whole structure (bone, cement & prosthesis) will bend altogether in medial direction creating large deformation to the prosthesis stem. For case 5, where the prosthesis is collarless, there is a chance to the stem to subside in to the cement mantle and at the same time move in the medial direction. In addition to this as it is known, the stiffness of the cement is much lower than that of the prosthesis, so the stem will be easy move around the cement mantle with less deformation. For this reason the stem of this design exposes to stresses lower than cases 2 and 4. When a smaller collared stem designed to seat just on the cement, case 3, the collar compels the cement mantle to move slightly down with the prosthesis when the load is applied. Because, in this case, the cement cuff acts as a support, the bending in the stem will be less than the collarless stem. The reason of less bending is because of the presence of soft cement under the collar. The prosthesis will subside slightly in the cement increasing bending to the stem in comparison to the case 1. That is why the stresses in this case are greater than that of the case 1 and less than case 5. The cement layer trapped between the collar and the surface of the resected neck, case 1, forms a soft bed, in addition to the soft cement mantle that surrounds the rigid stem. When the force is applied over the prosthesis head, the soft cement bed behaves like spring absorbing most of forces under the collar [80] leaving the prosthesis to tilt. Due to the pivot action of the collar the stem will expose to the lesser bending, because its stiffness large than that of cement. A large pressure and deformation will be created in the cement mantle directly under the collar in the proximo-medial side due to the movement of the rigid stem in the lateral direction within it. It has been shown in this case that the prosthesis has more chance to move quiet easily in the modularly canal, due to the action of the soft bed of the cement, producing lesser deformation and stresses in the stem comparing to

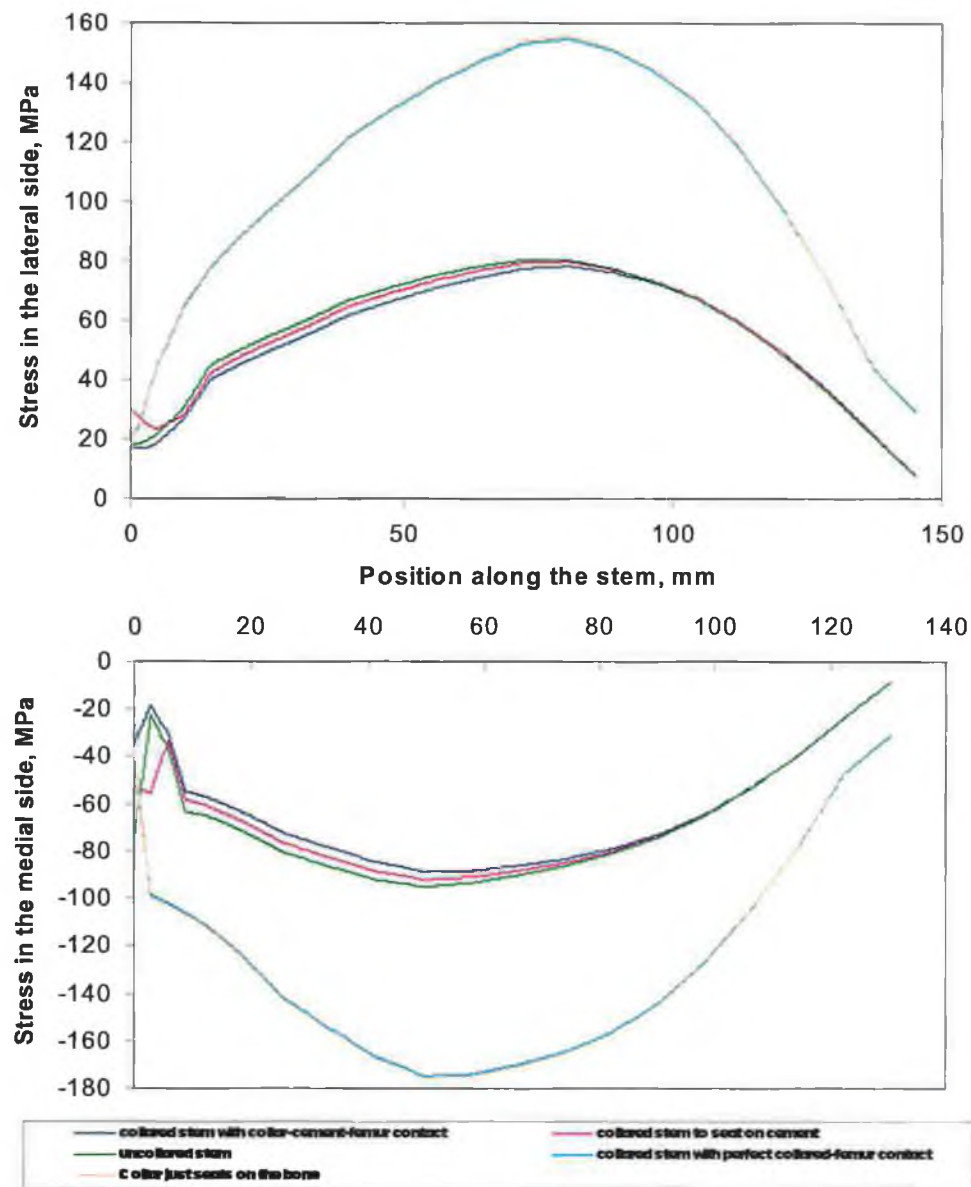


Figure 4.50A: Max. and min. principal stress distributions, in MPa, in the lateral and medial sides of the collared and uncollared stems made of CrCo.

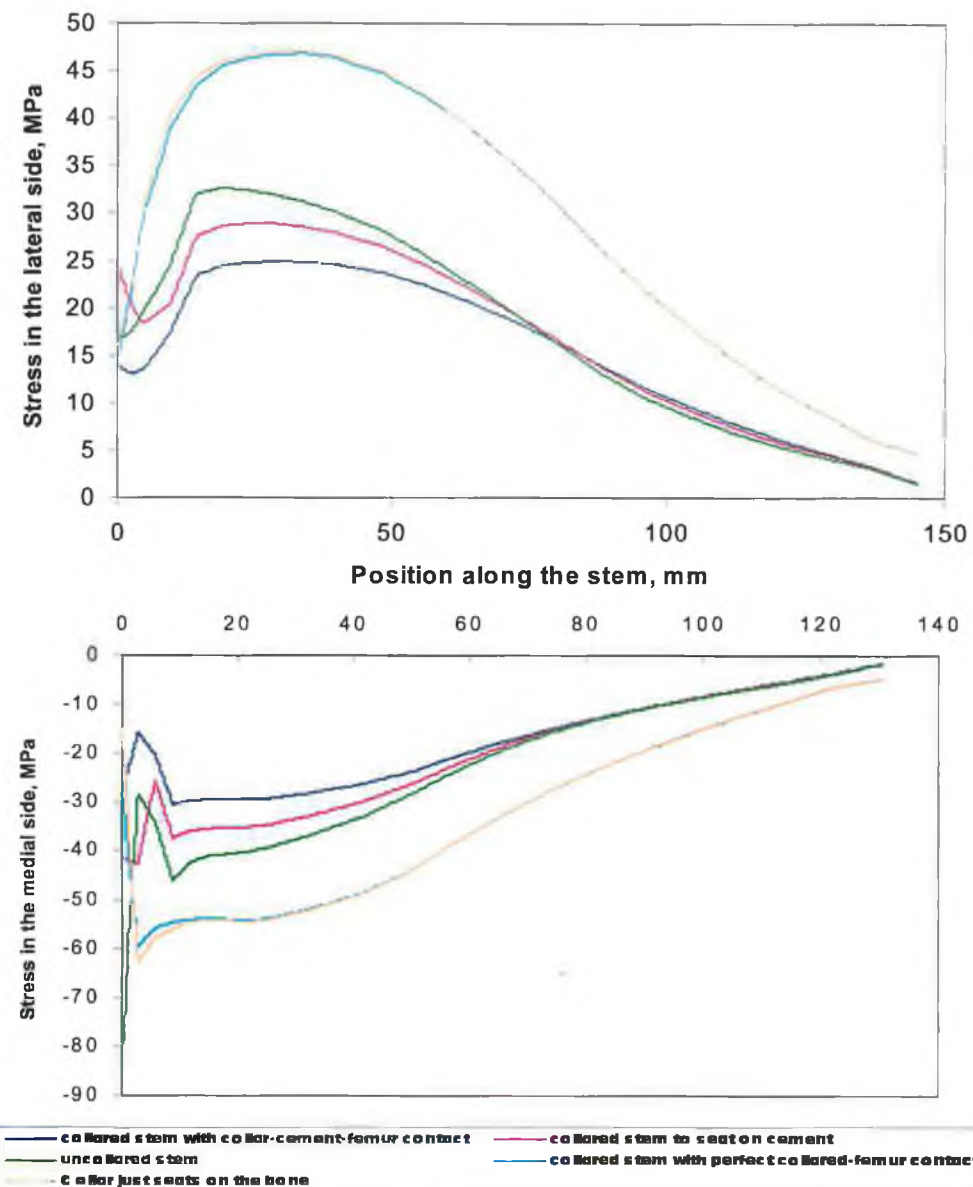


Figure 4.50B: Max. and min. principal stress distributions, in MPa, in the lateral and medial sides of the collared and uncollared stems made of polymer combisite.

The other cases mentioned above. By comparing Figures 4.50A and 4.50B, one can recognise that as the material stiffness increases the effects of cases 1, 3, and 5 on stress distributions on the stem become close.

The effect of case 4 on the stresses in the cement mantle is affected by the prosthesis stiffness. However, in the lower prosthesis stiffness, Figure 4.51B, the stress values are identical to that of case 2, while as the prosthesis stiffness increases the stress in the cement mantle developed on the strength of case 4 will be decreased remarkably, Figure 4.51A. The effects of cases 1, 3, and 5 on stress distributions in the cement mantle for prosthesis of high stiffness is negligible and all become so close as indicated in Figure 4.51A. While for that of lower stiffness, polymer composite, the effect is obvious only in the upper lateral side while distally is negligible. With an intervening layer of cement under the collar, a peak loading is recorded in the cement directly below the collar and this is in agreement with [80].

Figures 4.52A/B show the only region of the femur effected is the upper proximal third of the medial side, and this is in agreement with clinical observations where they note bone loss in this segment of the medial side of the femur after hip replacement [17, 126]. The stresses transferred to the bone due to the use of collared prosthesis is higher and is close to that of the intact femur in the case of using CrCo collared prosthesis. While in the case of low stiffness, the stresses developed in the bone exceed the physiological stresses in both cases, collared and uncollared prosthesis, Figure 4.53. Also, one can see that the effect of case 4, positioning the collar just on the surface of resected neck without any contact to the cement cuff, on the stress distributions in the medial side of the femur neck. In which its curve is close to that of intact femur, when CrCo prosthesis is used, and coincides to that of ideal case.

Considering hoop stresses, Fagan and Lee [80] reported compressive stress in the intact femur of maximum magnitude 3 MPa. However, Figure 4.54 shows that uncollared prostheses create tensile hoop stresses. This is attributable to the wedging effect of the tapered prosthesis stem. This is in agreement with results reported by Prendergast and Taylor [213], and Fagan and Lee [80]. For collared prosthesis this wedging effect does not operate and the results tend to be compressive hoop stress,

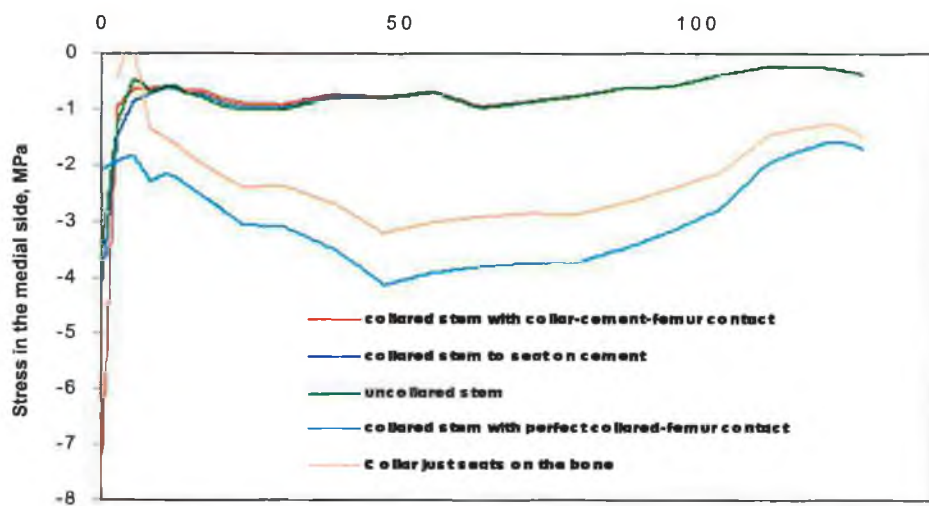
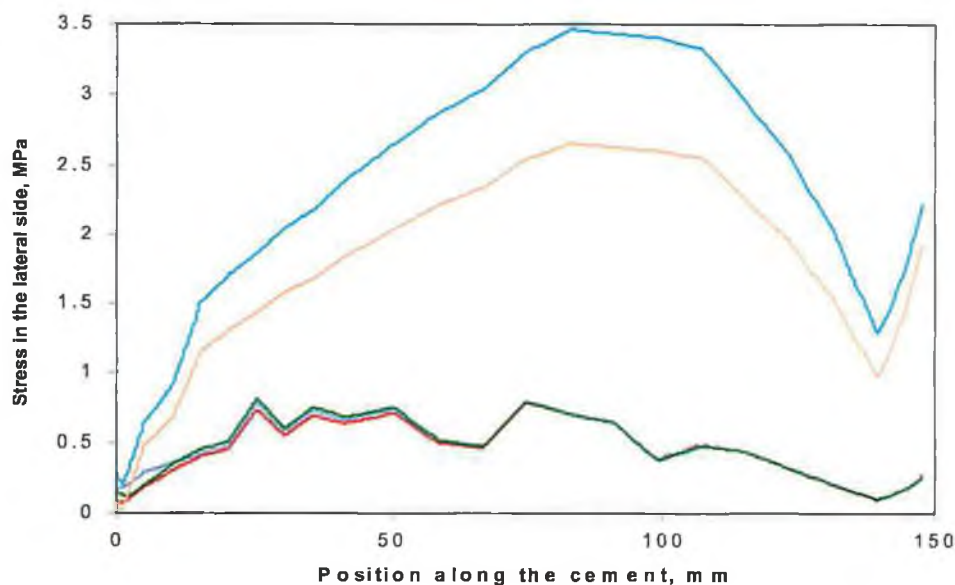


Figure 4.51A: Maximum and minimum principal stresses in the lateral and medial sides of the cement for collared and uncollared stems. Prosthesis Young's modulus = 196 GPa.

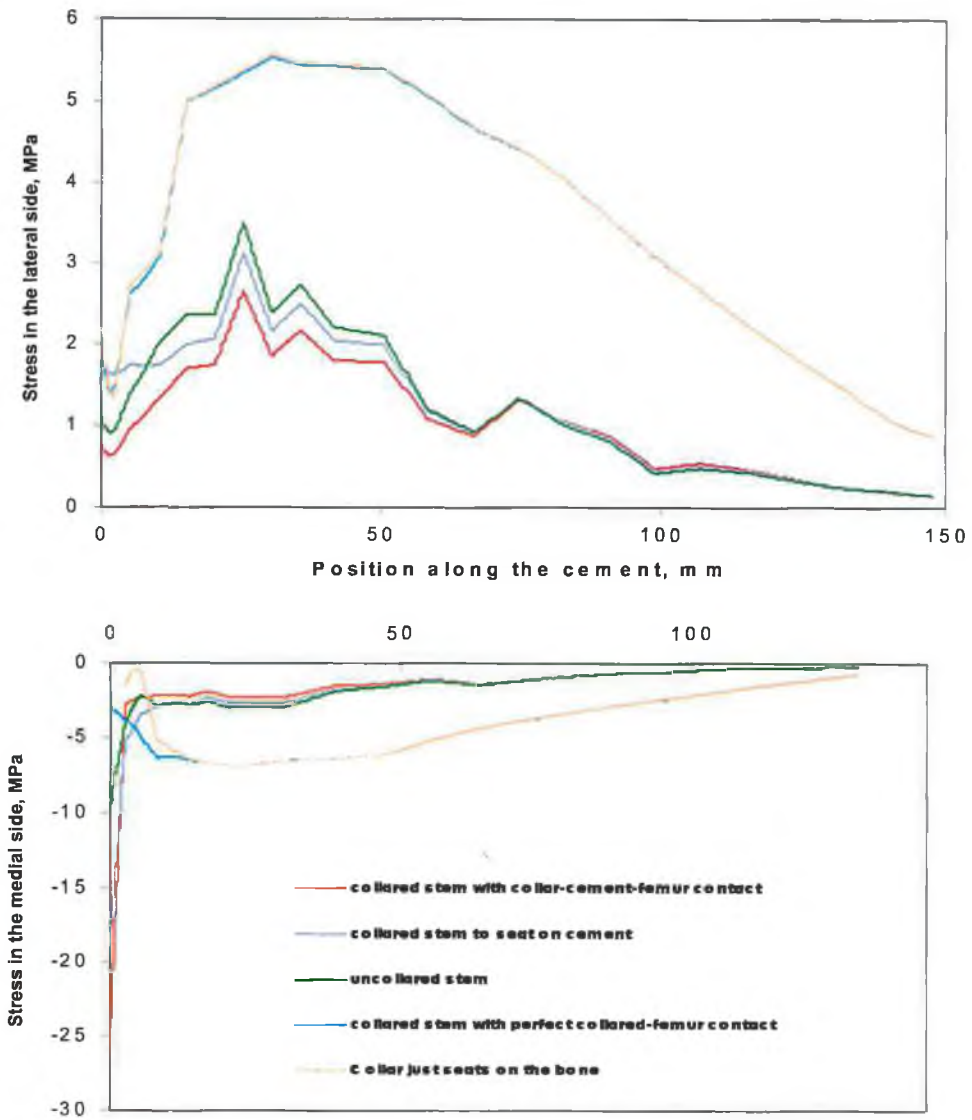


Figure 4.51B: Maximum and minimum principal stresses in the lateral and medial sides of the cement for collared and uncollared stems. Prosthesis Young's modulus = 25 GPa.

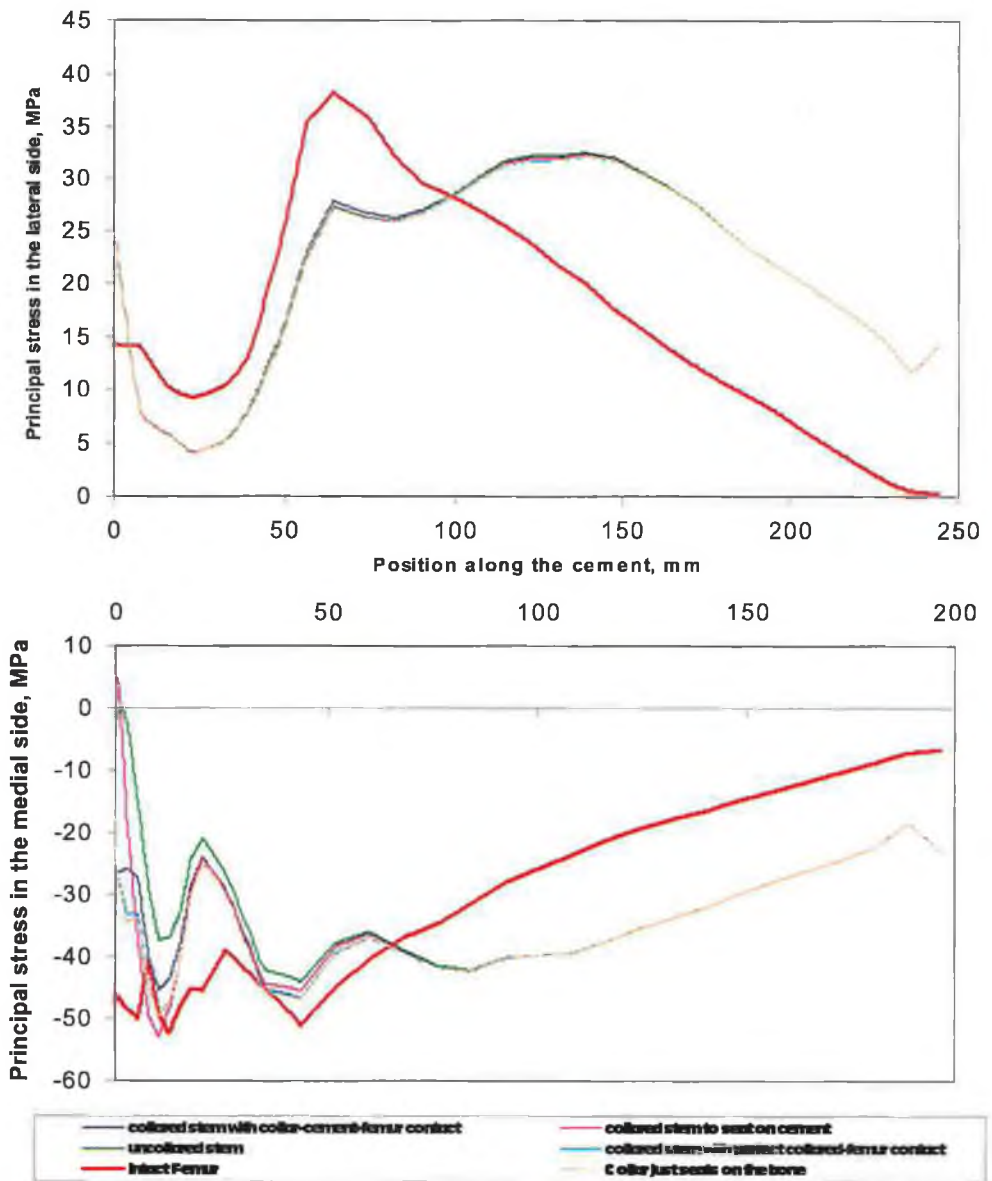


Figure 4.52A: Maximum and minimum principal stresses in the intact and implanted femur with collared and uncollared stems. Prosthesis Young's modulus = 196 GPa.

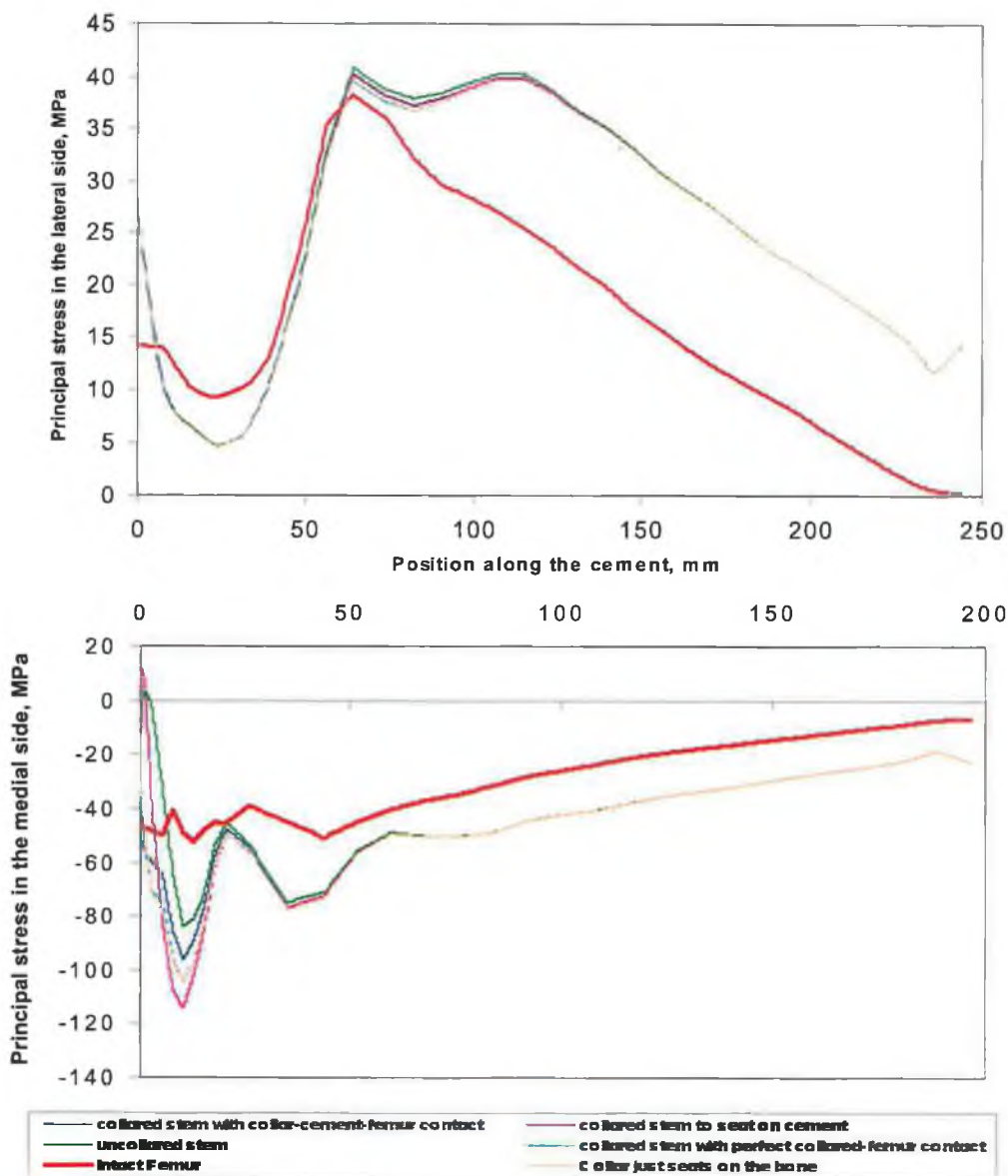


Figure 4.52B: Maximum and minimum principal stresses in the intact and implanted femur with collared and uncollared stems. Prosthesis Young's modulus = 196 GPa.

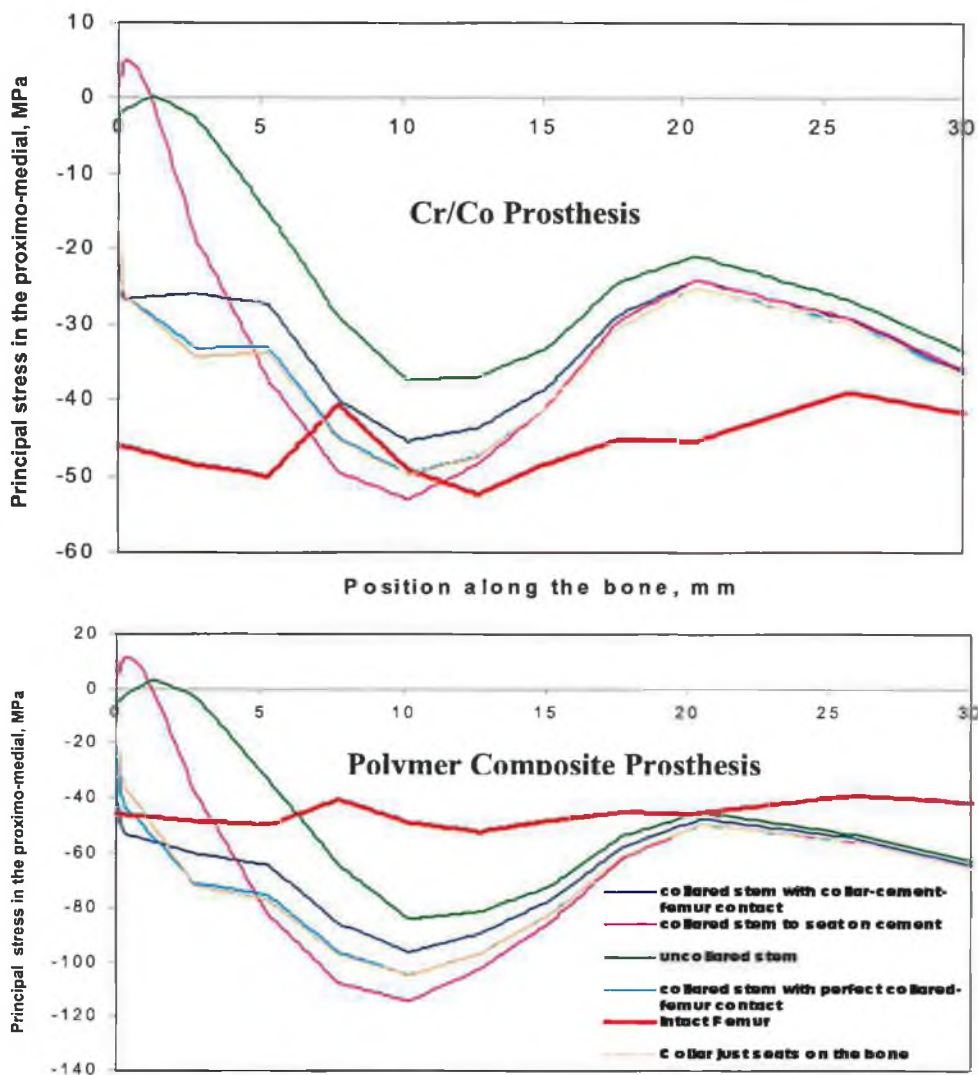


Figure 4.53: Minimum and maximum stresses in a region extending 30 mm below the femur neck for collared and uncollared stems.

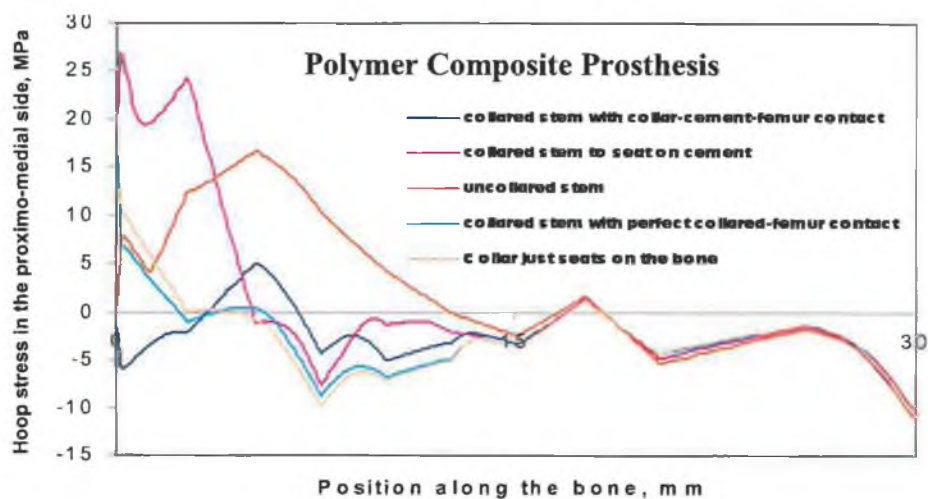
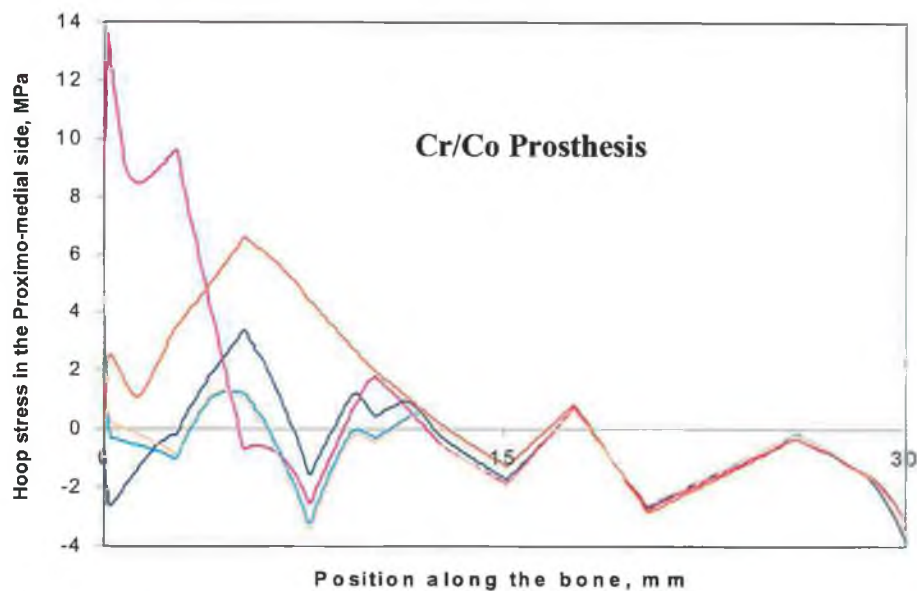


Figure 4.54: Hoop stresses in a region extending 30 mm below the femur neck for collared and uncollared stems.

Figure 4.54. Prendergast and Taylor [213], reported the same results which are in contrast with that reported by Fagan and Lee [80]. The greatest stresses, principal and hoop stresses, are produced by the (smaller) collared stem designed to seat on the cement and transmit the load into the femoral neck, Figures 4.53 and 4.54. The uncollared stem produces higher hoop stresses than the larger collared implants, presumably because of its ability to move further down into the cement, and thereby assert a greater internal pressure on the cement-bone composite. All of these were, also, in agreement with [80]. The value and sign of the hoop stress may be more critical than its magnitude would suggest [80, 213]. One could postulate that bone damage is more easily induced in the hoop direction than in the axial direction due to the fact that osteons are aligned axially.

The variations of the stem-cement and cement-bone interfacial shear stresses down the length of the model are presented in Figures 4.55 and 4.56 (A and B). At the stem-cement interface the highest shear stress value was that produced by using uncollared stem, that is this prosthesis has the ability to move within the cement mantle more than the collared ones. Only two cases, collared stem seats on the cement cuff and uncollared stem, have a sound effect on changing the shear stress distributions developed in the stem-cement interface, while the other cases do not. At the second distal half of the interface all the stresses are coincided, Figures 4.55A/B. It has been noted that the shear stress developed in the cement-bone interface, Figures 4.56A/B, is compressive in the upper proximo-medial side when an uncollared prosthesis is used, and then it tend to coincide to the other stress curves of the collared prostheses to be zero at the distal side. Also, was noted that the highest shear stress in the lateral side of the cement-bone interface was produced by using collared CrCo stem with perfect contact, case 2, Figure 4.56A. While it was highest by using polymeric uncollared prosthesis, Figure 4.56B. Case 4, collar sits on just the respected surface of the femoral nick, the shear stress in the cement-bone interface tend to be zero as the prosthesis stiffness increases. This because most of the shear stresses were absorbed by the stem-cement interface. However, after analysing the shear stresses in the cement-bone interface for different prosthesis configurations and materials it is not quiet understood what factors influenced the difference in these results.

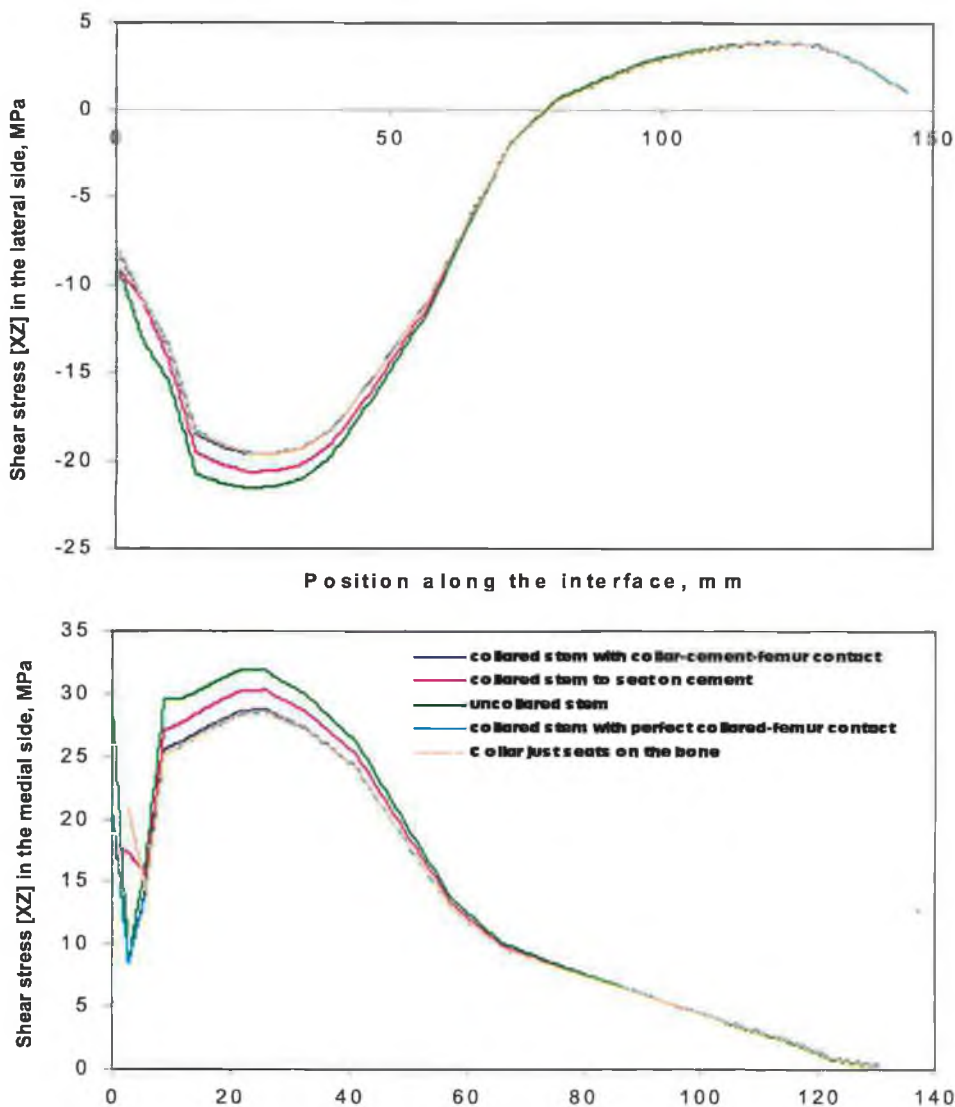


Figure 4.55A: Shear stresses in the stem-cement interface, in the lateral and the medial sides, for collared and uncollared stem. Prosthesis Young's modulus = 196 GPa.

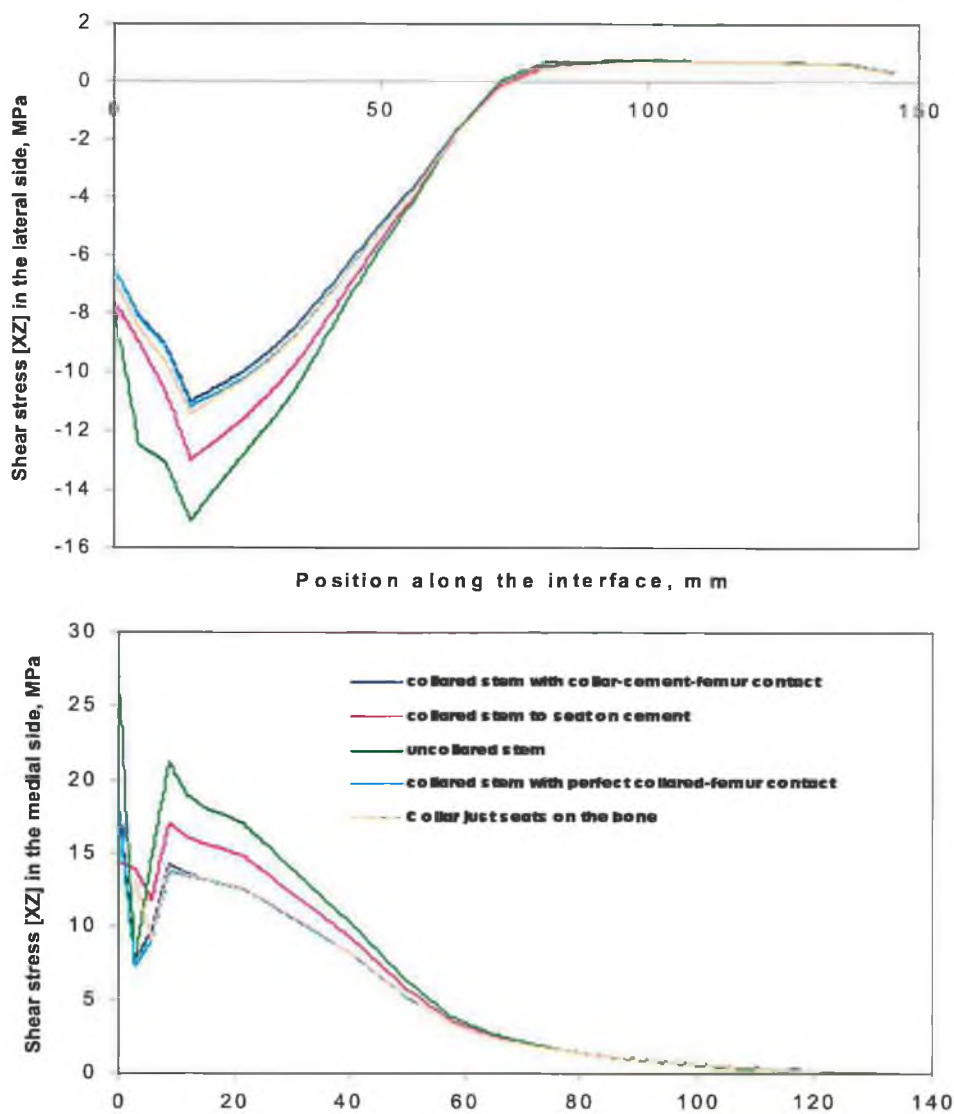


Figure 4.55B: Shear stresses in the stem-cement interface, in the lateral and medial sides, for collared and uncollared stem. Prosthesis Young's modulus = 25 GPa.

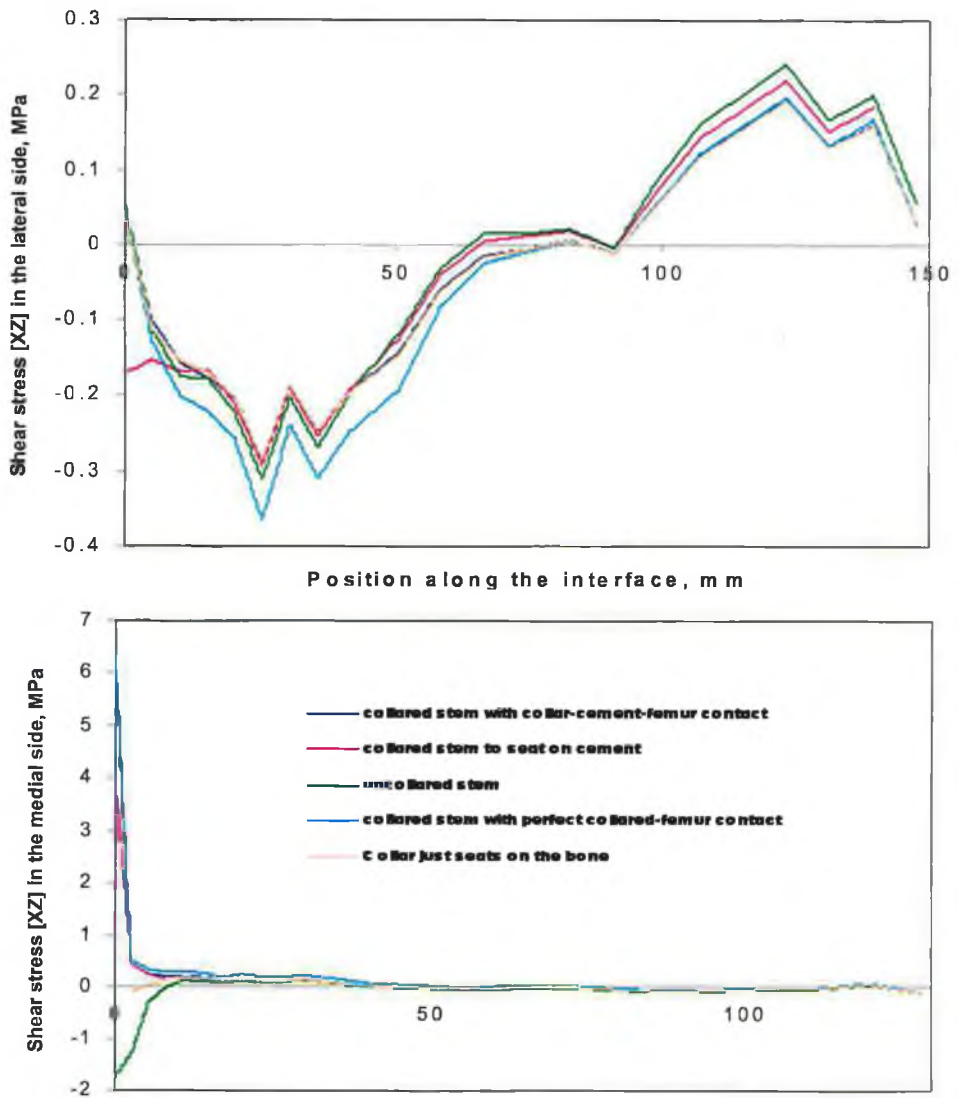


Figure 4.56A: Shear stresses in the cement-bone interface for collared and uncollared stem. Prosthesis Young's modulus = 196 GPa.

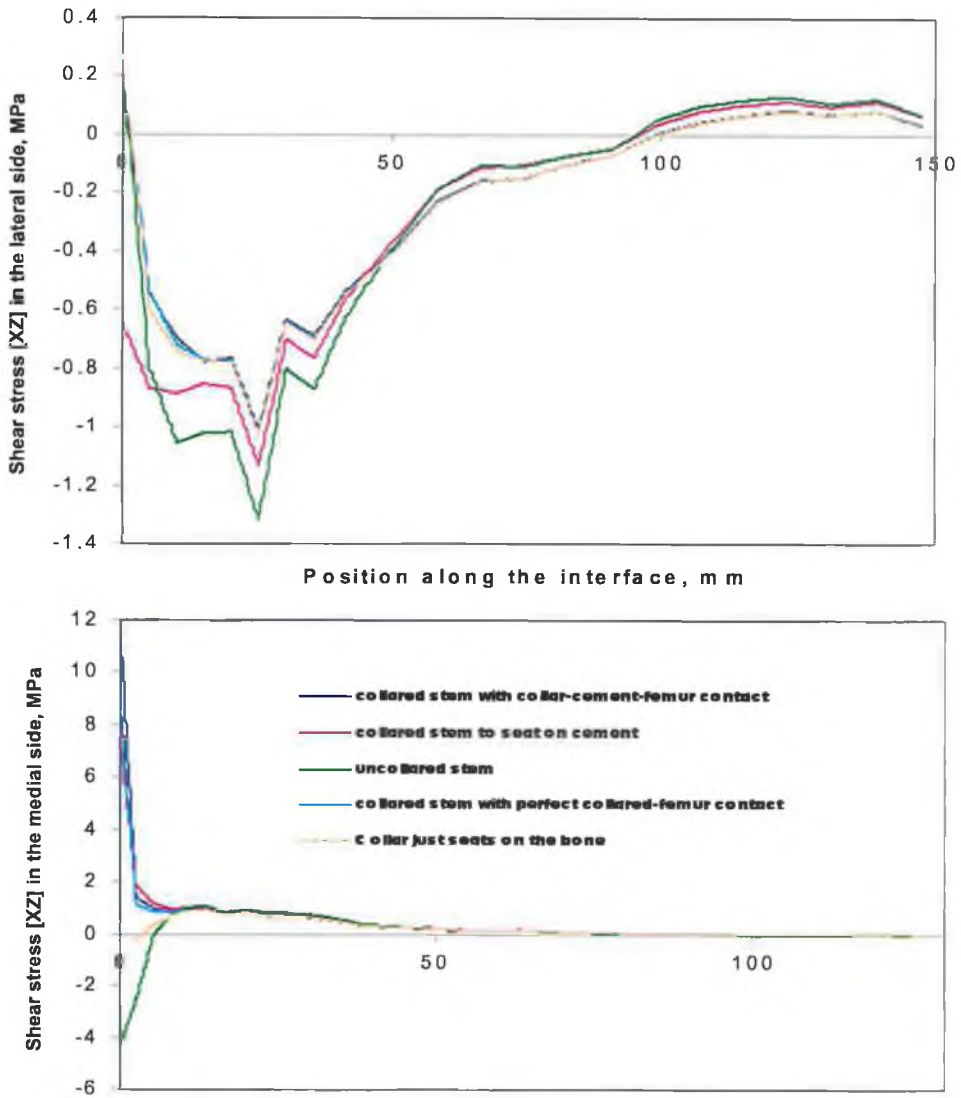


Figure 4.56B: Shear stresses in the cement-bone interface for collared and uncollared stem. Prosthesis Young's modulus = 196 GPa.

4.5.4. *Effect of Prosthesis Length Stem*

The stem of the prosthesis was successively shortened by 16 mm. Figure 4.59 shows the effect of stem shortening on the stresses developed in the medial and lateral sides of the prosthesis stem. As the prosthesis stem becomes shorter, the stresses on the stem decrease, this is in agreement with [29, 58]. This phenomenon was also noticed in the cement mantle as illustrated in Figure 4.60. However, it is noted that the stresses at the stem tip are increased by decreasing the stem length. This is because when the prosthesis stem becomes shorter it loses part of its flexibility; therefore the prosthesis toggles in the medullary canal, generating high stresses at the level of the prosthesis tip. The compressive and tensile stresses on the lateral and medial sides of the cement mantle, respectively, were not effected by the stem lengths as shown in Figure 4.60.

Hoop stresses in the cement/bone interface are shown in Figure 4.61 and shear stresses developed in the same interface are shown in Figure 4.62A, B, and C. It must be noted, however, that significant hoop stresses and shear stresses were observed in the extreme proximo-medial side in the cement/bone interface. These stresses tend to be close to zero from the position below the neck up to the distal tip, Figures 4.61, 4.62A, 4.62B, and 4.62C. Also it is obvious that the stresses in this side are not effected by the stem length while in the lateral side they are. As the prosthesis stem becomes shorter the hoop stress and the shear stress τ_{XZ} at the lateral side of bone/cement interface increase as shown in Figures 4.61 and 4.62B, while the shear stresses, τ_{YZ} and τ_{XY} , decrease as shown in Figures 4.62A, and 4.62C. Since splitting failure is more serious than compressive failure, the shortened prosthesis would become very dangerous [29]. Figure 4.63 shows the effect of stem length on the stresses developed in the bone. The stresses in the bone cortex are very sensitive to the prosthesis stem length; they increase with decreasing the stem length, this is in agreement with [29, 58]. The moment applied to the prosthesis is resisted by normal forces between the bone and prosthesis as suggested in Figure 4.57. These forces are reduced if their moment arm is increased. Thus, a long stem prosthesis will result in a smaller contact forces on the bone. These forces are 'foreign' to the normal loading of the bone. They produce circumferential stresses which are at right angles to the

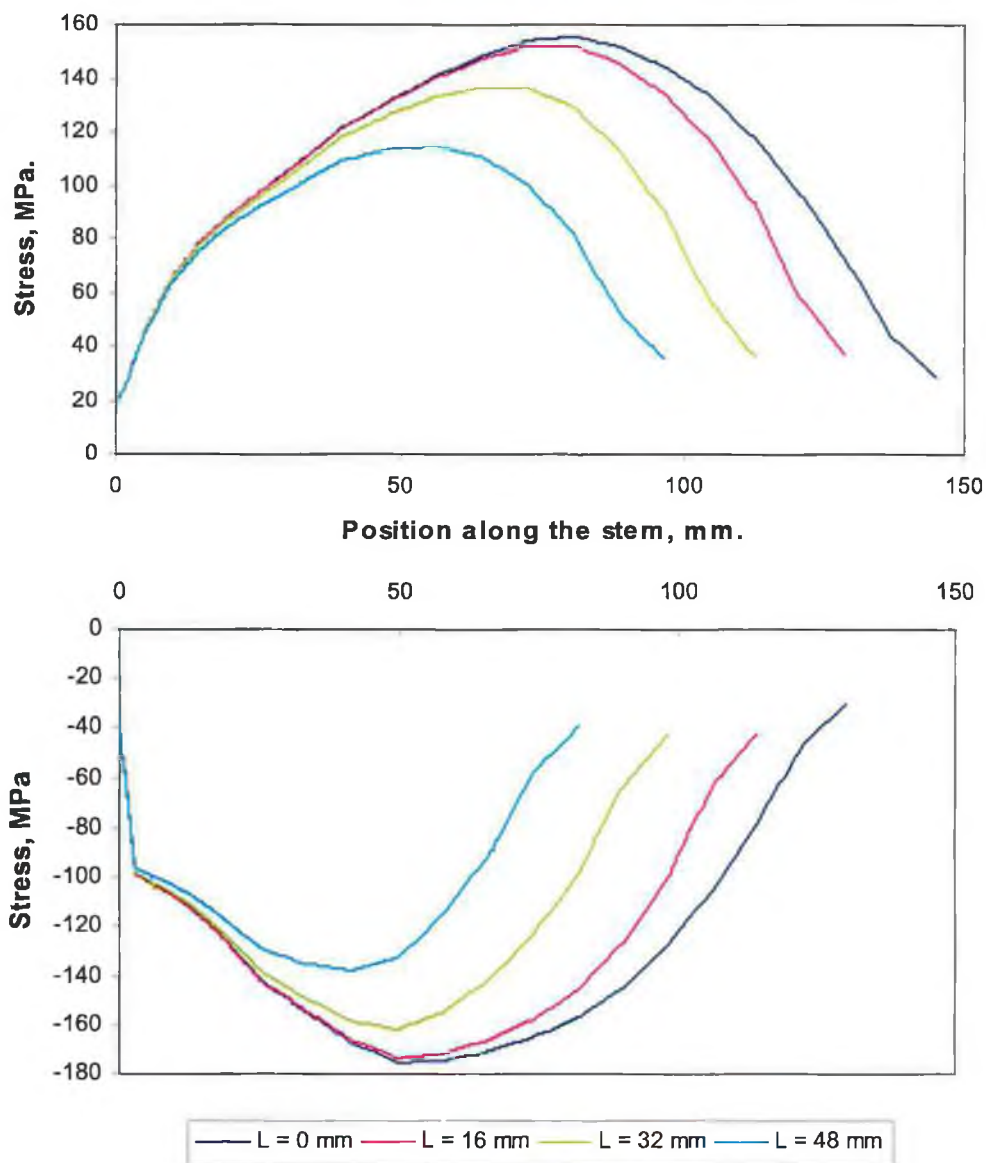


Figure 4.59, Minimum and maximum principal stress distributions, in MPa, in the lateral and medial sides of the prosthesis stem as a function of stem length.

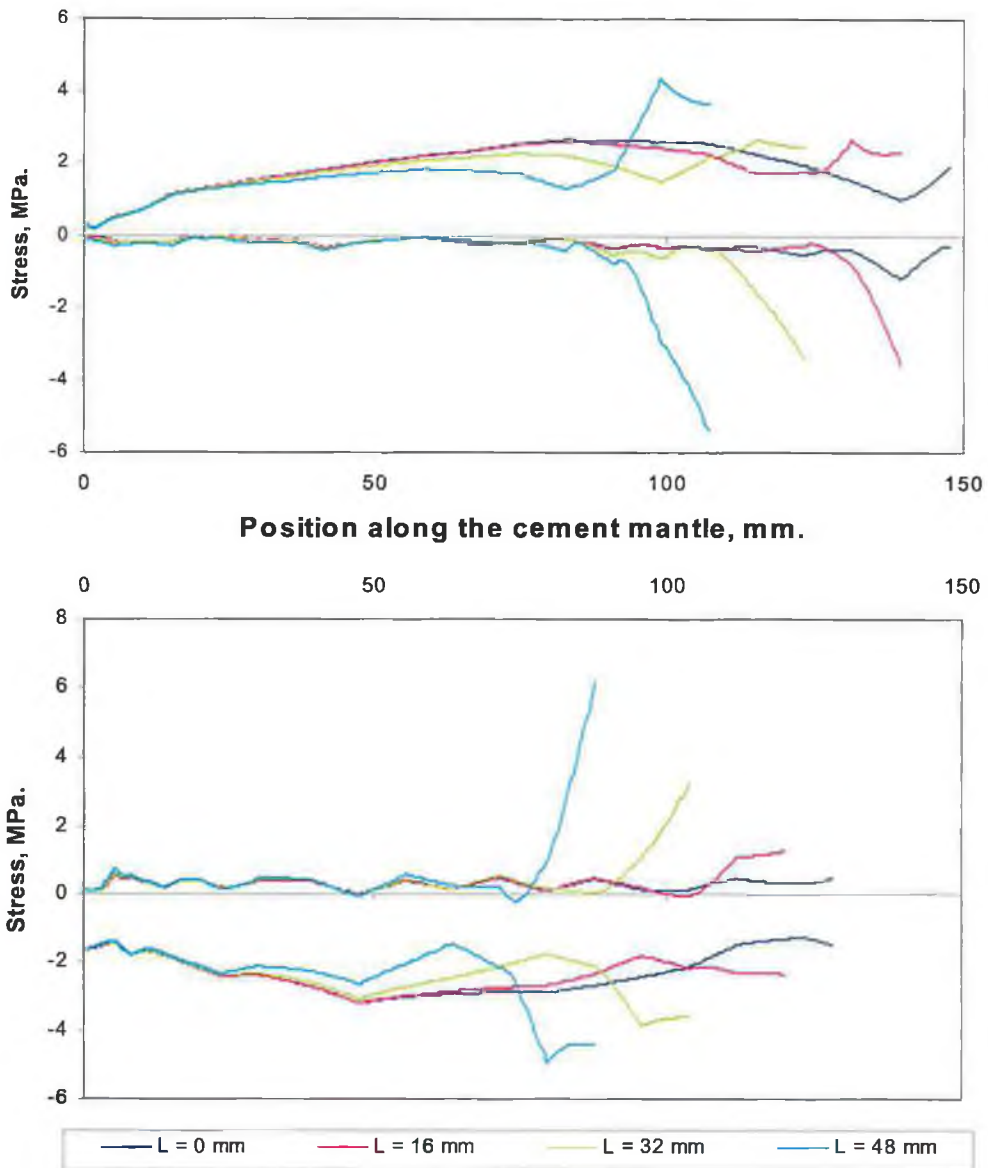


Figure 4.60, Minimum and maximum principal stress distributions, in MPa, in the lateral and medial sides of the cement mantle as a function of stem length.

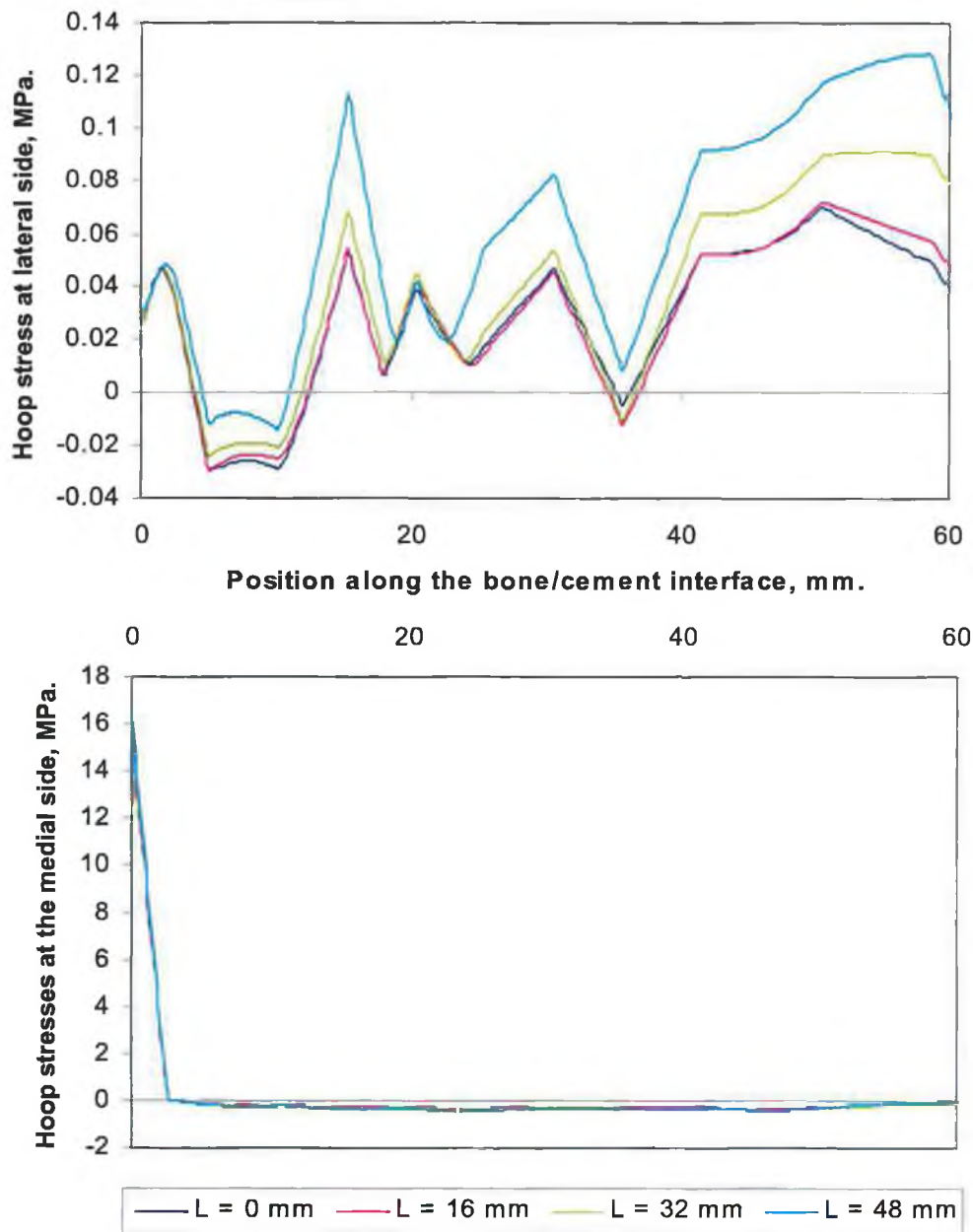


Figure 4.61, Hoop stress distributions, in MPa, in the lateral and medial sides of the bone/cement interface as a function of stem length.

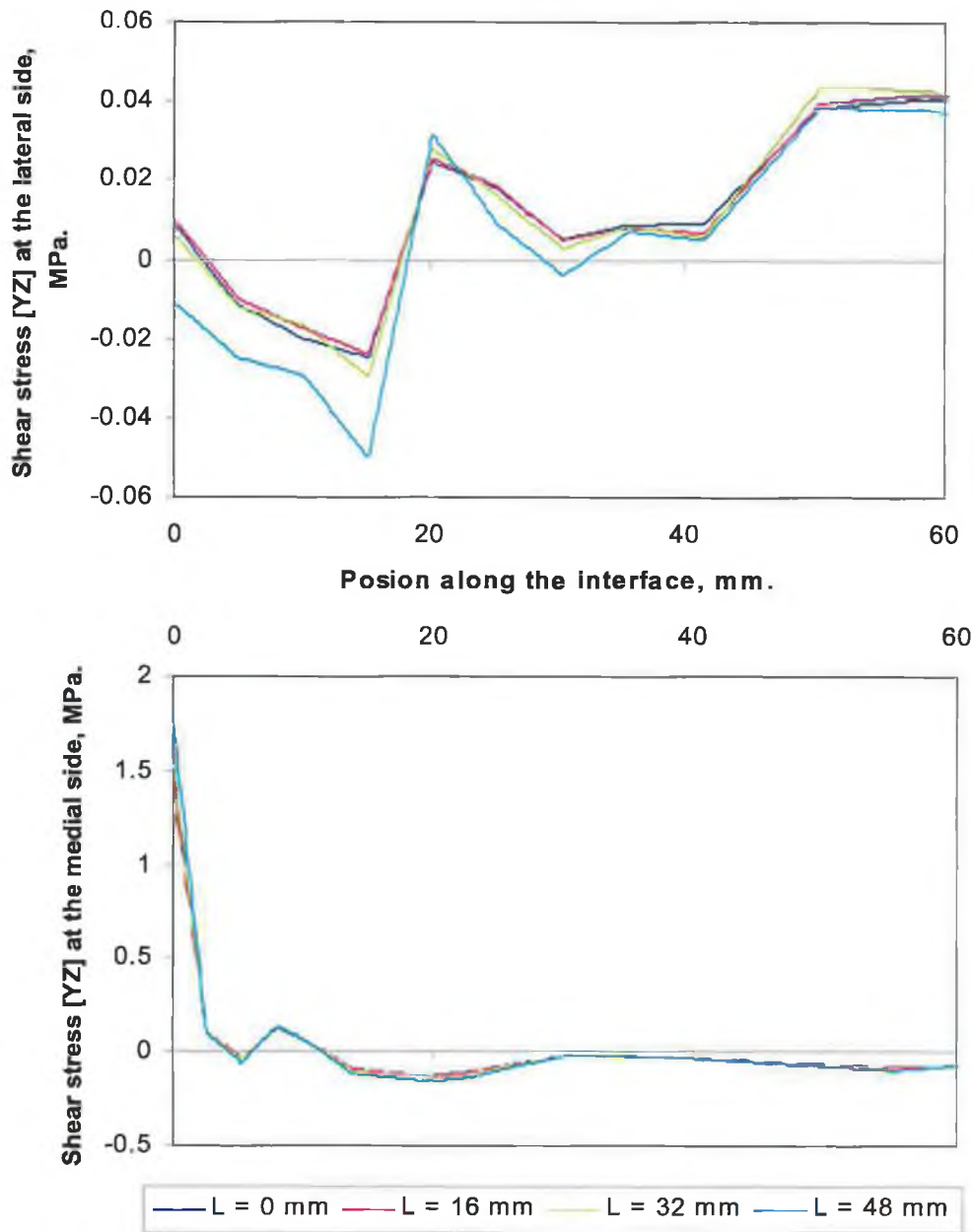


Figure 4.62A, Shear stress τ_{YZ} distributions, in MPa, in the lateral and medial sides of the bone/cement interface as a function of stem length.

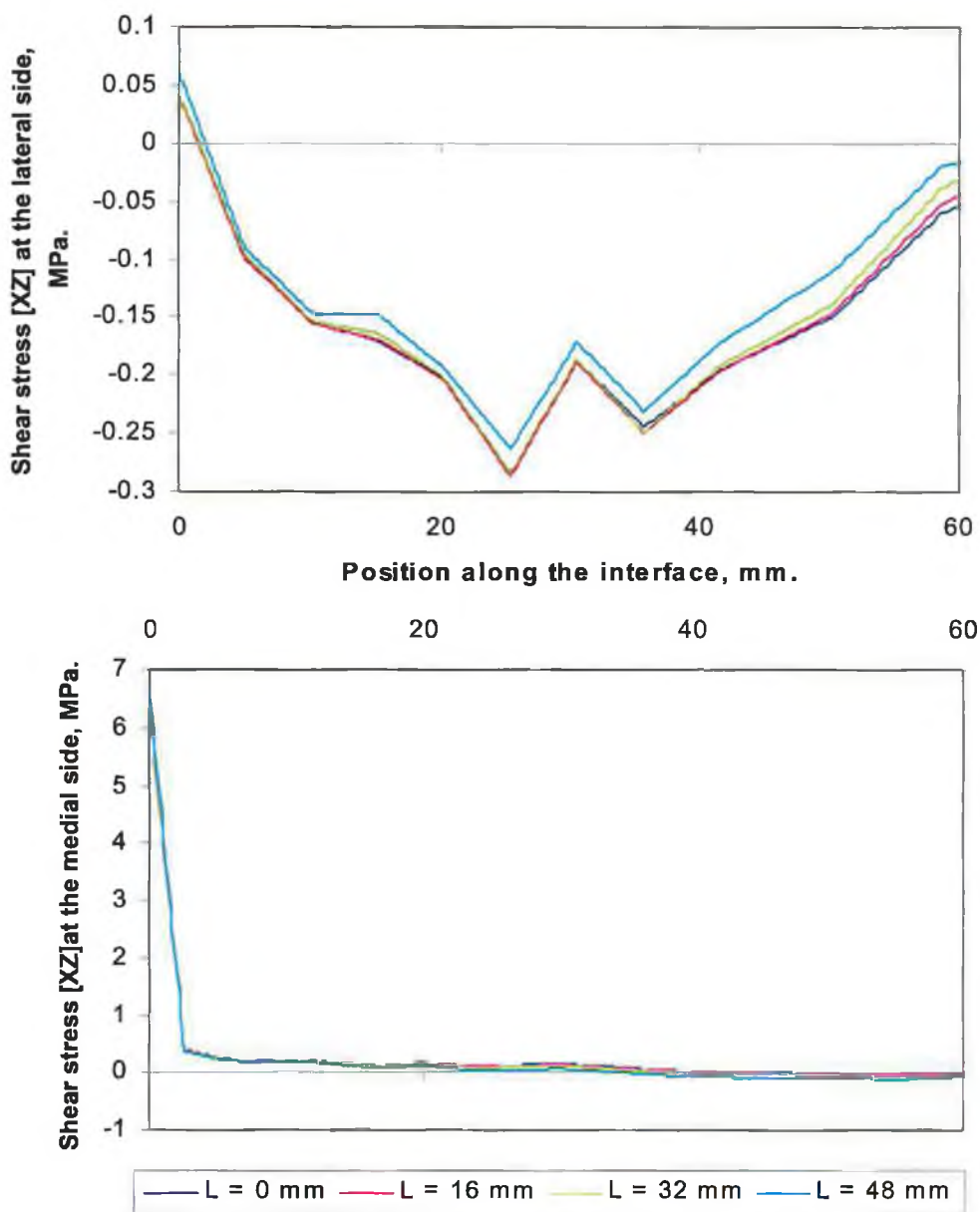


Figure 4.62B, Shear stress τ_{XZ} distributions, in MPa, in the lateral and medial sides of the bone/cement interface as a function of stem length.

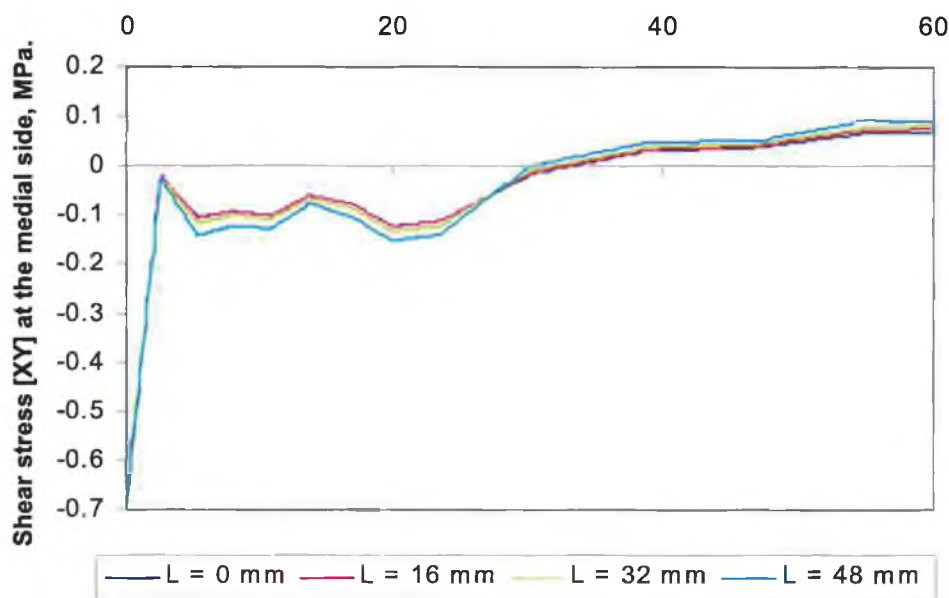
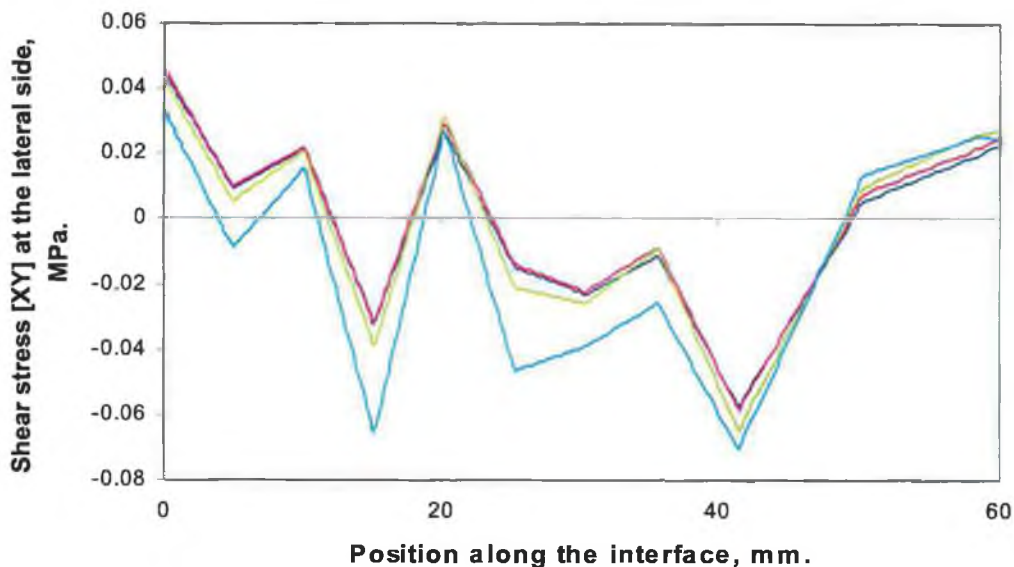


Figure 4.62C, Shear stress τ_{XY} distributions, in MPa, in the lateral and medial sides of the bone/cement interface as a function of stem length.

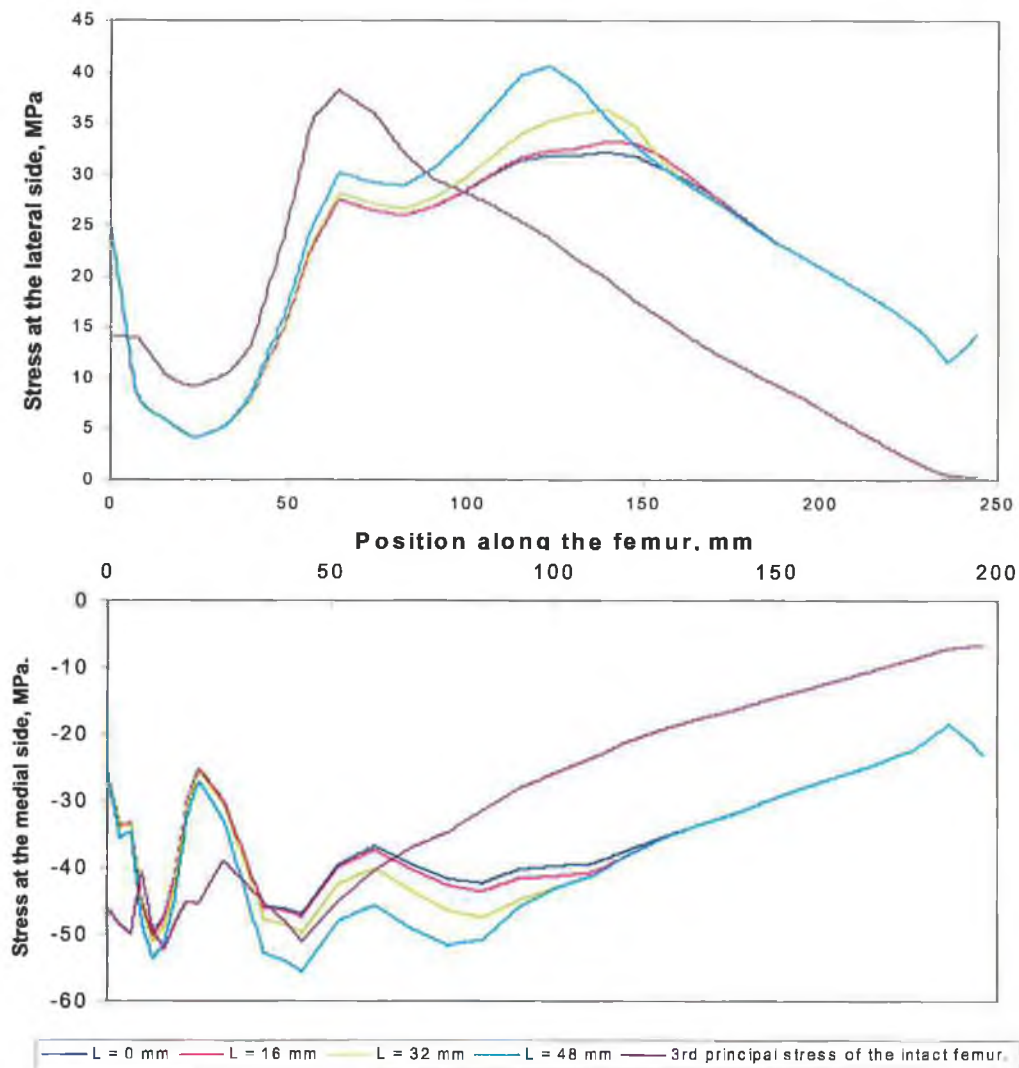


Figure 4.63: Minimum and maximum principal stress distributions, in MPa, in the lateral and medial sides of 1) treated femur, as a function of stem length; 2) an intact femur.

major fibre structure of the bone. Thus, whereas a shorter prosthesis does not cause additional stresses in the longitudinal direction, the circumferential stresses are increased alarmingly [29].

4.5.5. The Effect of the Stem Thickness

The effect of stem thickness on the load transferred was examined for the following two cases:

- A) The cross-section of the original stem prosthesis is reduced by removing 50% of the stem volume from the medial side, Figure 7.64 A, and
- B) The cross-section of the original stem prosthesis is reduced by removing total volume of 27% from the pesterious and anteriour stem sides, Figure 7.64 B.

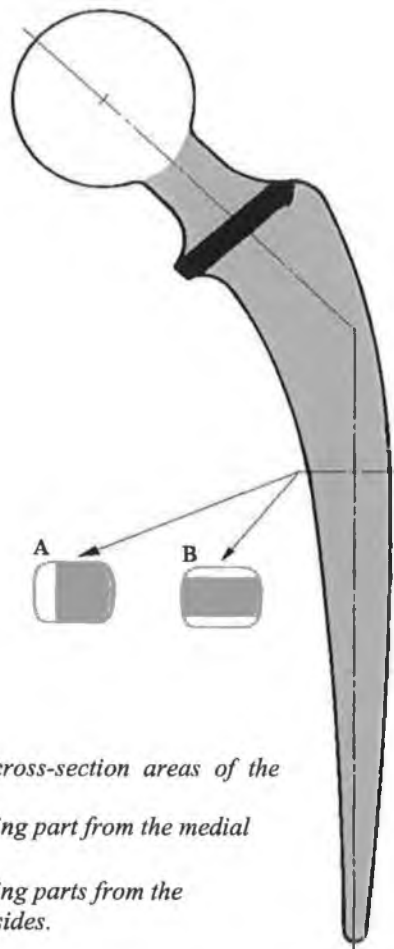


Figure 7.64: shows the cross-section areas of the stem prosthesis when:
A) It is reduced by removing part from the medial side.
B) It is reduced by removing parts from the pesterious / anteriour sides.

The stem thickness affects the stem rigidity, that is by reducing the stem prosthesis thickness the rigidity will decrease and reveal more flexibility [19]. By this there will be more load transferred to the bone cortex, Figure 7.65. It also shows that due to the high flexibility of stem's cross-section (A) the stresses transferred to the bone

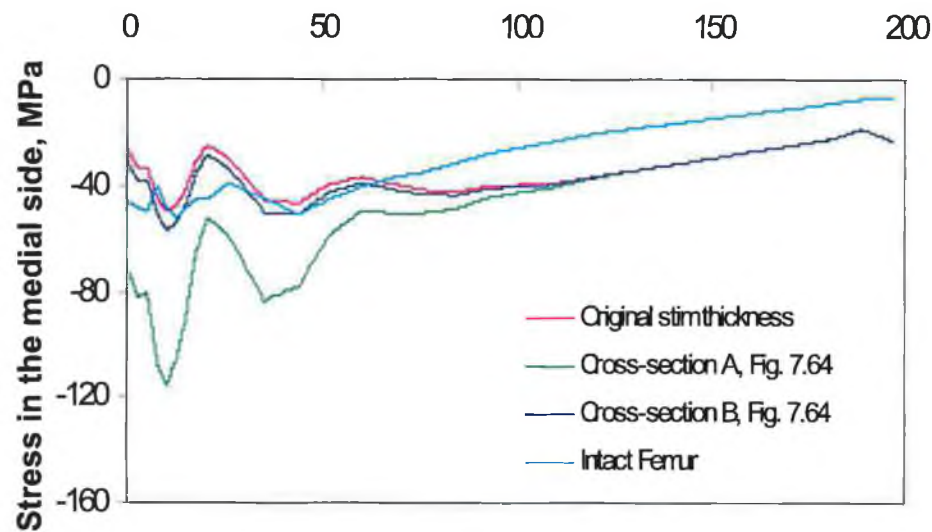
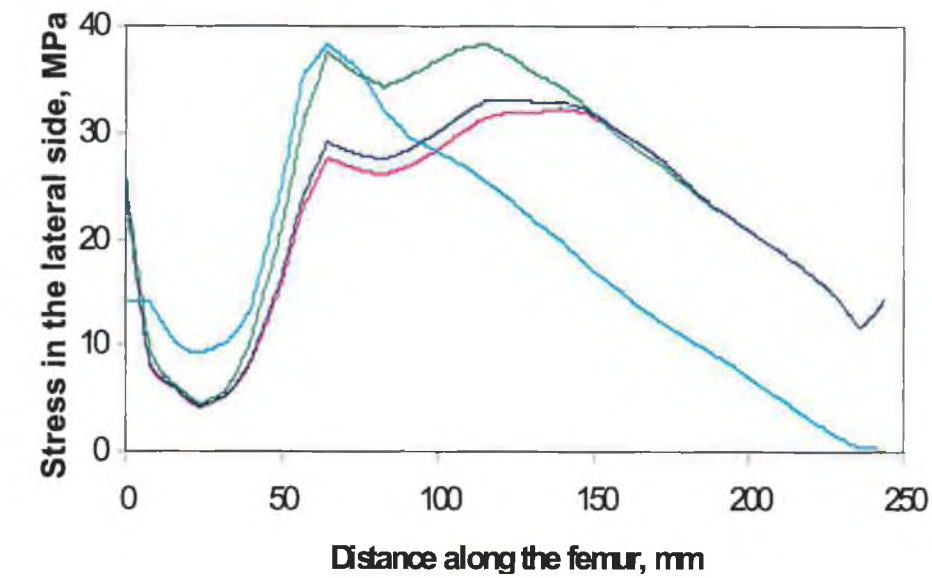


Figure 7.65: Minimum and maximum principal stress distribution, in MPa, in the lateral and medial sides of (1) treated femur as a function of stem thickness. and (2) intact femur.

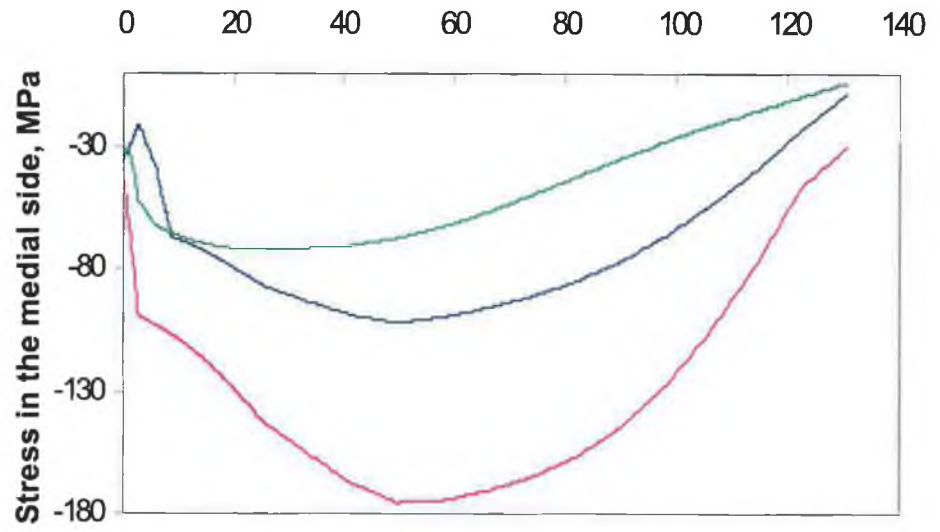
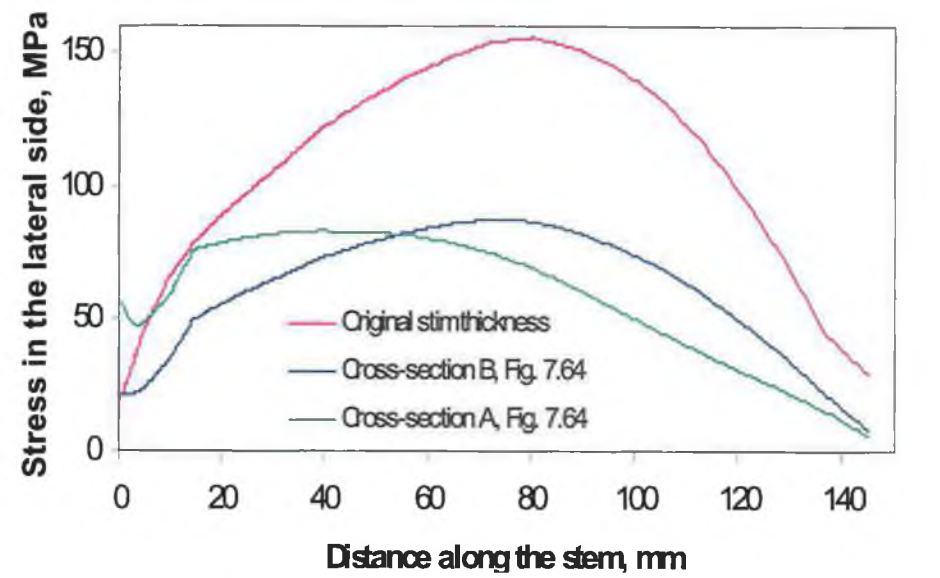


Figure 7.66: Minimum and maximum principal stress distribution, in MPa, in the lateral and medial sides of the prosthesis stem as a function of stem thickness.

cortex are highest compared to that of cross-section (B). They are, in fact, exceeded these of the intact femur in the medial side, but in the lateral side are close to them. Reducing stem thickness from the posterior and anterior sides, cross-section B, revealed relatively high rigidity by releasing stresses to bone cortex close to the original stem thickness, Figure 7.65.

Unexpected thing it was by increasing the stem cross-section the stresses along the stem increased since it is well known that $\tau = F/A$, Figure 7.66. According to Huiskes [35] work, the increase in the stem prosthesis cross-section does not imply an increase in the stem stresses, because a high internal bending moment does not necessarily result in higher maximal bending stresses, owing to the increased thickness of the stem. In fact, when the stem thickness increases in a given bone, the stem stresses initially increase, but later decrease, Figure 7.67.

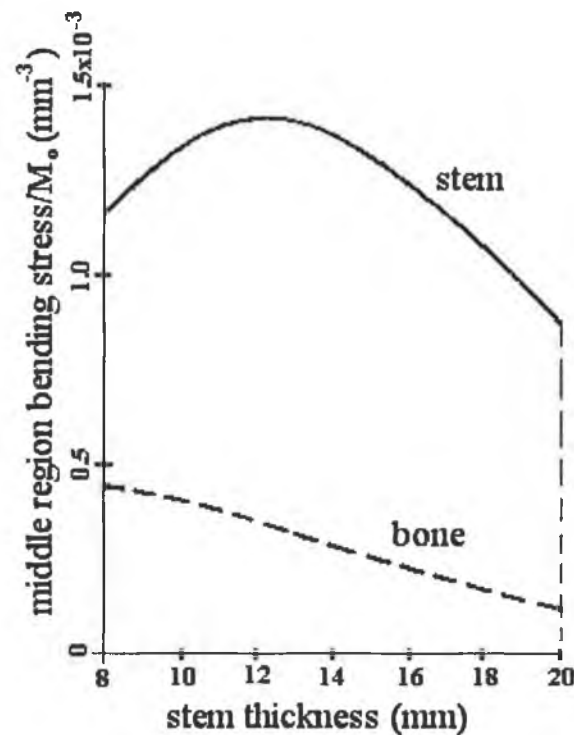


Figure 7.67: Bending stresses in bone and stem, occurring in the middle region of the structure, depending on the stem thickness for specific bone dimensions (medullary canal width 20 mm) [35].

Figure 7.66 shows that in spite the maximum stress in the lateral side are the same for stems cross-sections A and B, it is not in the medial side, since for stem cross-section A is more less in this side. Also, it reveals that the maximum tensile stress in the lateral side of the stem occurred in the middle region for stem of cross-section B, while for that of cross-section A it occurred in the proximal side.

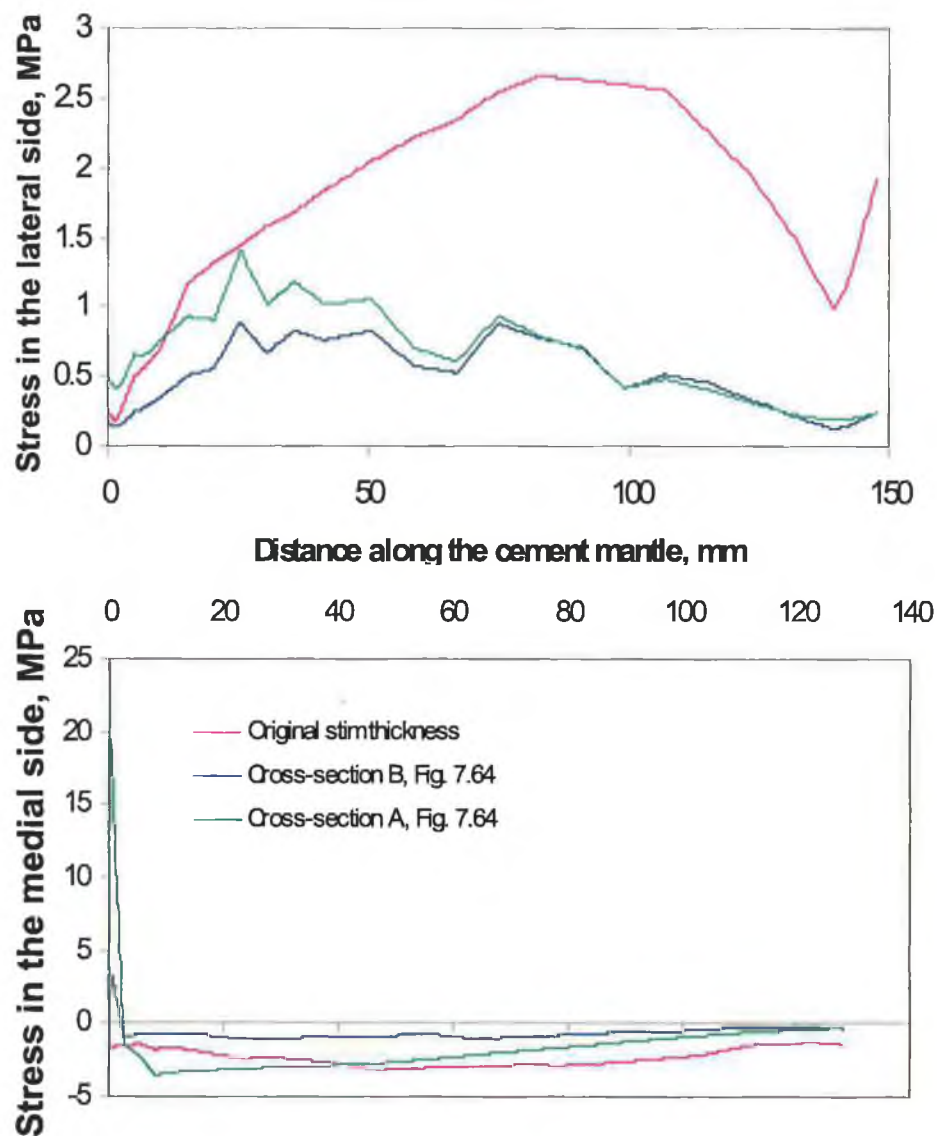


Figure 7.68: Minimum and maximum principal stress distribution, in MPa, in the lateral and medial sides of the cement mantle as a function of stem thickness.

As the stem thickness affects the stem rigidity, it also effects the transverse cement stiffness because the stem thickness determines, for a given bone, the cement-layer thickness as well [19]. The stem rigidity is very sensitive to the stem thickness, and so is the cement stiffness to cement thickness. Figure 7.68 shows that how large the cement/interface stresses in the lateral side is affected after reducing the stem thickness. It is clear that stresses in the medial side of the cement/interface is decreased as the stem thickness decreased owing to the increase of cement layer in this specific medullary bone's canal. Because stem of cross-section A reveals high bending deformation, the compressive stresses in the medial side of the cement/interface increased in the proximal part.

It is proposed that the prosthesis should be as thick as possible – particularly in the upper half. In the upper half the prosthesis itself carries most of the applied load. There is evidence to suggest that sometimes the stem is not sufficiently thick to resist fatigue loading. The results of experiments indicated that the stem of a prosthesis can be thickened a good deal without detriment to the force transfer from prosthesis to bone [6].

4.6 Summery of the Chapter

This chapter has presented a finite element model of the AHJ for the purpose of investigating its structural behaviour. This required 3 D model that could be relied upon for accuracy of numerical calculations. Results were presented which were used to analysis prosthesis fracture, cement fracture and fatigue crack growth and the stress patterns causing bone loss in the proximo-medial segment of the femur. In this study the important aspects of interface debonding was not simulated. Despite this neglected aspect, a useful and simple procedure for assessment of prosthesis material for primary stability was formulated. As regards cement failure, it has been shown that the reinforcement rout can have far less effectiveness than the increasing fatigue limit would indicate. Also, the stress vector plot of Figure 4.22 can be used to predict crack propagation paths in the cement mantle.

Chapter Five

A Comparison Study between Static and Dynamic Loading, and stress-Based Criteria Reliability

5.1. Introduction

Although pre-clinical validation procedures have significantly improved in the last few years, some important factors, affecting the biomechanical performance of hip implants, are still very difficult to account for. Using a clever combination of numerical models and experiments *in vivo* it is possible today to replicate the major part of the failure scenario previously observed in the clinical practice. However, many important factors are still very difficult to take into account during these studies. In particular, these aspects related to the patient (skeletal anatomy, bone quality, muscles, level of activity or biological response) or to the surgeon (bone surgery, implant position and fit, joint centre relocation or muscle surgery). Until now, models developed to predict stresses in total hip replacements have been generally poorly validated [93]. This could be because all the pre-clinical simulations were performed statically, that is by selecting the greatest load at a particular time of the activity cycle.

So far, all the results in these studies were conducted by assuming the peak loads during the normal gait at a particular time (static loads), but in fact the hip is exposed to varied loads, for example, when climbing the stairs, stumbling or jumping. These kind of loads could be considered as impact loads, and they could cause the artificial hip to fail.

This study aims to:

- (a) Take account of patient activity (stamping, jumping, walking, etc) when designing total hip replacement. In this regard the stress field in the artificial hip components (prostheses, cement mantle, and bone) is analyzed statically and dynamically with nonlinear simulation. In the

dynamic case, simulations have been conducted to investigate the effect of the loading pattern on the stress-based criteria to assess implant longevity.

(b) Also, in this study two quantitative measures were investigated; peak stress and stressed volume.

It has been shown that each measure may lead to differing conclusions.

5.2. *Finite Element Model*

The finite element models were generated using ANSYS finite element software (version 5.6). A standardized femur was used as a basis for the finite element model [97]. The geometry contained Linea Aspera on the posterior side and the femur displayed a noticeable bow in the anterior-posterior plane. A combination of free and mapped meshing was used to generate two hip prosthesis models for static and dynamic studies. The types and number of elements used are given in Table 5.1.

Table 5.1: Type and number of elements used in the dynamic and static analysis.				
Analysis Type	Dynamic Analysis		Static Analysis	
Element type	SOLID 164, 8-noded explicit brick element		SOLID 45, 8-noded isoparametric brick element	
AHJ Constitution	No. of elements	No. of nodes	No. of elements	No. of nodes
Prosthesis	1200	1690	1200	1690
Cement mantle	384	832	384	832
Cortical Bone	540	1375	540	1375
Concalleous Bone	4965	1426	1182	1108

The prosthesis was uncollared and its stem was designed to be tapered and follows the shape of internal cortical bone. Figure 5.1 shows a view of the mesh for the prosthesis, cement mantle and bone. The stem-cement interface was considered fully bonded.

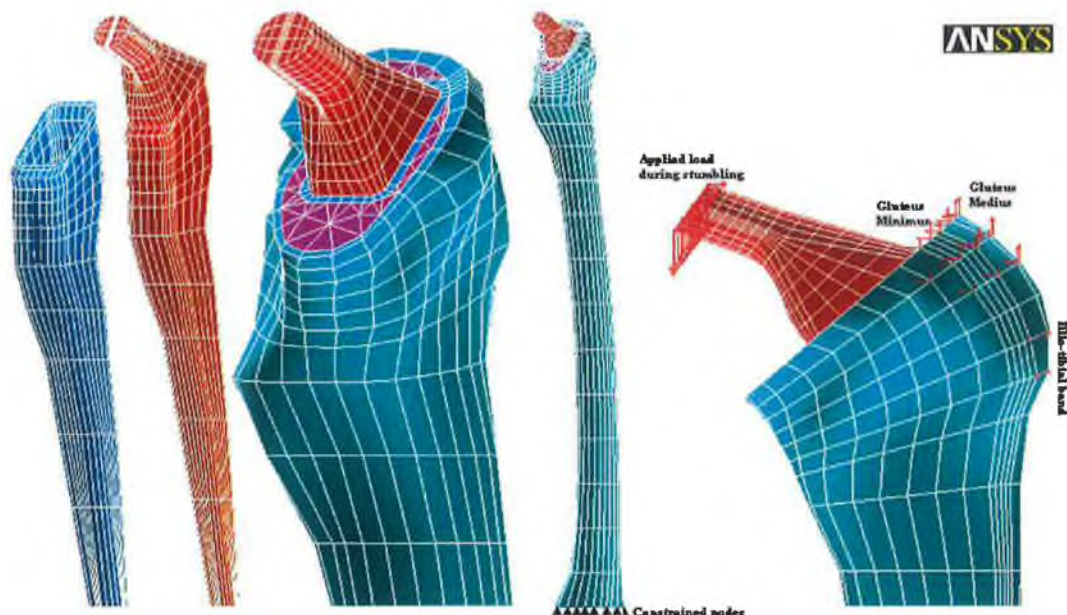


Figure 5.1: Finite element meshes of hip prosthesis components and the distribution of the applied and muscles forces.

5.3. Material Properties

In static analysis the material was assumed to be a linear elastic continuum with isotropic properties, whereas in dynamic analysis it was bi-linear elasto-plastic. Table 5.2 illustrates the material properties used:

Table 5.2: The artificial hip components material properties [24,79].				
Materials properties	Bone		Rostal Bone Cement (PMMA)	Prosthesis (Ti 6AL 4V)
	Cortical Bone	Concellleous Bone		
Young's Modulus [MPa]	16200	389	2.64×10^3	100,000
Poisson's Ratio	0.36	0.3	0.4	0.32
Density [ton / mm ³]	1.99×10^{-9}	0.5×10^{-9}	1.2×10^{-9}	4.43×10^{-9}
Yield Stress [MPa]	114	3.89	43.8	830
Tangent Modulus [MPa]	793	7.08	16.6×10^{-3}	1255.23
Ultimate Stress [MPa]	133	7.36	43.8	920

5.4. Loading Conditions

The loading applied was taken from the work of Berman et al. [20] and it is illustrated in Figure 5.2 which represent loading pattern for stumbling. In static

analysis, the maximum stumbling resultant force, F , on the head of the femur is 8.7 times the body weight ($BW = 70 \text{ kg}$) at 58 percent of the gait cycle. This can be resolved into:

$$F_x = 2188.86 \text{ [N]}, F_y = -669.53 \text{ [N]}, \text{ and } F_z = -5472.1 \text{ [N]}$$

At 85 percent of the gait cycle, a simplified set of active muscles are the abductor muscles, located on the greater trochanter (Gluteus medius and Gluteus minimus), and the ilio-tibial band (Gluteus maximus and Tensor fascia latae) [153], Table 5.3. For dynamic analysis these muscle forces have been considered to be constant during the entire loading cycle.

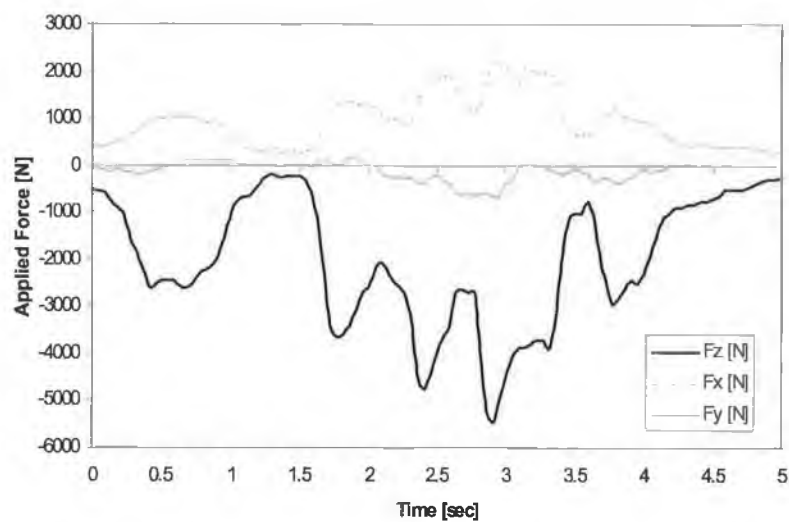


Figure 5.2: The variation of forces applied on the prosthesis during stumbling.

As shown in Figure 5.1, all nodes on the most distal section were fully restrained against displacements in all directions.

Table 5.3: Muscle load magnitudes applied to the FE model [153]			
Force component	Gluteus medius	Gluteus minimus	ilio-tibial band
F_x [N]	- 259	- 279	- 59
F_y [N]	160	269	- 74
F_z [N]	319	134	- 58

5.5. Results

For the purpose of comparison the analysis was performed by using the finite element package ANSYS for the static loading. Analysis was carried out using LS-DYNA for the dynamic loading case. The gait time of the highest force during stumbling was incorporated in the LS-DYNA solution routine.

To decrease the CPU time required to execute the dynamic solution, the gait time has been multiplied by a factor equal to 1×10^{-3} . However, the results were checked to ensure no unwanted dynamic effects were incorporated into the analysis as a result of this time change. This led to a solution time of 19 hours to carry out the dynamic solution.

5.5.1. Deformation Pattern

It is found that in representing the stumbling load case statically the x-component load has a major effect on the deformation of the treated femur. The resultant x-component force of 1592 N caused bending in the lateral side. While in the dynamic analysis the situation is completely different. Since the prosthesis components are exposed to a varied load, it is likely that the x-component of the applied load will be less than the counteracting muscle force (in case of muscle tension). The result was as expected, the vertical z-component load force played a major factor in deforming the treated femur in the medial direction at that time as seen in Figure 5.3. From these results one can conclude that the two approaches of analysis would have a large contrast.

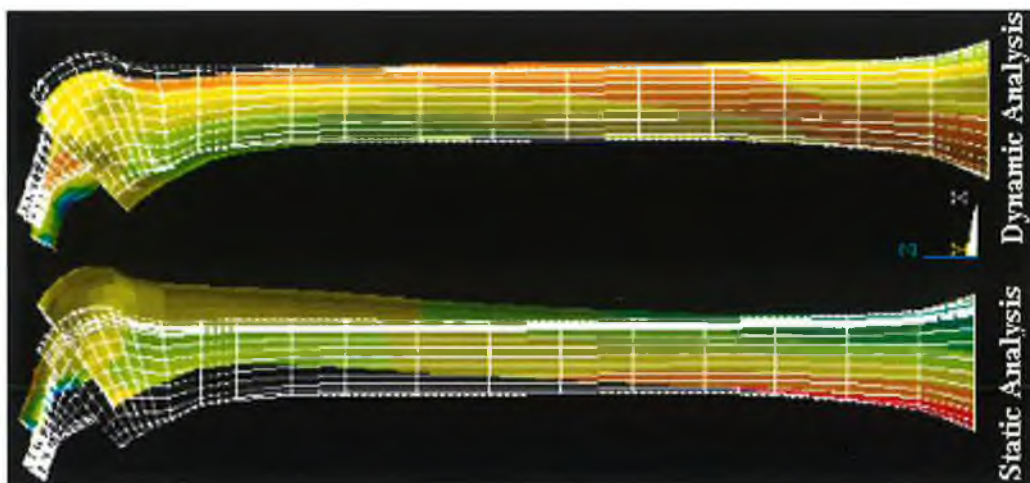


Figure 5.3: Deformation of the treated femur according to the static and dynamic analysis.

5.5.2. Contours and Peak Stresses

In spite of the fact that the maximum tensile stress being located in the middle of lateral side of the prosthesis stem with a peak stresses almost equal (95 MPa for static and 101.5 MPa for dynamic analysis), Figure 5.4, they are not in the cement mantle and bone cortex, Figures 5.5 and 5.6. Also, the tensile stress regions are obviously occupied more areas in the stem of static analysis rather than that of dynamic analysis.

For the cement mantle, in spite of the fact that the peak tensile stress for the static analysis is greater than that of dynamic one, Table 5.4, it was localized in a small region in the inner interior side of the upper proximal part, Figure 5.5. While that for the dynamic analysis is localized in the middle of the lateral side with large occupied area.

Table 5.4: Comparison of results of each criterion for each load approach analysis			
AHJ Component	Stress Criteria	Static Analysis	Dynamic Analysis
Prosthesis	Peak Stress [MPa]	95.047	101.491
	% Element > 90 MPa	0	0.667
Cement	Peak Stress [MPa]	4.922	3.595
	% Element > 3.5 MPa	0	4.43
Bone Cortex	Peak Stress [MPa]	97.685	27.515
	% Element > 90 MPa	0.37	0

Because that the x-component of the applied load plays a major component in deforming the treated femur towards the lateral side in the static analysis, the maximum tensile stress exists in the distal part with a value of 97.7 MPa which is greater than that for the dynamic analysis of 27.5 MPa, Table 5.4 and Figure 5.6. By using the dynamic approach the treated femur expected to bend in the medial side showed resistance to the vertical applied load. As a result, the peak tensile stress is localized in the upper third of the lateral side, Figure 5.6.

Figure 5.4: Comparison of maximum and minimum tensile axial stresses in the hip prosthesis for the static and dynamic analysis.

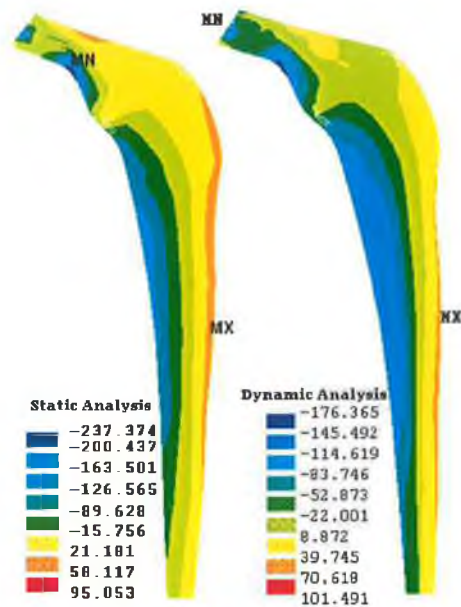


Figure 5.5: Comparison of maximum and minimum tensile axial stresses in the cement mantle for the static and dynamic analysis.

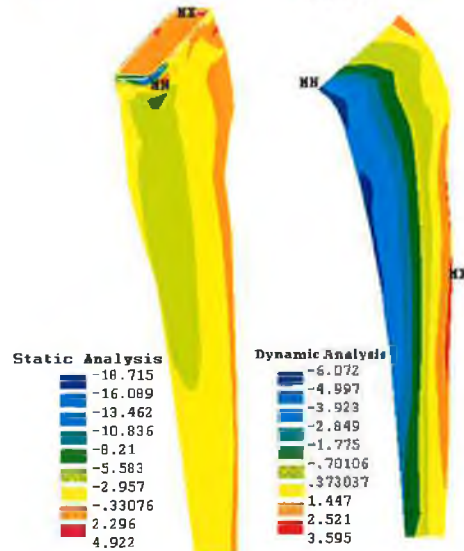
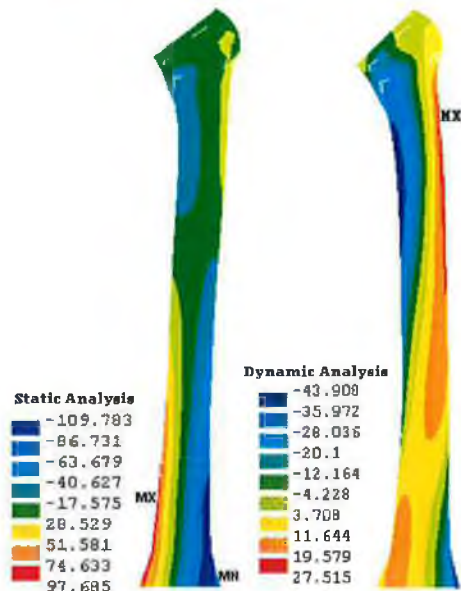


Figure 5.6: Comparison of maximum and minimum tensile axial stresses in the bone cortex for the static and dynamic analysis.



5.5.3. Axial Stresses

Based on the results from these two different deformations, the axial stresses along the medial and lateral side of each component of the hip prosthesis model system were higher in the dynamic approach than that of the static analysis, Figures 5.7, 5.8 and 5.9. They show high divergent curves in the distal direction. Because the prosthesis stem was designed to follow the shape of the internal cortical bone, and it is tilted slightly toward the anterior side in the upper proximal part, the cement mantle around it experienced high bending deformation in the anterior side during the static analysis. This may account for the compressive stresses in the extreme upper lateral and medial sides of the cement mantle, Figure 5.8.

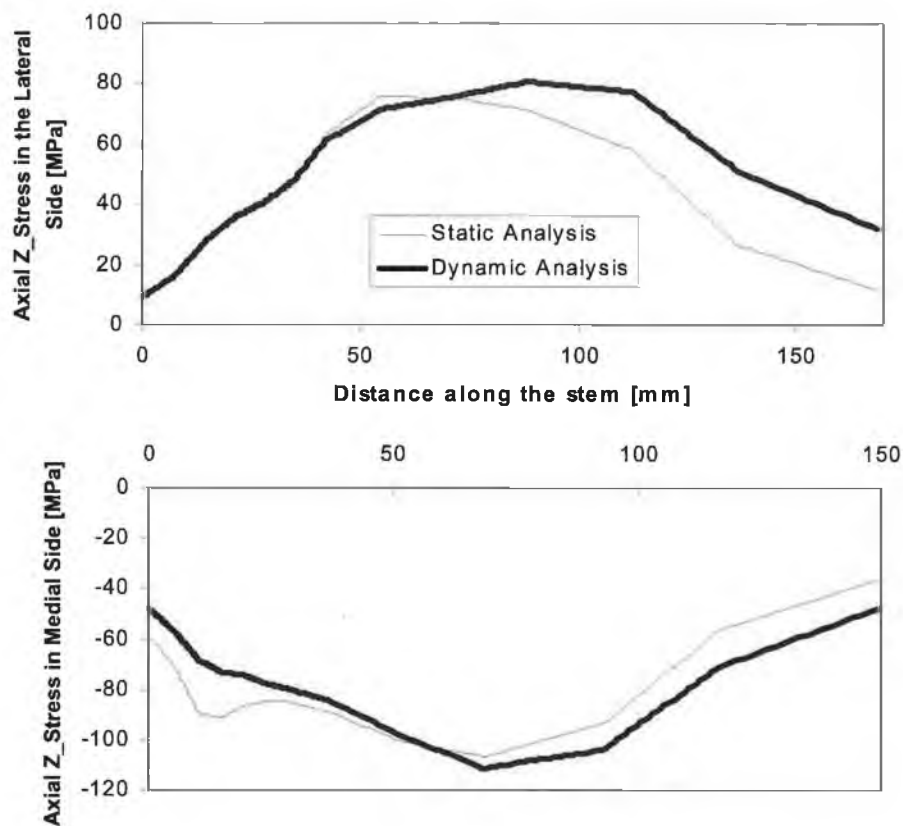


Figure 5.7: Axial z-stress distributed along the medial and the lateral side of the stem prosthesis.

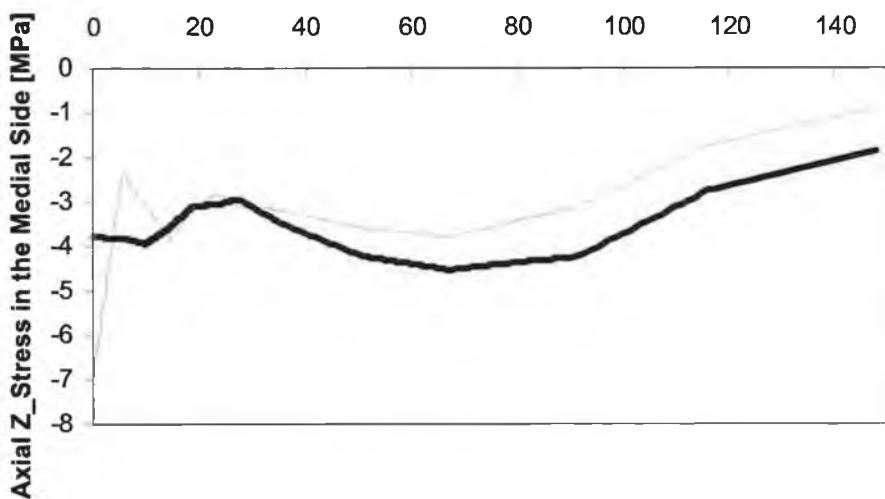
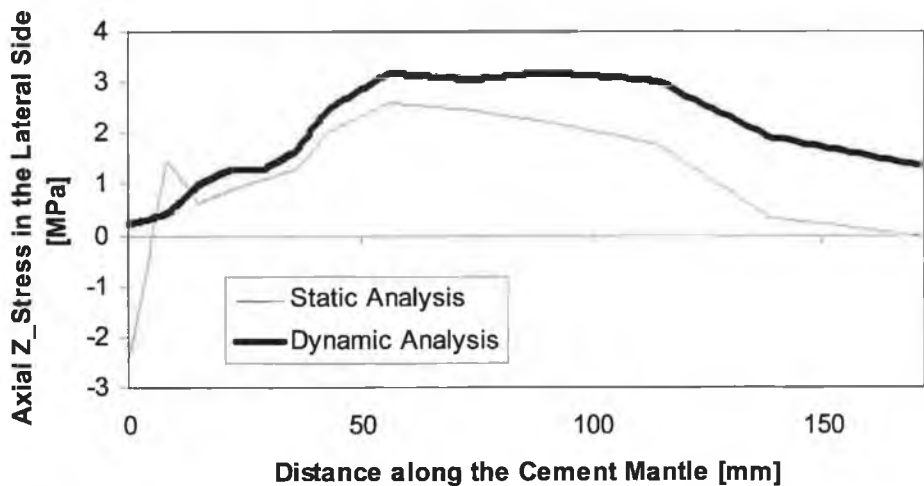


Figure 5.8: Axial z-stress distributed along the medial and the lateral side of the cement mantle.

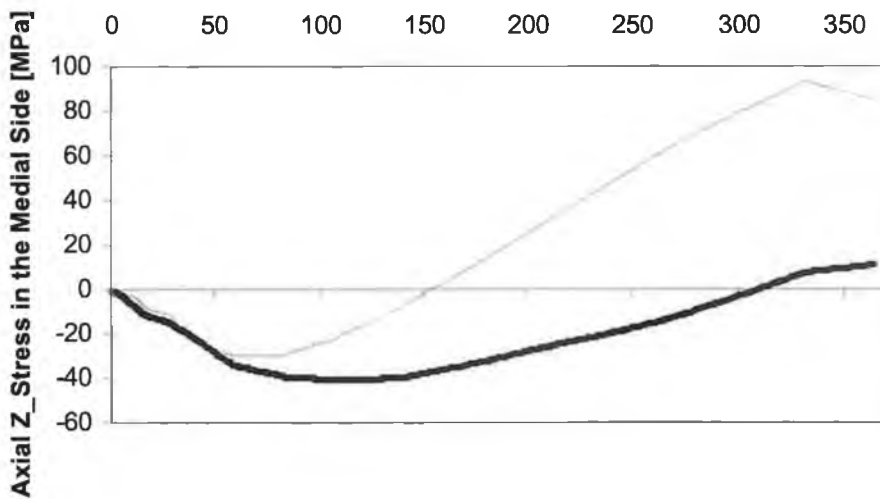
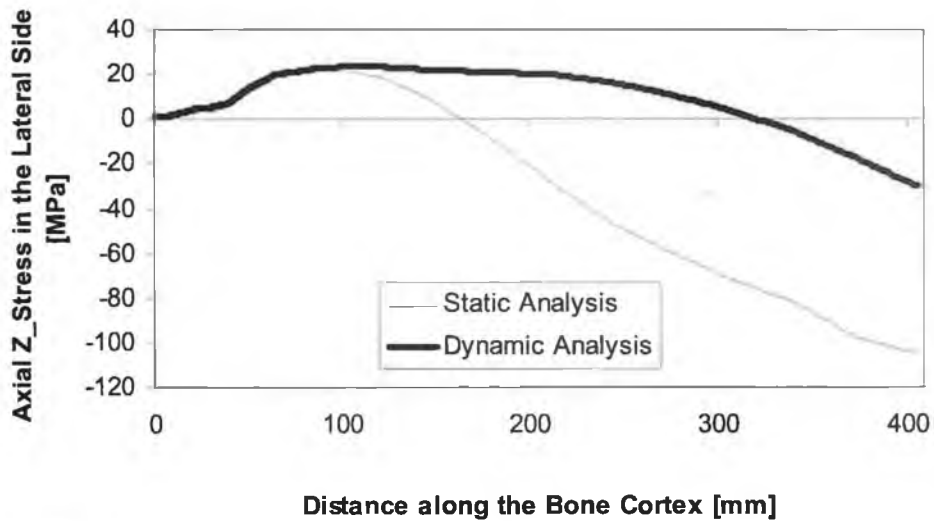


Figure 5.9: Axial z-stress distributed along the medial and the lateral side of the bone cortex.

5.5.4. Percentage of elements of prosthesis components at a given stress

To see the amount of stresses transferred to the prosthesis components, it would be of benefit to quantitatively examine the distribution of stress within them. The average stress for each element in each component was recorded and the elements were divided into groups with stress ranges. The total elements for each stress range could then be plotted, as shown in Figures 5.10, 5.11 and 5.12.

In spite of the fact that the bone cortex experiences higher stresses distributed over small amount of elements when the static analysis was used, Figure 5.12, this is not the case for both the prosthesis and the cement mantle, Figures 5.10 and 5.11. Furthermore, if a stress level of the cement mantle, e.g. of 3.5 MPa, is considered critical, it is clearly shown that the number of elements (and hence the volume) of endangered cement is greater when the dynamic load approach is used (4.4% out of 384 element in the dynamic analysis while 0 in the static analysis). This result was rather unexpected from the static analysis, see Table 5.4.

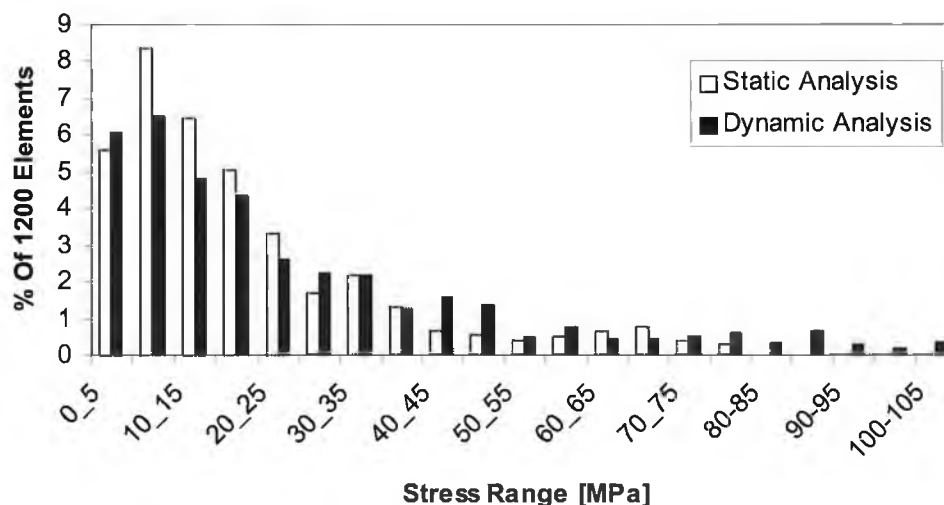


Figure 5.10: distribution of 1200 element of the prosthesis stem over a stress range of 0-105 MPa, for the two loads analysis.

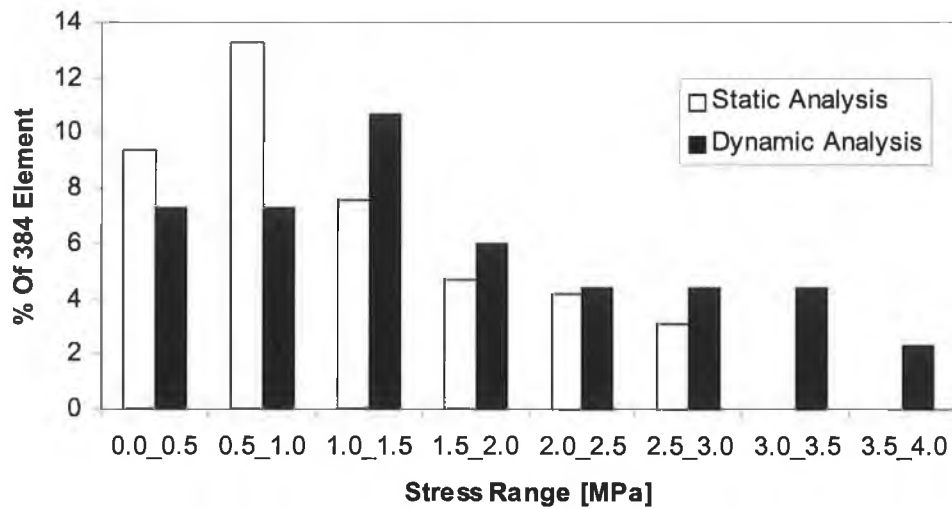


Figure 5.11: distribution of 384 element of the cement mantle over a stress range of 0-4.0 MPa, for the two loads analysis.

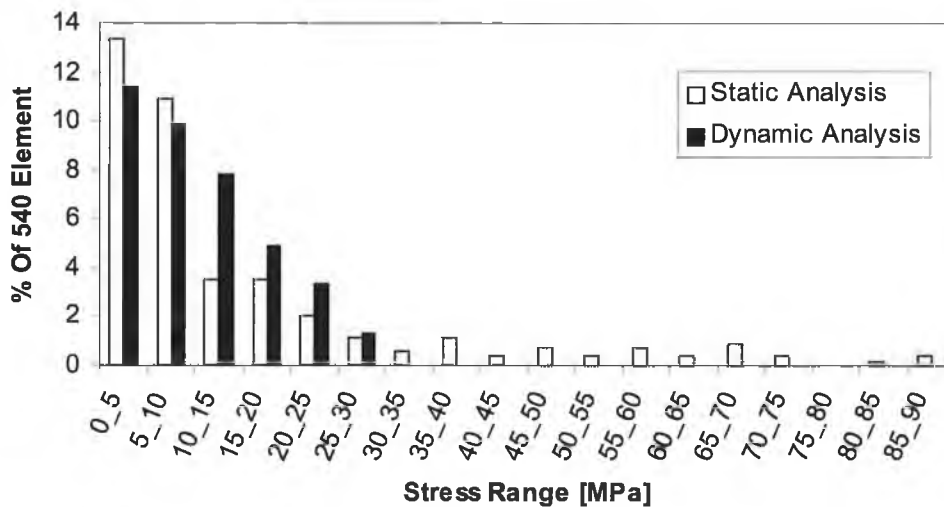


Figure 5.12: distribution of 1200 element of the prosthesis stem over a stress range of 0-105 MPa, for the two loads analysis.

Chapter Six

Dynamic Loading Simulation

6.1. Objective

Figure 6.1 shows schematic representation of the load transfer in the proximal femur before and after hip replacement. In the natural state, the stress is distributed over the entire cross section of the femur. Bending and axial compression are the major modes of loading. The postsurgery stress state is significantly different mainly due to the manner in which the load is transferred to the femur. In this case, the load is partially transferred through shear across the bone/cement/prostheses interfaces. This altered load transfer leads to increased stresses at the interface and unloading of the bone away from the prosthesis. The interface shear stresses are further increased due to the stiffness ratio between the prosthesis and the bone, typically of the order of 10 : 1 and higher.

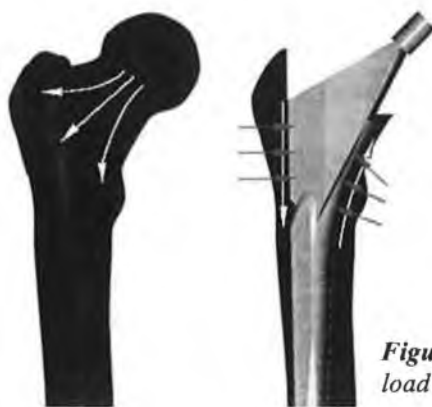


Figure 6.1: Schematic representation of the load transfer before and after THA.

In addition, the bending displacements in the bone surrounding the stem are reduced because of the relatively high flexural stiffness of the prosthesis. This reduced bending unloads the outer fibers of femur leading to a state of stress shielding. The change in the load distribution increases stresses in some regions and reduces them in others. If these changes are large enough, they can lead to adaptive bone remodeling. Areas that see higher loads, may experience an increase in bone mass, while areas that see a reduction in load may experience a decrease. The other factors mentioned earlier might also play a role in this remodeling but stress

shielding is often implicated. An apparent solution to the shielding problem would be a prosthesis which loads the proximal end of the femur in a manner similar to the natural state.

The motivating hypothesis for the current study, is “will an alternative femoral component design reduce the level of stress shielding in the femur following total hip arthroplasty and ease the impulse forces simultaneously?”. This study explores the hypothesis that through redesign, a total hip prosthesis can be developed to substantially reduce stress shielding. The description of the development of a new femoral hip prosthesis designed to alleviate this problem through a new geometry and system of proximal fixation based on the dynamic loading and finite element analysis. A compression study was undertaken to study the effect of the following types of the artificial hip prosthesis design, Figure 6.2, and the effect of selected material on the stress distributions in the entire model components (bone, cement, and the prosthesis) and the stress shielding:

- a) Collerless cemented hip prosthesis,
- b) Collared cemented hip prosthesis without skirt and damper,
- c) Skirt-Collared cemented hip prosthesis without damper, and
- d) Skirt-Collared cemented hip prosthesis with a damper.

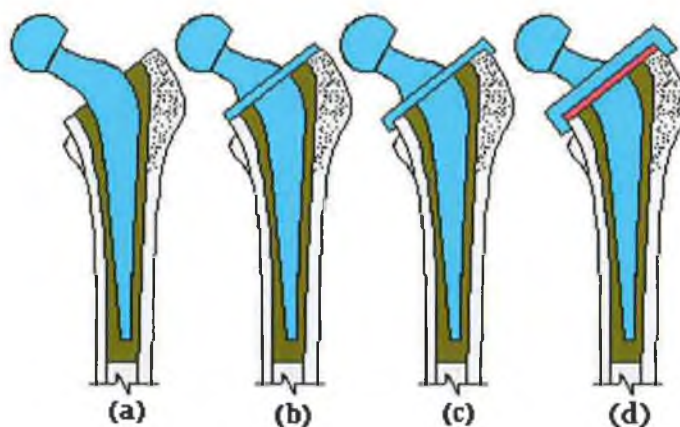


Figure 6.2: shows the four proposed prosthesis types to conduct the comparison;
d) Collerless cemented hip prosthesis.
e) Collared cemented hip prosthesis without skirt and damper.
f) Skirt-Collared cemented hip prosthesis without damper.
g) Skirt-Collared cemented hip prosthesis with a damper.

In spite of the fact that other issues will have a side effect, in this work the bone stress will be considered to be the primary design criterion.

In addition to this, the study will take into consideration for the three proposed models the displacements of the prosthesis inside the femoral bone during patient activity and it is subsequent.

6.2. Design Methodology

The current design and the approach of simulation are aim to:

- a) Develop a general prosthesis geometry to restore, as much as possible, the natural load-transfer mechanism through the proximal femur. Since the prosthesis collar helps to transfer the axial loads, it was designed to be mounted in a manner to cover all the resected area of the femur thoroughly. Beside that, it will cease prosthesis subsidence. But one should be aware that poor collar contact may cause proximal stress shielding.
- b) Prevent the radial displacements of the prosthesis relative to the femur by anchoring it firmly onto the resected part. As consequence, this will reduce shear forces and hence cement fragmentation and rifts that may occur in the proximal-lateral part due to the prosthesis bending and displacements. Also, it will help produce a more natural bending load over the cross section of the femur by fixing the trochanter to the implant. In this regard, a skirt was made around the collar to embrace tightly the proximal part of the femur to provide a metaphyseal fixation.
- c) Study the benefit of utilizing a damper placed between the resected femur surface and the prosthesis collar to absorb the sudden shocks caused by patient vigorous activities such as jumping and stumbling, which in turn may cause the artificial hip to fail as a result of the fatigue. It was proposed earlier in this study that damping the impulse forces, which carried out on the prosthesis head, may increase the prosthesis longevity. The use of high molecular weight polyethylene (HMWPE) articulation could absorb some of the impact force during gait [304]. In this regard, four different materials were undertaken in the analysis to examine their entire effects.
- d) Increase the design output effectiveness by utilizing both of:
 - Dynamic loading. More importantly, the hip biomechanics are very

different during normal gait compared with non-weight-bearing movements [304]. In this work the load was imposed over the prosthesis head as a function of time, and explicit dynamic finite element program (LS-DYNA) was used for solving this simulation.

- A finite element model close to the reality. A implant/cement interface was simulated to be in contact rather than bonded. Also, two layers of elements, represents a small cement layer, were located under the distal tip of the prosthesis stem, since subsidence of a stem can be increased when no distal cement exists to support it. In addition to a standardised femur was used as a basis for a finite element model of a composite femur [97].

6.3. Geometry Modelling

The primary strength of the finite element technique over strength of material methods is that, by defining local co-ordinates for elements, it can attempt to simulate the behavior of complex geometries. This is the reason for its wide application in orthopaedics.

The ANSYS Finite Element Package (version 5.6) was used to design and generate the three different cemented models mentioned above. The volumes of the resulting 3-D models were discretized using 8-node explicit brick elements. The number of elements used are given in Table 6.1.

Table 6.1: Type and number of elements used in the dynamic analysis.		
AHJ Constitution	No. of elements	No. of nodes
Skirt-Collared Prosthesis	6019	5403
Collared Prosthesis	7517	5890
Collaerless Prosthesis	3360	4615
Damper	1825	590
Cement mantle	1728	3490
Cortical Bone	1270	2560
Concelleous Bone	6014	3125

A combination of free and mapped meshing was used to generate models for a dynamic study. The bone-cement interface was considered to be fully bonded.

6.3.1. Prosthesis and cement

As Figure 6.3 shows, three different prosthesis models were generated. They all were characterized by a stem designed to be tapered and follows the shape of internal medullar channel. The cement mantle was taken to fill the space between the prosthesis and bone, and a layer was kept distal to the stem tip to prevent it from subsidence. This resulted in a cement mantle as shown in Figure 6.4.



Figure 6.3: 3-D finite element meshes of hip prosthesis. (a) Collarless cemented hip prosthesis, (b) Collared cemented hip prosthesis without skirt and damper, and (c) Skirt-Collared cemented hip prosthesis provided with a damper.



Figure 6.4: 3-D finite element meshes of cement mantle.

6.3.2. Damper

Figure 6.5 shows the geometry of the damper which is allocated between the resected femoral surface and the skirted-collar. It is 4 mm in thickness. Its xy plane has the same shape of the resected femur surface.

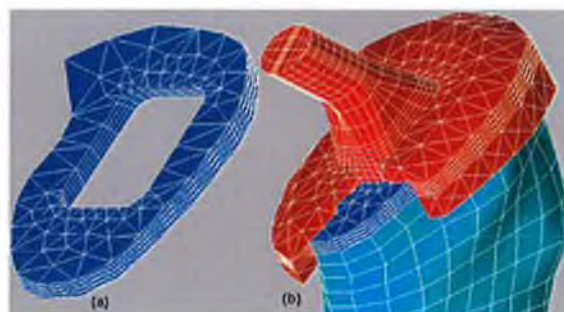


Figure 6.5: 3-D finite element meshes of prosthesis damper (a), which is allocated between the resected bone surface and the collar (b).

6.3.3. Femur

A standardized femur was used as a basis for the finite element model [97]. The femoral geometry contained Linea Aspera on the posterior side and the femur displayed a noticeable bow in the anterior-posterior plane, Figure 6.6.

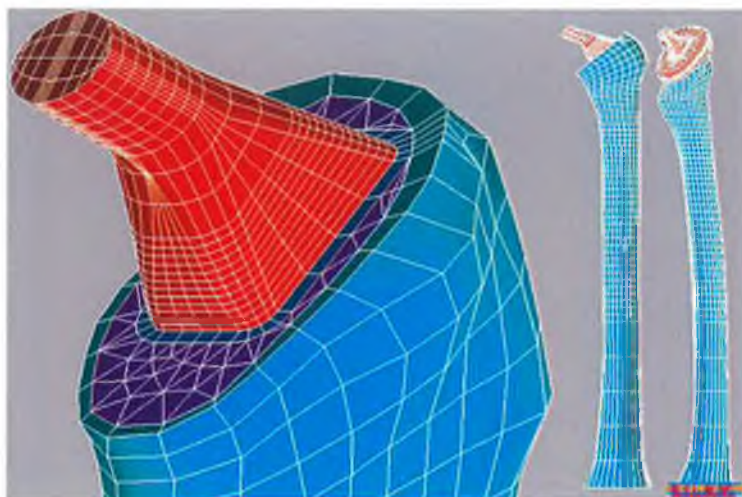


Figure 6.6: 3-D finite element meshes of the whole prosthesis components.

6.4. Boundary Conditions and loads applied

Just as geometry modeling is a strong aspect of the finite element technique, its weak aspect is in the modeling of interface conditions. This unfortunate since interface conditions play a dominant role in stress transfer in the artificial hip joint. To carry out a stress analysis of the post-operative case it is not necessary to model the soft tissue layer that builds up on the bone/cement interface. The cement/bone interface is of a different nature to that at the stem/cement junction. At the cement/bone interface the assumption of perfect bonding is not erroneous providing the cement penetrates sufficiently far into trabecular bone to produce a strong interlock between the two materials [81]. However the cement/stem interface debonds directly and may be regarded as the start of a mechanical failure train [37]. For this reason it comes within the scope of our problem and we should model it and allow for gaps forming under tension and slip under shear. By defining superimposed nodes of the prosthesis/cement interface it was possible to allow friction sliding. An eroding contact algorithm approach was selected in order to cope with the non-linear contact problem between the prosthesis and cement surfaces. The coefficient of friction was 0.32 and was determined from a pin-on-plate sliding test [153]. The

boundary condition at the distal end had no effect on the stresses in the proximal region. This was chosen as a fixed to avoid rigid-body motion.

The force applied to represent patient activity during stumbling and muscles forces were as demonstrated in the previous chapter, Figure 5.2 and Table 5.3.

6.5. *Material proposed*

All materials in the dynamic analysis, were assumed to be bi-linear elasto-plastic. The material properties of the hip prosthesis and bone cement were chosen to approximately represent Titanium alloy (Ti 6AL 4V) and unreinforced rostral bone cement PMMA, respectively. A wide range of different material Young's modulus were chosen to represent the damper plate to study their effects on the stress shielding and impulse force damping. Table 6.2 illustrates the material properties used:

Table 6.2: The artificial hip components material properties [24,79].						
Component	Material's Name	Young's Modulus [MPa]	Poisson's Ratio	Density [ton / mm ³]	Yield Stress [MPa]	Tangent Modulus [MPa]
Bone	Cortical Bone	16200	0.36	1.99×10^{-9}	114	793
	Concellleous Bone	389	0.3	0.5×10^{-9}	3.89	7.08
Rostal Bone Cement	(PMMA)	2.64×10^3	0.4	1.2×10^{-9}	43.8	10
Prosthesis	(Ti 6AL 4V)	100,000	0.32	4.43×10^{-9}	830	1255.23
	Epoxy Resin Composite	30,000	0.32	2×10^{-9}	700	-
Damper	Damper (1)	50,000	0.35	1.5×10^{-9}	-	-
	Damper (2)	1000				
	Damper (3)	1				
	Damper (4)	0.001				

6.6. *Simulation Results and Analysis*

To assess the benefits of using a skirt-collared cemented hip prosthesis (for a damperless and damped case) over the others, a comparison study has been made. This comparison gives an insight to the stem relative microdisplacements and stress distribution in each component of the artificial hip, including the bone and the cement mantle. Hence, the design justification effectiveness would essentially is based on:

- The potential of the joint design to withstand primary mechanical failure,

primary stability.

- b) The value of shielded stress in the bone cortex.

The gait time of the highest force during stumbling was incorporated in the LS-DYNA solver. However, the stresses developed on the artificial hip components were calculated at 2.9 sec during the stumbling, when the maximum load is occurred, see Figure 5.2. To decrease the CPU time required to execute the dynamic solution, the gait time has been multiplied by a factor equal to 1×10^{-3} . This led to about 38 hours to carry out the dynamic solution.

6.6.1. The Effect of Design Features

The following three different damperless prosthesis types have been undertaken:

- a) Skirt-Collared cemented hip prosthesis.
- b) Collared cemented hip prosthesis without skirt.
- c) Collarless cemented prosthesis.

The prostheses and cement mantle material stiffness were chosen to be 100 GPa and 2.64 GPa, respectively. A finite element model of the natural femur before arthroplasty was also produced to act as a reference for the bone stresses predicted by the models of the implanted components.

6.6.1.1. Prosthesis Displacements

The stability of the hip prosthesis has a major advantage in favour of its longevity and preserving the cement mantle from crumbling. Figures 6.7, 6.8, and 6.9 show the stem and cement displacements in Z, X, and Y axes, respectively. They were measured at two points in each side, one in the proximal tip and the other in the distal tip.

As expected the Z-axial displacements of the two collared prosthesis are upwards while the collarless one shows high subsidence at both the proximal and distal ends, see Figures 6.7 (a) and (b).

Figures 6.8 and 6.9 (a and b) show that the hip prosthesis and the cement mantle move together in the medial-posterior direction, and that the collared prostheses offers more resistance to the radial displacements than the collarless one. Because that skirt-collared prosthesis is rigidly held from the proximal end, it shows a pivot action while there are considerable movements towards the medial and posterior directions in the distal tip of its stem. However, this pivoted action could partly attribute to the high material stiffness of the prosthesis where less deformation and bending may happen to the prosthesis stem during the high stumbling loads.

It is evident that the stem and cement mantle do not undergo the same displacement after the commencement of the decrease in the stumbling load, Figures 5.2. This property is very common in a sandwich material. The cement property shows that it would not return into its initial state with the same rate of the stem material as the stumbling load decreases. This could account for the reason why the displacement for the collared prostheses at a certain stage (when the stumbling load starts decreasing) becomes greater.

6.6.1.2. Hip components Axial Stress

(A) Stem Prosthesis Stresses

Figure 6.10 shows the tensile and compressive axial z-stress of the prosthesis stem which occur at the prosthesis/cement interface for three different design types. It is evident that the maximum axial stress occurs medially, about the middle of the stem, for the three designs. Using collared prostheses shows a decrease in the stress along the stem compared to the collarless one. For the skirted and skirtless collared-prostheses, the maximum stress is not the same in the lateral side in spite of that it is equal in the medial sides. The skirtless collared prosthesis reveals less stress in that side. Because the crack initiation is caused by the tensile stresses, such stresses located in the lateral sides of the artificial hip components are of more concern.

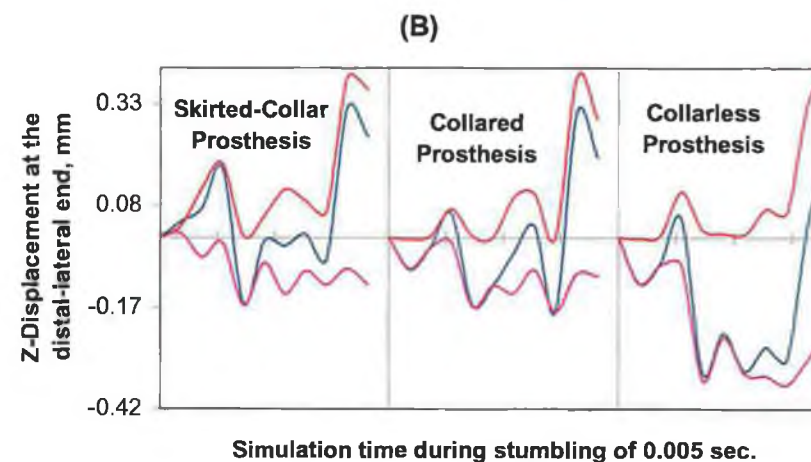
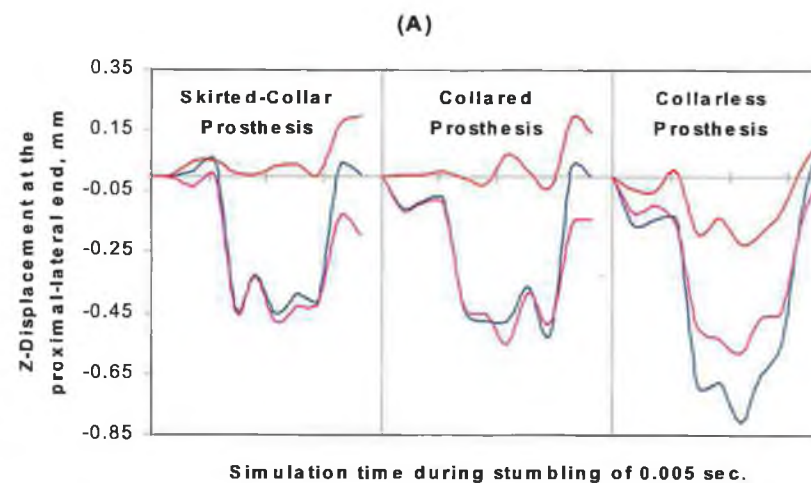
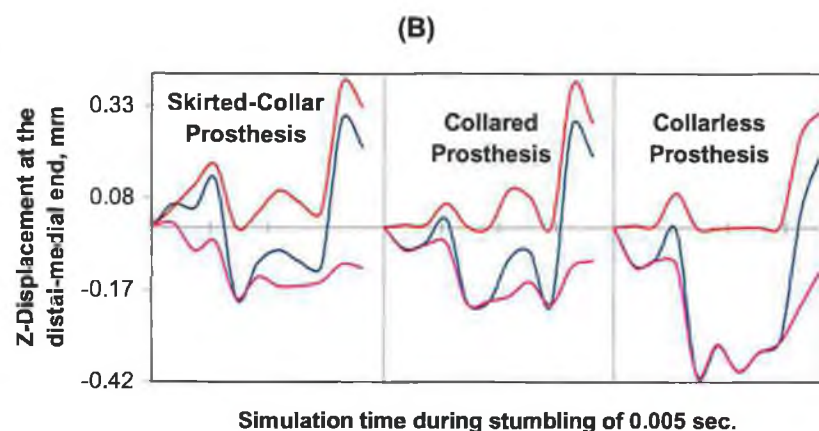
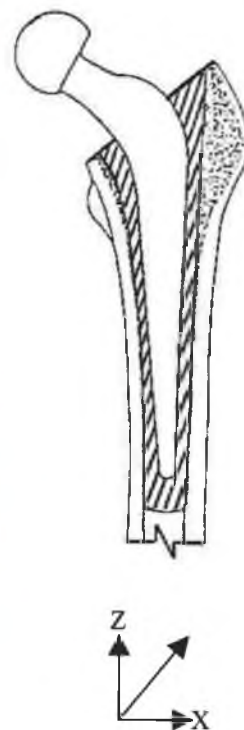
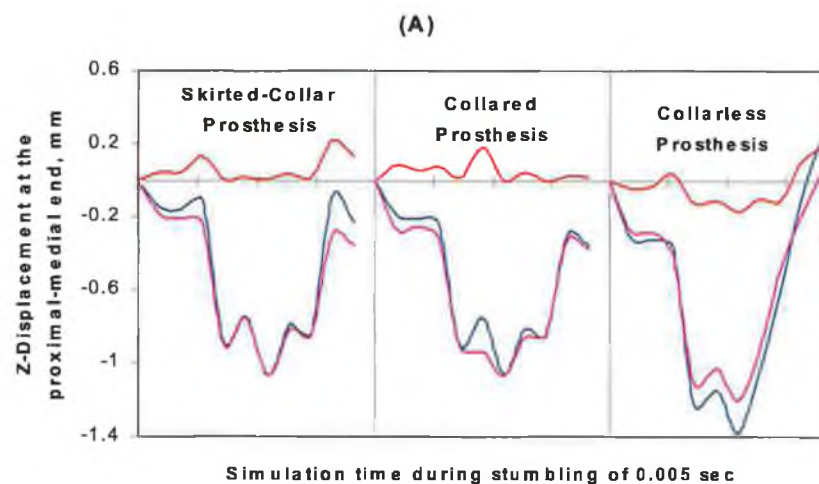


Figure 6.7(a): The stem and cement mantle displacements in z-direction, measured at A) the proximal and B) the distal ends of the medial and lateral sides, for three different prostheses types. (—) Artificial hip prosthesis, (—) Cement Mantle, and (—) The stem displacement relative to the cement.

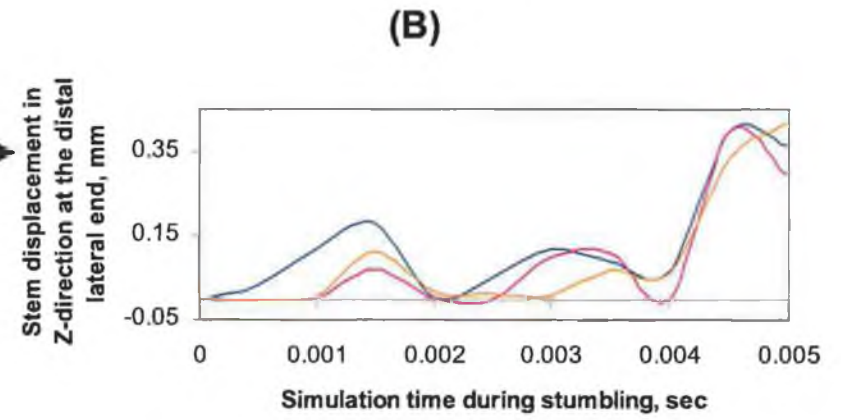
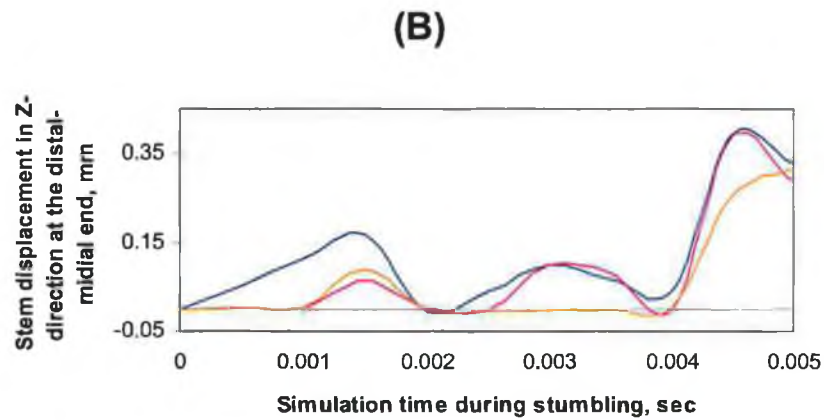
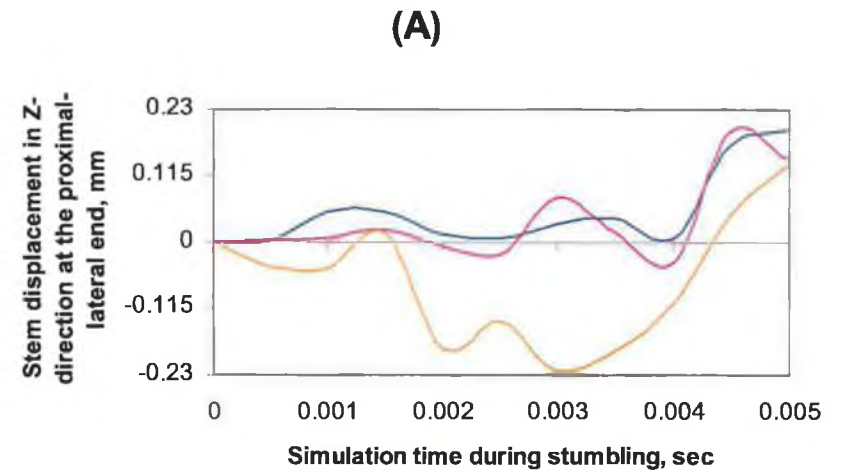
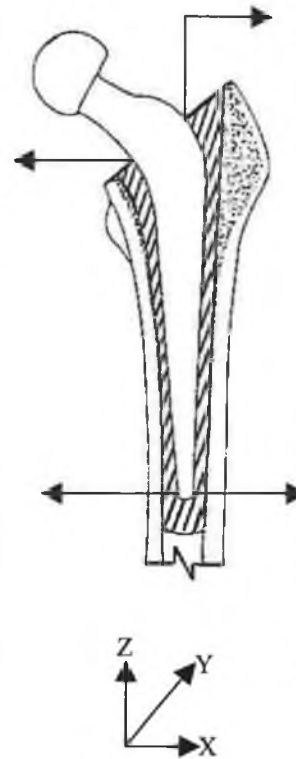
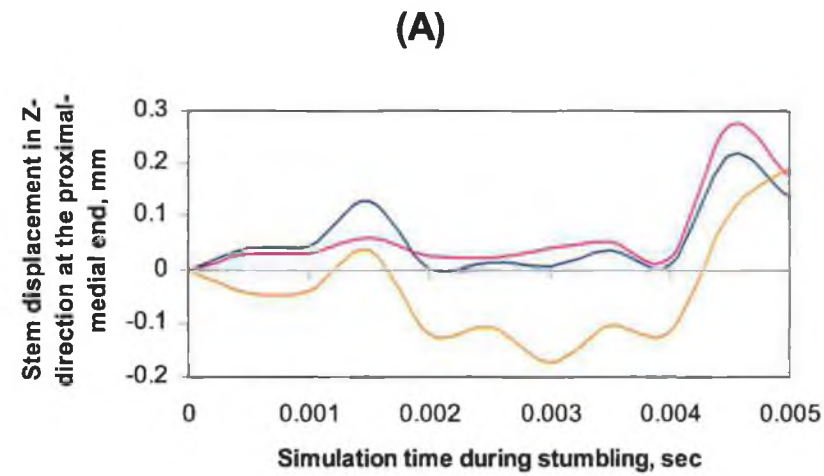


Figure 6.7(b): Stem displacements relative to the cement mantle in z-direction, measured at A) the proximal and B) the distal tips of medial and lateral sides, for three different prostheses types.

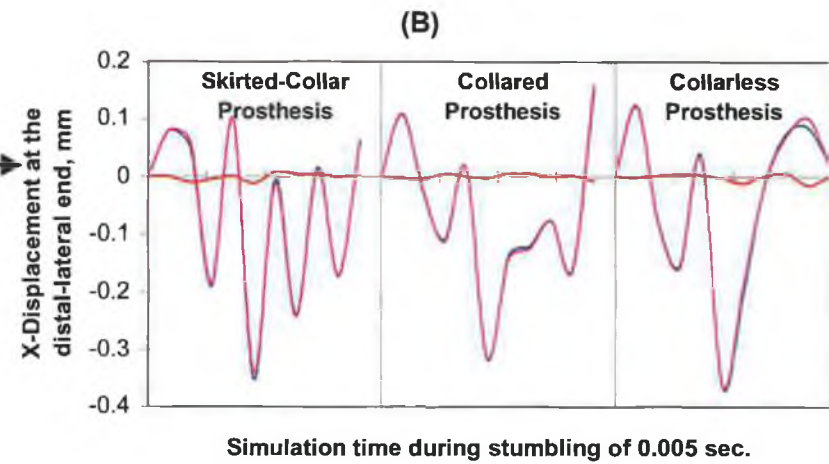
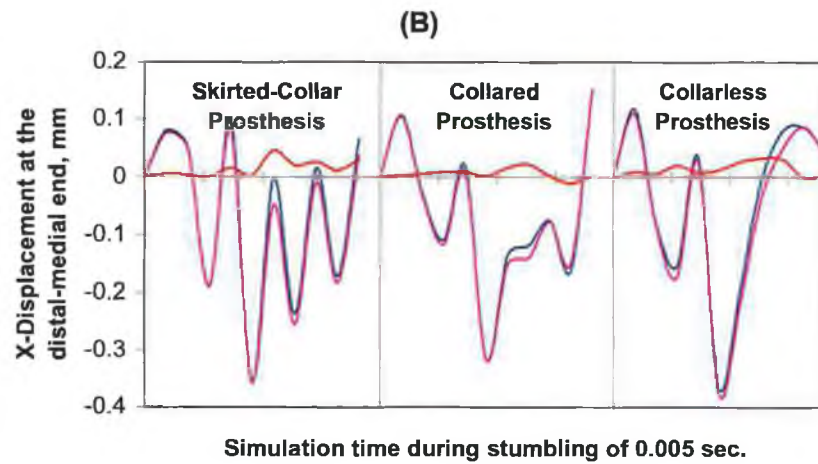
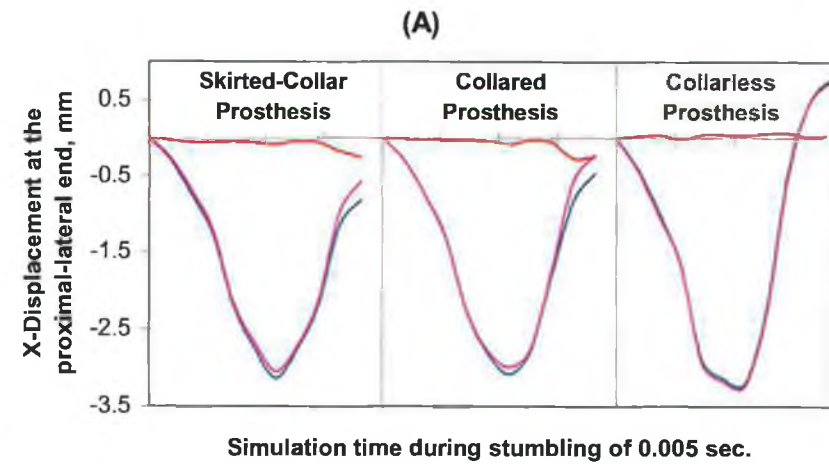
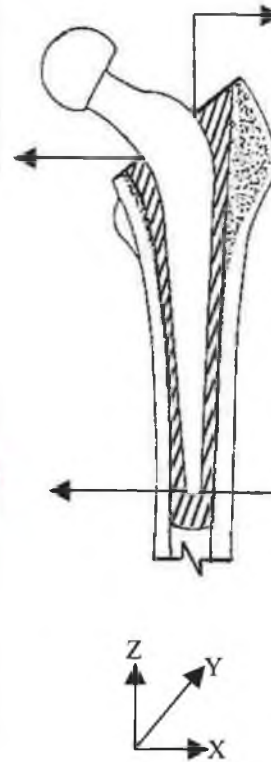
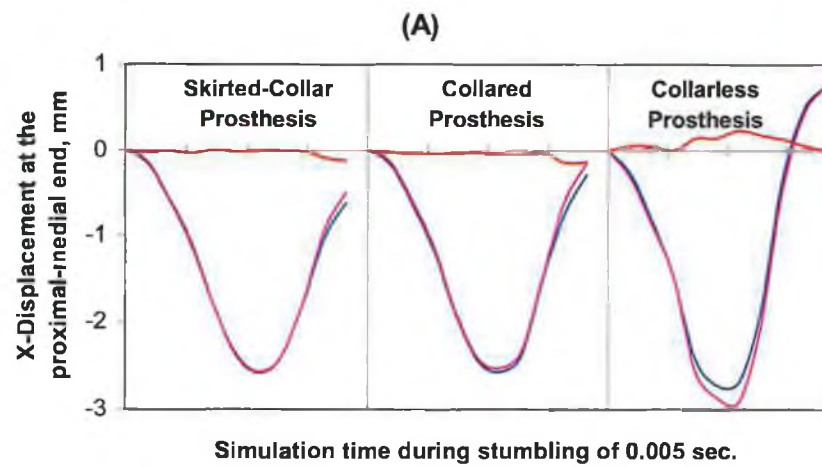


Figure 6.8(a): The stem and cement mantle displacements in x-direction, measured at A) the proximal and B) the distal ends of the medial and lateral sides, for three different prostheses types. (—) Artificial hip prosthesis, (—) Cement Mantle, and (---) The stem displacement relative to the cement.

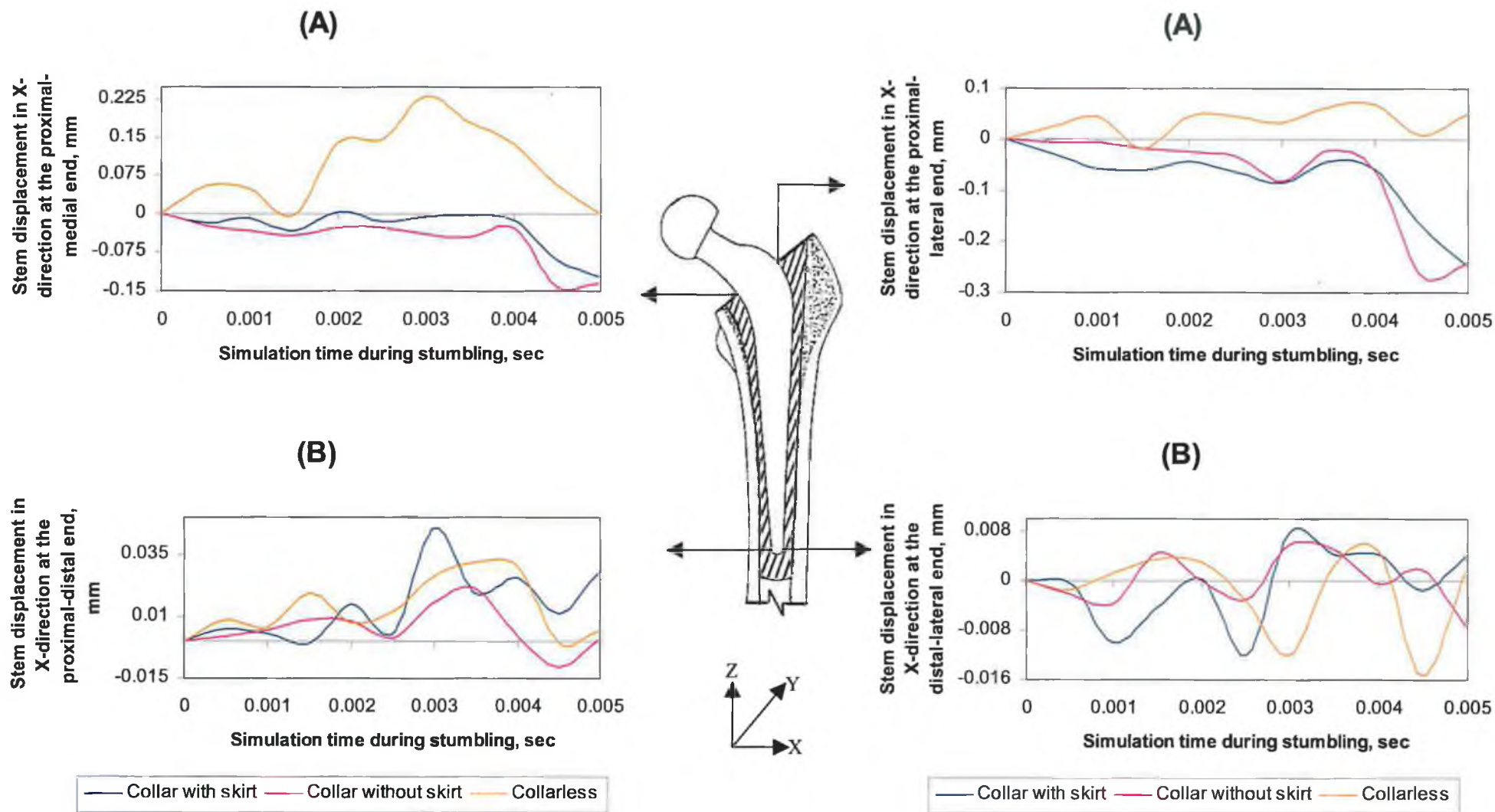


Figure 6.8(b): Stem displacements relative to the cement mantle in x-direction, measured at A) the proximal and B) the distal tips of medial and lateral sides, for three different prostheses types.

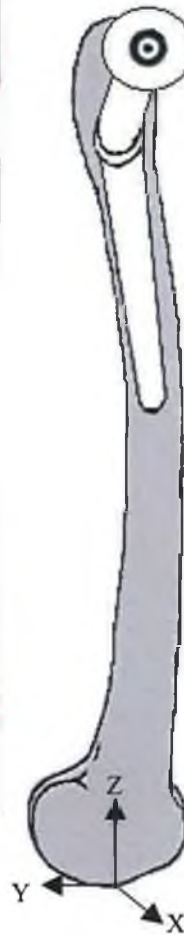
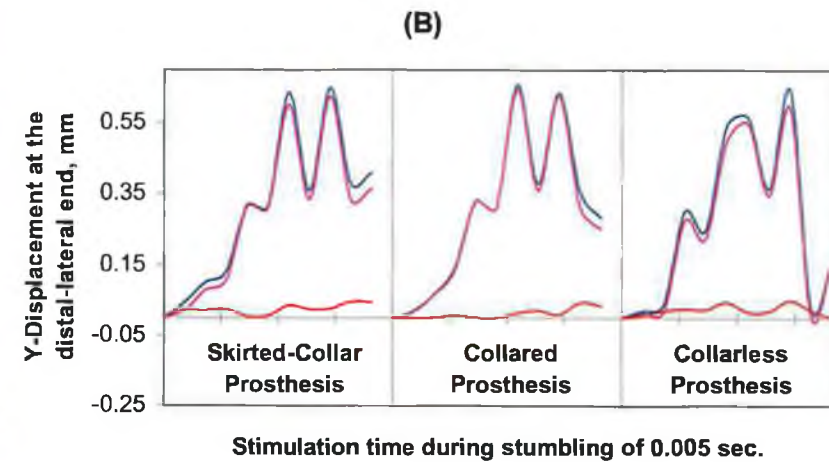
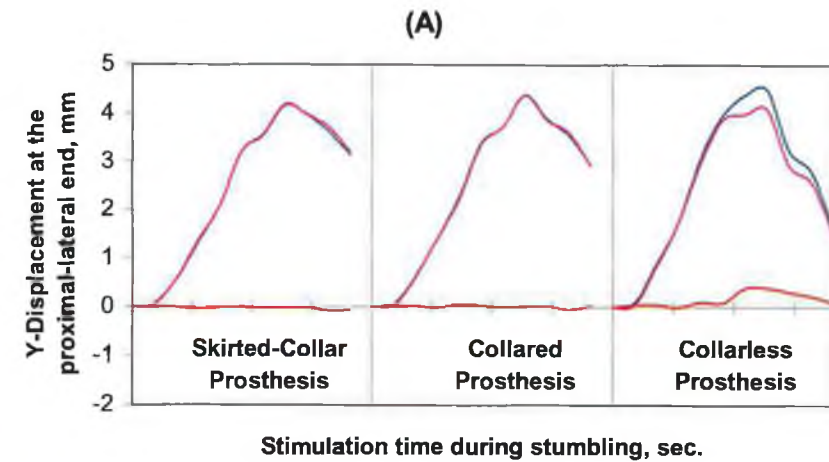
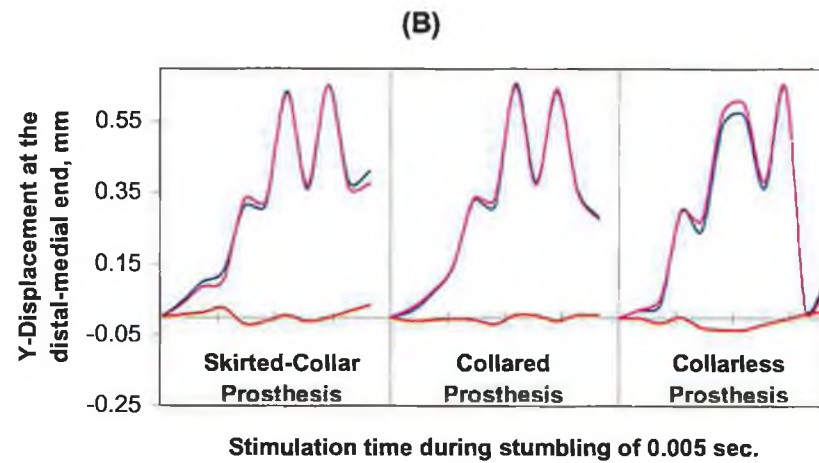
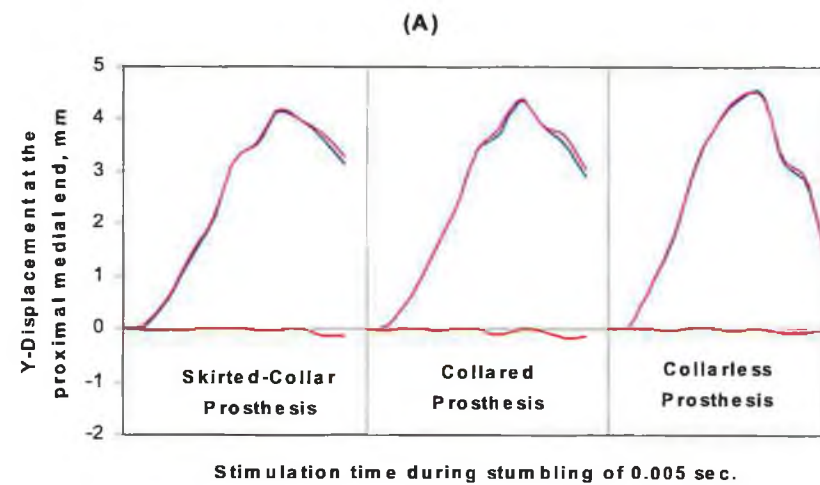


Figure 6.9(a): The stem and cement mantle displacements in z-direction, measured at (A) the proximal and (B) the distal tips of posterior and anterior sides, for three different prostheses types. (—) Artificial hip prosthesis, (—) Cement Mantle, and (—) The stem displacement relative to the cement

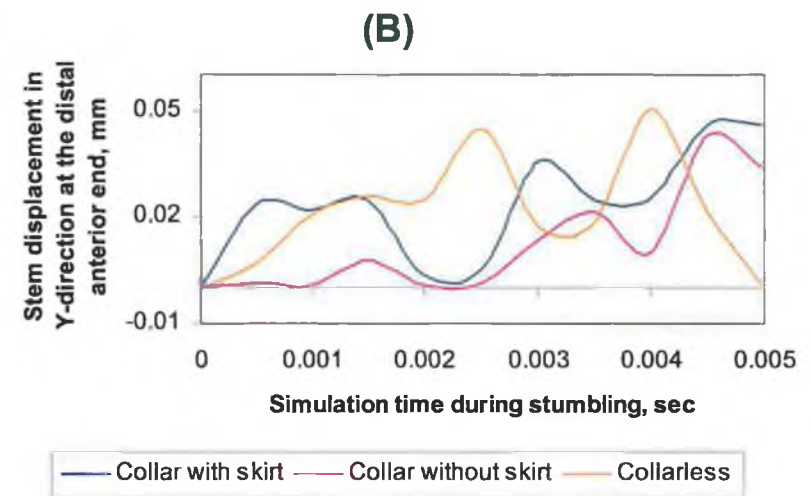
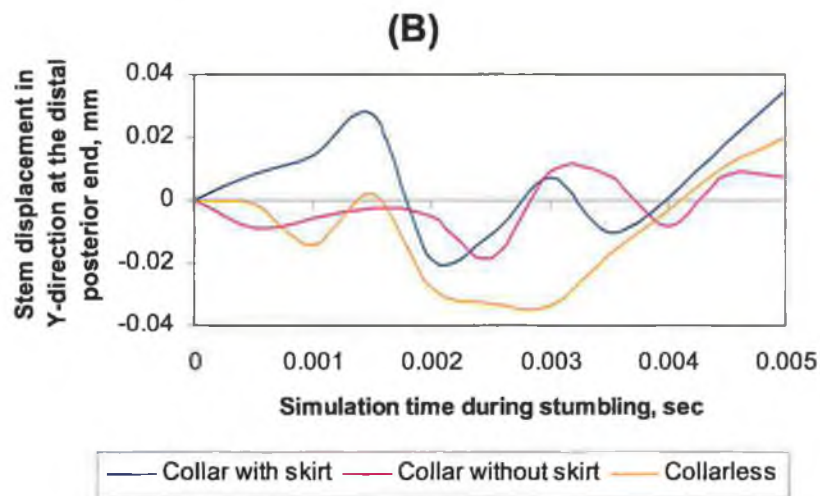
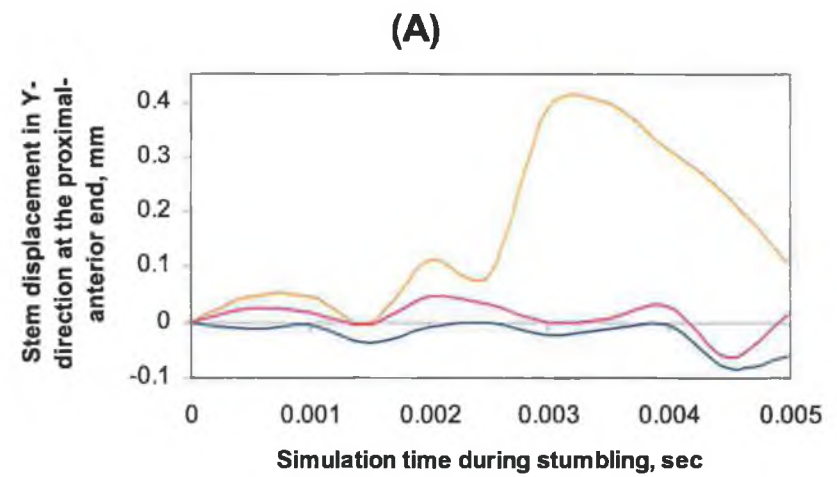
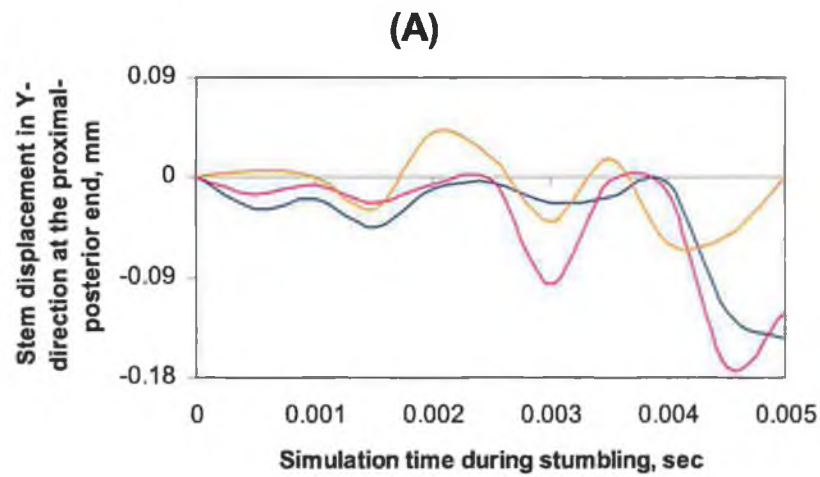


Figure 6.9(b): Stem displacements relative to the cement mantle in y-direction, measured at A) the proximal and B) the distal tips of posterior and anterior sides, for three different prostheses types.

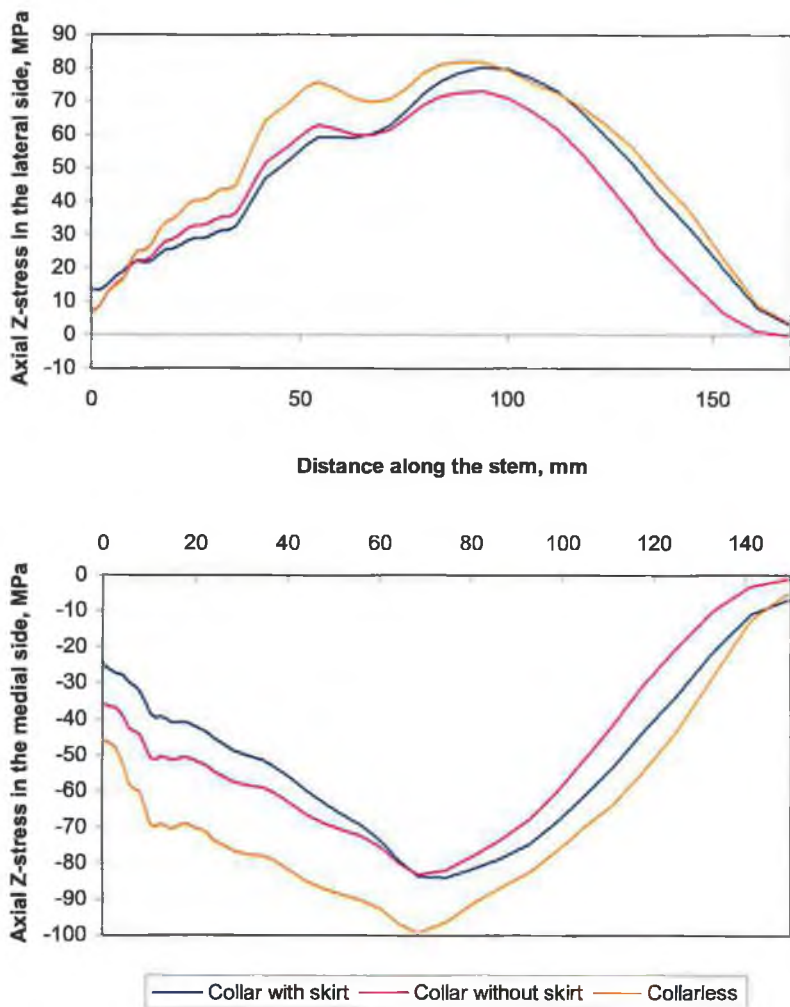


Figure 6.10: Minimum and maximum axial stress distributions, in MPa, in the lateral and medial sides of the stem as a function of prosthesis design. Note here, all the prostheses were damperless. Stem and cement Young's modulus are 100 GPa and 2.64 GPa respectively.

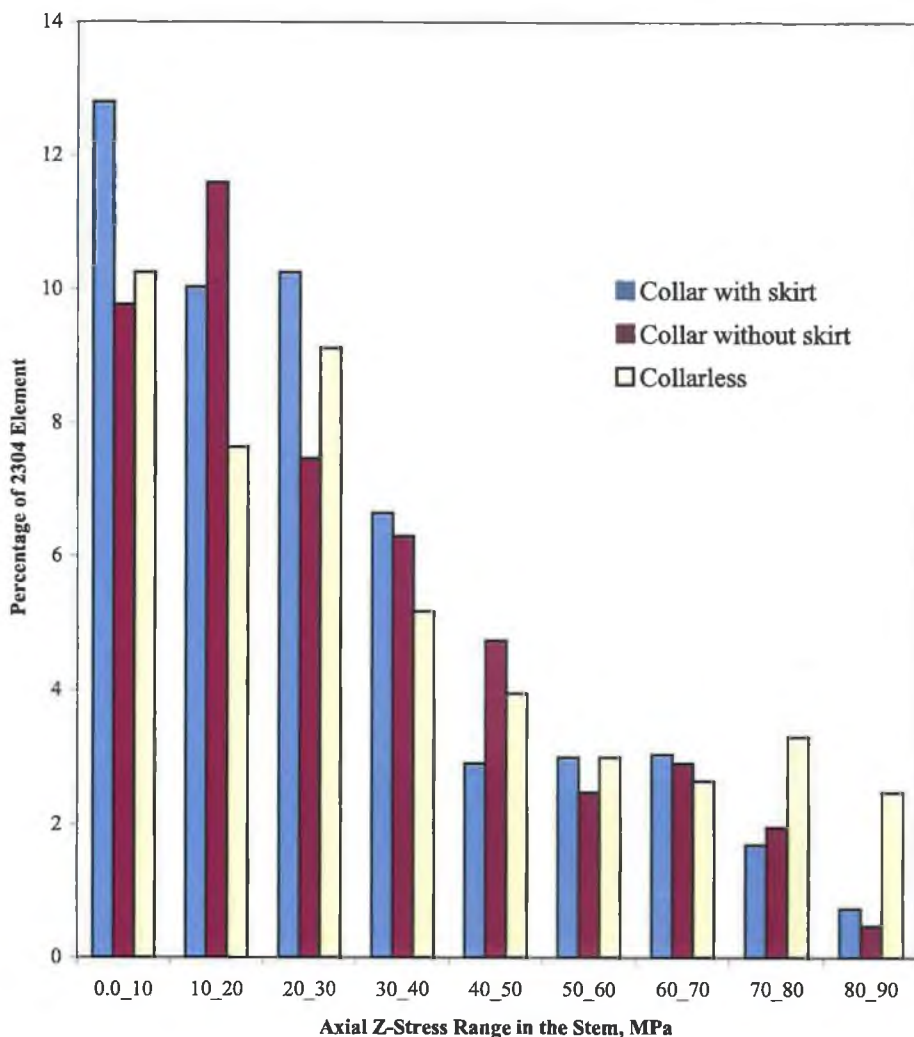


Figure 6.11: Distribution of 2304 element of the prosthesis stem over a stress range of 0-90 MPa as a function of prosthesis design. Note all the prostheses were damperless. Stem and cement Young's modulus are 100 GPa and 2.64 Gpa, respectively.

Figure 6.11 reveals that the collarless prosthesis experienced higher stresses distributed over a relatively large number of elements. This can also be seen from the contour plot of the axial z-stress distributions for the three prosthesis types, Figure 6.12. In spite of the fact that the maximum tensile stress is same for all prosthesis types, about 89 MPa, it is distributed over a broad area in the collarless and collared prosthesis stem and extends mostly along the lateral-posterior edge. This may give indication that they are exposed to a high deformation level. While for the skirted-collar prosthesis it is acting over a limited narrow area in the middle of the lateral side.

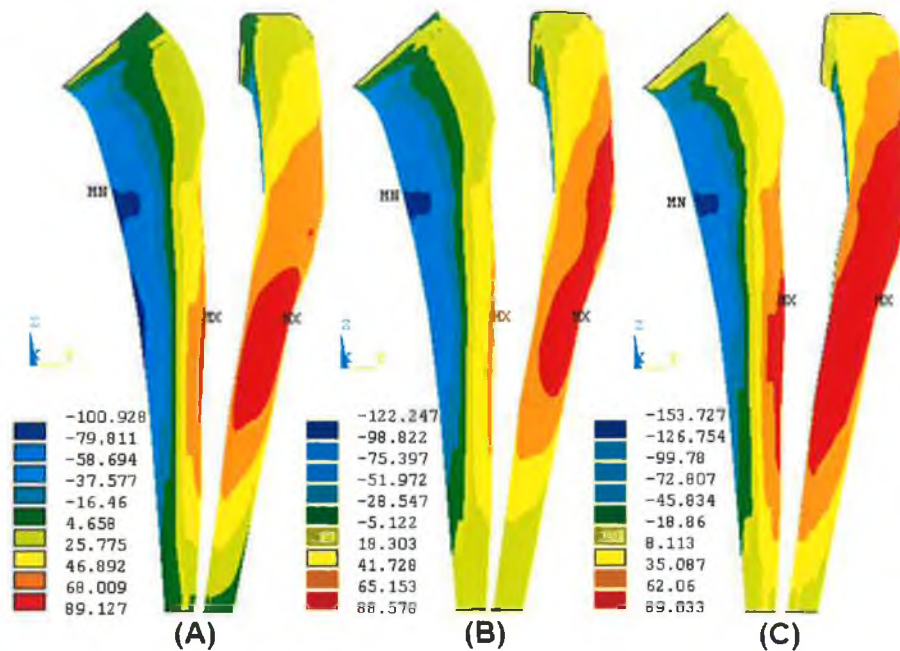


Figure 6.12: A contour plot of the axial z-stress (MPa) on the stem of (A) skirted-collar prosthesis, (B) collared prosthesis, and (C) collarless prosthesis.

(B) Neck Prosthesis Stresses

Figure 6.13 shows that the tensile and compressive stresses in the lateral and medial side of the prosthesis neck are equal and they amount to about 30 MPa and 165 MPa respectively for the three proposed designs whereas Figure 6.14 revealed that the tensile stresses could reach up to about 60 MPa somewhere in prosthesis neck. However this result is based on the element stresses which does not account the average of each element's nodes.

Figure 6.15 shows a contour plot of the axial z-stress distributions for the three prosthesis necks. In spite the fact that they are experiencing the same amount of maximum stresses, the uncollared prosthesis showed a different kind of bending deformation than the collared ones.

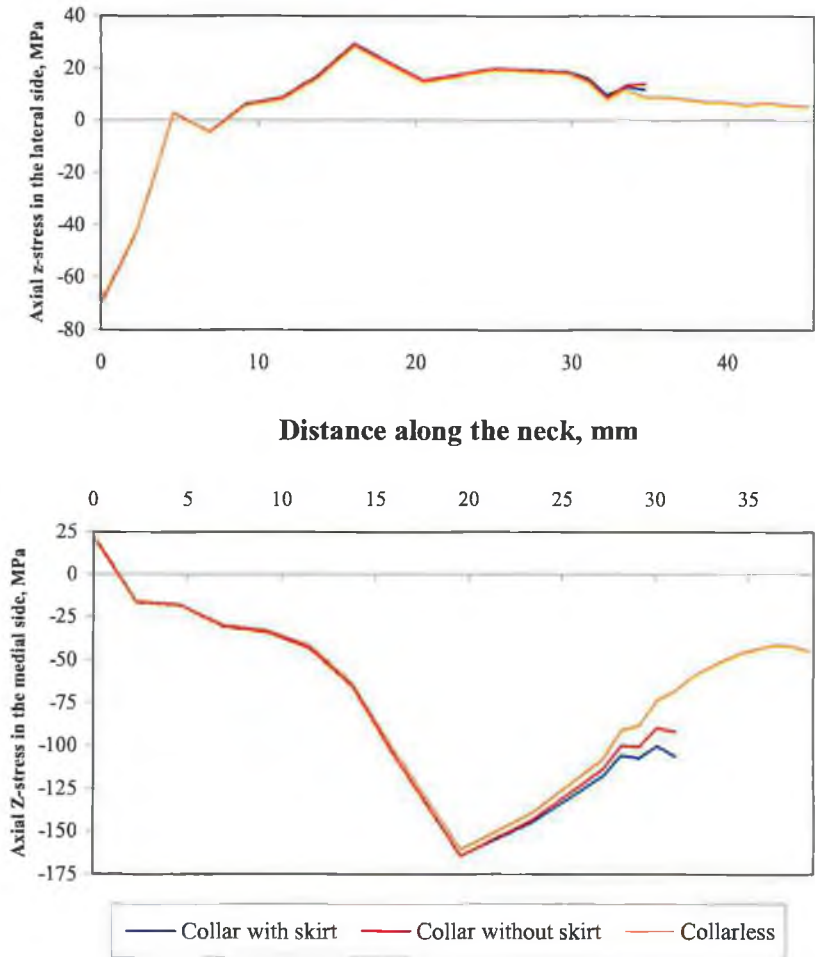


Figure 6.13: Minimum and maximum axial stress distributions, in MPa, in the lateral and medial sides of the prosthesis neck for three different prosthesis designs: Collar with skirt, Collared without skirt, and Collarless prosthesis. Stem and cement Young's modulus are 100 GPa and 2.64 GPa respectively.

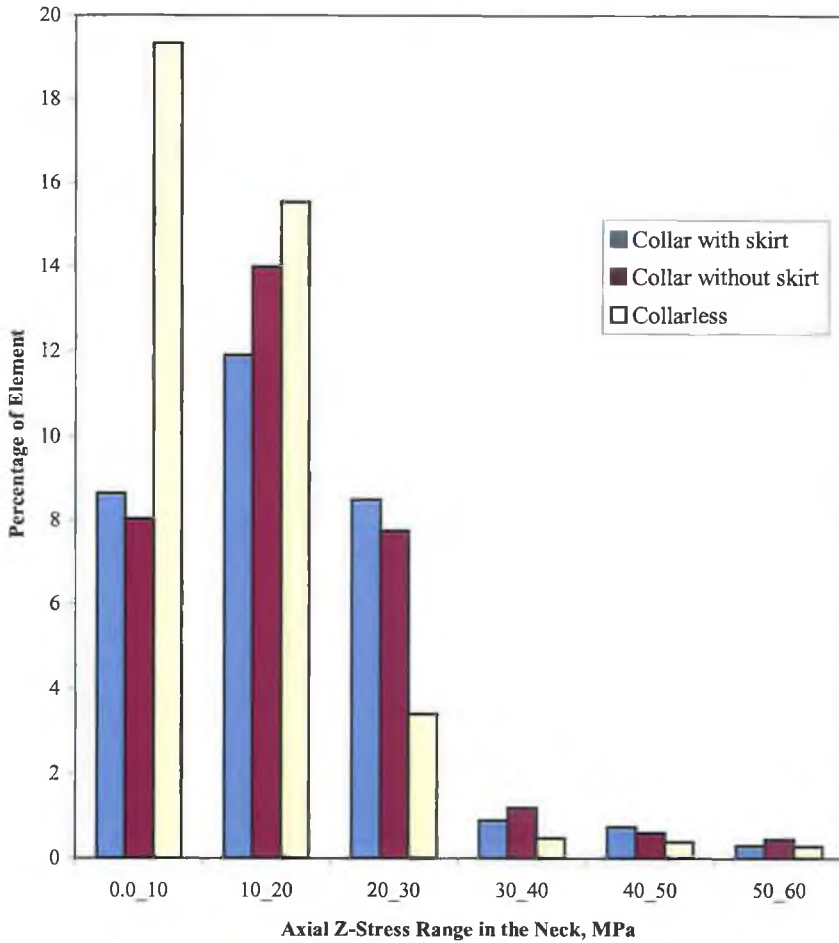


Figure 6.14: Distribution of elements (1056 element for the collarless prosthesis and 672 element for the rest) of the prosthesis neck over a stress range of 0-60 MPa for three different prosthesis designs: Collar with skirt, Collared without skirt, and Collarless prosthesis. Stem and cement Young's modulus are 100 GPa and 2.64 GPa respectively.

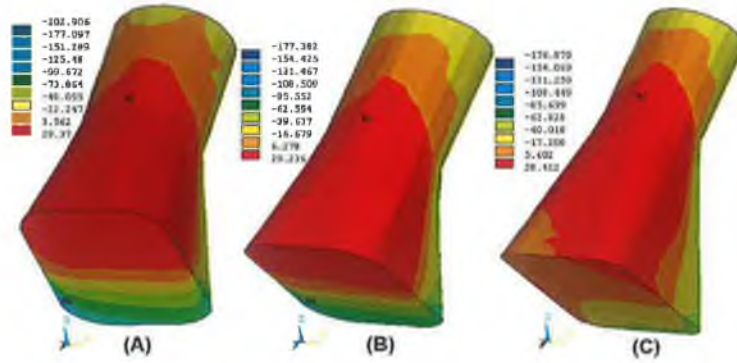


Figure 6.15: A contour plot of the axial z-stress (MPa) on the neck of (A) skirted-collar prosthesis, (B) collared prosthesis, and (C) collarless prosthesis.

(C) Cement Mantle Stresses

Stress distribution of the cement mantle is more complex than that of the prosthesis since it is subjected to multiple deformation modes [3]. Cement primarily undergoes a bending deformation, which generates tensile stresses laterally and compressive stresses medially. Additionally, due to the axial component of the joint, it deforms in shear. Moreover, it is deformed radially outwards because of the wedging action of the tapered stem.

Figure 6.16 shows the contour plot of the cement mantle axial z-stress distributions used for the three prostheses. Figure 6.17 shows the axial z-stress variation, as a function of prosthesis design features, in the medial and lateral sides of the cement mantle at the cement/bone interface. It is conspicuous that the use of

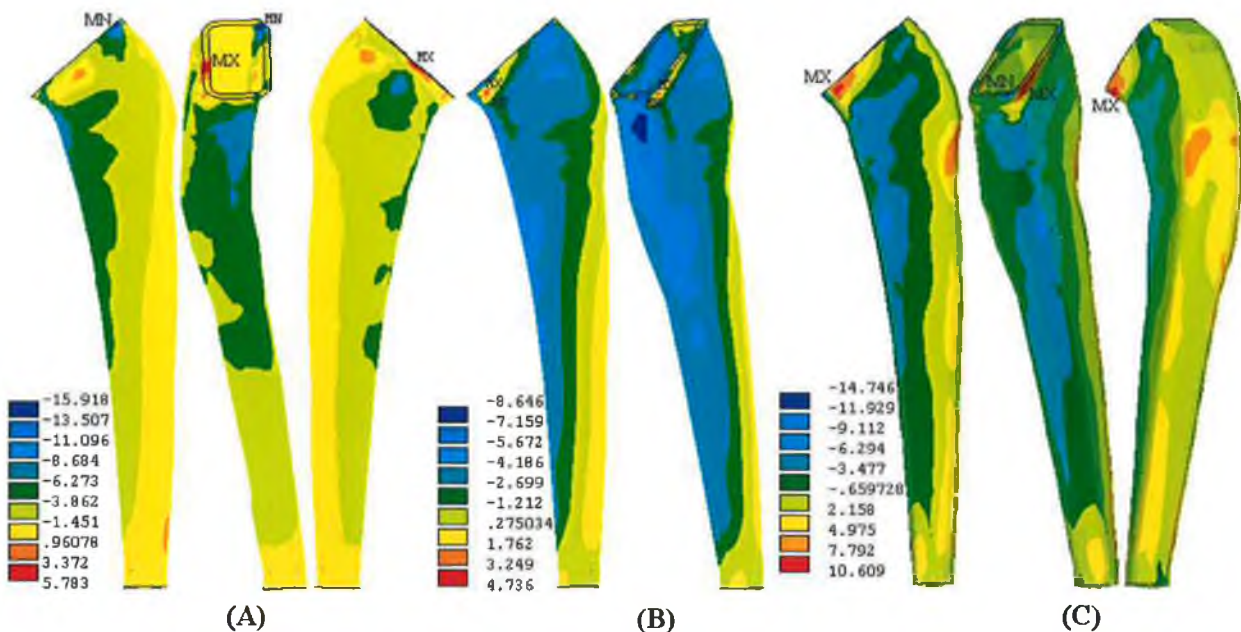


Figure 6.16: A contour plot of the axial z-stress (MPa) on the cement mantle of (A) skirted-collar prosthesis, (B) collared prosthesis, and (C) collarless prosthesis.

collarless prosthesis gives rise to a noticeable increase in the tensile stress in the lateral side of the cement mantle which may exceed more than 4 times of the stress caused by using collared prostheses. One can see, also, that the skirt-collared prosthesis revealed very low tensile stress magnitudes in that side. This is firstly because the collar acts in transferring part of the loads directly to the bone and hence this would ease the pressure on the cement and secondly due to the firm fixation in the proximal part of the femur by means of the skirted collar which in turn permits all the structures (prosthesis, cement, and bone) move together and prevent the excessive radial movements of the prosthesis stem inside the cement mantle. This could be considered as one advantage of using skirt-collared hip prosthesis over other configuration. The distal stresses in the lateral and medial sides of the cement mantle remain identical to those developed using skirted and skirtless collared prostheses, but the more proximal stresses are altered. However, some high lateral compressive cement stresses at the tip of the collarless prosthesis are also found. And this could be attributed to the high stiffness of the stem, since it deforms little; therefore the prosthesis toggles in the medullary canal, generating compressive stress on the lateral cement at the level of the prosthesis tip.

Maintaining the mechanical integrity of the mantle is not simply a matter of reducing the peak stress in the cement mantle or at the cement/bone and cement/prosthesis interfaces, although this criterion can be used to optimize a stem profile [120]. Mechanical integrity can only be maintained if the overall stress within the mantle is kept below some threshold over time. In theory, finite element modelling is the ideal tool for determining the stresses in the cement and hence the durability of the implant fixation. However, a significant problem is that the stress distribution in a cement mantle around an orthopaedic implant is very intricate, and furthermore, the influence of cement porosity may dominate the effect of the stress [106] to a degree that failure may not occur at the site of peak stresses in the cement mantle, but rather may occur where the pores are largest. In this respect, the peak stress may give an incorrect picture of the potential durability of a cemented fixation since it only occurs in a very small volume of the cement mantle. McCormack and Prendergast [306] reported that one important problem of cement stresses is that the critical peak stresses may occur at singularities in the stress field.

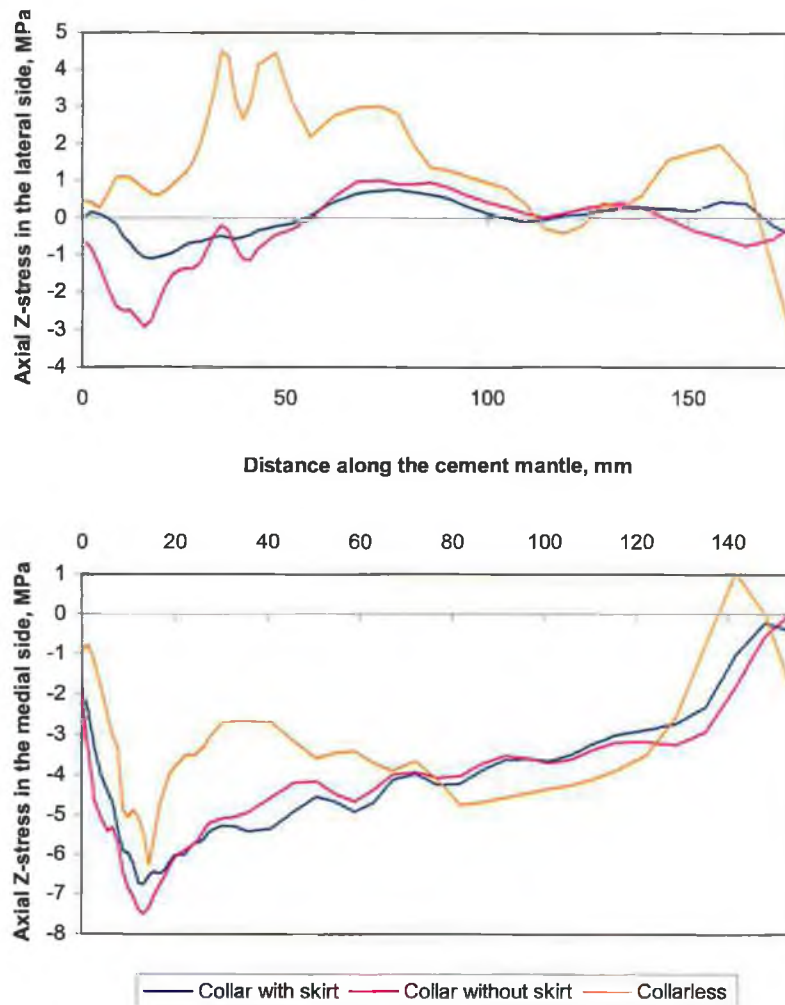


Figure 6.17: Minimum and maximum axial stress distributions, in MPa, in the lateral and medial sides of the cement mantle as a function of prosthesis design. Note here, all the prostheses were damperless. Stem and cement Young's modulus are 100 GPa and 2.64 GPa respectively.

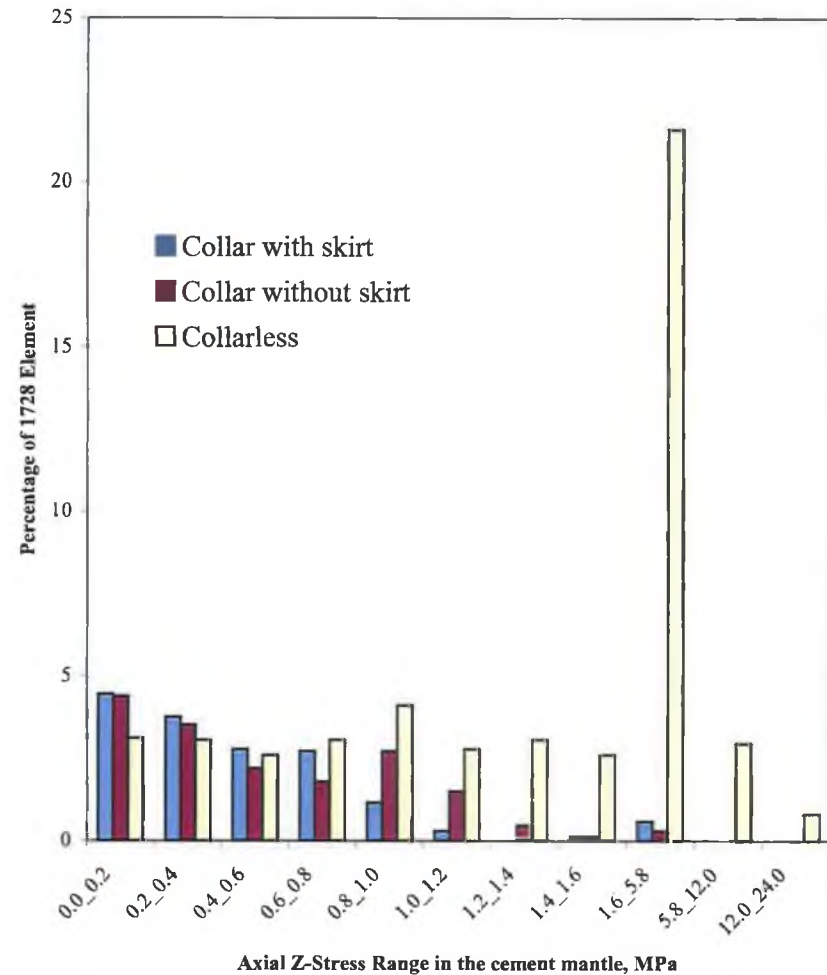


Figure 6.18: Distribution of 1728 element of the cement mantle over a stress range of 0-12 MPa as a function of prosthesis design. Note all the prostheses were damperless. Stem and cement Young's modulus are 100 GPa and 2.64 GPa, respectively.

One approach used to solve this problem is to use a non-local definition of stress [307], or to determine the volume of cement stressed above a certain level [269]. Furthermore, the use of the average stresses for an element diminishes the influence of any singularities in the stress field [153]. Reporting of peak stress alone would seem to be a particularly misleading measure of the durability of a cemented fixation as is clear in Figure 6.18. In spite of the fact that peak stress in the lateral side reached about 4.5 MPa using the collarless prosthesis (as depicted in Figure 6.7) plotting the total volume of elements for each stress range shows the stress to be 24 MPa (Figure 6.18). However, if a stress level, e.g. of 12 MPa, is considered critical, it is clear from Figure 6.18 that the volume of overstressed cement is greater when the collarless prosthesis is used. This result would not be expected from the peak stress only. Generally, one can deduce that the collarless prosthesis is capable of generating a very high tensile stress in the cement compared to the collared prosthesis.

(D) Bone Cortex Stresses

Figure 6.19 shows the comparison of axial stress distributions in the bone cortex for an intact femur with the treated femora. It demonstrates the stress distributions in the treated bone as a function of prosthesis feature design. It is obvious that in all regions, except that of greater trochanter, the three prostheses produce a significant stress shielding, Figure 6.20. In addition, the proximal fixed prosthesis design causes no significant change in the stresses in the diaphysis. The closer comparison between the proximally fixed design in Figure 6.20 clearly shows that the current design, skirted-collar prosthesis, produces lower magnitude stress shielding in the calcar region which is a site of major concern due to the common occurrence of bone resorption and hence a prosthesis failure [308]. Here, the new design produces less stress shielding than the skirtless-collared and collarless prostheses. In greater trochanter, a portion of the trochanter is removed to accommodate the prosthesis yet the trochanter muscle loads remain, so it is assumed to subject to be loading from the abductor muscles. Hence there is no significant difference between the pre and post-implantation stress states in the greater trochanter.

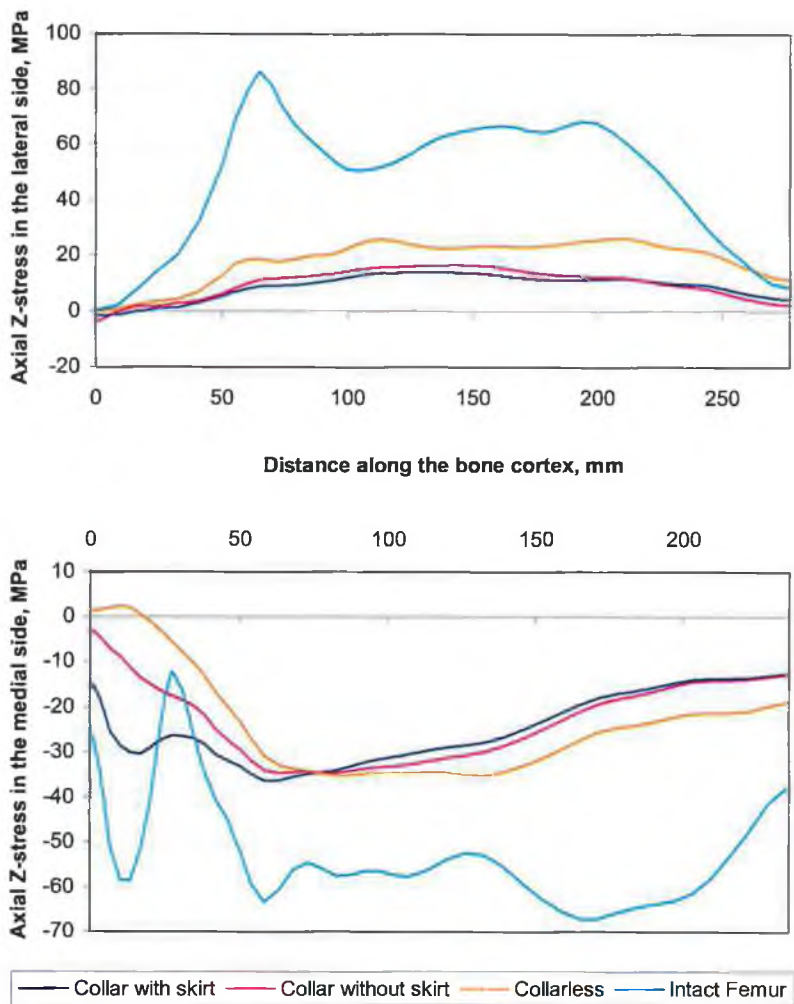


Figure 6.19: Minimum and maximum axial stress distributions, in MPa, in the lateral and medial sides of 1) treated femurs, as a function of prosthesis design, and 2) an intact femur. Note here, all the prostheses were damperless. Stem and cement Young's modulus are 100 GPa and 2.64 GPa, respectively.

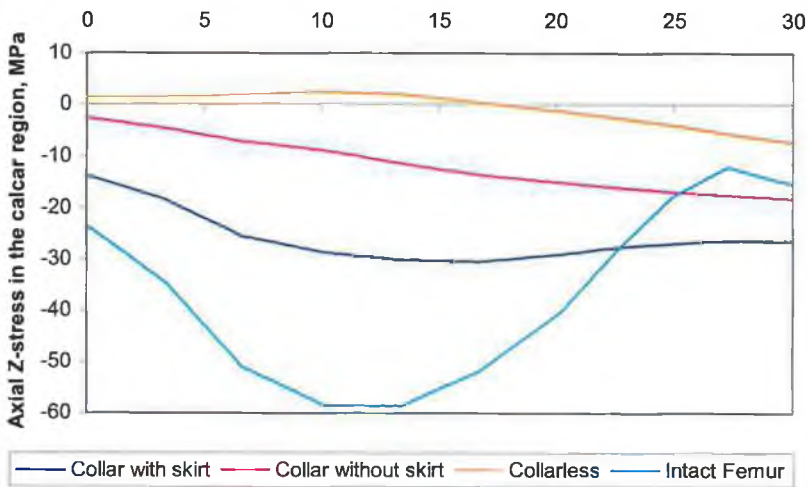
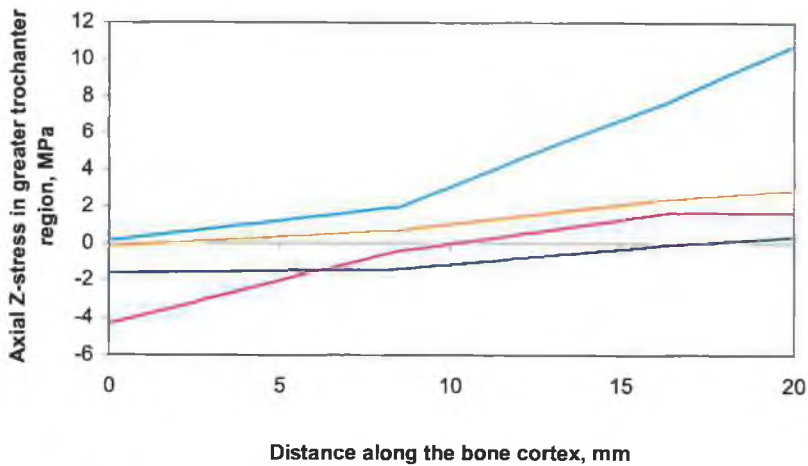


Figure 6.20: The variation of z-axial stresses in the calcar and the greater trochanter regions as a function of prosthesis type. Note that the axial stress of the natural femur before total hip implantation is used as a reference.

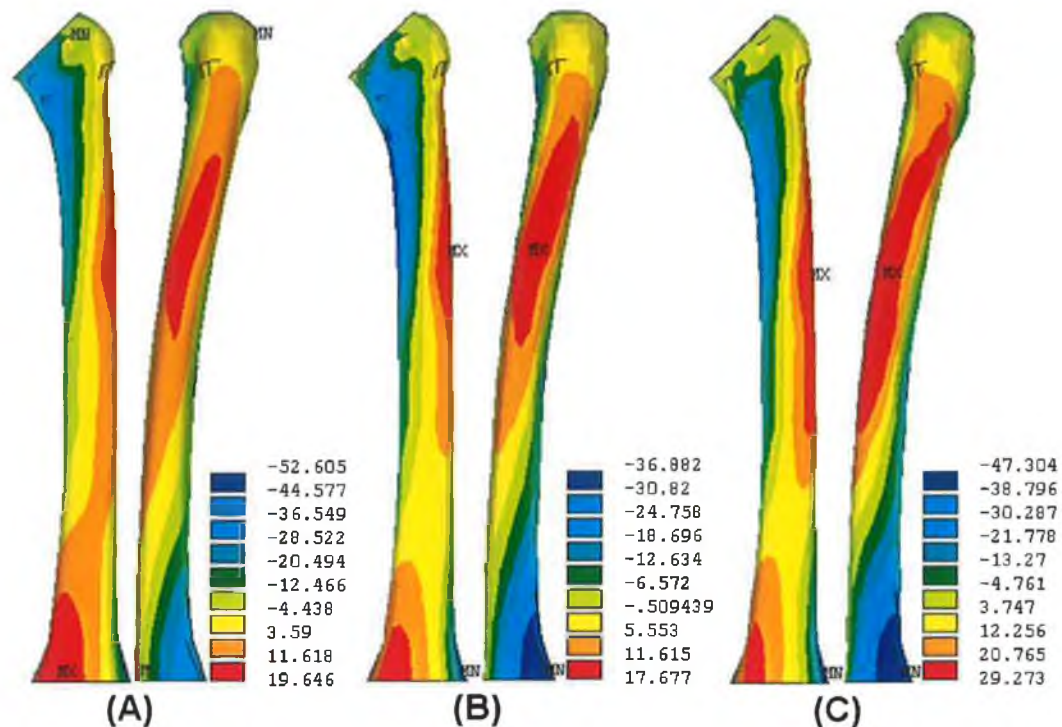


Figure 6.21: A contour plot of the axial z-stress (MPa) on the bone cortex of the femur when the following prostheses are used: (A) skirted-collar prosthesis, (B) collared prosthesis, and (C) collarless prosthesis.

Figure 6.21 shows a contour z-stresses based on nodal stresses of the bone cortex. It can be seen that the maximum stress for femur (A) is located in the distal anterior end as a result of the skirted-collar prosthesis which totally caused the femur to bend towards the medial-posterior direction. Aspect also quite noticable is that by increasing the tightening fixation in the proximal end the spread of maximum tensile stresses decreases. Rather, by using the collarless prosthesis the spread of maximum tensile stresses is over quite a large area compared to the other two collared prostheses.

6.6.2. The Effect of Prosthesis material

The use of metals for prosthesis material does present some difficulties, one of which is caused by their high stiffness relative to human bone. It can be appreciated then, that if part of the bone structure is replaced by a metal alloy the stress distribution of the system will change considerably. Two problems can be idenetified:

- a) A change to the stress conditions within the bone. Excessively high stresses can kill the bone (necrosis), unusually low stresses will lead to gradual loss of stiffness or complete dissolution of bone which is no longer required to bear load

(stress-shielding).

- b) The stiffness mismatch across the bone/cement/prosthesis interfaces will give rise to local stresses which encourage lack of interface adhesion and therefore lead to loosening.

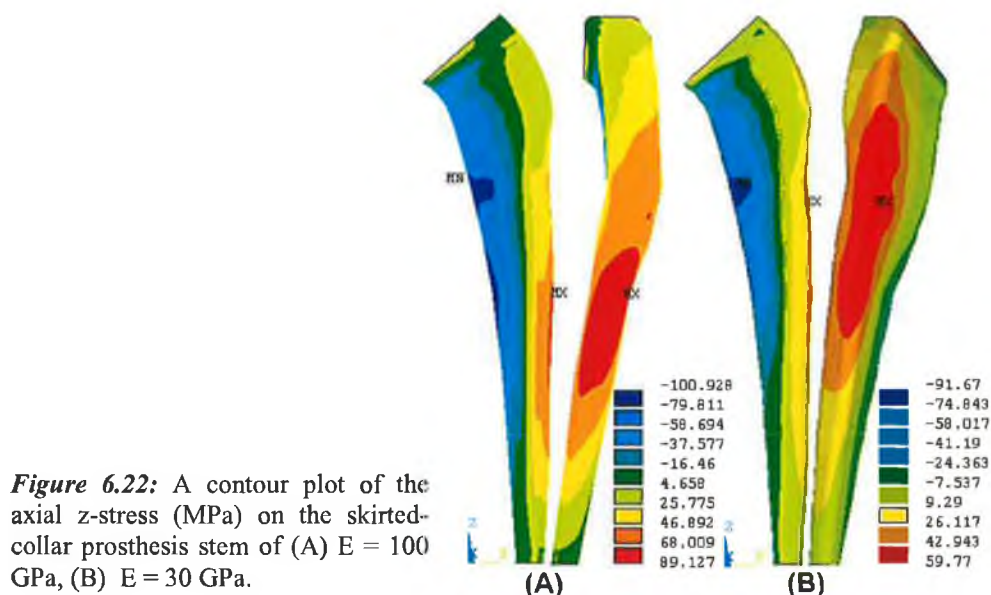
There is considerable interest, therefore, in manufacturing the prosthesis from a material which have the same stiffness as surrounding bone. Unfortunately, no metals are available, since all metals with Young's moduli less than 100 GPa can be ruled out on the basis of toxicity or on economic grounds. In this regard, polymer composites offer attractive mechanical properties since its stiffness and strength are increased by addition of carbon, glass or other materials. Similar materials are already being used extensively in the dental field, replacing metal alloys as fillings and repair materials.

The purpose of this study is to examine the behaviour of the skirt-collared prosthesis when it made of a material of low Young's modulus, such as reinforced Epoxy Resin Composite of Young's modulus 30 GPa, and compare it with that of Titanium alloy (Ti-6%Al-4%V).

6.6.2.1. Hip components Axial Stress

(A) Stem Prosthesis Stresses

Figure 6.22 shows that the stem of soft material exposed to minimal maximum axial stresses allocated along the lateral-posterior edge and extended on a



broad area of the stem. Whereas that of stiff material, 100 GPa, manifested higher stresses localized on a small area in the third middle of the lateral side.

Figure 6.23 shows the variation of axial stresses in the medial and lateral sides of the prosthesis stem, which occur at the prosthesis/cement interface, as a function of prosthesis material. Although the stresses are nearly identical for the two prosthesis materials in the proximal third and in the distal tip, there is a robust droop in the distal two-third part of the lower stiffness stem prosthesis of 30 GPa.

Figure 6.24 shows the amounts of stresses transferred to the prosthesis stem. It revealed that the polymeric prosthesis experienced low stresses distributed over a relatively large amount of elements compared to the Titanium prosthesis.

(B) Neck Prosthesis Stresses

There was not a noticeable change in the axial stresses in the prosthesis neck of 30 GPa stiffness compared to that of Titanium alloy, Figures 6.25, 6.26, and 6.27.

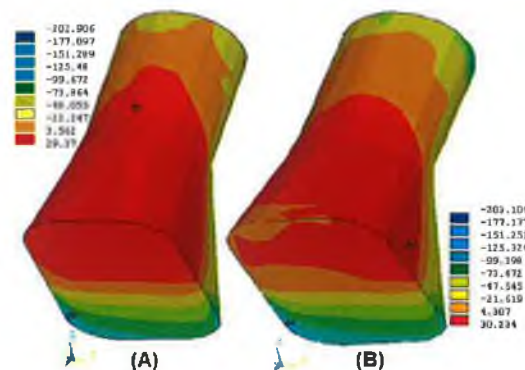


Figure 6.25: A contour plot of the axial z-stress (MPa) on the neck prosthesis of (A) $E = 100$ GPa, and (B) $E = 30$ GPa.

(C) Cement Mantle Stresses

Figure 6.26 shows the effect of prosthesis material on the cement stress pattern. Generally, decreasing prosthesis Young's modulus creates a higher stress in the cement mantle. This because prostheses of low stiffness, such as polymer composite, undergo high bending displacements, thereby transfer high stress to the cement mantle. The tensile stress in the lateral side worked out at about 2.1 MPa for the polymeric prosthesis, which is 3 times that of Titanium alloy. While the plot of cement volume at a given stress, Figure 6.27, reveals that polymeric prosthesis could raise the cement mantle stresses to more than 5.8 MPa (it was 7.4 MPa).

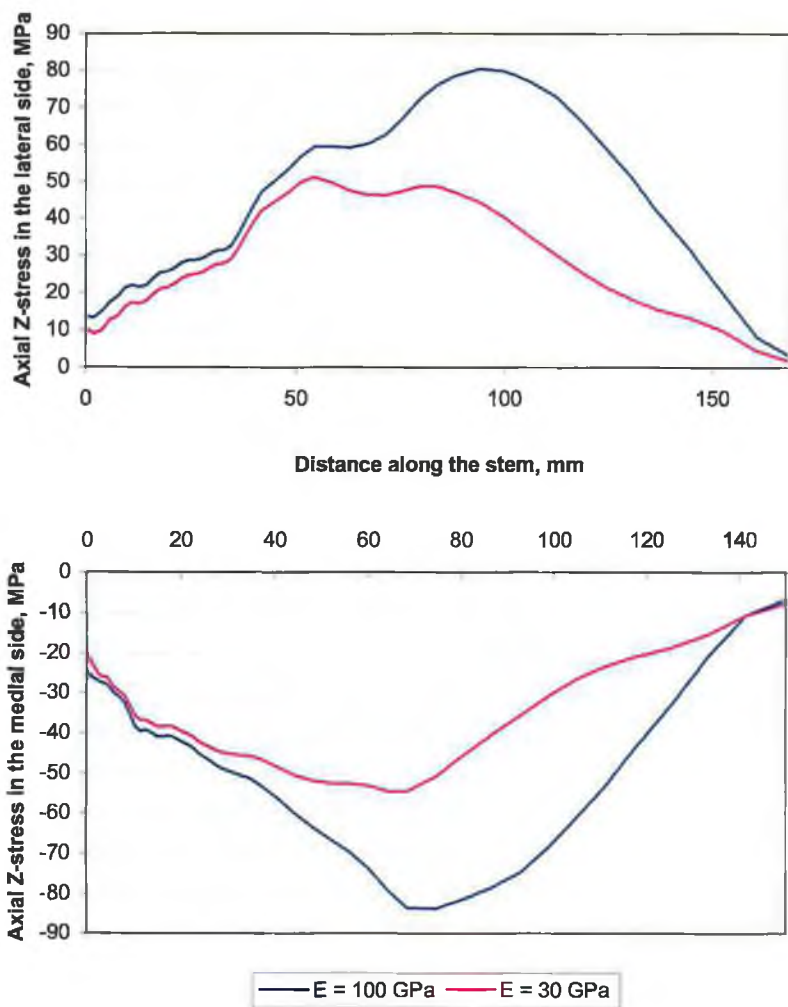


Figure 6.23: Minimum and maximum axial z-stress distributions, in MPa, in the lateral and medial sides of the stem as a function of prosthesis Young's modulus. The prostheses are damperless and cement Young's modulus is 2.64 GPa.

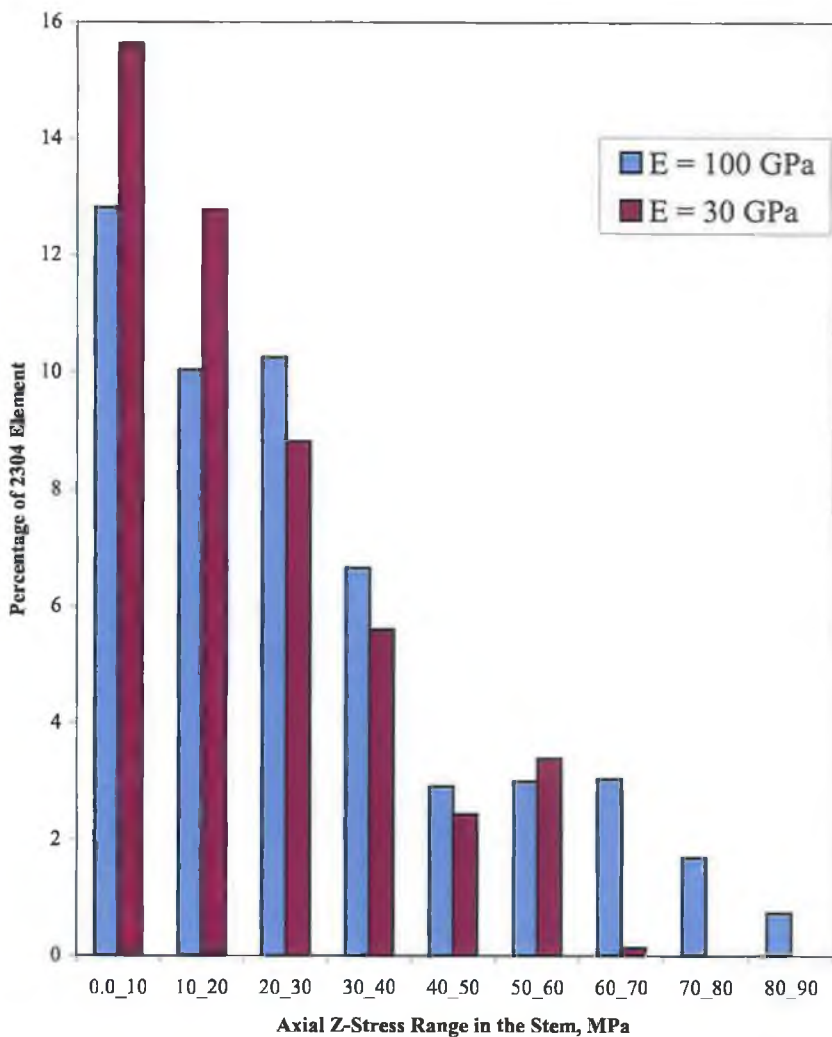


Figure 6.24: Distribution of 2304 element of the prosthesis stem over a stress range of 0-90 MPa as a function of prosthesis Young's modulus. The prostheses are damperless and cement Young's modulus is 2.64 GPa.

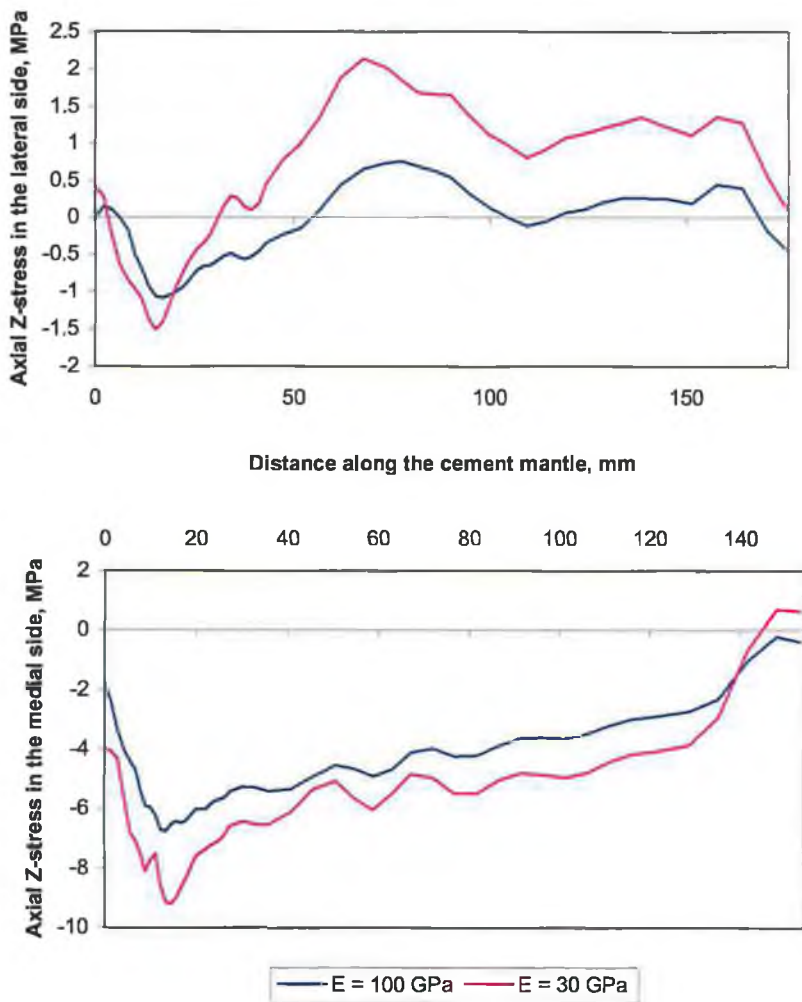


Figure 6.26: Minimum and maximum axial stress distributions, in MPa, in the lateral and medial sides of the cement mantle as a function of prosthesis Young's modulus. The prostheses are damperless and cement Young's modulus is 2.64 GPa.

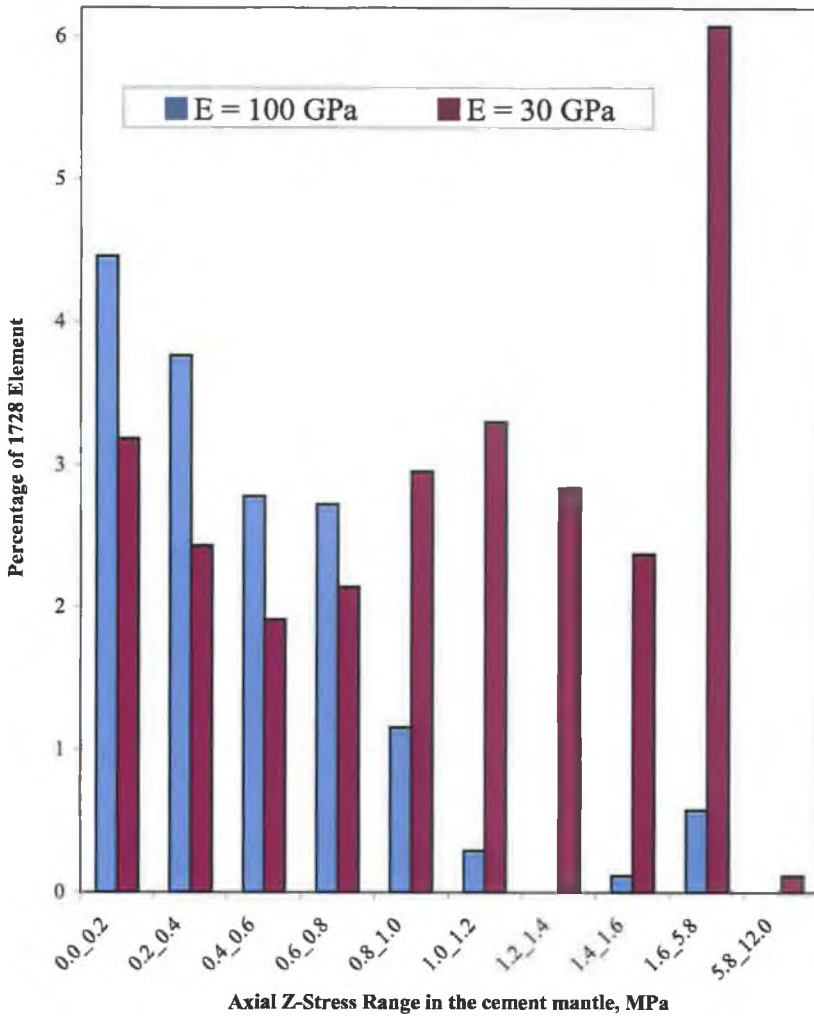


Figure 6.27: Distribution of 1728 element of the cement mantle over a stress range of 0-12 MPa as a function of prosthesis Young's modulus. The prostheses are damperless and cement Young's modulus is 2.64 GPa.

Figure 6.28 shows the effect of the cement mantle by the prosthesis material in form of contour stresses. And it clear that the lateral side of that used for interlocking the polymeric prosthesis is dominated with highest tensile stresses compared to that of titanium alloy, 100 GPa.

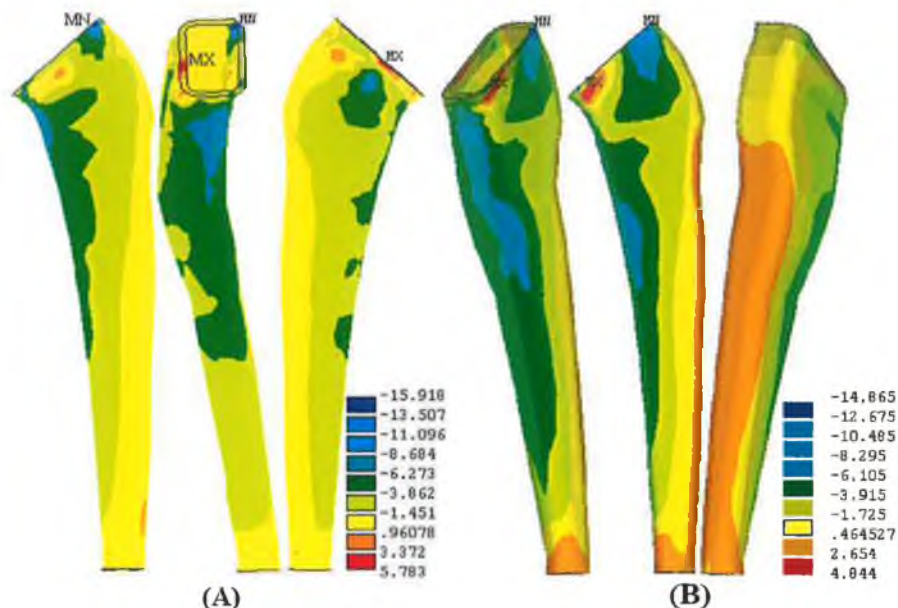


Figure 6.28: A contour plot of the axial z-stress (MPa) on the cement mantle of (A) $E = 100$ GPa, and (B) $E = 30$ GPa

(D) Bone Cortex Stresses

It was found that the stresses in the bone cortex are very sensitive to the prosthesis material and thus they increase with decreasing Young's modulus, except in the greater trochanter and the distal third, Figure 6.29. It can be noted that the compressive stresses are greatly increased with decreasing prosthesis stiffness untill they become close to the physiological stresses for the intact femur. The restored stresses in the medial calcar and diaphysis reached to about 86% as a result of using polymeric prosthesis whereas it was about 53% as a maximum restoration just in the calcar region when the Titanium prosthesis is utilized.

Figure 6.30 shows the contour stress in the bone cortex as a function of the prosthesis material, and it can be seen that the prosthesis of low stiffness capable of transferring more loads to the bone.

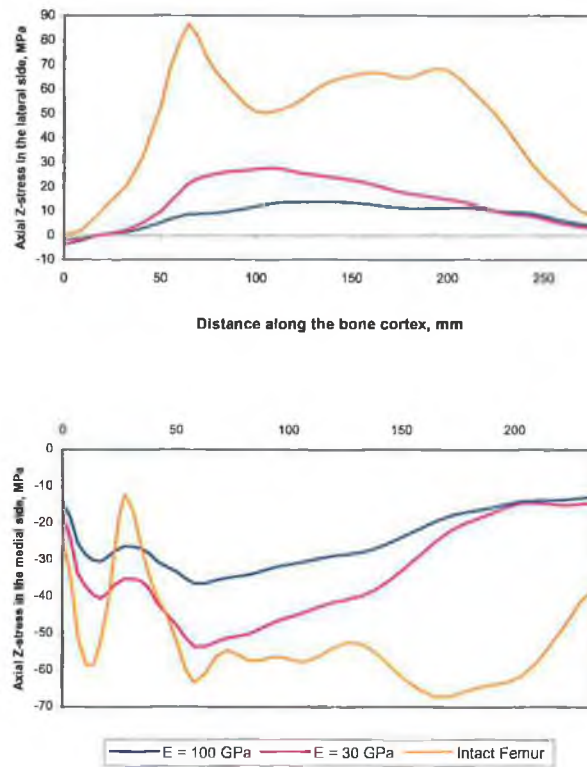


Figure 6.29: Minimum and maximum axial stress distributions, in MPa, in the lateral and medial sides of 1) treated femurs, as a function of prosthesis Young's modulus, and 2) an intact femur. The prostheses are damperless and cement Young's modulus is 2.64 GPa.

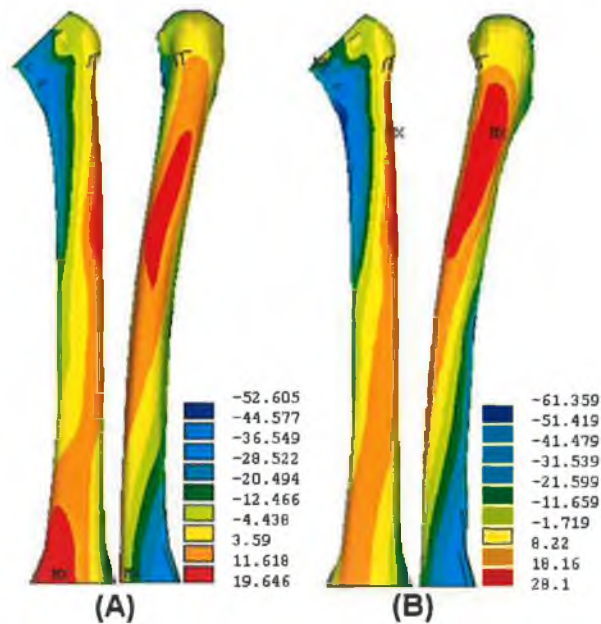


Figure 6.30: A contour plot of the axial z-stress (MPa) on the bone cortex of the femur as a function of using (A) $E = 100$ GPa, and (B) $E = 30$ GPa prosthesis.

6.6.3 Would proximal bound fixation alleviate stress shielding in the bone?

So far, the skirt-collared prosthesis revealed promising initial results in terms load transfer to the proximal femur bone in compression with the other two prosthesis types, figure 6.2. Therefore, was important to investigate further whether it is possible to improve its efficiency in terms of decreasing the stress shielding which occurred in the bone cortex. M. G. Joshi [165] demonstrated in his work that the relative motion across the interface might result in aseptic loosening as a result of stress shielding. Consequently, as revealed in the previous section that the current design still experiences of relative micromotions because it was not bound proximally to the bone. Thereby, in the current section the skirt-collared prosthesis will be bound proximally to the bone just from the inner surface of the skirt to investigate how far the stress shielding in the bone could be decreased. Two skirt-collared prostheses using proximal fixation of different material, 30 GPa and 100 GPa, were compared in one of 100 GPa hand with one normally fitted to the bone without binding, and in another hand they compared with each other numerically.

6.6.3.1. Stress Analysis

(A) Neck and stem prosthesis stresses

Figures 6.31 and 6.32 show a slight reduction in the axial stresses occurred in the medial and lateral sides of the bound prosthesis of 30 GPa compared to the others.

Whereas, the tensile axial stresses of the proximal bound prosthesis stems were lower than that of normal fixation, Figures 6.33 and 6.34, and it was noticeable that the tensile stress of the bound prosthesis of 30 GPa is reduced to the half of the other two.

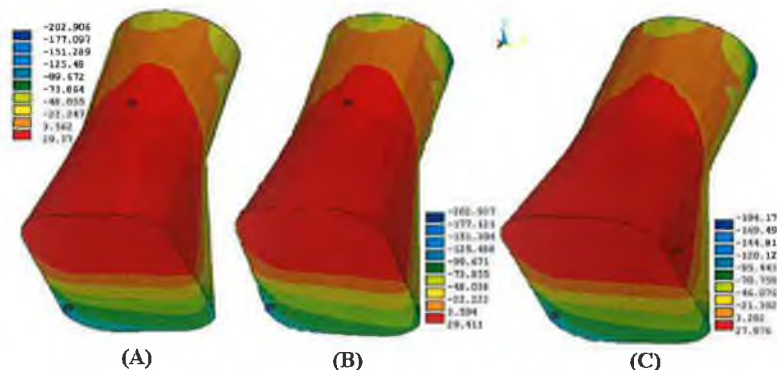


Figure 6.31: A contour plot of the axial z-stress (MPa) on the prosthesis neck for three different skirt-collared prostheses: (A) 100 GPa, normal fixation, (B) 100 GPa, bound proximal fixation, and (C) 30 GPa, bound proximal fixation.

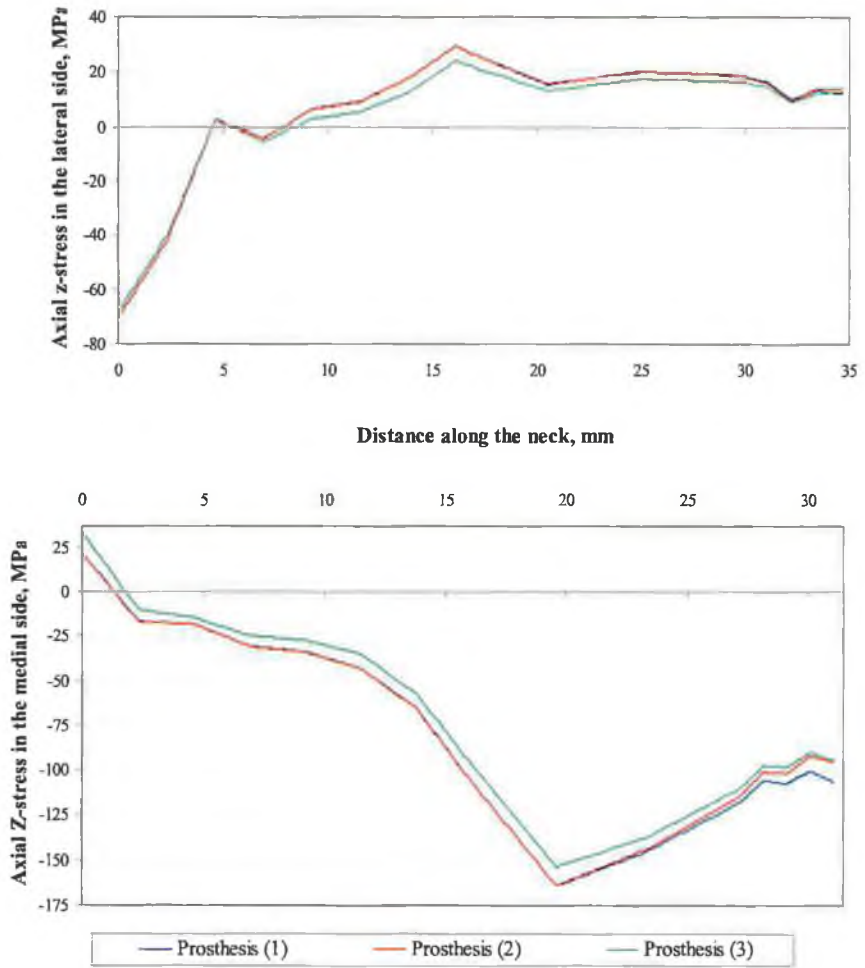


Figure 6.32: Minimum and maximum axial stress curves, in MPa, in the lateral and medial sides of the prosthesis neck for three different skirt-collared prostheses:

Prosthesis (1): 100 GPa, loose proximal fixation.

Prosthesis (2): 100 GPa, tight proximal fixation.

Prosthesis (3): 30 GPa, tight proximal fixation.

Cement Young's module is 2.64 GPa.

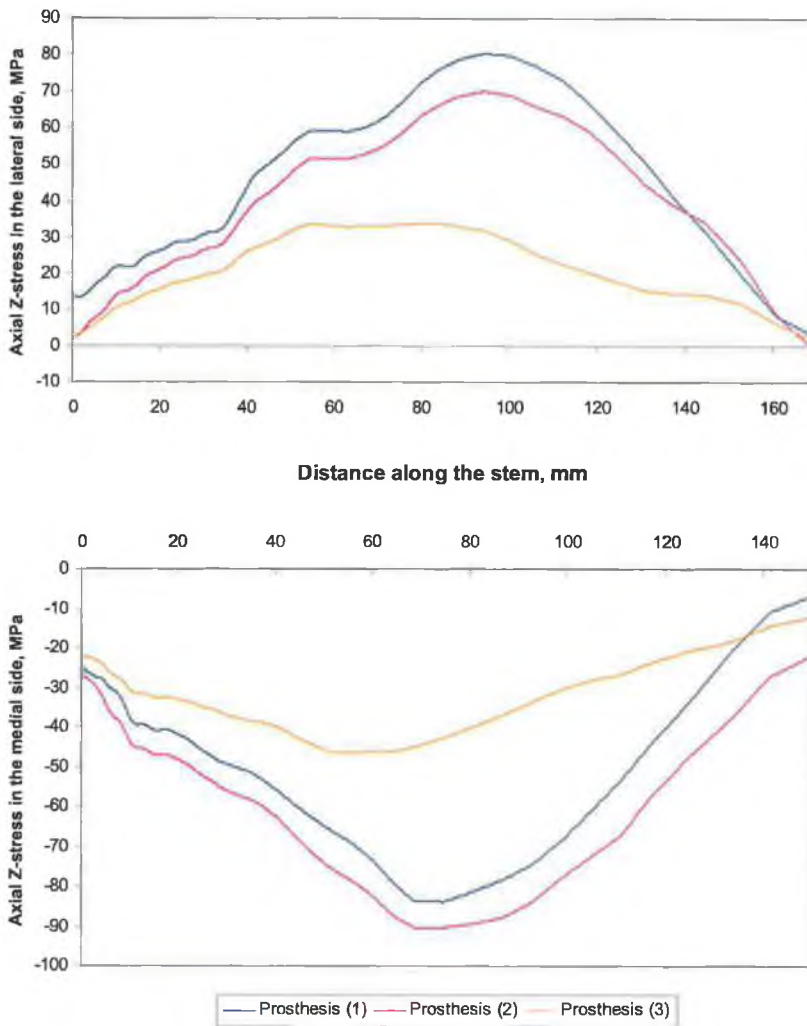


Figure 6.33: Minimum and maximum axial stress curves, in MPa, in the lateral and medial sides of the stem for three different skirt-collared prostheses:
 Prosthesis (1): 100 GPa, loose proximal fixation.
 Prosthesis (2): 100 GPa, tight proximal fixation.
 Prosthesis (3): 30 GPa, tight proximal fixation.
 Cement Young's module is 2.64 GPa.

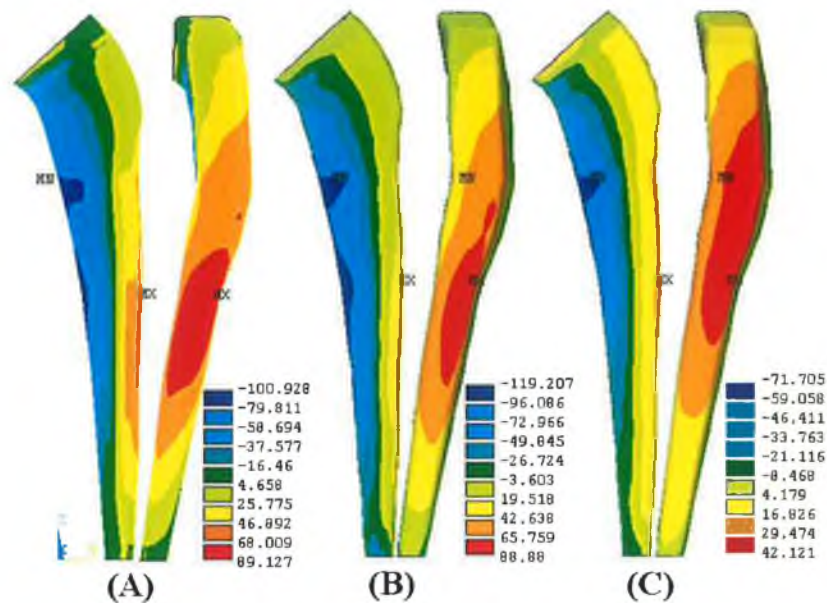


Figure 6.34: A contour plot of the axial z-stress (MPa) on the prosthesis stem for three different skirt-collared prostheses: (A) 100 GPa, normal proximal fixation, (B) 100 GPa, bound proximal fixation, and (C) 30 GPa, bound proximal fixation.

Also, by comparing the bound skirt-collared prosthesis of 30 GPa to that of normal fit of the same material, Figures 6.22 and 6.34, one can notice that the proximal bound of the prosthesis may act in a manner to reduce the tensile stresses located in the lateral side of the stem of soft material.

(B) Cement Mantle Axial Stress

The use of the proximal bound fixation technique, as revealed in Figures 6.35 and 6.37, could cause a dramatic rise in the tensile stresses located in the lateral side of the cement mantle specially for those used to interlock those stems of soft materials, 30 GPa. The stress could rise more than 6 times in the lateral side of the cement mantle due to the bound proximal fixation of the prosthesis which in turn forces it to bend extensively in the medial side without any possibility for slip.

In other hand, Figure 6.38 showed that the amounts of cement mantle elements that experience a certain value of stress, i.e. 1 to 5.8 MPa, are higher when prosthesis of 30 GPa is used for bound proximal fixation technique. This could increase the fragmentation risk and then fracture probability.

The element stress plot, Figures 6.36, revealed that both prostheses of bound proximal fixation exposed to the same value of maximum tensile stresses though they are not located in the same position in each cement mantle, i.e. for prosthesis 100 GPa maximum tensile stress located in the distal tip of the cement mantle while

for that of 30 GPa is located in the proximal third of lateral side. This result is hard to discover from the stress curves, Figure 6.37.

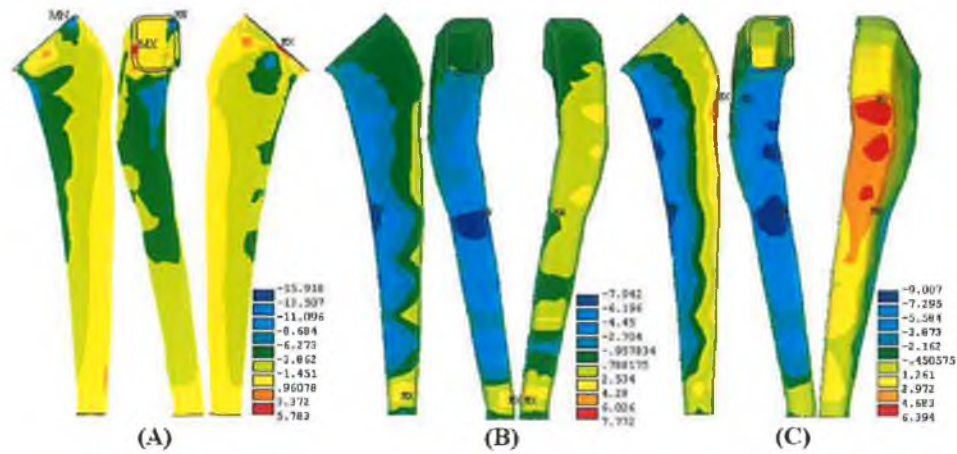


Figure 6.35: A contour plot of the axial z-stress (MPa) on the cement mantle as a consequence of using three different skirt-collared prostheses: (A) 100 GPa, normal proximal fixation, (B) 100 GPa, bound proximal fixation, and (C) 30 GPa, bound proximal fixation.

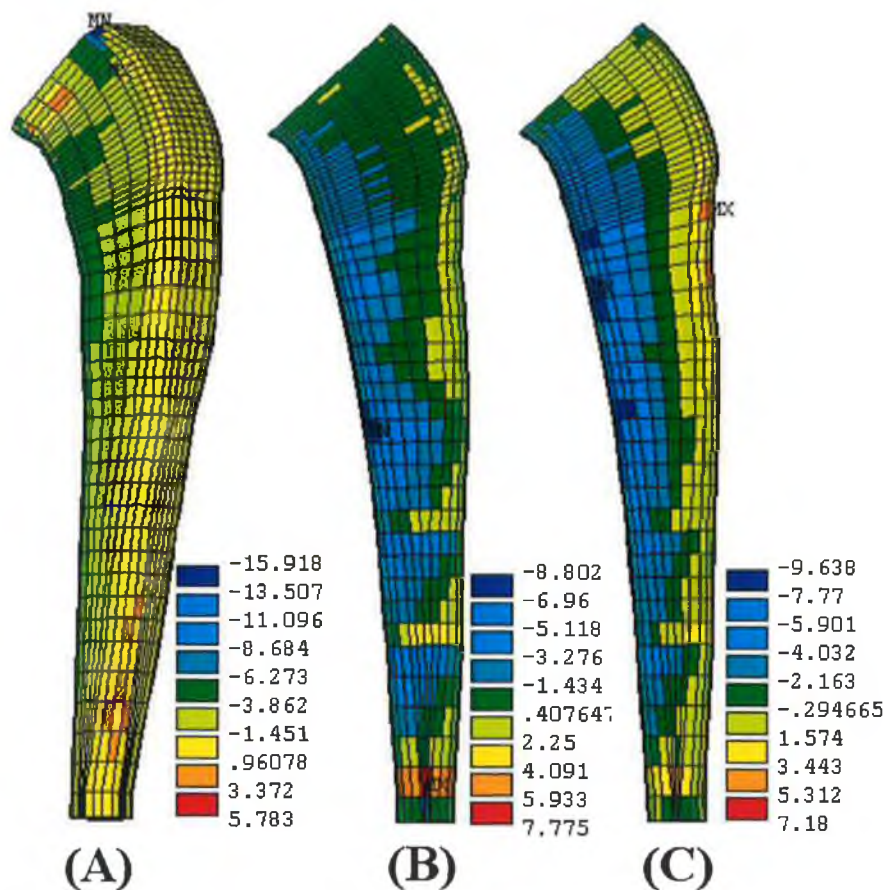


Figure 6.36: An element stress plot of the axial z-stress (MPa), based on element stress solution, on the cement mantle as a consequence of using three different skirt-collared prostheses: (A) 100 GPa, normal proximal fixation, (B) 100 GPa, bound proximal fixation, and (C) 30 GPa, bound proximal fixation.

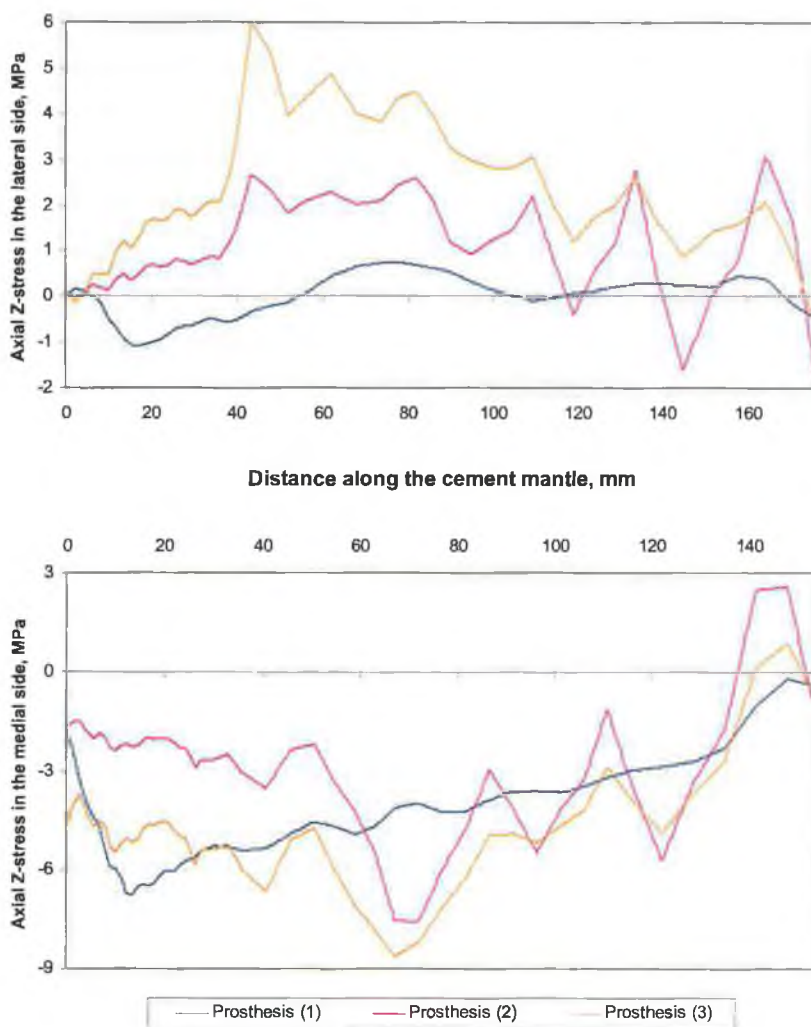


Figure 6.37: Minimum and maximum axial stress curves, in MPa, in the lateral and medial sides of the cement mantle used to interlock three different skirt-collared prostheses:

Prosthesis (1): 100 GPa, loose proximal fixation.

Prosthesis (2): 100 GPa, tight proximal fixation.

Prosthesis (3): 30 GPa, tight proximal fixation.

Cement Young's module is 2.64 GPa.

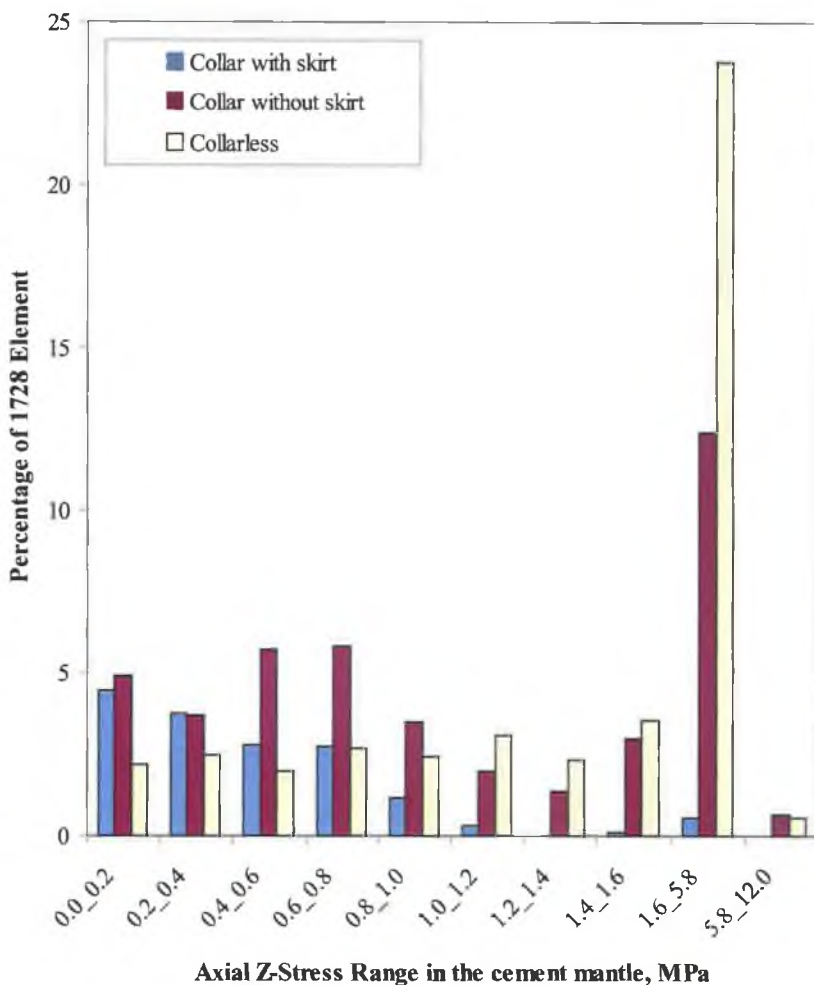


Figure 6.38: Distribution of 1728 element of the cement mantle over a stress range of 0-12 MPa. The cement mantle in these simulations was used for interlocking three different skirt-collared prostheses:

Prosthesis (1): 100 GPa, loose proximal fixation.

Prosthesis (2): 100 GPa, tight proximal fixation.

Prosthesis (3): 30 GPa, tight proximal fixation.

Cement Young's module is 2.64 GPa.

(C) Bone Cortex Axial Stress

In the present numerical studies, the use of the bound fixation technique of the skirt-collared prosthesis produced less stress shielding than the others which use ordinary proximal fixation, Figures 6.39 and 9.44. Also, using soft material prosthesis in this technique of fixation provides higher load transfer than the other as shown in the two figures.

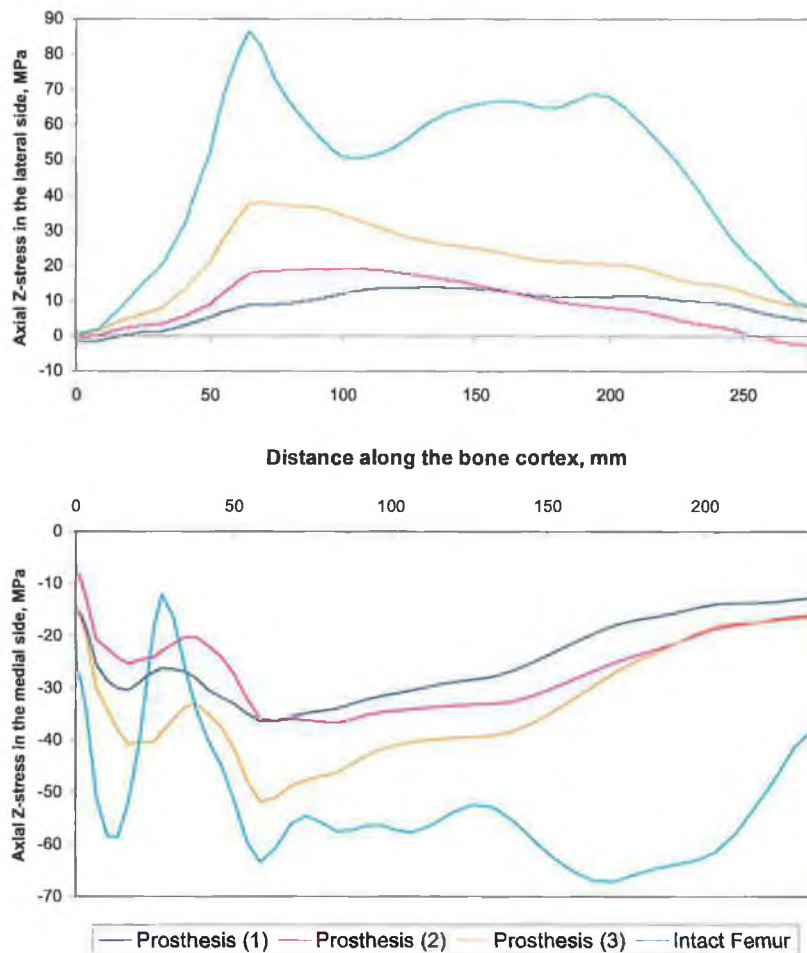


Figure 6.39: Minimum and maximum axial stress curves, in MPa, in the lateral and medial sides of the bone cortex as a function of using three different skirt-collared prostheses:

Prosthesis (1): 100 GPa, normal proximal fixation.

Prosthesis (2): 100 GPa, bound proximal fixation.

Prosthesis (3): 30 GPa, bound proximal fixation.

Cement Young's module is 2.64 GPa.

Figure 6.40 shows that as a consequence of using bound proximal fixation the femur exposed to high bending deformation, and the compression stresses are distributed broadly in the medial side.

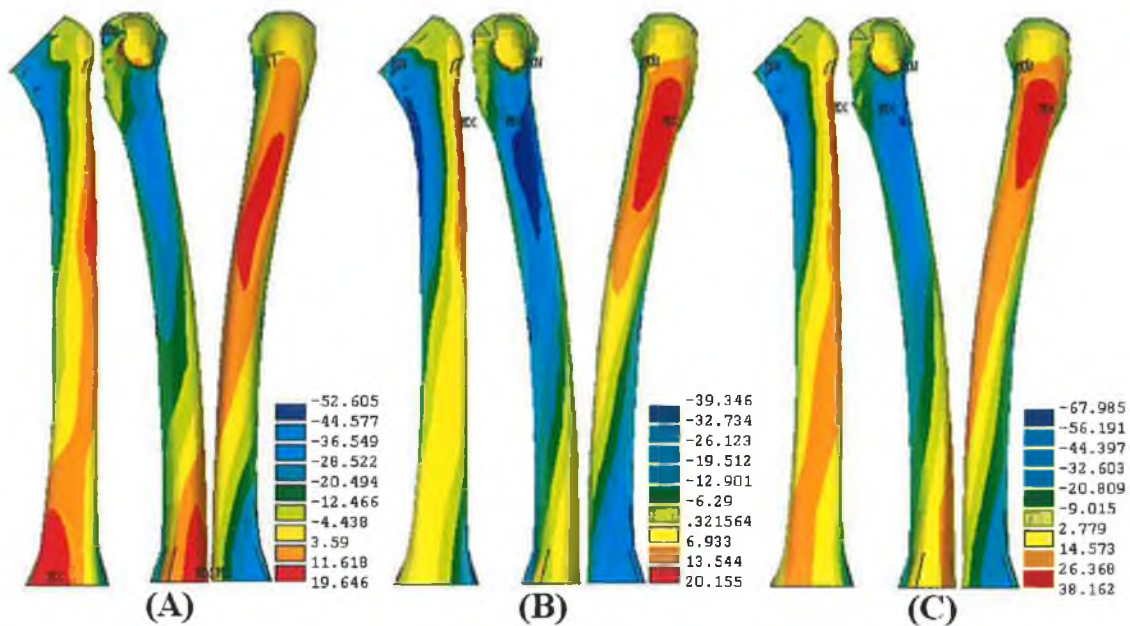


Figure 6.40: A contour plot of the axial z-stress, in MPa, for the bone cortex of the femur as a consequence of using three different skirt-collared prostheses: (A) 100 GPa, normal proximal fixation, (B) 100 GPa, bound proximal fixation, and (C) 30 GPa, bound proximal fixation.

6.6.4 Can a damper be used to alleviate impulse loads?

As was mentioned earlier this section will investigate whether it is possible to reduce the impulse loads, which arise from the patient activity and in turn may cause the artificial hip to fail as a result of the fatigue, by using the idea of damper. Therefore, this simulation inserted four layers of elements between the resected section of the femur and the collar of the prosthesis, Figure 6.5. These layers represented a damper of 4 mm thickness. To study the effectiveness of this configuration four different materials were investigated for the damper (Table 6.2).

6.6.4.1. Stress Analysis

(A) Neck and stem prosthesis stresses

Figures 6.41 and 6.42 show that there was not any effect on the neck in terms of tensile stress reduction at all by using different damper materials. While, as was expected, the tensile and compression axial stresses of the prosthesis stem are decreased by decreasing the damper material, Figure 6.43. Also, one can see from Figure 6.44 that although the tensile stress is decreased by decreasing the damper material stiffness, the area of the maximum tensile stress in the lateral side increases by decreasing the damper stiffness.

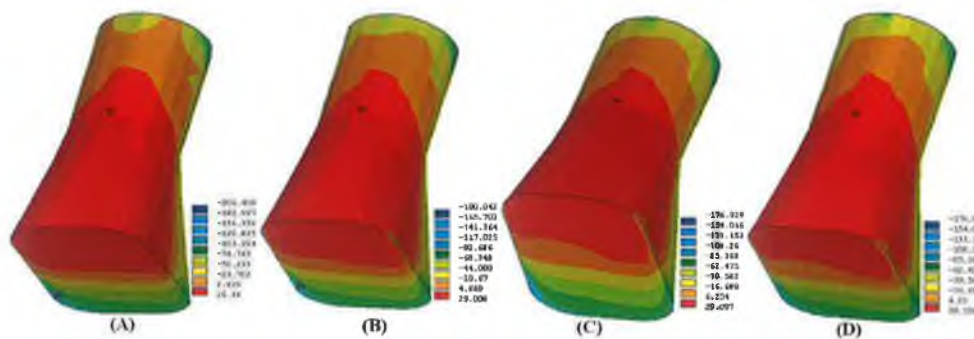


Figure 6.41: A contour plot of the axial z-stress (MPa) on the prosthesis neck as a function of damper material of (A) 50 GPa, (B) 1 GPa, (C) 1 MPa, and (D) 0.001 MPa.

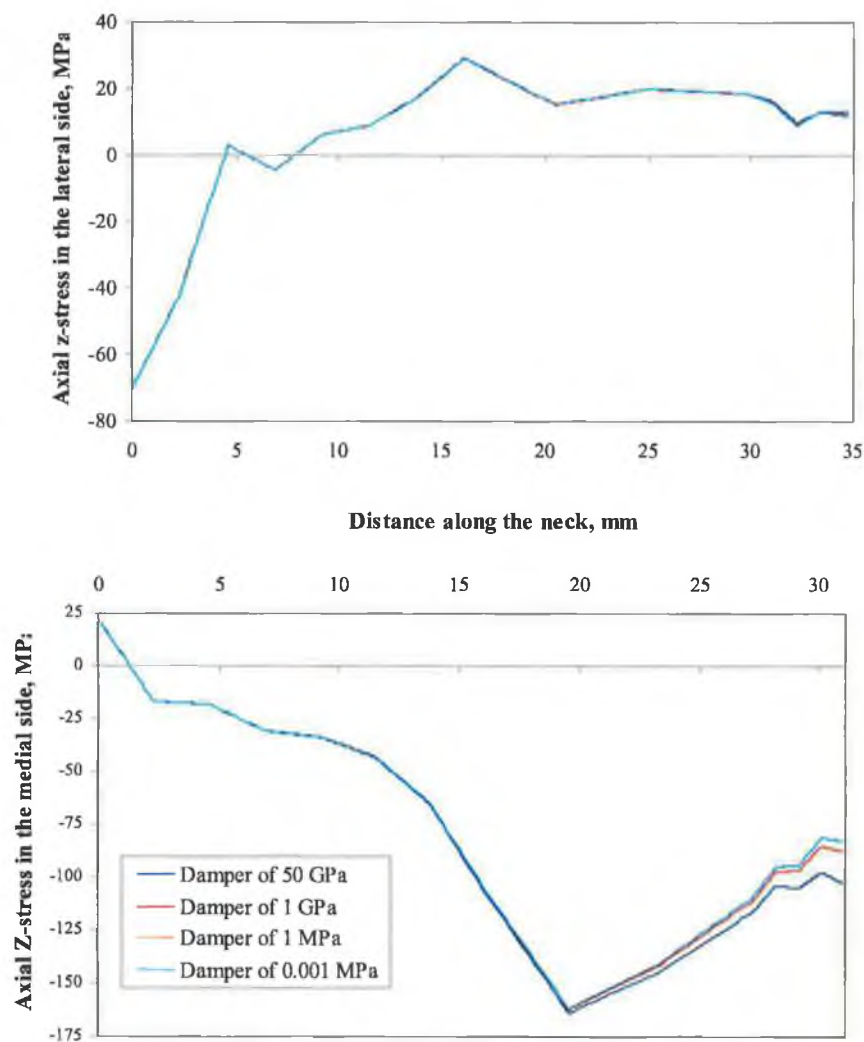


Figure 6.42: Minimum and maximum axial stress distributions, in MPa, in the lateral and medial sides of the prosthesis neck as a function of damper material. Stem and cement Young's moduli are 100 GPa and 2.64 GPa respectively.

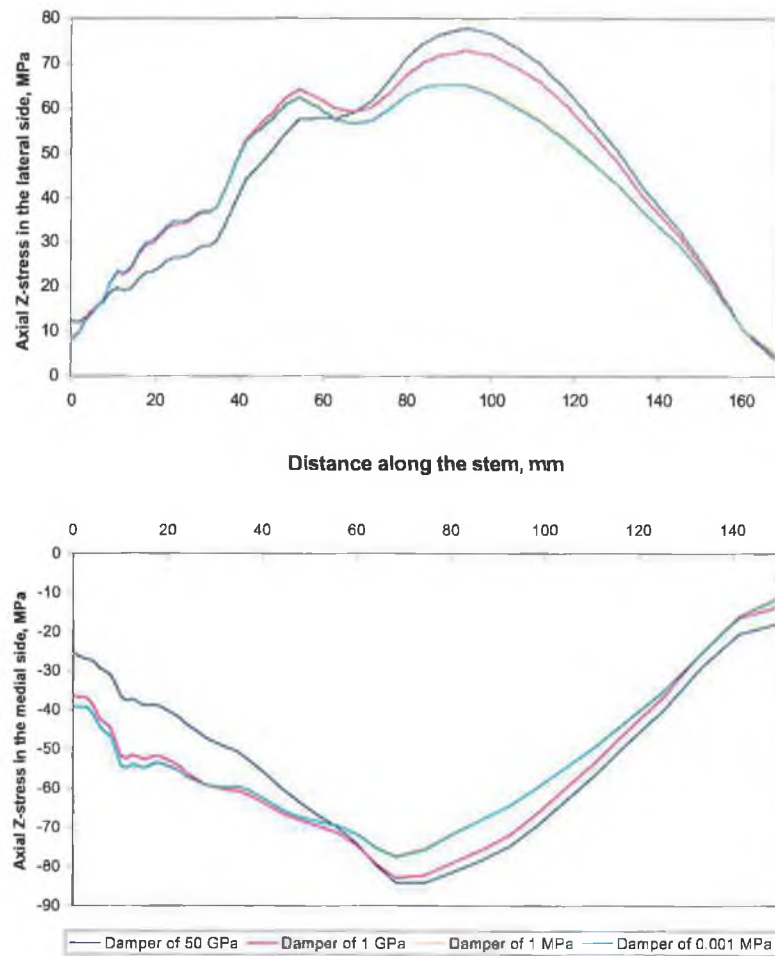


Figure 6.43: Minimum and maximum axial stress distributions, in MPa, in the lateral and medial sides of the stem as a function of damper material. The stem and cement Young's moduli are 100 GPa and 2.64 GPa respectively.

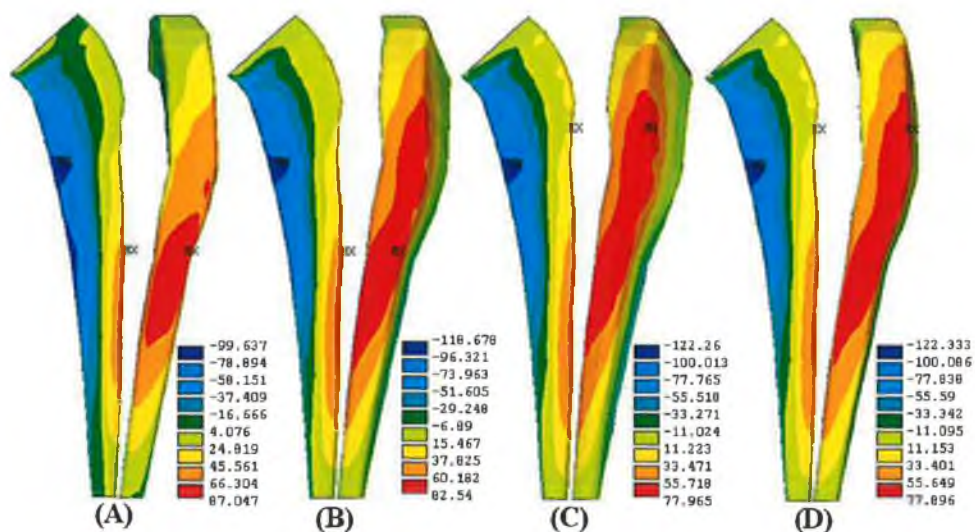


Figure 6.44: A contour plot of the axial z-stress (MPa) on the prosthesis neck as a function of damper material of (A) 50 GPa, (B) 1 GPa, (C) 1 MPa, and (D) 0.001 MPa.

(B) Cement Mantle Axial Stress

Figure 6.45 and 6.46 indicate that although by decreasing the damper's Young's modulus the compression stresses decrease, the tensile stresses increase. Also, Figure 6.45 made a comparison between a damperless and damperd prostheses, and it revealed that even a damper of relatively high material stiffness (50 GPa) could cause the cement mantle tensile stresses to increase.

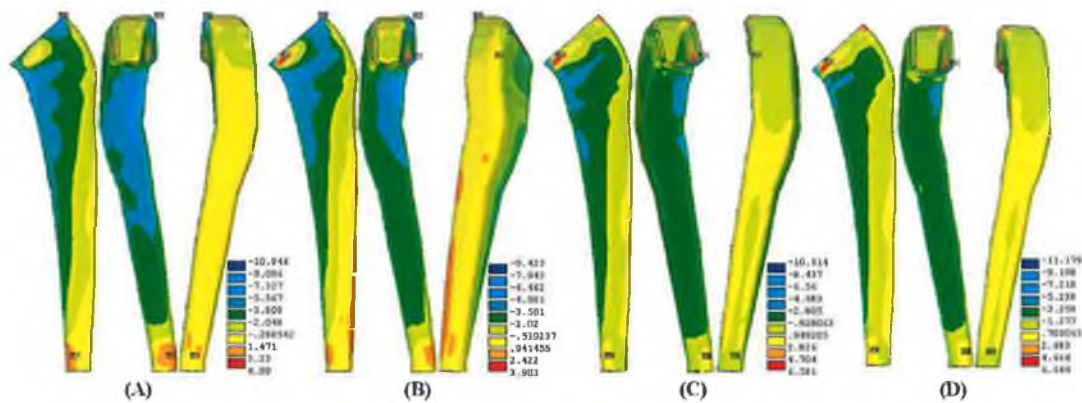


Figure 6.45: A contour plot of the axial z-stress (MPa) on the cement mantle as a function of damper material of (A) 50 GPa, (B) 1 GPa, (C) 1 MPa, and (D) 0.001 MPa.

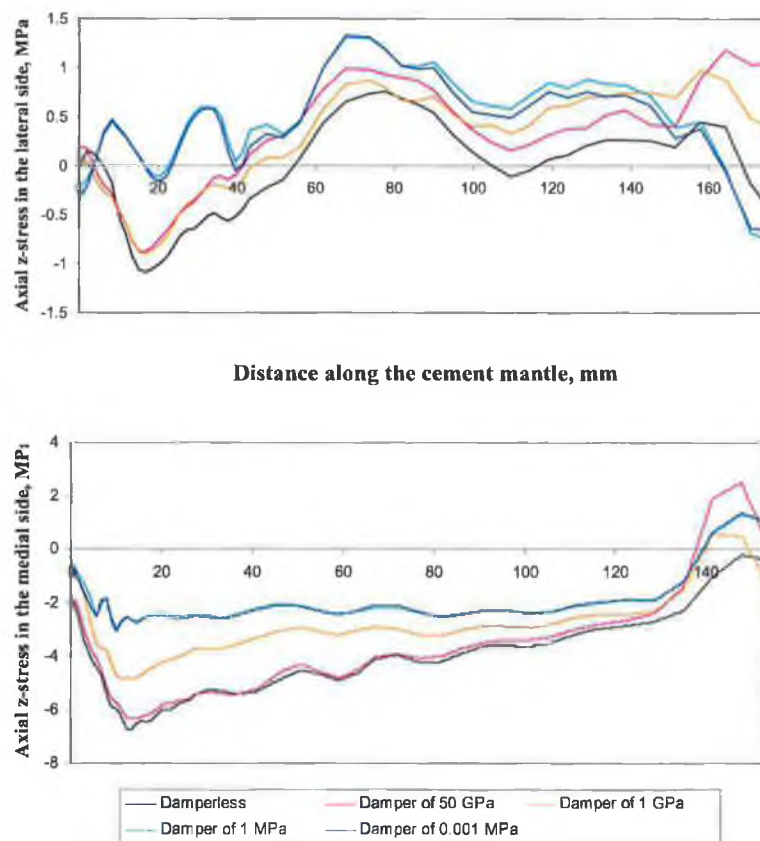


Figure 6.46: Minimum and maximum axial stress distributions, in MPa, in the lateral and medial sides of the cement mantle as a function damper material. The prosthesis and cement Young's modulus are 100 GPa and 2.64 GPa respectively.

It was found, also, that the amount of cement mantle elements that experienced a certain value of stress are higher in case of using dampers of soft material, Figure 6.47. And this could increase the risk of fragmentation and fracture likelihood when dampers of especially soft material are used.

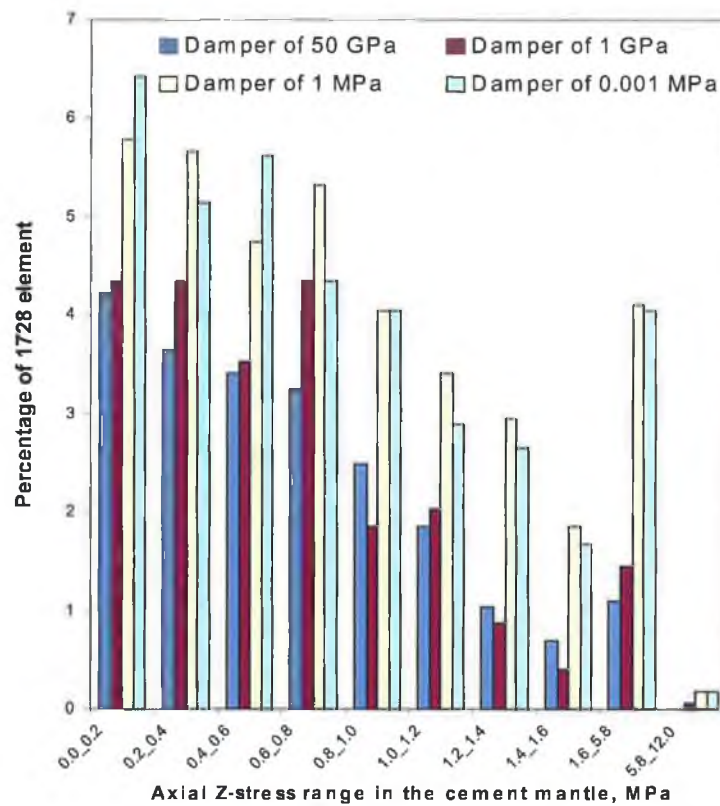


Figure 6.47: Distribution of 1728 element of the cement mantle over a stress range of 0-12 MPa as a function of damper's material. The prosthesis and cement Young's modulus are 100 GPa and 2.64 GPa, respectively.

(C) Bone Cortex Axial Stress

It was deduced that the presence of a damper between the collar and the resected cross section of the proximal part of the femur may lead to a decrease in the load transfer to the bone and hence could increase the bone stress shielding, Figure 6.48 and 6.49. In spite of the fact that a damper of 50 GPa has not any noticeable effect in terms of stress shielding in the bone, it has another side effect in the cement tensile stresses, Figure 6.46. Figure 6.49 shows that dampers made of soft material could increase the area of tensile stresses in the lateral side of the femur.

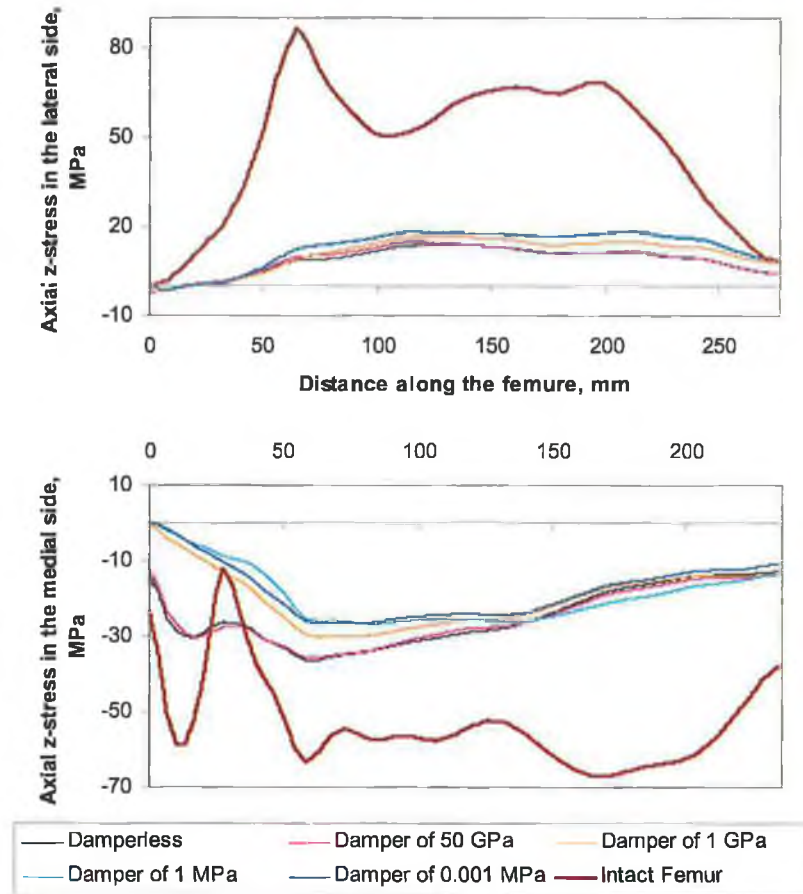


Figure 6.48: Minimum and maximum axial stress distributions, in MPa, in the lateral and medial sides of the bone cortex as a function damper material. The prosthesis and cement Young's modulus are 100 GPa and 2.64 GPa respectively.

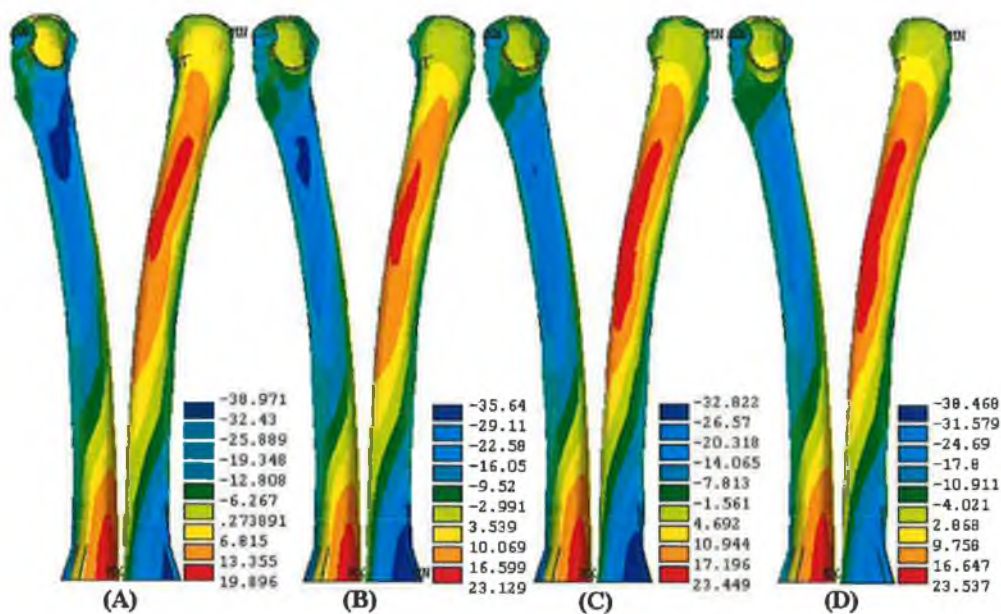


Figure 6.49: A contour plot of the axial z-stress (MPa) on the bone cortex as a function of damper material of (A) 50 GPa, (B) 1 GPa, (C) 1 MPa, and (D) 0.001 MPa.

6.6.3 Would proximal bound fixation alleviate stress shielding in the bone?

So far, the skirt-collared prosthesis revealed promising initial results in terms load transfer to the proximal femur bone in compression with the other two prosthesis types, figure 6.2. Therefore, was important to investigate further whether it is possible to improve its efficiency in terms of decreasing the stress shielding which occurred in the bone cortex. M. G. Joshi [165] demonstrated in his work that the relative motion across the interface might result in aseptic loosening as a result of stress shielding. Consequently, as revealed in the previous section that the current design still experiences of relative micromotions because it was not bound proximally to the bone. Thereby, in the current section the skirt-collared prosthesis will be bound proximally to the bone just from the inner surface of the skirt to investigate how far the stress shielding in the bone could be decreased. Two skirt-collared prostheses using proximal fixation of different material, 30 GPa and 100 GPa, were compared in one of 100 GPa hand with one normally fitted to the bone without binding, and in another hand they compared with each other numerically.

6.6.3.1. Stress Analysis

(A) Neck and stem prosthesis stresses

Figures 6.31 and 6.32 show a slight reduction in the axial stresses occurred in the medial and lateral sides of the bound prosthesis of 30 GPa compared to the others.

Whereas, the tensile axial stresses of the proximal bound prosthesis stems were lower than that of normal fixation, Figures 6.33 and 6.34, and it was noticeable that the tensile stress of the bound prosthesis of 30 GPa is reduced to the half of the other two.

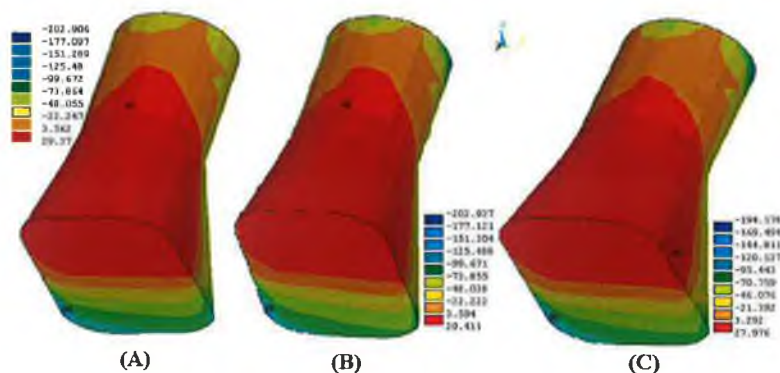


Figure 6.31: A contour plot of the axial z-stress (MPa) on the prosthesis neck for three different skirt-collared prostheses: (A) 100 GPa, normal fixation, (B) 100 GPa, bound proximal fixation, and (C) 30 GPa, bound proximal fixation.

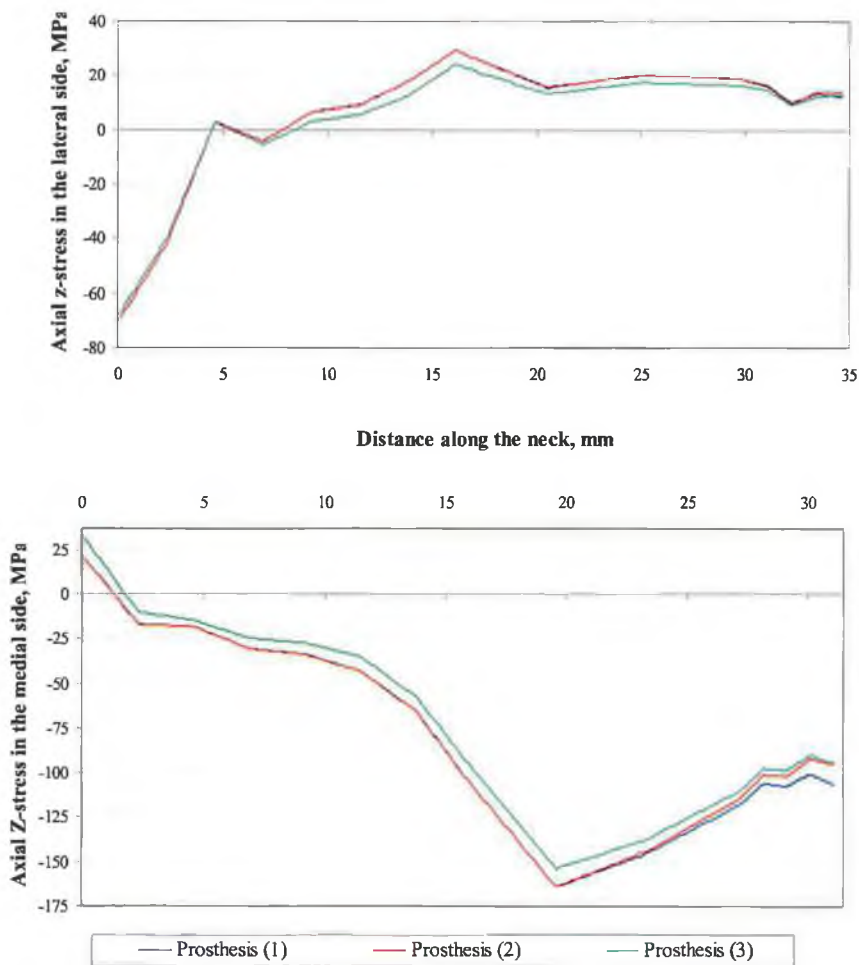


Figure 6.32: Minimum and maximum axial stress curves, in MPa, in the lateral and medial sides of the prosthesis neck for three different skirt-collared prostheses:

Prosthesis (1): 100 GPa, loose proximal fixation.

Prosthesis (2): 100 GPa, tight proximal fixation.

Prosthesis (3): 30 GPa, tight proximal fixation.

Cement Young's module is 2.64 GPa.

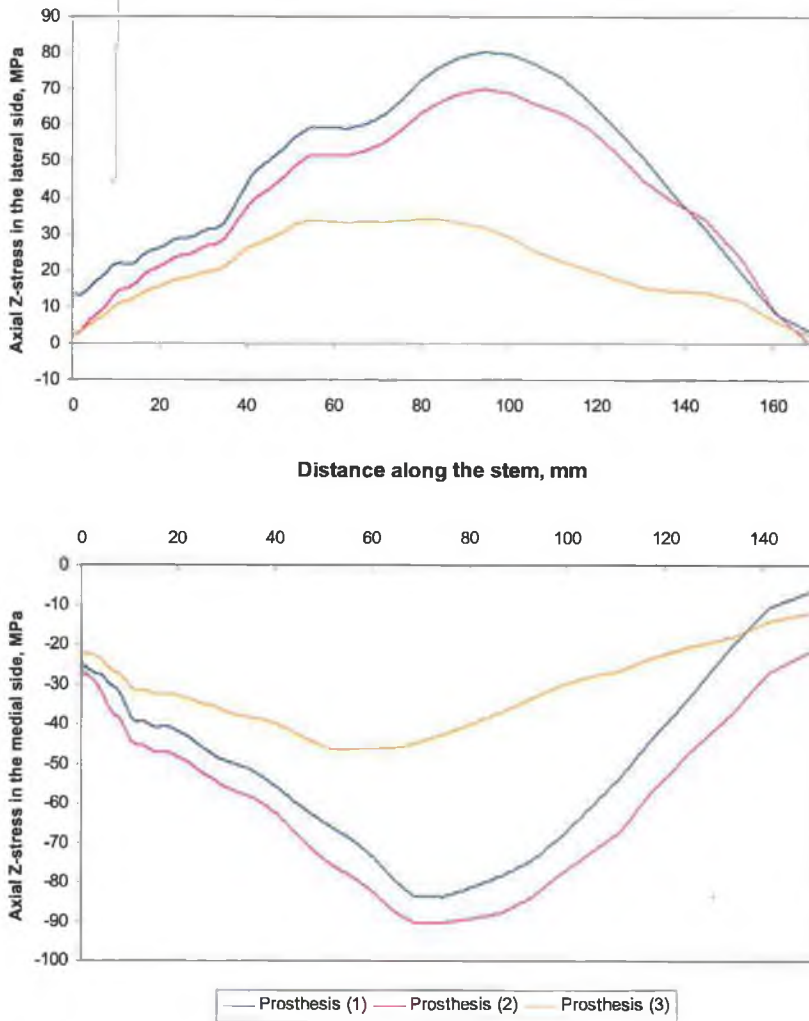


Figure 6.33: Minimum and maximum axial stress curves, in MPa, in the lateral and medial sides of the stem for three different skirt-collared prostheses:
 Prosthesis (1): 100 GPa, loose proximal fixation.
 Prosthesis (2): 100 GPa, tight proximal fixation.
 Prosthesis (3): 30 GPa, tight proximal fixation.
 Cement Young's module is 2.64 GPa.

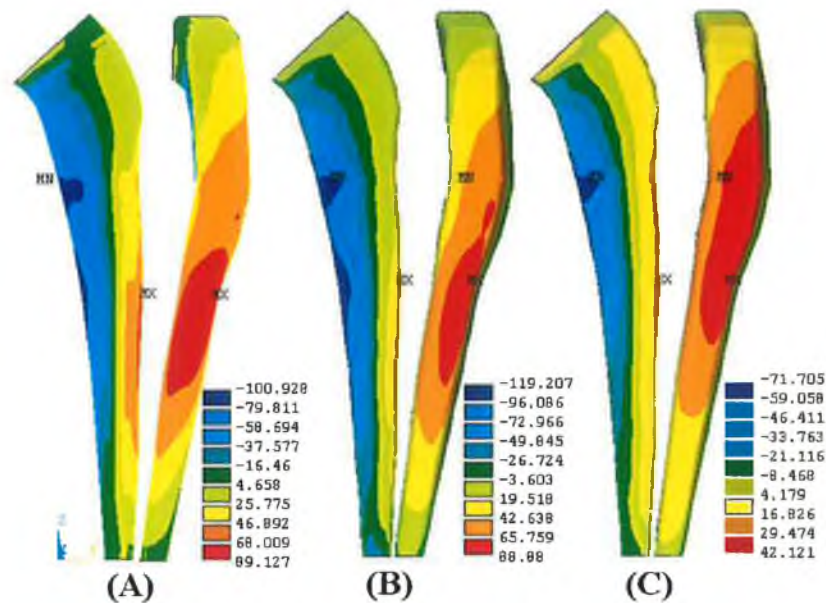


Figure 6.34: A contour plot of the axial z-stress (MPa) on the prosthesis stem for three different skirt-collared prostheses: (A) 100 GPa, normal proximal fixation, (B) 100 GPa, bound proximal fixation, and (C) 30 GPa, bound proximal fixation.

Also, by comparing the bound skirt-collared prosthesis of 30 GPa to that of normal fit of the same material, Figures 6.22 and 6.34, one can notice that the proximal bound of the prosthesis may act in a manner to reduce the tensile stresses located in the lateral side of the stem of soft material.

(B) Cement Mantle Axial Stress

The use of the proximal bound fixation technique, as revealed in Figures 6.35 and 6.37, could cause a dramatic rise in the tensile stresses located in the lateral side of the cement mantle specially for those used to interlock those stems of soft materials, 30 GPa. The stress could rise more than 6 times in the lateral side of the cement mantle due to the bound proximal fixation of the prosthesis which in turn forces it to bend extensively in the medial side without any possibility for slip.

In other hand, Figure 6.38 showed that the amounts of cement mantle elements that experience a certain value of stress, i.e. 1 to 5.8 MPa, are higher when prosthesis of 30 GPa is used for bound proximal fixation technique. This could increase the fragmentation risk and then fracture probability.

The element stress plot, Figures 6.36, revealed that both prostheses of bound proximal fixation exposed to the same value of maximum tensile stresses though they are not located in the same position in each cement mantle, i.e. for prosthesis 100 GPa maximum tensile stress located in the distal tip of the cement mantle while

for that of 30 GPa is located in the proximal third of lateral side. This result is hard to discover from the stress curves, Figure 6.37.

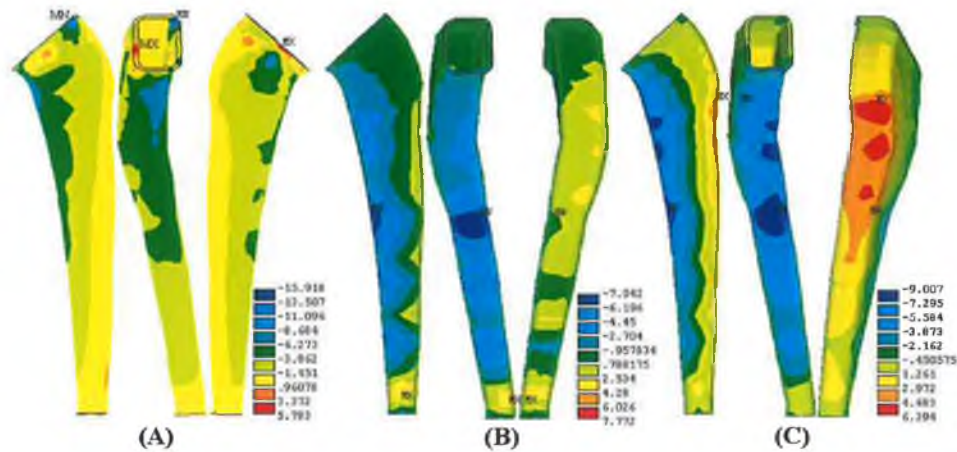


Figure 6.35: A contour plot of the axial z-stress (MPa) on the cement mantle as a consequence of using three different skirt-collared prostheses: (A) 100 GPa, normal proximal fixation, (B) 100 GPa, bound proximal fixation, and (C) 30 GPa, bound proximal fixation.

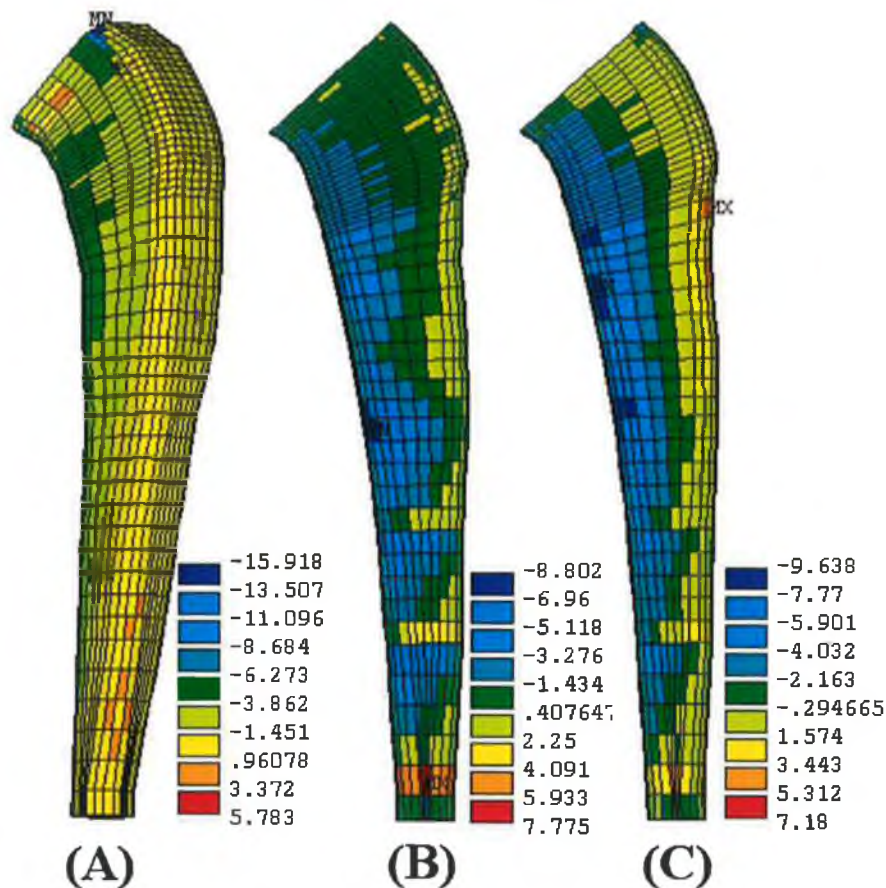


Figure 6.36: An element stress plot of the axial z-stress (MPa), based on element stress solution, on the cement mantle as a consequence of using three different skirt-collared prostheses: (A) 100 GPa, normal proximal fixation, (B) 100 GPa, bound proximal fixation, and (C) 30 GPa, bound proximal fixation.

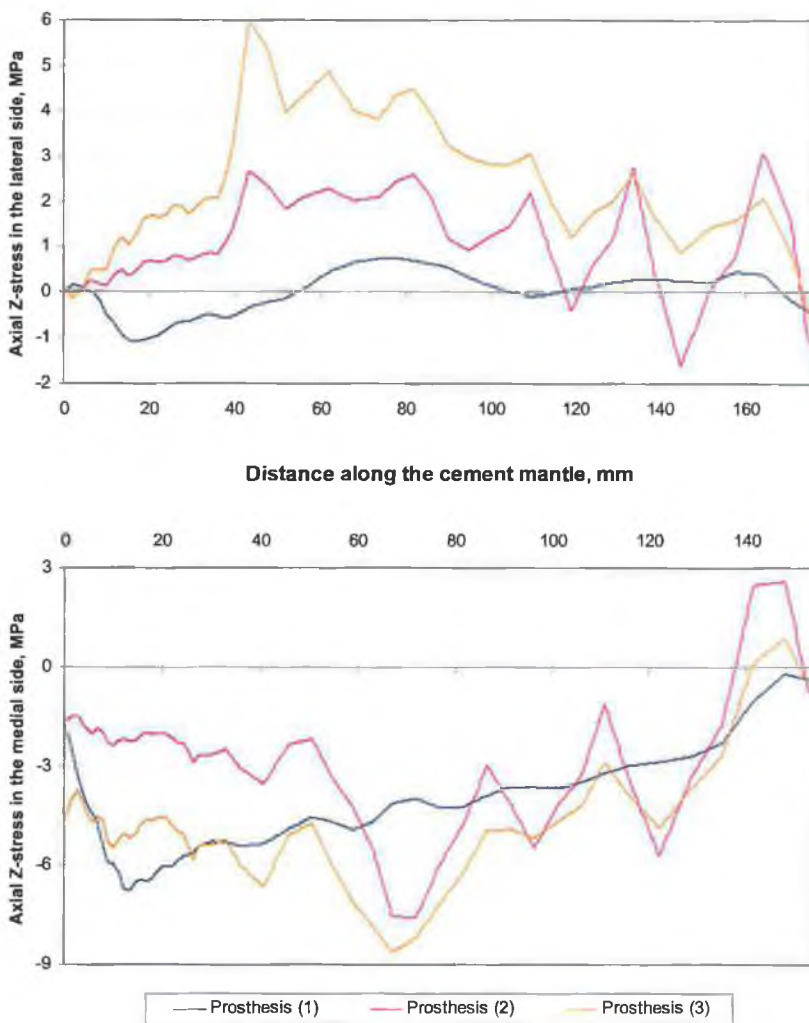


Figure 6.37: Minimum and maximum axial stress curves, in MPa, in the lateral and medial sides of the cement mantle used to interlock three different skirt-collared prostheses:

Prosthesis (1): 100 GPa, loose proximal fixation.

Prosthesis (2): 100 GPa, tight proximal fixation.

Prosthesis (3): 30 GPa, tight proximal fixation.

Cement Young's module is 2.64 GPa.

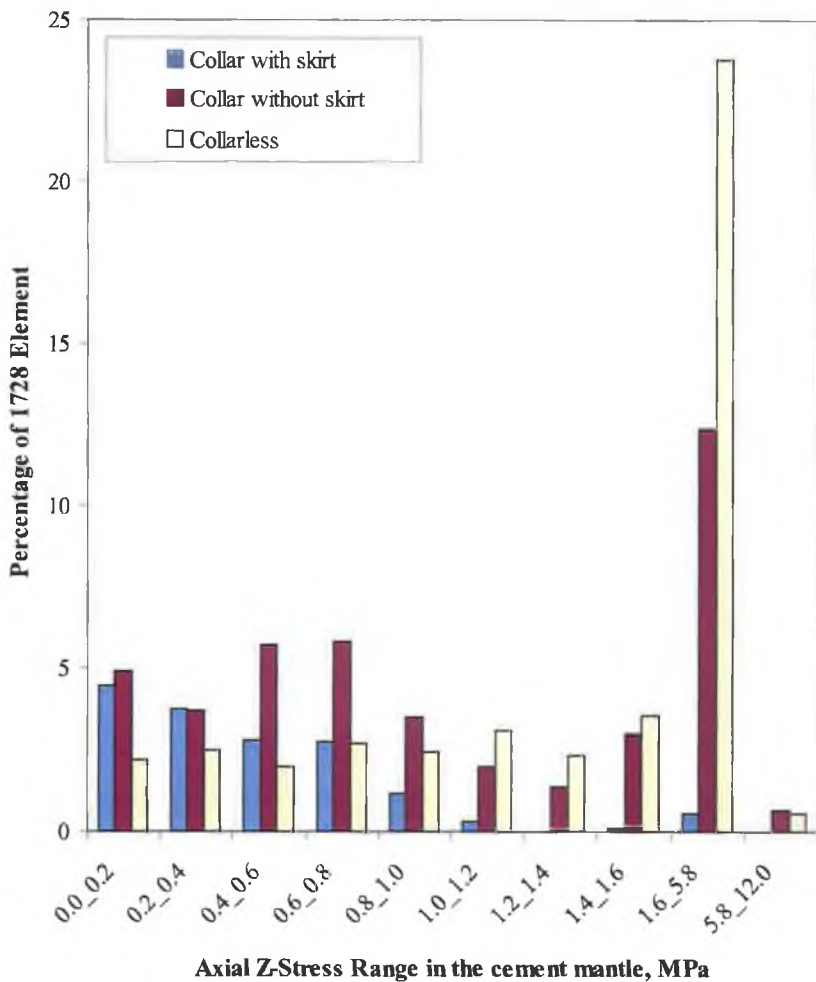


Figure 6.38: Distribution of 1728 element of the cement mantle over a stress range of 0-12 MPa. The cement mantle in these simulations was used for interlocking three different skirt-collared prostheses:
 Prosthesis (1): 100 GPa, loose proximal fixation.
 Prosthesis (2): 100 GPa, tight proximal fixation.
 Prosthesis (3): 30 GPa, tight proximal fixation.
 Cement Young's module is 2.64 GPa.

(C) Bone Cortex Axial Stress

In the present numerical studies, the use of the bound fixation technique of the skirt-collared prosthesis produced less stress shielding than the others which use ordinary proximal fixation, Figures 6.39 and 9.44. Also, using soft material prosthesis in this technique of fixation provides higher load transfer than the other as shown in the two figures.

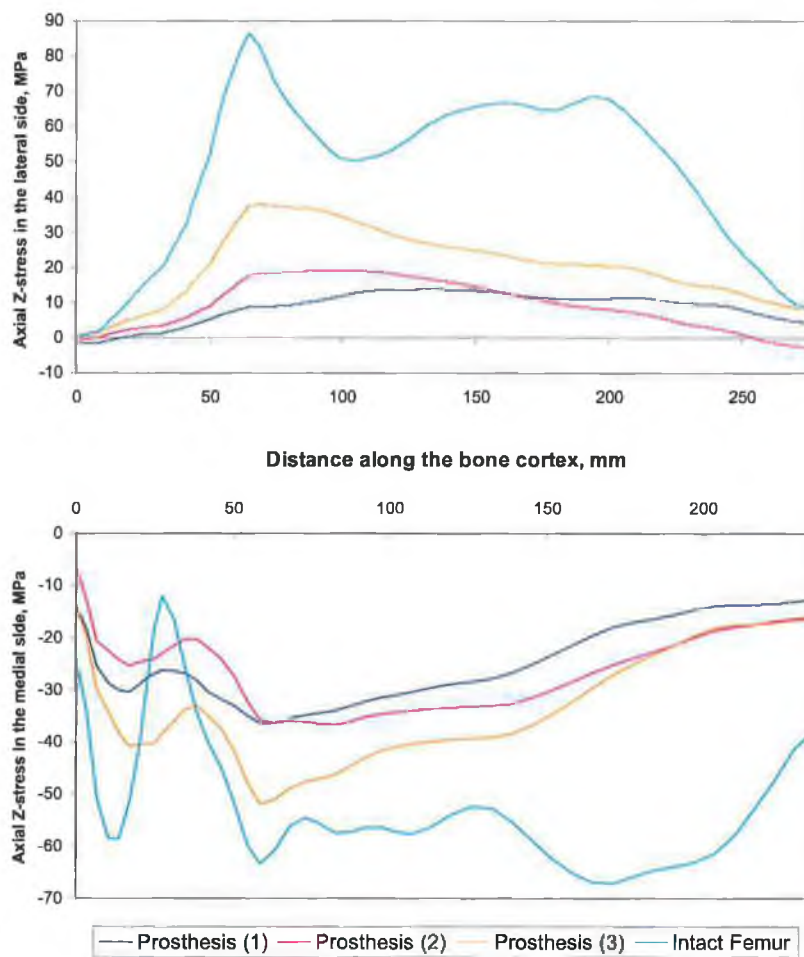


Figure 6.39: Minimum and maximum axial stress curves, in MPa, in the lateral and medial sides of the bone cortex as a function of using three different skirt-collared prostheses:

Prosthesis (1): 100 GPa, normal proximal fixation.

Prosthesis (2): 100 GPa, bound proximal fixation.

Prosthesis (3): 30 GPa, bound proximal fixation.

Cement Young's module is 2.64 GPa.

Figure 6.40 shows that as a consequence of using bound proximal fixation the femur exposed to high bending deformation, and the compression stresses are distributed broadly in the medial side.

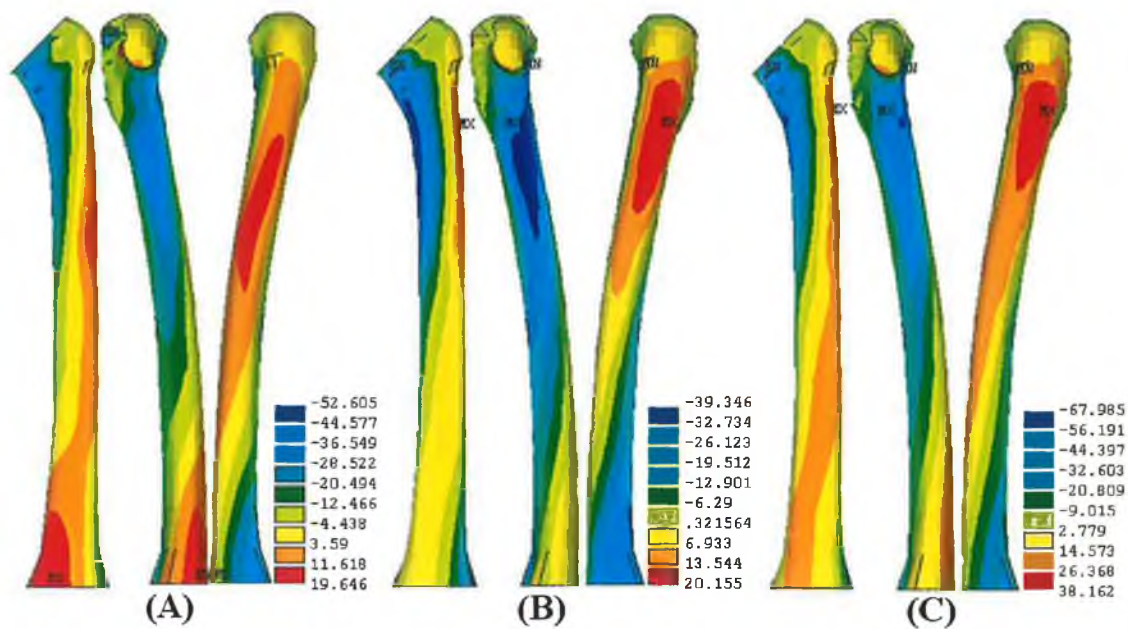


Figure 6.40: A contour plot of the axial z-stress, in MPa, for the bone cortex of the femur as a consequence of using three different skirt-collared prostheses: (A) 100 GPa, normal proximal fixation, (B) 100 GPa, bound proximal fixation, and (C) 30 GPa, bound proximal fixation.

6.6.4 Can a damper be used to alleviate impulse loads?

As was mentioned earlier this section will investigate whether it is possible to reduce the impulse loads, which arise from the patient activity and in turn may cause the artificial hip to fail as a result of the fatigue, by using the idea of damper. Therefore, this simulation inserted four layers of elements between the resected section of the femur and the collar of the prosthesis, Figure 6.5. These layers represented a damper of 4 mm thickness. To study the effectiveness of this configuration four different materials were investigated for the damper (Table 6.2).

6.6.4.1. Stress Analysis

(A) Neck and stem prosthesis stresses

Figures 6.41 and 6.42 show that there was not any effect on the neck in terms of tensile stress reduction at all by using different damper materials. While, as was expected, the tensile and compression axial stresses of the prosthesis stem are decreased by decreasing the damper material, Figure 6.43. Also, one can see from Figure 6.44 that although the tensile stress is decreased by decreasing the damper material stiffness, the area of the maximum tensile stress in the lateral side increases by decreasing the damper stiffness.

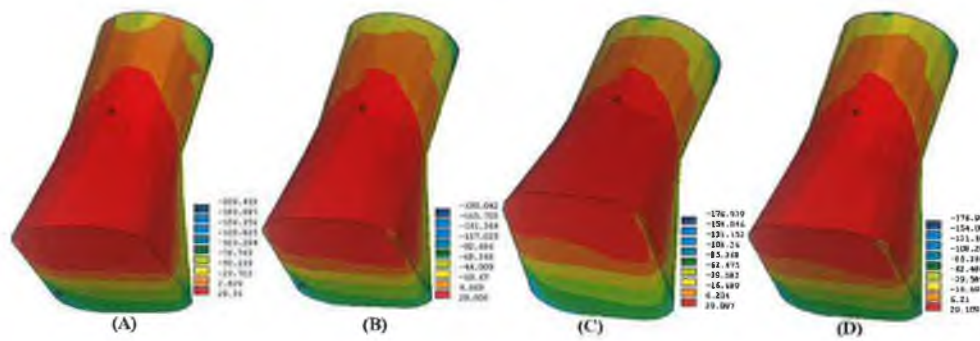


Figure 6.41: A contour plot of the axial z-stress (MPa) on the prosthesis neck as a function of damper material of (A) 50 GPa, (B) 1 GPa, (C) 1 MPa, and (D) 0.001 MPa.

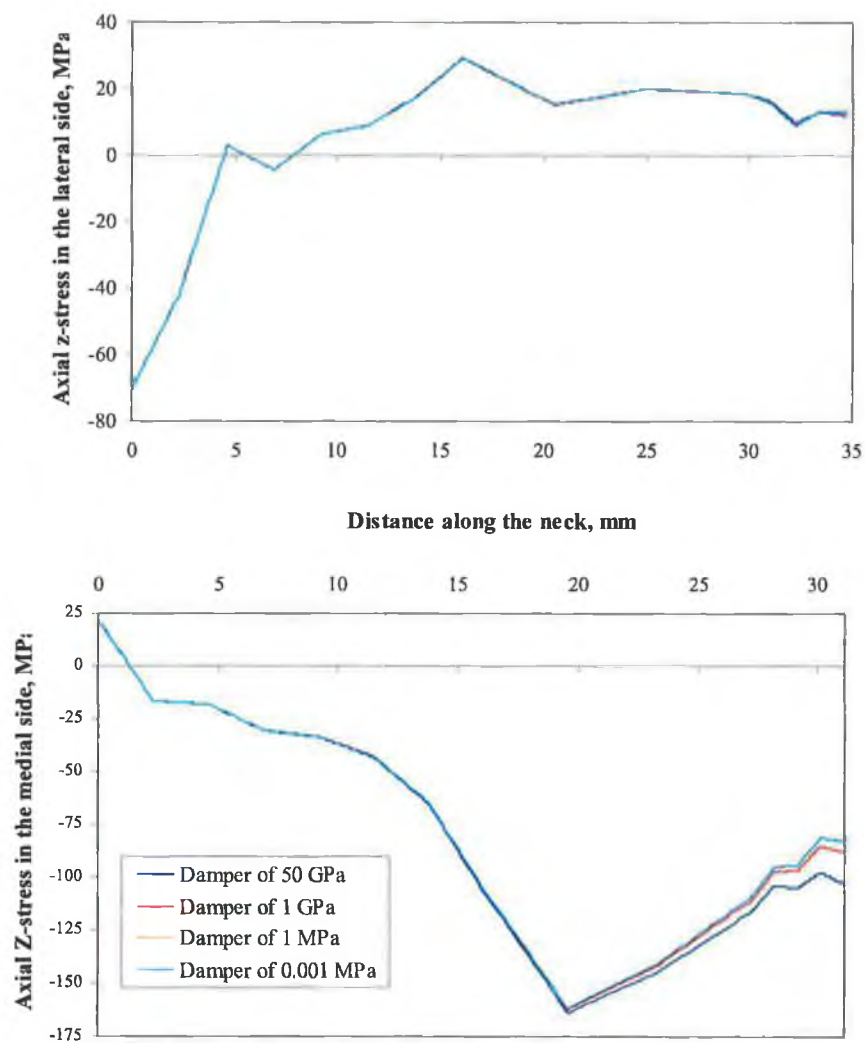


Figure 6.42: Minimum and maximum axial stress distributions, in MPa, in the lateral and medial sides of the prosthesis neck as a function of damper material. Stem and cement Young's moduli are 100 GPa and 2.64 GPa respectively.

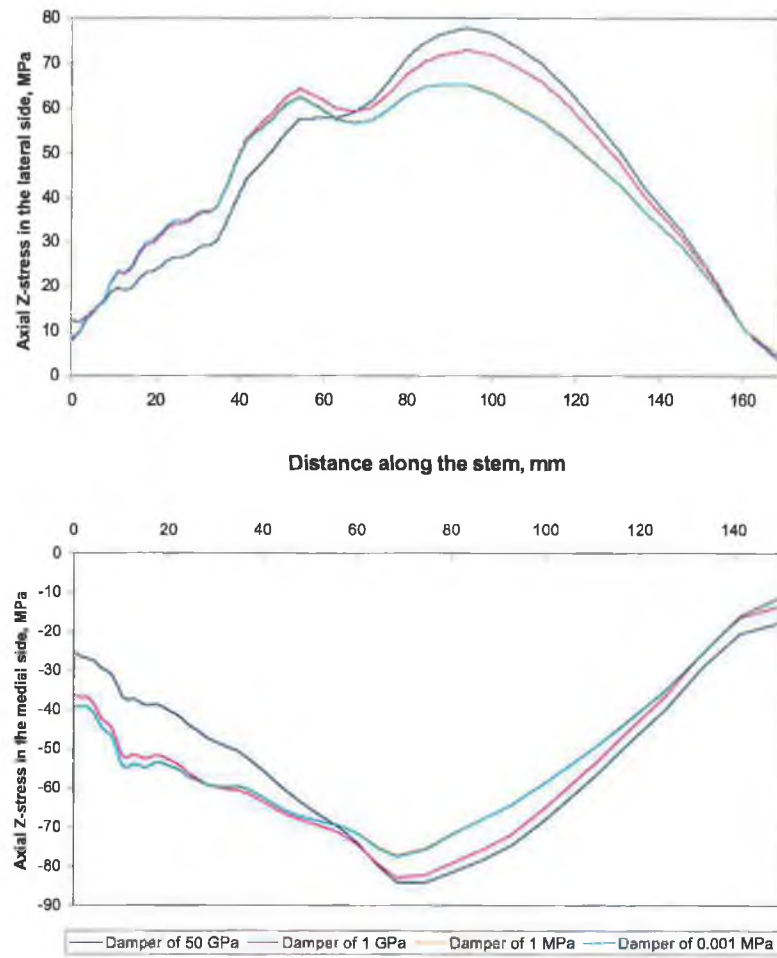


Figure 6.43: Minimum and maximum axial stress distributions, in MPa, in the lateral and medial sides of the stem as a function of damper material. The stem and cement Young's moduli are 100 GPa and 2.64 GPa respectively.

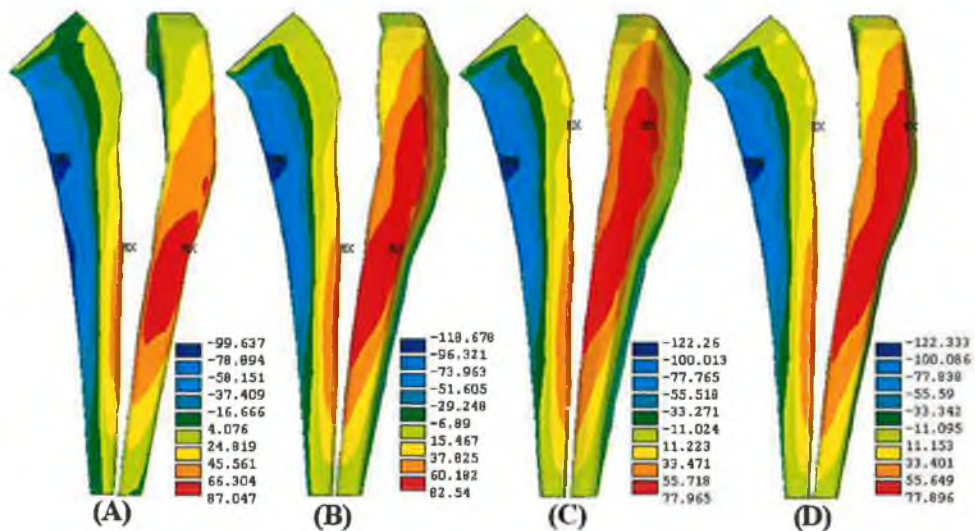


Figure 6.44: A contour plot of the axial z-stress (MPa) on the prosthesis neck as a function of damper material of (A) 50 GPa, (B) 1 GPa, (C) 1 MPa, and (D) 0.001 MPa.

(B) Cement Mantle Axial Stress

Figure 6.45 and 6.46 indicate that although by decreasing the damper's Young's modules the compression stresses decrease, the tensile stresses increase. Also, Figure 6.45 made a comparison between a damperless and damperd prostheses, and it revealed that even a damper of relatively high material stiffness (50 GPa) could cause the cement mantle tensile stresses to increase.

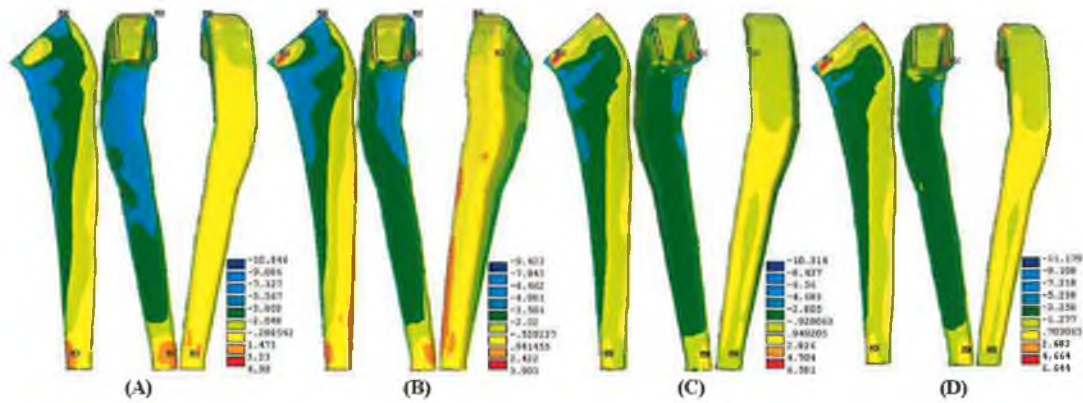


Figure 6.45: A contour plot of the axial z-stress (MPa) on the cement mantle as a function of damper material of (A) 50 GPa, (B) 1 GPa, (C) 1 MPa, and (D) 0.001 MPa.

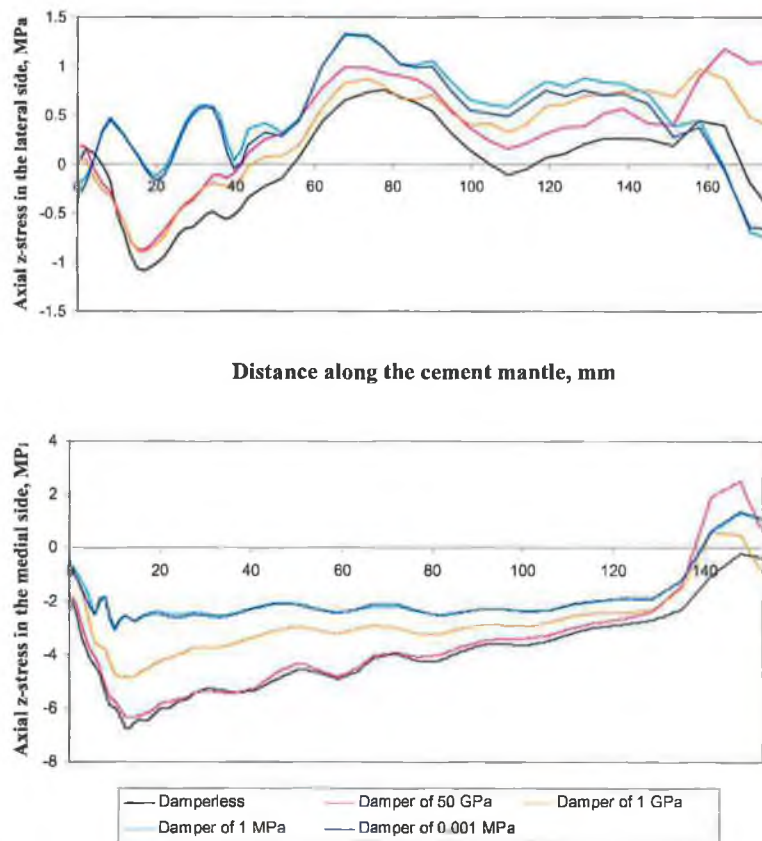


Figure 6.46: Minimum and maximum axial stress distributions, in MPa, in the lateral and medial sides of the cement mantle as a function damper material. The prosthesis and cement Young's modulus are 100 GPa and 2.64 GPa respectively.

It was found, also, that the amount of cement mantle elements that experienced a certain value of stress are higher in case of using dampers of soft material, Figure 6.47. And this could increase the risk of fragmentation and fracture likelihood when dampers of especially soft material are used.

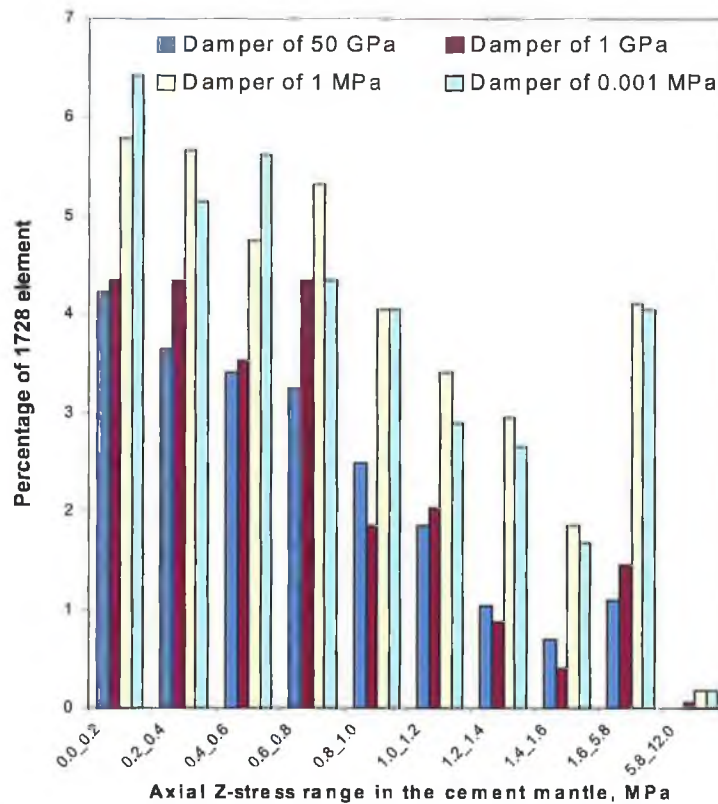


Figure 6.47: Distribution of 1728 element of the cement mantle over a stress range of 0-12 MPa as a function of damper's material. The prosthesis and cement Young's modulus are 100 GPa and 2.64 GPa, respectively.

(C) Bone Cortex Axial Stress

It was deduced that the presence of a damper between the collar and the resected cross section of the proximal part of the femur may lead to a decrease in the load transfer to the bone and hence could increase the bone stress shielding, Figure 6.48 and 6.49. In spite of the fact that a damper of 50 GPa has not any noticeable effect in terms of stress shielding in the bone, it has another side effect in the cement tensile stresses, Figure 6.46. Figure 6.49 shows that dampers made of soft material could increase the area of tensile stresses in the lateral side of the femur.

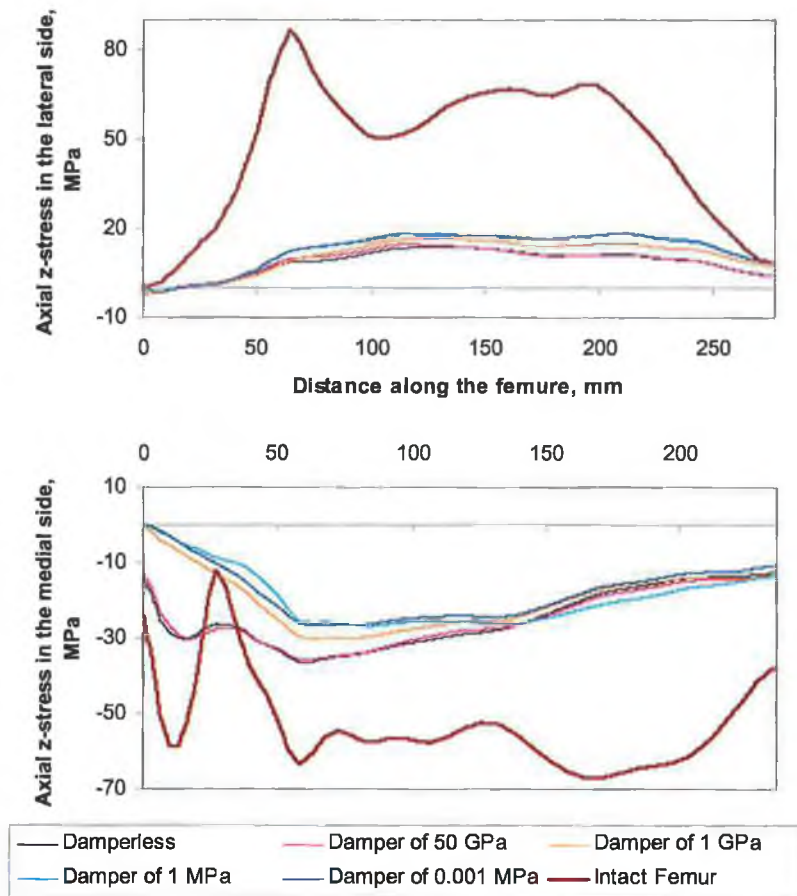


Figure 6.48: Minimum and maximum axial stress distributions, in MPa, in the lateral and medial sides of the bone cortex as a function damper material. The prosthesis and cement Young's modulus are 100 GPa and 2.64 GPa respectively.

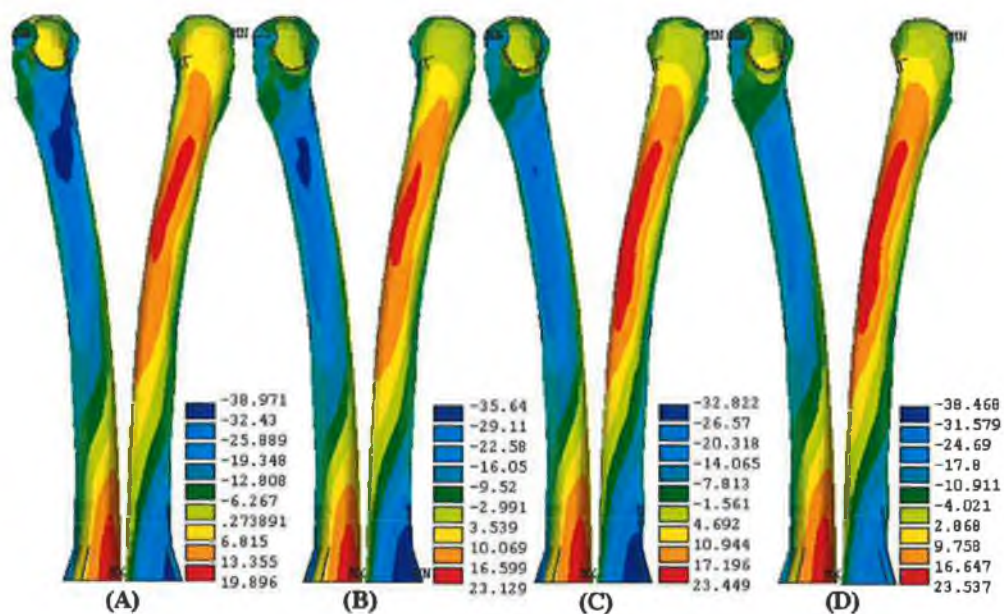


Figure 6.49: A contour plot of the axial z-stress (MPa) on the bone cortex as a function of damper material of (A) 50 GPa, (B) 1 GPa, (C) 1 MPa, and (D) 0.001 MPa.

Chapter Seven

Discussion

A number of approaches have been used in predicting stresses and strain patterns in biomechanical applications, including experimental techniques such as strain gauging and photoelastic analysis, and numerical procedures such as the finite element method (FEM) to obtain comprehensive information on the state of stress and strain in the intact and treated femur. The empirical approach of medicine has proved to be unsuitable for improving the design of biomechanical devices and mathematical models have been developed to simulate the features of real systems and so give us the capacity to predict how they would behave under changed circumstances. The versatile features of FEM analysis when compared to experimental methods are its potential for evaluating stresses/strains throughout the structure, in and between all materials concerned, and for parametric analysis. Material properties, and loading and boundary conditions are easily varied to investigate their influences. For these reasons the finite element method has been selected as a tool to investigate the factors that could contributed to the stress shielding in the bon cortex which in turn may reduce to bon atrophy. In the present study the design parameter factors, such as material properties, geometry parameters, and fixation approaches of the artificial hip prosthesis have been considered to assess its longevity. Also, this studied the effect of the static and dynamic loading of the individual, which carried over the joint head, on the artificial hip efficiency.

The problem is one of creating a valid model that satisfactorily represents the real structural behaviour of the artificial hip joint system. A balance has to be achieved between the complexity of the model and the required results. In order to assess the stresses disruption in the treated femur, a 3-D intact proximal femur was simulated for physiological loading conditions and validated by comparison with other validated FE models. It was found that there is a difference in the stress patterns in the intact femur and the femur with implant due to stiffness increment at

the femur's proximal end and 'stress shielding' by the implant. The ANSYS and LS-DYNA3D finite element packages were used for the simulations in this work.

The main simulations in this work are:

- 1) Static loading simulation:
 - (A) F.E. model validation.
 - (B) F.E. model of intact proximal femur.
 - (C) F.E. stress analysis of the artificial hip join.
 - (D) Material selection in the design of the femoral component of cemented total hip replacement.
 - (E) Design of an artificial hip replacement consisting of two materials to control stress shielding and migration phenomenon.
 - (F) The role of the collar on the femoral stem of cemented total hip replacements.
 - (G) The effect of prosthesis stem length.
 - (H) Effect of stem thickness.
- 2) A comparison study between static and dynamic loading, and stress-based criteria reliability.
- 3) Dynamic loading simulation:
 - (A) The effect of design features.
 - (B) The effect of skirt-collared prosthesis material.
 - (C) Would proximal bound fixation alleviate stress shielding in the bone?
 - (D) Can the use of a damper be used to alleviate impulse loads?

Findings from each of these simulation categories are presented in the following under separate heading.

7.1. Static Loading Simulation

7.1.1 F.E. Model Validation.

Simulation results of an intact femur subjected to a certain physiological loads have been verified with some experimental and theoretical results available in literature to establish the acceptability of the simulation results. The 3-D model of the intact femur was built using two kinds of meshing using 6-noded isoparametric elements and 4-noded isoparametric tetrahedral elements whereas the reference model was meshed with 8-noded isoparametric brick elements as shown in Figure 4.4. The reason for selecting two types of meshing was to approach to exact result relative to those in the literature. During the comparison it was concluded that the strains recorded by Akay [3] was very close to that obtained using tetrahedral elements, and the strains recorded by Oh and Harris [194] was very close to that obtained using hexahedral elements; whereas, the strains recorded by McNamara [179] agree in the calcar region but deviate significantly in the distal region as illustrated by Figures 4.8 and 4.9. This deviation may be due to the difference in the geometry dimensions of the intact femur model. Also if the average values of the two curves of Engelhardt and Saha [73] is taken one can get a curve close to the present work as shown in Figure 4.9. In general, one can say that the present model showed acceptable results compared to those presented else where, and accordingly is capable of providing information which is beyond the limitations of an experimental model, such as internal bone stress and interface analysis.

7.1.2 F.E. Model of Intact Proximal Femur

To be aware of the effect of the hip prosthesis on the stress/strain distribution in the bone after implantation, an intact proximal femur simulation was conducted. In this simulation the cancellous bone was excluded for simplification as tests conducted on cadaveric specimens showed that when the material is modelled as homogeneous, the absence of cancellous bone will only minimally affect the stiffness and failure mode of the femur [170, 179].

The results showed that under the applied loading the strains/stresses were higher on the concave side of the femur than in tension on the convex side and were greater in the coronal plane (Figures 4.10, 4.11 and 4.15) than in sagittal plane

(Figure 4.12 and 4.13). The distal portion of the posterior part of the neck of the femur was under tension with the loading conditions used and the posterior part of the femur distal to the lesser trochanter showed compressive axial strain/stress. While in the anterior side there was a compressive axial strain/stress.

7.1.3 Finite Element Stress Analysis of the AHJ

The results presented in this section were for AHJ combination of 196 GPa and 2.3 GPa for the prosthesis and cement mantle materials, respectively. It was found that bending was the primary deformation mode in the prosthesis stem (Figures 4.18 and 4.19). Fatigue cracking is most likely to initiate at the site of maximum principal stress, which dominate the middle region of the stem.

The stress in the cement mantle is more complex than that in the prosthesis stem. The dominant deformation mode is bending, generating medial compressive and lateral tensile stresses (Figures 4.20 and 4.21). It was shown that the principal stress is in the axial direction (Figure 4.22) and would cause cracks to initiate and grow in the lateral to the medial direction. It was also showed that these principal stresses were tensile and in the hoop direction. This would cause crack growth to be in the proximal to distal direction. The stress distribution in the bone cortex was noticeably effected and changed after the implantation.

7.1.4 Material Selection in the Design of the Femoral Component of Cemented Total Hip Replacement

The behaviour of the femoral prosthesis was examined when the stem and cement were manufactured from a wide range of different materials. Although the individual constituents may appear to have satisfactory mechanical properties, it is not until the composite structure of the bone, cement and stem is analysed; that the Factor-of-Safety can be generated and taken as an indictor of reliability. From the results, a design aid was developed by creating a mathematical model to facilitate the estimation of the maximum stresses produced in the stem and cement when it applied in any material combination.

It was concluded that increasing prosthesis stiffness could create higher prosthesis stresses and lower cement stresses. And that increasing cement Young's

modulus creates higher cement stresses, and insignificant decrease in prosthesis stresses. On the other hand maximum cement stresses was occur proximally, and might cause cracks to propagate in a distal direction down the stem.

As was expected prosthetic implants produced states of stress in bone which could differ widely from those produced under normal situations. The stresses in the bone cortex of the treated femur increased with decreasing prosthesis Young's modulus, except in the greater trochanter. Also an increase in the stresses in the bone of the treated femur was noted at the level of the tip of the stem, which then gradually decreases with the same slope of the intact femur.

Studying a range of materials for the stem and cement, enabled the derivation of two equations which enable prediction of the maximum critical principal stress in either material when any combination of materials is used.

7.1.5 Design of Artificial Hip Replacement consisting of Two Materials to Control Stress Shielding and Migration Phenomenon

By combining a stiff material with a more flexible one, it is possible to obtain prosthesis with controlled stiffness which meets the requirements of the compromise between the two parameters: stress shielding and migration. Concerning the materials structural point of view, a good success rate of a cemented prostheses can be obtained with controlled stiffness prosthesis, with less bone resorption. By composing two materials, one of low stiffness and the other of high stiffness, in designing the prosthesis stem one can realise the following advantages:

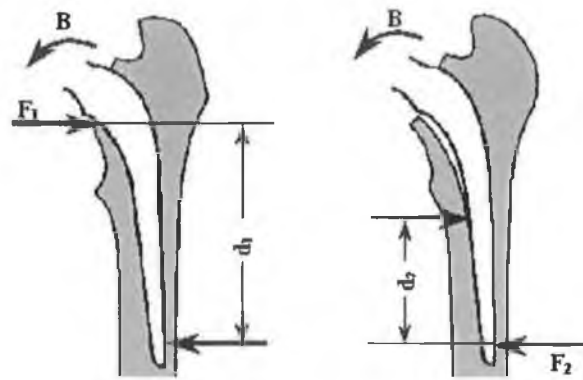
- (a) Minimising stress shielding, especially in the calcar region, therefore reducing the bone resorption.
- (b) Increasing the prosthesis reliability by reinforcing the material of low Young's modulus.

This study proved that designing a prosthesis stem consists of a low stiffness material along the medial half, and relatively high stiffness material in the lateral half gives good compromise between the stress shielding and mechanical performance of the artificial hip according to the finite element analysis results.

7.1.6 Role of the Collar on the Femoral Stem of Cemented Total Hip Replacements

Bone loss in the proximal segment of the medial side of the femur after hip replacement has been reported in many follow-up studies. The importance of the bone loss phenomenon is that it is one initiation mechanism for loosening of the prosthesis within the medullary canal. Hence to maximise joint lifetime particular attention must be given to the effect of prosthesis design on the stress distribution in this segment of the femur; not only on the stress immediately after insertion but also on how the stress changes as bone loss develops after insertion [126].

When designing Artificial Hip Joint (AHJ), from a consideration of load transfer path in intact femora, the initial response of using a large collar to reload the medial femoral cortex directly seems logical. The collared prostheses create higher compressive principal stress in the medial side and a hoop stress quiet close to the intact femora [80, 213]. It is intended that the collared prostheses will reduce the driving force for bone loss. This can only be the case if collar-on-femur support is permanent. The other approach is to use a small collar designed to transfer the load via bone cement to the inner surface of the medial femoral neck in the same way as the natural trabeculae. The simulation of this design (case 3) gives good results regarding to stress distributions in the stem, cement, and bone compared to the other design configurations. The totally collarless implant used the simple wedging action of the stem in the cement to transfer the axial component of the hip reaction to the femur. The finite element analyses show that the stress transfer to the proximal third of the medial side of the femur by using small collar (case 3) is better than that produced by collarless prosthesis because it tends to be close to the stresses of the intact femur (Figures 4.52A/B and 4.53). The clinical results from the use of these prostheses show that they can all operate successfully, although the effectiveness of the designs can vary significantly. Loss of proximal support while maintaining rigid distal fixation is widely reported to be a serious condition, indicating loosening in all types of prosthesis. In particular, resorption of the bone at the femoral neck is most frequently observed in this type of loosening. Fracture of the stem of femoral components appears likely where progressive absorption of the calcar femoral takes place. The combination of joint and muscle forces (Figure 7.1) produces a moment



$$\text{Moment} = F_1 \times d_1 = F_2 \times d_2$$

Figure 7.1: Resisting forces to balance hip movement. Note effect of resorption is to increase forces.

which is matched by a resisting couple consisting of a force acting on the lateral tip of the stem, and a force of the same magnitude and direction but opposite sign acting at the wedging action between the tapered stem and the bone. As absorption under the neck progresses, the distance between the forces of the couple decreases, and so the force must increase, and loosening eventually occurs. The bending moment applied to the stem will be a maximum at the point of application of the upper force. As resorption proceeds down the neck, the strength of the stem decreases rapidly, so that if loosening does not occur the stem will fail from overload, most likely by low cycle fatigue. If, in fact, prior absorption is an important factor as suggested loosening must occur even if fracture of the prosthesis does not. If the fixation of the stem is satisfactory, the deficiencies in the stem strength at the distal end will not be important. There is also the possibility that resorption under the upper medial stem may be due to some factors other than overload or excessive movement of the stem against the bone. Trauma from surgery, excessive heat from the acrylic cement, or the effect of adjacent soft tissue reaction may also produce absorption of bone, with consequent increase in the load exerted by the femoral stem on the bone. Provided the bone can withstand the loads applied to it after the resorption has taken place, and the prosthesis stem can withstand the bending moment applied to it, a satisfactory fixation will be maintained.

The presence of a large collar theoretically leads to the lowest stem and cement stresses in the proximal half of the joint (see Figures 4.50A/B and 4.51A/B for case 1) although a peak stress is recorded in the thin layer under the collar. At the stem-cement interface, the shear stresses are reduced by the collar, as would be

expected, although not enough to prevent failure of the joint. The large collared stems, also, minimise the shear stress at the lateral side of cement-bone interface (Figure 4.56A/B) and in the lateral and medial side when case 4 is applied, apparently restore as much as possible of the longitudinal stresses acting at the femoral neck of a natural femur, even though they some times gives a higher longitudinal stresses than those of the intact femur when low prosthesis stiffness is used, Figure 4.53. With uncollared stems, or those design to seat on the cement cuff, the principal stresses in the neck are too small/negligible (Figure 4.53). Fagan and Lee [80] found, by using FEA, that the hoop stresses developed in the cortex at the neck of intact femur are compressive, while all the models with implanted prostheses, predict the stress to be tensile. These finding is in contrast with what Prendergast and Taylor [213], and this present work. During this present work it was found some of the prosthesis designs gives tensile hoop stress, such as uncollared prosthesis and prosthesis of small collar to seat on the cement cuff, while others gives compressive hoop stress such as that collared stem seat on a layer of cement trapped between it and the surface of the resected neck (Figure 4.54). The hoop stresses have, however, measured with implanted Charnely and Charnely-Mullar stems in varying positions [174]. Compressive stresses were produced when the implants were placed in valgus, but in the natural femur, under the action of just the hip reaction, the hoop stress on the surface of the neck was reported to be tensile.

Clearly all hip replacement joints significantly alter the stressing regime in the femoral neck, so that some form of bone reaction can be expected with all implants. The view is held by some surgeons that the larger collared stems are the best design, since they should restore more of the longitudinal stress to the femoral neck, thus avoiding resorption of the bone. These implants certainly reload the femur more effectively than other designs when initially implanted; this is well established from experimental and theoretical examinations of collar performance. However, follow-up studies of uncollared and collared stems indicate that this cannot continue for long in clinical use; collared stems initiate bone resorption and uncollared versions can operate without bone resorption.

The concept of reducing the ‘stress shielding’, used to argue the case for the use of low stiffness, is not entirely adequate. As one theory suggests [55], bone will

remodel to change in any component of stress state. Hence, the fact that the tensile hoop stress is increased in uncollared low stiffness prostheses compared to with the hoop stress in uncollared higher stiffness prostheses cannot be overlooked when selecting prosthesis material. Further work to examine the importance of each component of the stress state is required before confident predictions of a reduction in bone loss with low stiffness prostheses can be made.

It has been postulated that the thin layer of cement trapped between the bone and the collar of the large collared stems may fracture *in vivo*, with the cement fragments then abrading the resected neck of the femur, leading to the resorption of the bone.

Consideration of the direction long-term migration of collared and uncollared stems may explain the mechanism of the resorption. When the stems are collared, they tend to move into a varus position, so that they move about the medial part of the collar [99], Figure 7.2. Uncollared stems on the other hand, appear to slide around the medial cement mass, moving into a valgus position [152], Figure 7.2. If the calcar loss is a function of stem position, it may be more likely to occur in the collared stems which move into varus, and consequently load the cortex in a manner different from the collarless implants. Such a hypothesis would explain why the smaller collared stems behave in a similar manner to the larger collared versions, and not like the uncollared versions. The pseudo-collars found with some uncollared stem cases must form an additional mechanism of bone destruction, resulting from micro-movement of the cement pseudo-collars over the cut surface of the bone.

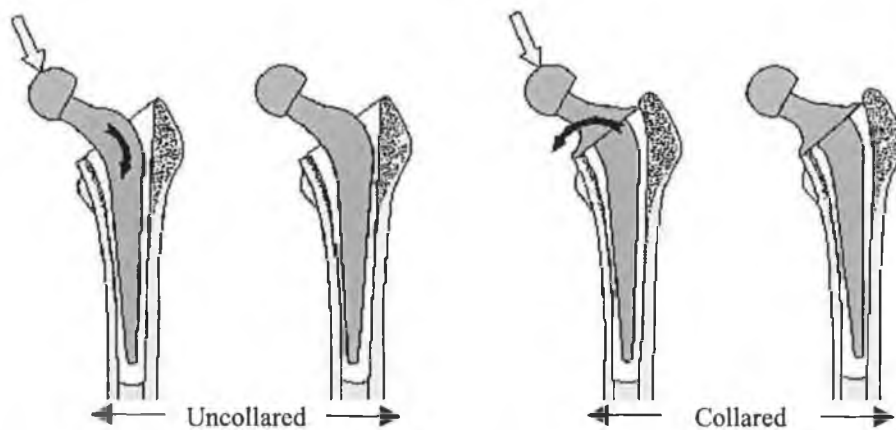


Figure 7.2: The different movement of collared and uncollared stems. When uncollared, failure of the stem-cement interface allows the stem to slide into valgus. When collared, the stem appears to pivot on the cement under the medial part of the collar, and move into varus.

7.1.7 Effect of Prosthesis Length Stem

It was shown that the stresses in the bone cortex were very sensitive to the prosthesis stem length; however, they increase with decreasing the stem length. On the other hand, this study proved that as the prosthesis stem becomes shorter, the stresses on the stem decrease and the stresses on the cement mantle decrease.

The shortness of the prosthesis stem may lead to increase the hoop stress and the shear stress τ_{XZ} at the lateral side of bone/cement interface as was shown in Figures 4.61 and 4.62B, while the shear stresses, τ_{YZ} and τ_{XY} , decrease as was shown in Figures 4.62A, and 4.62C. Since splitting failure is more serious than compressive failure, the shortened prosthesis would become very dangerous.

As a consequence, it was concluded from this investigation that the stem of the prosthesis should be as long as possible. Since the bearing pressure between prosthesis and bone (or cement and bone) is reduced and the circumferential stresses in the bone reduced. The shearing stresses at the acrylic/bone interface would also be reduced.

7.1.8 Effect of Stem Thickness

It was shown that by reducing the stem thickness from the medial side shows high flexibility by releasing more stresses to the bone cortex. While reducing the stem thickness from the posterior/anterior sides revealed high rigidity.

Unexpectedly it was found during this study that by increasing the stem cross-section the stresses along the stem increased (Figure 4.66). This in finding is, in fact, in contrast with the results of well known stress statement, $\tau = F/A$. But according to Huiskes [130] work, the increase in the stem prosthesis cross-section does not imply an increase in the stem stresses, because a high internal bending moment does not necessarily result in higher maximal bending stresses, owing to the increased thickness of the stem. In fact, when the stem thickness increases in a given bone, the stem stresses initially increase, but later decrease, Figure 4.67.

As the stem thickness affects the stem rigidity, it also effects the transverse cement stiffness because the stem thickness determines, for a given bone, the cement-layer thickness as well [69]. This result in, in this present work, a decrease in

the cement/interface stresses owing to an increase in the cement layer in this specific medullary bone's canal.

As a conclusion, it may be assumed using stem prosthesis of cross-section less than the original one may not be dangerous in terms of fatigue cracks, since in this work the stem and cement mantle stresses were dramatically decreased.

7.2. A Comparison Study between Static and Dynamic Loading, and Stress-Based Criteria Reliability

The loading methods used to determine the stresses in the prosthesis design can give quite different information, and could lead to different conclusions. To be close to the reality, a dynamic loading simulation is the only way to represent the effect of patient activity on prosthesis durability and design. This is important if finite element models are to achieve their potential as pre-clinical testing tools. The effects of the fatigue loads applied on the prosthesis head due to stumbling is well illustrated by dynamic analysis.

Irrespective of the method of analysis being used, maintaining the mechanical integrity is not a matter of reducing the peak stress in the cement mantle or on the cement/bone and cement/prosthesis interfaces, although this criterion can be used to optimize a stem profile [120]. Mechanical integrity can only be maintained if the overall stress is kept below some threshold over time. Another practical problem is that the influence of cement porosity may dominate the effect of the stress to a degree that failure may not occur at the site of peak stresses in the cement mantle, but rather may occur where the pores are largest. The peak stress predicted using the finite element method may give an incorrect picture of the potential durability of a cemented fixation since it only occurs in a very small volume of the cement mantle. One approach used to overcome this problem is to determine the volume of the composite joint stressed above a certain level. Furthermore, the use of the average stresses for an element diminishes the influence of any singularities in the stress field. In conclusion, the parameters used to report the stress in the prosthesis components can give quite different information (see Table 5.4) and could lead to different conclusions.

7.3. Dynamic Loading Simulation

7.3.1 The Effect of Design Features

Since the stability of the hip prosthesis has a major advantage in favour of its longevity it was shown that the collared prostheses offered more resistance to the radial and subsidence displacements than the collarless one. The skirt-collared prosthesis shows a pivot action which could partly attribute to the high material stiffness of the prosthesis, where less deformation and bending may occur to the prosthesis stem during the high stumbling loads. Also, it was shown that the wedge-shaped stem and the distal cement layer help in preventing the prosthesis subsidence specially for the collarless prosthesis.

Collared prostheses showed a decrease in the stresses along the stem compared to the collarless one. Since in the skirted-collar prosthesis the tensile stresses were concentrated in a limited narrow area in the middle of the lateral side which give indication that it was exposed to lower mechanical deformations, while in the collarless prosthesis higher stresses were distributed over a relatively large amount of elements (Figures 6.11 and 6.12). Because crack initiation is caused by tensile stresses, the fact that these are located in the lateral sides of the artificial hip components may be of serious concern.

However, on the other hand the numerical simulation showed that the tensile and compressive stresses in the lateral and medial side of the prosthesis neck are equal for the three different prosthesis types in spite of the fact that the uncollared prosthesis showed a different kind of bending deformation than the others (Figure 6.15).

As a consequence, it is important to note that the use of a collarless prosthesis gives rise to a noticeable increase in the tensile stresses in the lateral side of the cement mantle which may exceed by more than 4 times that of stresses caused by using collared prostheses, while skirt-collared prosthesis revealed very low tensile stress magnitudes in that side. This is firstly because the collar acts in transferring part of the loads directly to the bone and hence this would ease the pressure on the cement, and secondly due to the firm fixation in the proximal part of the femur by means of the skirted collar which in turn permits all the structures (prosthesis, cement, and bone) to move equally (together) and prevents the excessive radial

movements of the prosthesis stem inside the cement mantle. Generally, one can deduce that the collarless prosthesis is capable of generating a very high tensile stress in the cement compared to the collared prosthesis. In spite of the fact that the proximal fixed prosthesis design (skirted-collar prosthesis) causes no significant change in the stresses in the diaphysis., it produces lower magnitude stress shielding in the calcar region (Figure 6.20) which is a site of major concern due to the common occurrence of bone resorption and hence a prosthesis failure.

Table 7.1: A comparison between the three prosthesis types based on the maximum tensile stress for prosthesis components and restored stresses in the medial calcar region of the femur.				
Prosthesis Type	Prosthesis Neck, MPa	Prosthesis Stem, MPa	Cement Mantle, MPa	% stress restored in the Calcar region
Skirt-Collared Prosthesis	29.4	80.4	0.76	53 %
Collared Prosthesis	29.2	73.1	1.0	31 %
Collarless Prosthesis	28.4	82	4.5	12 %

The comparison would be clearer if the results of the three prosthesis types are seen as in Table 7.1 which shows the maximum tensile stress, quoted from the graphical results of stress curves because most of the fracture initiates in the lateral side in each component of the artificial hip construction and the percentage of the restored stresses in the calcar region of the femur. One can observe that the skirt-collared prosthesis offers least tensile stress in the cement mantle in the lateral side and a highest percentage of the resulting stress in the calcar region. This could be considered as a promising result and it could be affected by utilizing a material of lower stiffness instead of Titanium alloy. Therefore, according to this promising result the next simulation devoted to examine to how far the effectiveness of the skirt-collared prosthesis would be improved if it is made of softer material such as Epoxy Resin Composite.

7.3.2 The Effect of Skirt-Collared Prosthesis Material

Generally, it was shown that decreasing prosthesis stiffness creates lower prosthesis stresses and higher cement stresses. This is because prostheses of low

stiffness, such as polymer composite, undergo high bending deformation, thereby transferring high stress to the cement mantle. The prosthesis neck did not show any noticeable effect in terms of tensile stress quantity in spite of the fact that they show quite different deformation (Figure 6.25).

The best advantage is that by decreasing prosthesis Young's modulus the stress shielding in the bone cortex is decreased. Since in the present simulation the restored stresses in the medial calcar and diaphysis reached about 86% as a result of using polymeric prosthesis whereas it was about 53% as a maximum restoration just in the calcar region when the Titanium prosthesis is utilized.

Since failure of the prosthesis or the cement components generally occurs by fatigue, the important design parameter is not the maximum tensile stress but rather the factor of safety (FOS) of a given material that is the maximum tensile stress divided by the fatigue limit.

Table 7.2: Factor of Safety Estimates for Proposed Prosthesis and Cement Materials.				
Material	Young's Modulus, GPa	Tensile Stress, MPa	Fatigue Limit, MPa	FOS
PMMA Cement (when polymeric prosthesis is used)	2.64	7.4	10 [217]	1.4
PMMA Cement (when Titanium prosthesis is used)	2.64	5.8	10	1.7
Polymer Prosthesis	30	60.8	40 [113]	0.7
(Ti-6%Al-4%V) Prosthesis	100	89.1	550 [217]	6.2

The calculation of FOS will be based on element stress solution since the nodal solution of stress is created by averaging the element values at shared nodes. Figure 7.3 reveals the element stress solution for the hip prosthesis components as a function of prosthesis material for titanium and polymer prostheses.

It is evident from Table 7.2 that the fracture is inevitable for polymeric prosthesis since its FOS is less than one. In contrast, the 100 GPa material (Titanium Alloy) has clearly the higher FOS, and the prosthesis fracture is unlikely, unless stresses are increased by excessive loosening or by calcar bone loss. The assessment of the cement can be undertaken in a similar way, as shown in Table 7.2. From the results we can see that the FOS of the cement mantle used to interlock a stiff

prosthesis is slightly higher than that which is used to interlock the soft prosthesis.

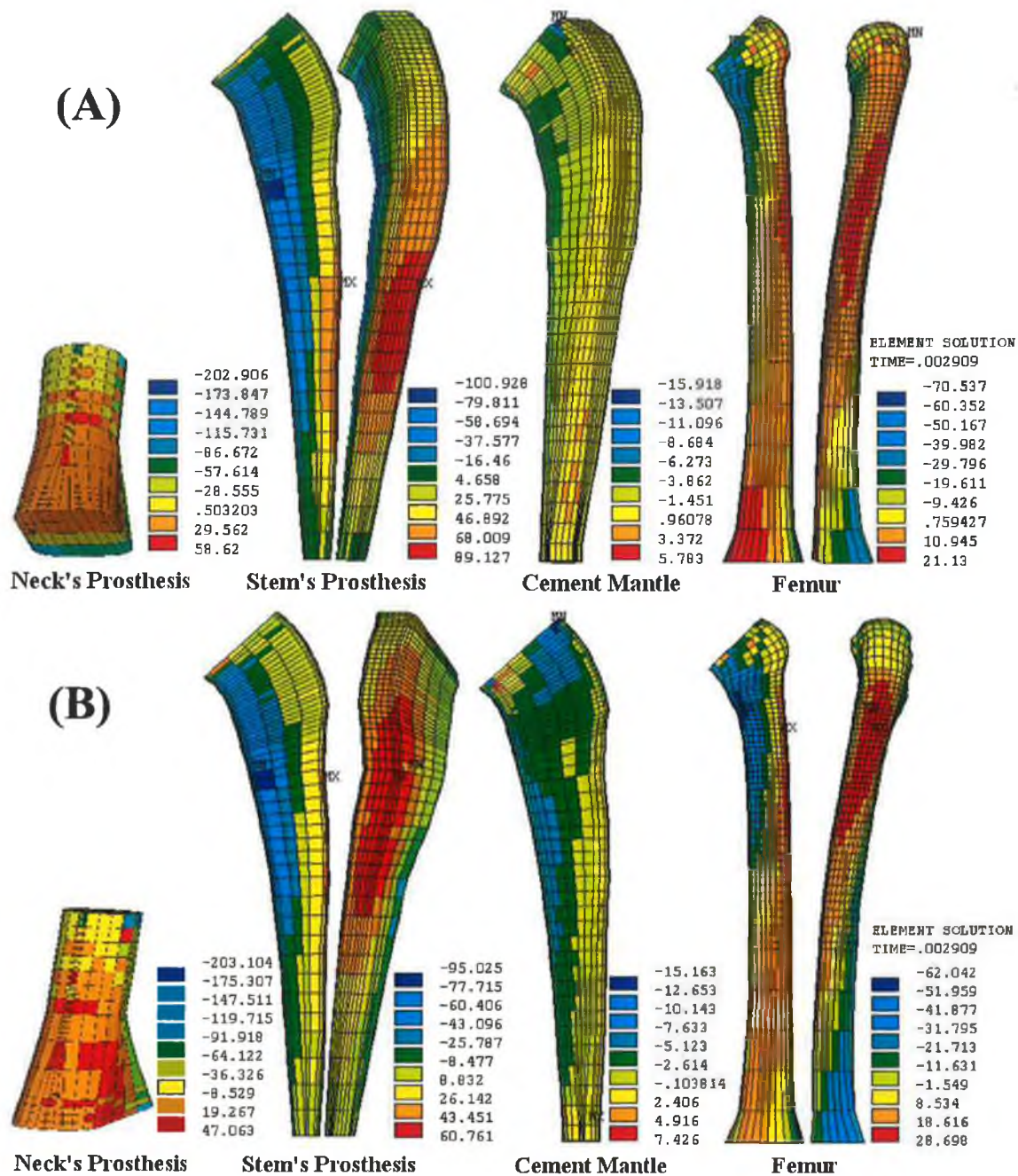


Figure 7.3: Shows the element stress solution for the hip prosthesis components as a function of prosthesis material. (A) Prosthesis of stiff material, $E = 100$ GPa, and (B) Prosthesis of soft material, $E = 30$ GPa.

7.3.3 Would the Proximal Bound Fixation Alleviate Stress Shielding in the Bone?

The total hip arthroplasty procedure employing intramedullary fixation has a lower long-term success rate in younger patients than older patients. This study

presents a design methodology and new design aimed at long-term fixation in the younger, more active population. The basis for this new design is an anchoring method providing proximal transfer of load. This prosthesis provides contact with entire cross section of the proximal femur resulting in much lower stress shielding when compared with others of ordinary fixation, or even with the other prosthesis types such as collarless prosthesis. In the numerical studies presented, the proposed design of proximal bound fixation consistently produces less stress shielding in the bone cortex. This can be considered as a promising result, however, the utilization of such this technique of fixation revealed to have the capability to aggravate the tensile stresses in the cement mantle. Which in turn needs more concentration on improving the cement mantle mechanical properties to avoid any deterioration that may happen due to consecutive load impact. On the other hand, it has been proved that the stresses in the stem can be significantly reduced by using the proximal bound fixation technique.

7.3.4 Can a Damper be Used to Alleviate the Impulse Loads?

This section showed an attempt to cushion the impulse loads occurring over the prosthesis neck, which implied the idea of shock absorption by using a soft material underneath the collar. In fact, this suggestion showed good results in terms of stem stresses alleviation (Figure 6.43), while the effect in the cement mantle and bone showed undesirable results. The tensile stresses in the cement mantle increased pronouncedly and this may increase its fragmentation and hence fracture probability. Also, the use of this kind of cushion revealed a very serious effect in regard to stress shielding in the bone which could accelerate bone atrophy and prosthesis loosening.

Chapter Eight

Conclusion and Proposal for Future Work

8.1. Static loading simulation

8.1.1 Finite element model

- Two 3-D finite element models of intact femur and treated femur has been generated for the purpose of investigating artificial hip joint behaviour under static and dynamic loading patterns. The intact model showed a good agreement with other validated numerical and experimental models.
- It was found there are difference in the stress patterns in the intact femur and the femur with implant due to stiffness increment at the femur's proximal end and 'stress shielding' by the implant.

8.1.2 Material Selection in the Design of the Femoral Component of Cemented Total Hip Replacement

- Prosthetic implants produce states of stress in bone which can differ widely from those produced under normal situations. The stresses in the bone cortex of the treated femur increase with decreasing prosthesis Young's modulus, except in the greater trochanter. Also an increase in the stresses in the bone of the treated femur is noted at the level of the tip of the stem, which then gradually decreases with the same slope of the intact femur.
- Increasing prosthesis stiffness creates higher prosthesis stresses and lower cement stresses.
- Increasing cement Young's modulus creates higher cement stresses, and a insignificant decrease in prosthesis stresses.
- Maximum cement stresses occur proximally, and may cause cracks to propagate in a distal direction down the stem.

- Although the individual constituents may appear to have satisfactory mechanical properties, it is not until the composite structure of the bone, cement and stem is analysed; that the Factor-of-Safety can be generated and taken as an indicator of reliability.
- Studying a range of materials for the stem and cement, enabled the derivation of two equations which enable prediction of the maximum critical principal stress in either material when any combination of materials is used.

8.1.3 Design of Artificial Hip Replacement Consisting of Two Materials to Control Stress Shielding And Migration Phenomenon

It has been proven that designing a prosthesis stem consisting of a low stiffness material along the medial half, and relatively high stiffness material in the lateral half gives a good compromise between the stress shielding and mechanical performance of the artificial hip according to the finite element analysis results.

8.1.4 Role of the Collar on the Femoral Stem of Cemented Total Hip Replacements

- Collared prosthesis creates a stress state that seems to approximate more closely to the intact femur stress state. We believe that the collar should reduce the driving force for bone loss. But this can only be the case if collar-on-femur support is permanent. The use of a collared stem that seats just on the cut surface of the femoral neck gives good results by FEA, since the stress on the cement mantle was reduced while that developed in the femur is close to that of the intact one. It should be noted, however, that this needs more experimental validation.
- A low stiffness prosthesis causes higher stresses, whether collared or uncollared. Therefore, the use of a low stiffness material such as a polymer composite should be advantageous.
- A low stiffness prosthesis causes higher tensile hoop stresses if uncollared or has small collar to seat on the cement cuff. Configurations of cases 2 and 4, result in small tensile hoop stresses just underneath the collar which changed to be compressive along the femur. While that of case 1, which assumed a thin layer of cement trapped between the collar and the cut surface of the femur neck, gives

almost compressive hoop stress. Fagan and Lee [80] they reported that the hoop stresses developed in the intact femur are compressive to the order of 3 MPa. This could suggest that the use of low stiffness material, with a collar that has long-term effectiveness, is an optimal prosthesis design in terms of reproducing the intact femur stress state.

8.1.5 Effect of Prosthesis Length Stem

- As the prosthesis stem becomes shorter, the stresses on the stem decrease.
- As the prosthesis stem becomes shorter, the stresses on the cement mantle decrease.
- As the prosthesis stem becomes shorter the hoop stress and the shear stress τ_{XZ} at the lateral side of bone/cement interface increase, while the shear stresses, τ_{YZ} and τ_{XY} , decrease. Since splitting failure is more serious than compressive failure, the shortened prosthesis would become very dangerous.
- The stresses in the bone cortex are very sensitive to the prosthesis stem length; they increase with decreasing the stem length.
- The stem of the prosthesis should be as long as possible. The bearing pressure between prosthesis and bone (or cement and bone) is reduced and the circumferential stresses in the bone reduced. The shearing stresses at the acrylic/bone interface would also be reduced.

8.1.6 Effect of Stem Thickness

- Reducing the stem thickness from the medial side shows high flexibility by releasing more stresses to the bone cortex.
- Reducing the stem thickness from the posterior/anterior sides still reveals high rigidity.
- It was found that by decreasing stem thickness the stem stresses decrease.
- As the stem thickness affects the stem rigidity, it also effects the transverse cement stiffness because the stem thickness determines, the cement-layer thickness as well. This resulted in a decrease in the cement/interface stresses

owing to an increase in the cement layer in this specific medullary bone's canal.

- Using stem prosthesis of cross-section less than the original one may be not dangerous in terms of fatigue cracks, since in the results presented here the stem and cement mantle stresses are dramatically decreased.

8.2. A Comparison Study Between Static and dynamic Loading, and Stress-Based Criteria Reliability

- The loading methods used to determine the stresses in the prosthesis design can give quite different information, and could lead to different conclusions.
- To be close to reality, dynamic loading simulation is the only way to represent the effect of the patient activity on the prosthesis durability and design. This is important if finite element models are used to achieve their potential as pre-clinical testing tools.
- The effects of the fatigue loads applied on the prosthesis head due to stumbling is well illustrated by dynamic analysis.
- The use of the average stresses for an element diminish the influence of any singularities in the stress field.

8.3. Dynamic Loading Simulation

8.3.1 The Effect of Design Features

It was proved that the skirt-Collared prosthesis could offer least tensile stress in the cement mantle in the lateral side, which is the expected place that the crack could initiate, and a highest percentage of resorted stress in the calcar region compared to the other prosthesis types.

8.3.2 The Effect of Skirt-Collared Prosthesis Material

- Decreasing prosthesis stiffness creates lower prosthesis stresses and higher cement stresses.
- Decreasing prosthesis Young's modulus causes the stress shielding in the bone cortex to be decreased.

- It was found that the polymeric prosthesis fracture is inevitable since its FOS is less than unity.
- The factor of safety of the cement mantle used to interlock a stiff prosthesis, titanium, is slightly higher than that which is used to interlock the soft prosthesis, polymer.

8.3.3 Would Proximal Bound Fixation Alleviate Stress Shielding in the Bone?

- In this numerical study, the proposed design of proximal bound fixation consistently produced less stress shielding in the bone cortex compared with conventional prosthesis.
- It has been proved that stresses in the stem can be alleviated by using the proximal bound fixation technique.

8.3.4 Can a Damper be Used to Alleviate Impulse Loads?

- The use of damper underneath the prosthesis collar revealed a very serious effect in regard to stress shielding in the bone, which could accelerate bone atrophy and prosthesis loosening.
- This suggestion showed good results in terms of stem stresses alleviation, while the effect in the cement mantle and bone was undesirable.

8.4. Recommendation for Further Work

- Currently the optimisation of a three dimensional artificial hip replacement is very difficult due to lack of adequate computational power. With increasing computational power available at reasonable cost and more efficient finite element software available it should be possible to optimise the hip prosthesis components in the near future. An algorithm can be adopted into the optimisation scheme which makes a compromise between the prosthesis and cement integrity and optimum resorted bone stresses.
- In this respect, the potential advantages of computer simulation vis-à-vis physical model testing may become considerable, but only if robust simulation algorithms can be developed to predict tissue adaptation (and this is still in the future).

- Research to date on bone adaptation in response to altered mechanical loading has provided much insight into the possible bio-mechanical factors which drive adaptation in biological systems such as bones. The phenomenon of Bone Adaptation is characterized by bone adapting its geometries definition and material characteristics with reference to its mechanical loading conditions. However, Proposed hypotheses showing varying degrees of success include stress, strain and micro-damage as the stimulus which drives adaptation of bone in response to altered mechanical load. Based on these hypotheses, this project could be proceeded to simulate this adaptation phenomenon and thus could provide a method/evaluation tool which could be used for evaluating different implant designs and also for optimizing a design based on maintaining the adaptation response to a minimum.

8.5. Thesis Contribution

The contribution made through the work presented in this thesis may be enumerated as follows: ✦

- A convincing argument has been put forward for the design of artificial hip replacement system to be based on patient activities giving rise to dynamic and impact loading.
- A new design of the implant for the artificial hip replacement has been proposed and its performance has been critically evaluated using FE analysis.
- A mathematical equation based approach has been proposed for selecting appropriate combinations for the cement mantle and the prosthesis.

References

- [1] A'Sheikh, H.F., MacDonald, B.J., and Hashmi, M.S.J., "Material selection in the design of the femoral component of cemented total hip replacement," Proceeding of the seventeenth conference of the Irish manufacturing committee: Building on manufacturing advances of the nineties IMC-17, Edited by Patrick Donnelln, Galway, Ireland, 23rd to 25th August 2000.
- [2] Ahmed AM, Raab S, Miller JE. "Metal/cement interface strength in cemented stem fixation", *J.Orthop Res.*, **2(2)**:105-118, 1984.
- [3] Akay, M. and Aslan, N., "Numerical and experimental stress analysis of polymeric composite hip joint prosthesis", *Journal of Biomedical Materials Research*, **31**: 167-182, 1996.
- [4] Amstutz, H.C., "Polymers as bearing materials for total hip replacement: A friction and wear analysis," *J. Biomed. Mater. Res.*, **3**: 568-587, 1968.
- [5] Amtmann, E., Kummer, B., "The demand of the human hip joint. Size and direction that of hip joint. Size and direction of the hip joint-resulting in the frontal level," Magazine for anatomy and history of the development (Zeitschrift für Anatomie und Entwicklungsgeschichte) **127**: 286, 1968.
- [6] Andrew T.A., Flanagan J.P., Gerundini M., Bombelli R., "The isoelastic non-cemented total hip arthroplasty: preliminary experience with 400 cases," *Clin Orthop Rel Res.*, **206**: 127-138, 1986.
- [7] Andriacch, T.P., Galante, J.O., Belytschko, T.B., and Hampton S., "A stress analysis of the femoral stem in total hip prostheses," *The Journal of Bone and Joint Surgery*, **58(A)**, No. 5, 618-624, July 1976.
- [8] Ascenzi, A. and Bonucci, E., "Orientation of collagen fibbers at the boundary between two successive osteonic lamellae and its mechanical interpretation," *J Biomechanical*, **19**: 455-463, 1986.
- [9] Ascenzi, A. and Bonucci, E., "The tensile properties of single osteons," *Anat. Rec.*, **158**: 375-386, 1966.
- [10] Ascenzi, A., "The micromechanics versus the macromechanics of cortical bone – A comprehensive presentation," *J. Biomechanics Eng.*, **110**: 357-363, 1988.
- [11] Ascenzi, A., Bonucci, E., Generali, P., Ripamonti, A. and Roveri, N., "Orientation of appetite in single osteon samples studied by pole figures, *Calcified Tissue International*, **29**: 101-105, 1979.
- [12] Ascenzi, A., Boyde, A., Porigliatti Barbos, M. and Carando, S., " Micro-biomechanics vs. macro-biomechanics in cortical bone. A micromechanical

- investigation of femur deformed by bending," *J. Biomechanics*, **20**: 1045-1053, 1987.
- [13] Bannister G.C, Miles A.W., "The influence of cementing technique and blood on the strength of the bone-cement interface", *Eng Med*, **17(3)**: 131-133, 1988.
 - [14] Bassett, C.A.L., "Electrical effects in bone," *Sci. Amer.*, **213**: 18-25, 1965.
 - [15] Bathe, K. J., "Finite Element Procedures," Prentice-Hall International, 1996.
 - [16] Bechtol, C.O., "Low-friction arthroplasty using a two-part prosthesis with acrylic cement," Richards Mfg. Co., 1971.
 - [17] Beckenbaugh R.D., and Ilstrup, D.M.; "Total hip arthroplasty – a review of three hundred and thirty three cases with long follow up," *J. Bone Joint Surg*, **60A**: 306 – 313, 1978.
 - [18] Bergman G., Graichen F., and Rohlmann A., Hip joint loading during walking and running, measured in two patients, *J. Biomechanics*, **26**: 969, 1993
 - [19] Bergmann G., Graichen F., Rohlmann A., Verdonschot N., and van Lenthe G.H., "Frictional heating of total hip implants. Part 2: finite element study", *Journal of Biomechanics*, **34(4)**: 429-435, April 2001
 - [20] Bergmann, G., Graichen, F, Rohlmann, A., Verdonschot, N., and van Lengthe, G.H., "Friction heating in and around total hip implants," Proceedings of the 12th Conference of the European Society of Biomechanics, edited by Prendergast, P.J., Lee, T.C. and Carr, A.J., Trinity College, Dublin, 28-30 August 2000.
 - [21] Besong, A.A., Farrar, R., and Jin, Z.M., "Contact mechanics of a novel metal-on-metal total hip replacement," Proceedings of the 12th Conference of the European Society of Biomechanics, edited by Prendergast, P.J., Lee, T.C. and Carr, A.J., Trinity College, Dublin, 28-30 August 2000.
 - [22] Besong, A.A., Jin, Z.M., and Fisher, J., "Importance of pin geometry on screening wear testing of orthopaedic bearing materials," Proceedings of the 12th Conference of the European Society of Biomechanics, edited by Prendergast, P.J., Lee, T.C. and Carr, A.J., Trinity College, Dublin, 28-30 August 2000.
 - [23] Bishop N.E., Ferguson S, Tepic S., "Porosity reduction in bone cement at the cement-stem interface", *J Bone Joint Surg*; **78(3)**:349-56, 1996.
 - [24] Black J. and Hastings G., "Handbook of Biomaterial Properties", Chapman and Hall 1998.
 - [25] Bobyn, J. D., Mortimer, E. S., Glassman, A. H., Engh, Ch. A., Miller, J. E. and Brooks C. E., "Producing and avoiding stress shielding. Laboratory and clinical

- observations of non-cemented total hip arthroplasty", *Clin. Orthop.*, **274**: 79-96, 1992.
- [26] Bobyn, J.D., Glassman, A.H., Goto, H., Krygier, J.J., Miller, J.E., Brooks, C.E., "The effect of stem stiffness on femoral bone resorption after canine porous coated total hip replacement.", *Clinical Orthopaedics and Related Research*, **261**: 196-213, 1990.
 - [27] Bocco, F., Langan, P. and Charnley, J., "Change in the Calcar Femoris in Relation to Cement Technology in Total Hip Replacement," *Clin. Orthop. Rel. Res.*, **128**: 287-295, 1977.
 - [28] Bonfield, W., "Material for the Replacement of Osteoarthritic Hip Joints," *J. Inst. Materials*, **3**: 712-716, 1987.
 - [29] Brockhurst, P. J., and Svensson, N. L., "Design of total hip prosthesis: the femoral stem," *Med. Progr. Technology*, **5**: 73-102, 1977.
 - [30] Bühler DW, Berlemann U, Lippuner K, Jaeger P, Nolte L-P. "Three-dimensional primary stability of cementless femoral stems", *Clin Biomech*, **12(2)**: 75-86, 1997.
 - [31] Burke DW, Gates EI, Harris WH. "Centrifugation as a method of improving tensile and fatigue properties of acrylic bone cement", *J Bone Joint Surg (Am)*; **66(8)**: 1265-1273, 1984.
 - [32] Burr, D.B., Schaffler, M.B. and Frederickson, R.G., "Composition of the cement line and its possible mechanical role as a local interface in human compact bone," *J. Biomechanics*, **21**: 939-945, 1988.
 - [33] Butel J., and Robb J. E., "The isoelastic hip prosthesis followed for 5 years," *Acta Orthop Scand*, **59**: 258-262, 1988.
 - [34] Cameron, H. U., Pilliar, R. M. and MacNab, I., "The effect of movement on the bonding of porous metal to bone. Biomed", *Mater. Res.*, **7**: 301-311, 1973.
 - [35] Carlsson, L., Röstlund, T., Albrektsson, B. and Albrektsson, T., "Implant fixation improved by close fit", *Acta Orthop. Scand.*, **59**: 272-275, 1988.
 - [36] Carter, D.R., Hayes, W.C., and Schurman, D.J., "Fatigue life of compact bone _2: Effects of microstructure and density," *J. Biomechanics*, **9**: 211-218, 1976.
 - [37] Chao, E. Y. S. and An, K. A., "Perspectives measurements and modeling of musculoskeletal joint dynamics," in *Biomechanics: Principles and Applications*. Huiskes, R., van Campen, D. H., and de Wijn, J. R., Eds., Martinus Nijhoff. The Hague, 1982.
 - [38] Charnley, J. "The bonding of prostheses to bone by cement," *J. Bone Joint Surg.*, **46B**: 518-529, 1964.

- [39] Charnley, J., "Acrylic Cement in Orthopaedic Surgery," London: Livingstone 1970.
- [40] Charnley, J., "Arthroplasty of the hip. A new operation," *Lancet*, 1129-1132, 1961.
- [41] Charnley, J., "Factors in the design of an artificial hip joint," *Inst. Mech. Eng., Proc.*, 181, 1976.
- [42] Charnley, J., "Low-friction arthroplasty of the hip," Springer-Verlag, Berlin, 1979.
- [43] Charnley, J., "Surgery of the hip joint," *Brit. Med. J.*, III, 821-826, 1960.
- [44] Charnley, J., Fallacci, F.M., Hammond, B.T., "The long term reaction of bone to self-curing acrylic cement," *J. Bone Joint Surg.*, **50B**: 822-829, 1968.
- [45] Charnley, J., Ferreira, A. de S.D., "Transplantation of the greater trochanter in arthroplasty of the hip," *J. Bone Joint Surg.*, **46B**: 191-197, 1964.
- [46] Charnley, J., Kamangar, A., Longfield, M.D., "The optimum size of prosthetic heads in relation to wear of plastic sockets in total replacement of the hip," *Med. Biol. Eng.*, 7: 31-39, 1969.
- [47] Charnley, J., Kettlewell, J., "The elimination of slip between prosthesis and femur," *J. Bone Joint Surg.*, **47B**: 56-60, 1965.
- [48] Chi-Chung Hu, Chun-Hsiung, Fang-Yung Ho, and Cheng-Kung Cheng, "Finite element analyses for frictional heating in total hip prosthesis," Proceedings of the 12th Conference of the European Society of Biomechanics, edited by Prendergast, P.J., Lee, T.C. and Carr, A.J., Trinity College, Dublin, 28-30 August 2000.
- [49] Christainson, T., "A combined endo-and total hip prosthesis with trunnion-bearing," *Acta lin. Scand.*, **140**: 185-188, 1974.
- [50] Christal, P., Meunier, A., Leclercq, S., Bouquet, Ph. And Buttazzoni, B., "Development of a carbon-carbon hip prosthesis," *J. Biomed. Mater. Res.*, **21**: 191-218, 1987.
- [51] Claes I., Burri C., Neugebauer R., Gruber U., "Experimental investigations on hip prostheses with carbon fibre reinforced carbon shafts and ceramic heads," In: P. Vincenzini, editor. *Ceramics in Surgery*. Amsterdam, 243-250, 1983..
- [52] Collier, J. P., Bauer, T. W., Bloebaum, R. D., Bobyn, J. D., Cook, S. D., Galante, J. O., Harris, W. H., Head, W. C., Jasty, M. J., Mayor, M. B., Sumner, D. R. and Whiteside, L. A., "Results of implant retrieval from postmortem specimens in patients with well-functioning long-term total hip replacement", *Clin. Orthop.*, **274**: 97-112, 1992.

- [53] Cook S.D., Thongpreda N., Anderson R.C., Thomas K.A., Haddad R.J.J., GriÅn C.D., "Optimum pore size for bone cement fixation", *Clin Orthop*, **223**: 296-302, 1987.
- [54] Cotterill P., Hunter G. A. and Tile M. A., "A radiographic analysis of 166 charnley-muller total hip arthroplasties," *Clin Orthop. Rel. Res.*, **163**: 120-126, 1982.
- [55] Cowin, S.C., "bone remodelling of diaphyseal surfaces by tortional loads: theoretical predictions," *J. Biomech.*, **20**: 1111-1120, 1987.
- [56] Cowin, S.C., "Strain assessment by bone cells," In *Tissue Engineering*, R. Skalak and C.F. Fox (eds.) Alan Liss, New York, 181-188, 1988.
- [57] Cowin, S.C., and Hegedus, D.H., "Bone remodeling I: Theory of adaptive elasticity," *Journal of Elasticity*, **6 (3)**: 313-326, 1976.
- [58] Crowninshield, R.D., Brand, R.A., Johnston, R.C. and Milroy, J.C., "An analysis of femoral component stem design in total hip arthroplasty," *J Bone Joint Surg.*, **62A**: 68-78, 1980.
- [59] Crowninshield, R.D., Brand, R.A., Johnston, R.C., Milroy, J.C., "The effect of femoral stem cross section geometry on cement stresses in total hip reconstruction", *Clinical Orthopaedics and Related Research*, **146**: 71-77, 1980
- [60] Crowninshield, R.D., Pedersen, D.R., and Brand, R.A., "A measurement of proximal femur strain with total hip arthroplasty," *J. Biomech. Eng.*, **102**: 230-233, 1980.
- [61] Davidson JA. "The challenges and opportunity for composites in structural orthopaedics applications", *J Comp Tech Res.*, **9**: 151-161, 1987.
- [62] Davidson R., Brabon S., Lee R.J., Nelson K., Unwin P., Roughley P., "The development of CFRP based hip stems," In: *Proceedings of the 7th European conference on composite materials, ECCM-7*, London, 513-517, 1996.
- [63] de Wijn, J.R., Driessens, F.C.M., and Sloof, T.J.J.H., "Dimensional behavior of curing bone cement masser," *J.Biomed. Material Res. Symp.*, **6**: 99, 1975.
- [64] Debrunner, H. And, " studies to the bio mechanics of the hip joint. A new model for calculation Hip loads", *Magazine for orthopaedie*, **113**: 377, 1975.
- [65] Devanathan D., "Orthopaedic composites," In: Lee SM, editor. *International encyclopaedia of composites*, **4**, New York, 74-86, 1991.
- [66] Deyerle, W.M., "A total hip unit with replaceable non-cemented parts," *Clin. Orthop.*, **99**: 103-119, 1974.

- [67] Dietrick, J.E., Whedon, G., and Shorr, E., "Effect of immobilization upon various metabolic and physiological functions of normal man," *Am. J. Med.*, **4**: 3-36, 1948.
- [68] Dowson, D. "Bio-mechanics of the lower limb," In An introduction to biomechanics of joints and joint replacements (Edited by Dowson, D. and Wright, V.), pp. 68-73, MEP, London, 1981.
- [69] Ducheyne, P. and Hasting, G. W., "Functional behavior of orthopedic biomaterials, Volume I: Fundamentals," CRC Series in Structure-Property Relationships of Biomaterials, 1984.
- [70] Ducheyne, P. and Hastings, G.W., "Fundamental behavior of Orthopedic biomaterials," Vol. II, Chap. 2, p. 21, CRC series in structure-property relationships of biomaterials, CRC Press, Inc., Boca Raton, Florida, 1984.
- [71] Duff-Barclay, I., Scales, J.T., Wilson, J.N., "The development of the Stanmore total hip replacement," *Proc. Roy. Soc. Med.*, **59**: 948-951, 1966.
- [72] Duff-Barclay, I., Spillmann, D.T., "Total human hip joint prosthesis – a laboratory study of friction and wear," *Inst. Mech. Eng. Proc.*, **181**: 90-103, 1966.
- [73] Engelhardt, J. A., and Saha, S., "The effect of femoral component cross section modulus on the stress distribution in the proximal human femur," *Med. Biol. Eng. Comp.*, **26**: 38-45, 1988.
- [74] Eriksen, E.F., Kassem, M., "The cellular basis of bone remodeling," *Sandoz J. Med. Sci.*, **31**: 45-57, 1992.
- [75] Evans, F. G., "The mechanical properties of bone," *Artificial Limbs*, **13**: 37-48, 1969.
- [76] Evans, F.G. and Lebow, M., "Strength of human compact bone under repetitive loading," *J. appl. Physiol.*, **10** (1): 127-130, 1957.
- [77] Evans, F.G., "The mechanical properties of bone," *Artificial Limbs*, **13**: 37-48, 1969.
- [78] Evans, S.L., "Computational simulation of fatigue crack propagation in PMMA bone cement around an Exeter hip prosthesis, using a boundary element approach," Proceedings of the 12th Conference of the European Society of Biomechanics, edited by Prendergast, P.J., Lee, T.C. and Carr, A.J., Trinity College, Dublin, 28-30 August 2000.
- [79] Fagan M. J. & Lee A.J.C., "Finite element analysis of the loading mechanism of the femoral component of total hip replacement joints," Material Properties and Stress Analysis in Biomechanics. Institute of Physics Conference, Brunel University; 1985.

- [80] Fagan M.J. and Lee A. J. C., "Role of the collar on the femoral stem of cemented total hip replacements," *J. Biomed. Eng.*, **8**: 295-304, 1986.
- [81] Fagan, M. J., and Lee, A. J. C., "Material selection in the design of the femoral component of cemented total hip replacements," *Clinical Materials*, **1**: 151-167, 1986.
- [82] Fagan, M. J., "Finite Element Analysis: Theory and practice", University of Hull, 1992.
- [83] Feith, R., "side effects of acrylic cement implanted into bone," *Acta Orthop. Scand.*, 161, 1975.
- [84] Fielder J.H, Black J., "But doctor, it's my hip! The fate of failed medical devices", *Kennedy Inst. Eth. J.*, **5**:113-131, 1995.
- [85] Frankel, A., Balderston, R., Rothman, R., "Radiographic demarcation of acetabular bone-cement interface," *J. of Arthrop.*, Vol. 5, Supp Oct 1990.
- [86] Freeman, M. A. R., Miller, A. J. and Vernon-Roberts, B., "Metal sensitivity as of bone necrosis and loosening of the prosthesis in total joint replacement", *J. Bone Jt Surg.*, **56B**: 626-642, 1974.
- [87] Fritz, W., Hüttner, W., and Hartwig, G., "Carbon-fiber-reinforced carbon composite: processing, room temperature properties, and expansion behavior at low temperatures," 245-266, 1979.
- [88] Frost, H.M., Guise, E.R., "A replacement prosthesis for the hip," *Henry Ford Hosp. Med. J.*, **29**: 3-14, 1971.
- [89] Fung, Y.C., "Biomechanics: Mechanical Properties of Living Tissues," 2nd edition, Springer publication, 1990.
- [90] Galante, J. O., Rostoker, W. and Doyle, I. M., "Failed femoral stems in total hip prostheses," *JBJS*, **57(A)**: 230-236, 1975.
- [91] Gallagher, R. H., Simon, B. R., Johnson, P. C., and Gross, J. F., Eds., "Finite Elements in Biomechanics", *John Wiley & Sons*, New York, 1982.
- [92] Giovetti, F., Dovesi, A., Mingozi, F., Perissinotto, A., "Modular hip prosthesis N.D.S.1: Design purpose, mechanical testing and preliminary results and considerations," Proceedings of the 12th Conference of the European Society of Biomechanics, edited by Prendergast, P.J., Lee, T.C. and Carr, A.J., Trinity College, Dublin, 28-30 August 2000.
- [93] Godest A.C., Beaugonin M., Haug E., Taylor M., and Gregson P.J., Dynamic simulation of a knee joint replacement during gait using explicit FEA, Proc. 12th Conf. European Society of Biomechanics, Trinity College, Dublin, 28-30 August, 2000.

- [94] Gola, M.M. and Gugliotta, A.A., "Analytical estimate of stresses in bones and prosthesis stems," *J. Strain Analysis*, **14**: 29-33, 1979.
- [95] Graichen, F., Bergmann, G., and Rohlmann, A., "Hip endoprosthesis for in vivo measurement of joint forces and temperature," *J. Biomechanics*, **10**: 1113-1117, 1999.
- [96] Greenwald, A. S., O'Connor, J. J., "The transmission of load through the human hip joint," *J. Biomechanics*, **4**: 507-516, 1971.
- [97] Greer, B. "Finite element modeling and analysis of the proximal femur," Master Thesis, University of Nevada-Reno, 1999.
http://www.cinea.it/hosted/LTM-IOR/back2net/ISB_mesh/mesh_list.html.
- [98] Gross1, S. and Abel, E.W., "A finite element analysis of hollow stemmed hip prostheses as a means of reducing stress shielding of the femur", *Journal of Biomechanics*, **34**: 995–1003, 2001.
- [99] Gruen, T. A., McNeice, G. M. and Amstutz, H. C., "modes of failure of cemented femoral components – a radiological analysis of loosening," *Clin. Orthop. Rel. Res.*, **141**: 17-27, 1979.
- [100] Gualtieri, G., Gualtieri, I., Gagliardi, S., Hendriks, M. and Giunti, A., "I reimpianti con artroprotesi in bioceramica," *Giornale Ital. Ortop. Traum.*, **16**: 311-317, 1990.
- [101] Hallquist J.O. and Benson D.J., "Explicit Finite Element Methods for Impact Engineering", *Proc. of First Australasian Congress on Applied Mechanics, Melbourne*, 11-16, 1996.
- [102] Hallquist J.O., LS-DYNA3D Theoretical Manual, Livermore Software Technology Corporation, California, USA, 1993.
- [103] Ham, A.W., "Histology," 6th edition. Lippincott, Philadelphia, 1969.
- [104] Hamid Katoozian, H., Davy, D.T., Arshi, A. and Saadati, U., "Material optimization of femoral component of total hip prosthesis using fiber reinforced polymeric composites", *Medical Engineering & Physics*, **23**: 503–509, 2001.
- [105] Harrigan T.P., Kareh J.A., O'Connor D.O., Burke D.W., and Harris W.H., "A finite element study of the initiation of failure of fixation in cemented femoral total hip components", *J. Orthopaedic Res.*, **10**: 134, 1992.
- [106] Harrigan, T.P. and Harris, W.H., "A finite element study of the effect of diametral interface gaps on the contact areas and pressures in uncemented cylindrical femoral total hip components," *J Biomech*, **24**: 87-91, 1991.

- [107] Harrigan, T.P. and Harris, W.H., "A three-dimensional non-linear finite element study of the effect of cement-prosthesis debonding in cemented femoral total hip components," *J Biomech*, **24**: 1047-1058, 1991.
- [108] Hastings, G.W. and Mahmud, F.A., "Electrical effects in bone," *J. Biomedical Eng.*, **10**: 515-521, 1988.
- [109] Haynes, D. R., Rogers, S. D., Hay, S., Percy, M. J. and Howie, D. W., "The difference in toxicity and release of bone-resorbing mediators induced by titanium and cobalt-chromium-alloy wear particles", *J. Bone Jt Surg.*, **75A**: 825-834, 1993.
- [110] Hedia, H. S., Barton, D. C., and Fisher, J., "Shape optimisation of a Charnley prosthesis based on the fatigue notch factor," *Bio-Materials and Engineering*, **6**: 199-217, 1996.
- [111] Hedia, H.S., Barton, D.C., Fisher, J., and Elmidany, T.T., "Effect of idealization, load conditions and interface assumptions on the stress distribution and fatigue notch factor in the human femur with an endoprosthesis," *Bio-Medical Materials and Engineering*, **6**: 135-152, 1996.
- [112] Heimke, G., Jentschura, G., and Werner, E., "Direct anchorage of Al₂O₃ ceramic hip components: Three years of clinical experience and results of further animal studies," *J. Biomed. Mater. Res.*, **12**: 57-65, 1979.
- [113] Henn, G., Prendergast, P. J., and Taylor, D., "Assessment of particulate composite material for use in hip joint prostheses," In Proceedings of the sixth Irish Materials Forum (Edited by Taplin, D.M.R. and Taylor, D.), pp. 283-232, Elsevir Applied Science, 1989.
- [114] Hert, J., Sklenska, A., Liskova, M., "Reaction of bone to mechanical stimuli. Part 5. Effect of intermittent stress on the rabbit tibia after reaction of the peripheral nerves," *Folia Morphol.*, **19**: 378-387, 1971.
- [115] Hertzler J., Miller M.A., and Mann K.A., "Fatigue crack growth rate does not depend on mantle thickness: an idealized cemented stem construct under torsional loading", *Journal of Orthopaedic Research*, 2002
- [116] Hochman R.F., US patient 3, **893**: 196, 1975.
- [117] Hoffman, O., "The brittle strength of orthotropic materials," *J. Composite Mater.*, **1**: 200-207, 1967.
- [118] Hozack WJ, Rothman RH, Booth REJ, Balderston RA. "Cemented versus cementless total hip arthroplasty. A comparative study of equivalent patient populations", *Clin Orthop*; **289**:161-165, 1993.
- [119] Huiskes R. "Failed innovation in total hip replacement: Diagnosis and proposals for a cure," *Acta Orthop Scand* , **64 (6)**: 699-716, 1993.

- [120] Huiskes R. and Boeklagen R., "Mathematical shape optimization of hip prosthesis design", *J. Biomechanics*, **22**: 793-804, 1989
- [121] Huiskes, R. and Chao, E.Y.S., "A survey of finite element analysis in orthopaedic biomechanics: the first decade," *J Biomech.*, **16**: 385-409, 1983.
- [122] Huiskes, R. and Nunamaker, D., "Local stresses and bone adaptation around orthopedic implants", *Calcif Tissue Int.*, **36**: 110-117, 1984.
- [123] Huiskes, R. and Vroemen, W., "A standardized finite element model for routine comparative evaluations of femoral hip prostheses," *Acta Orthop Belg*, **52**: 258-261, 1986.
- [124] Huiskes, R. H., van Heck, J., Walker, P. S., Green, D. J., and Nunamaker, D., "A three -dimensional stress analysis of a new finger-joint prosthesis fixation system". In Proc. Finite Elements Biomechanics. Vol.2, Simon, B. R., Ed., University of Arizon, Tucson, pp. 749, 1980.
- [125] Huiskes, R., "Principal methods of solid biomechanics," Chapter 4 In Functional behavior of orthopedic materials. 1- Fundamentals. (Edited by Hastings, G.W. and Ducheyne, P.), pp. 51-97, CRC Press, Boca Raton, 1984.
- [126] Huiskes, R., "Stress patterns, failure modes and bone remodeling". In Non-Cemented Total Hip Arthroplasty (Edited by Fitzgerald, R. Jr.), pp. 283-302, Raven Press, New York, 1988.
- [127] Huiskes, R., Janssen, J.D. and Slooff, T.J., "A detailed comparison of experimental and theoretical stress analyses of the human femur," In Mechanical Properties of Bone (Edited by Cowin, S.C.) AMD-Vol.45, pp. 211-234, American Society of Mechanical Engineers, New York, 1981
- [128] Huiskes, R., "Some fundamental aspects of human joint replacement: analyses of stresses and heat-condition in bone-prosthesis structures", *Acta Orthop. Scand. Suppl.*, pp.185, 1979.
- [129] Huiskes, R., Weinans H. and van Riebergen, B., "The relationship between stress shielding and bone resorption around total hip stems and the effect of flexible materials", *Clin. Orthop.* **274**: 124-134, 1992.
- [130] Huiskess, R., "Optimal stem dimensions for intramedullary fixated custom-fit joint prostheses," ZWO Scientific Report, Grant No. S.95-118, The Netherlands Organization for the Advancement of Pure Research, The Hague, 1981.
- [131] Introduction to ANSYS – Release 5.3, 000777, July 24, 1996Ansys
- [132] Jacob, H.A.C. and Huggler, A.H., "An investigation into the biomechanical causes of prosthesis stem loosening within the proximal end of the human femur," *J. Biomechanics*, **13**: 159-173, 1980.

- [133] Jacobsson S.A., Djerf K., Gillquist J., Hammerby S., Iversson I., "A prospective comparison of Butel and PCA hip arthroplasty," *J. Bone Joint Surg.*, **75B**: 624-629, 1993.
- [134] Jin Z.M., Dowson D., Fisher J., "A parametric analysis of the contact stress in ultra-high molecular weight polyethylene acetabular cups", *Med. Eng. Phys.*, **16**: 398-405, 1994.
- [135] Johnston R. C., Brand R.A., Crowninshield, R.D., "Reconstruction of the human hip: a mathematical approach to determine optimum geometrical relationships," *J. BIOMECH*, **61A**: 5, 1979.
- [136] Justus, R. and Luft, J.H., "A mechanochemical hypothesis for bone remodeling induced by mechanical stress," *Calcified Tissue International*, **5**: 222-235, 1970.
- [137] Katoozian, H., Davy, D.T., "Three-dimensional shape optimization of femoral components of total hip prostheses, Bioengineering Conference", BED-Vol. 24, ASME, pp. 552-555, 1993.
- [138] Katoozian, H; Davy, D T; Arshi, A; Saadati, U., "Material optimization of femoral component of total hip prosthesis using fiber reinforced polymeric composites", *Medical Engineering and Physics*, **23(7)**: 505-511, September 2001
- [139] Keaveny TM, Bartel DL. "Mechanical consequences of bone ingrowth in a hip prosthesis inserted without cement", *J Bone Joint Surg*; **6**: 911-923, 1995.
- [140] Keaveny, T.M., and Bartel, D.L., "Effect of porous coating and collar support on early load transfer for a cementless hip prosthesis," *J Biomech*, **26**: 1205-1216, 1993.
- [141] King, A.I., "A review of biomechanical models," *J. Biomechanical Eng.*, **106**: 97-104, 1984.
- [142] Klabunde, R., and Portmann, D., "Consequences of dislocation on hard-hard bearings in total hip arthroplasty," Proceedings of the 12th Conference of the European Society of Biomechanics, edited by Prendergast, P.J., Lee, T.C. and Carr, A.J., Trinity College, Dublin, 28-30 August 2000.
- [143] Kohnke, P., "ANSYS User's Manual", Rev. 5.1, Vol. 4, theory, Swanaon Analysis Systems Inc., Houston, 1994.
- [144] Kuiper J.H., Huiskes R., "Numerical optimization of hip-prosthetic stem material," In: Middleton et al., editors. Computer methods in Biomechanics and biomedicine, 76-84, 1993.
- [145] Kuiper, J.H. and Huiskes, R., "Friction and stem stiffness affect dynamic interface motion in total hip replacement," *J Orthop res*, **14**: 36-43, 1996.

- [146] Kummer, B., "Bio mechanics of the joints. The demand of the joint cartilage," 7 Wiss. Konf. Interpret of natural scientists and physicians (Deutsher Naturforscher und Ärzte), 19-28, 1974.
- [147] Kummer, B., "The demand of the joints, represented by the example of the human hip joint. Negotiations of the German orthopedic society," 55. Konger. Kassel 1968, 301-311, 1969.
- [148] Kummer, B.K.F., "Biomechanics of bone: Mechanical properties, functional structure, and functional adaptation," In Biomechanics: Its Foundations and Objectives, Y.C. Fung, N. Perrone, and M. Anliker (eds.) Prentice-Hall, Englewood Cliffs, NJ, 237-271, 1972.
- [149] Kwarteng KB. "Carbon fiber reinforced PEEK (APC-2/AS-4) composites for orthopaedic implants", *Journal of Biomedical Materials Research*, **29**: 10-14, 1990.
- [150] Lanyon, L. E., "The measurement and biological significance of bone strain in vivo, in Mechanical Properties of Bone" (AMD – Vol. 45), Cowin, S. C., Ed., American Society of Mechanical Engineers, New York, pp. 93, 1981.
- [151] Lanyon, L.E., "Osteocytes, strain direction, bone modeling and remodeling," *Calcif. Tissue Int.* 53(Supl.), S102-S107, 1993.
- [152] Lee A. J. C. and Ling R. S. M., "The Exeter Hip System," Seminar and Workshop Handbook, University of Exeter, Devon, 1983.
- [153] Lennon A.B. and Prendergast P.J., Stress-based criteria to compare cement stresses between finite element models of cemented joint replacements, *J. Biomechanical Eng.*, 2001.
- [154] Lennon A.B., Prendergast P.J., "Residual stress due to curing can initiate damage in porous bone cement: experimental and theoretical evidence", *Journal of Biomechanics*, **35**: 311-321, 2002
- [155] Lennon, A. and Prendergast, P. J., privet communication, 24.Nov 1999.
- [156] Lewis, J.L., Askew, M.J., Wixson, R.L., Kramer, G.M., and Tarr, R.R., "The influence of prosthetic stem stiffness and of a calcar collar on stresses in the proximal end of the femur with a cemented femoral component," *J Bone Joint Surg*, **66A**: 280-286, 1984.
- [157] Linder L., "Implant stability, histology, RSA and wear-more critical questions are needed: a viewpoint," *Acta Orthop Scand*, **65**: 654-658, 1994.
- [158] Ling, R. A., Lee, A. C. J., and Vangala, S. S., "The effect of implant design on fixation and performance", in Trans. 3rd Annu. Meeting Society for Biomaterials, New Orleans, 1977, 14.

- [159] Little, G.W., "Strain measurements of a model of the Geomedic knee," Ph.D. Thesis in mechanical engineering, University of Dublin, 1983.
- [160] Lotz, J.C., Cheal, E.J., and Hayes, W.D., "Fracture prediction for the proximal femur using finite element models. Part I: Linear analysis. Part II: Nonlinear analysis," *J. Biomech. Eng.*, **113**: 353-365, 1991.
- [161] Macey, A. C., McManus, F. and Taylor, D., "Subcapital fracture in a femoral prosthesis," *Proc. I. Mech. E. Part H* 203, 171-172, 1989.
- [162] Mackerle, J. "Finite and poundary element methods in biomechanics: a bibliography (1976-1991). *Eng. Comput*, Vol. 9, 403-435, 1992.
- [163] Mackerle, J. "Finite and poundary element techniques in biomechanics: a bibliography (1991-1993). *Finite Elem. Anal. Design*, 16, 163-174, 1994.
- [164] Magee FP, Weinstein AM, Longo J. "A canine composite femoral stem: an in vivo study", *Clin Orthop Res*, **235**: 237-53, 1998.
- [165] Makarand G. Joshi, Suresh G. Advani, Freeman Miller, Michael H. Santare, "Analysis of a femoral hip prosthesis designed to reduce stress shielding", *Journal of Biomechanics*, **33**: 1655-1662, 2000.
- [166] Maloney, W. J., Jasty, M., Burke, D. W., O'Connor, D. O., Zalenski, E. B., Bragdon, Ch. And Harris, W. H., "Biomechanical and histologic investigation of cemented total hip arthroplasties. A study of autopsy-retrieved femurs after in vivo cycling", *Clin. Orthop.*, **242**: 129-140, 1989.
- [167] Maloney, W. J., Jasty, M., Rosenberg, A. and Harris, W. H., "Bone analysis in well-fixed cemented femoral components", *J. bone Jt Surg.* **72B**: 966-970, 1990.
- [168] Maloney, W. J., Lane Smith, R., Castro, F. and Schurman, D. J., "Fibroblast response to metallic debris in vitro", *J. Bone Jt Surg.*, **75A**: 835-844, 1993.
- [169] Martens, M., Aermoudt Ettiene, De Meester, P., Ducheyne, P., Mulier, J.C., de Langh, I.R.K., Kestellin, P., "Factors in the mechanical failure of the femoral component in total hip prosthesis," *Acta. Orthop. Scand.*, **45**: 693-710, 1974.
- [170] Martens, M., Van Audekercke, R., Delpont, P., De Meester, P. and Mulier, J.C., "The mechanical characteristics of cancellous bone at the upper femoral region," *J. Biomech.* **16**: 971-983, 1983.
- [171] Martin, R.B. and Ishida, J., "The relative effects of collagen fiber orientation, porosity and mineralization on bone strength," *J. Biomechanics*, **22**: 419-426, 1989.
- [172] Martin, R.B., Burr, D.B., "Structure, Function and Adaptation in Compact bone," Raven Press: New York, 1989.

- [173] Maxian T.A., Brown T.D., Pedersen D.R., et al., "A sliding-distance-couple finite element formulation for polyethylene wear in total hip arthroplasty", *J. Biomech.*, **29(5)**: 687-692, 1996.
- [174] McBeath, A.A., Schpler, S.A., and Seireg, A.A., "circumferencetial and longitudinal strain in the proximal femur as determined by prosthesis (thr) type and position," Proc. 25th Ann. Mtg Othop. Res. Soc., San Francisco, California, Vol. 36, 1979.
- [175] McKee, G.K., "Development in total hip joint replacement," *Inst. Mech. Eng. Proc.*, 181, 1967.
- [176] McLeish, R.D. and Charnley, J., "Abduction forces in the one legged stance," *J. Biomechanics*, **3**: 191-209, 1970.
- [177] McNamara, B. P., Prendergast, P. J., Taylor, D., and Toni, A., "Prediction of bone remodelling around hip prosthesis stems based on altered microdamage accumulation in bone tissue," 41 Annual Meeting, Orthopaedic Research Society, Orlando, Florida, February 13-16, 1995.
- [178] McNamara, B.P. "Damage Stimulated Bone Remodeling", Ph.D. Thesis, University of Dublin, 1995.
- [179] McNamara, B.P., Cristofolini, L., Toni, A., and Taylor, D., "Relationship between bone-prosthesis bonding and load transfer in total hip reconstruction," *J Biomechanics*, **30(6)**: 621-630, 1997.
- [180] McNamara, P. P., Taylor, D. and Prendergast, P. J., "Computer prediction of adaptive bone remodeling around non-cemented femoral prostheses: the relationship between damage-based and strain-based algorithms," *Med. Eng. Phys.*, **19(5)**: 454-463, 1997.
- [181] Miller, J., Burke, D.L., Stachiewicz, J.W., and Kelebay, L., "A study of the interface between polymetacrylate and living cortical bone under conditions of load bearing," In Proc. 22nd Annu. Meeting, Orthopedic Research Society, New Orleans, 1976.
- [182] Moalic, J. M., "Fatigue of fibre reinforced polymethylmethracrylate," M.Sc. Thesis in mechanical engineering, University of Dublin, 1987.
- [183] Moaveni, S., "Finite element analysis, Theory and Application with ANSYS." Prentice-Hall, New Jersey, 1999.
- [184] Moore, A.T., "The self-locking metal hip prosthesis," *J. Bone Joint Surg.*, **39A**: 811-827, 1957.
- [185] Morley, J. G., "High performance composites," publ. Academic Press, 1987.

- [186] Morscher E.W., Dick W., "Cementless fixation of 'isoelastic' hip endoprostheses manufactured from plastic materials," *Clin Orthop Rel Res*, **176**: 77-87, 1983.
- [187] Müller, M.E., "Total hip prosthesis," *Clin. Orthop.*, **72**: 46-68, 1970.
- [188] Munting, E. and Verhelpen, M., "Fixation and effect on bone strain pattern of stemless hip prosthesis", *J. Biomechanics*, **8**: 949-961, 1995.
- [189] Natalie AN, Meroi EA. "A review of the biochemical properties of bone as a material", *J Biomed Eng*, **11**:266-76, 1989.
- [190] Niinimäki T., Puranen J., Jalovaara P., "Total hip arthroplasty using isoelastic femoral stems," *J. Bone Joint Surg.*, **76B(3)**: 413-418, 1994.
- [191] Nistor L., Blaha J.D., Kjellstrom U., and Selvik G., "In vivo measurements of relative motion between an uncemented femoral total hip component and the femur by roentgen stereophotogrammetric analysis," *Clin Orthop*, **269**: 220-227, 1991.
- [192] Norman, T., Saligrama, V.C., Hustosky, K.T., Gruen, T.A. and Blaha, J.D., "Axisymmetric finite element analysis of debonded total hip stem with an unsupported distal tip," *J Biomech Eng*, **118**: 399-404, 1996.
- [193] O'Brien, B. M., "Isoelastic hip prosthesis design," Ms.C. Thesis in mechanical engineering, University of Dublin, 1991.
- [194] Oh J. and Harris, W. H., "Proximal strain distribution in the loaded femur. An in vitro comparison of the distributions in the intact femur and after insertion of different hip replacement femoral components," *J. Bone Jt. Surg.*, **60a**: 75-86, 1978.
- [195] Orr, J.F., "Experimental measurement of stresses in bone and joint replacements," Ph.D. Thesis in Mechanical Engineering, The Queens University of Belfast, 1985.
- [196] Park S. H., Llinás A., Goel V. K., Keller J. C., "Bone Repair and Joint Implant," CRC Press, Inc. 1995.
- [197] Park, H. C., Liu, Y. K. and Lakes, R. S., "The mechanical properties of bone-particle impregnated PMMA," *J. Biomechanical Eng.*, **108**: 141-148, 1986.
- [198] Park, S-H., Llinas, A., Goal, V.K. & Keller, J.C. "Hard Tissue Replacement", CRC Press, Inc., 1995
- [199] Paul, J. P., "Approaches to design. Force actions transmitted by joints in the human body," *Proc. R. Soc. Lond. B.*, **192**: 163-172, 1976b.

- [200] Paul, J. P., "Loading on normal hip and knee joints and on replacements, " in Advances in artificial hip and knee joint technology (Edited by Holmann, D. and Schaldach, M.), *Eng. In Med* 2, 1976a
- [201] Paul, J.P., "Bioengineering studies of the force s transmitted by joints. ii. engineering analysis," In: Kendi, R.M., ed. Biomechanics and Related Topics. Pergamon Press, 1964.
- [202] Pauwels, F., "Atlas to the bio mechanics of the healthy and ill hip," Berlin, Heidelberg, New York, 1973.
- [203] Pauwels, F., "The bio mechanics of the movement apparatus," Berlin, Heidelberg, New York: Springer 1965.
- [204] Pauwels, F., "Biomechanics of the locomotion apparatus", Springer-Verlag, Berlin, 1980.
- [205] Pauwes, F., "The static significance of the linea aspera," In Biomechanics of the locomotor apparatus (Translated from the 1965 German edition by Manquet, P. and Furlong, R.) pp. 223-228, 1980a
- [206] Piekarsk, K.R., "Analysis of bone as a composite material," *Int. J. Engng. Sci.*, **11**: 557-565, 1973.
- [207] Piekarski, K.R., "Morphology and fracture of bone," In Fracture '77 (Edited by Taplin, D.M.R.), Pergamon Press, London, 607-641, 1977.
- [208] Pietrabissa R., Rainmondi M., Martino E.D., "Wear of polyethylene cups in total hip arthroplasty: a parametric mathematical model", *Med. Eng. Phys.*, **20**: 199-210, 1998.
- [209] Pilliar R.M., Lee J.M., Maniopoulos C., "Observations on the effect of movement on bone ingrowth into porous-surfaced implants," *Clin Orthop Rel Res*, **208**: 103-108, 1986.
- [210] Pilliar, R. M., Blackwell, R., MacNab, I. and Cameron, H. U., "Carbon fibre reinforced bone cement in orthopaedic surgery," *J. Biomat. Mater. Res.*, **10**: 893-906, 1979.
- [211] Poss, R., "Natural factors that affect the shape and strength of aging human femur", *Clin. Orthop.*, **274**: 194-201, 1992.
- [212] Prendergast P. J., "A structural analysis of the artificial hip joint with a damage model to simulate bone adaption," Ph. D. Thesis, Trinity College, 1991.
- [213] Prendergast P. J., and Taylor D., "Stress analysis of the proximo-medial femur after total hip replacement," *J. Biomed. Eng.*, **12**: 379-382, 1990.

- [214] Prendergast P.J. and Taylor D., "Prediction of bone adaptation using damage accumulation," The 8th meeting of the European Society of Biomechanics, Rome, June 21-24, 1992.
- [215] Prendergast P.J., "Bone prostheses and implants", in: S.C. Cowin (Ed.), Handbook of Bone Mechanics, CRC Press, Boca Raton, FL, Chapter 35.
- [216] Prendergast, P. J., "Finite element models in tissue mechanics and orthopaedic implant design," *Clinical Biomechanics*, **12(6)**: 343-366, 1997.
- [217] Prendergast, P. J., Monaghan, J., and Taylor, D., "Material selection in the artificial hip joint using finite element stress analysis," *Clinical Materials*, **4**: 361-376, 1989.
- [218] Prendergast, P.J., and Huiskes, R., "The biomechanics of Wolff's law: recent advances," *Irish J. Med. Sci.*, **164(2)**: 152-154, 1995.
- [219] Raftopolous, D., Katsamanis, E., Saul, F., Liu, W. and Saddemi, S. "An intermediate loading rate technique for the determination of mechanical properties of human femoral cortical bone," *J. Biomed. Eng.*, **12**, 379-382, 1993.
- [220] Reilly, D.T. and Burstein, A. H., "The elastic and ultimate properties of compact bone tissue," *J. Biomechanics*, **8**: 393-405, 1975.
- [221] Rhinelander, F.W., "Circulation of bone," In The Biochemistry and Physiology of Bone, 2nd edition, G.H. Bourne (ed.) Academic, New York, pp. 2-78, 1972.
- [222] Ring, P.A., "Complete replacement arthroplasty of the hip by the ring prosthesis," *J. Bone Joint Surg.*, **50B**: 720-731, 1968.
- [223] Ring, P.A., "Use of cobalt-chromium-molybdenum in total hip replacements," *J. Bone Joint Surg.*, **53B**, 344 – 357, 1971.
- [224] Ritter, M., Stringer, E., Littrell, D., Williams, J., "Correlation of prosthetic femoral head size and/or design with longevity of total hip arthroplasty," *Clin Orthop. And Rel. Res.*, 179, June 1983.
- [225] Rohlmann, A., Cheal, E.J., Hayes, W.C., and Bermann, G.A., "Nonlinear finite element analysis of interface conditions in porous coated hip endoprostheses," *J biomech*, **21**: 605-611, 1988.
- [226] Rohlmann, A., Mossner, U., Bergmann, G. and Kolbel, R. "Finite element analysis and experimental investigation in femur with hip endoprosthesis," *J. Biomechanics* **16**, 727-742, 1983.
- [227] Rohlmann, A., Mössner, U., Bergmann, G., Hees, G. and Kölbel, R., " Effects of stem design and material properties on stresses in hip endoprostheses," *J biomech Eng*, **9**: 77-83, 1987.

- [228] Rublin, P.J., Rakotomanana, R.L., Leyvraz, P.F., Zysset, P.K., Curnier, A., and Heegaard, J.H., "Frictional interface micromotions and anisotropic stress distribution in a femoral total hip component," *J Biomech*, **26**: 725-739, 1993.
- [229] Sasaki, N., Matsushima, Ikawa, T., Yamamura, H. and Fukuda, A., "Orientation of bone mineral and its role in the anisotropic mechanical properties of bone – transverse anisotropy," *J. Biomechanics*, **22**, 157-164, 1989.
- [230] Scales, J.T., "Arthroplasty of the hip using foreign materials: A history," *Inst. Mech. Eng. Proc.*, **181**: 3, 1966.
- [231] Scales, J.T., "The unsuitability of nylon weight bearing prosthesis articulating with bone or cartilage," *Acta. Orthop. Scand.*, **27**: 13-20, 1957.
- [232] Scales, J.T., Kelly, P., Goddard, D., "Friction torque studies of total joint replacements – the use of a simulator," *Ann. Rheum. Dis. Suppl.*, **28**: 30-35, 1969.
- [233] Schmidt, J., Hackenbroch, M.H., "The cenos hollow stem total hip arthroplasty: first experiences in a prospective study", *Archives of the Orthopaedic Trauma Surgery*, **113**: 117–120, 1994.
- [234] Semlitsch, M., "Artificial joint material development," *Engineering in Medicine*, **2**: 89-97, 1973.
- [235] Semlitsch, M., "Technical progress in artificial hip joints," *Engineering in Medicine*, **3**: 10-19, 1974,
- [236] Shorbe, H.B., "Total hip replacement without cement," *Clin. Orthop.*, **72**: 186-200, 1970.
- [237] Sih, G.C., Connelly, G.M., and Berman, A.T., "The effect of thickness and pressure on the curing of PMMA bone cement for the total hip joint replacement," *J. Biomechan.*, **13**: 347, 1980.
- [238] Simoes J.A., Marques A.T., Jeronimidis G., "Design of a controlled-stiffness composite proximal femoral prosthesis," *Composites Science and Technology*, **60**: 559-567, 2000.
- [239] Simoes J.A., Taylor M., "Comparison of conventional and hybrid modulus press-fit proximal femoral prostheses," In: M Cerrolaza, D Jugo, CA Brebbia, editors. *Simulation modelling in bioengineering. Computational Mechanics Publications*, pp. 127-139, 1996.
- [240] Simoes J.A., Taylor M., Marues A.T., Jeronimidis G., "Preliminary investigation of novel controlled stiffness proximal prosthesis," *Proc Inst Mech Engrs Part H*, **212**: 165-175, 1998.

- [241] Simoes J.A.O., Antonio C.A.C., Marques A.T., "Material stiffness optimisation for a composite hip prosthesis," In: S Adali, VE Verijenko, editors. 1st International conference on Composite Science and Technology, Durban, South Africa, Department of Mechanical Engineering, University of Natal, pp. 477-482, 1996.
- [242] Simões, J.A., Marues, A.T., and Jeronimidis, G., "Design of a controlled-stiffness composite proximal femoral prosthesis," *Composite Science and Technology*, **60**: 559-567, 2000.
- [243] Sivash, K.M., "The development of a total metal prosthesis for the hip joint from a partial joint replacement," *Reconstr. Surg. Traumat.*, **11**, 53-62, 1969.
- [244] Skinner HB. Composite technology for total hip arthroplasty. *Clin Orthop Res*; **235**: 224-36, 1988.
- [245] Sloof, T.J.J.H., "Stress pattern in the proximal femur with cemented femoral prostheses," (Ger.) *Arch. Orthop. Unfallchir*, **71**: 281-289, 1971.
- [246] Smith, R.P., "Total hip replacement," *Clin. Orthop.*, **72**: 177-185, 1970.
- [247] Smyth, E.H.J., "The mechanical problem of the artificial hip," *J. Bone Joint Surg.*, **40B**: 778-798, 1958.
- [248] Søballe, K., Hansen, E., Brockstedt-Rasmussen, H. and Bünger, C., "Gap healing enhanced by hydroxyapatite coating", *Clin. Orthop.* **272**: 300-307, 1991.
- [249] Spector, M., Shorkroff, S., Hsu, H. P., Lane, N., Sledge, C. B. and Thornhill, T. S., "Tissue changes around loose prostheses. A canine model to investigate the effects of an anti-inflammatory agent", *Clin. Orthop.*, **261**: 140-150, 1990.
- [250] Speirs A.D., Slomczykowski M.A., Orr T.E., Siebenrock K., Nolte L.P., "Three-dimensional measurement of cemented femoral stem stability: an in vitro cadaver study", *Clinical Biomechanics*, **15**: 248-255, 2000.
- [251] Stolk J., Verdonschot N., and Huiskes R., "Hip-joint and abductor-muscle forces adequately represent in vivo loading of a cemented total hip reconstruction", *J. Biomech*, **34(7)**: 917-926, July 2001
- [252] Stolk, J., Verdonschot, N., and Huiskes, R., "FE simulation of damage accumulation in cement around a prosthetic hip stem," Proceedings of the 12th Conference of the European Society of Biomechanics, edited by Prendergast, P.J., Lee, T.C. and Carr, A.J., Trinity College, Dublin, 28-30 August 2000.
- [253] Stone MH, Wilkinson R, Stother IG. "Some factors affecting the strength of the cement-metal interface", *J Bone Joint Surg*, **71(2)**:217-221, 1989.
- [254] Stone, J.L., Beaupre, G.S., and Hayes, W.O., "Multiaxial strength characteristics of trabecular bone," *J. Biomech.*, **16**: 743-752, 1983.

- [255] Svensson, N.L., Valliappan, S. and Wood, R.D., "Stress analysis of human femur with implanted charnly prosthesis," *J. Biomechanics*, **10**: 581-588, 1977.
- [256] Szivek, J.A. and Gealar, R.L., "Comparison of the deformation response of synthetic and cadaveric femora during simulated one-legged stance," *J. Appl. Biomater.* **2**: 277-280, 1991.
- [257] Täger, K.H., The new spongiosa hip joint endoprosthesis (SHEP)., *Acta Orthopaedica Belgica*, 59 (Suppl. 1), 351-353, 1993.
- [258] Taylor, D., and Delestre, C., "The use of textiles for the reinforcement of bone cement," in *Textiles in Medicine and Surgery*, UMIST, Manchester, England, 1989.
- [259] Tensi, H.M., Gese, H., and Ascherl, R., "Non-linear three-dimensional finite element analysis of a cementless hip endoprosthesis," *Proc Inst Mech Eng (Lond)*, **203H**: 215-222, 1989.
- [260] Thompson, F.R., "Two and a half years experience with a vitallium intermedullary hip prosthesis," *J. Bone Joint Surg.*, **36A**: 489-502, 1954.
- [261] Timoshenko, S. P. and Goudier, J. N., "Theory of Elasticity", McGraw-Hill, Kogachucha, 1970.
- [262] Torino, A.J., Davidson, C.L., Kloppe, P.J. and Linclau, L.A., "Protection from stress in bone and its effects: Experiments with stainless steel and plastic plates in dogs," *J. Bone Joint Surg.*, **58**: 107-113, 1976.
- [263] Trager D. "The 5 to 7 year follow-up results with the RM isoelastic hip prosthesis," *Unfallchirurg*, **92**: 301-304, 1989.
- [264] Treharne, R.W., "Review of Wolff's law and its proposed means of operation," *Orthopaedic Review*, **10**: 35-47, 1981.
- [265] Tronzo, R.G., "Surgery of the hip Joint," Chap. 3, p. 46, Philadelphia: Lea and Febeger, 1973.
- [266] Tronzo, R.G., "Total hip arthroplasty using a universal joint device," Memphis: Richards Mfg. Co. 1970.
- [267] Uhthoff, H. H. and Germain, J. P., The reversal of tissue differentiation around screws., *Clin. Orthop.* **123**, 248-252, 1977.
- [268] van Lenthe, G.H., Verdonschot, N., Bergmann, G., and Huiskes, R., "The effect of implant material on friction induced heating around total hip implants," *Proceedings of the 12th Conference of the European Society of Biomechanics*, edited by Prendergast, P.J., Lee, T.C. and Carr, A.J., Trinity College, Dublin, 28-30 August 2000.

- [269] Verdonshot N. and Huiskes R., "Mechanical effects of stem cement interface chrematistics in total hip replacement", *Clinical Orthopaedics and Related Res.*, **329**: 326-336, 1996.
- [270] Verdonshot, N. and Huiskes, R., "Subsidence of THA stem due to acrylic cement creep is extremely sensitive to interface friction," *J Biomec*, **29**: 1569-1575, 1996.
- [271] Viceconti, M., Bernakiewicz, M., Taddei, F., Zannoni, C., Toni, A., "Pre-clinical validation total hip replacement: how to take into account the surgeon and the patient?", Proceedings of the 12th Conference of the European Society of Biomechanics, edited by Prendergast, P.J., Lee, T.C. and Carr, A.J., Trinity College, Dublin, 28-30 August 2000.
- [272] Viceconti, M., Toni, A., Giunti, A., "Effects of some technological aspects on the fatigue strength of a cementless hip stem", *Journal of Biomedical Materials Research*, **29**, 875-881, 1995.
- [273] Vichnin, H.H. and Betterman, S.C., "Stress analysis and failure prediction in the proximal femur before and after total hip replacement," *J Biomech Eng*, **108**: 33-41, 1986.
- [274] Vincent, J., "Materials technology from nature," *J. Inst. Metals*, **6**: 1-11, 1990.
- [275] Wang, A., Stark, C., Dumbleton, J.H., Mechanistic and morphological origins of ultra-high molecular weight polyethylene wear debris in total joint replacement prostheses, *Proc. Instn. Mech. Eng.*, **210**: 141-155, 1996.
- [276] Weber, B.C., "Total hip replacement with rotation-endo-prosthesis (trunnion-bearing prosthesis)," *Clin. Orthop.*, **72**: 79-84, 1970.
- [277] Weinans H. Mechanically induced bone adaptations around orthopaedic implants. Ph.D. thesis, University of Nijmegen, The Netherlands; 1992.
- [278] Weinans, H., Huiskes, R., and Grootenboer, H.J., "Effects of material properties of femoral hip components on bone remodeling," *Journal of Orthopaedic Research*, **10**: 845-853, 1992.
- [279] Wenz LM, Merritt K, Brown SA, Moet A. "In vitro biocompatibility of polyetheretherketon and polysulphone composites", *J Biomed Mater Res.*, **24**:207-215, 1990.
- [280] Wettstein, P., "The bone response of the upper femur in total hip replacement," *SICOT* **12**, Abstract, p. 322, 1972.
- [281] Widmer M., Callenbach T, Isler J., Frohlich M., Meier D., Mayer J., "Injection moulding of carbon fibre reinforced PEEK for anistropic hip-prostheses: Preliminary results," In: Proceeding of the III Portuguese Congress in Biomedical Engineering, Porto, 1995.

- [282] Wiles, P., "The surgery of the osteoarthritic hip," *Brit. J. Surg.*, **45**: 488, 1957.
- [283] Willert, H. G., Bertram, H. and Buchhorn, G. H., "Osteolysis in alloarthroplasty of the hip. The role of bone cement fragmentation", *Clin. Orthop.* **258**: 108-121, 1990.
- [284] Willert, H.G. and Semlitsch, M., "Problems associated with the anchorage of artificial joint," In *Advances in Artificial Hip and Knee Joint Technology*, Schaldach, N. and Hohmann, D., Eds., Springer-Verlag, Berlin, 1976.
- [285] Willert, H.G., and Semlitsch, M., "Reactions of the articular capsule to wear products of artificial joint prostheses," *J. Biomed. Material Res.*, **2**: 157-163, 1977.
- [286] Willert, H.G., Semlitsch, M., "Reaction of the articular capsule to plastic and metallic wear products from joint endoprotheses," *Sulzer Tech. Rev.*, No. 2, 119-133, 1975.
- [287] Williams DF, McNamara A, "Turner RM. Potential of polyetheretherketon and carbon-fibre-reinforced PEEK in medical applications" *J Mater Sci*; **6**:188-90, 1987.
- [288] Williams, D.F., Roaf, R., "Implants in surgery," Chap. 6, London: Sauners 1973.
- [289] Winter, G.D., "Prosthesis and tissue: the interface problem," *Biol. Eng.*, 390-394, 1974.
- [290] Woo, S.L.Y., Akeson, W.H., Coutts, R.D., Rutherford, L., Doty, D., Jemmott, G.F., and Amiel, D., "A comparison of cortical bone atrophy secondary to fixation with plates with large differences in bending stiffness," *J. Bone Joint Surg.*, **58**: 190-195, 1976.
- [291] Wood, R.D., "Stress analysis of the femur," Ph.D. Thesis, University of New South Wales, Australia, 1975.
- [292] Wroblewski, B. M., "The mechanism of fracture of the prosthesis in total hip replacement," *Int. Orthop. (SICOT)*, **3**, 137-139, 1979.
- [293] Wu J.S.S., Hung J.P., Shu C.S., Chen J.H, "The computer simulation of wear behavior appearing in total hip prosthesis", *Computer Methods and Programs in Biomedicine*, 2002
- [294] Yamada, H., "Strength of biological materials," Translated by F.G. Evans. Williams and Wilkins, Baltimore, 1970.
- [295] Yoon, Y.S., Jang, G.H., Kim, Y.Y., Shape optimal design of the stem of a cemented hip prosthesis to minimise stress concentration in the cement layer., *Journal of Biomechanics*, **22**: 1279-1284, 1989.

- [296] Zaki, M., Hamed, M., and Abu-Mansour, T., "3D Finite Analysis of Natural and Artificial Hip Joints," *Advances in Bioengineering*, BED-Vol. 31, ASME 1995.
- [297] Zienkiewicz, O. C., *The Finite Element Method*, 3rd ed., McGraw-Hill, London, 1977.
- [298] Eftekhari NS., "Total hip arthroplasty," (it was quoted from the net), 1993.
- [299] Carter, D.R. and Hayes, W.C., "Fatigue life of compact bone_1: Effects of stress amplitude, temperature and density," *J. biomechanics*, **9**: 27-34, 1977a.
- [300] Hert, J., Liskova, M. and Landa, J., "Reaction of bone to mechanical stimuli. Part 1. Continuous and intermittent loading of tibia in rabbit," *Folia Morphol.*, **19**: 290-317, 1971.
- [301] Hedia, H.S., Barton, D.C., Fisher, J., Elmidany, T.T., "A method for shape optimisation of a hip prosthesis to maximise the fatigue life of the cement", *Medical Engineering and Physics* **18**: 647-654, 1996.
- [302] Huiskes, R., "The various stress patterns of press-fit, ingrown and cemented femoral stems", *Clinical Orthopedics* **261**: 27-38, 1990.
- [303] Huiskes, R., "Bone remodeling around implants can be explained as an effect of mechanical adaptation". In: Galante, J.O., Rosenberg, A.G., Gallagher, J.J. (Eds.), *Total Hip Revision Surgery*. Raven Press, New York, 159-171, 1995.
- [304] Gaine, W. J, Sanville, P. R., and Bamford, D. J., "The Charnley-Hastings bipolar prosthesis in femoral neck fractures: a study of dynamic motion", *Injury, Int. J. Care Injured*, **31**: 257-263, 2000.
- [305] Prendergast, P. J., "A structural Analysis of the artificial hip joint with a damage model to simulate bone adaption", Ph.D. Thesis, University of Dublin, Trinity College, 1991.
- [306] McCormack, B.A.O. and Prendergast, P.J., "Microdamage accumulation in the cement layer of hip replacements under flexural loading". *J. Biomechanics*, **32**: 467-475, 1999.
- [307] Stolk, J., Verdonschot, N., and Huiskes, R., "Management of strain fields around singular point: comparison of FE simulations and experiments". In Middleton, J., Jones, M. N., and Pande, G. N., *4th International Symposium on Computer Methods in Biomechanics and Biomedical Engineering*. Gordon and Breach, 1999.
- [308] Engh, C.A., Culpepper, W.J., "Long term results of the use of the anatomic medullary locking prosthesis," *Clinical Orthopaedics and Related Research*, 340-349, 1997.
- [309] Hitti, Y.K., "Hitti's medical dictionary: English-Arabic", 4th Edition, 1982, Librairie du liban, Beirut – Lebanon.

- [310] Dowson D., Unswsorth A., Cooke A. F. and Gvozdanvic D., "Lubrication of Joint"; In An introduction to biomechanics of joints and joint replacements (Edited by Dowson, D. and Wright, V.), pp. 68-73, MEP, London, 1981.
- [311] Jayson M. and Charnley J. "Total Hip Replacement", Sector Publishing Limited, London, 1971.

APPENDIX 1

LIST OF PUBLICATIONS

- [1] H. F. El-Sheikh, B. J. MacDonald and M. S. J. Hashmi, "Numerical Analysis of a Femoral Hip Prosthesis Designed to Reduce Stress Shielding", ESDA2002, 6th Biennial Conference on Engineering Systems Design And Analysis, Istanbul, Turkey, July 8-11, 2002 (to be held).
- [2] H. F. El-Sheikh, B. J. MacDonald and M. S. J. Hashmi, "Finite Element Simulation of The Hip joint During Stumbling: A Comparison between Static and Dynamic Loading", International Conference on Advances in Materials and Processing Technologies, 18 – 21 September 2001, Madrid, Spain, pp..
- [3] H. F. El-Sheikh, B. J. MacDonald and M. S. J. Hashmi, "Material Selection in the Design of the Femoral Component of Cemented Total Hip Replacement", Journal of materials processing technology, 122, (2001), pp.309-317.

Poster Presentation

- [1] H. F. El-Sheikh, B. J. MacDonald and M. S. J. Hashmi, "Effect of Design Features of AHJ: Role of Collar on the Femoral Stem of Cemented Total Hip Replacements", National Committee for engineering science conference: Engineering Design in an Academic Environment, 12 –13 October 2000, Academy House, 19 Dawson St., Dublin 2, Ireland (Abstract).